

“Man would not have attained the possible unless
time and again he had reached out for the impossible.”

— Max Weber

THE UNIVERSITY OF CALGARY

Synthesis, Structure and Reactivity of β -Diketiminato

Supported Organoscandium Cations

by

Paul George Hayes

A DISSERTATION

SUBMITTED TO THE FACULTY OF GRADUATE STUDIES
IN PARTIAL FULFILMENT OF THE REQUIREMENTS FOR THE
DEGREE OF DOCTOR OF PHILOSOPHY

DEPARTMENT OF CHEMISTRY

CALGARY, ALBERTA

APRIL, 2004

© Paul George Hayes 2004

UNIVERSITY OF CALGARY
FACULTY OF GRADUATE STUDIES

The undersigned certify that they have read, and recommend to the Faculty of Graduate Studies for acceptance, a thesis entitled “Synthesis, Structure and Reactivity of β -Diketiminato Supported Organoscandium Cations” submitted by Paul George Hayes in partial fulfilment of the requirements for the degree of Doctor of Philosophy.

Supervisor, Dr. Warren E. Piers, Department of Chemistry

Dr. Tristram Chivers, Department of Chemistry

Dr. George K. H. Shimizu, Department of Chemistry

Dr. Hans J. Vogel, Department of Biological Sciences

External Examiner, Dr. John E. Bercaw, California Institute of Technology

Date

Abstract

A variety of β -diketiminato supported mononuclear dialkyl scandium compounds have been synthesized and fully characterized in both the solid and solution states. The 4-coordinate species exhibit fluxional behaviour in solution which has been quantitatively studied and is interpreted as a dynamic process which equilibrates two structures *via* a C_{2v} symmetric transition state. At elevated temperatures these compounds have been determined to undergo an intramolecular metallation process with loss of RH. Polymerization experiments revealed that several of the organoscandium complexes are effective catalysts for the polymerization of ethylene.

The reactivity of the neutral dialkyl organoscandium species was examined leading to the synthesis of a family of highly reactive organoscandium alkyl cations. Deactivation pathways, most notably C_6F_5 transfer to the metal centre and metallation of an *isopropyl* group were observed. While C_6F_5 transfer impeded subsequent reactivity studies, metallation proceeded sufficiently slowly so as not to hinder the development of their organometallic chemistry. Quantitative analysis of ion-pair dynamics established that intermolecular anion exchange likely occurs by way of a highly ordered transition state, most likely a low energy associative anion displacement by an incoming arene molecule.

A unique class of isolable solvent separated organoscandium methyl cations was synthesized by reaction of dialkyl scandium compounds with $[CPh_3][B(C_6F_5)_4]$. These complexes have been found to be resistant to both C_6F_5 transfer and metallation decomposition pathways. The molecular structures show stabilization of the alkyl cations

through η^6 arene binding to the metal centre. These aromatic solvent molecules are bound sufficiently loose to permit the study of their chemistry. Quantitative kinetic experiments for arene exchange imply a partially dissociative mechanism whereby the rate-limiting step involves dissociation to lower hapticity. The mechanism for arene displacement was further investigated upon exploring the reactivity of these compounds with diphenylacetylene. In this situation it was determined that rate-limiting coordination of the alkyne to the metal centre had a slightly higher barrier than arene ring slipping.

Preliminary work demonstrated that the β -diketiminato ancillary can also be used to prepare organoyttrium species with potential for further derivatization to the corresponding organoyttrium cations.

Acknowledgements

I would like to thank my supervisor, Dr. Warren Piers, for his direction and mentoring throughout this degree. His enthusiasm and insight have both challenged and inspired me by providing an exceptional scientific environment in which to develop as a chemist. His unrelenting work ethic, scientific integrity and amazing efficiency have made a lasting impression which I will continue to strive towards. He made this thesis possible. Thank you.

I would like to extend my gratitude to all my fellow labmates whom have made my time here both productive and fun, especially: Dr. Lawrence (Larry) Lee, Dr. Suobo Zhang, Dr. James Blackwell, Dr. Kevin Cook, Bryon Carpenter (thank you for Easter 2000), Dr. Lisa Knight (my nacnac partner), Dr. Preston Chase, Lee Henderson, Darryl Morrison, Dr. Roland Roesler, Dr. Andy McWilliams, Greg “The Hammer” Welch, Heather Phillips, Glen McInnis, Dr. Ioan Ghesner, Dr. Marcus Schaefer, Allison Kenward, and Mike Bosdet.

A significant quantity of time and energy was expended by Dr. Stuart Dubberley, Patricio Romero (my Chilean brother), and Korey “Papa” Conroy (I’ll miss the B&G) proofreading various portions of this thesis. These efforts contributed significantly to the overall quality of this work, and as such, are greatly appreciated.

A special thank you is extended to Dr. David Emslie, the eternal postdoc, for countless chemistry discussions, lunches on “the hill”, and for continuously keeping my spirits high. It is impossible not to be excited about science in your presence.

I thank Drs. Tristram Chivers, George Shimizu and Hans Vogel for excellent suggestions, numerous reference letters and all else on the extensive list of duties which

sitting on my Ph.D. committee encompassed. I would like to thank Dr. Rupert E. v. H. Spence and Dr. Brian Keay for being members of my Candidacy Committee. Gratitude is extended to Dr. John Bercaw for attending my Ph.D. defence and contributing his knowledge and expertise on mechanistic organometallic chemistry.

Many thanks go to Mrs. Dorothy Fox, Ms. Qiao Wu, Mrs. Roxanna Smith, Dr. Raghav Yamdagni, Mark Toonen, Dave Malinsky, Keith Collins, Kim Wagstaff, Mike Siewert and Ed De Bruyn for expert technical assistance. Dr. Masood Parvez is acknowledged for X-ray crystal structure determinations. I am grateful to Ms. Greta Prihodko and Ms. Bonnie King for keeping me organized. I want to thank Dr. Adrien Côté for his assistance with X-ray crystallography and the DSC/TGA analyzer.

The University of Calgary, the Natural Sciences and Engineering Research Council of Canada, the Killam Foundation, and the Alberta Heritage Foundation are acknowledged for their generous financial support in the form of teaching assistantships and scholarships throughout my graduate career. Gratitude is extended to Dr. Q. Wang of NOVA Chemicals LTD for performing polymerization experiments.

I would like to thank friends Allan MacMillan, Todd Lacey and Drs. Michael and Naomi Kruhlak for extracurricular activities – I owe you my sanity.

I am indebted to the excellent teachers in my life: Gus Pike, Michael Gaudet and Dr. Stephen Westcott. Thank you for nurturing my passion for science.

Finally I wish to extend my utmost gratitude to my parents, George and Christine, my grandparents, Winston, Madeline, Johnnie and Mabel, my siblings, Stephanie and Ian, and my wife Joanne. Without your continual love, guidance and encouragement I would not be where I am today. Thank you for believing in me.

Time transcends inequalities, borders and generations equally
and unforgivingly; it is the most valuable gift one can give.

Thus, I dedicate the following to my eternal supporter and loving wife, Joanne.

Table of Contents

Approval Page.....	ii
Abstract.....	iii
Acknowledgements.....	v
Dedication.....	vii
Table of Contents.....	viii
List of Compounds.....	xi
List of Tables.....	xiii
List of Figures.....	xv
List of Schemes.....	xx
List of Abbreviations and Symbols.....	xxiv
Chapter 1: Introduction	
1.1 Historical Account of Organoscandium Chemistry and Chapter Content.....	1
1.2 Scandocene Chemistry.....	2
1.3 Mixed Cp* - Amido Scandium Chemistry.....	6
1.4 Non-Cp Supported Organoscandium Compounds.....	7
1.5 Cationic Organoscandium Compounds.....	9
1.6 Thesis Goals.....	11
Chapter 2: Synthesis, Characterization and Thermal Decomposition of Dialkylscandium Complexes Supported by the β -Diketiminato Ligand	
2.1 Introduction – β -Diketiminato Ancillary Ligand.....	13
2.1.1 Synthesis and Structural features of the β -Diketiminato Ligand.....	13
2.1.2 Electronic Features and Bonding Modes of the β -Diketiminato Ligand.....	18
2.2 Results.....	23
2.2.1 Synthesis of $L^{\text{Me}}\text{ScR}_2(\text{THF})_x$	23
2.2.2 Synthesis of $L^{\text{tBu}}\text{ScR}_2$	25
2.2.3 X-ray Crystal Structures.....	30

2.2.4	Solution Structures and Dynamic Behaviour.....	47
2.2.5	Reaction of $L^{tBu}ScR_2$ with H_2	56
2.2.6	Thermal Decomposition <i>via</i> Metallation of Aryl <i>Isopropyl</i> Group	63
2.2.7	Ethylene Polymerization Data for $L^{Me}ScCl_2(THF)$, $L^{Me}ScMe_2(THF)$, $L^{tBu}ScCl_2$ and $L^{tBu}ScMe_2$	72
2.3	Proposed Directions for the Acquisition of Organoscandium Catalyzed Ethylene Polymerization Data	74
2.4	Conclusions.....	76

Chapter 3: Activation of Neutral Organoscandium Complexes with Borane-Based Lewis Acids

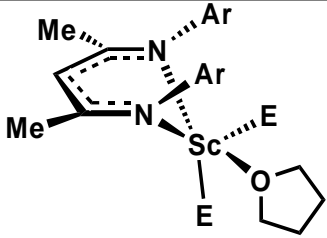
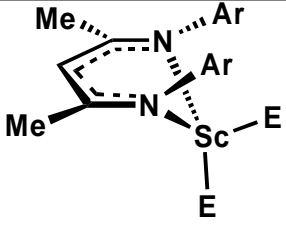
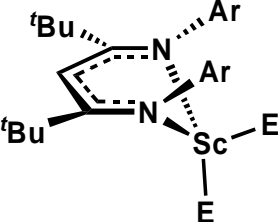
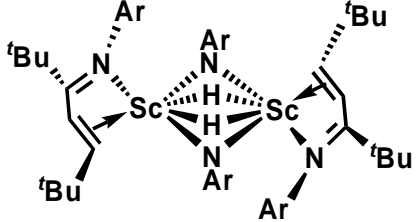
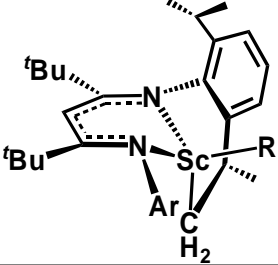
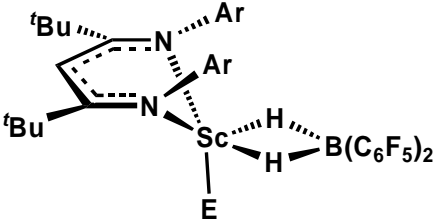
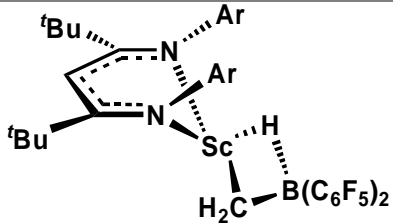
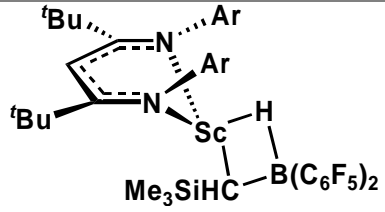
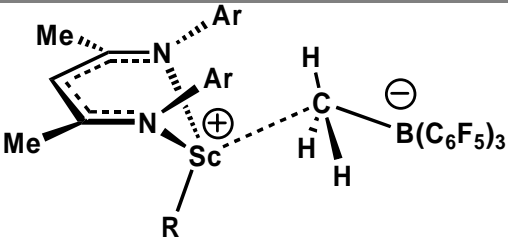
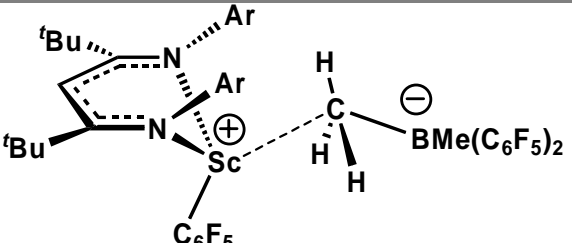
3.1	Introduction.....	78
3.1.1	Triarylborane Lewis Acid Activation of Metallocenes	78
3.1.2	Diarylborane Lewis Acid Activation of Metallocenes	88
3.2	Results.....	91
3.2.1	Reactivity of $L^{tBu}ScR_2$ with $HB(C_6F_5)_2$	91
3.2.2	Reactivity of $L^{Me}ScMe_2$, 1-Me , with $B(C_6F_5)_3$	98
3.2.3	Reactivity of $L^{tBu}ScMe_2$, 2-Me , with $B(C_6F_5)_3$	102
3.2.4	Reactivity of 2-CH₂SiMe₃ with $B(C_6F_5)_3$	111
3.2.5	Thermal Decomposition of Organoscandium Cations <i>via</i> Metallation of an <i>Isopropyl Methyl</i> Group.	119
3.2.6	Ion-Pair Dynamics of 10-Me	124
3.2.7	Ion-pair Dynamics of 10-CH₂SiMe₂CH₂SiMe₃	133
3.2.8	Conclusions.....	141

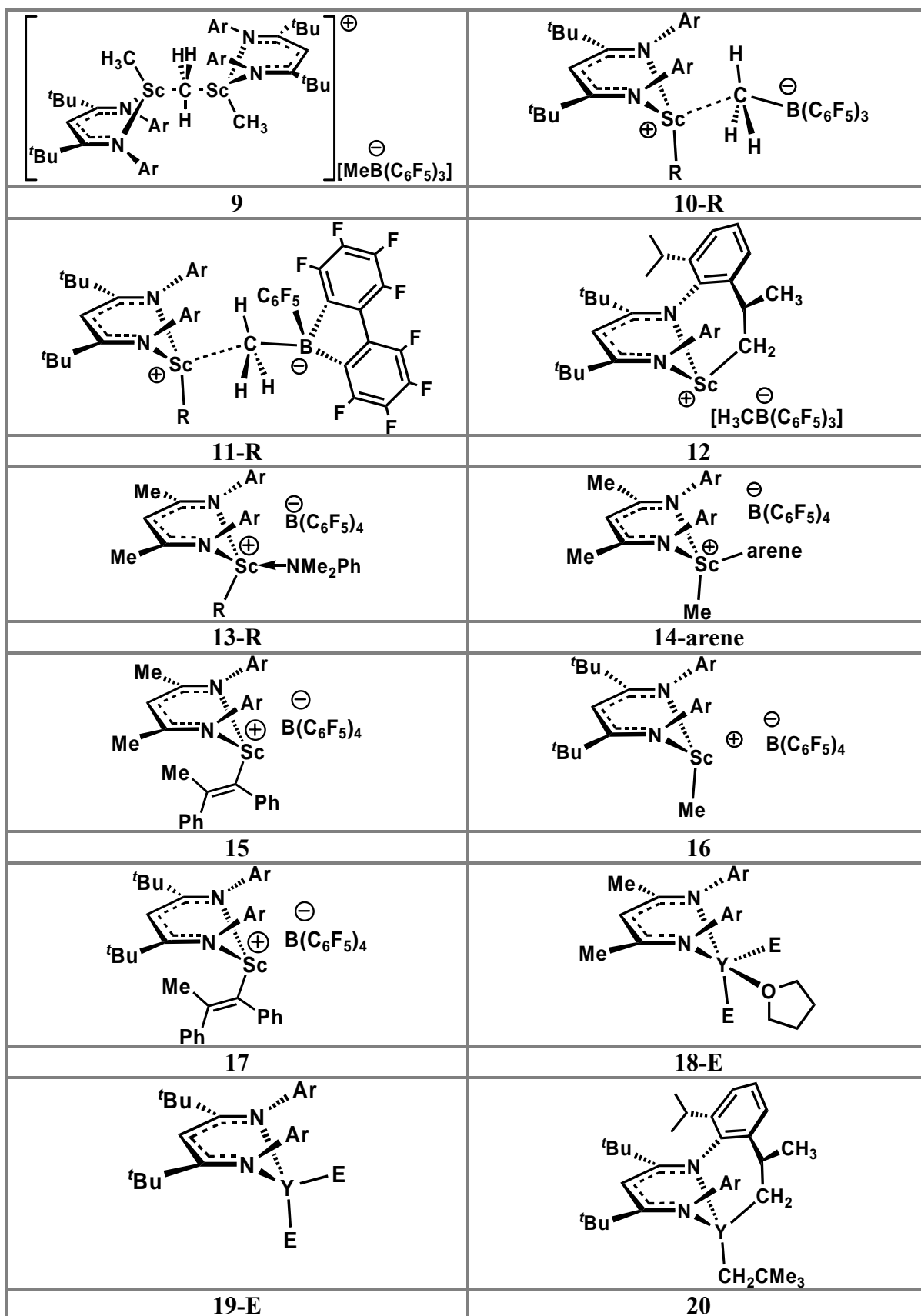
Chapter 4: Activation of Neutral Organoscandium Complexes with Non-Borane-Based Lewis Acids

4.1	Introduction.....	143
4.1.1	Activation of Metallocenes with Protic Activators – $[HNMe_2Ph][B(C_6F_5)_4]$	143
4.1.2	Activation of Metallocenes with $[CPh_3][B(C_6F_5)_4]$	146
4.2	Results.....	147
4.2.1	Reactivity of $L^{Me}ScR_2$ with $[HNMe_2Ph][B(C_6F_5)_4]$	147
4.2.2	Reactivity of $L^{Me}ScR_2$ with $[CPh_3][B(C_6F_5)_4]$	149

4.2.3	Arene Exchange Between 14-C₉H₁₂ and 14-C₇H₈	156
4.2.4	Insertion of Diphenylacetylene into 14-C₉H₁₂	166
4.2.5	Conclusions.....	179
Chapter 5: Future Work: Synthesis of Cationic Organoyttrium Complexes		
5.1	Introduction.....	181
5.1.1	Cationic Organoyttrium Compounds.....	181
5.2	Preliminary Results.....	182
5.2.1	Synthesis and Reactivity of L ^{Me} YR ₂ (THF).....	182
5.2.2	Synthesis and Reactivity of [L ^{tBu} YR ₂] ₂	186
5.3	Conclusions.....	192
Chapter 6: Experimental Methods		
6.1	General.....	193
6.1.1	Laboratory Equipment and Apparatus.....	193
6.1.2	Solvents.....	193
6.1.3	Instrumentation and details for NMR experiments.....	194
6.1.4	Other Instrumentation and Analysis	195
6.1.5	NMR tube Reactions.....	196
6.1.6	Starting Materials.....	197
6.2	Experimental Procedures Pertaining to Chapter 2.....	198
6.2.1	Synthetic Procedures.....	198
6.3	Experimental Procedures Pertaining to Chapter 3.....	220
6.3.1	Synthetic Procedures.....	220
6.4	Experimental Procedures Pertaining to Chapter 4.....	236
6.4.1	Synthetic Procedures.....	236
6.5	Experimental Procedures Pertaining to Chapter 5.....	245
6.5.1	Synthetic Procedures.....	245
6.6	Kinetic Experiments.....	249
	References.....	255
Appendix 1:	Crystallographic Data Tables, Atomic Coordinates, Anisotropic Displacement Parameters and Metrical Data.....	267
Appendix 2:	Publications Arising from Thesis.....	343

List of Compounds

	
1-E(THF)	1-E
	
2-E	2-H
	
3-R	4-E
	
5	6
	
7-R	8



List of Tables

Table 2.1	UV-Vis Data for Scandium Nacnac Compounds	30
Table 2.2	Selected Metrical Data for L ^{Me} ScE ₂ (THF) _x Compounds: 1-Cl(THF) , 1-Me(THF) , and [1-Me]₂	32
Table 2.3	Selected Metrical Data for L ^{tBu} ScE ₂ Compounds: 2-Cl , 2-Me , 2-Et , 2-CH₂Ph , and 2-CH₂SiMe₃	36
Table 2.4	Selected Metrical Data for Mixed Alkyl and Alkylhalide Compounds: 2-Cl(CH₂SiMe₃) , 2-CH₂SiMe₃(CH₂CMe₃) and 2-Br(C₃H₅)	41
Table 2.5	Comparison of Ligand Bond Distances in Complexes of form L ^{tBu} ScR ₂ ..	46
Table 2.6	Selected ¹ H NMR Data of 4-Coordinate Compounds	49
Table 2.7	Selected ¹³ C NMR Data of 4-Coordinate Compounds	50
Table 2.8	Free Energies of "Ligand Flip" in 4-Coordinate Compounds	53
Table 2.9	Isomeric Ratios of Mixed Substituent Compounds	54
Table 2.10	Rate Data for Ligand Flip within 2-CH₂SiMe₃	55
Table 2.11	Selected Metrical Data for 3-CH₂SiMe₃	65
Table 2.12	Half Lives and k _{exp} for Metallation Reactions	68
Table 2.13	Ethylene Polymerization Data for β-Diketiminato Scandium Complexes.....	73
Table 3.1	Selected Metrical Data for 4-H₂B(C₆F₅)₂	95
Table 3.2	Selected Metrical Data for 7-C₆F₅	101
Table 3.3	Selected Metrical Data for 10-Me	108

Table 3.4	Selected Metrical Data for 10-CH₂SiMe₂CH₂SiMe₃	115
Table 3.5	Half-Lives and k_{exp} for Metallation Reactions.....	124
Table 3.6	Rate Data for Exchange Reactions Between 10-Me and 11-Me	130
Table 3.7	Activation Parameters for Exchange Reactions Between 10-Me and 11-Me	132
Table 3.8	Rate Data for Intermolecular Anion Exchange Between 10-CH₂SiMe₂CH₂SiMe₃ and 11-CH₂SiMe₂CH₂SiMe₃	137
Table 4.1	Selected Metrical Data for 14-C₆H₅Br , 14-C₇H₈ and 14-C₉H₁₂	154
Table 4.2	Reaction Rates and Half-Lives for the Arene Exchange of 14-C₉H₁₂ to 14-C₇H₈	160
Table 4.3	Temperature Dependence of K_{eq} for the Addition of 1 Equivalent of Toluene to 14-C₆H₅Br	163
Table 4.4	Reaction Rates and Half-Lives for the Reaction of PhC≡CPh with 14-C₉H₁₂	170
Table 4.5	[Diphenylacetylene] vs. k_{exp} of Reaction with 14-C₉H₁₂	171
Table 4.6	Reaction Rates and Half-Lives for the Reaction of PhC≡CPh with 14-arene.....	172
Table 5.1	Selected Metrical Data for 18-I(THF)	185
Table 5.2	Selected Metrical Data for 19-I	187

List of Figures

Figure 1.1	Olefin Insertion vs. σ -Bond Metathesis for Cp^*_2ScR and Propylene.....	3
Figure 2.1	Acetylacetonato and β -Diketiminato Ligands	14
Figure 2.2	Typical β -Diketiminato Bonding mode between κ^2 and η^5	19
Figure 2.3	Numerous Bonding Modes in a Ba_2L_3 Unit.....	20
Figure 2.4	Proposed Transition State for Halide/Alkyl Redistribution to 2-R(Cl)	28
Figure 2.5	Numbering Scheme of Sc-nacnac Framework	31
Figure 2.6	X-ray Molecular Structure of 1-Me(THF) . Thermal ellipsoids are drawn at the 30% probability level. Hydrogen atoms omitted for clarity.	31
Figure 2.7	X-ray Molecular Structure of 2-Et . Thermal Ellipsoids are drawn at the 30% probability level. Front aryl group and hydrogen atoms are removed for clarity.....	34
Figure 2.8	X-ray Molecular Structure of 2-CH₂Ph . Thermal Ellipsoids are drawn at the 30% probability level. Front aryl group and hydrogen atoms are removed for clarity.....	35
Figure 2.9	X-ray Molecular Structure of 2-Br(C₃H₅) . Thermal Ellipsoids are Drawn at the 30% probability level. Hydrogen atoms are removed for clarity.....	37
Figure 2.10	X-ray Molecular Structure of 2-Cl(CH₂SiMe₃) . Thermal ellipsoids are drawn at the 30% probability level. Hydrogen atoms are removed for clarity.	39
Figure 2.11	X-ray Molecular Structure of 2-CH₂SiMe₃(CH₂CMe₃) . Thermal ellipsoids are drawn at the 30% probability level. Hydrogen atoms are removed for clarity.....	40

Figure 2.12	X-ray Molecular Structure of [1-Me]₂ . Thermal ellipsoids are drawn at the 30% probability level. Hydrogen atoms and aryl groups are removed for clarity.....	42
Figure 2.13	Proposed Qualitative Energy Profile for Scandium Deviating From Planarity: Differences Invoked as a Result of the Size of the Metal Substituents.....	44
Figure 2.14	Potential β -diketiminato Resonance Structures.....	45
Figure 2.15	Top: Mirror Plane Reflecting Right and Left Sides of LScE ₂ ; Bottom: Mirror Plane Reflecting Top and Bottom of LScE ₂	48
Figure 2.16	Variable Temperature ¹ H NMR Spectra of 2-Et in <i>d</i> ₈ -toluene.....	51
Figure 2.17	Eyring Plot for Ligand Flip Within 2-CH₂SiMe₃	56
Figure 2.18	L ^t BuScR ₂ + D ₂ ; Left: H-D Coupling in Backbone Region. Right: Production of H-D and H ₂	58
Figure 2.19	X-ray Crystal Structure of 3-CH₂SiMe₃ . Thermal ellipsoids drawn at the 30% probability level. Hydrogen atoms and rear aryl group are removed for clarity.....	64
Figure 2.20	Series of ¹ H NMR Spectra Acquired in <i>d</i> ₈ -toluene at 333 K Monitoring the Thermal Decomposition of 2-CH₂SiMe₃	66
Figure 2.21	Top: Metallation of 2-CH₂SiMe₃ , Monitored Quantitatively at Various Temperatures; Bottom: Eyring Plot of Metallation of 2-CH₂SiMe₃	67
Figure 2.22	Top: TGA Trace for Thermal Decomposition of Solid 2-CH₂SiMe₃ ; Bottom: TGA Trace for Thermal Decomposition of Solid 2-Et	71
Figure 2.23	Scandium Complexes Tested for Ethylene Polymerization Activity.....	73
Figure 3.1	¹ H NMR Spectrum of 4-Me	92

Figure 3.2	Top: $^{11}\text{B}\{^1\text{H}\}$ NMR of 4-H₂B(C₆F₅)₂ ; Bottom: ^{11}B NMR of 4-H₂B(C₆F₅)₂	93
Figure 3.3	X-ray Molecular Structure of 4-H₂B(C₆F₅)₂ . Thermal ellipsoids are drawn at the 30% probability level. Hydrogen atoms and aromatic groups are removed for clarity.....	94
Figure 3.4	X-ray Molecular Structure of 7-C₆F₅ . Thermal ellipsoids are drawn at the 30% probability level. Hydrogen atoms and aryl groups are removed for clarity.....	100
Figure 3.5	^1H NMR Spectra of 10-Me at 263 K (Top) and 213 K (Bottom).....	105
Figure 3.6	^1H - ^1H 2D ROESY Spectrum of 10-Me	106
Figure 3.7	X-ray Molecular Structure of 10-Me . Thermal ellipsoids are drawn at the 30% probability level. Hydrogen atoms and aryl groups are removed for clarity.....	107
Figure 3.8	^1H NMR of 10-MeB(C₆F₅)₃ in C ₆ D ₆ at Room Temperature.....	110
Figure 3.9	X-ray Molecular Structure of 10-CH₂SiMe₂CH₂SiMe₃ . Thermal ellipsoids are drawn at the 30% probability level. Hydrogen atoms and aryl groups are removed for clarity.....	114
Figure 3.10	Series of ^{19}F NMR Spectra Acquire in <i>d</i> ₈ -toluene at 308K Monitoring the Thermal Decomposition of 10-CH₂SiMe₂CH₂SiMe₃	121
Figure 3.11	Top: Metallation of 10-CH₂SiMe₂CH₂SiMe₃ , Monitored Quantitatively at Various Temperatures; Bottom: Eyring Plot of Metallation of 10-CH₂SiMe₂CH₂SiMe₃	123
Figure 3.12	Top: Exchange Processes Between 10-Me and 11-Me ; Bottom: ^1H - ^1H 2D EXSY of 10-Me and 11-Me	129
Figure 3.13	Eyring Plot of Intermolecular Anion Exchange Between endo_{Me}-10-Me and endo_{Me}-11-Me	130
Figure 3.14	Crossover Products from Reaction of 10-CH₂SiMe₂CH₂CMe₃ and 11-CH₂SiMe₂CH₂SiMe₃	133

Figure 3.15	^1H NMR Spectra of the Independently Synthesized Products from the Crossover Experiment Between 10-CH₂SiMe₂CH₂CMe₃ and 11-CH₂SiMe₂CH₂SiMe₃	134
Figure 3.16	Top: Manually Summed ^1H NMR Spectra of Independently Synthesized Crossover Products. Bottom: Actual ^1H NMR Spectrum of Crossover Experiment	135
Figure 3.17	^1H - ^1H 2D EXSY NMR Spectrum of 10-CH₂SiMe₂CH₂SiMe₃ and 11-CH₂SiMe₂CH₂SiMe₃	136
Figure 3.18	Eyring Plot of Intermolecular Anion Exchange Between 10-CH₂SiMe₂CH₂SiMe₃ and 11-CH₂SiMe₂CH₂SiMe₃	138
Figure 4.1	^1H NMR Spectrum of 13-Me	148
Figure 4.2	^1H NMR Spectrum of 14-C₆D₅Br Generated <i>In Situ</i>	150
Figure 4.3	X-ray Structure of 14-C₆D₅Br . Thermal Ellipsoids are drawn at the 30% probability level. Hydrogen atoms and [B(C ₆ F ₅) ₄] ⁻ are removed for clarity	151
Figure 4.4	Top: X-ray structure of 14-C₇H₈ . Front aryl group, hydrogen atoms and [B(C ₆ F ₅) ₄] ⁻ removed for clarity. Bottom: X-ray structure of 14-C₉H₁₂ . Hydrogen atoms and [B(C ₆ F ₅) ₄] ⁻ removed for clarity. Thermal ellipsoids are at the 30% probability level.	153
Figure 4.5	^1H NMR Spectrum of 14-C₇H₈ in C ₆ D ₅ Br at Room Temperature	156
Figure 4.6	Relative Arene Binding to [L ^{Me} ScMe][B(C ₆ F ₅) ₄]	157
Figure 4.7	Series of ^1H NMR Spectra Exhibiting Arene Exchange from 14-C₉H₁₂ to 14-C₇H₈ at 266.0 K	158
Figure 4.8	Top: Arene Exchange from 14-C₉H₁₂ to 14-C₇H₈ , Monitored Quantitatively at Various Temperatures; Bottom: Eyring Plot of Arene Exchange from 14-C₉H₁₂ to 14-C₇H₈	161

Figure 4.9	[Toluene] vs. Rate of Arene Exchange from 14-C₉H₁₂ to 14-C₇H₈	162
Figure 4.10	Van't Hoff Plot for the Addition of 1 Equivalent of Toluene to 14-C₆H₅Br	164
Figure 4.11	Series of ¹ H NMR Spectra for Reaction of PhC≡CPh with 14-C₉H₁₂ at 306 K.....	168
Figure 4.12	Top: Reaction of PhC≡CPh and 14-C₉H₁₂ , Monitored Quantitatively at Various Temperatures; Bottom: Eyring Plot of Reaction of PhC≡CPh and 14-C₉H₁₂	169
Figure 4.13	[Diphenylacetylene] vs. k _{exp} for Reaction of [Diphenylacetylene with 14-C₉H₁₂	171
Figure 4.14	Effect of Bound Arene on k _{exp} for Alkyne Insertion	172
Figure 4.15	Double Reciprocal Plot (1/k _{exp} vs. 1/[Diphenylacetylene]) for Reaction of Diphenylacetylene with 14-C₉H₁₂	174
Figure 5.1	¹ H NMR Spectrum of 18-I(THF)	183
Figure 5.2	X-ray Molecular Structure of 18-I(THF) . Thermal ellipsoids are drawn at the 30% probability level. Hydrogen atoms are removed for clarity.....	184
Figure 5.3	¹ H NMR Spectrum of 19-I at 370K.....	187
Figure 5.4	X-ray Molecular Structure of 19-I . Thermal ellipsoids are drawn at the 30% probability level. Hydrogen atoms are removed for clarity.	188
Figure 5.5	¹ H NMR Spectrum of 19-CH₂SiMe₃	190
Figure 5.6	¹ H NMR Spectrum of 20	191

List of Schemes

Scheme 1.1	Synthesis and Reactivity of Cp* ₂ ScR.....	2
Scheme 1.2	Mechanism for σ -Bond Metathesis	3
Scheme 1.3	Synthesis of Cp' Cp* ScMe.....	4
Scheme 1.4	Reaction of CpCp*ScMe(PMe ₃) with H ₂	5
Scheme 1.5	Synthesis of [DpScCl] _n	5
Scheme 1.6	Synthesis of [(Cp*SiMe ₂ N ^t Bu)Sc(PMe ₃)](μ -H) ₂	6
Scheme 1.7	Synthesis of PNPSc(Cp)(H).....	8
Scheme 1.8	Synthesis of (C ₅ H ₅ BPh)ScPh ₂ (THF)	8
Scheme 1.9	Synthesis of TpSc(CH ₂ SiMe ₃) ₂ (THF) _n	9
Scheme 1.10	Synthesis of [(Me ₃ [9]aneN ₃)ScMe ₂][MeB(C ₆ F ₅) ₃].....	10
Scheme 1.11	Synthesis of (N ₃ O ^{Me})Sc(CH ₂ SiMe ₃) ₂	10
Scheme 2.1	Synthesis of β -Diketiminato Ligands <i>via</i> Condensation Route	14
Scheme 2.2	Synthesis of Bulky β -Diketiminato Ligands.....	15
Scheme 2.3	Observed Tautomers for the β -Diketiminato Ligand.....	15
Scheme 2.4	Synthesis of β -Diketiminato Magnesium Alkyl Complexes	16
Scheme 2.5	Addition of Ethylene Across the Metal and Nacnac Backbone.....	17
Scheme 2.6	Reduction of the β -Diketiminato Ligand Upon Reaction with Li	18
Scheme 2.7	Reaction of Cp* ₂ ScMe with RNC	22
Scheme 2.8	Synthesis of L ^{Me} ScR ₂ Compounds.....	24

Scheme 2.9	Synthesis of $L^{tBu}ScR'_2$ Compounds.....	26
Scheme 2.10	Synthesis of Mixed Alkyl 2-Me(CH₂SiMe₃)	27
Scheme 2.11	Synthesis of Mixed Alkyl Compounds of Form $L^{tBu}Sc(CH_2SiMe_3)(R')$.	28
Scheme 2.12	Synthesis of 2-Br(C₃H₅)	29
Scheme 2.13	Proposed Mechanism of "Ligand Flip" for 4-Coordinate Compounds....	52
Scheme 2.14	Fluxional Process Exchanging Structural Isomers.....	54
Scheme 2.15	Synthetic Strategy for Production of a Monomeric Scandium Dihydride	57
Scheme 2.16	Representative Series of Reversible Metallation Processes.....	59
Scheme 2.17	Deuterium Labelling of <i>Isopropyl</i> Groups <i>via</i> Reversible β -H Elimination	60
Scheme 2.18	Reaction Pathway of 2-Cl(CH₂SiMe₃)₃ , with H ₂	61
Scheme 2.19	Proposed Mechanism of Formation of Scandium Imido Hydride	62
Scheme 2.20	Metallation of 2-CH₂SiMe₃	64
Scheme 2.21	Direct Metallation of <i>d</i> ₁₀ - 2-Et	69
Scheme 2.22	β -Deuteride Elimination/Metallation Mechanism.....	70
Scheme 3.1	Activation of Cp ₂ ZrMe ₂ with B(C ₆ F ₅) ₃	80
Scheme 3.2	Ion-Pair Dynamic Processes Distinguished Using [1,2-Me ₂ C ₅ H ₃) ₂ ZrMe][MeB(C ₆ F ₅) ₃].....	82
Scheme 3.3	Anion Exchange <i>via</i> Ion-Pair Quadruples	84
Scheme 3.4	Ion-Pair Decomposition by C ₆ F ₅ Transfer to the Metal Centre.....	87

Scheme 3.5	Reaction of Cp_2ZrR_2 with Varying Equivalents of $\text{HB}(\text{C}_6\text{F}_5)_2$	89
Scheme 3.6	Reactivity of Cp_2ZrR_2 with $\text{HB}(\text{C}_6\text{F}_5)_2$ in Hexanes	89
Scheme 3.7	Reactivity of $\text{L}^{\text{tBu}}\text{ScR}_2$ with $\text{HB}(\text{C}_6\text{F}_5)_2$	91
Scheme 3.8	Proposed Mechanism for Reaction of 1 Equivalent of $\text{HB}(\text{C}_6\text{F}_5)_2$ with 2-Me , in Hydrocarbon Solvents.....	96
Scheme 3.9	Reactivity of 2-Me(CH₂SiMe₃) with $\text{HB}(\text{C}_6\text{F}_5)_2$	97
Scheme 3.10	Possible Mechanistic Pathway for Reactivity of 2-Me(CH₂SiMe₃) with $\text{HB}(\text{C}_6\text{F}_5)_2$	98
Scheme 3.11	Reactivity of 1-Me with $\text{B}(\text{C}_6\text{F}_5)_3$	99
Scheme 3.12	Reactivity of Varying Equivalents of $\text{B}(\text{C}_6\text{F}_5)_3$ with 2-Me	103
Scheme 3.13	Proposed Decomposition of 9	104
Scheme 3.14	Synthesis of 11-Me	111
Scheme 3.15	Reaction of 2-CH₂SiMe₃ with $\text{B}(\text{C}_6\text{F}_5)_3$	113
Scheme 3.16	Proposed Mechanistic Pathways for formation of 10-CH₂SiMe₂CH₂SiMe₃	117
Scheme 3.17	Metallation of Cationic Organoscandium Species	120
Scheme 3.18	Proposed Ligand Flip Mechanism Within Metallated Ion Pair.....	122
Scheme 3.19	¹ H- ¹ H 2D EXSY NMR of 10-Me	125
Scheme 3.20	Top: Synthesis of $[\text{L}^{\text{tBu}}\text{ScCD}_3][\text{H}_3\text{CB}(\text{C}_6\text{F}_5)_3]$, d₃-10-Me ; Bottom: Comparison of ¹ H NMR Spectra of with 10-Me and d₃-10-Me	127
Scheme 3.21	Proposed Mechanism for Intermolecular Anion Exchange	140

Scheme 4.1	Protic Activation of Cp ₂ TiMe ₂ with [NH ₄][X]; X = PF ₆ ⁻ , ClO ₄ ⁻	143
Scheme 4.2	NMe ₂ Ph Coordination upon Activation of Me ₂ Si(NCMe ₃) ₂ Zr(CH ₂ Ph) ₂ with [HNMe ₂ Ph][B(C ₆ F ₅) ₄]	145
Scheme 4.3	Activation of Cp ₂ ZrMe ₂ with [CPh ₃][B(C ₆ F ₅) ₄]	146
Scheme 4.4	Synthesis of [L ^{Me} ScR(NMe ₂ Ph)][B(C ₆ F ₅) ₄].....	147
Scheme 4.5	Synthesis of [L ^{Me} ScMe(arene)][B(C ₆ F ₅) ₄]	150
Scheme 4.6	Proposed Mechanism for Arene Exchange	162
Scheme 4.7	Equilibrium Upon Addition of 1 Equivalent of Toluene to 14-C₉H₁₂	163
Scheme 4.8	Proposed Reaction Profile for Arene Exchange from 14-C₉H₁₂ to 14-C₇H₈ at 298 K.....	165
Scheme 4.9	Reaction of 14-C₉H₁₂ with PhC≡CPh.....	166
Scheme 4.10	Proposed Mechanism for Reaction of Diphenylacetylene with 14-C₉H₁₂	175
Scheme 4.11	Preparation of 16	176
Scheme 4.12	Competing Pathways Upon Addition of PhC≡CPh to 16	177
Scheme 4.13	Proposed Reaction Profile for Reaction of PhC≡CPh with 14-C₉H₁₂ ...	178
Scheme 5.1	Synthesis of 18-I(THF)	183
Scheme 5.2	Synthesis and Reactivity of 18-CH₂SiMe₃(THF)	185
Scheme 5.3	Synthesis of 19-I	186
Scheme 5.4	Synthesis and Metallation of 19-CH₂SiMe₃	189

List of Abbreviations and Symbols

Å	Angstrom
Anal Calcd	calculated (elemental) analysis
Ar	aryl
br	broad
C	Celsius
CIP	contact ion-pair
Cp	cyclopentadienyl
Cp'	cyclopentadienyl or 1,3,4-trimethylcyclopentadienyl
Cp*	pentamethylcyclopentadienyl
d	doublet
Dp	<i>bis(3-tertiarybutylcyclopentadienyl)dimethylsilane</i>
DSC	differential scanning calorimetry
Et	ethyl
EXSY	exchange spectroscopy
g	gram(s)
h	hour(s)
HMQC	heteronuclear correlation through multiple quantum coherence
HOMO	highest occupied molecular orbital
Hz	hertz
I	nuclear spin quantum number
ⁱ Pr	<i>isopropyl</i>
<i>J</i>	symbol for coupling constant

k	rate constant
K	Kelvin
K_{eq}	equilibrium constant
LUMO	lowest unoccupied molecular orbital
M	molarity (mol/L)
m	multiplet
MAO	methylaluminoxane
Me	methyl
$Me_3[9]aneN_3$	1,4,7-trimethyl-1,4,7-triazacyclononane
<i>m</i> -F	<i>meta</i> -fluorine
MHz	megahertz
mL	millilitre(s)
min	minute(s)
mmol	millimole(s)
nacnac	β -diketiminato
NMR	nuclear magnetic resonance
Np	neopentyl
<i>o</i> -F	<i>ortho</i> -fluorine
Op	<i>bis</i> (tetramethylcyclopentadienyl)dimethylsilane
ov	overlapping
<i>p</i> -F	<i>para</i> -fluorine
Ph	phenyl
PNP	amido-diphosphine

ppm	parts per million
psi	pounds per square inch
q	quartet
R	alkyl or aryl group
ROESY	rotating frame overhauser effect spectroscopy
rpm	revolutions per minute
s	singlet
SBR	slurry batch reactor
Sol	solvent
sp	septet
SSIP	solvent separated ion-pair
t	triplet
^t Bu	<i>tertiary</i> butyl
TGA	thermogravimetric analysis
THF	tetrahydrofuran
TMS	trimethylsilylmethyl
tol	toluene
UV	ultraviolet
ϵ	absorption coefficient
δ	chemical shift (parts per million)
°	degree(s)
μM	micromole
$^1J_{\text{X-Y}}$	one bond coupling constant between atoms X and Y

1D	one dimensional
{ ¹ H}	proton decoupled
² J _{X-Y}	two bond coupling constant between atoms X and Y
2D	two dimensional
λ	wavelength

Chapter 1:

Introduction

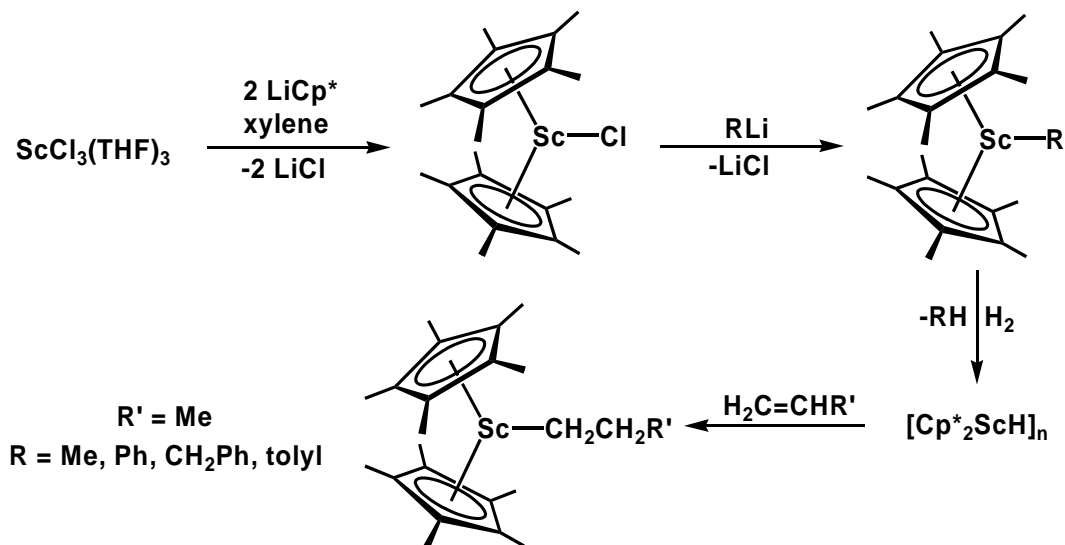
1.1 Historical Account of Organoscandium Chemistry and Chapter Content

The first organoscandium compound, Cp_3Sc ($\text{Cp} = \text{C}_5\text{H}_5$), was reported by Birmingham and Wilkinson in early 1956.¹ Interestingly, this milestone was punctuated by an opening sentence which cast doubt on the possibility of ever isolating scandium alkyl or aryl compounds. Perhaps partially as a consequence of this statement, organoscandium chemistry received little attention with only a handful of compounds published through the end of the 1970's.² Indeed, even in the 1980's organoscandium chemistry appeared only sparsely throughout the literature until in 1984 Bercaw *et al.* reported the synthesis of Cp^*_2ScR ($\text{Cp}^* = \text{C}_5\text{Me}_5$).³ This preliminary account was followed soon thereafter by a seminal contribution which detailed the mechanistic aspects of the reactions between Cp^*_2ScR and alkane/aryl C-H bonds.⁴ From this point forward the development of sophisticated organoscandium systems was greatly accelerated until the present where a plethora of ancillary ligand scaffolds and synthetic strategies have been successfully implemented.

The following chapter is not designed to be a comprehensive review of this field (the reader is referred to several recent reviews on this subject⁵⁻⁸), but to chronicle highlights so as to place the remainder of the thesis in the appropriate context with respect to the challenges which currently face this discipline.

1.2 Scandocene Chemistry

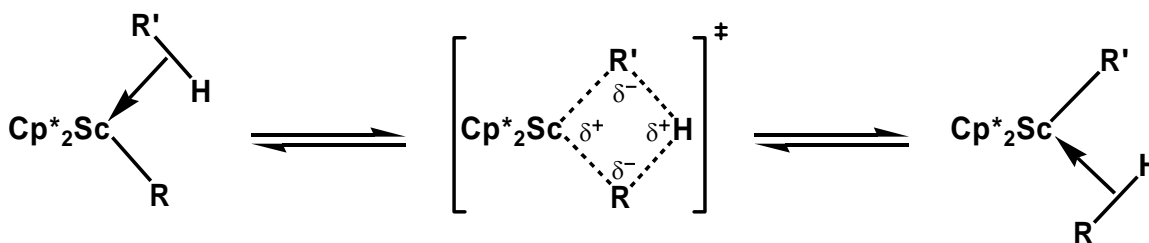
As previously discussed, the development of complexes of the type Cp^*_2ScR was important in the synthetic challenge to isolate mononuclear base free organoscandium complexes. Unlike its smaller and more electron-deprived Cp analogue, Cp^*_2ScCl is monomeric in aromatic solvents.⁴ Although this species will coordinate THF, it was possible to remove it by sublimation under dynamic vacuum at 120 °C or upon alkylation with one equivalent of alkyl lithium (Scheme 1.1). The corresponding monoalkyls, upon reaction with 4 atmospheres of H_2 , afforded the expected scandium hydride. Although the nuclearity of this compound was not unambiguously established, the THF adduct is indeed mononuclear.



Scheme 1.1 Synthesis and Reactivity of Cp^*_2ScR

Although $[\text{Cp}^*_2\text{ScH}]_n$ was capable of inserting ethylene, similar reactions of Cp^*_2ScR with α -olefins resulted in products arising from loss of R-H and formation of vinyl derivatives $\text{Cp}^*_2\text{ScCH}=\text{CHR}'$ (Scheme 1.2).⁴ This unique reactivity was

thoroughly studied and dubbed “ σ -bond metathesis” by analogy with the common reaction of olefins with transition metal alkylidenes. Mechanistic experiments revealed that this pathway was operative in the reaction between Cp^*ScR and alkanes, arenes, alkynes and bulky olefins.⁹ The transition state has been determined to be a 4-coordinate



Scheme 1.2 Mechanism for σ -Bond Metathesis

species with partial positive charge on both the metal centre and hydrogen. There is a strong preference for non-directional (s -character) at the β -position, and as a consequence the hydrogen always occupies this site (Scheme 1.2). Unfortunately, this renders it impossible to promote reactions which result in C-C bond formation.

It was speculated that σ -bond metathesis (as opposed to insertion) dominates between Cp^*_2ScR and α -olefins because steric interactions between R' and Cp^* disfavour olefin approach where the π -orbital is directed towards the frontier molecular

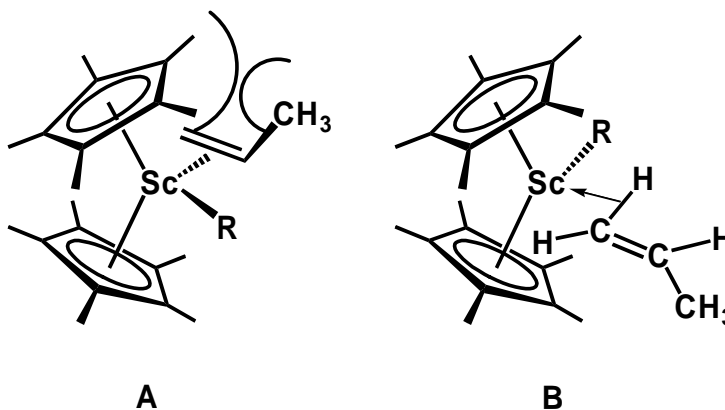
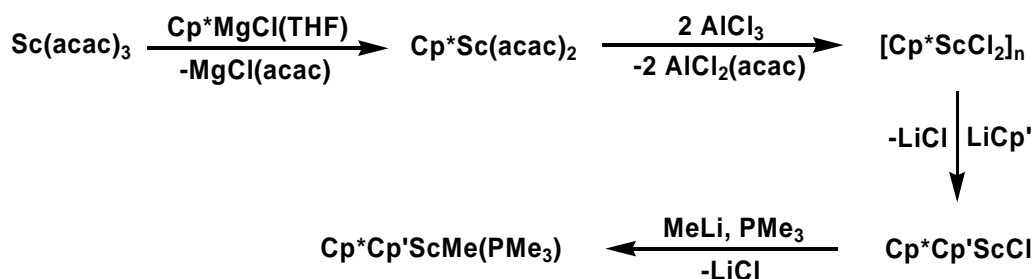


Figure 1.1 Olefin Insertion vs. σ -Bond Metathesis for Cp^*_2ScR and Propylene

orbitals of the Cp^*_2ScR . An orthogonal approach, which results in σ -bond metathesis, minimizes these repulsions, and is thus preferred (Figure 1.1).⁹

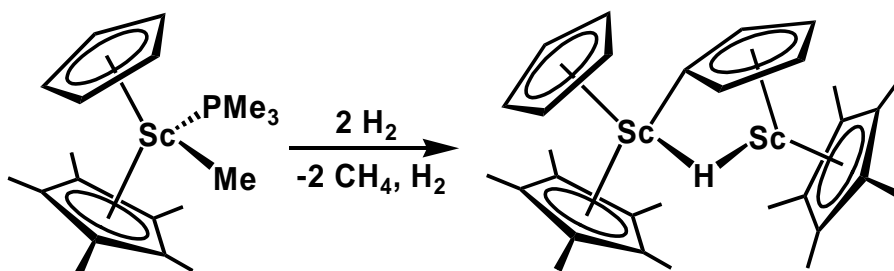
It was hypothesized that the inability of olefins to insert into the Sc-R bond of Cp^*_2ScR could be remedied by reducing the steric bulk at the metal centre. One strategy to accomplish this involved the mixed Cp'/Cp^* ($\text{Cp}' = \text{C}_5\text{H}_5$ or $1,3,4\text{-C}_5\text{H}_2\text{Me}_3$) derivative, $\text{Cp}'\text{Cp}^*\text{ScR}$. This necessitated the synthesis of Cp^*ScCl_2 which was cleverly accomplished by reacting $\text{Sc}(\text{acac})_3$ with $\text{Cp}^*\text{MgCl}(\text{THF})$ to afford $\text{Cp}^*\text{Sc}(\text{acac})_2$.² $\text{Cp}^*\text{Sc}(\text{acac})_2$ was then converted to the dichloride variant upon addition of 2 equivalents



Scheme 1.3 Synthesis of $\text{Cp}'\text{Cp}^*\text{ScMe}$

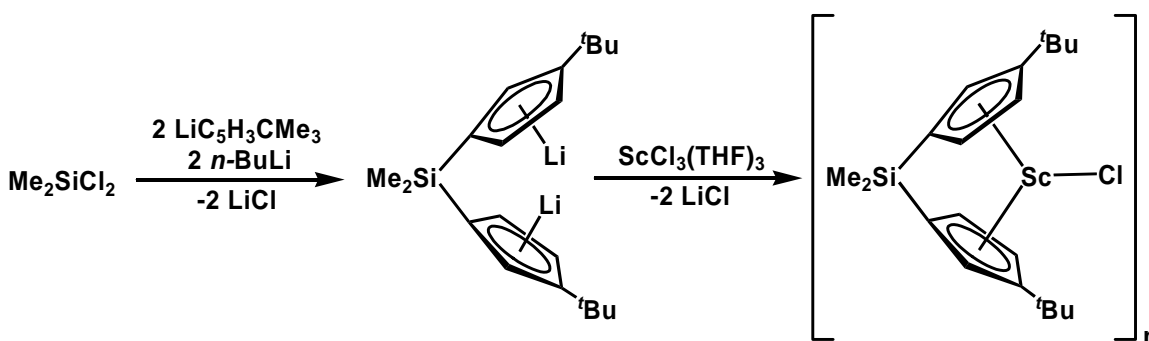
of AlCl_3 . Reaction of the oligomeric $[\text{Cp}^*\text{ScCl}_2]_n$ with $\text{Cp}'\text{Li}$ yielded the desired mixed Cp'/Cp^* complexes. The decreased bulk of the ancillary ligand in this system required that the alkylations be performed in the presence of PMe_3 so that the resultant scandocene alkyl could be isolated as the base stabilized monomer (Scheme 1.3).² Although hydrogenolysis of $\text{Cp}'\text{Cp}^*\text{ScMe}(\text{PMe}_3)$ afforded the expected scandium hydride, it reacted with itself through a σ -bond metathesis reaction between Sc-H and a Cp C-H bond to yield the corresponding dinuclear complex (Scheme 1.4).

Another approach to reduce crowding at the metal centre was to tie back the Cp^* ligands with a SiMe_2 bridge. The resulting *ansa*-metallocene complex contains a scandium centre with an enhanced coordination sphere. Through variation of the Cp



Scheme 1.4 Reaction of CpCp*ScMe(PMe₃) with H₂

moieties it was possible to prepare numerous scandocene complexes, however, for simplicity most early work concentrated on two ancillaries, Op and Dp (Op = (C₅Me₄)₂SiMe₂, Dp = (C₅H₃CMe₃)₂SiMe₂).² Attachment of these ligands to scandium was straightforward (Scheme 1.5), although the Dp supported dichloride was oligomeric and the Op analogue retained one equivalent of LiCl. Nonetheless, alkylation of both compounds with appropriate groups (-CH₂SiMe₃ for DpScR and -CH(SiMe₃)₂ for OpScR) afforded the desired monomeric scandocene alkyls. Hydrogenolysis gave the corresponding scandium hydrides; DpScH was isolated as a dimer and OpScH was best



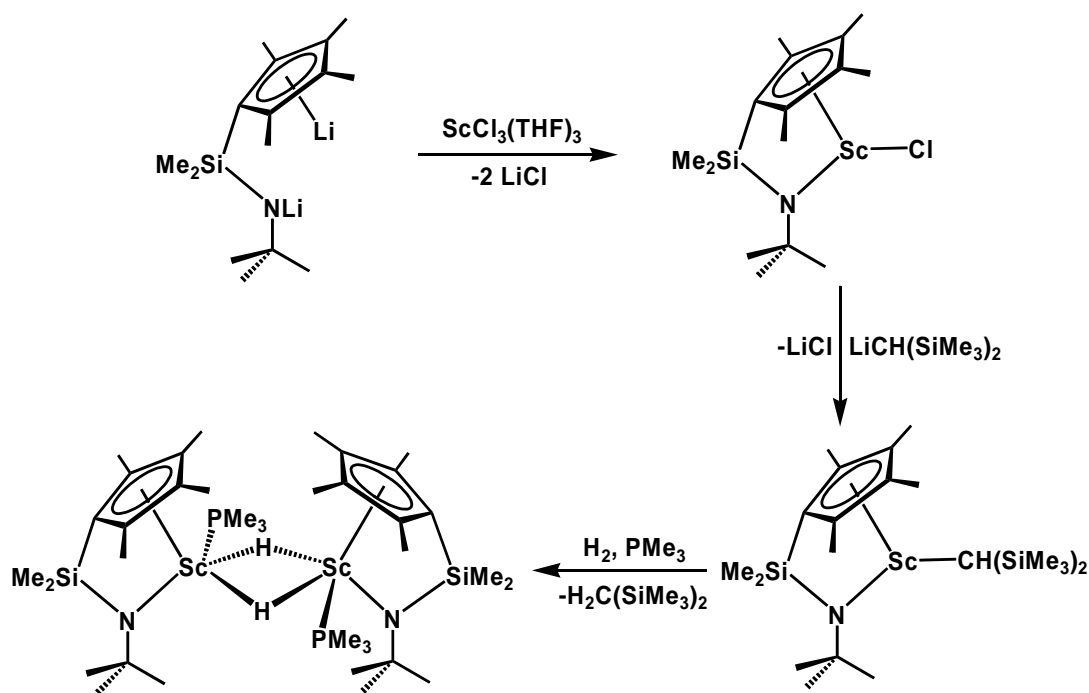
Scheme 1.5 Synthesis of [DpScCl]_n

prepared as the PMe₃ adduct. In comparison to the permethylscandocene system, these compounds exhibited improved reactivity with α -olefins, however, the chemistry was limited exclusively to head-to tail dimerization. These species also served as excellent

candidates to probe the mechanism of Ziegler-Natta polymerization.¹⁰

1.3 Mixed Cp* - Amido Scandium Chemistry

The reactivity of the scandium centre towards unsaturated molecules was further enhanced by moving to an even more sterically open Cp* – amido ancillary set. Reaction of $\text{ScCl}_3(\text{THF})_3$ with $\text{LiCp}^*\text{SiMe}_2\text{NRLi}$ afforded the metal chloride as a LiCl and THF free monomer (Scheme 1.6).² Alkylation with $\text{LiCH}(\text{SiMe}_3)_2$ generated the desired alkyl derivative, which served as a convenient starting material for the metal hydride. If the



Scheme 1.6 Synthesis of $[(\text{Cp}^*\text{SiMe}_2\text{N}^t\text{Bu})\text{Sc}(\text{PMe}_3)](\mu\text{-H})_2$

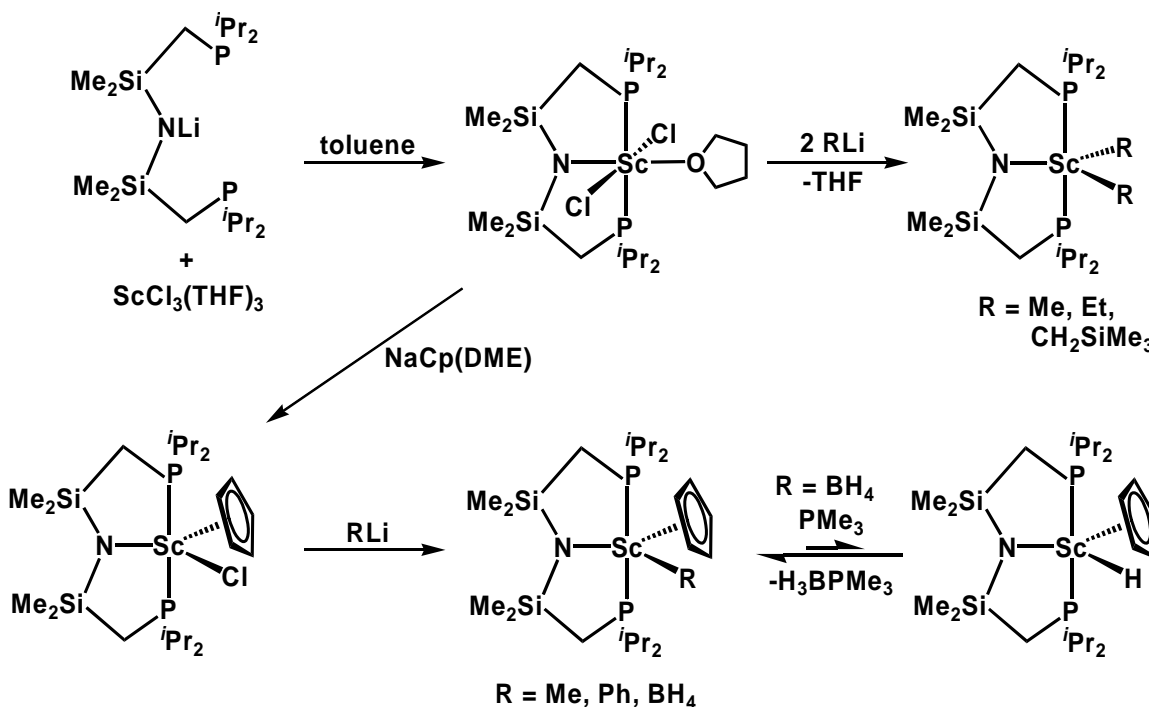
hydrogenolysis was conducted in the presence of excess PMe_3 $[(\text{Cp}^*\text{SiMe}_2\text{N}^t\text{Bu})\text{Sc}(\text{PMe}_3)](\mu\text{-H})_2$ could be isolated as a well behaved solid in 80% yield. The solid state structure of this complex revealed a long Sc-P bond length of

almost 3 Å; variable temperature NMR studies indicated a low barrier for phosphine dissociation. As in the *ansa*-scandocene examples, α -olefins were coupled in a head-to-tail fashion, however, much higher activities (*e.g.* polymerization of 1-butene resulted in molecular weights of approximately 4000) were realized in these sterically less demanding complexes.²

1.4 Non-Cp Supported Organoscandium Compounds

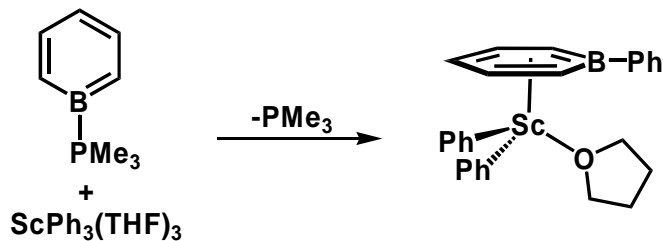
Although a veritable wealth of organometallic chemistry originated from the previously discussed scandocene systems, inherent limitations in the *bis*-Cp ancillary set prompted a search for new ligand environments, most notably, one which leaves at least 2 valences for reactive hydrocarbyl ligands. One successful example is the amido-diphosphine (PNP) ligand reported by Fryzuk and co-workers. This ligand was employed in the synthesis of the first non-Cp Group 3 dialkyl compounds.¹¹ Reaction of LiPNP with $\text{ScCl}_3(\text{THF})_3$ at 100 °C in toluene afforded $\text{PNPScCl}_2(\text{THF})$ in high yield. While the dichloride complex retained one THF molecule, it was precluded upon conversion to mononuclear dialkyl derivatives (Scheme 1.7). Unfortunately, this class of dialkyl complexes exhibit reactivity patterns complicated by decomposition and facile ligand loss; clean reactions were not observed with H_2 , CO or ethylene. In order to increase electronic saturation at the metal centre a mixed Cp/PNP system was synthesized through addition of NaCp to $\text{PNPScCl}_2(\text{THF})$.¹² The resultant THF free monohalide complex reacts cleanly with typical lithium reagents. $\text{PNPSc}(\text{Cp})(\text{BH}_4)$ can be converted to the corresponding metal hydride by employing PMe_3 to sequester the Lewis acidic

borane (Scheme 1.7). Unfortunately it was not possible to prepare $\text{PNPSc}(\text{Cp})(\text{H})$ by reaction of $\text{PNPSc}(\text{Cp})(\text{Me})$ with H_2 .



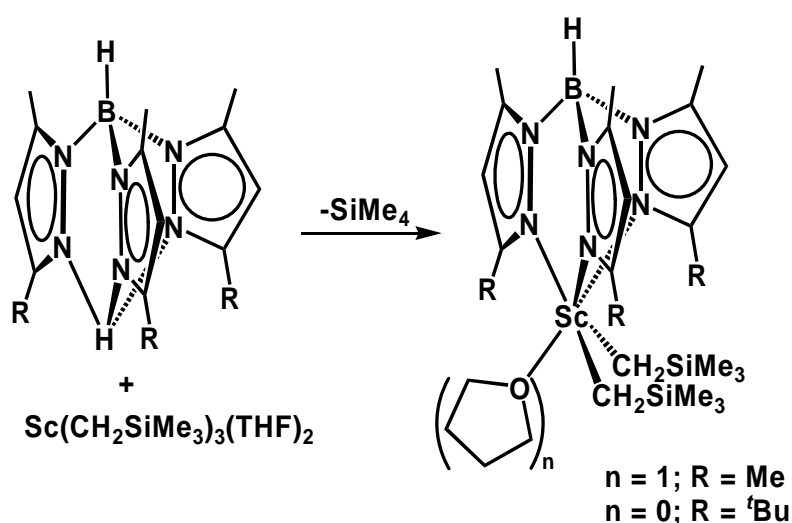
Scheme 1.7 Synthesis of $\text{PNPSc}(\text{Cp})(\text{H})$

A rather novel Cp alternative was reported by Bazan *et al.* where addition of $\text{C}_5\text{H}_5\text{BPMe}_3$ to $\text{ScPh}_3(\text{THF})_3$ affords the boratabenzene supported dialkyl complex depicted in Scheme 1.8.¹³ Although this species represents a unique class of dialkyl scandium compounds whose reactivity may prove fruitful, no such studies involving boratabenzene stabilized scandium complexes have yet been published.



Scheme 1.8 Synthesis of $(\text{C}_5\text{H}_5\text{BPh})\text{ScPh}_2(\text{THF})$

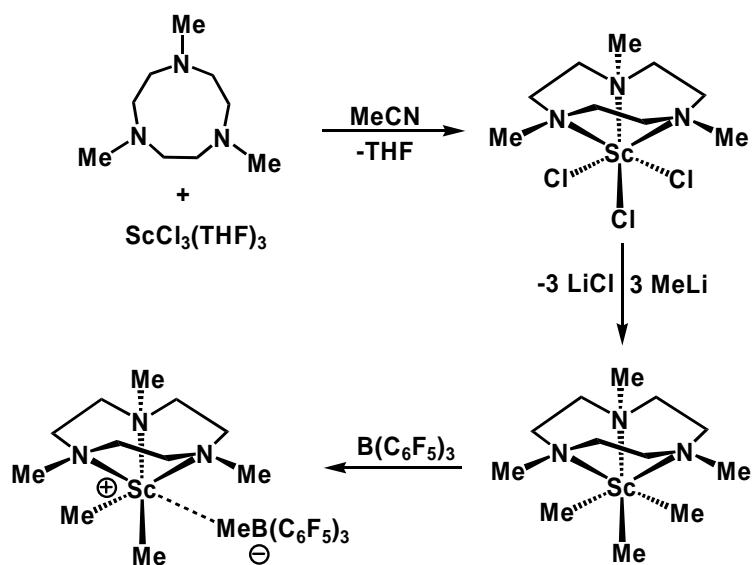
A more thoroughly explored monoanionic ancillary is the readily modified *tris*(pyrazolyl)borate (Tp) ligand. It was established in the late 1990's, with the report of a variety of dialkyl scandium complexes, that these are suitable ligands for group 3 metals.¹⁴⁻¹⁷ Although the scandium dichloride species could be isolated, subsequent reactions with RLi were problematic, restricting the institution of organic groups to alkane elimination procedures (Scheme 1.9). The chemistry of the resultant dialkyls was limited due to general unreactivity and loss of ligand under forcing conditions. Nonetheless, the relative ease and degree to which the Tp ligand can be fine tuned render it potentially useful for the synthesis of more reactive species.



Scheme 1.9 Synthesis of $\text{TpSc}(\text{CH}_2\text{SiMe}_3)_2(\text{THF})_n$

1.5 Cationic Organoscandium Compounds

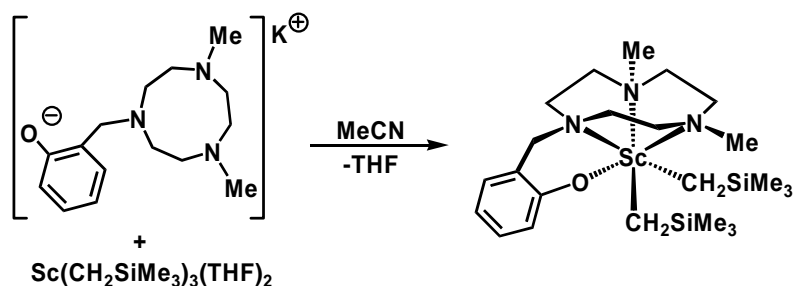
The development of non-Cp supported species permitted the generation of cationic organoscandium compounds akin to group 4 metallocenes used in olefin polymerization. Examples of this class of compounds are exceedingly rare, the first of



Scheme 1.10 Synthesis of $[(\text{Me}_3[9]\text{aneN}_3)\text{ScMe}_2][\text{MeB}(\text{C}_6\text{F}_5)_3]$

which was suggested in 1997 by Bercaw and colleagues.¹⁸ Reaction of 1,4,7-trimethyl-1,4,7-triazacyclononane ($\text{Me}_3[9]\text{aneN}_3$) with $\text{ScCl}_3(\text{THF})_3$ afforded the THF free trihalide which could be cleanly alkylated with 3 equivalents of MeLi (Scheme 1.10). Although $(\text{Me}_3[9]\text{aneN}_3)\text{ScMe}_3$ is relatively unreactive towards unsaturated organic substrates, addition of $\text{B}(\text{C}_6\text{F}_5)_3$ afforded an active ethylene polymerization catalyst. While it was not possible to isolate the ion-pair, spectroscopic data were consistent with the proposed compound.

A variation of the $\text{Me}_3[9]\text{aneN}_3$ ligand, which incorporated a pendant phenoxide arm, was recently communicated.⁶ The now monoanionic ligand was successfully



Scheme 1.11 Synthesis of $(\text{N}_3\text{O}^{\text{Me}})\text{Sc}(\text{CH}_2\text{SiMe}_3)_2$

employed in the generation of organoscandium complexes (Scheme 1.11). Unfortunately, reaction of these compounds with Lewis acidic boranes led only to ill-defined mixtures. Mountford and colleagues have also reported, however, neutral trialkyl compounds supported by *tris*(pyrazolyl)methane ligands.¹⁹ These complexes can indeed be converted to cationic derivatives upon introduction of either $\text{B}(\text{C}_6\text{F}_5)_3$ or $[\text{CPh}_3][\text{B}(\text{C}_6\text{F}_5)_4]$.

While these examples suggest cationic species are viable compounds, isolable organoscandium cations remained virtually absent from the literature at the time the research presented in this thesis began.

1.6 Thesis Goals

Since the late 1980's organoscandium chemistry has blossomed, and although elegant work has been performed, there are only a limited number of well defined examples of mononuclear base free dialkyl scandium complexes. These species, which necessitate alternative ancillaries to the ubiquitous Cp ligand, are often prone to undesirable reaction pathways involving the supporting ligand itself. As a result, the chemistry of such compounds remains relatively unexplored.

Thus, it was the goal of this research to develop and employ a synthetic strategy towards thermally stable mononuclear dialkyl scandium compounds and subsequently explore their reactivities. In particular, it was the objective to isolate organoscandium cations, and examine the reactivity of this virtually unprecedented class of compounds.

The synthesis, solution and solid state structures as well as thermal stability and

preliminary polymerization data of a family of β -diketiminato supported dialkyl scandium compounds are described in detail in Chapter 2. The reactivity of these species with electrophilic boranes, namely $\text{HB}(\text{C}_6\text{F}_5)_2$, $\text{B}(\text{C}_6\text{F}_5)_3$ and $(\text{C}_6\text{F}_5)\text{B}(\text{C}_{12}\text{F}_8)$ comprises Chapter 3. The dialkyl compounds introduced in Chapter 2, were reacted with $[\text{CPh}_3][\text{B}(\text{C}_6\text{F}_5)_4]$, leading to the formation of aromatic solvent separated ion-pairs. This is a topic of acute interest because these types of compounds are often speculated to be intermediates in olefin polymerization processes. Mechanistic studies exploring the pathways by which unsaturated molecules react with these arene bound scandium cations were undertaken and are summarized in Chapter 4. Finally, Chapter 5 addresses initial results focusing on the extension of this chemistry to yttrium. Future directions for this area are discussed in depth. More detailed introductory material is presented at the beginning of each chapter where it was felt to be more pertinent and thereby more beneficial to the reader.

Chapter 2:

Synthesis, Characterization and Thermal Decomposition of Dialkylscandium Complexes Supported by the β -Diketiminato Ancillary Ligand

2.1 Introduction – β -Diketiminato Ancillary Ligand

2.1.1 Synthesis and Structural features of the β -Diketiminato Ligand

The development of well-behaved and clearly defined diorganoscandium species necessitates the use of a carefully designed ancillary ligand. Since scandium exists almost exclusively in the +3 oxidation state (although several unusual examples have recently been reported where scandium is in a lower oxidation state),²⁰⁻²⁷ only one valence can be used for the ancillary framework if one wishes to leave two for reactive hydrocarbyl fragments. Thus, one must utilize a monoanionic ligand with the appropriate steric balance to sufficiently protect the metal centre against aggregation, Lewis base ligation and ligand redistribution reactions without completely quenching the desired reactivity of the resultant organometallic complexes.

While a variety of non-cyclopentadienyl alternatives exist⁵ the β -diketiminato ligand²⁸ was chosen for several reasons. The nacnac²⁹ ancillary is the nitrogen analogue to the acetylacetonato or acac ligand, which is ubiquitous throughout coordination chemistry (Figure 2.1). Unlike the acac ligand, however, the coordination chemistry of the β -diketiminato ancillary has remained, until recently, largely unexplored.³⁰ Although there are several structural similarities between the two classes of ligand, the nacnac

framework is advantageous for use in organoscandium chemistry as the nitrogen atoms allow the addition of readily tuned bulky substituents near the coordination sphere of the metal. This, in combination with the ability to modify the R groups, allows

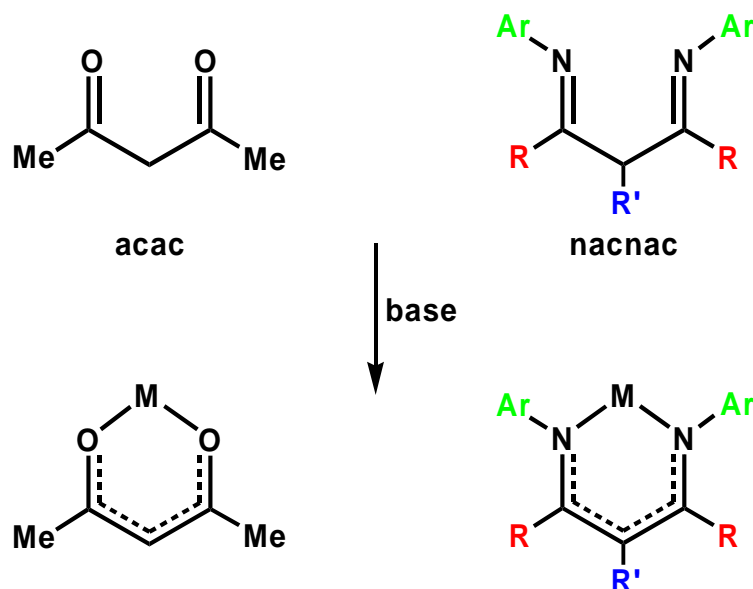


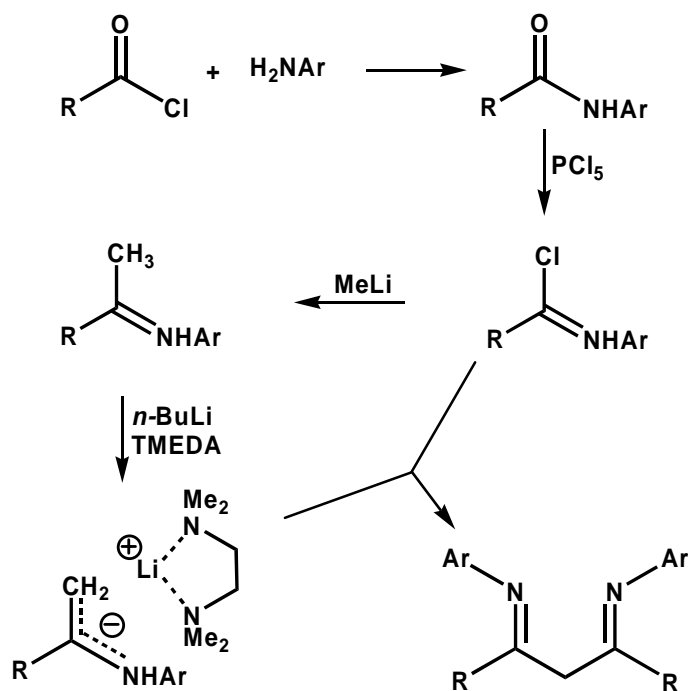
Figure 2.1 Acetylacetonato and β -Diketiminato Ligands

straightforward fine tuning of both steric and electronic ligand properties. In particular, Coates *et al.* have shown that substitution at R' has a dramatic effect on the electron donating ability of the nacnac ligand.³¹⁻³³ Furthermore, these ligands can be synthesized on multi-gram scale in good to high yield from inexpensive commercially available starting materials.³⁴ Although several synthetic strategies exist,^{30,34-36} the most commonly used route involves the condensation of a primary amine with a β -diketone



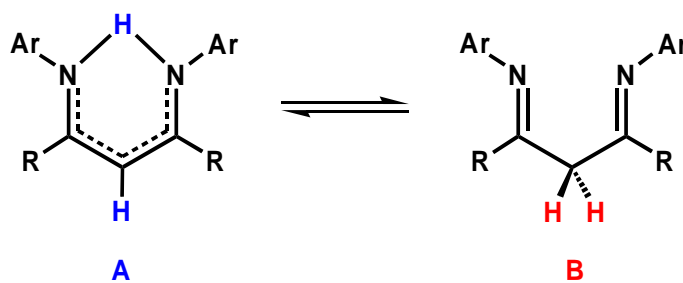
Scheme 2.1 Synthesis of β -Diketiminato Ligands *via* Condensation Route

(Scheme 2.1). For β -diketiminato variants with bulky R groups (i.e. t Bu) it is not always possible to achieve the second condensation step, forcing the use of a time demanding, albeit more versatile convergent synthesis (Scheme 2.2).



Scheme 2.2 Synthesis of Bulky β -Diketiminato Ligands

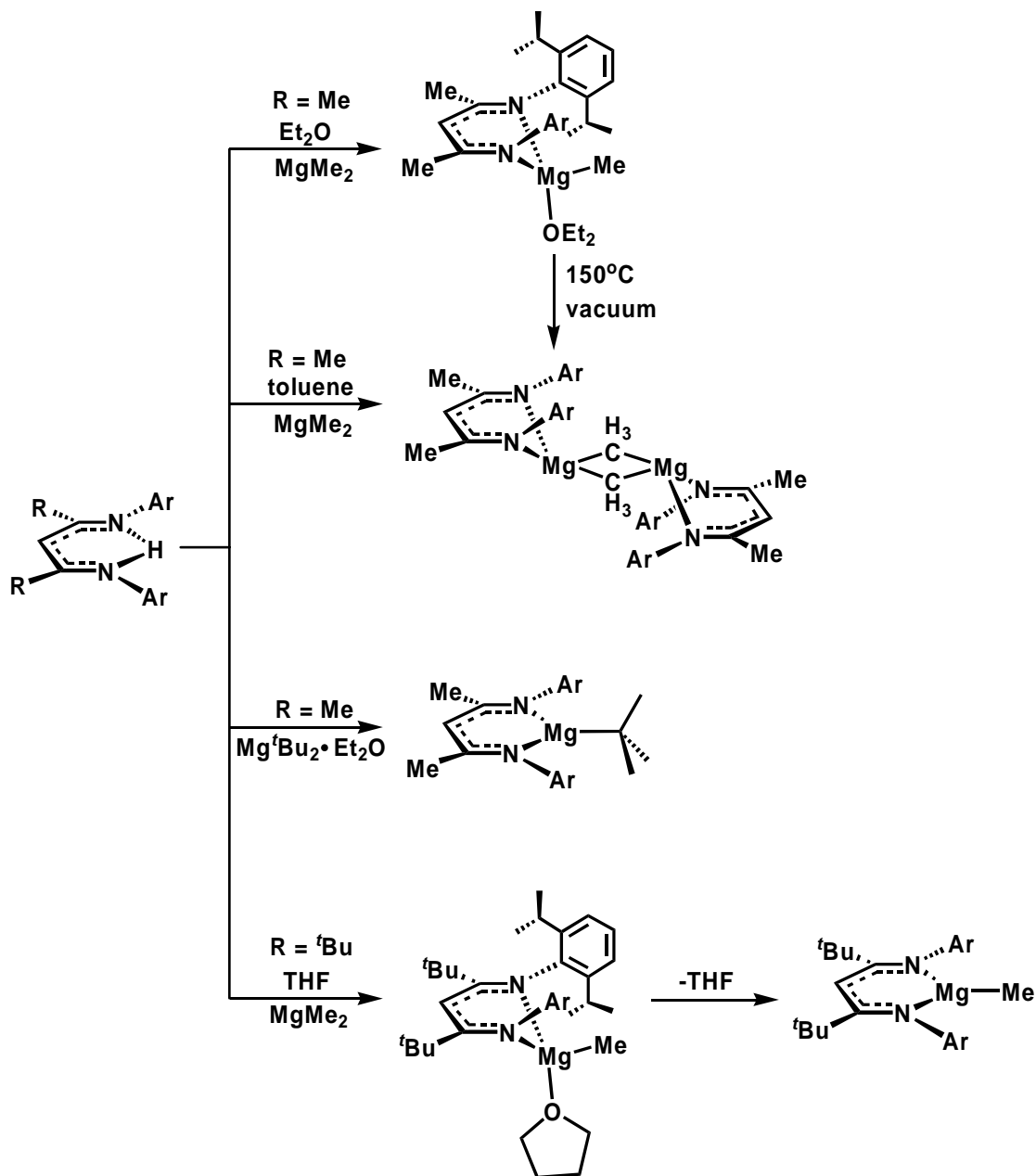
Although the R group is easily modified, its proximity to the metal's coordination sphere is secondary to the nitrogen substituents. Nonetheless, it has a sizeable impact on the ensuing reactivity of the metal complexes, as it forces the N-Ar groups towards the



Scheme 2.3 Observed Tautomers for the β -Diketiminato Ligand

metal centre (*vide infra*).

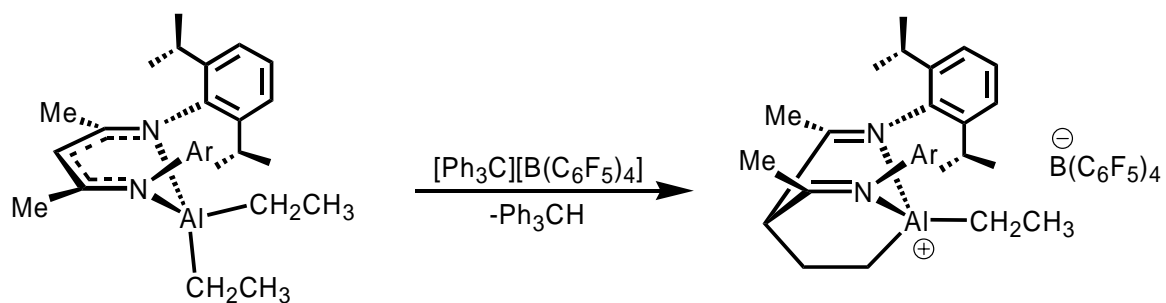
The protio nacrnac ligands can exist as a mixture of tautomers in solution; when R = Me, form A is observed exclusively, as evidenced by an N-H resonance downfield of 11 ppm in the ^1H NMR spectrum. Alternatively, if R = $t\text{Bu}$, a 1 : 4 ratio of A : B is observed in chloroform while only B is detected in benzene (Scheme 2.3).



Scheme 2.4 Synthesis of β -Diketiminato Magnesium Alkyl Complexes

The nacnac ligand has proven successful in stabilizing extremely reactive species, for example, Roesky and co-workers have demonstrated that when R = methyl and Ar = 2,6-*i*-Pr₂-C₆H₃, the β-diketiminato ligand is capable of stabilizing the first reported example of a monomeric aluminum (I) complex.³⁷ Similarly, a rare example of a low valent Ga (I) compound was recently reported by Power and colleagues.³⁸ Bailey *et al.* have found that upon increasing the steric bulk of the R group from Me to ^tBu, it is possible to isolate a base-free monomeric magnesium methyl compound (Scheme 2.4).³⁹ Interestingly, when R = Me only the diethylether and THF adducts could be obtained; all attempts to remove these bases resulted in a dimeric structure.^{40,41}

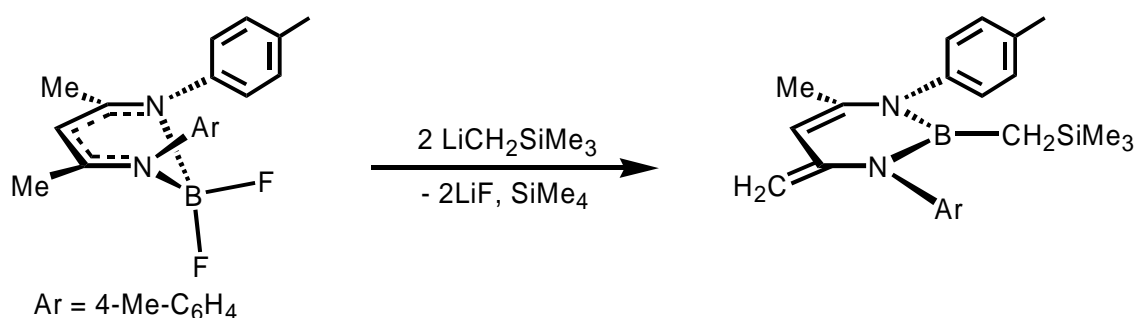
Jordan and co-workers have demonstrated that the β-diketiminato framework can be successfully implemented to synthesize well defined organoaluminum compounds. Reaction of monomeric dialkyl aluminum nacnac compounds with [CPh₃][B(C₆F₅)₄] or B(C₆F₅)₃, generated a family of alkylaluminum cations.^{42,43} Although these species do



Scheme 2.5 Addition of Ethylene Across the Metal and Nacnac Backbone

not decompose *via* β-elimination, they do undergo an unusual addition reaction whereby olefins add across the nacnac backbone and metal centre (Scheme 2.5). Nonetheless, similarities between Group 3 and 13 suggest that cationic organoscandium compounds may be feasible targets.

The above example illustrates that the nacnac ligand is not always an innocuous observer in the chemical reactivity of β -diketiminato supported complexes. It has also been shown that it is possible to deprotonate the methyl R groups in the ligand backbone. Attempts by Smith III and co-workers to alkylate a nacnac boron difluoride compound with 2 equivalents of $\text{LiCH}_2\text{SiMe}_3$ resulted in the production of a reduced nacnac complex (Scheme 2.6).⁴⁴ A one electron ligand reduction was reported by Lappert *et al.* upon reaction of L_2YbCl ($\text{L} = \text{Me}_3\text{SiNC}(\text{Ph})\text{CHC}(\text{Ph})\text{NSiMe}_3$) with Li in THF.⁴⁵



Scheme 2.6 Reduction of the β -Diketiminato Ligand Upon Reaction with Li

2.1.2 Electronic Features and Bonding Modes of the β -Diketiminato Ligand

From an electronic perspective, the β -diketiminato ligand is theoretically capable of stabilizing a metal through a host of bonding modes with donation of 2 – 10 electrons; η^1 , κ^2 and η^5 bonding are the most prevalent.³⁰ Although the purely κ^2 bonding motif, whereby the metal resides in the plane of the nacnac ligand is rare, it predominates for 3-coordinate Group II and XII compounds. One such example was published by Roesky and co-workers where $\text{L}^{\text{Me}}\text{ZnCCPh}$, is clearly trigonal planar in the solid state.⁴⁶ Compounds of higher coordination number usually exist in a geometry where the metal is

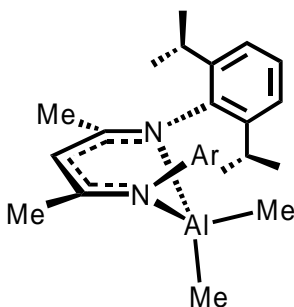


Figure 2.2 Typical β -Diketiminato Bonding mode between κ^2 and η^5

displaced out of the plane of the ligand by varying degrees. In these situations the electron donation to the metal centre is considerably more ambiguous, ranging the entire bonding spectrum from κ^2 to η^5 . This intermediate bonding dominates most β -diketiminato complexes; a typical example is reported by Smith III and is shown in Figure 2.2.⁴⁷ Metals with significantly larger coordination spheres, such as the lanthanides, are occasionally observed to lie at the latter extreme.⁴⁸ Since there is no clear cut classification established for such bonding modes a large degree of discrepancy exists. For example, Collins and colleagues have reported several zirconium complexes in which the metal is described to be bonded in a purely η^5 fashion akin to that observed in cyclopentadienyl complexes,^{49,50} however, careful scrutiny of the solid state metrical parameters suggest otherwise.

There are also a plethora of highly unusual bonding modes, such as the η^1 - η^5 - κ^2 / η^3 - κ^2 bonding mode which has been observed for barium. In this situation one metal centre is bound to the ligand through only one nitrogen atom. A second nacnac ligand bonds to the metal in an η^5 fashion while a third is bound κ^2 . A second barium centre bonds to the first ligand in an η^3 mode and the second in a κ^2 motif such that the solid state structure portrays a Ba_2L_3 unit whereby both barium atoms are involved in multiple

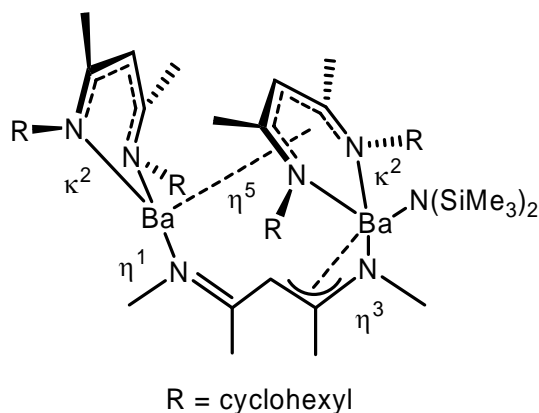


Figure 2.3 Numerous Bonding Modes in a Ba_2L_3 Unit

bonding modes to different β -diketiminato ligands (Figure 2.3).⁵¹

Although analogies between the electronics of cyclopentadienyl η^5 bonding and “out-of-the-plane” β -diketiminato structures have been made,^{49,50,52,53} a DFT study by Tolman *et al.* suggest that this type of comparison may not be accurate.⁵⁴ These calculations, which analyze the bonding between a Cu(I) centre and a β -diketiminato ancillary, reveal that five occupied molecular orbitals are associated with the ligand, and as such it is possible to have a donation of 10 electrons from the ligand to the metal centre. In reality, however, the picture is more complicated; most of the bonding interactions take place with 5b2 and 6a1 which are representative of in-plane σ -bonding from the nitrogen atoms to the metal centre. The out-of-plane π orbitals, 1b1, 1a2 and 2b1, which could interact in cyclopentadienyl-like bonding play a significantly less important role. In particular, orbitals 1b1 and 1a2 were found to lie too deep in energy to contribute to bonding to a meaningful extent. Thus, the nacnac ligand can be envisioned as a κ^2 , 4 electron donor (2σ) for in-plane structures, and for the most part a κ^3 ,⁵⁵ 6 electron donor (2σ , 1π) for out-of-plane structures, depending on the degree to which the

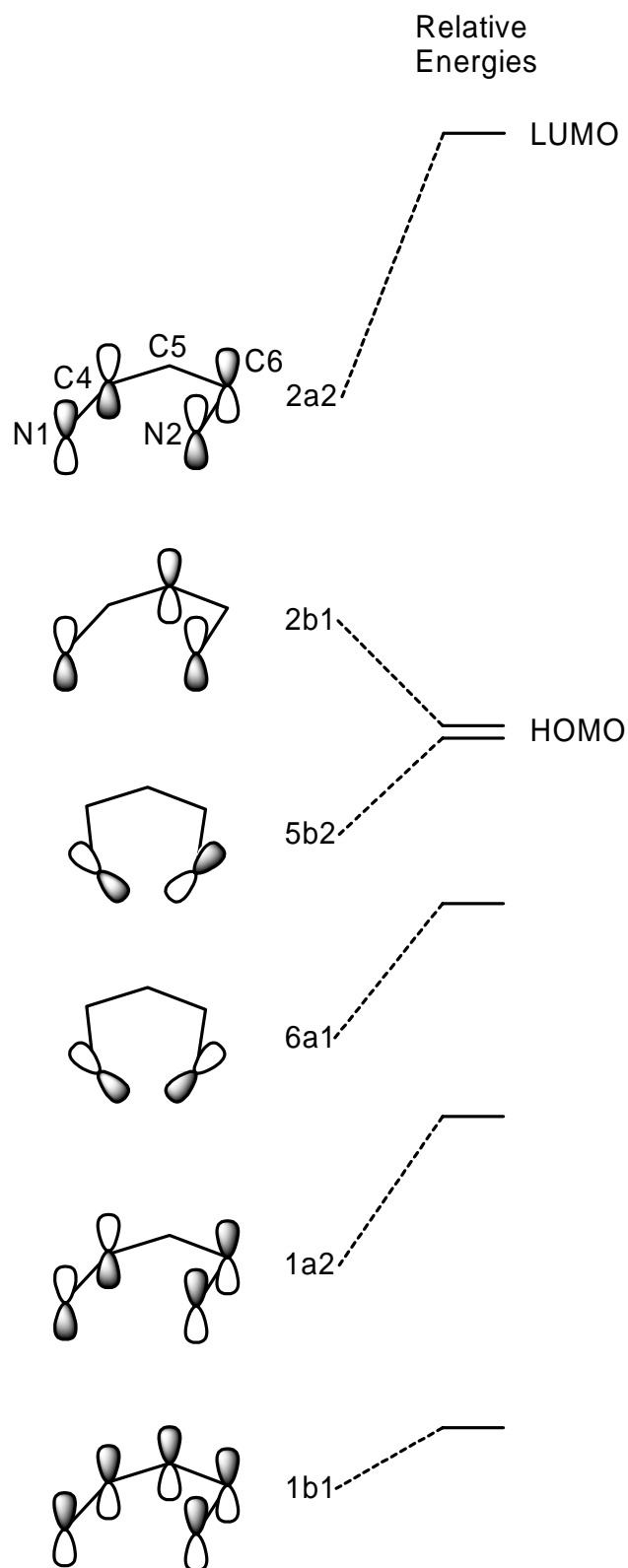
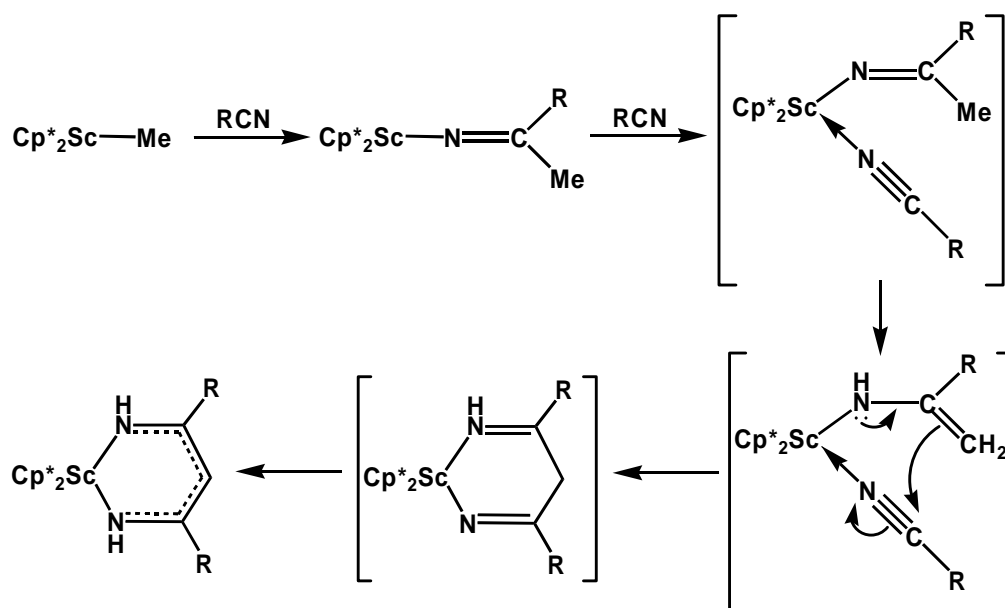


Chart 2.1 Frontier Molecular Orbitals of the β -Diketiminato Ligand

metal is removed from the ligand plane and the quantity of backbone puckering (Chart 2.1). It should be noted that out-of-plane structures appear to have little disruption in the σ -bonding as the ligand backbone is quite flexible, and as such the aforementioned 6 electron donation in these structures remains reasonable. It should also be pointed out that the N-aromatic substituents lie perpendicular to the ligand plane, and therefore are not part of the conjugated π -system. The LUMO of the nacnac ligand, 2a2, which is of relevance in spectroscopic studies, is depicted as the π -antibonding analogy of 1a2. The HOMO-LUMO gap was calculated to be approximately 2.3 eV. A more comprehensive account of β -diketiminato ligand complexes and their properties can be found in a recent review by Lappert *et al.*³⁰

The structural and electronic diversities, the ability to stabilize reactive species and an inexpensive and straightforward synthesis made the nacnac ligand an excellent candidate as an ancillary in our quest to generate stable dialkylscandium complexes and



Scheme 2.7 Reaction of Cp^*_2ScMe with RNC

explore their reactivity and efficacy as catalysts for olefin polymerization. It is important to point out that a β -diketiminato supported scandium species was previously reported by Bercaw *et al.* upon reaction of Cp^*_2ScMe with 2 equivalents of isonitrile (Scheme 2.7).⁵⁵

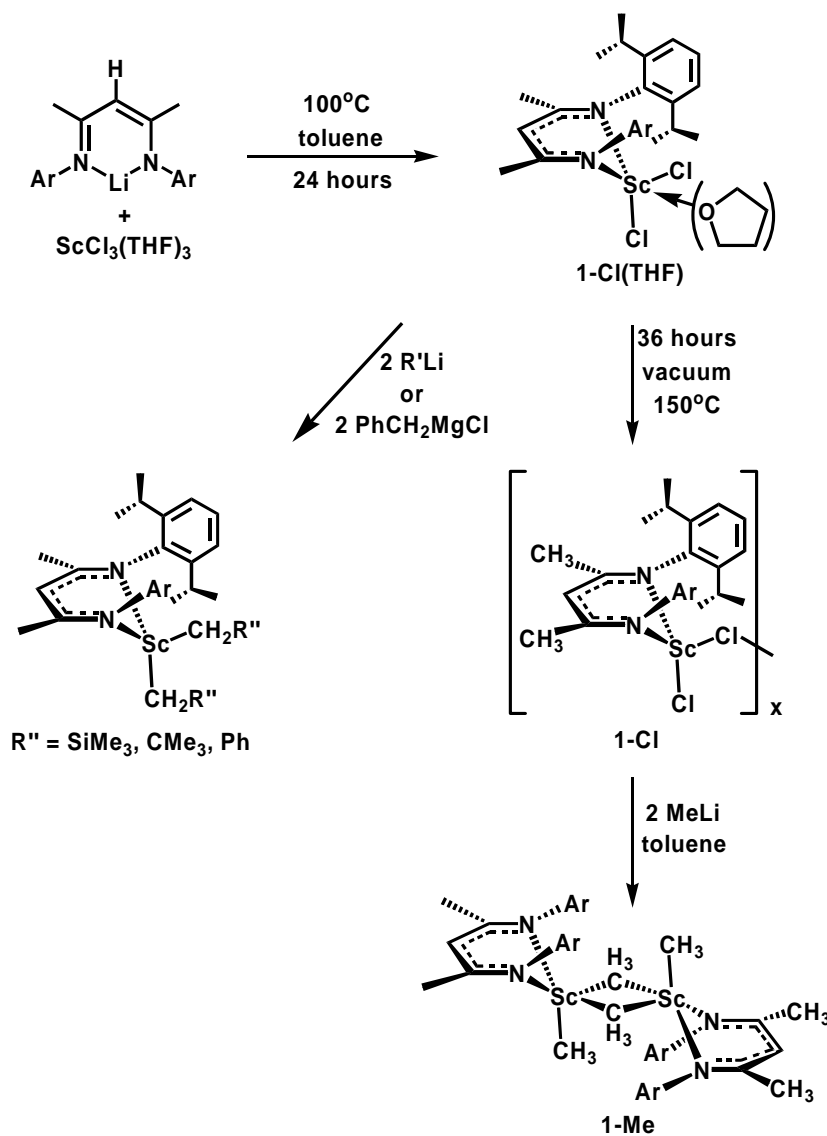
Throughout this thesis two different β -diketiminato ligands were employed: the less bulky methyl backbone derivative, denoted as L^{Me} , and the more sterically encumbered $t\text{Bu}$ compound, $\text{L}^{t\text{Bu}}$. Both ligands incorporate the N-2,6- $t\text{Pr}_2\text{-C}_6\text{H}_3$ group, and as such it will be abbreviated as Ar.

2.2 Results

2.2.1 Synthesis of $\text{L}^{\text{Me}}\text{ScR}_2(\text{THF})_x$

Initial results reported that reaction of $\text{ScCl}_3(\text{THF})_3$, with one equivalent of LiL^{Me} at 100 °C in toluene for 24 hours cleanly generated the dichloride $\text{L}^{\text{Me}}\text{ScCl}_2(\text{THF})$, **1-Cl(THF)**, as a crystalline white solid in high yield (80%).⁵⁶ This monomeric dichloride serves as an excellent starting material that can be alkylated under mild conditions (room temperature, 1-2 hours) with two equivalents of $\text{R}'\text{Li}$ ($\text{R}' = \text{CH}_3$, **1-Me(THF)**, CH_2SiMe_3 , **1-CH₂SiMe₃**, CH_2CMe_3 , **1-CH₂CMe₃**) in aromatic solvents.⁵⁷ Although the dibenzyl compound, **1-CH₂Ph**, can be generated using benzyl potassium,⁵⁸ sizeable quantities of potassiated ligand, KL^{Me} , are formed as an undesirable side product. The reaction proceeds more cleanly if the milder Grignard reagent, PhCH_2MgCl , is utilized. The dimethyl compound, **1-Me(THF)**, exists as a five coordinate THF adduct.⁵⁶ Unfortunately, all attempts to remove the ligated THF, including prolonged exposure to high vacuum and addition of Lewis acids to sequester a

potentially labile THF were unsuccessful. Interestingly, the THF ligand can be precluded upon alkylation if the alkyl group is sufficiently bulky; the dibenzyl, dineopentyl and *bis*((trimethylsilyl)methyl) derivatives are monomeric and free of Lewis bases (Scheme 2.8).⁵⁹



Scheme 2.8 Synthesis of $\text{L}^{\text{Me}}\text{ScR}_2$ Compounds

Alternatively, in a manner similar to that reported by Bercaw for $\text{Cp}^*\text{ScCl}(\text{THF})$,⁴ heating dichloride **1-Cl(THF)** at 130 °C under reduced pressure for 36

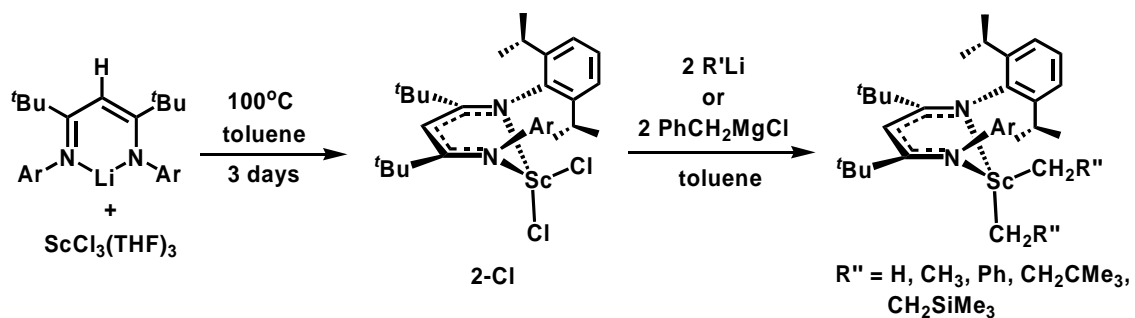
hours affords a pale yellow insoluble powder. Surprisingly, despite the almost complete lack of solubility of this presumed oligomeric species, reaction with 2 equivalents of MeLi in toluene proceeds smoothly to afford base-free $L^{\text{Me}}\text{ScMe}_2$, **1-Me**, upon workup. Although the compound exists as a dimer in the solid state (Figure 2.12), its marked increase in solubility compared to its dichloride precursor, possibly indicates it exists as a monomer in solution. Likewise, the ^1H NMR spectrum exhibits only one Sc-Me resonance which is due either to a monomeric structure or rapid exchange of bridging and terminal Me groups within a dimer. Furthermore, its reactivity with Lewis acids, which will be discussed in future chapters, also supports an accessible monomeric structure in solution. In order to completely eliminate ambiguity regarding the nuclearity of **1-Me** in solution, however, cryoscopic measurements would need to be conducted.

2.2.2 Synthesis of $L^{\text{tBu}}\text{ScR}_2$

In an attempt to avoid THF retention altogether, the significantly more bulky β -diketiminato ligand L^{tBu} was employed with the idea that the ^tBu groups would push the aromatic substituents sufficiently forward into the coordination sphere of the scandium centre, thus completely eliminating coordinated THF.^{34,60} The desired steric saturation at the metal centre was indeed achieved; the dichloride, **2-Cl**, even upon exposure to excess Lewis bases, such as diethyl ether or THF remains base-free. A further testament to the encompassing steric bulk imposed by this scaffold is the harsh conditions required in the metathesis reaction. The reaction between $\text{ScCl}_3(\text{THF})_3$ and $\text{Li}L^{\text{tBu}}$ proceeds to completion after three days at 100 °C in toluene whereas only one day

is required for L^{Me} . Another successful ligand attachment strategy involves conducting the reaction at 180 °C which reduces the required time to an impressive 15 minutes. Although the latter route was not quite as clean as the former (88%), at 68% the yield is still quite good. Alkylation procedures analogous to those utilized with the smaller L^{Me} , afforded the corresponding family of monomeric, base-free dialkyl scandium complexes ($L^{\text{tBu}}\text{ScR}_2$, $R = \text{Me}$, **2-Me**, Et, **2-Et**, CH_2Ph , **2-CH₂Ph**, CH_2CMe_3 , **2-CH₂CMe₃**, CH_2SiMe_3 , **2-CH₂SiMe₃**) as yellow crystalline solids in good to high yield (Scheme 2.9).

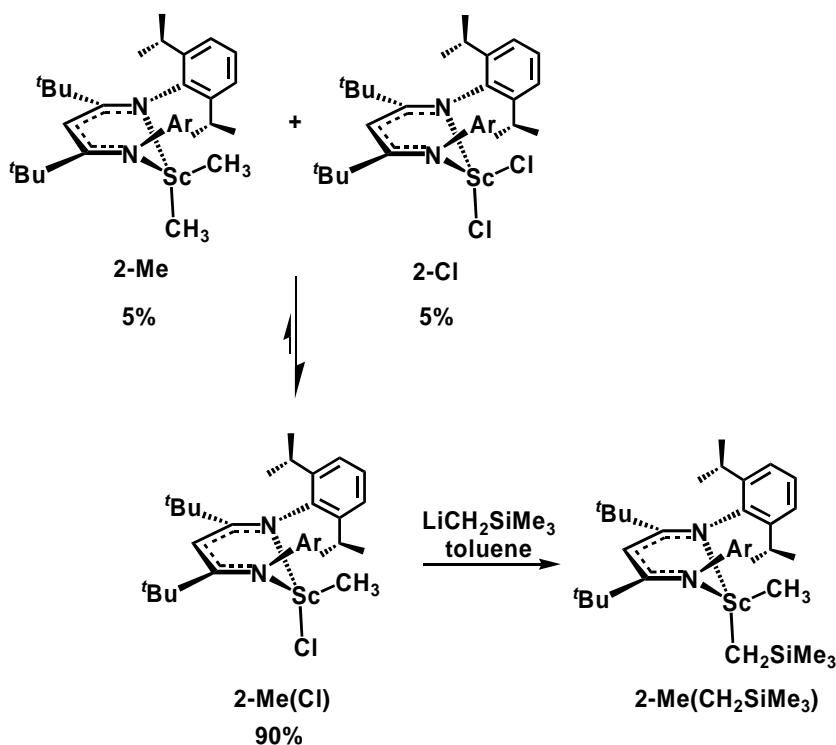
Mixed alkyl derivatives can be synthesized *via* two separate routes. The first involves the reaction of **2-Cl**, and **2-Me**, to give solution mixtures comprising of 90% the desired methylchloro derivative, **2-Me(Cl)**, along with 5% of both **2-Me** and **2-Cl**.



Scheme 2.9 Synthesis of $L^{\text{tBu}}\text{ScR}'_2$ Compounds

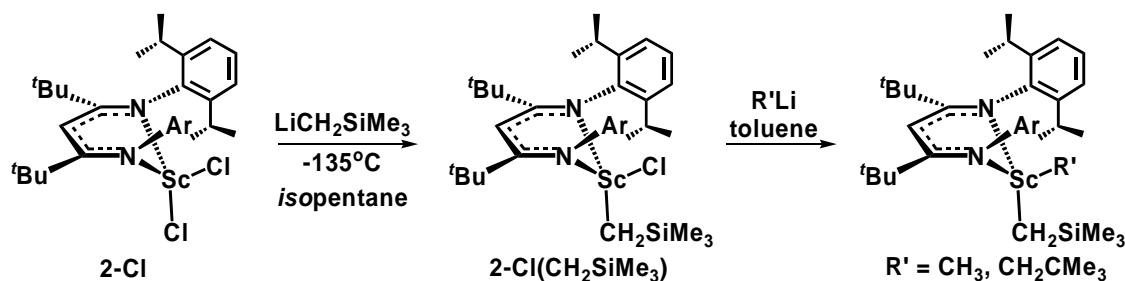
Attempts to further alter this ratio towards the mixed alkyl species were fraught with failure, suggesting that the observed mixture is an equilibrium ratio. Likewise, attempts to catalyze the exchange with $\text{B}(\text{C}_6\text{F}_5)_3$ were unsuccessful. Nonetheless, addition of $\text{LiCH}_2\text{SiMe}_3$ to the mixture affords the mixed alkyl species, $L^{\text{tBu}}\text{Sc}(\text{Me})(\text{CH}_2\text{SiMe}_3)$, **2-Me(CH₂SiMe₃)**, contaminated with residual **2-Me** and **2-Cl** (Scheme 2.10). The desired mixed alkyl compound could be obtained in >95% purity upon successive recrystallizations from cold hexanes.

A vastly improved procedure for the synthesis of mixed alkyls was established by adding a dilute toluene solution of one equivalent of $\text{LiCH}_2\text{SiMe}_3$ dropwise to a cold



Scheme 2.10 Synthesis of Mixed Alkyl $\text{2-Me(CH}_2\text{SiMe}_3)$

($-135\text{ }^\circ\text{C}$) solution of dichloride 2-Cl at a rate of 0.11 mL/minute *via* syringe pump (Scheme 2.11). If the addition takes place at a faster rate or at higher temperatures, a mixture of dialkyl, dichloride and the desired alkylchloride results. Upon complete addition, the reaction mixture was slowly (6 hours) warmed to room temperature whereupon workup gave pure $\text{2-Cl(CH}_2\text{SiMe}_3)$, in 70% yield. Interestingly, $\text{2-Cl(CH}_2\text{SiMe}_3)$ is stable towards decomposition by redistribution to 2-Cl , and $\text{2-CH}_2\text{SiMe}_3$. Likewise, it is not possible to generate alkylchloride $\text{2-Cl(CH}_2\text{SiMe}_3)$,



Scheme 2.11 Synthesis of Mixed Alkyl Compounds of Form $L^{t\text{Bu}}\text{Sc}(\text{CH}_2\text{SiMe}_3)(\text{R}')$

through reaction of **2-CH₂SiMe₃** and **2-Cl**. Presumably, the bulkier CH₂SiMe₃ group, renders the likely halide/alkyl bridged transition state too high in energy (Figure 2.4). Exploratory reactions into this phenomenon suggest that the redistribution is still viable if R = CH₂CH₃, although the equilibrium lies slightly further towards the starting materials (10% of both the dialkyl and dichloride compounds remain). No production of mixed alkyls was observed when R = CH₂Ph or CH₂CMe₃.

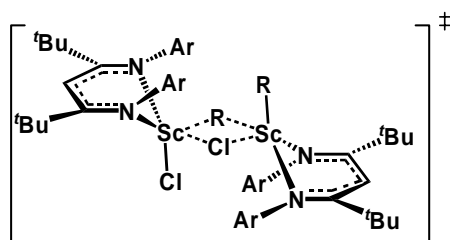
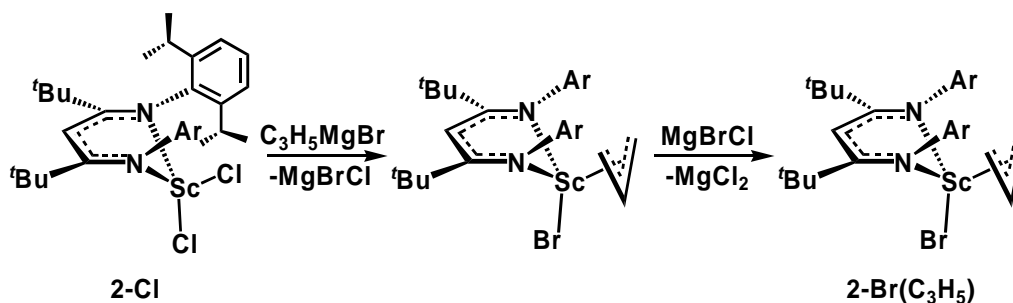


Figure 2.4 Proposed Transition State for Halide/Alkyl Redistribution to **2-R(Cl)**

Alkylation of **2-Cl(CH₂SiMe₃)** is readily achieved in good yields (50-70%) upon reaction with one equivalent of the appropriate alkylating reagent (MeLi, LiCH₂CMe₃) to give **2-Me(CH₂SiMe₃)** and $L^{t\text{Bu}}\text{Sc}(\text{CH}_2\text{CMe}_3)(\text{CH}_2\text{SiMe}_3)$, **2-CH₂SiMe₃(CH₂CMe₃)**, respectively. Higher combined yields for the two steps responsible for alkyl group introduction can be accomplished through a one-pot synthesis; upon allowing the crude reaction mixture of **2-Cl** and LiCH₂SiMe₃ to gradually warm to room temperature the

solution can be cooled back to $-78\text{ }^{\circ}\text{C}$ whereupon the second alkyl lithium can be added from a solid addition piece. Slow warming to room temperature and subsequent workup cleanly produced the mixed alkyl compounds in $>80\%$ yield.

It is also possible to alkylate with unsaturated groups; reaction of dichloride **2-Cl** with one equivalent of $\text{C}_3\text{H}_5\text{MgBr}$ cleanly installed one allyl group, producing the allylhalide compound, $\text{L}^{\text{tBu}}\text{Sc}(\text{Br})(\text{C}_3\text{H}_5)$, **2-Br(C₃H₅)**. Intriguingly, there appears to be rapid halogen exchange between $\text{L}^{\text{tBu}}\text{ScCl}(\text{C}_3\text{H}_5)$, and the newly formed MgBrCl , presumably due to the driving force of MgCl_2 formation (Scheme 2.12). It was not possible to introduce a second allyl group, even when excess Grignard reagent was used.



Scheme 2.12 Synthesis of **2-Br(C₃H₅)**

The halogen exchange observed during the production of **2-Br(C₃H₅)** prompted exploratory reactions involving both scandium dichloride and mixed alkylchloride species with LiI ; these reactions showed rapid halogen exchange as the iodide was incorporated at expense of the chloride. Since it was not possible to push the reaction completely towards $\text{L}^{\text{tBu}}\text{ScI}_2$, even with a large excess of LiI , it would seem that the halogen exchange is an equilibrium process. In slightly different scandium dichloride compounds, it may, however, be possible to drive the reaction to completion, a desirable

transformation if one is seeking low valent Sc(I) compounds, since metal iodides are frequently much easier to reduce than their chloride analogues.³⁷

All of the compounds vary little in colour ranging from white to pale yellow with intense ligand to metal charge transfer (LMCT) absorptions occurring in the UV region of the UV-visible spectra recorded in hexane. The 5-coordinate compounds exhibit maximum absorptions at shorter wavelength (higher energy) than their 4-coordinate congeners due to the different geometry and greater degree of electronic saturation at the metal. Likewise, 4-coordinate dialkyl compounds supported by L^{Me} afforded absorptions 10-15 nm lower than their L^{tBu} stabilized counterparts (Table 2.1).

Table 2.1 UV-Vis Data for Scandium Nacnac Compounds

Compound	λ	ϵ	Compound	λ	ϵ
1-Cl(THF)	322	3800	2-Cl	358	10800
1-Me(THF)	318	20600	2-Me	366	11000
1-CH₂Ph	348	4300	2-Et	366	20800
1-CH₂CMe₃	346	28900	2-CH₂Ph	366	11300
1-CH₂SiMe₃	344	19400	2-CH₂CMe₃	367	22100
			2-CH₂SiMe₃	370	22200

* λ = wavelength (nm); ϵ = molar absorptivity ($M^{-1}cm^{-1}$); solvent = hexane

2.2.3 X-ray Crystal Structures

A number of solid state structures have been determined for the previously discussed nacnac supported complexes and are presented in the following section. Several important features will be addressed including the effects of substitution in the ligand backbone and the degree to which the scandium centre is displaced from the plane made by the β -diketiminato framework. The fact that the metal centre does not lie in the plane of the ligand renders the two alkyl sites inequivalent. The differences between

these positions and the rationale for site preference will be addressed. Finally, the observation of a localized ligand backbone structure will be elaborated upon.

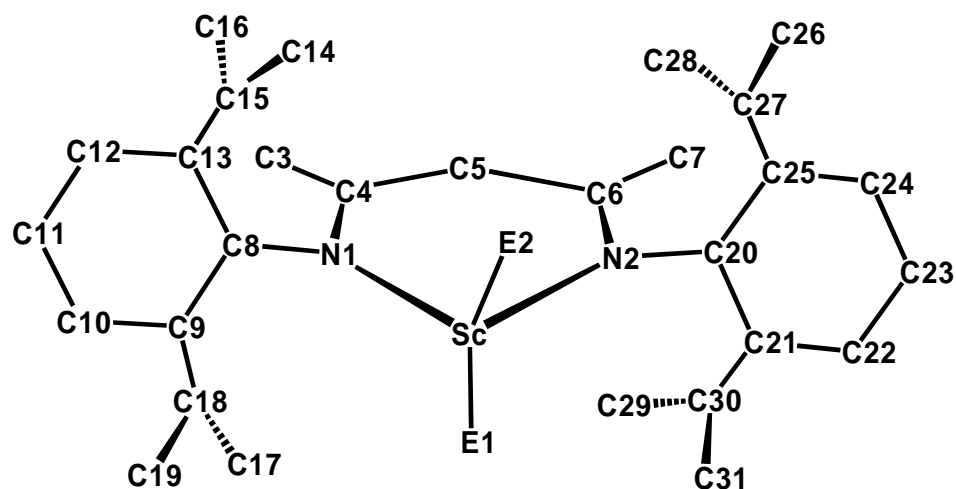


Figure 2.5 Numbering Scheme of Sc-nacnac Framework

The β -diketiminato framework has proven useful in its ability to impart crystallinity in the scandium complexes, and as such, a variety of X-ray quality crystals

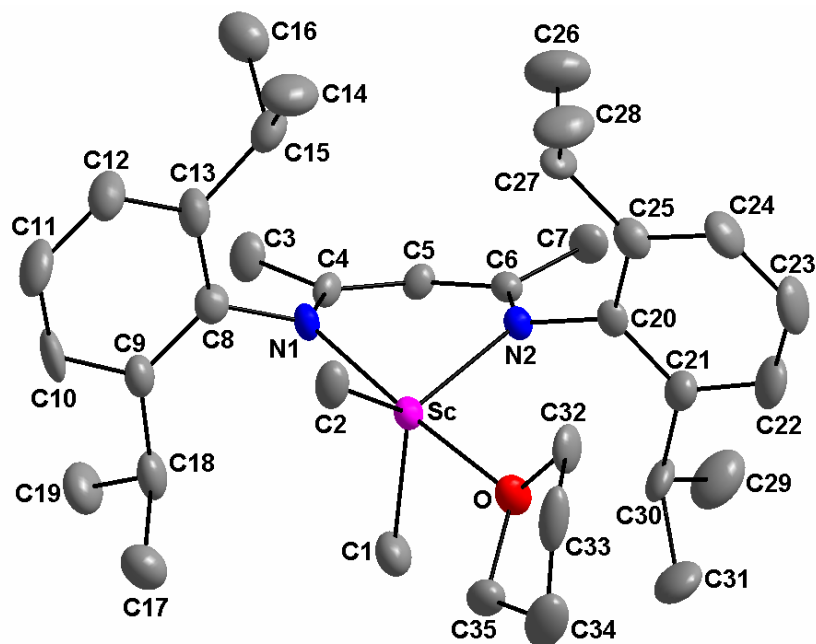


Figure 2.6 X-ray Molecular Structure of **1-Me(THF)**. Thermal ellipsoids are drawn at the 30% probability level. Hydrogen atoms omitted for clarity.

Table 2.2 Selected Metrical Data for $L^{\text{Me}}\text{ScE}_2(\text{THF})_x$ Compounds: **1-Cl(THF)⁵⁶, **1-Me(THF)**, and **[1-Me]₂****

Parameter ^a	1-Cl(THF)	1-Me(THF)	[1-Me] ₂
Bond Distances (Å)			
Sc-N(1)	2.175(4)	2.201(6)	2.2230(15)
Sc-N(2)	2.107(4)	2.190(7)	2.2230(16)
Sc-O(1)	2.203(4)	2.228(5)	N/A
Sc-E(1)	2.3556(17)	2.210(9)	2.208(2)
Sc-E(2)	2.3795(18)	2.245(9)	2.303(5)
			2.364(10)
Sc-C(4)	3.066(5)	3.116(9)	3.123(2)
Sc-C(5)	3.327(6)	3.383(9)	3.382(2)
Sc-C(6)	3.062(6)	3.098(9)	3.126(2)
Sc-N ₂ C ₃ plane	0.694(6)	0.815(9)	0.879(2)
Bond Angles (°)			
E(1)-Sc-E(2)	131.47(8)	123.8(4)	99.9(5)
			116.7(3)
N(1)-Sc-E(1)	94.85(13)	96.4(3)	100.63(8)
N(1)-Sc-E(2)	92.33(12)	93.1(3)	90.4(2)
			86.3(2)
N(2)-Sc-E(1)	104.53(11)	105.9(3)	101.10(8)
N(2)-Sc-E(2)	123.79(13)	130.1(3)	159.0(5)
			142.2(3)
N(1)-Sc-N(2)	86.77(17)	85.2(3)	85.46(6)
N(1)-Sc-O(1)	175.31(16)	175.5(3)	N/A
N(2)-Sc-O(1)	95.82(16)	93.7(2)	N/A
Sc-N(1)-C(4)	121.1(4)	121.5(8)	120.40(12)
N(1)-C(4)-C(5)	123.5(5)	124.0(8)	124.57(17)
C(4)-C(5)-C(6)	130.4(5)	129.3(8)	129.96(17)
C(5)-C(6)-N(2)	122.9(5)	124.7(8)	124.57(17)
C(6)-N(2)-Sc	122.4(3)	122.6(6)	120.67(12)

^aE = Cl for **1-Cl(THF)** and Me for **1-Me(THF)** and **[1-Me]₂**

were grown from cold hydrocarbon mixtures. A number of representative solid state structures are presented in Figures 2.6 – 2.12 with a selection of relevant metrical data in Tables 2.2 – 2.4. The numbering of the ligand framework is held consistent throughout this thesis with E1 and E2 being reserved for alkyl groups bonded to scandium, C3 – C7 representing the ligand backbone core, which is in common to both nacnac variants, and C8 – C19 and C20 – C31 numbering the *diisopropylphenyl* moieties (Figure 2.5).

The structures of the 5-coordinate THF ligated compounds **1-Cl(THF)** and **1-Me(THF)** are quite similar with the metal centre exhibiting distorted trigonal bipyramidal geometry. N1 and O1 occupy the apical sites with N1-Sc-O1 bond angles just shy of linear at approximately 175 °. The equatorial sites are occupied by N2, C1(C11) and C2(C12) with angles ranging from 104 – 131 °. The scandium centre is symmetrically bound to the nacnac ligand with typical Sc-N bond distances of 2.107(4) – 2.201(6) Å.⁷ Likewise, the Sc-Cl and Sc-C bond lengths are unremarkable, ranging from 2.3556(17) – 2.3795(18) Å for the former and 2.210(9) – 2.245(9) Å for the latter.⁸ Although the metal is displaced from the plane of the ligand (0.694 – 0.815 Å) it is not sufficiently great to suspect significant π -donation from the 2b1 orbital. Indeed, the distances of 3.062(6) – 3.383(9) Å between C4, C5 and C6 and Sc, coupled with the lack of puckering of these atoms towards the metal (the five atoms within the ligand backbone are virtually coplanar with a maximum standard deviation of 0.064(8) Å from planarity), suggest these complexes are best described as having a 2 σ , 4 electron donation from the nitrogens of the nacnac ligand to the scandium centre. The torsion angles about the N-C_{aryl} bonds are in good agreement with the calculations reported by Tolman *et al.*;⁵⁴ the

aromatic rings lie almost completely perpendicular to the plane of the ligand with torsion angles approaching 90° in all cases.

The structures of the 4-coordinate complexes are the first reported for the L^{tBu} ancillary and are quite symmetrical with the metal centre adopting a slightly distorted tetrahedral geometry; the N1-Sc-N2 bond angles deviate from ideality with values ranging from $92 - 96^\circ$ for the L^{tBu} derivatives and approximately 91° for the L^{Me} compounds.⁵⁷ This marked increase in the angle for the bulkier L^{tBu} species is likely due

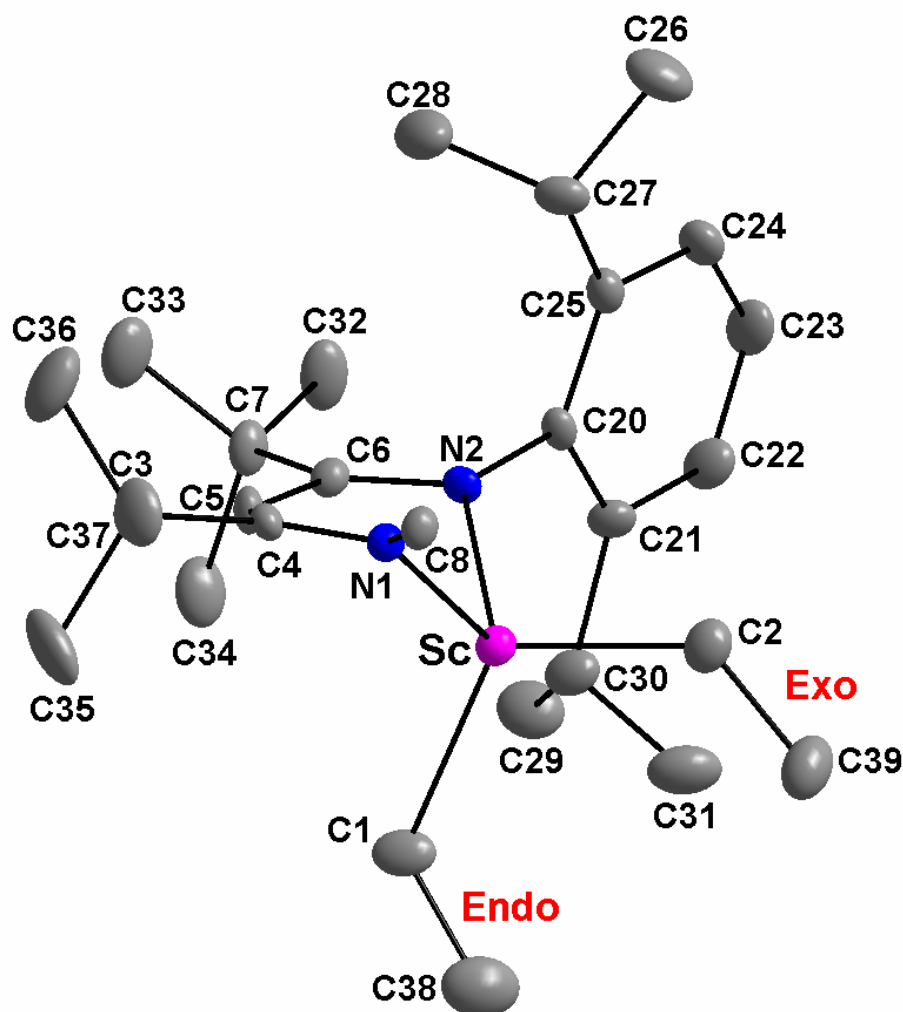


Figure 2.7 X-ray Molecular Structure of 2-Et. Thermal Ellipsoids are drawn at the 30% probability level. Front aryl group and hydrogen atoms are removed for clarity.

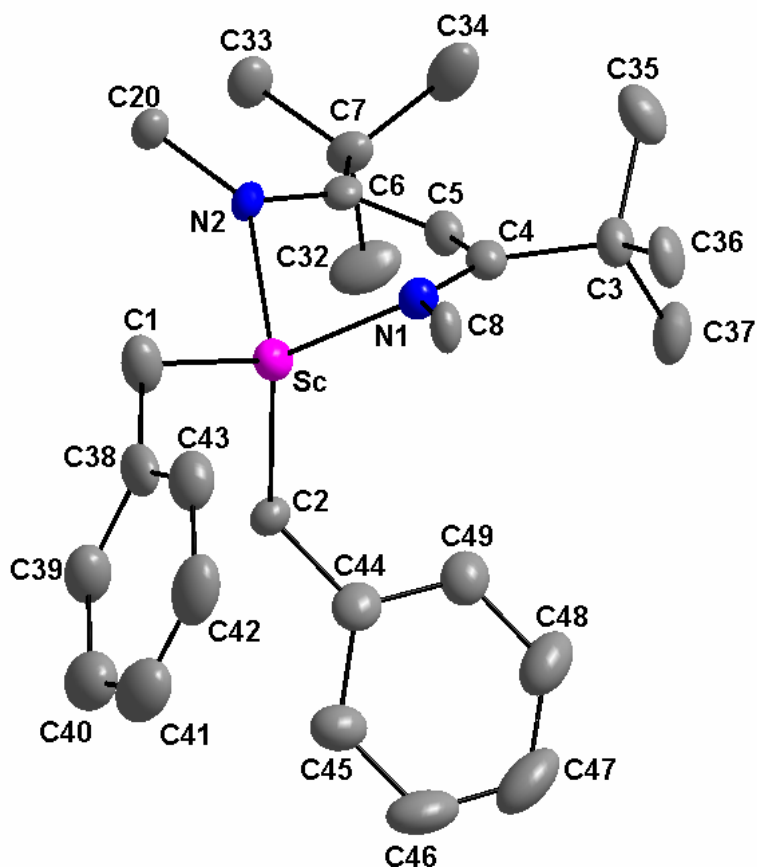


Figure 2.8 X-ray Molecular Structure of **2-CH₂Ph**. Thermal Ellipsoids are drawn at the 30% probability level. Front aryl group and hydrogen atoms are removed for clarity.

to increased steric interactions between the aromatic groups and substituents attached to scandium. The increased steric crowding at the metal centre is also obvious upon perusal of the C4-N1-C8 and C6-N2-C20 angles which have been forced open by an additional 5 – 6° in comparison to their L^{Me} analogues. Although the Sc-C and Sc-N bond distances remain within normal ranges⁸ the scandium is forced significantly further from the plane of the ligand with values up to 1.295(6) Å (cf. 0.694(6) – 0.879(2) Å for five-coordinate L^{Me} structures). As a result, the structures exhibit C_s symmetry with a mirror plane

Table 2.3 Selected Metrical Data for L^{tBu}ScE₂ Compounds: **2-Cl**, **2-Me**, **2-Et**, **2-CH₂Ph**, and **2-CH₂SiMe₃**⁵⁹

Parameter	2-Cl	2-Me	2-Et	2-CH ₂ Ph	2-TMS
Bond Distances (Å)					
Sc-N(1)	2.046(6)	2.1029(10)	2.125(5)	2.091(5)	2.091(5)
Sc-N(2)	2.099(6)	2.1451(10)	2.118(5)	2.118(5)	2.144(5)
Sc-E(1)	2.352(3)	2.2197(15)	2.244(6)	2.265(6)	2.229(7)
Sc-E(2)	2.326(3)	2.2219(16)	2.204(6)	2.203(7)	2.202(7)
Sc-C(4)	2.628(7)	2.7289(12)	2.777(7)	2.722(7)	2.808(7)
Sc-C(5)	2.700(7)	2.8775(12)	2.832(6)	2.796(7)	2.934(7)
Sc-C(6)	2.738(7)	2.8770(12)	2.767(7)	2.796(7)	2.890(7)
Sc-N ₂ C ₃ plane	1.295(6)	1.2621(21)	1.240(5)	1.244(4)	1.146(6)
Bond Angles (°)					
E(1)-Sc-E(2)	115.00(12)	109.46(6)	117.6(3)	114.4(3)	109.4(3)
N(1)-Sc-E(1)	113.5(2)	110.80(5)	111.4(2)	109.7(2)	119.3(2)
N(1)-Sc-E(2)	112.2(2)	123.27(6)	109.2(2)	105.7(3)	105.3(3)
N(2)-Sc-E(1)	116.0(2)	112.64(5)	113.2(2)	123.9(2)	120.2(2)
N(2)-Sc-E(2)	102.2(2)	107.17(5)	108.9(2)	105.6(3)	107.3(2)
N(1)-Sc-N(2)	95.9(2)	92.20(4)	94.00(16)	94.7(2)	93.5(2)
Sc-N(1)-C(4)	100.0(5)	101.77(7)	105.1(3)	102.0(4)	107.4(4)
N(1)-C(4)-C(3)	126.4(8)	124.60(10)	126.8(5)	125.2(6)	124.6(6)
N(1)-C(4)-C(5)	120.0(8)	121.33(11)	121.2(5)	120.3(6)	120.9(6)
C(3)-C(4)-C(5)	113.0(8)	113.71(10)	111.9(5)	114.2(6)	114.2(6)
C(4)-C(5)-C(6)	134.8(8)	133.43(11)	136.4(5)	136.1(7)	134.7(6)
C(5)-C(6)-C(7)	112.6(7)	113.28(10)	113.4(5)	112.6(6)	112.0(6)
C(5)-C(6)-N(2)	119.7(8)	119.23(10)	120.5(5)	120.0(6)	120.2(6)
C(7)-C(6)-N(2)	127.7(8)	127.50(10)	125.9(5)	127.4(6)	127.8(6)
C(6)-N(2)-Sc	104.2(5)	110.28(8)	104.1(3)	106.3(4)	110.6(4)
Torsion Angles (°)					
C(6)-N(2)-C(20)-C(25)	95(0)	98.31(15)	89.3(7)	98.2(8)	94.2(8)
C(6)-N(2)-C(20)-C(21)	-92.0(10)	-87.90(15)	-95.4(7)	-88.8(9)	-91.5(9)
C(4)-N(1)-C(8)-C(9)	115.1(9)	124.69(13)	104.1(7)	110.7(8)	105.7(7)
C(4)-N(1)-C(8)-C(13)	-69.6(11)	-59.56(16)	-80.8(7)	-74.3(9)	-82.0(8)

reflecting the right and left sides of the complexes; consequently, the two alkyl or chloride substituents are inequivalent. The chemical difference between the two environments is important and throughout this thesis the substituent which occupies the site pointing “out and away” from the ligand is denoted as the *exo* position while the site “below” the nacnac plane is distinguished as the *endo* position (Figure 2.7). It appears that the *isopropyl* aryl groups tilt away from the *endo* position to alleviate steric strain. In this case the *isopropyl* groups above the *exo* position are forced close together while the *isopropyls* in closer proximity to the *endo* substituents are allowed to bend away (Figure

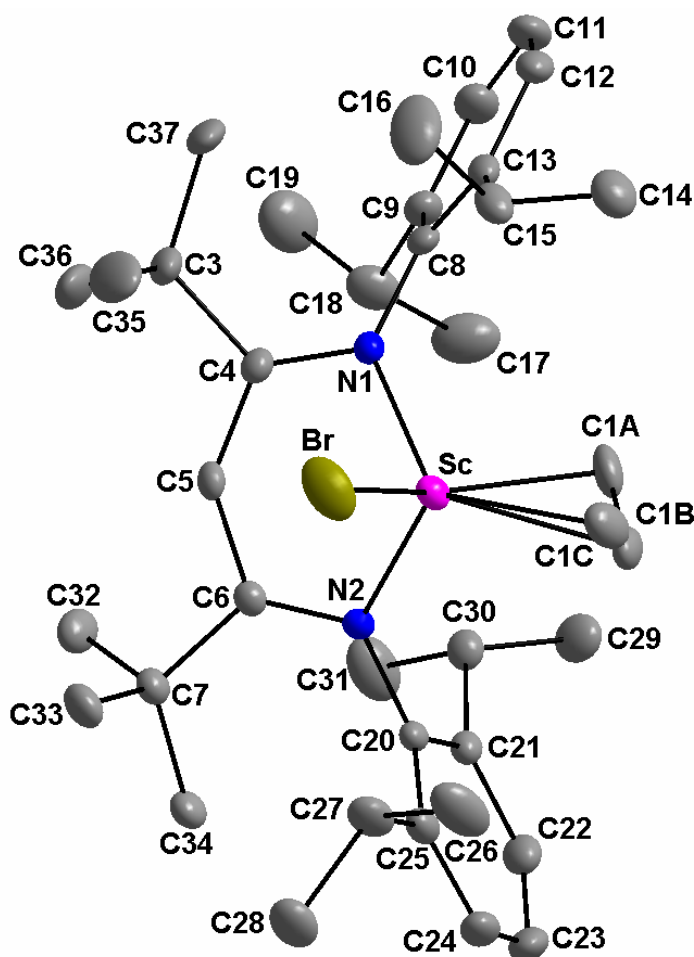


Figure 2.9 X-ray Molecular Structure of 2-Br(C₃H₅). Thermal Ellipsoids are Drawn at the 30% probability level. Hydrogen atoms are removed for clarity.

2.10). This steric relief becomes more important the further the metal is out of the ligand plane and is likely not possible to the same extent for the 5-coordinate structures because the “top” aryl groups, upon bending towards one another, would encounter the fifth metal substituent.

Interestingly, the diethyl derivative, **2-Et**, has large Sc-C1-C38 and Sc-C2-C39 values of 119.4(5) and 129.0(5) ° which argue against β -agostic interactions like that found in Cp*₂ScEt.⁴ This feature is likely due to the steric crowding at the metal centre. In agreement with this finding, L^{tBu}ScEt₂ was not found to decompose *via* β -H elimination, whereas the less crowded L^{Me}ScEt₂ rapidly decomposes upon initial formation to a variety of uncharacterized products. Similarly, the dibenzyl complex, **2-CH₂Ph**, has normal Sc-C1-C38 and Sc-C2-C44 angles of 127.0(4) and 115.3(5) ° which argue against any η^2 bonding interactions (Figure 2.8).

The X-ray crystal structures have also been determined for the mixed alkylhalide compounds **2-Br(C₃H₅)**, and **2-Cl(CH₂SiMe₃)**. The former compound adopts a structure akin to the various 4-coordinate dialkyl species, with the allyl functionality symmetrically bound with Sc-C1A and Sc-C1C bond distances of 2.414(3) and 2.437(3) Å respectively (Figure 2.9). The allyl resides in the *exo* site in a vertical arrangement, that is, the C3 unit lies in a plane parallel to the aromatic rings. It appears that the *exo* position is less sterically demanding, thus it is not surprising the bulky C₃H₅ substituent is found in this location. The solid state structure of **2-Cl(CH₂SiMe₃)**, however, appears to contradict this trend; it has been shown that π -donors appear to favour the *exo* site.^{61,62} Nonetheless, the structure for L^{tBu}Sc(CH₂CMe₃)(CH₂SiMe₃) lends support to the concept with the bulky neopentyl group lying exclusively in the *exo* site (Figure 2.11). In this situation the

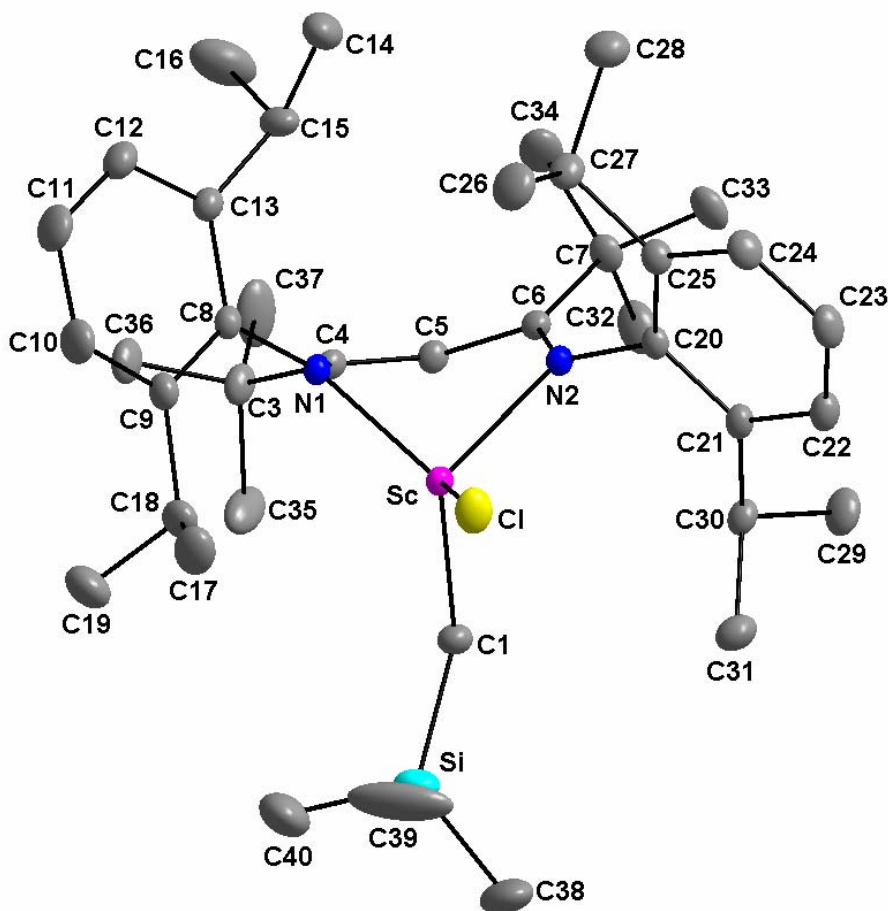


Figure 2.10 X-ray Molecular Structure of 2-Cl(CH₂SiMe₃). Thermal ellipsoids are drawn at the 30% probability level. Hydrogen atoms are removed for clarity.

longer C-Si bond length of 1.848(6)Å in comparison to the C-C bond distance of 1.516(5)Å within the neopentyl group results in the bulk of the CH₂SiMe₃ group being further removed from the metal centre. The non-bonding distances between scandium and the β-C and β-Si of 3.314(3) and 3.763(2)Å respectively, illustrate this fact.

The solid state structure of the THF free complex [1-Me]₂, has been determined as a dimer with the two bridging methyl groups having rather long Sc-C distances of

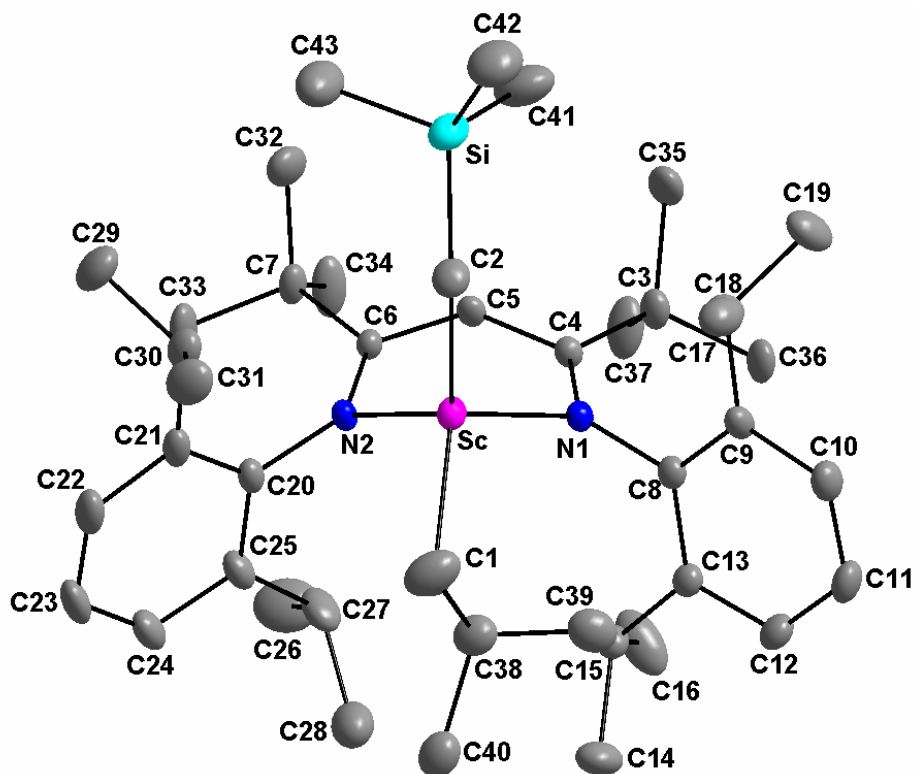


Figure 2.11 X-ray Molecular Structure of 2-CH₂SiMe₃(CH₂CMe₃). Thermal ellipsoids are drawn at the 30% probability level. Hydrogen atoms are removed for clarity.

2.372(12) and 2.303(11) Å and 2 terminal methyls with a typical Sc-C distance of 2.208(2) Å. Although the metal centre is 5 coordinate and the structure can be viewed as a rather distorted trigonal bipyramid with C2' and N2 in the apical positions (C2'-Sc-N2 = 159.03(20)°) and the equatorial plane comprised of C1, C2 and N1 (with angles ranging from 100.63(8) - 151.4(25)°), it can also be viewed as a slightly skewed tetrahedron with the bridging methyl groups together representing one vertex of the tetrahedron (Figure 2.12). In this scenario, with an imaginary atom placed between the two bridging methyl groups, the angles about the tetrahedron range from 100.63(8) – 128.07(4)°. In view of the previous discussion, it is not surprising that the bridging methyls (and remainder of the dimer) are located in the *exo* site with the terminal methyl in the *endo* position.

Table 2.4 Selected Metrical Data for Mixed Alkyl and Alkylhalide Compounds:
2-Cl(CH₂SiMe₃), 2-CH₂SiMe₃(CH₂CMe₃) and 2-Br(C₃H₅)

Parameter	2-Cl(CH ₂ SiMe ₃)	2-CH ₂ SiMe ₃ (CH ₂ CMe ₃)	2-Br(C ₃ H ₅)
Bond Distances (Å)			
Sc-N(1)	2.0747(12)	2.144(3)	2.0965(19)
Sc-N(2)	2.1435(12)	2.126(3)	2.1081(18)
Sc-E(1)	2.2098(16)	2.239(3)	2.437(3)
			2.381(3)
			2.414(3)
Sc-E(2)	2.3493(5) ^b	2.234(4)	2.5524(5)
Sc-C(4)	2.6528(14)	2.939(3)	2.765(2)
Sc-C(5)	2.7695(15)	3.036(3)	2.867(2)
Sc-C(6)	2.8262(14)	2.903(3)	2.831(2)
Sc-N ₂ C ₃ plane	1.328(1)	1.031(3)	1.164(2)
Bond Angles (°)			
E(1)-Sc-E(2)	111.90(5) ^b	113.28(14)	91.28(9) ^a
N(1)-Sc-E(1)	118.75(6)	109.11(12)	132.70(9) ^a
N(1)-Sc-E(2)	116.32(4) ^b	115.18(13)	105.02(5)
N(2)-Sc-E(1)	111.00(6)	103.58(11)	121.82(9) ^a
N(2)-Sc-E(2)	103.22(4) ^b	120.17(13)	107.97(5)
N(1)-Sc-N(2)	92.49(5)	93.32(10)	95.23(7)
Sc-N(1)-C(4)	98.63(9)	113.2(2)	104.42(15)
N(1)-C(4)-C(5)	120.35(12)	120.8(3)	121.5(2)
C(4)-C(5)-C(6)	132.71(13)	135.7(3)	136.6(2)
C(5)-C(6)-N(2)	118.60(13)	121.2(3)	119.8(2)
C(7)-C(6)-N(2)	127.69(13)	125.4(3)	127.42(19)
C(6)-N(2)-Sc	107.40(9)	11.56(19)	108.51(13)
Torsion Angles (°)			
C(6)-N(2)-C(20)-C(25)	98.05(19)	79.59(42)	-90.10(28)
C(6)-N(2)-C(20)-C(21)	-90.24(19)	-105.85(38)	96.38(27)
C(4)-N(1)-C(8)-C(9)	123.71(16)	82.56(39)	-69.43(31)
C(4)-N(1)-C(8)-C(13)	-60.31(20)	-93.72(39)	115.72(26)

^aWhenever E1 is listed, C1B, the central carbon of the symmetrically bound allyl group is used to determine the angle; ^bE2 = Cl

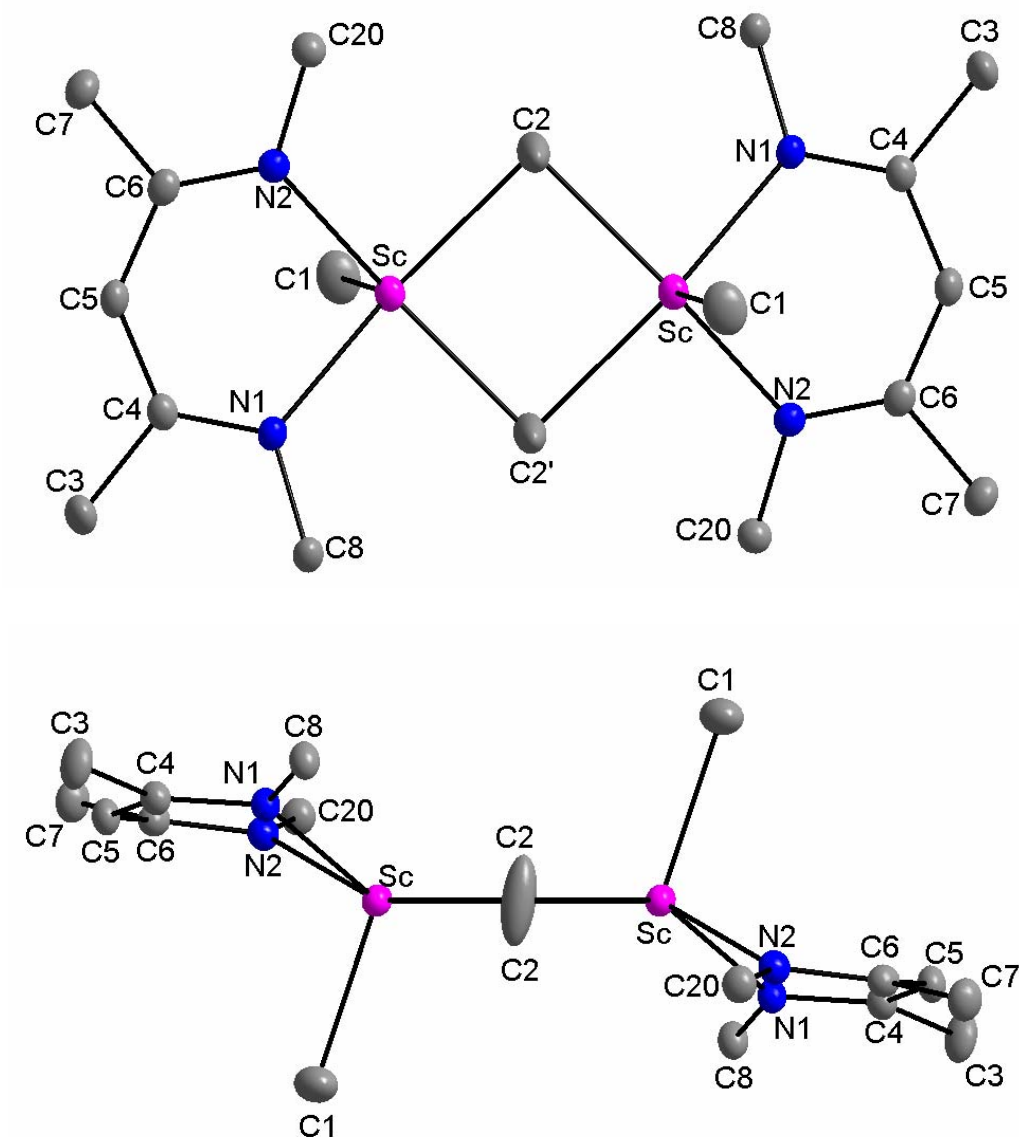


Figure 2.12 X-ray Molecular Structure of $[1\text{-Me}]_2$. Thermal ellipsoids are drawn at the 30% probability level. Hydrogen atoms and aryl groups are removed for clarity.

While it appears that the metal sits significantly out of the plane mainly due to steric interactions between the aryl *isopropyl* groups and the metal substituents, potential electronic stabilization through donation from the 2b1 orbital must also be considered. In contrast to the five coordinate structures, the metal is further from the ligand plane and there is significant puckering of the ligand, most notably C4 and C5. Both of these

factors result in the scandium centre lying dramatically closer to the ligand backbone, thus allowing for greater orbital overlap and more donation from a filled 2b1 orbital into a metal orbital of appropriate symmetry. Indeed, with distances as low as 2.628(7) and 2.700(7) Å between Sc and C4 and C5 respectively, the bonding should be considered to incorporate a degree of π donation to the metal. Another argument which suggests that the metal's residence out of the plane is partially electronic is the fact that the most pronounced metal – backbone interactions are observed for **2-Me**, the complex with the smallest metal substituents. In fact, the degree to which the metal is displaced from the plane correlates reasonably well with the electron donating ability of the metal's substituents; the less the metal is electronically stabilized by its alkyl groups, the more it is out of the plane, and hence the greater degree of electronic stabilization available from interaction with the 2b1 ligand orbital.

Conversely, the bulkier the alkyl group, the less the metal is out of the plane. Although this may seem counterintuitive, more sterically encumbered groups may render the metal incapable of further displacement due to growing unfavourable interactions with the aryl *isopropyl* moieties. The energetic benefits achieved by dipping out of the plane gradually diminish as steric interactions between the *exo* substituent and the lower aryl *isopropyl* group increases (Figure 2.7).

Thus, while it appears that displacement from the plane of the ligand alleviates steric interactions between the metal substituents and the aryl *isopropyl* groups, the degree to which this stabilization can occur would seem to be a fine balance between energy gained by dipping from the plane and growing destabilization occurring between the *exo* substituent and the lower *isopropyl* groups; as such this process is highly

dependent upon the size of the *exo* group. Hence, despite the fact that the *exo* position is believed to be more sterically accessible, it becomes less so the more the metal is displaced from the plane, and for this reason, smaller *exo* groups permit larger deviation from planarity. This phenomenon is shown pictorially by a qualitative energy profile in Figure 2.13.

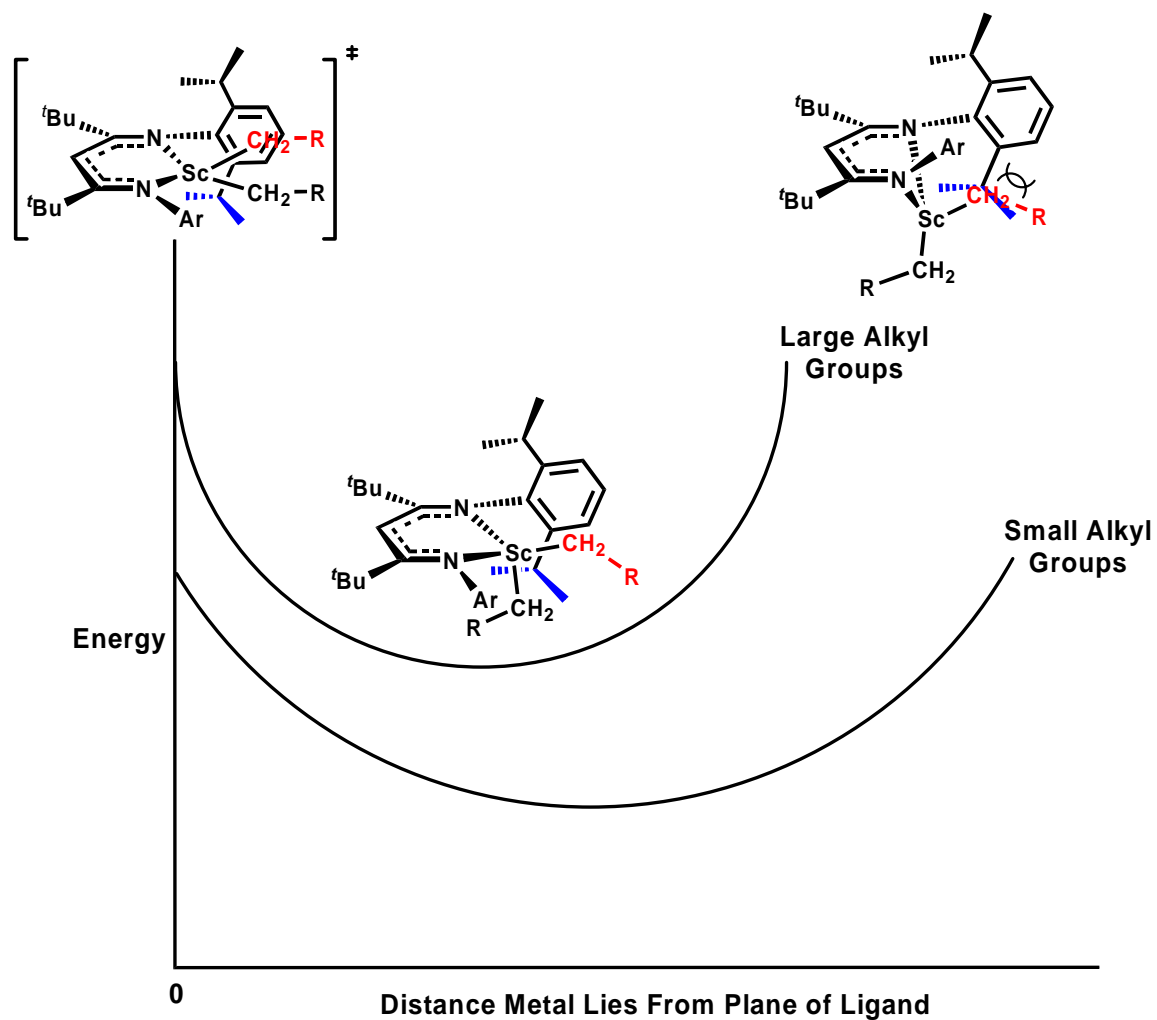


Figure 2.13 Proposed Qualitative Energy Profile for Scandium Deviating From Planarity: Differences Invoked as a Result of the Size of the Metal Substituents

In the case of mixed alkylchloride **2-Cl(CH₂SiMe₃)**, it would appear that substantial energetic benefits result from the metal dipping out of the nacnac plane. Meanwhile negligible interactions result between the *exo* Cl and the lower *isopropyl* groups because the steric bulk associated with the chloride is small and not sufficiently removed from the metal centre to significantly interact with the lower *isopropyl* aryl moieties. The net result is a scandium species whereby at 1.328(1) Å, the metal is the furthest from the β-diketiminato plane of all structurally characterized compounds in this family.

A careful analysis of the metrical parameters associated with the ligand backbone exposes a partially localized ligand backbone structure, resulting from an amido-imine resonance contribution, Table 2.5. The bond lengths for several of the dialkyl structures

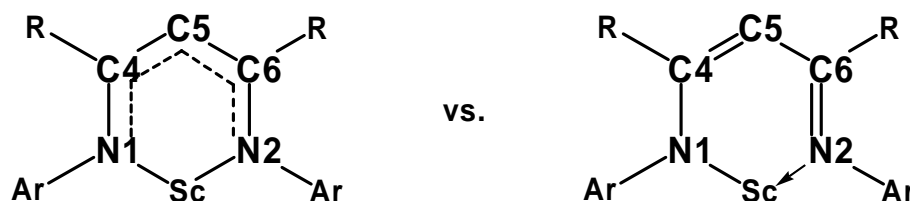


Figure 2.14 Potential β-diketiminato Resonance Structures

suggest the bonding is not completely symmetrical, most notably L^{*t*Bu}ScMe₂, which also has the largest deviation from planarity in the ligand plane; C6 is 0.321 Å from the plane made by the other four atoms. The Sc-N1, N2-C6 and C4-C5 lengths are somewhat shorter than Sc-N2, N1-C4 and C5-C6 indicating a partially alternating series of bond lengths and localized electron distribution (Figure 2.14). It is difficult to say how important this resonance structure is as there does not appear to be a clear correlation between the sterics or electronics of the alkyl group and the severity of perturbation from

Table 2.5 Comparison of Ligand Bond Distances in Complexes of form L^{tBu}ScR₂

Parameter	2-Me	2-CH ₂ Ph	2-Et	2-CH ₂ SiMe ₃ ⁵⁹	2-CH ₂ SiMe ₃ CH ₂ CMe ₃
	Bond Distances (Å)				
Sc-N(1)	2.1029(10)	2.091(5)	2.125(5)	2.091(5)	2.144(3)
Sc-N(2)	2.1451(10)	2.118(5)	2.118(5)	2.144(5)	2.126(3)
Δ	0.0422	0.027	-0.007	0.053	-0.018
N(1)-C(4)	1.3622(15)	1.361(8)	1.318(6)	1.349(8)	1.332(4)
N(2)-C(6)	1.3127(15)	1.325(8)	1.338(7)	1.325(7)	1.345(4)
Δ	0.0495	0.036	-0.02	0.024	-0.013
C(4)-C(5)	1.3962(16)	1.399(8)	1.418(7)	1.400(9)	1.422(4)
C(5)-C(6)	1.4475(16)	1.431(9)	1.423(7)	1.447(8)	1.413(4)
Δ	0.0513	0.032	0.005	0.047	-0.009
E Δ	0.143	0.095	-0.022	0.124	0.040
Sc-C(4)	2.7289(12)	2.722(7)	2.777(7)	2.808(7)	2.939(3)
Sc-C(6)	2.8770(12)	2.796(7)	2.767(7)	2.890(7)	2.903(3)
Δ	0.1481	0.074	-0.01	0.082	-0.036
Sc Out of Plane	1.2621(12)	1.244(4)	1.240(5)	1.146(6)	1.031(3)

a delocalised symmetric structure. For example, **2-Et**, is the most symmetrical compound. There is likely to be a very low energy difference between the two structures.

In conclusion to this section, straightforward routes have been developed for the preparation of base-free dialkyl scandium compounds on a multi-gram scale. A variety of dialkyl and mixed alkyl halide synthetic strategies have proven successful and a number of these compounds have been characterized by X-ray crystallography. The solid

state structures exhibit C_s symmetry with two distinct metal substituent environments denoted *exo* for the position out and away from the metal, and *endo* for the more sterically encumbered site beneath the ancillary framework. The mixed alkyl and alkyl halide complexes generally adopt a geometry which places the largest group in the *exo* position; exceptions to this rule are limited.^{61,62} Finally, it appears that while steric interactions between the metal substituents and the aryl *isopropyl* moieties force the metal out of the plane of the ligand, the degree to which this is possible is dictated by the size of the metal bound groups.

2.2.4 Solution Structures and Dynamic Behaviour

The solution NMR spectra of the 5-coordinate compounds at room temperature display higher symmetry than observed in the solid state structures, exhibiting only one *isopropyl* methine resonance, two *isopropyl* methyl resonances, and one scandium alkyl resonance. Evidently the compounds are fluxional at room temperature, likely as a consequence of THF lability or Berry pseudorotation. This is a low energy process as no changes were observed in the NMR spectra upon cooling the samples to 200K.

The solution ^1H NMR spectra of the various 4-coordinate dialkyls also indicate a more symmetric, in-plane structure than that observed in the solid state. If the solution structure mimicked that observed in the solid state, the NMR spectra would be expected to indicate C_s symmetry, with the only symmetry element being a plane bisecting the *nacnac* ligand. There would be two distinct *isopropyl* groups on each aromatic ring as rotation about the N-aryl groups is inhibited due to the steric properties of the ligand. As

such, there should be right – left symmetry, but top – bottom asymmetry resulting in 2 distinct resonances in the ^1H NMR attributable to the *isopropyl* methines and 4 signals for the corresponding methyls (Figure 2.15). The actual spectra, however, are reflective of an in-plane or time averaged structure of C_{2v} symmetry, whereby only one *isopropyl*

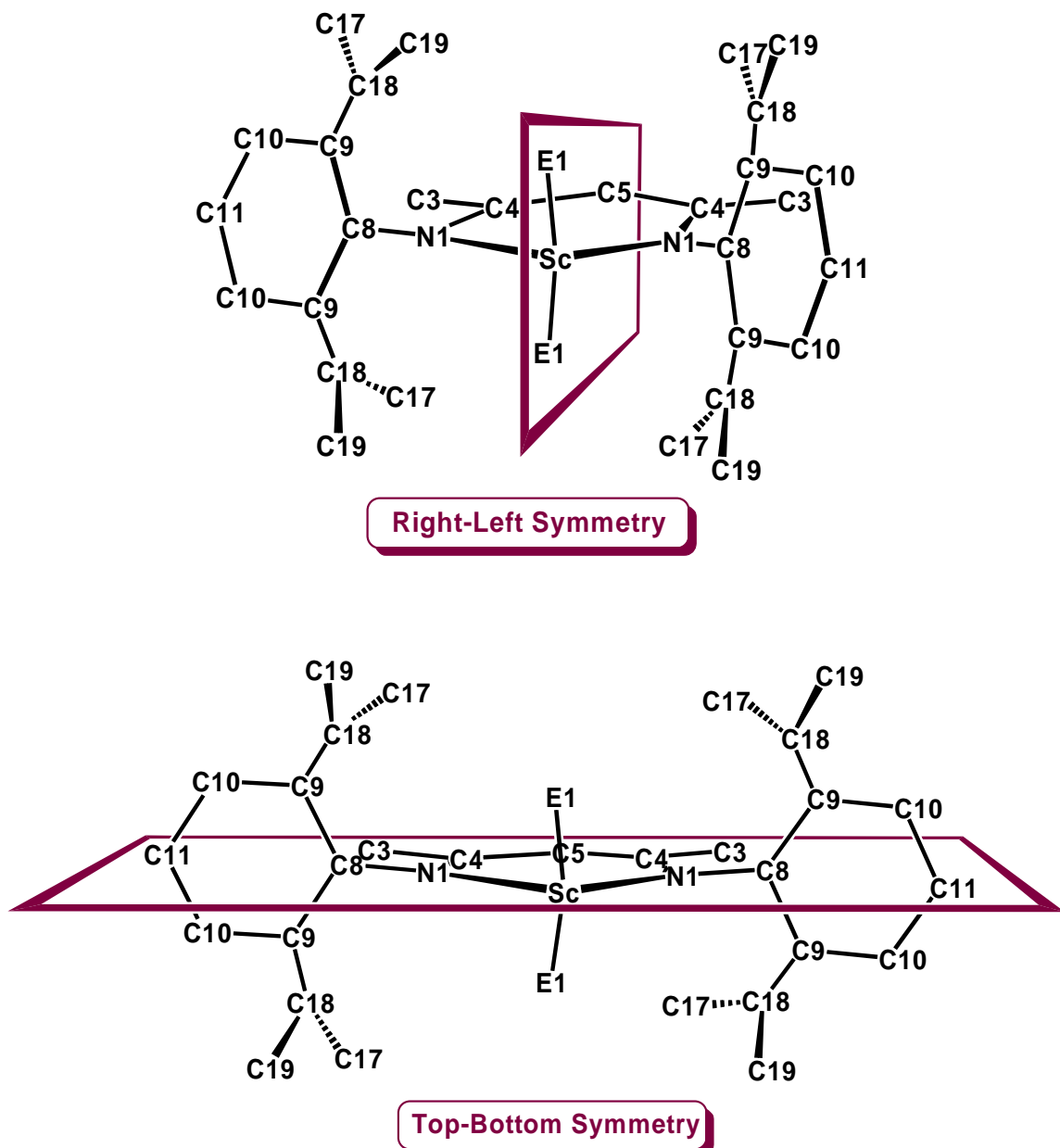


Figure 2.15 Top: Mirror Plane Reflecting Right and Left Sides of LScE_2 ; Bottom: Mirror Plane Reflecting Top and Bottom of LScE_2

Table 2.6 Selected ^1H NMR Data of 4-Coordinate Compounds

Compound ^a	T (K)	H _{Backbone}	CH- <i>i</i> Pr	CH ₃ - <i>i</i> Pr	Sc-CH ₂ R	Sc-CH ₂ R
2-Cl	298	6.01	3.10	1.26, 1.43		
2-Me	298	5.77	3.52	1.41, 1.47	0.00	
2-Et	298	5.70	3.38	1.43, 1.50	0.32	1.25
1-CH₂Ph	298	5.01	3.08	1.06, 1.22	2.10	6.70-7.16
2-CH₂Ph	298	5.62	2.50-3.65	1.18-1.23	2.12	6.70-7.20
1-CH₂CMe₃	298	5.00	3.47	1.17, 1.47	0.87	1.03
2-CH₂CMe₃	242	5.58	2.86, 4.12	1.23, 1.23, 1.46, 1.74	0.75, 0.78	1.35
1-CH₂SiMe₃	298	5.00	3.31	1.16, 1.44	0.18	0.08
2-CH₂SiMe₃	298	5.68	2.70-3.95	1.20-1.75	0.00	0.13
2-Me(Cl)	298	5.87	3.15, 3.43	1.27, 1.37, 1.37, 1.46	0.16	
2-Cl CH₂SiMe₃	298	5.84	3.04, 3.60	1.22, 1.29, 1.32, 1.54	0.23	-0.04
2-CH₂SiMe₃ CH₂CMe₃	298	5.64	2.88, 3.85	1.25, 1.34, 1.47, 1.72	0.26, 0.72	0.11, 1.26
2-Me CH₂SiMe₃	298	5.73	3.12, 3.55	1.27, 1.30, 1.32, 1.48	-0.08, -0.09	0.00
endo_{Me}-2-Me CH₂SiMe₃	200	5.69	2.87, 3.91	1.18, 1.38, 1.73, 1.74	0.03, 0.12	0.09
exo_{Me}-2-Me CH₂SiMe₃	200	5.74	2.73, 3.79	1.18, 1.34, 1.46, 1.69	0.01, 0.12	0.50

methine and 2 methyls, integrating as 4H and 24H respectively, are observed (Figure 2.16). Likewise, the two separate signals expected for the *exo* and *endo* positions are not realized. The selected ^1H and ^{13}C NMR data acquired in C_6D_6 , (Tables 2.6 and 2.7), shows that most of the data is consistent with this, however, the room temperature ^1H NMR spectrum of **2-CH₂SiMe₃**, is broad and featureless, indicative of dynamic

Table 2.7 Selected ^{13}C NMR Data of 4-Coordinate Compounds

Compound ^a	T (K)	ⁱ Pr	Sc-CH ₂ R	Sc-CH ₂ R
2-Cl	298	24.4, 26.9, 29.9		
2-Me	298	24.5, 26.9, 29.7	27.6	
2-Et	298	26.6, 26.7, 29.2	40.8	13.2
1-CH₂Ph	298	24.8, 24.9, 28.8	61.6	120.3, 124.9, 129.6, 149.3
2-CH₂Ph	265	24.6, 25.3, 26.2, 27.0, 28.9, 29.8	57.5, 64.3	119.7, 119.8, 125.2, 126.0 128.5, 128.7, 149.0, 151.6
1-CH₂CMe₃	298	25.0, 25.3, 28.8	72.3	34.9, 35.4
2-CH₂CMe₃	242	25.1, 25.6, 26.7, 27.5, 28.8, 29.9	69.9, 75.5	35.3, 35.6
1-CH₂SiMe₃	298	24.9, 25.7, 28.6	44.9	3.4
2-CH₂SiMe₃	233	24.7, 25.4, 26.5, 28.4, 28.8, 29.4	41.8, 48.7	3.4, 4.7
2-Me(Cl)	298	24.0, 24.1, 26.3, 26.6, 29.1, 29.7	25.8	
2-Cl(CH₂SiMe₃)	298	24.0, 24.2, 24.3, 26.0, 28.9, 31.8	47.8	3.3
2-CH₂SiMe₃ CH₂CMe₃	218	24.1, 24.2, 25.0, 25.1, 26.0, 26.3, 27.2, 27.6, 28.1, 28.3, 28.6, 29.4	40.8, 47.3, 69.5, 75.5	2.9, 4.2, 34.7, 35.2, 35.2, 35.9
2-Me CH₂SiMe₃	298	24.4, 24.6, 25.1, 26.6, 27.0, 29.6	27.3, 45.5	3.9

behaviour near its coalescence temperature. Indeed, upon cooling the sample, a spectrum reflective of the C_s symmetric solid state structure is observed. This corroborates the notion of a low energy exchange process which equilibrates two out-of-plane C_s symmetric structures *via* an in-plane, C_{2v} symmetric transition state (Scheme 2.13). As such, a complete variable-temperature study was conducted on all the 4-coordinate

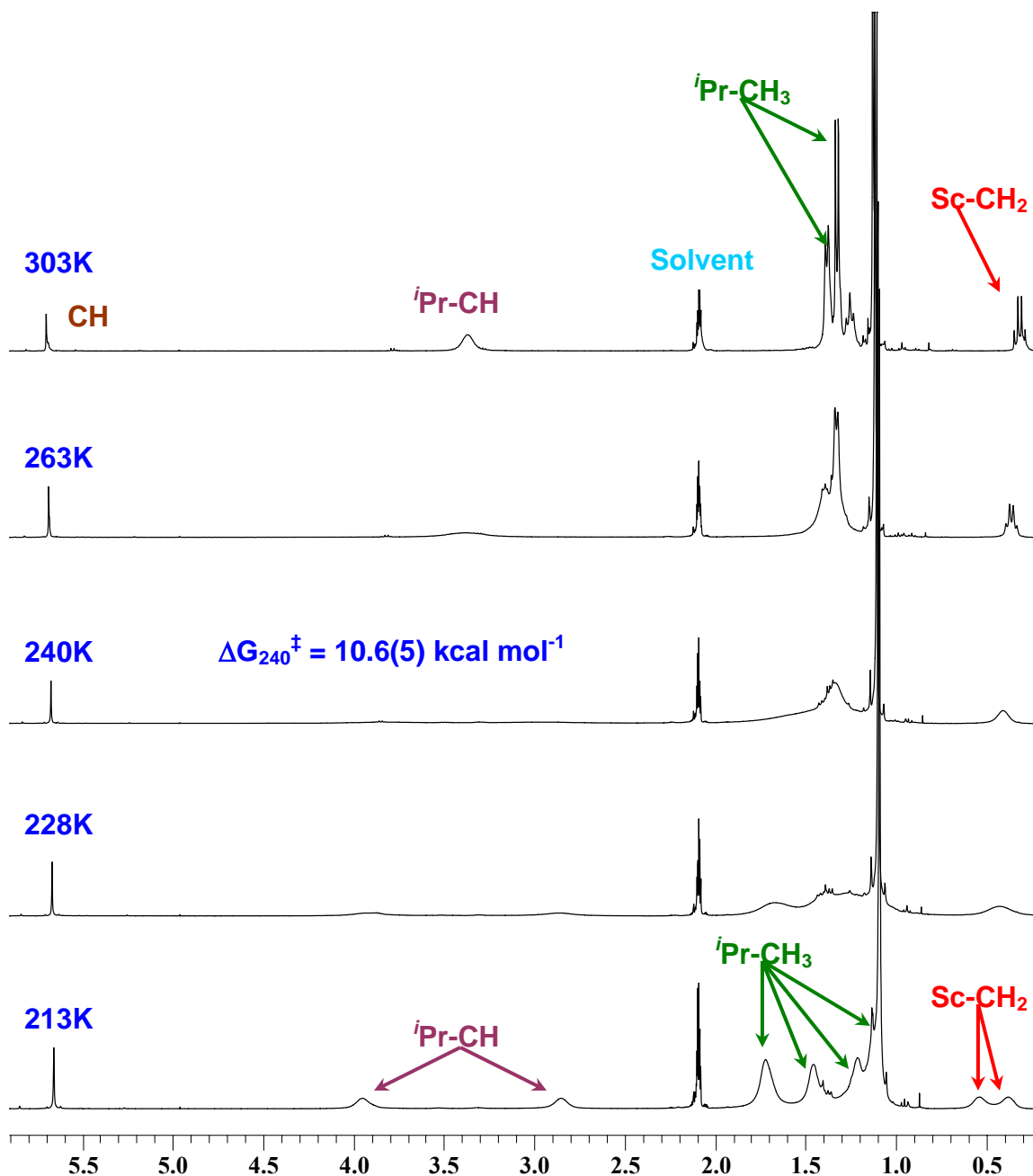
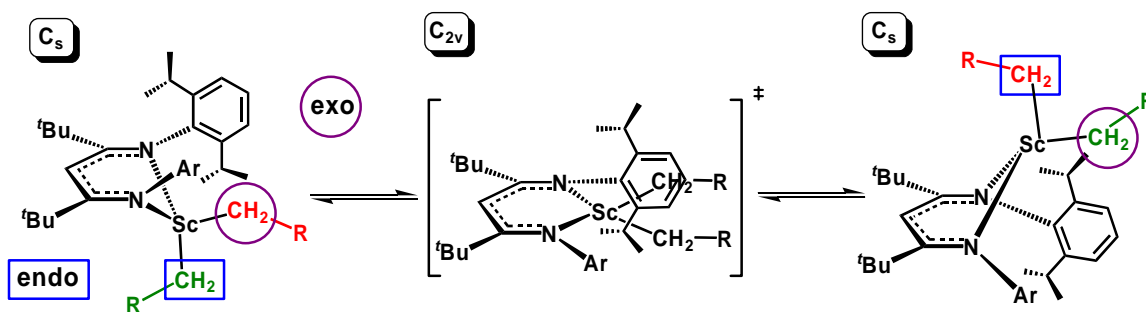


Figure 2.16 Variable Temperature ^1H NMR Spectra of **2-Et** in d_8 -toluene

compounds, a representative series of spectra using **2-Et** is shown in Figure 2.16. At room temperature all four methine protons are equivalent and appear as a septet at approximately 3.4 ppm. Likewise, two corresponding *isopropyl* methyls are seen in the aliphatic region and both scandium ethyl groups are equivalent. As in the solid state

structure, there is no evidence of β -H agostic interactions, a typical C-H coupling ($^1J_{\text{C-H}} = 122$ Hz) is observed. As the temperature is lowered the spectrum becomes increasingly broad until at 240 K the coalescence temperature is reached. Further cooling slows the exchange process to below that of the NMR timescale resulting in a freezing out of the C_s symmetric out-of-plane structure. Two inequivalent ethyl groups have now emerged along with the expected number of *isopropyl* resonances.

The energy barrier for this process was calculated according to Equation 2.1, and found to be quite low with $\Delta G^\ddagger = 10.6(5)$ kcal mol $^{-1}$. This equation, reported by Sandström *et al.*, contains two experimental variables, the temperature of coalescence, and the maximum separation, in Hertz, of the two equilibrating signals.⁶³ A complete list of the barriers for all 4-coordinate compounds at their coalescence temperature are reported in Table 2.8. A close inspection of the energy barrier associated with “ligand flipping” reveals a general correlation with the size of alkyl group; the



Scheme 2.13 Proposed Mechanism of "Ligand Flip" for 4-Coordinate Compounds

larger the steric bulk, the higher the barrier. This supports the previously discussed idea that the metal centre is displaced from the plane of the ligand due to steric interactions between the metal substituents and the aryl *isopropyl* moieties. It should be noted, however, that several of the values lie in contrast to this trend, specifically those for **2-Cl**,

and **1-CH₂Ph**.

$$\Delta G^{\ddagger}_{coal} (kcal\ mol^{-1}) = \frac{1.914 \times 10^{-2} (T_{coal}) [9.972 + \log \frac{T_{coal}}{\Delta\nu}]}{4.184} \quad (2.1)$$

T_{coal} = coalescence temperature (K)

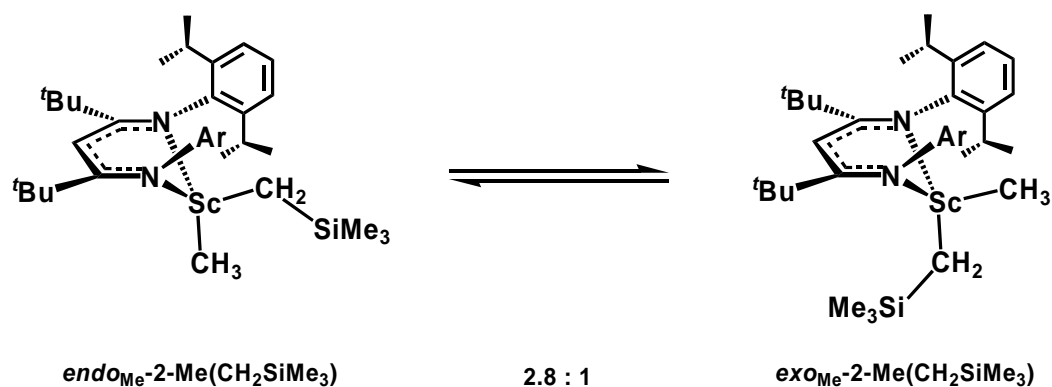
$\Delta\nu$ = maximum peak separation (Hz)

Table 2.8 Free Energies of "Ligand Flip" in 4-Coordinate Compounds

Compound	T_{coal} (K)	$\Delta G^{\ddagger}_{T_{coal}}$ (kcal mol ⁻¹)
1-CH₂Ph	187	8.2(5)
1-CH₂CMe₃	275	12.3(6)
1-CH₂SiMe₃	210	9.5(5)
2-Cl	263	12.3(6)
2-Me	213	9.6(5)
2-Et	240	10.6(5)
2-CH₂Ph	298	13.4(6)
2-CH₂CMe₃	242	10.7(5)
2-CH₂SiMe₃	303	13.7(6)

^b This is an estimated value due to inability to achieve full separation of peaks

The NMR spectra for the mixed alkyl complexes exhibited the expected patterns with a loss of top – bottom symmetry even in the fast exchange regime. As the samples are cooled, however, a different dynamic process, one which exchanges structural isomers, as opposed to equivalent structures, is frozen out (Scheme 2.14). In the case of **2-Me(CH₂SiMe₃)**, the coalescence temperature is observed at 255 K with a complete set of isomer resonances emerging at 210 K. The two isomers are present in a 2.8 : 1 ratio; a 2D NMR ROESY spectrum permitted the assignment of *endo*_{Me} as the major isomer with



Scheme 2.14 Fluxional Process Exchanging Structural Isomers

observed crosspeaks between the methyl group and the lower *isopropyl* methine. In light of the various solid state structures of other mixed substituent compounds, which favour the large group in the *exo* position (*vide supra*), the prevalence of this isomer is not surprising. Most of the other mixed substituent compounds have similar isomeric ratios with **2-Cl(CH₂SiMe₃)**, having the most extreme preference of 4 : 1 (Table 2.9). Interestingly, the presence of two isomers was not observed for **2-Br(C₃H₅)**, even at temperatures which approach the freezing point of *d*₈-toluene (-95 °C). In addition, the ¹H NMR spectrum of **2-Br(C₃H₅)** exhibits only two resonances at 3.4 and 5.7 ppm (in an AX₄ splitting pattern) attributable to the allyl group, suggesting rapid η¹ – η³ – η¹ fluxionality.⁶⁴ The barriers for such exchange mechanisms are likely to be quite low in

Table 2.9 Isomeric Ratios of Mixed Substituent Compounds

Compound	T _{coal} (K)	Isomeric Ratio
2-Me(Cl)	250	2.3 : 1
2-Cl(CH₂SiMe₃)	263	4 : 1
2-Me(CH₂SiMe₃)	260	2.8 : 1
2-CH₂SiMe₃(CH₂CMe₃)	292	1.9 : 1

energy as it was not possible to distinguish between the 4 methylene protons at low temperature.

Additional energetic information regarding the fluxional process within the 4-coordinate dialkyl species can be garnered utilizing the 2D EXSY technique.⁶⁵ It is

$$k = \frac{1}{T_m} \times \ln \frac{(r+1)}{(r-1)} \quad (2.2)$$

T_m = mixing time

$$r = \frac{(I_{AA} + I_{BB})}{(I_{AB} + I_{BA})}$$

I_{AA} & I_{BB} = Intensity of Diagonal Peaks

I_{AB} & I_{BA} = Intensity of Cross-peaks

possible to use this approach to determine accurate rates of exchange, according to Equation 2.2. In order to obtain definitive values it is necessary to have two exchanging resonances which are baseline resolved both from each other and any other signals; in this case, the *isopropyl* methines were used. The rate of the ligand flip process

Table 2.10 Rate Data for Ligand Flip within **2-CH₂SiMe₃**

Compound	T(K)	k_{exp} (s⁻¹)
2-CH₂SiMe₃	247.3	10.0(3)
2-CH₂SiMe₃	235.0	2.58(3)
2-CH₂SiMe₃	235.0	2.59(3)
2-CH₂SiMe₃	235.0	2.56(3)
2-CH₂SiMe₃	235.0	2.62(3)
2-CH₂SiMe₃	228.0	0.95(3)
2-CH₂SiMe₃	214.1	0.15(2)

was quantitatively determined for **2-CH₂SiMe₃** (Table 2.10), at various temperatures and an Eyring plot which showed an excellent fit, allowed the extraction of the activation parameters $\Delta H^\ddagger = 12.9(2)$ kcal mol⁻¹ and $\Delta S^\ddagger = -1.6(5)$ e.u. (Figure 2.17). Calculation of ΔG^\ddagger agreed within experimental error to that obtained at T_{coal} using Sandström's method. Given the unimolecular nature of the process it is not surprising that it is essentially entropically neutral.

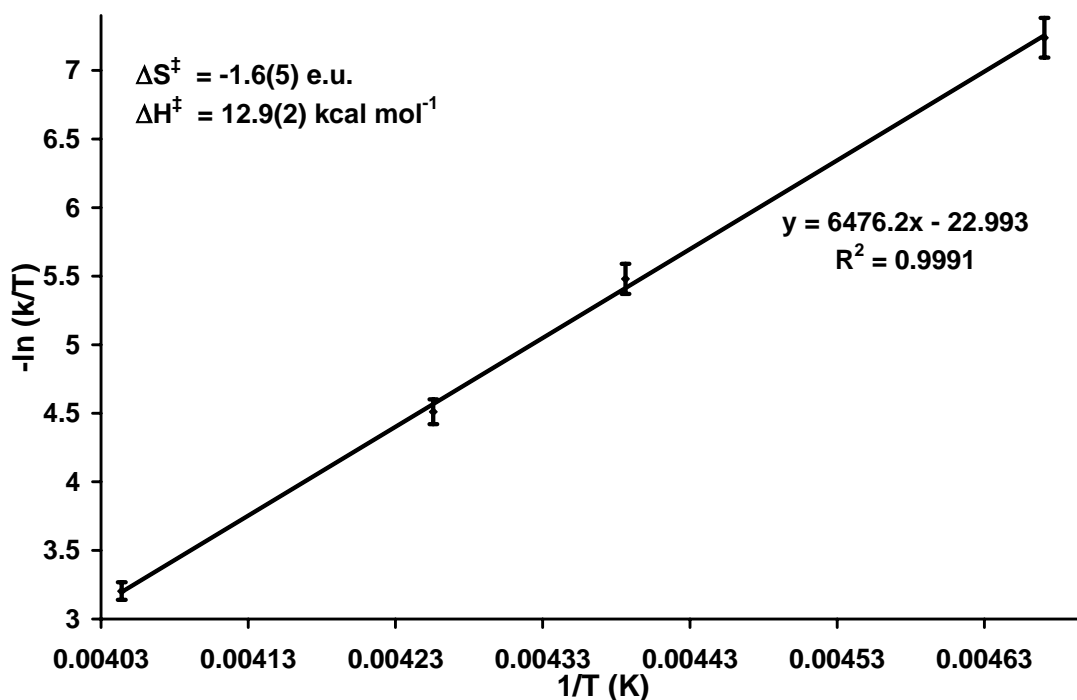
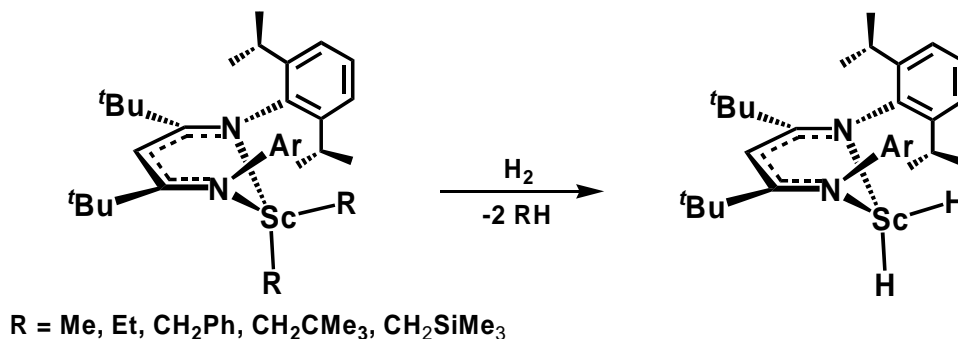


Figure 2.17 Eyring Plot for Ligand Flip Within **2-CH₂SiMe₃**

2.2.5 Reaction of L^tBuScR₂ with H₂

In an effort to generate a monomeric Group III dihydride, the reactivity of the 4-coordinate dialkyl compounds with H₂ was explored.⁶⁶ Upon introduction of 1 atmosphere of dihydrogen gas into a cooled (-196 °C) NMR tube charged with L^tBuScR₂

in d_8 -toluene, the tube was sealed and allowed to gradually warm to room temperature (See Section 6.1.5 for complete experimental details) creating an H_2 pressure of approximately 4 atmospheres. Monitoring of the reaction over the course of several days showed evidence for loss of RH, presumably by a σ -bond metathesis reaction,⁴ however, various aspects of the 1H NMR spectrum did not agree with production of the anticipated



Scheme 2.15 Synthetic Strategy for Production of a Monomeric Scandium Dihydride product (Scheme 2.15). Since the experiment progressed most cleanly when **2-CH₂SiMe₃** was utilized, the reaction was scaled up under similar conditions to produce the unidentified product as a red oil. Repeated washing with hexamethyldisiloxane and recrystallization afforded a bright orange solid which was characterized by a host of 2D and multinuclear NMR techniques.

A close examination of the 1H NMR spectrum, which did not show evidence of fluxional behaviour upon a variable temperature study, showed loss of right – left symmetry within the β -diketiminato framework, as evidenced by 2 inequivalent ^tBu signals. Additional conflicting evidence was observed between 5 and 6 ppm, the region of the spectrum where the diagnostic singlet from the backbone proton usually appears, where 2 doublets, with a very large coupling constant of 16.4 Hz, were observed.

Although initial speculation involved a process whereby the desired dihydride species formed and subsequently decomposed *via* hydride attack at the imine carbon, as seen for salicylaldehyde scandium complexes,⁶⁷ the downfield chemical shift reflective of olefinic protons and the large coupling constant indicative of *trans* coupling, negate this product.

Although selective irradiation of one of the doublets confirmed the two resonances were coupled to each other, it did not authenticate the origin of either proton. In order to determine if these resonances could be attributed to the original H₂ unit a deuterium labelling experiment was performed whereby the analogous procedure was repeated using D₂ gas. Indeed, the ¹H NMR spectrum revealed a 1:1:1 triplet at 5.7 ppm with a coupling constant of 2.7 Hz verifying that a deuterium had been installed adjacent to the original backbone proton. Interestingly, however, this 1:1:1 triplet had not completely replaced the original signals, but rather, was overlapping with it. The ¹H NMR spectrum was acquired numerous times over the course of 24 hours unveiling a characteristic 1:1:1 triplet ($J_{\text{H-D}} = 44$ Hz) at 4.50 ppm attributable to significant H-D production. Further monitoring of the reaction showed the eventual growth of a singlet due to H₂ generation (Figure 2.18). The ²H NMR spectrum for the same reaction mixture

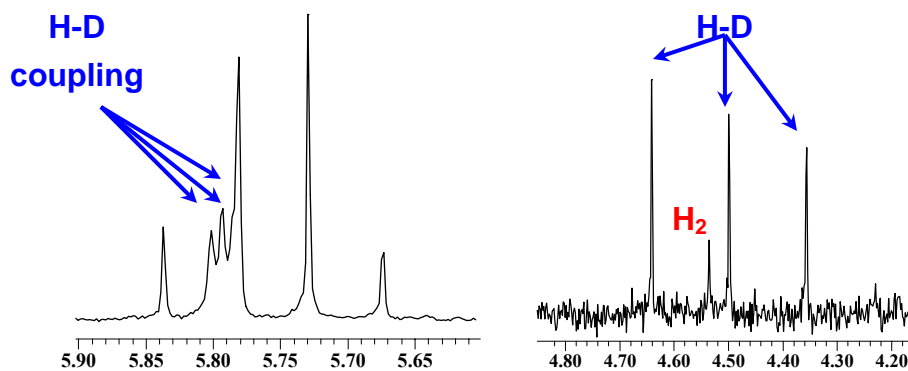
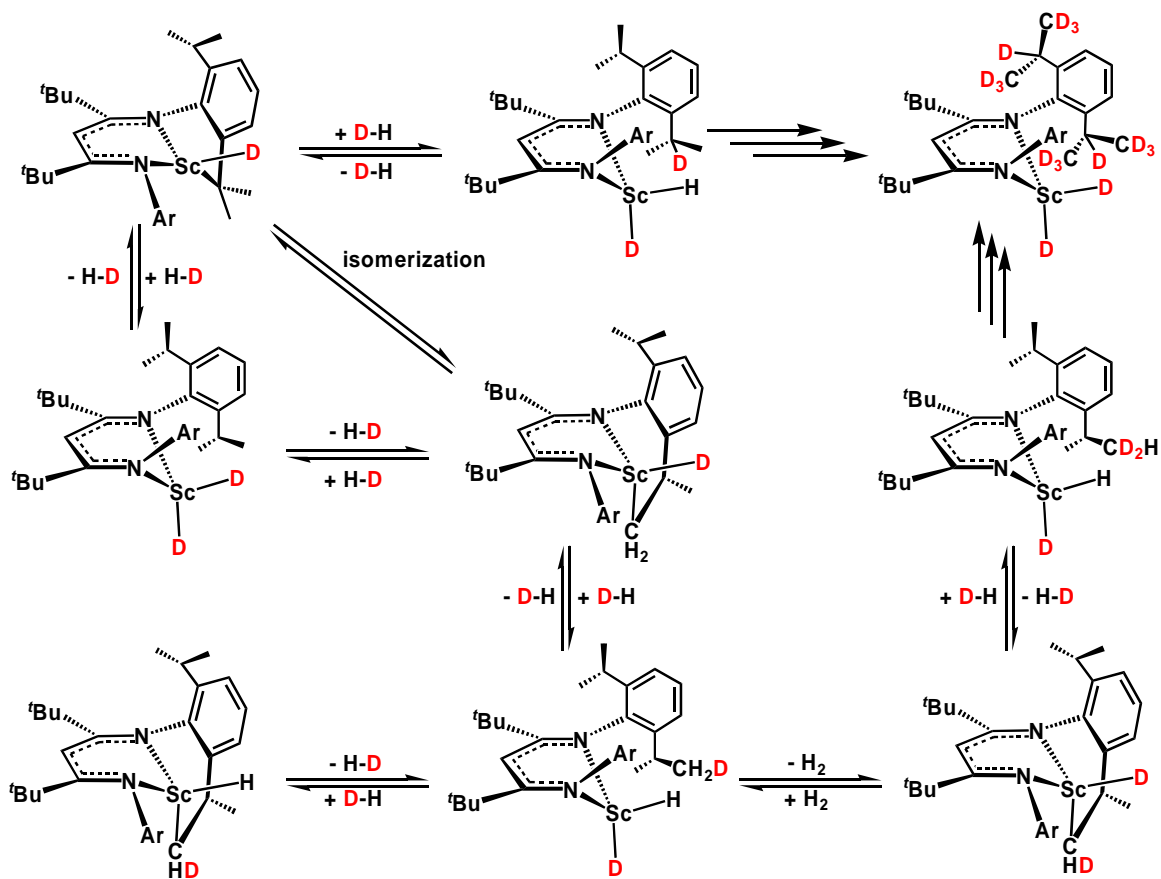


Figure 2.18 L^tBuScR₂ + D₂; Left: H-D Coupling in Backbone Region. Right: Production of H-D and H₂

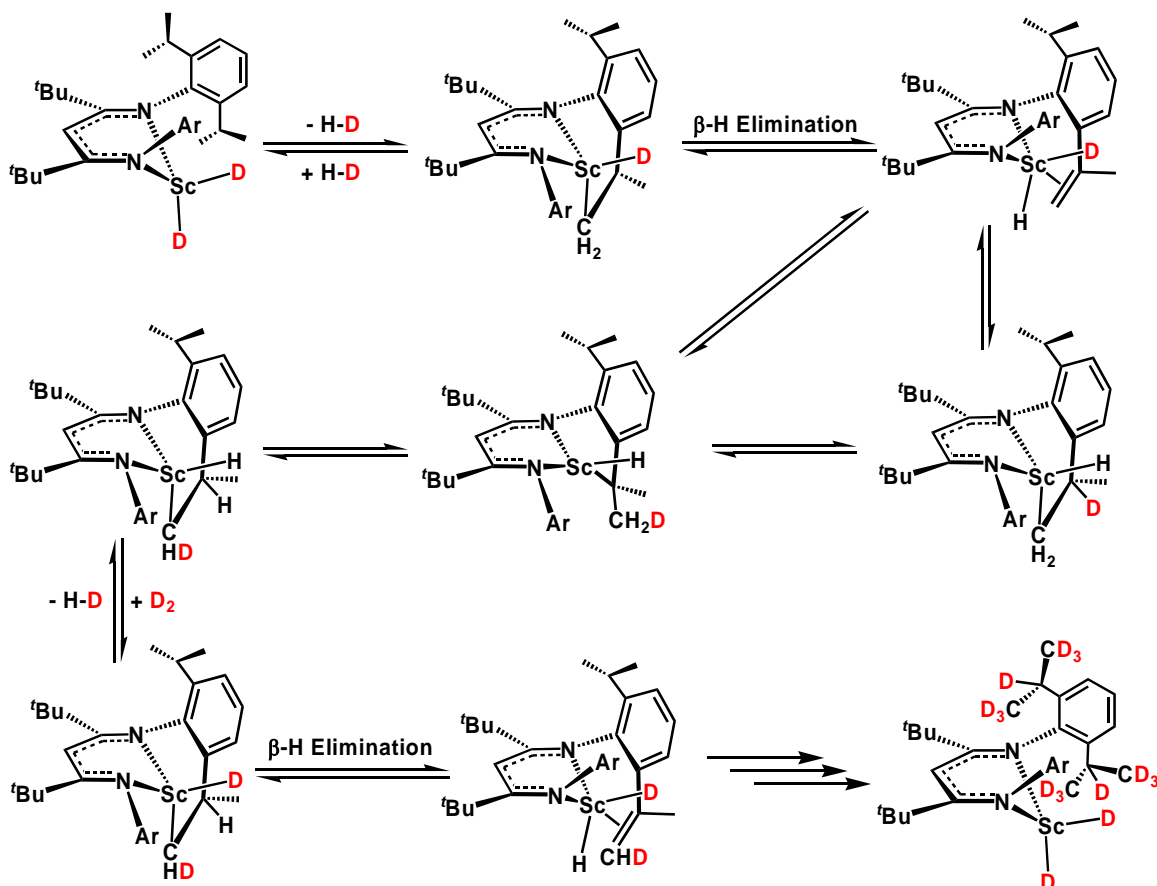
exhibited the expected resonances at 5.8 and 0.0 ppm for the backbone and $\text{Me}_3\text{SiCH}_2\text{D}$, respectively, as well as a signal at 4.54 ppm for H-D and signs of significant deuterium incorporation into both the *isopropyl* methine and methyl resonances. These results can be explained by a competing reversible metallation mechanism as depicted in Scheme 2.16. Although the majority of *isopropyl* labelling occurs in the methine position in the



Scheme 2.16 Representative Series of Reversible Metallation Processes

scandium nacnac compounds, significant incorporation into the methyl substituents suggests that either metallation is competitive at both sites or that upon reaction at one position, an isomerization results. Alternatively, metallation in conjunction with a reversible β -Hydride elimination process, as observed by Goldberg *et al.* for nacnac

supported platinum compounds, would also explain the labelling of the *isopropyl* groups and production of H-D and H₂ (Scheme 2.17).^{68,69} Presumably repeated replenishment of D₂ over time would lead to complete labelling of the *isopropyl* groups similar to the facile deuteration of the Cp* methyls in decamethyl scandocene compounds.⁴

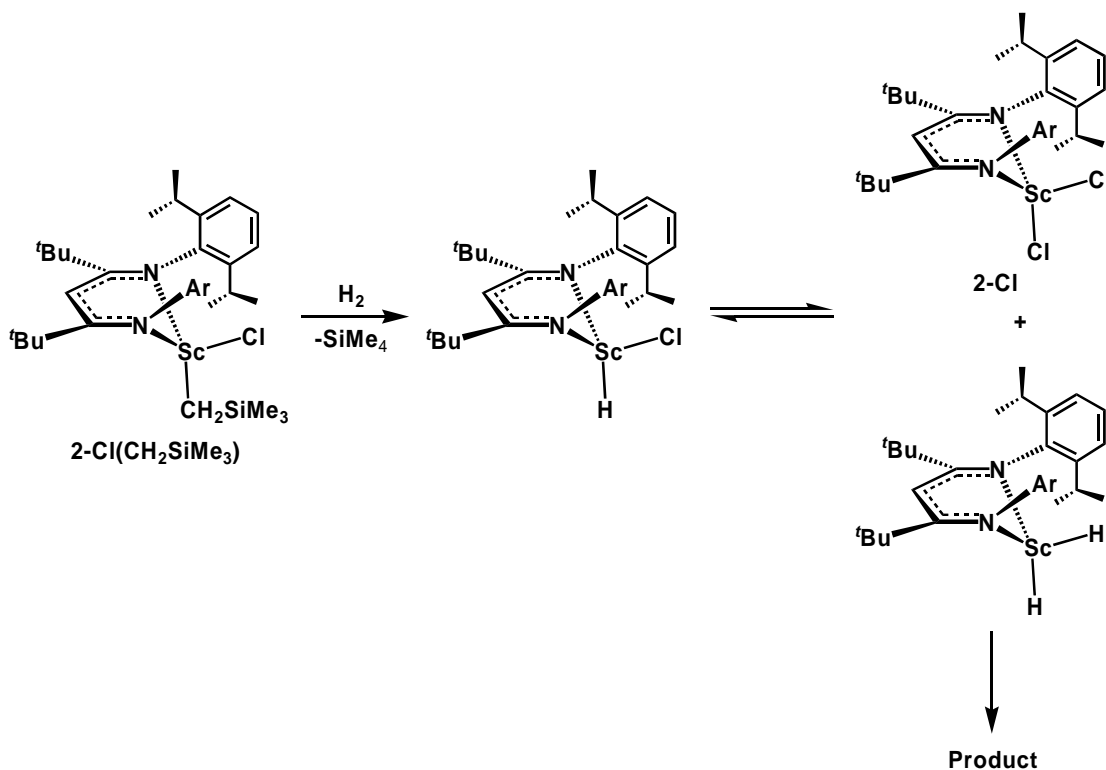


Scheme 2.17 Deuterium Labelling of *Isopropyl* Groups *via* Reversible β-H Elimination

The reaction of H₂ with 2-Cl(CH₂SiMe₃), was explored in hopes that a mixed hydride/halide compound, akin to Schwartz's reagent⁷⁰ would be more stable towards decomposition. In this case, a 1 : 1 ratio of 2-Cl, and the unidentified product resulted, likely through initial formation of the desired L^{tBu}ScH(Cl), followed by redistribution to

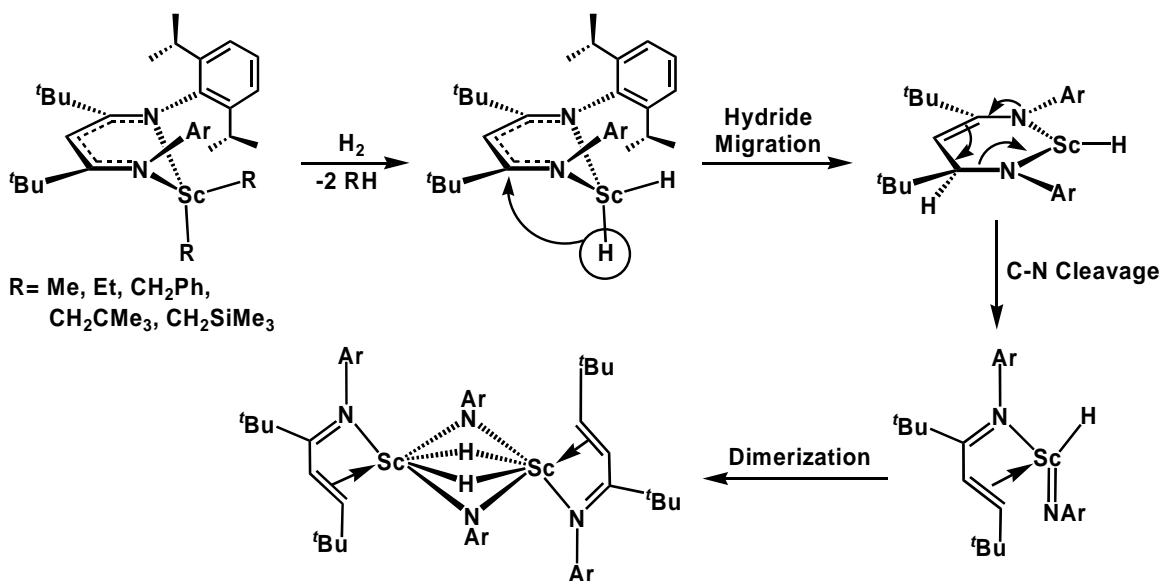
an equilibrium mixture of **2-Cl** and the putative $L^{tBu}ScH_2$. From this point $L^{tBu}ScH_2$ rapidly and irreversibly decomposes in a similar fashion to that observed for the dialkyls (Scheme 2.18). In light of the precedent for equilibrium mixtures for mixed alkyl/halide compounds (*vide supra*), this reactivity is not surprising.

A combination of these facts led to the proposal of a novel bridging imido scandium hydride dimer depicted in Scheme 2.19. This highly unusual species would likely form by hydride attack at the imine carbon, followed by carbon nitrogen cleavage to yield an imido – hydride species which is likely to dimerize immediately upon formation. Although repeated attempts to grow crystals suitable for a single crystal X-ray diffraction study were unsuccessful, Mindiola and co-workers recently reported a similar C-N cleavage within a titanium β -diketiminato derivative yielding a compound supported



Scheme 2.18 Reaction Pathway of **2-Cl(CH₂SiMe₃)**, with H₂

by comparable nacnac remnants.⁷¹ The reported spectroscopic data is in excellent agreement with that observed for this compound.



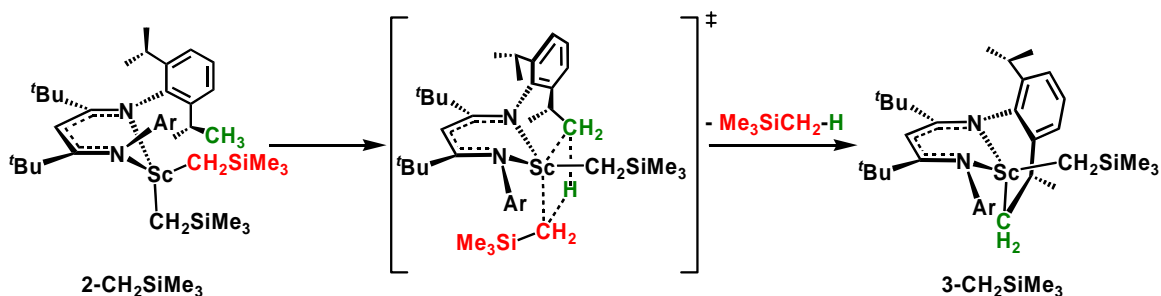
Scheme 2.19 Proposed Mechanism of Formation of Scandium Imido Hydride

The final experiment responsible for the confirmation of the proposed compound involves hydrolysis of the organometallic species, followed by an organic work-up to isolate a mixture of the associated organic compounds. Analysis by GC-MS showed peaks corresponding to ArNH₂ and ArN=C(^tBu)CH=CH(^tBu) with molecular masses of 177 and 327 g/mol respectively, as the only high weight species. In order to ensure the observed signals were not artefacts from residual proteo nacnac, it too was analyzed by GC-MS with no sign of peaks at either 177 or 327 g/mol.

2.2.6 Thermal Decomposition *via* Metallation of Aryl *Isopropyl* Group

The possibility of metallation (*vide supra*) prompted the examination of the thermal decomposition of the 4-coordinate dialkyl compounds. Indeed, at elevated temperatures in aromatic solvent a metallation process involving one of the C-H bonds of an aryl *isopropyl* group and loss of R-H was observed. Interestingly, no intermolecular σ -bond metathesis reactions were observed with the solvent. While the L^{tBu} stabilized dialkyl complexes decompose cleanly to the metallated product (R = CH₃, **3-Me**, CH₂CH₃, **3-Et**, CH₂Ph, **3-CH₂Ph**, CH₂CMe₃, **3-CH₂CMe₃**, CH₂SiMe₃, **3-CH₂SiMe₃**), those supported by L^{Me} have a more complicated decomposition which is plagued by further ill-defined processes. This additional deleterious reactivity is likely due to the greater thermal stability, and thus higher temperatures and longer reaction times which must be used to induce metallation.

The ¹H NMR spectra of the L^{tBu} metallated compounds are quite diagnostic with loss of both right – left and top – bottom symmetry; seven doublets for the *isopropyl* methyls and four multiplets for the methines are exhibited, suggesting the end product involves bond formation between scandium and a former *isopropyl* methyl carbon (Scheme 2.20). Compounds with alkyl groups of the form CH₂R, where R \neq H exhibit 2 doublets upfield of 0 ppm for the now diastereotopic CH₂ protons of the remaining alkyl moiety. The solid state structure of the metallated product starting from **2-CH₂SiMe₃**, was determined by X-ray crystallography and confirmed its identity as κ^3 -[ArNC(^tBu)CHC(^tBu)N-*i*Pr- C₆H₃]ScCH₂SiMe₃, **3-CH₂SiMe₃**, with scandium bound



Scheme 2.20 Metallation of 2-CH₂SiMe₃

to a former *isopropyl* methyl carbon (Figure 2.19). The Sc-C bond distances of 2.26(2) and 2.263(3) Å agree well with other Sc-C bonds within this family of compounds. The metal centre is significantly closer to the plane of the ligand (0.540(5) Å) than that observed in other structures, however, this is expected as the constraints imposed by bonding to the *isopropyl* group

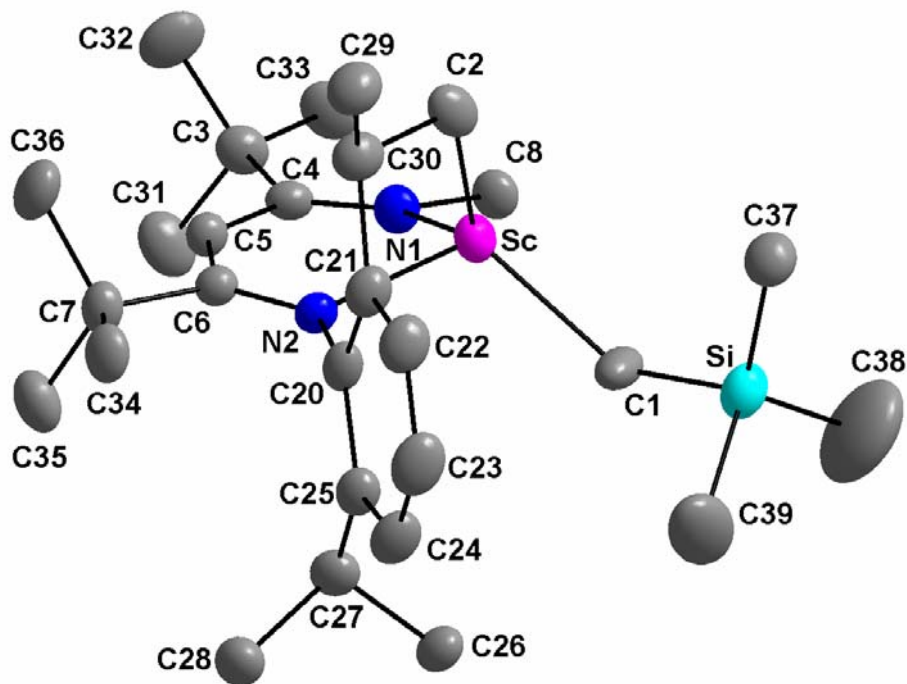


Figure 2.19 X-ray Crystal Structure of 3-CH₂SiMe₃. Thermal ellipsoids drawn at the 30% probability level. Hydrogen atoms and rear aryl group are removed for clarity.

Table 2.11 Selected Metrical Data for **3-CH₂SiMe₃**

Atoms	Bond Lengths (Å)	Atoms	Bond Angles (°)
Sc-N(1)	2.126(3)	N(1)-Sc-N(2)	82.84(12)
Sc-N(2)	2.136(3)	C(1)-Sc-C(2)	117.4(6)
Sc-C(1)	2.26(2)	N(1)-Sc-C(1)	118.5(6)
Sc-C(2)	2.263(9)	N(1)-Sc-C(2)	122.0(2)
Sc-C(4)	3.154(4)	N(2)-Sc-C(1)	114.5(5)
Sc-C(5)	3.454(4)	N(2)-Sc-C(2)	87.8(3)
Sc-C(6)	3.141(4)	Sc-N(1)-C(4)	130.5(2)
Sc-N ₂ C ₃ Plane	0.540(5)	C(3)-C(4)-N(1)	125.7(3)
Atoms	Torsion Angles (°)	N(1)-C(4)-C(5)	120.2(3)
C(6)-N(2)-C(20)-C(25)	95.09(44)	C(4)-C(5)-C(6)	130.8(4)
C(6)-N(2)-C(20)-C(21)	-93.90(45)	C(5)-C(6)-N(2)	120.1(3)
C(4)-N(1)-C(8)-C(9)	109.45(46)	C(7)-C(6)-N(2)	125.8(3)
C(4)-N(1)-C(8)-C(13)	-82.42(53)	C(6)-N(2)-Sc	128.6(2)

prevent further deviation from planarity (Table 2.11).

The metallation process was quantitatively monitored for **2-CH₂SiMe₃** using ¹H NMR spectroscopy (Figure 2.20); concentration dependence studies found the reaction to be first order in metal complex, indicative of an intramolecular pathway. Upon following the reaction at a variety of temperatures an Eyring plot was constructed which permitted the extraction of the activation parameters $\Delta H^\ddagger = 19.7(6)$ kcal mol⁻¹ and $\Delta S^\ddagger = -17(2)$ e.u. (Figure 2.21). The negative entropy of activation is expected for the highly ordered σ -bond metathesis transition state, although the magnitude is perhaps greater than expected; Bercaw and co-workers reported $\Delta S^\ddagger = -23(2)$ e.u. for the intermolecular reaction between *d*₃₀-Cp*₂ScCH₃, and C₆H₆.⁴ It may be possible that the fluxionality of the ligand is contributing to the negative activation entropy. The ΔH^\ddagger agrees well with the reported value of -18.9(2) kcal mol⁻¹ for the metallocene.

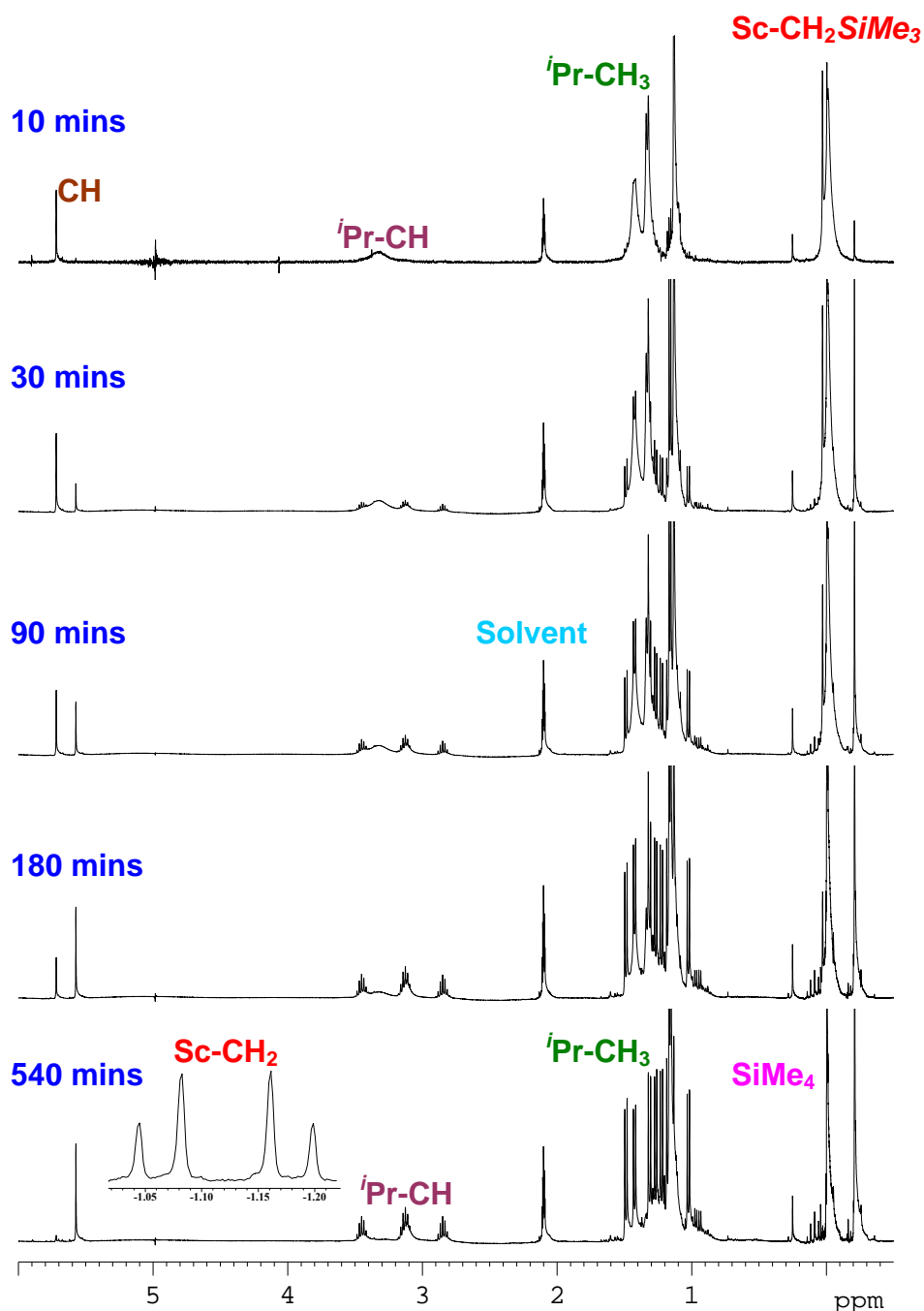


Figure 2.20 Series of ^1H NMR Spectra Acquired in d_8 -toluene at 333 K Monitoring the Thermal Decomposition of $2\text{-CH}_2\text{SiMe}_3$

In order to obtain comparative values to draw meaningful trends between metallation rates and compound structure, a kinetic investigation was conducted (Table 2.12). Monitoring the metallation of some $\text{L}^{\text{Me}}\text{ScR}_2$ species was complicated by competing reactions and as such the values should be considered semiquantitative

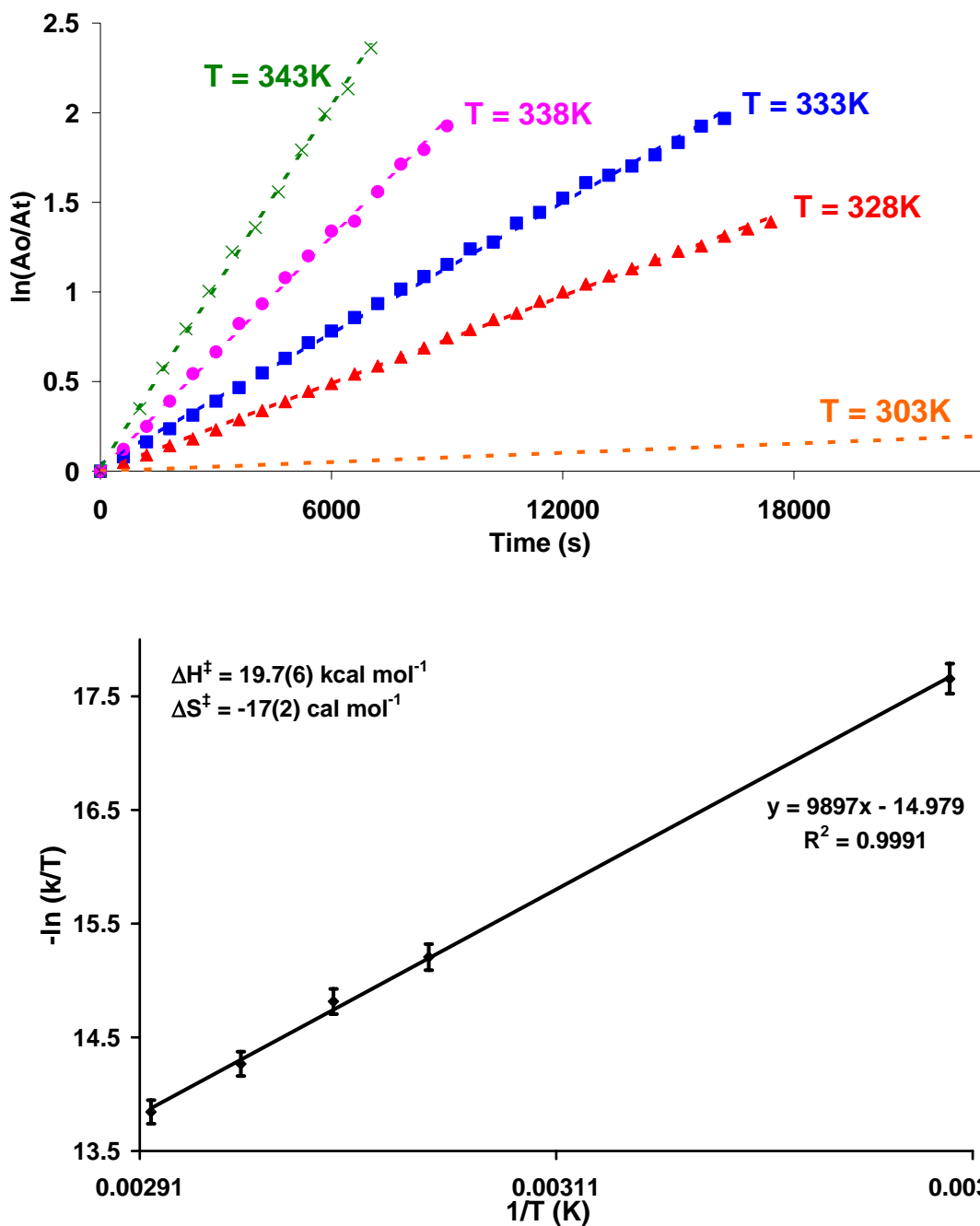


Figure 2.21 Top: Metallation of **2-CH₂SiMe₃**, Monitored Quantitatively at Various Temperatures; Bottom: Eyring Plot of Metallation of **2-CH₂SiMe₃**

estimates at best. They are, however, sufficiently reliable to establish that L^{Me} supported compounds are drastically more metallation resistant than their L^{iBu} counterparts. This

Table 2.12 Half Lives and k_{exp} for Metallation Reactions

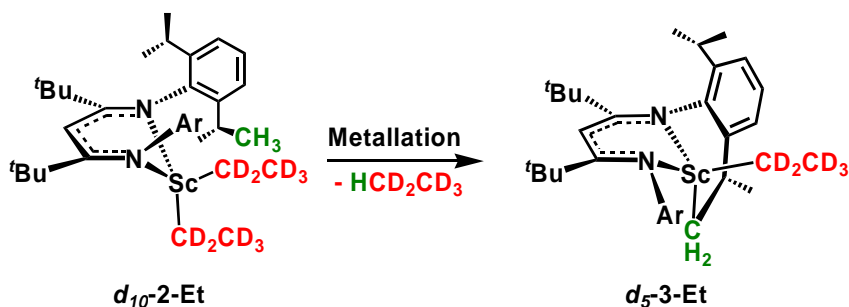
Compound	T (K)	$t_{1/2}$ (h)	k_{exp} (s^{-1})
1-CH₂Ph	360	7.2	$2.68(5) \times 10^{-5}$
1-CH₂CMe₃	360	0.37	$5.32(3) \times 10^{-4}$
1-CH₂SiMe₃	360	3.8	$5.09(6) \times 10^{-5}$
2-CH₂SiMe₃	360	0.13	$1.47(2) \times 10^{-3}$
2-Me	333	0.53	$3.59(3) \times 10^{-4}$
2-Et	333	0.15	$1.34(2) \times 10^{-3}$
2-CH₂Ph	333	11.7	$1.65(4) \times 10^{-5}$
2-CH₂CMe₃	333	0.33	$5.86(3) \times 10^{-4}$
2-CH₂SiMe₃	333	1.6	$1.22(3) \times 10^{-4}$
2-CH₂SiMe₃	333	1.6	$1.25(3) \times 10^{-4}$
2-CH₂SiMe₃	333	1.6	$1.19(3) \times 10^{-4}$
2-CH₂SiMe₃	333	1.6	$1.17(2) \times 10^{-4}$
2-CH₂SiMe₃	303	29.5	$6.52(6) \times 10^{-6}$
2-CH₂SiMe₃	328	2.36	$8.16(5) \times 10^{-5}$
2-CH₂SiMe₃	338	0.90	$2.15(4) \times 10^{-4}$
2-CH₂SiMe₃	343	0.58	$3.34(4) \times 10^{-4}$

fact is best illustrated by comparison of **1-CH₂SiMe₃**, and **2-CH₂SiMe₃**, which at 360K were found to have metallation half-lives of 3.8 hours and 8 minutes respectively. This decreased stability observed for L^{tBu} vs. L^{Me} compounds is presumably because the ^tBu groups within the nacnac framework force the *isopropyl* aryl groups significantly closer to the metal centre. Unfortunately, it is difficult to draw conclusions regarding the nature of the alkyl group and its effect on metallation, as there appear to be no consistent trends; evidently, the steric and electronic factors involved in the σ -bond metathesis transition state are complex in these systems.

It is well established that metallation processes occur much more readily in sterically crowded environments.^{72,73} Since the *endo* position is thought to be more sterically demanding and there is little to no correlation between rate of metallation and the barrier to *exo/endo* exchange, it was anticipated that metallation does not take place from an in-plane structure, but rather, from the out-of-plane structure with loss of the

endo substituent. Thus, it was not surprising that the solid state structure confirmed this; the metallated compound clearly showed loss of the *endo* substituent. This was corroborated by the fact that heating of **2-Me(CH₂SiMe₃)**, showed preferential loss of CH₄ over SiMe₄ in an 8 : 1 ratio which correlated well since the major isomer has been assigned to have the methyl group in the *endo* position. Metallation at the *endo* site was further supported upon comparing non-bonding distances in the **2-CH₂SiMe₃** starting material; the *exo* CH₂SiMe₃ lies significantly further from the *isopropyl* groups involved in the metallation process with an average distance of 4.54 Å from the bottom *isopropyl* methines. The more crowded *endo* CH₂SiMe₃ group is substantially closer, at only 3.83 Å.⁵⁹

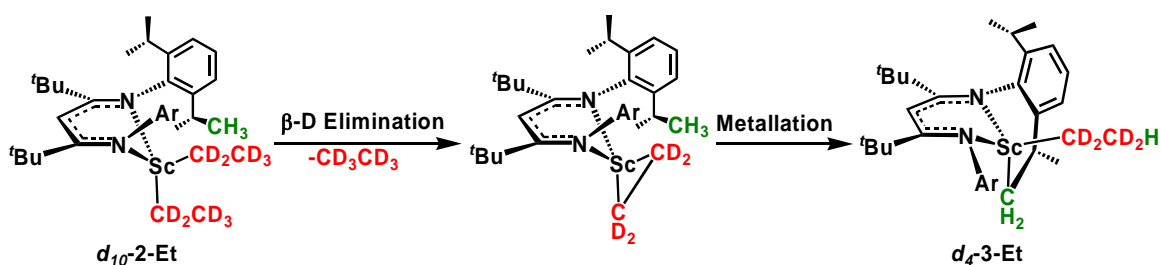
As the only compound with β-hydrogens, **2-Et**, was of interest as additional decomposition pathways, namely those involving β-hydride elimination⁹ or β-hydrogen abstraction,⁷⁴ can also be envisioned. Although these processes could combine with



Scheme 2.21 Direct Metallation of *d*₁₀-**2-Et**.

metallation yielding the same net result, it appears that a direct σ-bond metathesis reaction is operative. This was proven by monitoring metallation of *d*₁₀-**2-Et**, which had fully deuterated ethyl groups (Scheme 2.21). The only product observed from metallation was *d*₅-κ³-[ArNC(*t*Bu)CHC(*t*Bu)N-*i*Pr-C₆H₃]ScCD₂CD₃, *d*₅-**3-Et**, as indicated

by two resonances appearing at 0.6 and -0.6 ppm integrating in a 3 : 2 ratio, in the ^2H NMR spectrum. The only alkane liberated was $\text{CD}_3\text{CD}_2\text{H}$, whereas production of C_2D_6 and $d_4\text{-}\kappa^3\text{-}[\text{ArNC}(\text{tBu})\text{CHC}(\text{tBu})\text{N-}i\text{Pr-C}_6\text{H}_3]\text{ScEt}$, ***d*₄-3-Et** would be observed if the mechanism first proceeded *via* β -deuteride elimination to generate a scandacyclopropane, followed by subsequent ring opening by metallation of an *isopropyl* moiety (Scheme 2.22). It is intriguing that the only other reported $\text{LSc}(\text{CH}_2\text{CH}_3)_2$ is also immune to β -hydride elimination processes.¹¹



Scheme 2.22 β -Deuteride Elimination/Metallation Mechanism

Although thermolysis of the mixed alkyl halide compounds was attempted, it was discovered that under reasonable experimental conditions metallation does not occur. Perhaps the halide increases stability through π -electron donation into empty metal orbitals.^{61,62} It is also noteworthy that base-free **1-Me**, is quite metallation resistant with no signs of metallation after 12 hours at 100 °C. Monitoring over prolonged periods at 100 °C yielded a variety of unidentifiable products.

In interest of harvesting information regarding whether or not similar metallation processes occur in the solid state a variety of the dialkyl compounds were examined using TGA. The solid samples were sealed in aluminum pans in the glovebox and pierced with

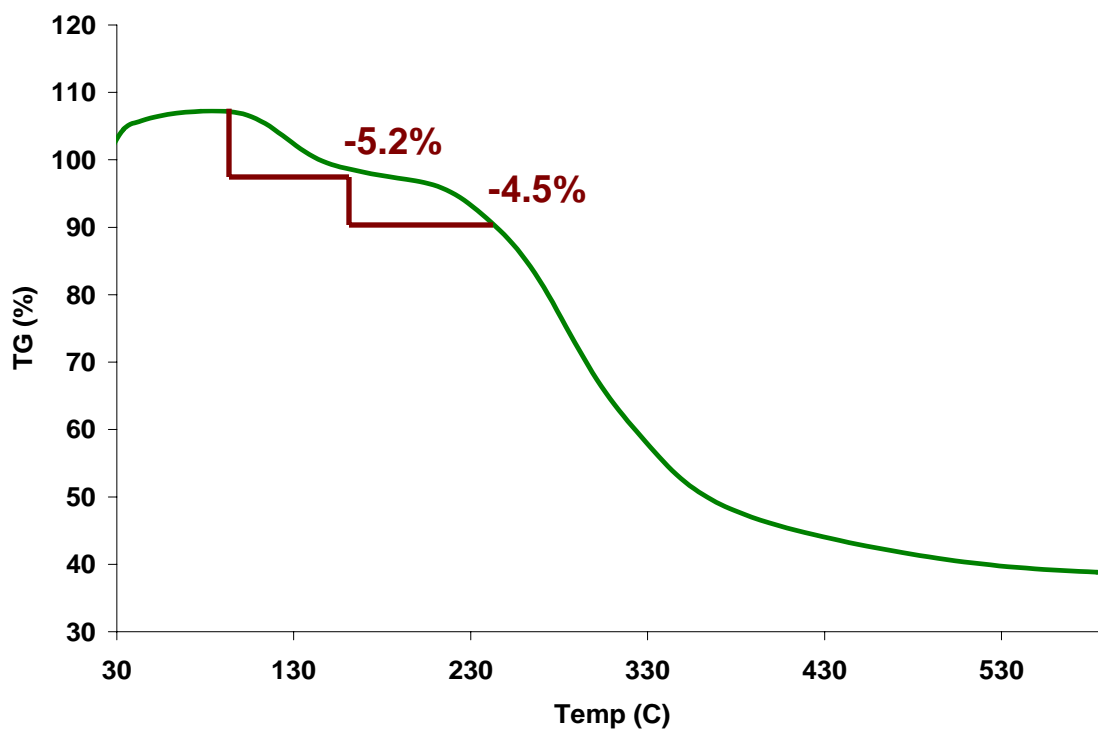
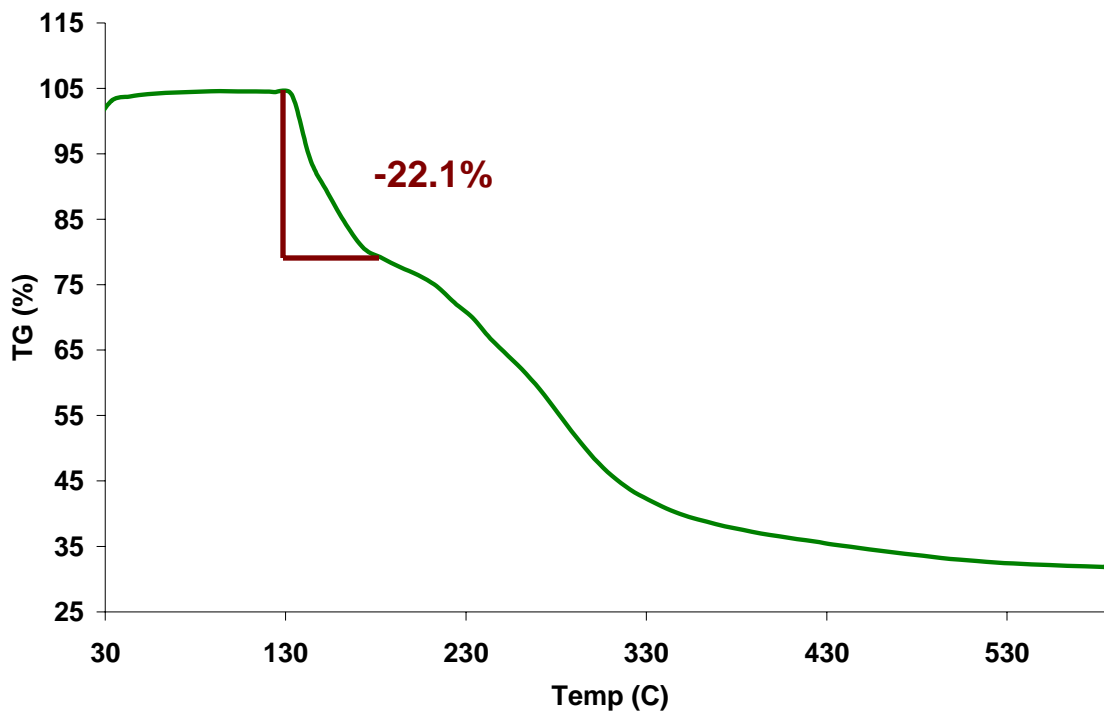


Figure 2.22 Top: TGA Trace for Thermal Decomposition of Solid 2-CH₂SiMe₃;
Bottom: TGA Trace for Thermal Decomposition of Solid 2-Et

a small bore needle under a flow of N₂ immediately prior to insertion into the instrument. The samples were then heated at a rate of 10 °C/minute and the mass loss recorded to the nearest microgram. In all cases a sharp mass loss was observed at low temperatures, between 100 and 150 °C, which corresponded to loss of one or two equivalents of RH, followed by complete ligand decomposition beginning at approximately 200 °C. For example, the thermogram of **2-CH₂SiMe₃** shows two overlapping peaks which correspond to a loss of 22.1% of the mass of the starting material; loss of SiMe₄ through metallation would result in a mass decrease of 12.1% (Figure 2.22). Although it is impossible to confirm the operative mechanism of decomposition, these findings support sequential loss of both alkyl groups as RH, potentially by a metallation pathway. The thermogram of **2-Et**, is more diagnostic with two distinctly separated processes giving rise to mass losses of 5.2 and 4.5%. Each of these quantities corresponds excellently with the theoretical value of 5.0% for ethane.

2.2.7 Ethylene Polymerization Data for L^{Me}ScCl₂(THF), L^{Me}ScMe₂(THF), L^{tBu}ScCl₂ and L^{tBu}ScMe₂

The development of well defined dialkyl scandium species provided a variety of compounds which had potential to be effective catalysts for ethylene polymerization. In a quest to gain insight into the relationship between catalyst structure and polymerization activity, four nacnac supported scandium complexes were tested as ethylene polymerization catalysts (Figure 2.23). In order to determine their activities under

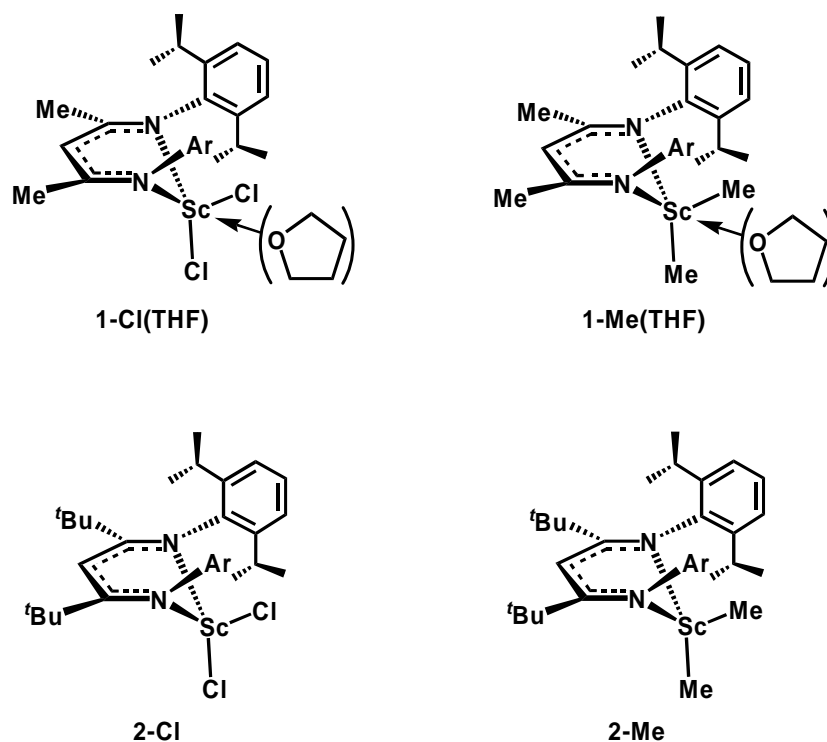


Figure 2.23 Scandium Complexes Tested for Ethylene Polymerization Activity

industrially relevant conditions, NOVA Chemicals Ltd. (Calgary, AB) performed the experiments using a small scale SBR (slurry batch reactor). All polymerizations were conducted at 50 °C with 300 psi ethylene pressure in a cyclohexane/toluene mixture. Stirring was at a rate of 2000 rpm and a catalyst concentration of 300 μM was used. The results are displayed in Table 2.13.

Table 2.13 Ethylene Polymerization Data for β -Diketiminato Scandium Complexes

Catalyst	Co-catalyst	Activity ^a	M_w (K)	M_w/M_n
1-Cl(THF)^b	PMAO-IP	4.7×10^3	973	3.18
1-Me(THF)^b	PMAO-IP	1.2×10^4	711	6.53
2-Cl^b	PMAO-IP	9.9×10^4	1357	2.20
2-Me	none	4.6×10^5	1039	1.68
2-Me^b	PMAO-IP	1.2×10^6	1866	1.98
2-Me	$\text{B}(\text{C}_6\text{F}_5)_3$	3.0×10^5	1051	1.70
2-Me	$[\text{CPh}_3][\text{B}(\text{C}_6\text{F}_5)_4]$	4.8×10^5	851	2.48

^aActivity in g polyethylene mol Sc^{-1} h⁻¹ atm⁻¹, ^bAl/Sc = 20.

Polymerization activities are significant for all 4 compounds, with **2-Me** being the most active. Relatively high molecular weights and low polydispersities, consistent with a single site catalysis model, are observed. The lower activities for the dichlorides, upon MAO activation, may indicate that alkylation of the scandium centre by organoaluminum species is relatively slow. The high polydispersities for the THF ligated complexes suggest that the Lewis base is interfering with the polymerization process. Perhaps the THF is in equilibrium between the scandium and aluminum centres thus providing two or more different scandium species responsible for polymerization. Nonetheless, the activities are generally promising as they approach that reported for metallocenes and other group 4 catalysts under similar conditions.^{6,19,75-78} Interestingly, these activities were measured in the presence of the potentially coordinating toluene.

2.3 Proposed Directions for the Acquisition of Organoscandium Catalyzed Ethylene Polymerization Data

While the preliminary polymerization results suggest β -diketiminato supported scandium compounds have potential as industrially applicable ethylene polymerization catalysts, a number of experiments could provide the necessary understanding to further enhance catalytic activity.

Although THF ligation appears to hamper polymerization activity in these systems no direct comparisons have yet been conducted. The ability to remove THF

from **1-Cl(THF)** provides the opportunity to test 2 sets of compounds (**1-Cl/1-Cl(THF)** and **1-Me/1-Me(THF)**) which differ only by their nuclearity and the presence of 1 molecule of THF. The enhanced thermal stability of **1-Me**, in comparison to its L^{tBu} analogue **2-Me**, will also supply information regarding the effects of metallation on polymerization activity.

No polymerization testing has yet been conducted on the SSIPs described in Chapter 4. These compounds are particularly interesting because mechanistic studies suggest that the arenes are easily displaced by arenes and acetylenes. These species exhibit significant thermal stability and will allow the direct comparison of isostructural contact ion-pairs (CIPs) and solvent separated ion-pairs (SSIPs). In light of the arene exchange studies on these complexes the presence of a vast excess of a more coordinating solvent (i.e. toluene) is expected to have a dramatic effect on polymerization activity. As such, it will be informative to obtain polymerization data in a variety of solvents ranging from cyclohexane to bromobenzene to toluene. It is plausible that the high pressures of ethylene may be sufficient to displace toluene. Such experiments should make it possible to draw correlations between the mechanistic studies described in Chapter 4 and polymerization activity, thus providing direction for future structural improvements.

Perhaps the most intriguing set of compounds to study in an industrial setting is the series of CIPs described in Chapter 3. Although the activity of **2-Me** has already been investigated, the ability to generate isolable pre-activated catalysts ensures that the observed polymerization activity is a result of the intended organoscandium cations. This will alleviate uncertainties about incomplete activation as well as solubility issues which may arise if the dialkyl species is activated *in situ*. For example, if significant quantities

of insoluble dimers formed, the observed catalyst activity would be significantly skewed as only a small percentage of the scandium catalyst would be available for ethylene polymerization. In short, preformed ion-pairs will essentially eliminate ambiguity that the intended catalyst is indeed what is being studied.

Upon amassing sufficient data, it may be possible to draw correlations between the energetics of intermolecular anion exchange and polymerization activity. It will also be possible to compare activity data for various alkyl substituents (e.g. **10-Me** and **10-CH₂SiMe₂CH₂SiMe₃**) to determine if increased steric bulk at the metal centre results in longer initiation periods. Finally, the broad range of well defined CIPs will also allow investigation into differences arising from B(C₆F₅)₃ vs. (C₆F₅)B(C₁₂F₈) activated complexes.

2.4 Conclusions

In summary, facile routes have been established to previously elusive base-free dialkyl scandium compounds, opening up opportunities to investigate the organometallic chemistry of this family of compounds in detail. A variety of dialkyl and mixed alkyl/halide synthetic strategies have been developed and several of the derivatives have been structurally characterized by X-ray crystallography. The 4-coordinate species exhibit fluxional behaviour in solution which has been quantitatively studied and is interpreted as a dynamic process which equilibrates two out-of-plane structures *via* a C_{2v} symmetric in-plane transition state. The thermal stability of these compounds has been thoroughly explored and although they undergo an intramolecular metallation process

with loss of RH, the reactions are sufficiently slow on the chemical timescale to not effectively compete with their desired reactivities. For example, reaction with H₂ gas has yielded a highly unusual imido hydride *via* a complicated rearrangement mechanism; future studies involving this species are currently underway. The details of the rich organometallic chemistry of this novel group of compounds, namely their reactivity with Lewis acids to enhance their efficacy as olefin polymerization catalysts, will unfold in the remaining chapters of this dissertation.

Chapter 3:

Activation of Neutral Organoscandium Complexes with Borane-Based Lewis Acids

3.1 Introduction

This chapter focuses upon the reactivity of neutral dialkyl scandium compounds (see Chapter 2) with electrophilic boranes and the subsequent reactivities therein. Since both $B(C_6F_5)_3$ and $HB(C_6F_5)_2$ are integral reagents in this chapter their synthesis and chemistry is introduced according to the chronology in which it was developed. Due to the more in depth studies pursued with $B(C_6F_5)_3$, however, their reactivities with neutral scandium complexes will be addressed in the opposite order, so as to improve the overall flow of the discussion.

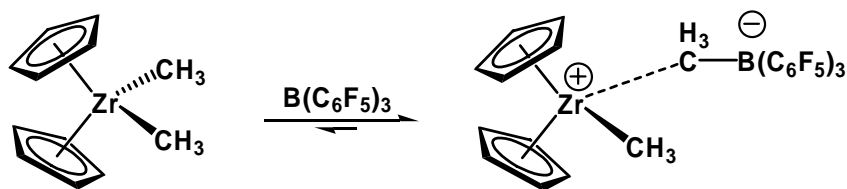
3.1.1 Triarylborane Lewis Acid Activation of Metallocenes

It was well established in the 1980's that the olefin polymerization activity of group 4 catalysts could be greatly enhanced upon the addition of methylaluminoxane (MAO) as a co-catalyst.⁷⁵ MAO, which is synthesized by the controlled hydrolysis of trimethylaluminum, was serendipitously discovered to aid in the polymerization process in 1980 upon reaction of a transition metal water adduct with trimethylaluminum.⁷⁹ Although there have since been a plethora of synthetic⁸⁰⁻⁸⁶ and computational studies⁸⁷⁻⁸⁹ undertaken to determine the exact mechanism by which this co-catalyst activates a

metallocene complex, its heterogeneity renders this task exceedingly difficult.⁸⁵ This is further complicated by the fact that only a small percentage of the MAO is capable of functioning as an activator, thus necessitating the addition of vast excesses of MAO (measured by the Al : transition metal ratio), often greater than 1000 equivalents.^{80,86} This ill-defined mixture is also difficult to systematically synthesize, requiring the careful characterization of each batch to determine the percentage of aluminum – slight variations from batch to batch can have drastic and deleterious effects on the resultant polymerization activity.⁸⁵ Nonetheless, it is generally accepted that MAO acts both as an alkylating agent and a Lewis acid which abstracts a methyl group from the metal centre to generate the active catalyst.⁷⁵

It was in this context that several research groups sought the development of a new co-catalyst system involving a Lewis acid which could be utilized to stoichiometrically activate dialkyl metallocenes in a well defined manner. In 1991, Marks,⁹⁰ Ewen⁹¹ and Turner⁹² reported that *tris*(pentafluorophenyl)borane, B(C₆F₅)₃, was a useful reagent for this purpose. Although the synthesis of B(C₆F₅)₃ was originally published by Massey, Park and Stone in the early 1960's,^{93,94} it had received little attention until its applicability towards olefin polymerization was demonstrated. Since these original papers B(C₆F₅)₃ has received wide appeal within the chemical community through a breadth of studies concerning the mechanism by which this Lewis acid activates dialkyl metallocenes and the dynamics of the ensuing ion-pair.⁹⁵

Reaction of B(C₆F₅)₃ with dialkyl metallocenes results in a “tug-of-war” between the metal centre and borane for the abstracted methyl group (Scheme 3.1). The resultant



Scheme 3.1 Activation of Cp_2ZrMe_2 with $\text{B}(\text{C}_6\text{F}_5)_3$

zwitterionic species has an extremely elongated Zr-C bond as the methyl group is usually more strongly associated with the boron atom.⁹⁶ This institutes a partial positive charge upon the metal centre and a partial negative charge on boron. The effect on the metal is two-fold as it becomes significantly more electron deficient, and thus reactive, while at the same time a vacant coordination site, necessary for alkene coordination, the first step of the well established Cossee polymerization mechanism,⁹⁷ is partially formed. As one might expect, the degree to which the alkyl group is abstracted, plays a significant role in dictating the polymerization activity of the ion-pair. A number of strategies can be exploited for probing this phenomenon, with the most obvious being X-ray crystallography. Most solid state structures exhibit similar features with elongated Zr-C distances ranging from approximately 2.4 – 2.7 Å and Zr-C-B angles approaching linearity with typical values between 160 – 180 °.^{75,96,98}

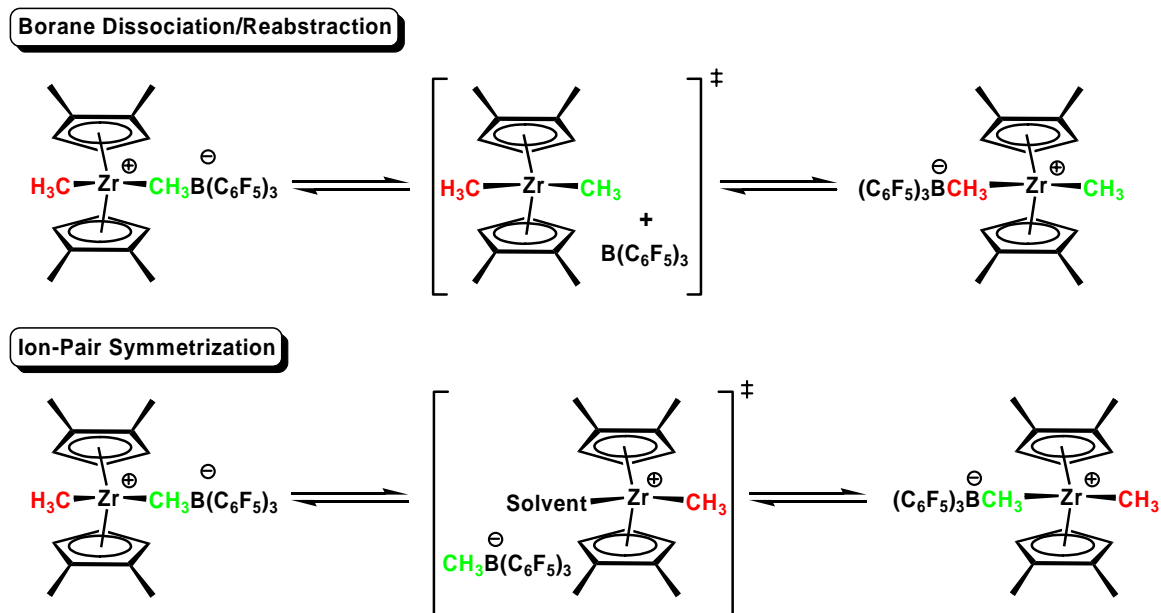
It is possible to examine the nature of the cation – anion interactions in solution using multinuclear NMR techniques. The degree to which the methide is abstracted can be measured by both ^{19}F and ^{11}B NMR spectroscopy: the difference between the *para* and *meta* resonances ($\Delta\delta_{\text{m,p}}$) in the ^{19}F NMR spectrum is inversely dependent on negative charge at the boron (*i.e.* greater degree of methide abstraction). A gap greater than 12 ppm is common for 3-coordinate boranes ($\text{B}(\text{C}_6\text{F}_5)_3$ has a $\Delta\delta_{\text{m,p}} = 18$ ppm in non-

coordinating solvents), 4 – 8 ppm is indicative of 4-coordinate neutral species and a difference of 2.5 ppm is reflective of a 4-coordinate anionic borate, or in respect to this system, a fully separated ion-pair.⁹⁹ Although it is possible to invoke resonance effects to explain the ¹⁹F NMR spectra, the complete picture is significantly more complicated; it is usually treated simply as an empirical tool to help classify ion-pair separation. Likewise, ¹¹B NMR chemical shifts provide information about the boron environment: 3 coordinate boranes have positive chemical shifts while anionic 4-coordinate borates generally appear upfield of 0 ppm.⁷⁵

Deck and Marks have developed an elegant zirconocene system to provide insight into the nature of the cation – anion interaction and have shown that methide abstraction from metallocenes is usually reversible. As such, two dynamic processes exist that exchange the zirconium methyls, the first of which involves B(C₆F₅)₃ dissociation/reabstraction.⁹⁸ In this case the borane relinquishes its hold on the methyl group, whereby it is then free to abstract either of the two, now equivalent, methyl groups. The second process, referred to by Marks as “ion-pair symmetrization” involves dissociation of the entire borate anion into a solvent separated ion-pair (SSIP), followed by recombination on the other side of the zirconocene wedge (Scheme 3.2). Since the latter pathway is speculated to proceed *via* a solvent stabilized transition state, it is not surprising that it is significantly accelerated in polar solvents.¹⁰⁰ Marks has demonstrated that it is possible to distinguish between these competing exchange mechanisms using [1,2-Me₂C₅H₃)₂ZrMe][MeB(C₆F₅)₃], since ion-pair symmetrization only exchanges the diastereotopic metallocene methyl groups while B(C₆F₅)₃ dissociation/reabstraction exchanges both the ring substituents and the Zr methyls (Scheme 3.2). Ion-pair

symmetrization was found to dominate for zirconocene compounds, while dissociation/reabstraction governs if the metal is replaced with hafnium.¹⁰⁰

It was realized that it should be possible to quantitatively evaluate the coordinative ability of the anion by measuring the energetics of structural reorganization, namely ion-pair symmetrization. It is likely that the activation barrier for this rearrangement is essentially that required for complete ion-pair dissociation (presumably within a solvent cage). The study of anion dissociation is pertinent to olefin polymerization because it is necessary to generate a vacant coordination site for the incoming monomer, thus, the energetics of this process should have a direct bearing on catalyst activity.



Scheme 3.2 Ion-Pair Dynamic Processes Distinguished Using $[1,2\text{-Me}_2\text{C}_5\text{H}_3]_2\text{ZrMe}[\text{MeB}(\text{C}_6\text{F}_5)_3]$

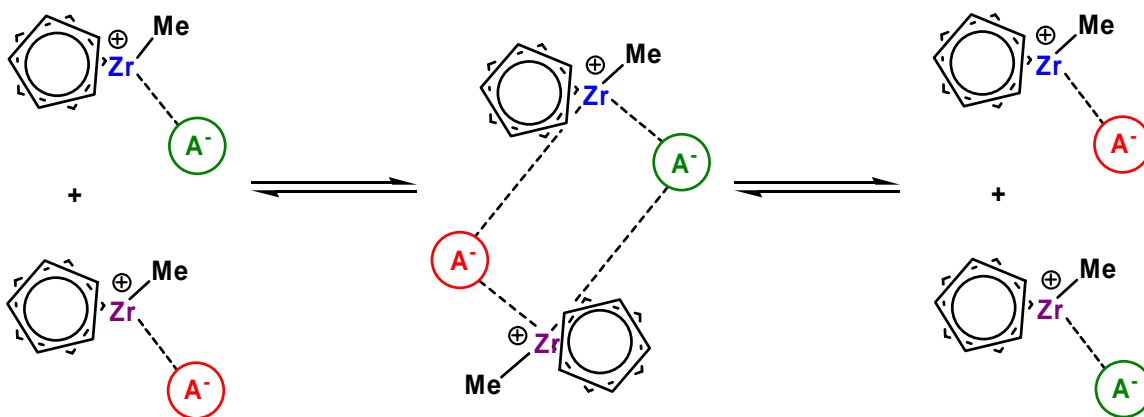
Indeed, line broadening, 2D EXSY, and variable temperature NMR techniques have proven invaluable for measuring the energy barriers for the two exchange processes. $\text{B}(\text{C}_6\text{F}_5)_3$ dissociation/reabstraction is often considered an undesired competing

mechanism as it makes it difficult to acquire accurate rate data for ion-pair symmetrization. As such, a great deal of effort has been expended on fine-tuning the metallocene microstructure and exploring experimental conditions in order to obtain a system where the latter process can be measured exclusively. Numerous publications detail such studies, with similar activation parameters found in a wide variety of contact ion-pairs (CIPS) possessing $[\text{MeB}(\text{C}_6\text{F}_5)_3]^-$ counterions; ΔH^\ddagger ranges from 20 – 30 kcal mol⁻¹ and ΔS^\ddagger is generally positive, usually with values of significant magnitude (*ca.* 10 – 20 e.u.).^{98,100-103} These findings have been interpreted to suggest that anion displacement occurs *via* a dissociative mechanism proceeding through a solvent stabilized zirconocene cation (Scheme 3.2). The barrier for this exchange process is believed to be a good representation of the energy requirements to displace the anion in a polymerization reaction. Indeed, Marks observes the expected inverse correlation between catalyst polymerization activity and strength of cation – anion ion-pairing.⁷⁵

Marks *et al.* have determined that solvent can have a considerable effect upon the rate of ion-pair symmetrization; polar solvents with high dielectric constants can increase the observed rates by more than an order of magnitude.¹⁰¹ A rough relationship between the ¹³C NMR chemical shift for the Me group of $[\text{MeB}(\text{C}_6\text{F}_5)_3]^-$ and polymerization activity has also been noted,¹⁰¹ however, these findings should be considered approximate at best, as there is very little difference in the chemical shift of the various species. In addition, only a small population of compounds was compared and only weak correlations can be drawn.

In contrast, Brintzinger and co-workers have tackled the same task using 2D EXSY NMR with *ansa*-zirconocenes and have obtained data which conflicts with Marks'

findings; the values of ΔH^\ddagger are similar, however, negative values for ΔS^\ddagger are found.^{104,105} Addition of excess $[\text{MeB}(\text{C}_6\text{F}_5)_3]^-$ anion in the form of $[\text{Li}][\text{MeB}(\text{C}_6\text{F}_5)_3]$ gives rise to dramatic enhancements in exchange rates. These results have prompted an explanation which involves the formation of higher aggregates, primarily ion-pair quadruples, as the intermediates responsible for anion exchange. One can easily envision a productive anion exchange if the two ion-pairs associate and then disperse with separate partners (Scheme 3.3). The observed negative ΔS^\ddagger would be expected for an associative ion-pair



Scheme 3.3 Anion Exchange *via* Ion-Pair Quadruples

metathesis. It is important to realize that although Brintzinger's results contradict Marks' interpretations, these experiments were conducted at much greater concentrations (*ca.* 10 – 15 mM) than those employed in Marks' studies (*ca.* 0.2 – 2 mM). Furthermore, Brintzinger's experiments focus on a slightly different zirconocene framework and considerable caution should be exercised when making comparisons between systems. It is also feasible that these results are representative of a different associative process, one where the anion is displaced by an incoming aromatic solvent molecule, as opposed to associative formation of ion-pair quadruples.

Marks has since countered Brintzinger's claims using the 1D DPGSE-NOE (differential pulse field gradient spin-echo nuclear Overhauser effect) technique to estimate the average size of the species in solution.^{104,106,107} In these cases the various exchange processes were not studied directly, but rather, the nature of ion-pair structures was examined. Excellent fits were established between calculated and experimental results which suggest no signs of ion-pair aggregation for CIPs, even at relatively high concentrations (10 – 20 mM). It is speculated that the residual coordinative ability of the anion is sufficient to prevent significant ion-pair mobility. As such, the solid state structures appear to be reasonable approximations of the species present in solution.

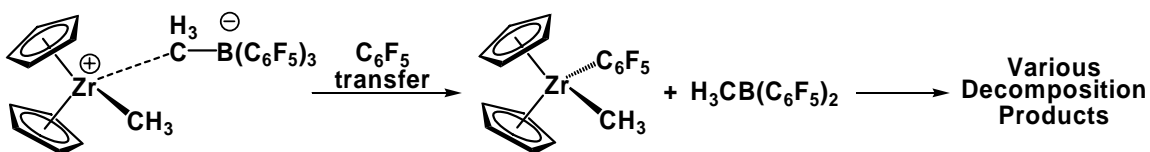
Analysis of SSIPs possessing perfluoroaryl borate anions, $(B(Ar_F)_4)$, established the presence of observable ion-pair quadruples and higher aggregates if concentrations exceed 0.5 mM.¹⁰⁷ It is reasoned that for these species the lack of residual coordination between the cation and anion permits a greater degree of orientational flexibility and as such, the X-ray structures should not be considered representative models of the solution state. It was further noted that higher aggregates are unlikely to play significant roles in an industrial polymerization setting as the extremely low concentrations would necessarily negate such formation. Also, when using 1D DPGSE-NOE it is difficult to approximate the expected ionic radius, and upon utilization of spherical models significant deviation may result between calculated and actual volumes which could seriously skew the findings.

This hotly debated area has also been explored by Landis *et al.* who have undertaken sophisticated NMR studies and managed to elucidate numerous additional dynamic processes.¹⁰⁸ Interestingly no evidence of ion-pair aggregation has been found

and rate enhancement upon addition of excess $[\text{MeB}(\text{C}_6\text{F}_5)_3]^-$ has been attributed to changes in solution dielectric constant. This is corroborated in that the same rate augmentations were achieved upon addition of chemically inert polar additives, such as $[\text{NBu}_4][\text{B}(\text{C}_6\text{F}_5)_4]$. Conclusions have been drawn that the conflicting reports from Marks and Brintzinger are likely due to differences in concentration, temperature and metallocene scaffold.

The possibility of SSIPs as intermediates in the ion-pair symmetrization process, and as viable intermediates in olefin polymerization, is substantiated by several theoretical investigations by Ziegler *et al.*^{109,110} The barrier for complete dissociation of $[(1,2\text{-Me}_2\text{C}_5\text{H}_3)_2\text{ZrMe}][\text{MeB}(\text{C}_6\text{F}_5)_3]$, into “naked” ions was calculated to be 38.0 kcal mol⁻¹, significantly greater than the 24.2 kcal mol⁻¹ found experimentally.¹⁰⁰ Interestingly, however, there is much better agreement upon comparison of the barrier for SSIP formation which was determined to be 18.7 kcal mol⁻¹.

While $\text{B}(\text{C}_6\text{F}_5)_3$ has proven its utility as an efficient co-catalyst for olefin polymerization, several undesirable deactivation pathways have been established and must be addressed. The most prevalent reactivity involves B-C cleavage with concomitant C_6F_5 transfer from the borate to the highly electron deficient metal centre (Scheme 3.4).^{98,111-113} This pathway, which predominates for sterically less encumbered species, is a dead-end route as the resultant M- C_6F_5 species can further decompose *via* various mechanisms including F-abstraction to generate dormant metal fluorides. Furthermore, competitive pathways also exist between the now liberated Lewis acid and the neutral metal complex usually leading to a mixture of intractable products. Direct fluoride abstraction from the borate moiety has also been observed and ultimately



Scheme 3.4 Ion-Pair Decomposition by C_6F_5 Transfer to the Metal Centre

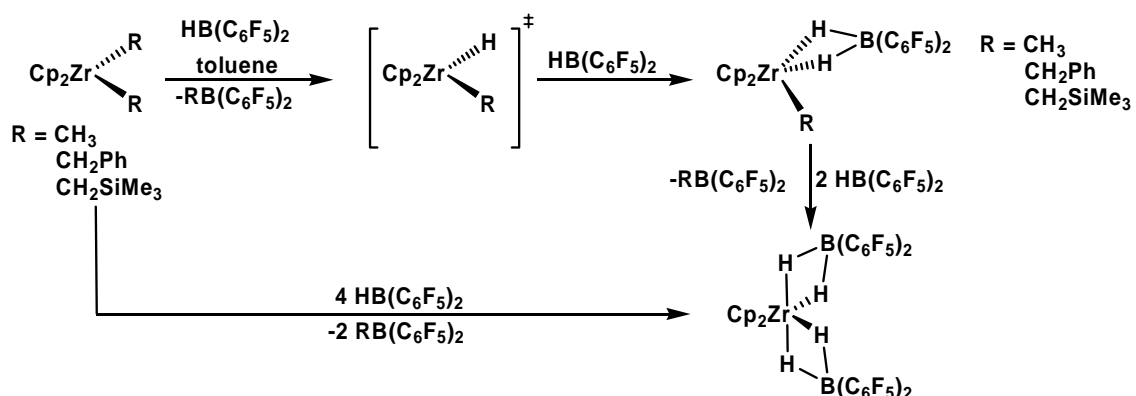
leads to complete Lewis acid degradation rendering the system inactive towards polymerization processes.^{90,114,115} In unusual cases decomposition involving both C_6F_5 transfer and F-abstraction can occur.¹¹⁶

Nonetheless, the debate over dynamic processes proliferates; it appears that one thing is certain – subtle differences in ion-pairing and their resultant dynamic processes are important to probe as cation – anion interactions have been shown to effect catalyst activity, stability, polymerization selectivity and polymer microstructure.¹¹⁷⁻¹²¹ Much work remains, however, especially with regard to non-Cp supported catalysts. Significant advances have been accomplished in the synthesis of non-metallocene compounds,^{5,77} however, with all the work dedicated to the development of these systems the paucity of ion-pair dynamic evaluations is apparent. This is especially notable in light of the drastic differences observed with only minute structural deviations within metallocene frameworks. As such, the substantial changes in ancillaries associated with non-metallocene catalysts will inevitably have huge effects on the dynamic processes available. An improvement in our understanding of these processes, in conjunction with the ability to alter them, as shown for metallocene examples, is bound to open new doors for homogeneously catalyzed olefin polymerization.

3.1.2 Diarylborane Lewis Acid Activation of Metallocenes

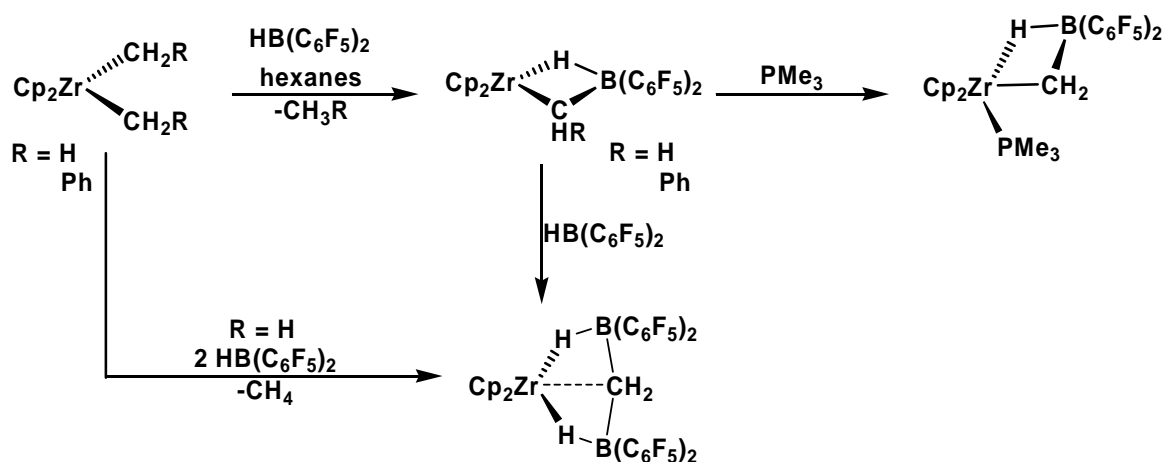
The utility found for aryl boranes in inorganic chemistry was recently extended to include the secondary borane, $\text{HB}(\text{C}_6\text{F}_5)_2$.¹²² This highly electrophilic borane, which can be prepared in multigram quantities, exists as a dimer in the solid state but in a monomer – dimer equilibrium in non-polar solvents. Unlike its triaryl congener, $\text{HB}(\text{C}_6\text{F}_5)_2$ has the added advantage of a B-H functionality from which desirable chemical transformations can result. For example, *bis*(pentafluorophenyl)borane is an exceptional hydroborating agent, capable of adding a B-H bond across virtually all unsaturated organic fragments with the only exception being tri- or tetra-substituted olefins with one or more strongly electron withdrawing substituents.^{123,124} These transformations are exceedingly rapid, usually complete within seconds at room temperature, while still offering improved regio- and chemo-selectivity in comparison to traditional hydroborating agents.¹²⁵

From an organometallic perspective, one might expect similar Lewis acid abstracting abilities to that observed for $\text{B}(\text{C}_6\text{F}_5)_3$, however, the resultant chemistry is both more rich and complex. Reactivity studies of $\text{HB}(\text{C}_6\text{F}_5)_2$ with Cp_2ZrR_2 ($\text{R} = \text{CH}_3$, CH_2Ph , and CH_2SiMe_3) have established that if two equivalents of borane are permitted to react in toluene the product is a dihydrido *bis*(pentafluorophenyl)borate species.^{126,127} These complexes are the result of alkyl group abstraction, followed by hydride delivery and trapping of the alkylhydride with the second equivalent of borane in rapid succession (Scheme 3.5). Addition of two more equivalents of borane afforded the expected tetrahydrido *bis*(pentafluorophenyl)borate complex. While this pathway was prevalent for reactions carried out in toluene, if the solvent was switched to hexanes, a competing



Scheme 3.5 Reaction of Cp_2ZrR_2 with Varying Equivalents of $\text{HB}(\text{C}_6\text{F}_5)_2$

process emerged whereby RH was lost and borane stabilized alkylidene species were realized (Scheme 3.6). Although the parent methylidene compound was not stable in solution at room temperature it was successfully trapped with PMe_3 . In the absence of added Lewis base a second equivalent of borane reacted to yield the structurally intriguing species, $\text{Cp}_2\text{Zr}=\text{CH}_2 \cdot 2\text{HB}(\text{C}_6\text{F}_5)_2$, which possesses a unique 5-coordinate carbon atom. If $\text{Cp}_2\text{Zr}(\text{CH}_2\text{Ph})_2$ was used as the starting material, the corresponding benzyl alkylidene, $\text{Cp}_2\text{Zr}=\text{CHPh} \cdot \text{HB}(\text{C}_6\text{F}_5)_2$, was stable and trapping with a Lewis base was no longer warranted. Upon switching to the smaller group 4 metal, titanium,



Scheme 3.6 Reactivity of Cp_2ZrR_2 with $\text{HB}(\text{C}_6\text{F}_5)_2$ in Hexanes

different reactivities involving reduction of the metal, and generation of the Ti(III) complex, $\text{Cp}_2\text{Ti}(\text{H}_2\text{B}(\text{C}_6\text{F}_5)_2)$, were observed.^{128,129}

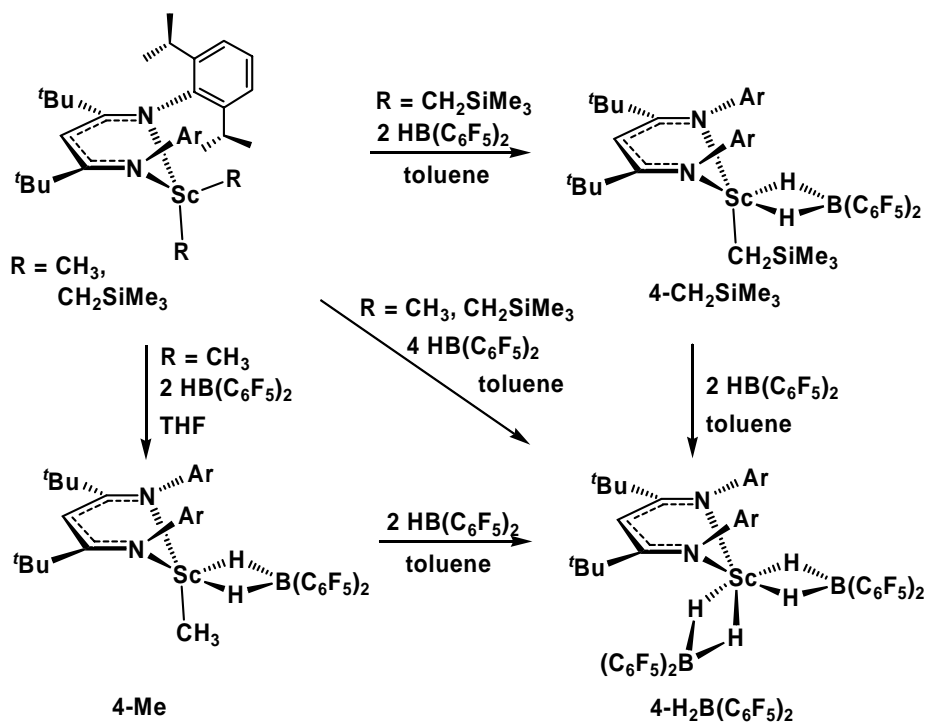
Reactions of $\text{HB}(\text{C}_6\text{F}_5)_2$ with species possessing metal carbon unsaturated functionalities, namely Schrock's $\text{Cp}_2\text{Ta}=\text{CH}_2(\text{CH}_3)$ ¹³⁰⁻¹³³ and $(\text{dmpe})_2\text{W}(\text{X})\equiv\text{CH}$ (dmpe = dimethylphosphinoethane; X = Cl, OSO_2CF_3) have also been examined.¹³⁴ In both of these cases unprecedented reactivities and bonding modes, namely the borataalkene and borylalkylidene ligands, were discovered.

While the reactivity of $\text{HB}(\text{C}_6\text{F}_5)_2$ has been carefully examined with group 4 carbon single bonds, Ta=C bonds, $\text{W}\equiv\text{C}$ bonds and even group 6 carbides,¹³⁵ little to no work has been reported on its chemistry with metal-carbon group 3 single bonds. Indeed, the observed reactions of Cp_2ZrMe_2 and $\text{Cp}_2\text{Zr}(\text{CH}_2\text{Ph})_2$ with one equivalent of $\text{HB}(\text{C}_6\text{F}_5)_2$ in hexane are especially intriguing as the ensuing intermediate can be viewed as a zirconium alkylidene in an arrested state of hydroboration. As such, this process might open avenues to generate alkylidene complexes for metals where this functionality has not yet been realized. Furthermore, the novel bonding modes and formation of unprecedented ligands, such as the borataalkene fragment, have proven useful from both practical and fundamental perspectives. It was with this rationale that the reactivity of various stoichiometries of $\text{HB}(\text{C}_6\text{F}_5)_2$ with the nacnac supported organoscandium complexes described in Chapter 2 was investigated.

3.2 Results

3.2.1 Reactivity of $L^{tBu}ScR_2$ with $HB(C_6F_5)_2$

An exploratory series of reactions conducted between $L^{Me}ScR_2$ ($R = CH_3$, **1-Me**, CH_2Ph , **1-CH₂Ph**, CH_2SiMe_3 , **1-CH₂SiMe₃**) and varying stoichiometries of *bis*(pentafluorophenyl)borane led to competing pathways which ultimately yielded an intractable mixture of unidentifiable products. Upon implementing the bulkier L^{tBu} , however, the various pathways were more easily controlled and well defined products could be isolated. As in the zirconocene examples,^{126,127} reaction of 2 equivalents of $HB(C_6F_5)_2$ with $L^{tBu}ScR_2$ ($R = CH_3$, **2-Me**, CH_2SiMe_3 , **2-CH₂SiMe₃**) in THF resulted in rapid alkyl-hydride exchange to produce $L^{tBu}Sc(R)(H)$ ($R = CH_3$, CH_2SiMe_3) and $RB(C_6F_5)_2$. The resultant mixed alkyl hydride complex is trapped with the second



Scheme 3.7 Reactivity of $L^{tBu}ScR_2$ with $HB(C_6F_5)_2$

equivalent of $\text{HB}(\text{C}_6\text{F}_5)_2$ (Scheme 3.7). Upon cold filtration in hexanes the desired scandium species can be isolated as pale yellow semi-crystalline solids in quantitative yields. The second equivalent of borane is required for the reaction to proceed; if only one equivalent of $\text{HB}(\text{C}_6\text{F}_5)_2$ is utilized, a 1:1 ratio of $\text{L}^{\text{tBu}}\text{ScR}_2$ starting material and $[\text{L}^{\text{tBu}}\text{ScR}][\text{H}_2\text{B}(\text{C}_6\text{F}_5)_2]$ ($\text{R} = \text{CH}_3$, **4-Me**, CH_2SiMe_3 , **4-CH₂SiMe₃**) is formed. Evidently $\text{HB}(\text{C}_6\text{F}_5)_2$ traps the incipient $\text{L}^{\text{tBu}}\text{Sc}(\text{H})(\text{R})$ faster than H migrates to the ligand (see section 2.2.5).

The ^1H NMR spectra are diagnostic for these compounds; aliquots of the crude reaction mixtures exhibit resonances at 1.32 and 2.00 ppm assigned as $\text{MeB}(\text{C}_6\text{F}_5)_2$ and $\text{Me}_3\text{SiCH}_2\text{B}(\text{C}_6\text{F}_5)_2$ respectively.¹²⁶ Despite the quadrupolar nature of scandium ($^{45}\text{Sc} = 100\%$, $I = 7/2$) the bridging hydride resonances are observed as broad 1:1:1:1 quartets centred around 2.7 ppm and possessing typical $^1J_{\text{B-H}}$ values ranging from 58 – 85 Hz (Figure 3.1). The ^{11}B NMR spectra exhibit sharp triplets, upfield of 0 ppm, with the expected coupling constant.

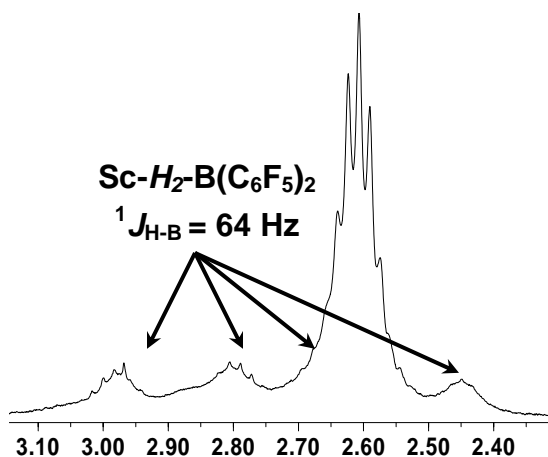


Figure 3.1 ^1H NMR Spectrum of **4-Me**

If four equivalents of $\text{HB}(\text{C}_6\text{F}_5)_2$ are employed both alkyl groups can be

exchanged for dihydridoborate ligands (Scheme 3.7). The two borate fragments are inequivalent as evidenced by 2 overlapping triplets observed in the ^{11}B NMR spectrum (Figure 3.2). Crystals suitable for an X-ray diffraction analysis were grown from cold hexanes and confirmed the identity of $4\text{-H}_2\text{B}(\text{C}_6\text{F}_5)_2$ (Figure 3.3). Although the solid state structure shows a quasi 7-coordinate scandium atom, its geometry is better described as distorted tetrahedral with the two $\text{H}_2\text{B}(\text{C}_6\text{F}_5)_2$ units occupying two vertices of the tetrahedron. The two borate units occupy the *exo* and *endo* positions, with the sterically less encumbered *exo* site permitting one of the C_6F_5 rings to approach sufficiently close to the metal to allow a close contact between one of the *ortho* fluorines (F5) and the metal centre. There is precedent for this type of stabilizing interaction; a similar bonding motif between an *ortho* C_6F_5 fluorine and yttrium was reported by Bochmann *et al.* in $[\text{Cp}_2\text{Y}][\text{MeB}(\text{C}_6\text{F}_5)_3]$.¹³⁶ The fluorine atom, which roughly caps one

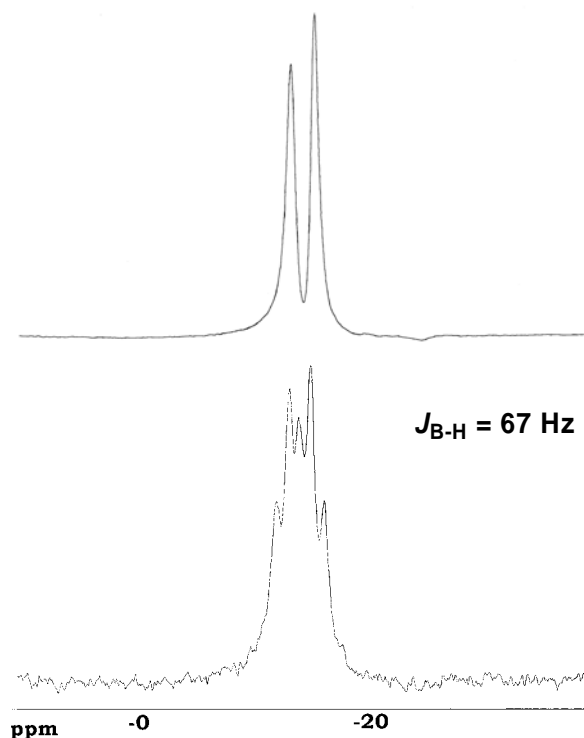


Figure 3.2 Top: $^{11}\text{B}\{^1\text{H}\}$ NMR of $4\text{-H}_2\text{B}(\text{C}_6\text{F}_5)_2$; Bottom: ^{11}B NMR of $4\text{-H}_2\text{B}(\text{C}_6\text{F}_5)_2$

of the tetrahedral faces, lies quite close to the scandium centre at a distance of 2.370(1) Å. Although the solid state structure might seem to suggest the possibility of decomposition *via* fluoride abstraction, the interaction is thought to be mainly a solid state phenomenon. No signs of the F-contact are observed in the room temperature ^{19}F NMR with a time averaged spectrum exhibiting two distinct sets of C_6F_5 resonances each integrating as two C_6F_5 groups. No change is observed in the spectrum upon cooling the sample to $-90\text{ }^\circ\text{C}$; evidently any Sc-F contacts must be fluxional in solution with a low

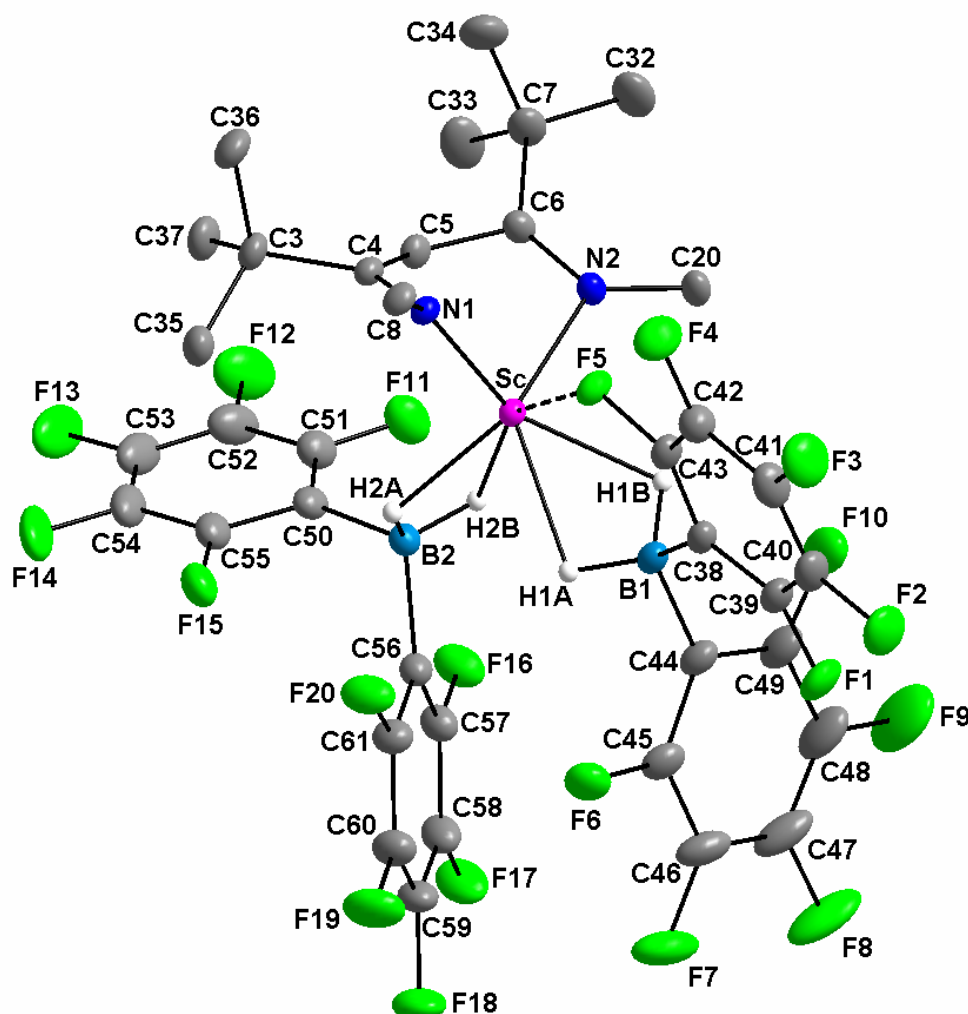


Figure 3.3 X-ray Molecular Structure of 4-H₂B(C₆F₅)₂. Thermal ellipsoids are drawn at the 30% probability level. Hydrogen atoms and aromatic groups are removed for clarity.

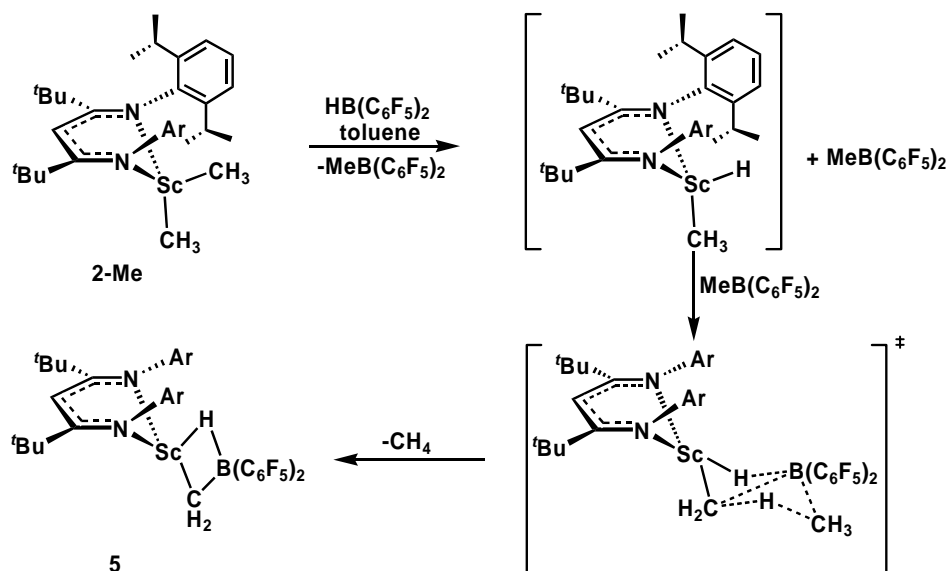
energy barrier for interconversion between structures. Furthermore, the compound is quite robust with no signs of decomposition upon heating at 100 °C in toluene for 6 hours. Three of the four bridging hydrides were located in the solid state structure and have short Sc-H distances ranging from 2.063(1) – 2.202(1) Å (Table 3.1).

While the choice of solvent does not affect the reactivity if R = CH₂SiMe₃, a different product is realized if one equivalent of HB(C₆F₅)₂ is allowed to react with **2-Me** in hydrocarbon solvents. In this case, evolution of methane is observed as evidenced by a resonance at 0.16 ppm in the ¹H NMR spectrum acquired in *d*₈-toluene, along with the final product, **5**. This presumably occurs *via* a similar mechanistic pathway to that proposed by Piers *et al.* for the zirconocene analogue whereby initial alkyl – hydride

Table 3.1 Selected Metrical Data for **4-H₂B(C₆F₅)₂**

Atoms	Bond Lengths (Å)	Atoms	Bond Angles (°)
Sc-N(1)	2.0517(15)	N(1)-Sc-N(2)	96.18(6)
Sc-N(2)	2.1475(15)	N(1)-Sc-B(1)	135.85(6)
Sc-F(5)	2.370(5)	N(1)-Sc-B(2)	112.48(6)
Sc-C(4)	2.5911(17)	N(2)-Sc-B(1)	103.73(6)
Sc-C(5)	2.6302(18)	N(2)-Sc-B(2)	114.39(6)
Sc-C(6)	2.7642(18)	Sc-N(1)-C(4)	96.58(11)
Sc-N ₂ C ₃ Plane	1.309(2)	C(3)-C(4)-N(1)	123.75(17)
Atoms	Torsion Angles (°)	N(1)-C(4)-C(5)	118.86(16)
C(6)-N(2)-C(20)-C(25)	108.32(22)	C(4)-C(5)-C(6)	133.75(17)
C(6)-N(2)-C(20)-C(21)	-77.16(25)	C(5)-C(6)-N(2)	118.20(16)
C(4)-N(1)-C(8)-C(9)	108.28(21)	C(7)-C(6)-N(2)	128.73(18)
C(4)-N(1)-C(8)-C(13)	-76.32(23)	C(6)-N(2)-Sc	103.54(12)

exchange is followed by subsequent reaction of the newly formed MeB(C₆F₅)₂ and L^{*t*Bu}ScMe(H) before the borane is released from the coordination sphere of the metal (Scheme 3.8).¹²⁶ Unlike the zirconocene species, however, the scandocyclic product did not require trapping with a Lewis base. In fact, the compound is stable for weeks in toluene at room temperature with little evidence of decomposition.

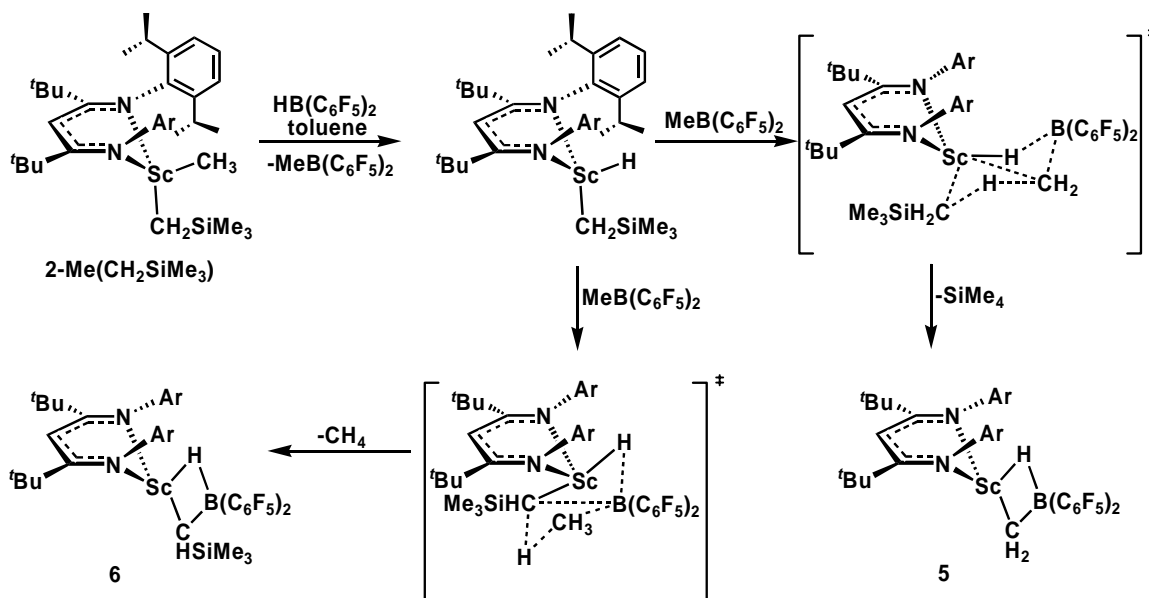


Scheme 3.8 Proposed Mechanism for Reaction of 1 Equivalent of $\text{HB}(\text{C}_6\text{F}_5)_2$ with **2-Me**, in Hydrocarbon Solvents

Although attempts to grow single crystals suitable for X-ray diffraction were unsuccessful, the compound has been identified by multinuclear NMR and elemental analysis. As expected, the $^{11}\text{B}\{^1\text{H}\}$ NMR spectrum had a single resonance at -21.0 ppm which upon acquiring the ^1H coupled spectrum, became a doublet with a characteristic B-H coupling of 64 Hz. Likewise, the ^1H NMR spectrum exhibited a broad 1:1:1:1 quartet integrating as 1H at 2.95 ppm and a broadened resonance at -0.13 ppm attributed to the bridging methylene moiety.

This intriguing complex can be described as a borane stabilized scandium methylene, akin to Tebbe's reagent,¹³⁷ a well known $\text{Cp}_2\text{Ti}=\text{CH}_2$ synthon, and as such, it represents an unprecedented class of compounds. To this end, several attempts to remove the coordinated $\text{HB}(\text{C}_6\text{F}_5)_2$, including addition of Lewis bases (PMe_3 and pyridine) to sequester the borane as a Lewis acid – base adduct were performed. These reactions were unsuccessful. Likewise, clean products were not obtained upon reaction

established, only preliminary work has been completed in this direction.



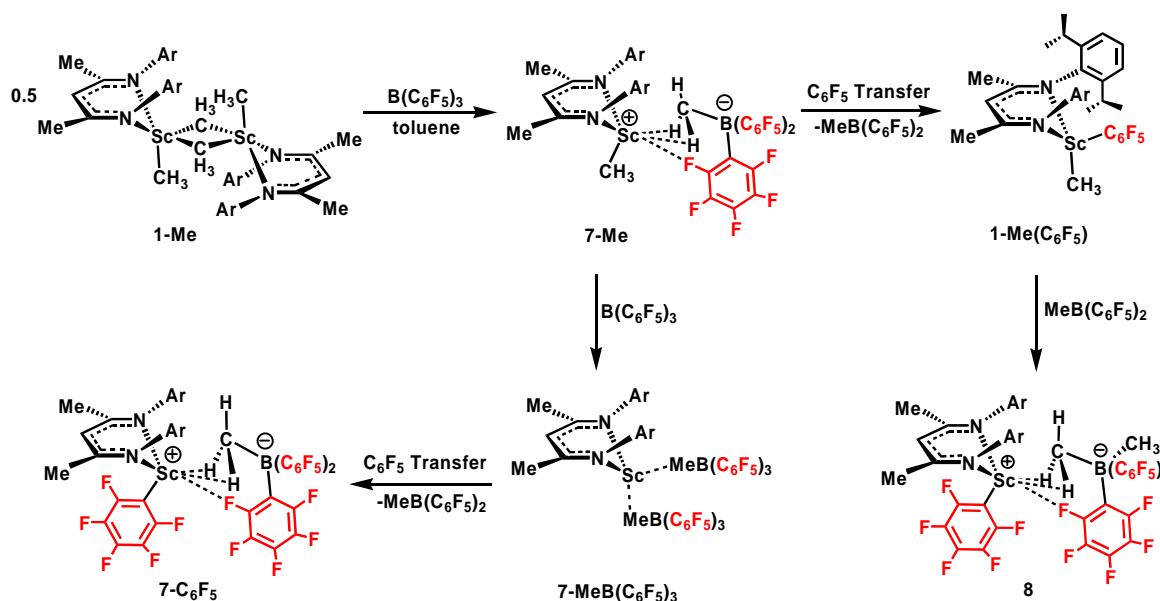
Scheme 3.10 Possible Mechanistic Pathway for Reactivity of **2-Me(CH₂SiMe₃)** with $\text{HB}(\text{C}_6\text{F}_5)_2$

3.2.2 Reactivity of $\text{L}^{\text{Me}}\text{ScMe}_2$, **1-Me**, with $\text{B}(\text{C}_6\text{F}_5)_3$

Since activation with the Lewis acidic $\text{B}(\text{C}_6\text{F}_5)_3$ was anticipated to increase the metal's electrophilicity and hence reactivity, it was speculated that the resultant cationic organoscandium species would have a heightened affinity for metallation. Because the neutral dialkyl compounds, $\text{L}^{\text{Me}}\text{ScR}_2$, were found to be substantially more metallation resistant than their L^{tBu} analogues (see section 2.2.6) it was decided to initially focus on these systems.

Reaction of $\text{L}^{\text{Me}}\text{ScMe}_2$, **1-Me**, with one equivalent of $\text{B}(\text{C}_6\text{F}_5)_3$ in toluene at -35°C afforded the desired ion-pair $[\text{L}^{\text{Me}}\text{ScMe}][\text{MeB}(\text{C}_6\text{F}_5)_3]$, **7-Me**, as monitored by ^1H , ^{11}B and ^{19}F NMR spectroscopy. A broad resonance at -16.8 ppm in the ^{11}B NMR spectrum, in combination with a $\Delta\delta_{\text{m,p}} = 4.2$ ppm in the ^{19}F NMR spectrum supported the formation

of a loosely bound CIP. While no evidence of metallation was observed at $-35\text{ }^{\circ}\text{C}$, upon gradual warming to room temperature, rapid C_6F_5 transfer from the borate to scandium generated the neutral complex $\text{L}^{\text{Me}}\text{Sc}(\text{Me})(\text{C}_6\text{F}_5)$, **1-Me(C₆F₅)**, with concomitant loss of $\text{MeB}(\text{C}_6\text{F}_5)_2$. Although **1-Me(C₆F₅)** reacted further with the liberated $\text{MeB}(\text{C}_6\text{F}_5)_2$ to produce $[\text{L}^{\text{Me}}\text{Sc}(\text{C}_6\text{F}_5)][\text{Me}_2\text{B}(\text{C}_6\text{F}_5)_2]$, **8**, the extreme solubility and thermal instability of **8** rendered it impossible to grow high quality crystals for an X-ray diffraction study. If two equivalents of $\text{B}(\text{C}_6\text{F}_5)_3$ were utilized, however, the more Lewis acidic $\text{B}(\text{C}_6\text{F}_5)_3$ successfully competed for the second abstraction resulting in $[\text{L}^{\text{Me}}\text{Sc}][\text{MeB}(\text{C}_6\text{F}_5)_3]_2$, **7-MeB(C₆F₅)₃**,¹³⁸ as evidenced by the disappearance of both Sc-CH₃ resonances in the ^1H NMR spectrum and the emergence of 2 sets of $[\text{MeB}(\text{C}_6\text{F}_5)_3]^-$ signals in the ^{19}F NMR spectrum. This doubly activated species is also prone to C_6F_5 transfer, ultimately giving rise to the much less soluble and more stable $[\text{L}^{\text{Me}}\text{Sc}(\text{C}_6\text{F}_5)][\text{MeB}(\text{C}_6\text{F}_5)_3]$, **7-C₆F₅**, (Scheme 3.11) which was characterized by X-ray crystallography (Figure 3.4).



Scheme 3.11 Reactivity of **1-Me** with $\text{B}(\text{C}_6\text{F}_5)_3$

The solid state structure of **7-C₆F₅** exhibits a symmetrically bound β -diketiminato ancillary with the metal lying only 0.645(5) Å from the plane formed by the nacnac backbone (Table 3.2). The most notable feature of the structure involves the cation – anion interactions; an extremely elongated Sc-C1 distance of 2.699(4) Å (cf. an average Sc-C distance of 2.29 Å for **1-Me**) is indicative of a weakly coordinating [MeB(C₆F₅)₃]⁻ anion. The Sc-C1-B angle of 133.42(25) ° is far from linearity as usually observed for activated metallocene structures.¹³⁹ This bending allows for a rather strong interaction between Sc and F1 as evidenced by a short contact of only 2.221(2) Å; this non-bonding

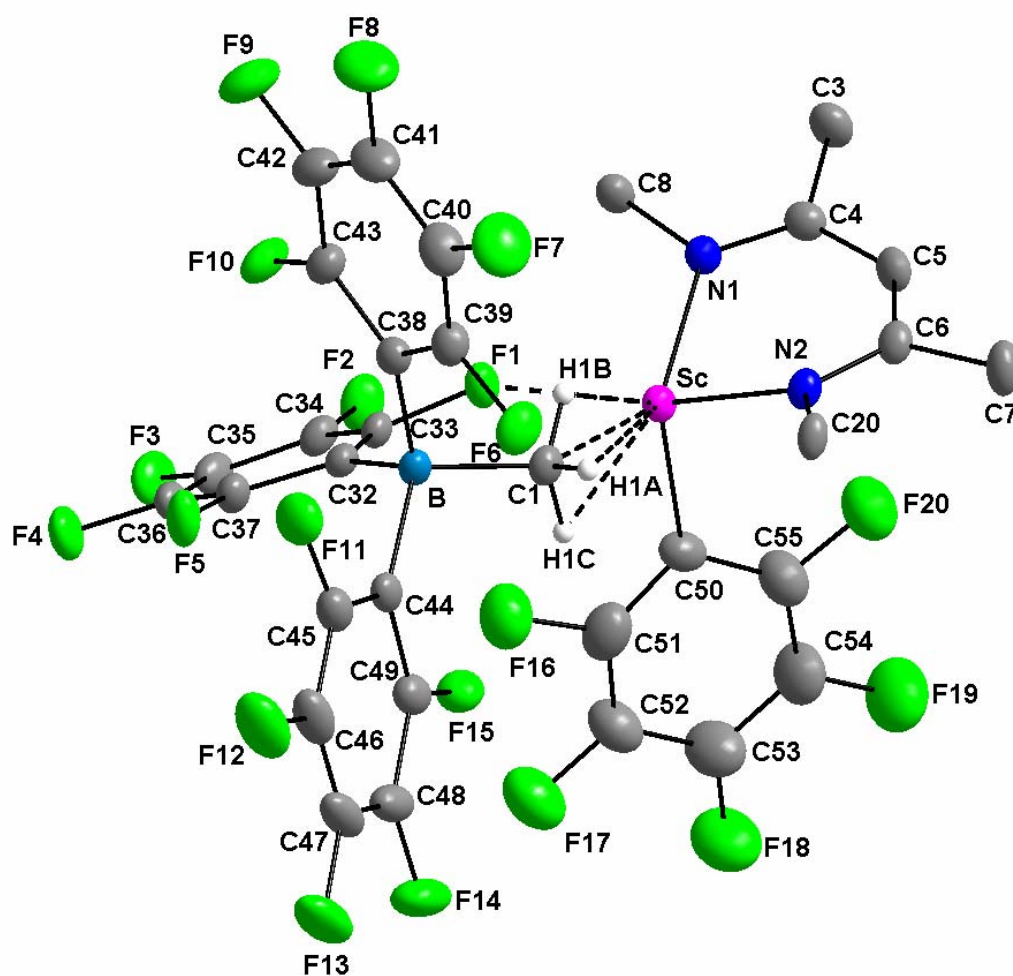


Figure 3.4 X-ray Molecular Structure of **7-C₆F₅**. Thermal ellipsoids are drawn at the 30% probability level. Hydrogen atoms and aryl groups are removed for clarity.

distance deviates only modestly from the bridging Sc-F distances (2.039(23) – 2.070(24) Å) found in $[\text{Cp}_2\text{ScF}]_3$ ¹⁴⁰ and is suggestive of possible decomposition *via* complete F-abstraction. This Sc-F interaction can be envisioned as a contest between C33 and Sc for the fluoride, in a similar fashion to that observed between Sc and B for the abstracted methyl group. This interpretation is corroborated by a rather long C33-F1 bond distance of 1.413(5) Å which deviates significantly from the average C-F distance in the structure of 1.349(5) Å. There are also two weak C-H interactions between the metal centre and the abstracted methyl group. The remaining Sc-C and Sc-N distances agree well with typical values.

Table 3.2 Selected Metrical Data for **7-C₆F₅**

Atoms	Bond Lengths (Å)	Atoms	Bond Angles (°)
Sc-N(1)	2.094(3)	N(1)-Sc-N(2)	87.9(3)
Sc-N(2)	2.087(3)	C(1)-Sc-C(50)	111.7(2)
Sc-C(1)	2.699(4)	N(1)-Sc-C(1)	139.9(2)
Sc-C(50)	2.220(5)	N(1)-Sc-C(50)	106.5(3)
Sc-F(5)	2.221(2)	N(2)-Sc-C(1)	93.6(3)
Sc-C(4)	3.052(5)	N(2)-Sc-C(50)	105.2(3)
Sc-C(5)	3.343(6)	Sc-N(1)-C(4)	124.1(3)
Sc-C(6)	3.045(6)	C(3)-C(4)-N(1)	120.7(4)
Sc-N ₂ C ₃ Plane	0.645(5)	N(1)-C(4)-C(5)	123.5(4)
Atoms	Torsion Angles (°)	C(4)-C(5)-C(6)	129.2(4)
C(6)-N(2)-C(20)-C(25)	83.66(50)	C(5)-C(6)-N(2)	123.2(4)
C(6)-N(2)-C(20)-C(21)	-98.44(48)	C(7)-C(6)-N(2)	119.4(4)
C(4)-N(1)-C(8)-C(9)	78.52(55)	C(6)-N(2)-Sc	123.0(3)
C(4)-N(1)-C(8)-C(13)	-103.39(50)	Sc-C(1)-B	133.4(2)

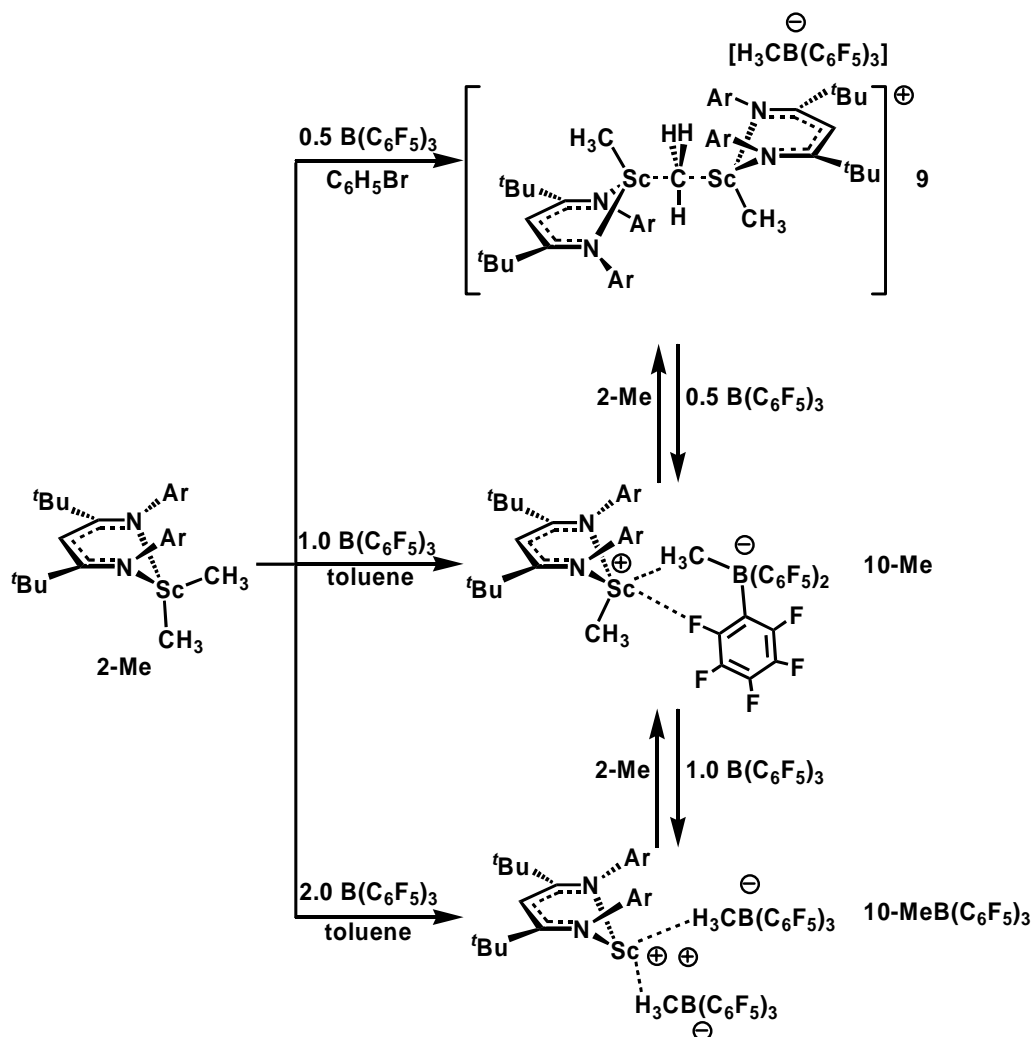
The low temperature ¹H and ¹⁹F NMR spectra of both **7-C₆F₅** and **8** do not exhibit a solution structure consistent with that observed by X-ray crystallography; there are no resonances indicative of a Sc-F interaction. Likewise there is no indication of restricted rotation about the Sc-C₆F₅ bond, with only three diagnostic resonances attributable to the C₆F₅ group in the low temperature ¹⁹F NMR spectrum. It is interesting to note, however,

that while two isomers (*exo*_{Me} and *endo*_{Me}) are observed in a 7 : 3 ratio for **7-C₆F₅**, only one is observed for **7-Me**. While it is presumed that the major isomer has the larger MeB(C₆F₅)₃ group in the *exo* position, as observed in the solid state, this was not unequivocally established.

3.2.3 Reactivity of L^{tBu}ScMe₂, **2-Me**, with B(C₆F₅)₃

Due to the deactivation by C₆F₅ transfer observed for L^{Me} supported complexes, a move to L^{tBu} supported compounds was made on the rationale that the enhanced steric bulk would circumvent C₆F₅ transfer by preventing the borate from approaching within sufficient proximity to efficiently deliver the C₆F₅ group to the scandium centre. At the same time it was necessary to be wary of decomposition by a metallation route, which was the original reason for utilizing the smaller β-diketiminato ancillary.

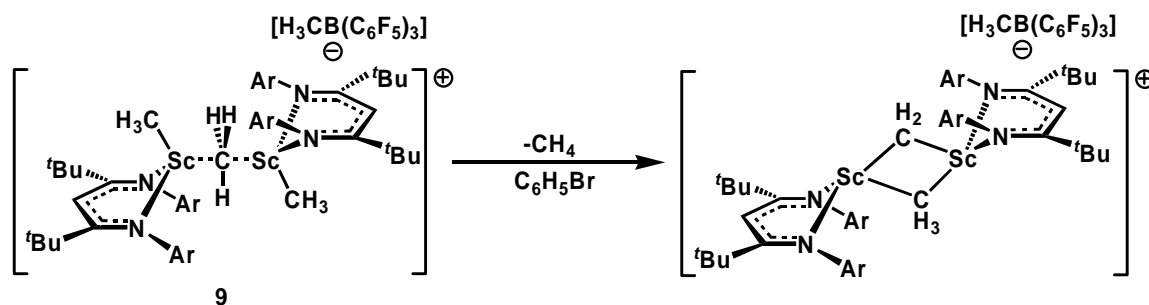
The reaction of varying equivalencies of B(C₆F₅)₃ with **2-Me** was examined and a variety of ion-pairs were formed (Scheme 3.12).¹⁴¹ Reaction of **2-Me** with 0.5 equivalents of borane results in a μ-methyl dimer, **9** as indicated by the characteristic ¹H NMR resonances for the terminal Sc-Me groups at -0.29 ppm and the bridging Sc-Me-Sc group at 0.10 ppm. The ¹J_{C-H} coupling constant of 132 Hz for the latter signal is indicative of an sp² hybridized carbon with interaction between the two metal centres via a filled p-orbital.^{139,142} Although it was not possible to isolate **9** it has been fully characterized by a host of multinuclear and 2D NMR techniques which confirm its identity. A very small Δδ_{m,p} of 2.4 ppm in the ¹⁹F NMR spectrum, along with a ¹¹B NMR resonance at -15.0 ppm suggest that the ion pair is completely separated due to the steric



Scheme 3.12 Reactivity of Varying Equivalents of $\text{B}(\text{C}_6\text{F}_5)_3$ with **2-Me**

constraints imposed by the μ -methyl dimer. Likewise, the expected low solubility in hydrocarbon solvents is also realized; **9** is not soluble in typical aromatic solvents, necessitating the use of the more polar bromobenzene ($\epsilon = 5.45$).¹⁴³ Even with the added stabilizing effect of bromobenzene, **9** slowly decomposes at temperatures higher than 270 K *via* loss of CH_4 . Although it was not possible to fully characterize the decomposition product due to additional competing pathways, it is possible that the first step results in formation of a methylene/methyl bridged dimer through loss of methane, as observed in

the decomposition of group 4 μ -methyl dimers (Scheme 3.13).^{139,144}



Scheme 3.13 Proposed Decomposition of **9**

Upon treatment of **2-Me** with a stoichiometric equivalent of $B(C_6F_5)_3$ in cold (-35 °C) hexanes the desired monomeric ion-pair, **10-Me**, precipitated as a crystalline yellow solid in quantitative yields.¹⁴¹ Alternatively, **10-Me** can be produced upon addition of 0.5 equivalents of $B(C_6F_5)_3$ to **9**. **10-Me** was stable as a solution in toluene for prolonged periods below 0 °C and indefinitely as a solid under an inert atmosphere at low temperature. Although no sign of decomposition *via* C_6F_5 transfer occurred upon gradual warming to room temperature, **10-Me** slowly evolved methane through a metallation pathway similar to that observed for the neutral dialkyl species. It is important to note that while metallation is an undesirable reactivity, it proceeds sufficiently slowly so as to not present a serious problem for subsequent mechanistic studies; a complete account on the kinetics of metallation of cationic complexes is presented in section 3.2.6.

The solution NMR spectra of **10-Me** in d_8 -toluene are indicative of fluxional behaviour; the 1H NMR spectrum at room temperature was broad and featureless, however, upon cooling to 213 K the spectrum sharpened considerably and resonances attributed to two isomers in a 2.2 : 1 ratio emerged (Figure 3.5). The ΔG^\ddagger was calculated at the coalescence temperature (263 K) to be $12.4(5)$ kcal mol $^{-1}$ which is a relatively low

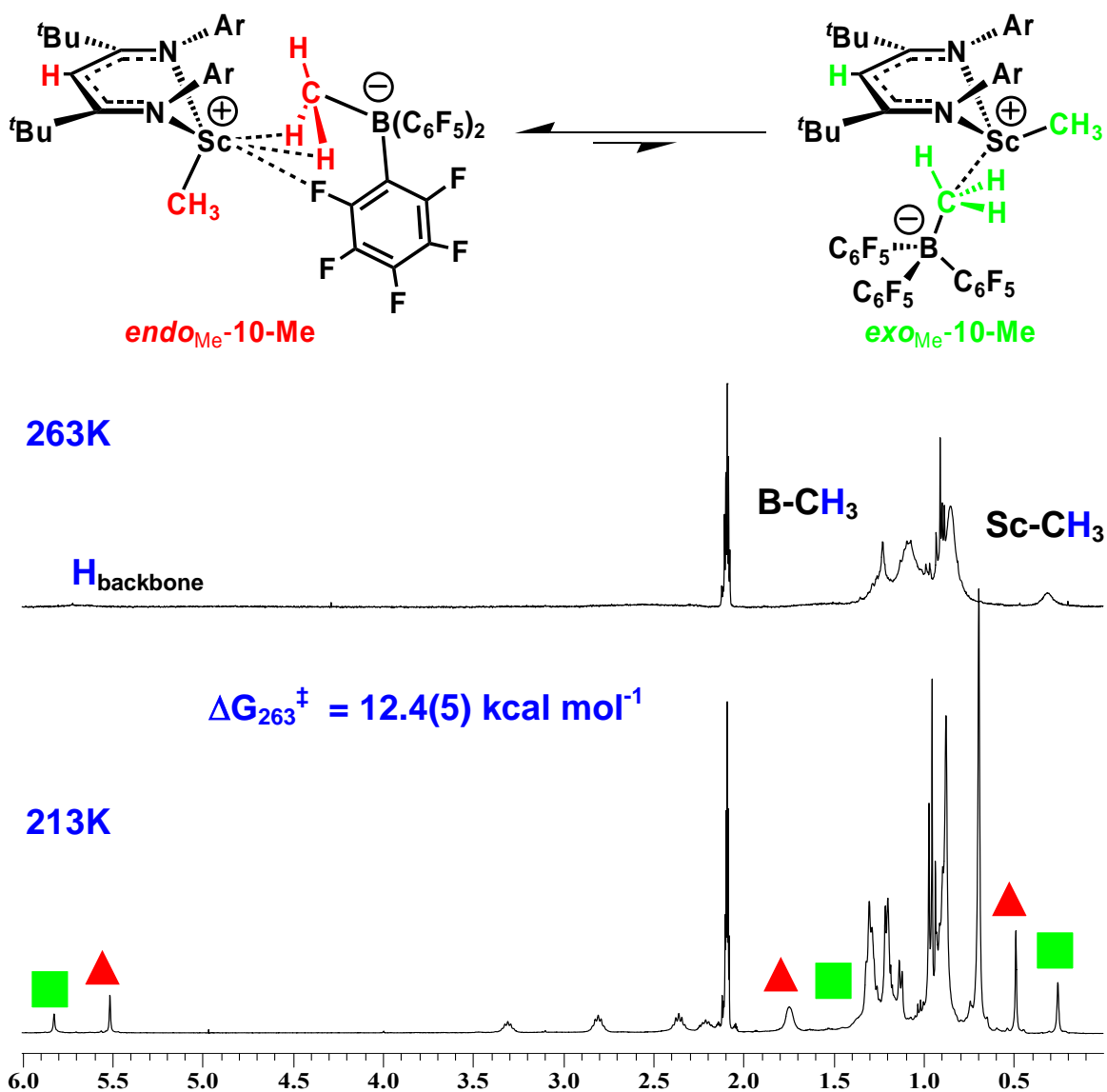


Figure 3.5 ^1H NMR Spectra of **10-Me** at 263 K (Top) and 213 K (Bottom).

barrier for interconversion between isomers and comparable to that determined for the more sterically encumbered dialkyl compounds (see section 2.2.4). In light of the discussion presented in Chapter 2, it was anticipated that *endo*_{Me}-**10-Me** was the energetically favourable isomer and thus responsible for the dominant isomer resonances in solution. As with the neutral compounds, a ^1H - ^1H 2D-ROESY NMR experiment

allowed the tentative assignment of isomers; through space interactions were observed between the *exo* Sc-Me and the lower aryl *isopropyl* groups for the minor isomer (Figure 3.6). Likewise, the major isomer showed a distinct crosspeak between the $[\text{MeB}(\text{C}_6\text{F}_5)_3]^-$ and the same *isopropyl* substituents. This finding agrees with the expected isomeric ratio where the bulky $[\text{MeB}(\text{C}_6\text{F}_5)_3]^-$ anion preferentially occupies the *exo* position. The ^{19}F NMR spectrum exhibited 2 isomers; the major isomer had the larger $\Delta\delta_{m,p}$ difference of 4.9 ppm. While this may seem to contradict the isomeric assignments it is difficult to speculate which isomer would have the tighter cation – anion contacts in solution. As such, the assignments given to the major and minor isomers in solution should not be considered unambiguous. The ^{11}B NMR spectrum, exhibited two overlapping resonances at -16.6 ppm.

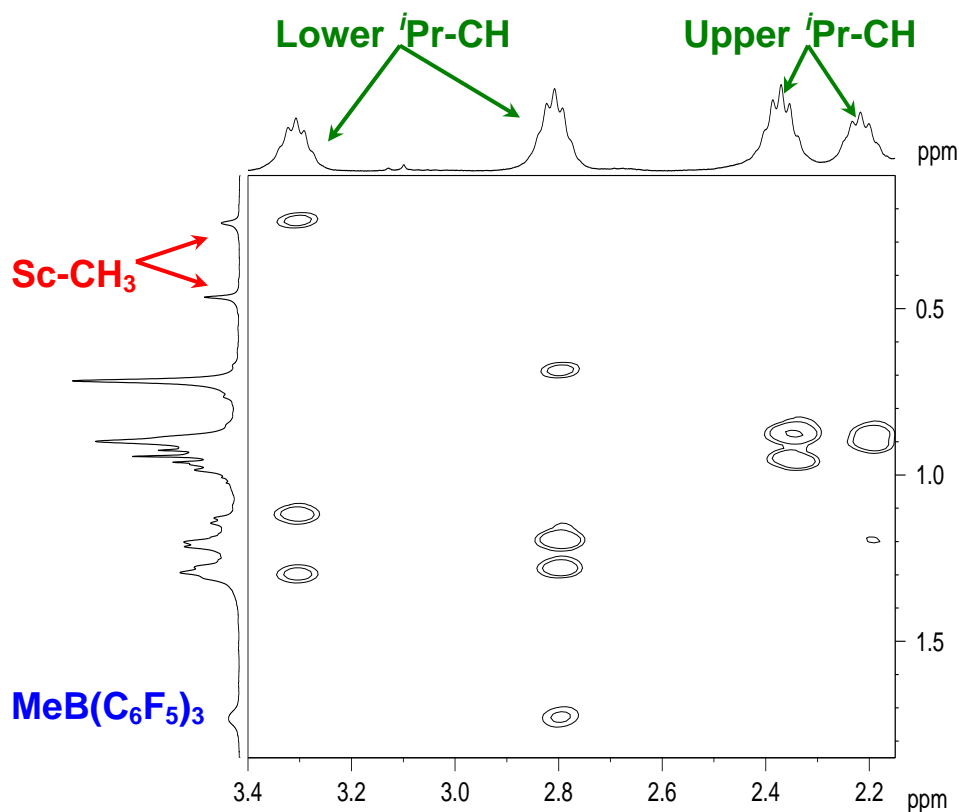


Figure 3.6 ^1H - ^1H 2D ROESY Spectrum of 10-Me.

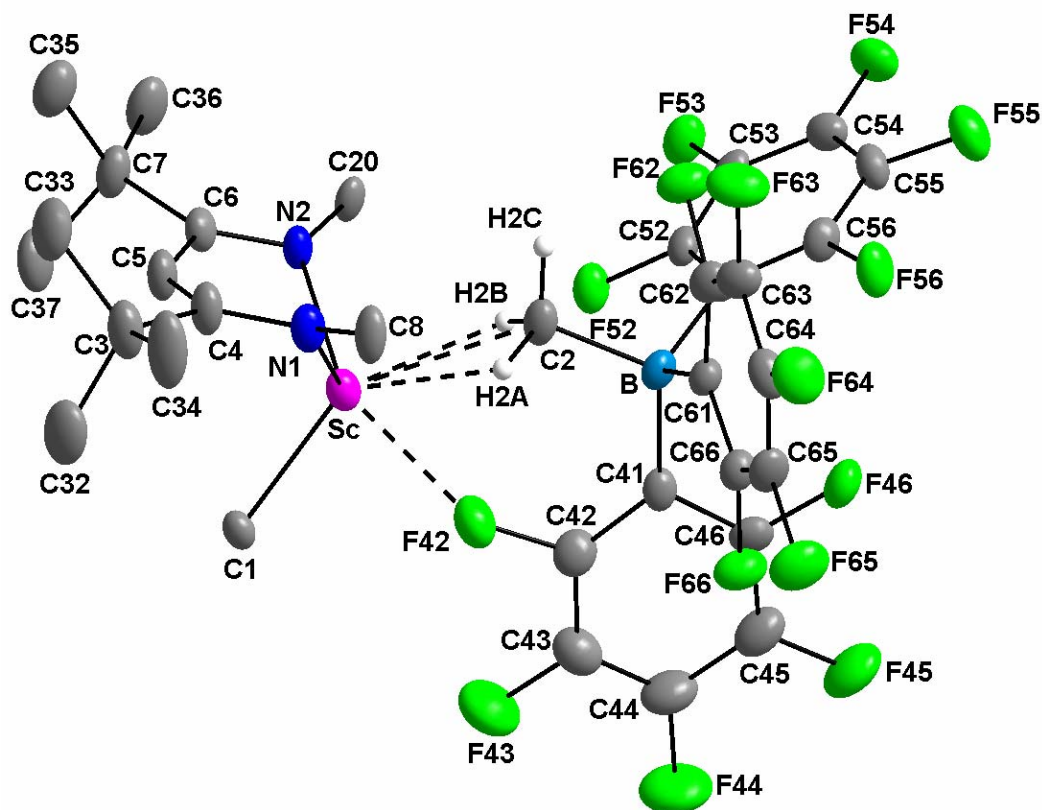


Figure 3.7 X-ray Molecular Structure of **10-Me**. Thermal ellipsoids are drawn at the 30% probability level. Hydrogen atoms and aryl groups are removed for clarity.

The inherent insolubility of ion-pair **10-Me** in hexanes made it an excellent candidate from which to grow high quality single crystals; an X-ray diffraction study confirmed its identity as the first fully characterized group 3 alkyl cation (Figure 3.7). The major isomer in solution agrees with that observed in the solid state; the $[\text{MeB}(\text{C}_6\text{F}_5)_3]^-$ counterion resides in the *exo* site with a Sc-C2 bond which has been elongated from 2.2219(16) Å to a length of 2.703(6) Å (Table 3.3). As observed for **7-C₆F₅**, the bent Sc-C2-B geometry (138.72(18) °) allows the newly formed vacant coordination site to be partially blocked through a weak Sc-F42 interaction of 2.390(4) Å.

Table 3.3 Selected Metrical Data for **10-Me**

Atoms	Bond Lengths (Å)	Atoms	Bond Angles (°)
Sc-N(1)	2.060(5)	N(1)-Sc-N(2)	95.06(19)
Sc-N(2)	2.093(5)	C(1)-Sc-C(2)	146.55(18)
Sc-C(1)	2.221(5)	N(1)-Sc-C(1)	110.14(19)
Sc-C(2)	2.703(6)	N(1)-Sc-C(2)	88.5(3)
Sc-F(42)	2.390(4)	N(2)-Sc-C(1)	110.32(19)
Sc-C(4)	2.688(6)	N(2)-Sc-C(2)	94.73(16)
Sc-C(5)	2.773(6)	Sc-N(1)-C(4)	102.7(4)
Sc-C(6)	2.757(6)	C(3)-C(4)-N(1)	126.1(5)
Sc-N ₂ C ₃ Plane	1.232(5)	N(1)-C(4)-C(5)	120.5(5)
Atoms	Torsion Angles (°)	C(4)-C(5)-C(6)	135.4(6)
C(6)-N(2)-C(20)-C(25)	92.8(7)	C(5)-C(6)-N(2)	120.0(5)
C(6)-N(2)-C(20)-C(21)	-90.9(7)	C(7)-C(6)-N(2)	127.8(5)
C(4)-N(1)-C(8)-C(9)	108.3(8)	C(6)-N(2)-Sc	105.4(4)
C(4)-N(1)-C(8)-C(13)	-75.8(9)	Sc-C(2)-B	138.72(18)

There is no evidence for this interaction in solution and as such, the solid state structure may not be representative of the solution structure. While the crystal data implies that it may be difficult to make isomeric assignments using 2D EXSY NMR (both the *endo* and *exo* positions are similar distances to the lower *isopropyl* groups), it is speculated that upon removal of the Sc-F42 interaction in solution, a more linear Sc-C2-B angle would be expected. This would likely place the [MeB(C₆F₅)₃]⁻ group in a more typical *exo* site, hence placing it much closer to the lower aryl *isopropyl* substituents and thereby rendering the isomeric assignment valid.

The Sc-F42 interaction is substantially longer than that in **7-C₆F₅** (2.221(2) Å) which is presumably due to the difficulty the anion has in accessing the coordination sphere of the metal. This crowding is imposed by the ^tBu groups on the nacnac which force the N-aryl groups further forward. Likewise, the C42-F42 bond distance of 1.400(8) Å shows only marginal elongation in comparison to the other C-F bonds within the structure (average C-F = 1.355(8) Å). From an electronic perspective, **10-Me** can

also be viewed as more saturated than the electron deprived **7-C₆F₅**. The remainder of the cation – anion bonding motif is also similar to that observed in **7-C₆F₅** with two Sc-H interactions (2.297(1) and 2.302(2) Å) located in the Fourier difference map and typical Sc-N and Sc-C1 bond distances.

Thus, moving from L^{Me} to the bulkier L^{tBu} ancillary has provided a two-fold benefit: increased thermal stability has been achieved in addition to a further separation of the ions. As such, the weaker coordinating anion in **10-Me** should be less prone to deactivation pathways such as C₆F₅ transfer or F atom abstraction in a polymerization setting. Indeed, **10-Me** is a highly active polymerization catalyst; complete polymerization details are outlined in section 2.2.7.

If **2-Me**, is allowed to react with 2 equivalents of B(C₆F₅)₃ in toluene, the unusual doubly activated species, [L^{tBu}Sc][MeB(C₆F₅)₃]₂, **10-MeB(C₆F₅)₃**, forms as a pale yellow solid with high solubility in aromatic solvents.¹⁴¹ It can also be synthesized through addition of one equivalent of B(C₆F₅)₃ to the previously formed **10-Me**. While double activation of dialkyl group 4 complexes is quite uncommon, Stephan and co-workers recently reported a crystallographically characterized titanium example,¹³⁸ [(^tBu₃PN)₂Ti][MeB(C₆F₅)₃]₂. The solution ¹H NMR data of **10-MeB(C₆F₅)₃** was diagnostic with no Sc-Me resonances and two distinct [MeB(C₆F₅)₃]⁻ signals at 1.55 and 1.92 ppm for the chemically inequivalent *exo* and *endo* anions (Figure 3.8). The ¹⁹F NMR spectrum also exhibited two sets of C₆F₅ resonances with Δδ_{m,p} = 4.3 and 5.8 ppm (assigned by ¹⁹F-¹⁹F 2D COSY). These values correlate well to those observed for the two isomers of **10-Me** and as such, it is presumed that the resonances with the larger *meta* – *para* gap are due to the *exo* MeB(C₆F₅)₃ group. While a ¹⁹F-¹⁹F 2D EXSY

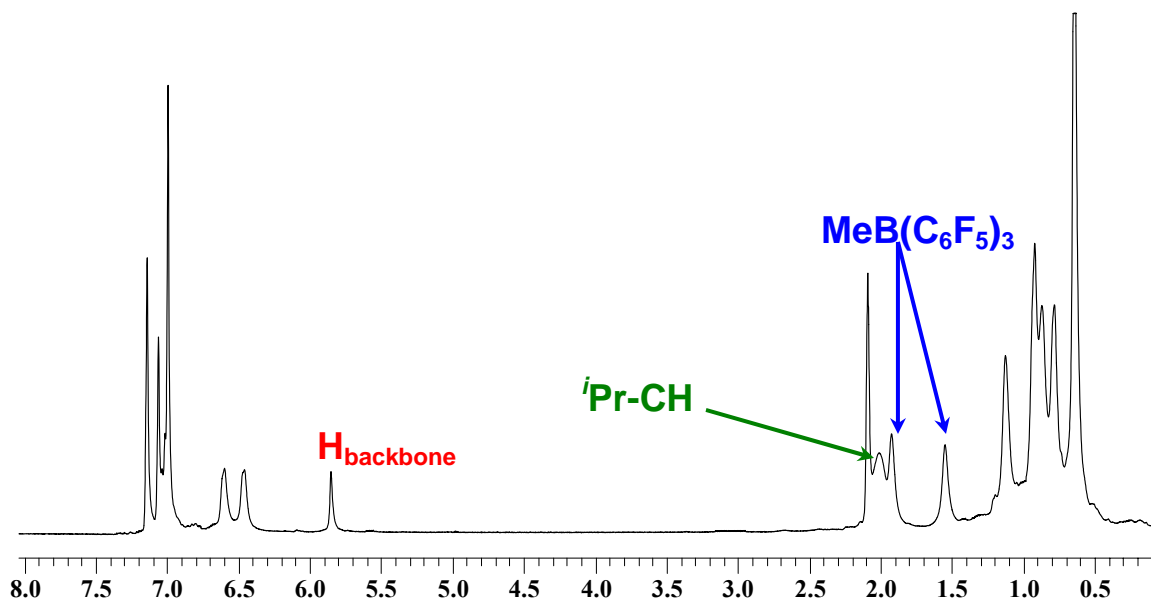
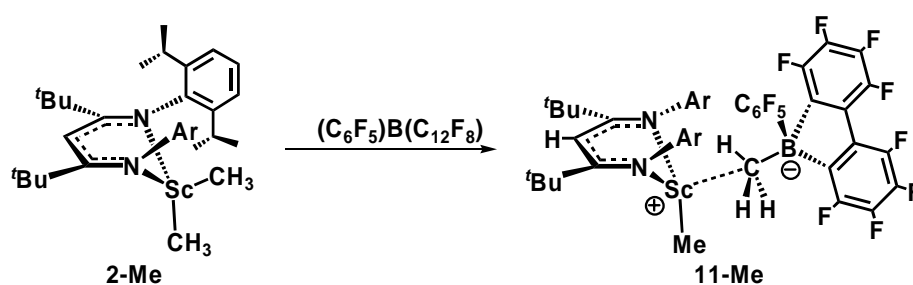


Figure 3.8 ^1H NMR of **10-MeB(C₆F₅)₃** in C_6D_6 at Room Temperature.

experiment confirmed the two anions were indeed exchanging, it was not possible to coalesce the process on the 1D ^1H NMR timescale.

Interestingly, while $[(^t\text{Bu}_3\text{PN})_2\text{Ti}][\text{MeB}(\text{C}_6\text{F}_5)_3]_2$ is inactive towards olefin polymerization, **10-MeB(C₆F₅)₃** has been qualitatively found to be an ethylene polymerization catalyst. Presumably one of the $\text{B}(\text{C}_6\text{F}_5)_3$ groups is capable of relinquishing its Me group in a similar manner to the borane dissociation/reabstraction mechanism proposed by Marks, thus providing a Sc-C bond into which an incoming olefin can insert. It is also interesting to note that **10-MeB(C₆F₅)₃** exhibits a significant thermal stability enhancement over both **9** and **10-Me** with no noticeable evidence of decomposition after 6 hours in solution at room temperature. Although it is quite surprising that **10-MeB(C₆F₅)₃** is immune to C_6F_5 transfer and fluoride abstraction, it is not unforeseen that the lack of a readily available Sc alkyl group for σ -bond metathesis would negate a metallation pathway.

In order to conduct an experiment on ion-pair dynamics (*vide infra*), it was necessary to synthesize an ion-pair of the same ilk as **10-Me**, but possessing a different anion. As such, the perfluorinated 9-borafluorene, $(\text{C}_6\text{F}_5)\text{B}(\text{C}_{12}\text{F}_8)$, which had recently been reported by Piers and co-workers, was employed.¹⁴⁵ Similar synthetic procedures to that utilized for **10-Me** quantitatively produced $[\text{L}^{\text{tBu}}\text{ScMe}][\text{MeB}(\text{C}_6\text{F}_5)(\text{C}_{12}\text{F}_8)]$, **11-Me**, as an analytically pure crystalline yellow solid (Scheme 3.14). Likewise, it was also possible to generate the doubly activated species, $[\text{L}^{\text{tBu}}\text{Sc}][\text{MeB}(\text{C}_6\text{F}_5)(\text{C}_{12}\text{F}_8)]_2$,



Scheme 3.14 Synthesis of **11-Me**

11-MeB(C₆F₅)(C₁₂F₈). The solution ¹H NMR confirmed the identity of **11-Me** with a spectrum analogous to **10-Me**; two isomers were present in a 1.6 : 1 ratio at 213 K. There was one important exception, however; the chemical shift of the ligand backbone protons differed sufficiently to allow differentiation between **10-Me** and **11-Me**. The ¹⁹F NMR spectrum remains a useful tool to provide information regarding ion-pairing;¹⁴⁵ the $\Delta\delta_{\text{m,p}}$ for the C₆F₅ group of the two isomers was 4.8 and 4.5 ppm respectively.

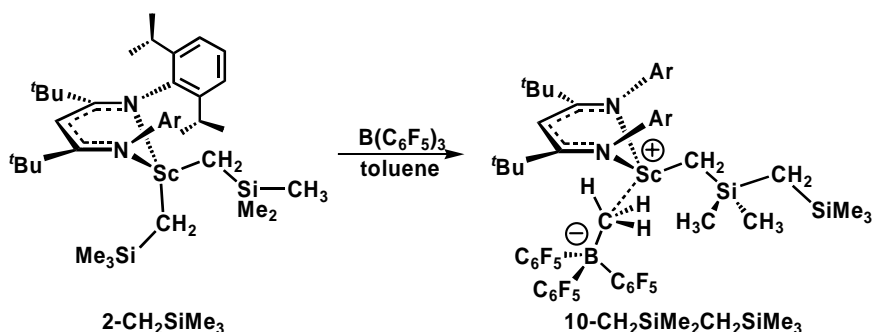
3.2.4 Reactivity of 2-CH₂SiMe₃ with B(C₆F₅)₃

In order to deconvolute complications in the examination of ion-pair dynamics (*vide infra*) which arose from the presence of two isomers in solution (two isomers for

each **10-Me** and **11-Me**), namely, competing ligand flip processes and different concentrations of isomers, a system was sought where only one isomer existed at low temperature. It was assumed that an ion-pair which possessed a bulky Sc-alkyl group, in addition to the large anion, would accomplish this. The fact that both **10-Me** and **11-Me** exist as two isomers in solution would seem to suggest that the bulk of the anion is sufficiently removed from the metal center so that there is little preference for one isomer over the other. As such, if the alkyl group could be substantially increased in steric bulk, it may cause a preference for one isomer.

With this idea in mind, one equivalent of $\text{B}(\text{C}_6\text{F}_5)_3$ was reacted with **2-CH₂SiMe₃** in toluene at low temperature to afford a highly unusual ion-pair. The ^1H NMR spectrum acquired in *d*₈-toluene exhibited three resonances upfield of 0 ppm in a 9:6:2 ratio. In addition, a broad peak which integrated as 3H was observed at 1.51 ppm, the region where the methylborate signals in the previously generated ion pairs (**10-MeB(C₆F₅)₃**, **10-Me**, **11-MeB(C₆F₅)(C₁₂F₈)** and **11-Me**) are present. Perhaps the most intriguing spectroscopic feature from the various NMR active nuclei was the fact that only one isomer was observed at all temperatures. The combined information garnered from these experiments led to the deduction that an alkyl group rearrangement produced $[\text{L}^{\text{tBu}}\text{ScCH}_2\text{SiMe}_2\text{CH}_2\text{SiMe}_3][\text{MeB}(\text{C}_6\text{F}_5)_3]$, **10-CH₂SiMe₂CH₂SiMe₃**, as the resultant ion-pair (Scheme 3.15).

Although **10-CH₂SiMe₂CH₂SiMe₃** exhibited a marked increase in solubility in hydrocarbon solvents in comparison to the other organoscandium ion-pairs it was still possible to obtain high quality single crystals from cold hexanes. An X-ray diffraction study confirmed the identity of **10-CH₂SiMe₂CH₂SiMe₃**, its molecular structure is



Scheme 3.15 Reaction of **2-CH₂SiMe₃** with B(C₆F₅)₃.

depicted in Figure 3.9. The solid state structure of **10-CH₂SiMe₂CH₂SiMe₃** exhibited several noteworthy parameters including a Sc-C1 bond distance of 2.499(3) Å. While this distance represents a significant elongation from approximately 2.20 Å in the neutral starting material, it is vastly shorter than that observed in either **7-C₆F₅** or **10-Me**. Also unlike these structures, the Sc-C1-B bond angle approaches linearity at 176.76(17) ° (Table 3.4). Consequently, the borate anion is not appropriately configured to permit Sc-F interactions; the closest Sc-F non-bonding distance is that observed between Sc and F6 at 3.937(2) Å. The rationale for the difference between these structures, and perhaps the most unique feature of this compound is that the [MeB(C₆F₅)₃]⁻ anion occupies the *endo* site as opposed to the more spacious *exo* position. This difference is likely due to a combination of electronic stabilization (the [MeB(C₆F₅)₃]⁻ appears to be able to approach the metal centre closer in the *endo* position) and the very bulky CH₂SiMe₂CH₂SiMe₃ alkyl group which, especially if one considers rotational flexibility about the Si-C bonds, render it more sterically encompassing than the anionic ligand. As such, it fits with the majority of previous findings that the smaller group resides in the *endo* position.

Since the counterion is forced into the more encumbered site, it does not have the

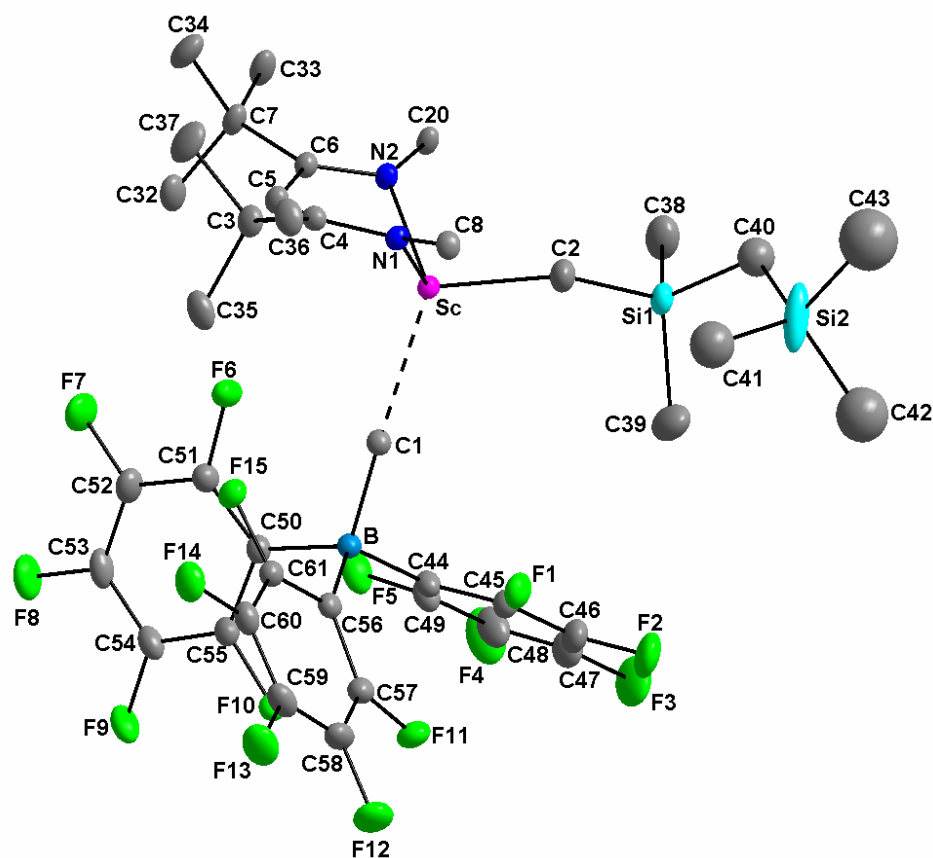


Figure 3.9 X-ray Molecular Structure of **10-CH₂SiMe₂CH₂SiMe₃**. Thermal ellipsoids are drawn at the 30% probability level. Hydrogen atoms and aryl groups are removed for clarity.

conformational freedom to permit a Sc-F interaction. This may also be an explanation as to why the anion approaches the metal more closely than that observed for other similar structures; the inability of the anion to flex and electronically stabilize the metal center through Sc-F interactions results in a more Lewis acidic metal center, thus drawing the methylborate closer. Although the Sc-C distance is shorter than that in **10-Me**, the majority of the steric bulk of the borate is actually further removed. This can be seen from the bending of the C₆F₅ groups away from the cationic fragment, as well as the imposed linearity of the Sc-C1-B bond angle which forces a Sc-B distance of 4.163(3) Å in comparison to only 4.083(7) Å in **10-Me** (cf. 2.499(2) vs 2.699(3) Å for Sc-C1). The

steric bulk of the $\text{CH}_2\text{SiMe}_2\text{CH}_2\text{SiMe}_3$ alkyl is also apparent in the Sc-C2-Si1 bond angle of $144.47(15)^\circ$ which deviates drastically from the ideal tetrahedral value of 109.5° ; presumably the angle is enlarged in order to further remove the steric bulk from the crowded metal centre.

Table 3.4 Selected Metrical Data for **10-CH₂SiMe₂CH₂SiMe₃**

Atoms	Bond Lengths (Å)	Atoms	Bond Angles (°)
Sc-N(1)	2.0722(18)	N(1)-Sc-N(2)	96.65(7)
Sc-N(2)	2.0858(18)	C(1)-Sc-C(2)	113.49(10)
Sc-C(1)	2.499(2)	N(1)-Sc-C(1)	116.51(8)
Sc-C(2)	2.133(3)	N(1)-Sc-C(2)	99.29(11)
Sc-C(4)	2.746(2)	N(2)-Sc-C(1)	121.29(8)
Sc-C(5)	2.785(2)	N(2)-Sc-C(2)	106.34(10)
Sc-C(6)	2.755(2)	Sc-N(1)-C(4)	104.81(14)
Sc-N ₂ C ₃ Plane	1.193(2)	C(3)-C(4)-N(1)	125.7(2)
Atoms	Torsion Angles (°)	N(1)-C(4)-C(5)	120.06(19)
C(6)-N(2)-C(20)-C(25)	95.3(3)	C(4)-C(5)-C(6)	135.2(2)
C(6)-N(2)-C(20)-C(21)	-89.3(3)	C(5)-C(6)-N(2)	120.28(19)
C(4)-N(1)-C(8)-C(9)	94.4(4)	C(7)-C(6)-N(2)	126.68(19)
C(4)-N(1)-C(8)-C(13)	-91.1(3)	C(6)-N(2)-Sc	105.07(14)
		Sc-C(1)-B	176.77(17)

Both the ^{11}B and ^{19}F NMR spectra support the solid state structure with only one isomer observed and indications of close cation – anion connectivity; the ^{11}B resonance at -15.2 ppm is slightly more downfield than that observed for **10-Me** and the $\Delta\delta_{m,p}$ difference of 4.6 ppm is slightly larger than that obtained for **10-Me**. Unlike **2-Me**, reaction of 2 equivalents of borane with **2-CH₂SiMe₃** does not result in double activation. Likewise, if only 0.5 equivalents of activator are employed, a 1:1 mixture of **10-CH₂SiMe₂CH₂SiMe₃** and starting material results.

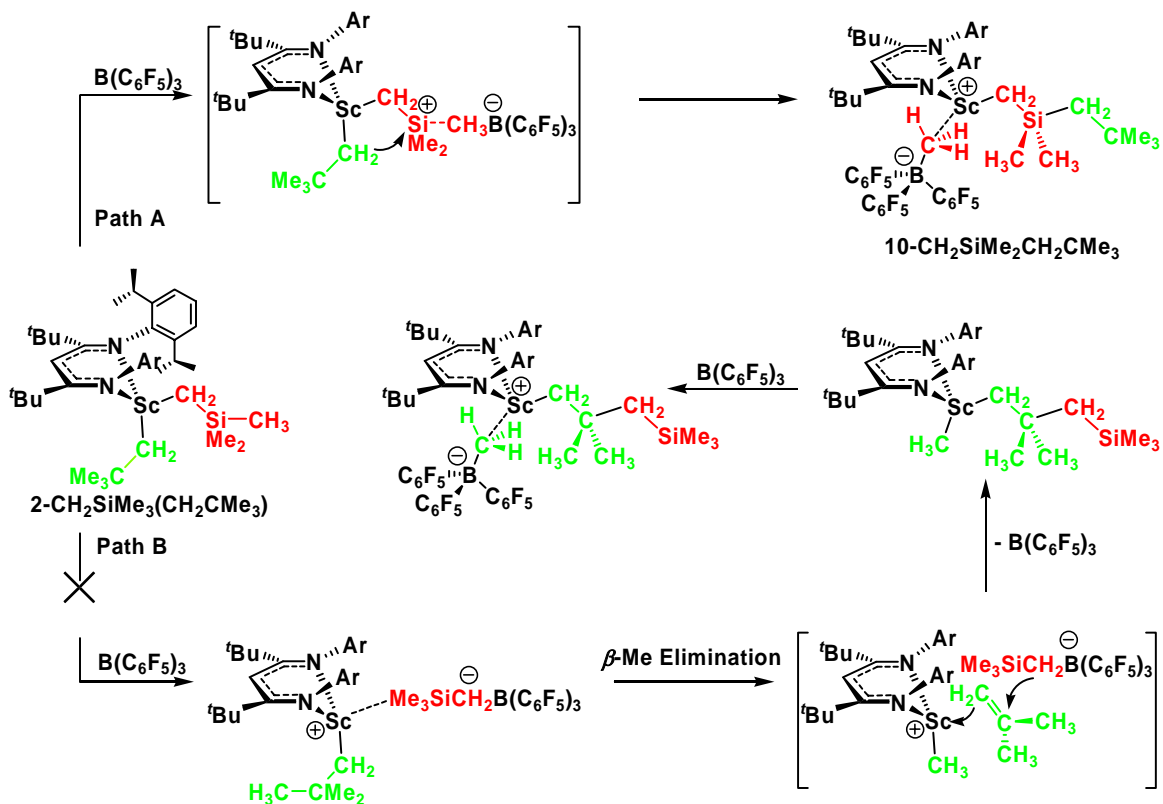
With this novel compound in hand, the mechanism of formation was of keen interest from a fundamental perspective. Two reasonable pathways can be envisioned,

the first involves abstraction of an entire CH_2SiMe_3 moiety,^{146,147} followed by β -Me elimination, and subsequent attack by the abstracted alkyl on the intermediate silene species. The newly formed $\text{L}^{\text{tBu}}\text{Sc}(\text{CH}_3)(\text{CH}_2\text{SiMe}_2\text{CH}_2\text{SiMe}_3)$, is then free to react with the liberated borane, ultimately affording **10-CH₂SiMe₂CH₂SiMe₃** (Scheme 3.16). Precedent for this type of reactivity has been reported by Young and co-workers in the thermal decomposition of various organoplatinum compounds.¹⁴⁸ Likewise, Horton has reported β -Me elimination with loss of *isobutene* from cationic zirconium neopentyl species.⁹⁹ Alternatively, the borane may abstract a Si-Me group through cleavage of a Si-C bond. The dissociation of the borate would likely be accompanied by simultaneous migration of the remaining CH_2SiMe_3 group to the incipient silicon cation. There have been two reports of this type of rearrangement, however, **10-CH₂SiMe₂CH₂SiMe₃** represents the first structurally characterized example.^{149,150}

In order to distinguish between the two possible mechanisms, several experiments were conducted. The most straightforward experiment was the reaction of $\text{L}^{\text{tBu}}\text{Sc}(\text{CH}_2\text{CMe}_3)_2$, **2-CH₂CMe₃**, with $\text{B}(\text{C}_6\text{F}_5)_3$ which showed no sign of reaction even at elevated temperatures. If the former pathway was operative, one might expect to see similar reactivity whereby an entire neopentyl group could be abstracted. This mechanism would likely be more facile for **2-CH₂CMe₃** than **2-CH₂SiMe₃** because β -Me elimination would produce *isobutene* which is significantly more stable than dimethyl silene (Scheme 3.16). Conversely, if the latter scenario is prevalent then reaction might not take place since a C-C bond at $82.6 \text{ kcal mol}^{-1}$ is significantly more difficult to break than a Si-C bond (76 kcal mol^{-1}).¹⁵¹

In an attempt to lend further support to one mechanism over the other, another

study, which took advantage of the ability to generate mixed alkyl compounds, was undertaken. In this experiment the mixed alkyl, $L^{t\text{Bu}}\text{Sc}(\text{CH}_2\text{SiMe}_3)(\text{CH}_2\text{CMe}_3)$, **2-CH₂SiMe₃(CH₂CMe₃)**, was permitted to react with one equivalent of $\text{B}(\text{C}_6\text{F}_5)_3$. If the entire alkyl group is abstracted it can be assumed that it will be the CH_2SiMe_3 group,



Scheme 3.16 Proposed Mechanistic Pathways for formation of **10-CH₂SiMe₂CH₂SiMe₃**

since no reaction took place between **2-CH₂CMe₃** and $\text{B}(\text{C}_6\text{F}_5)_3$. In this case, path B in Scheme 3.16 would produce $[\text{L}^{t\text{Bu}}\text{ScCH}_2\text{CMe}_2\text{CH}_2\text{SiMe}_3][\text{MeB}(\text{C}_6\text{F}_5)_3]$. Alternatively, if Si-C bond cleavage occurs, path A would be followed and the final product, $[\text{L}^{t\text{Bu}}\text{ScCH}_2\text{SiMe}_2\text{CH}_2\text{CMe}_3][\text{MeB}(\text{C}_6\text{F}_5)_3]$, **10-CH₂SiMe₂CH₂CMe₃**, would have silicon, as opposed to carbon in the β -position. Upon completion of the reaction, integration of

the SiMe₂ and CMe₃ resonances in the ¹H NMR spectrum unambiguously determined **10-CH₂SiMe₂CH₂CMe₃** as the end-product, thus supporting path A.

The preferred reactivity at the Si-C position over the Sc-C is likely due to the steric constraints imposed by the bulky alkyl groups. Simply put, there is not enough space for B(C₆F₅)₃ to approach in sufficient proximity to abstract the entire alkyl group. An experiment between L^tBuSc(CD₃)(CH₂SiMe₃), **d₃-2-Me(CH₂SiMe₃)**, and B(C₆F₅)₃ appears to corroborate this as [L^tBuScCH₂SiMe₃][D₃CB(C₆F₅)₃], **d₃-10-CH₂SiMe₃**, was the only product formed. Evidently, if the sterics permit, the borane preferentially cleaves the weaker Sc-C bond.¹⁰² One final experiment supported path A; no reaction was observed upon addition of the borane to **2-Cl(CH₂SiMe₃)**, even at elevated temperatures. Presumably B(C₆F₅)₃ is not capable of abstracting the entire CH₂SiMe₃ group, nor can it abstract the Si-Me group as the chloride cannot migrate from scandium to silicon.

In conclusion to this section, the success realized with **10-CH₂SiMe₂CH₂SiMe₃** was four-fold: the ion-pair was substantially more soluble, only one isomer was present in solution, it had added thermal stability and was a more realistic model for what is actually present in an industrial polymerization setting as the longer alkyl group represents a growing polymer chain and thus, provides a novel glimpse into previously unstudied ion-pair dynamics. One final obstacle, however, still had to be overcome in order to study intermolecular anion exchange, a comparable ion-pair with a different anion had to be synthesized.

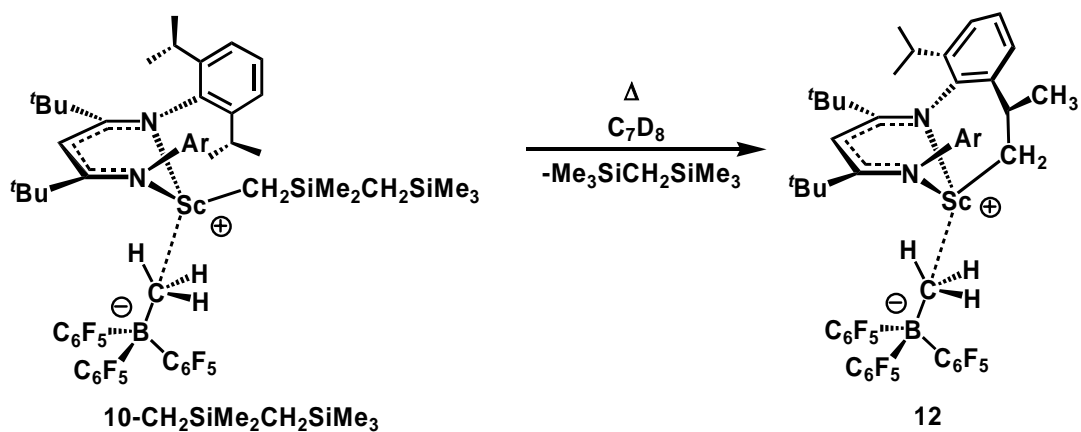
The reactivity established with the C₆F₅ substituted 9-borfluorene and **2-Me** made this activator a logical choice. Reaction of one equivalent of (C₆F₅)B(C₁₂F₈) with

2-CH₂SiMe₃, according to the same experimental protocol employed with B(C₆F₅)₃, cleanly produced the expected ion-pair [L^{tBu}ScCH₂SiMe₂CH₂SiMe₃][MeB(C₆F₅)(C₁₂F₈)], **11-CH₂SiMe₂CH₂SiMe₃** in high yield.

3.2.5 Thermal Decomposition of Organoscandium Cations *via* Metallation of an Isopropyl Methyl Group.

Although the previously discussed organoscandium cations were sufficiently thermally stable to allow detailed mechanistic studies, decomposition by metallation of an *isopropyl* methyl with concomitant loss of RH, as observed for the neutral analogues, indeed occurred over prolonged periods in solution at room temperature (Scheme 3.17). Despite the fact that the process appeared qualitatively slow, and thus was not anticipated to be capable of effectively competing with olefin coordination and insertion in an industrial polymerization setting, a detailed quantitative study was conducted to garner further insight into the decomposition pathway.

While the metallation process can be monitored by ¹H NMR spectroscopy, as with the neutral complexes, the cationic species were advantageous in that they possessed additional NMR active nuclei, namely ¹¹B and ¹⁹F. The ¹⁹F NMR spectrum was especially useful as there were only 3 signals in the cationic starting material attributable to the *ortho*, *para* and *meta* fluorines on the C₆F₅ rings. As the reaction progressed, it was possible to monitor the growth of the new signals for the decomposition product as shown in Figure 3.10. The ¹H NMR spectrum was similar to that observed for the neutral compounds exhibiting a loss of right – left symmetry and growth of RH. Unlike the



Scheme 3.17 Metallation of Cationic Organoscandium Species

neutral complexes, however, the metallated compound, $[\kappa^3\text{-}\{\text{ArNC}(\text{tBu})\text{CHC}(\text{tBu})\text{N-}i\text{Pr-C}_6\text{H}_3\}\text{Sc}][\text{MeB}(\text{C}_6\text{F}_5)_3]$, **12**, existed as two isomers in a 2.5 : 1 ratio. While this would seem to suggest that metallation can occur from either the *exo* or *endo* sites, the fact that an identical ratio is obtained regardless of cationic starting material implies this is actually an equilibrium mixture. Likewise, it was not possible to selectively precipitate one isomer in order to affect the isomeric ratio. Although no sign of ligand flipping was observed for the neutral metallation products, it may be possible for the cationic derivatives as the remaining alkyl group has been replaced with a significantly more mobile $[\text{MeB}(\text{C}_6\text{F}_5)_3]^-$ anion, providing the necessary flexibility to accomplish the flip. This process is likely to be relatively high in energy as it would require partial rotation about the C-N bond. Thus it is not surprising that it was not possible to study this process; no changes were observed in the NMR spectra upon heating the sample to 350 K (Scheme 3.18). The presence of two isomers for **12** was apparent in the ^{19}F NMR spectrum whereby two new sets of C_6F_5 resonances appeared in the same 2.5 : 1 ratio; the *meta* and *para* signals are indistinguishable as they overlap.

The metallation process was quantitatively followed for **10-CH₂SiMe₂CH₂SiMe₃** using both ¹H and ¹⁹F NMR and the reaction was found to be first order in ion-pair. As with the neutral compounds the reaction was followed at a variety of temperatures and the activation parameters of $\Delta S^\ddagger = -7.0(7)$ e.u. and $\Delta H^\ddagger = 21.5(2)$ kcal mol⁻¹ were extracted (Figure 3.11). The enthalpic barrier is similar to that observed for the neutral analogues (cf. 19.7(6) kcal mol⁻¹), however, the entropy of activation, while still negative indicative of an ordered transition state, is significantly lower in magnitude (cf. -17(2) and thus e.u.). This can likely be attributed to the enhanced spatial freedom of the weakly coordinating [MeB(C₆F₅)₃]⁻ anion in the σ -bond metathesis transition state.

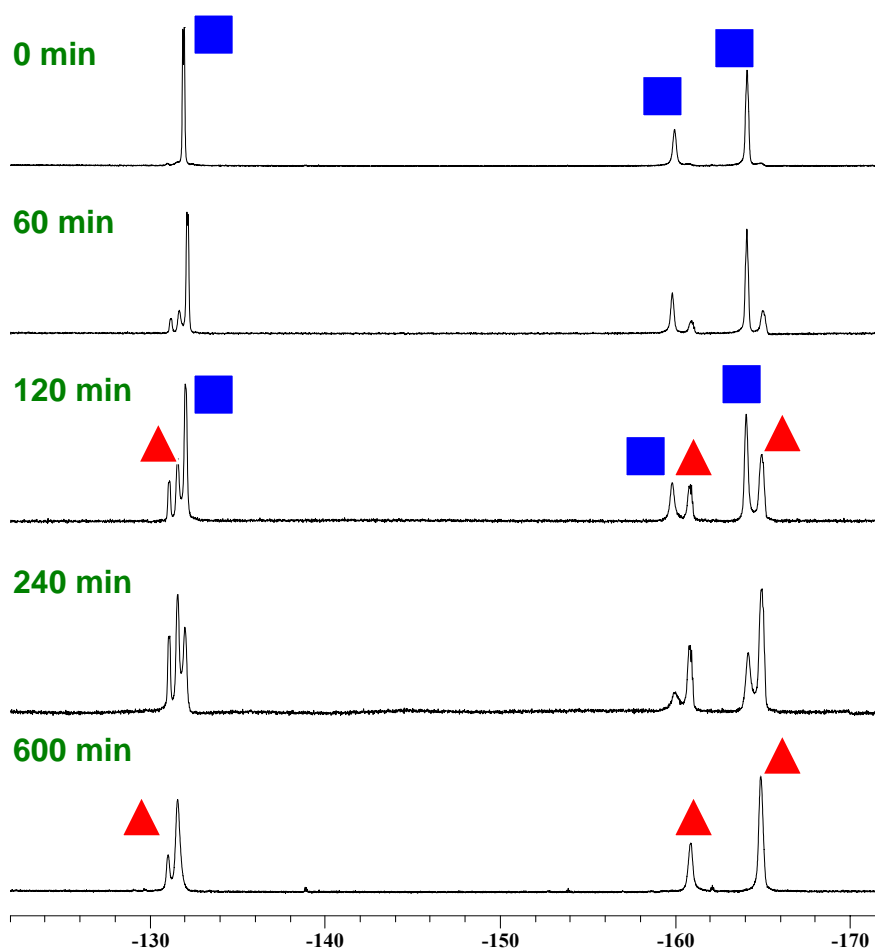
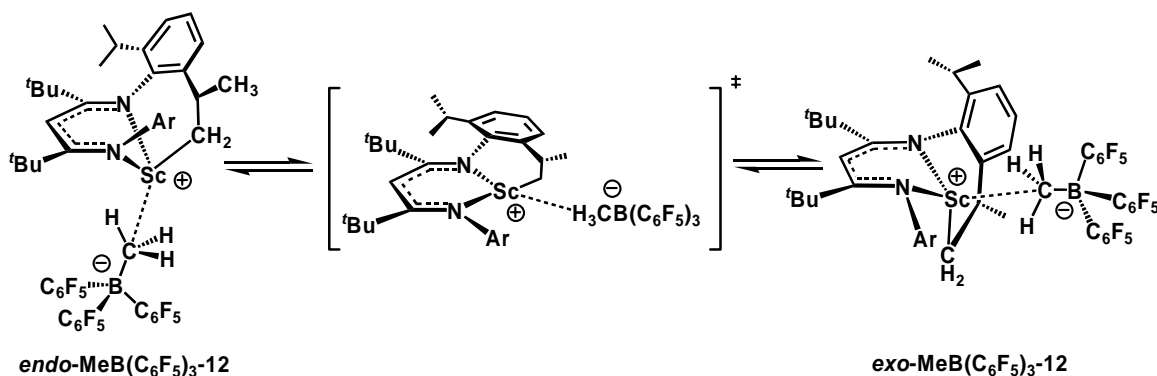


Figure 3.10 Series of ¹⁹F NMR Spectra Acquire in *d*₈-toluene at 308K Monitoring the Thermal Decomposition of **10-CH₂SiMe₂CH₂SiMe₃**.

In order to obtain comparative values and observe meaningful trends between metallation rates and ion-pair structure, a kinetic investigation was completed (Table 3.5). The measured rates for the various ion-pairs were approximately an order of magnitude



Scheme 3.18 Proposed Ligand Flip Mechanism Within Metallated Ion Pair

greater than that determined for the neutral dialkyl species, with the nature of the alkyl group having little impact on the rates. Nonetheless, the deactivation process is remarkably slow with half lives greater than 1 hour at 35 °C in all cases. Both B(C₆F₅)₃ and (C₆F₅)B(C₁₂F₈) activated complexes were studied with similar rates observed for **10-Me** and **11-Me**. Curiously, however, a dramatic rate diminution was observed for the borole activated **11-CH₂SiMe₂CH₂SiMe₃** in comparison to **10-CH₂SiMe₂CH₂SiMe₃**. This enhanced thermal stability may be attributable to the steric properties of the flat borole core which permits the anion to reside in closer proximity to the metal centre than the more sterically encumbered [MeB(C₆F₅)₃]⁻. This notion is substantiated by the ¹⁹F NMR solution data wherein **10-CH₂SiMe₂CH₂SiMe₃** exhibited a Δδ_{m,p} = 4.6 ppm while **11-CH₂SiMe₂CH₂SiMe₃** had a Δδ_{m,p} = 5.1 indicative of tighter ion-pairing. A more tightly bound anion should result in a less electronically deficient, and thus more thermally stable metal centre. These marked differences in decomposition

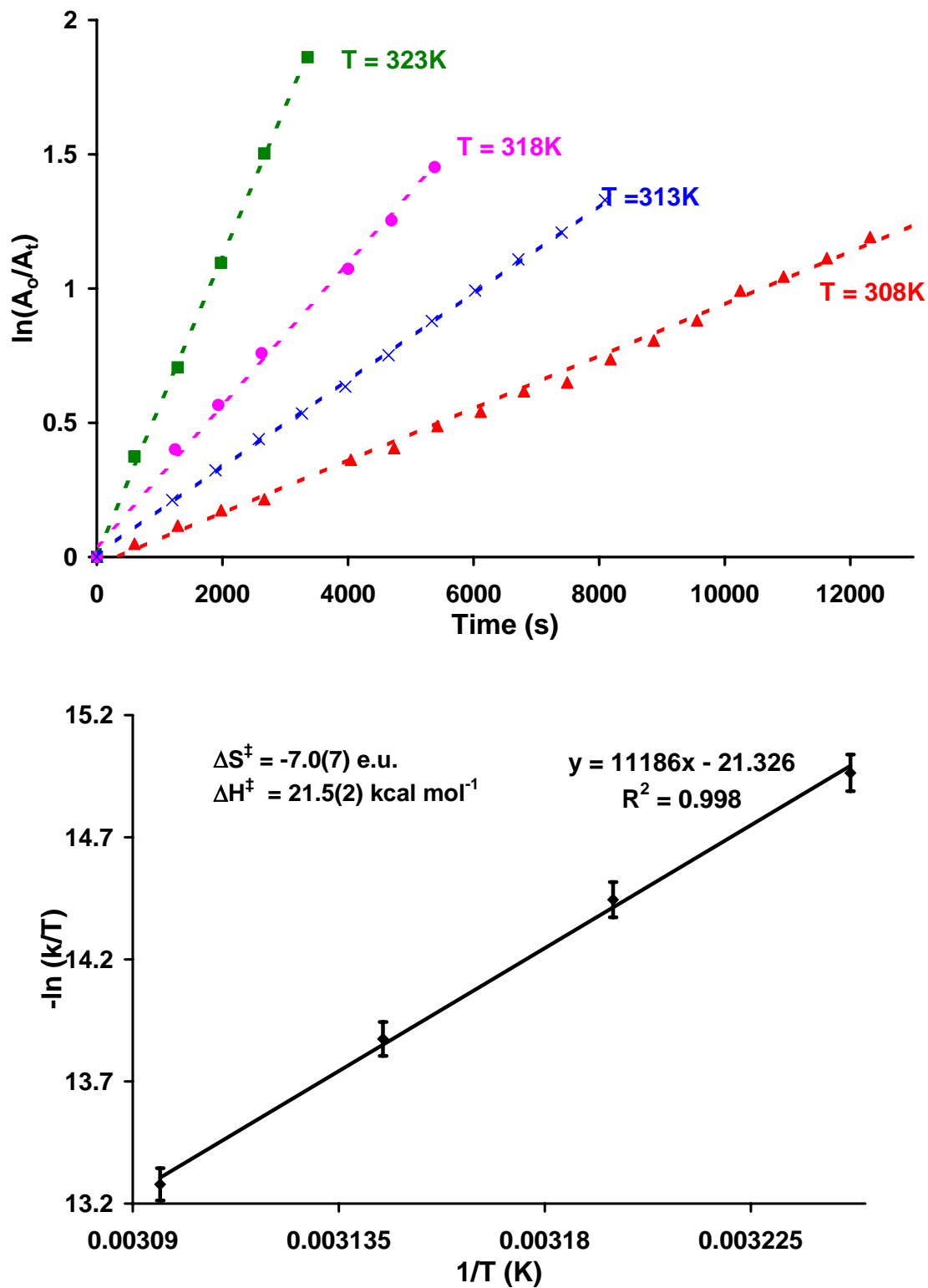


Figure 3.11 Top: Metallation of $10\text{-CH}_2\text{SiMe}_2\text{CH}_2\text{SiMe}_3$, Monitored Quantitatively at Various Temperatures; Bottom: Eyring Plot of Metallation of $10\text{-CH}_2\text{SiMe}_2\text{CH}_2\text{SiMe}_3$

Table 3.5 Half-Lives and k_{exp} for Metallation Reactions

Compound	Borane	Temp (K)	$t_{1/2}$ (hr)	k_{exp} (s^{-1})
Ion-Pairs				
10-Me	$\text{B}(\text{C}_6\text{F}_5)_3$	308	1.83	$1.05(2) \times 10^{-4}$
11-Me	$(\text{C}_6\text{F}_5)\text{B}(\text{C}_{12}\text{F}_8)$	308	1.32	$1.46(2) \times 10^{-4}$
10-CH₂SiMe₂CH₂SiMe₃	$\text{B}(\text{C}_6\text{F}_5)_3$	308	1.97	$9.77(3) \times 10^{-5}$
11-CH₂SiMe₂CH₂SiMe₃	$(\text{C}_6\text{F}_5)\text{B}(\text{C}_{12}\text{F}_8)$	308	7.70	$2.50(3) \times 10^{-5}$
10-CH₂SiMe₂CH₂SiMe₃	$\text{B}(\text{C}_6\text{F}_5)_3$	308	2.0	$1.02(3) \times 10^{-4}$
10-CH₂SiMe₂CH₂SiMe₃	$\text{B}(\text{C}_6\text{F}_5)_3$	308	2.0	$9.79(3) \times 10^{-5}$
10-CH₂SiMe₂CH₂SiMe₃	$\text{B}(\text{C}_6\text{F}_5)_3$	308	2.0	$9.77(3) \times 10^{-5}$
10-CH₂SiMe₂CH₂SiMe₃	$\text{B}(\text{C}_6\text{F}_5)_3$	313	1.2	$1.67(2) \times 10^{-4}$
10-CH₂SiMe₂CH₂SiMe₃	$\text{B}(\text{C}_6\text{F}_5)_3$	318	0.6	$3.00(2) \times 10^{-4}$
10-CH₂SiMe₂CH₂SiMe₃	$\text{B}(\text{C}_6\text{F}_5)_3$	323	0.4	$5.53(3) \times 10^{-4}$
Neutral Compounds				
2-Me	N/A	308	12.26	$1.57(3) \times 10^{-5}$
2-CH₂SiMe₃	N/A	308	17.99	$1.07(2) \times 10^{-5}$

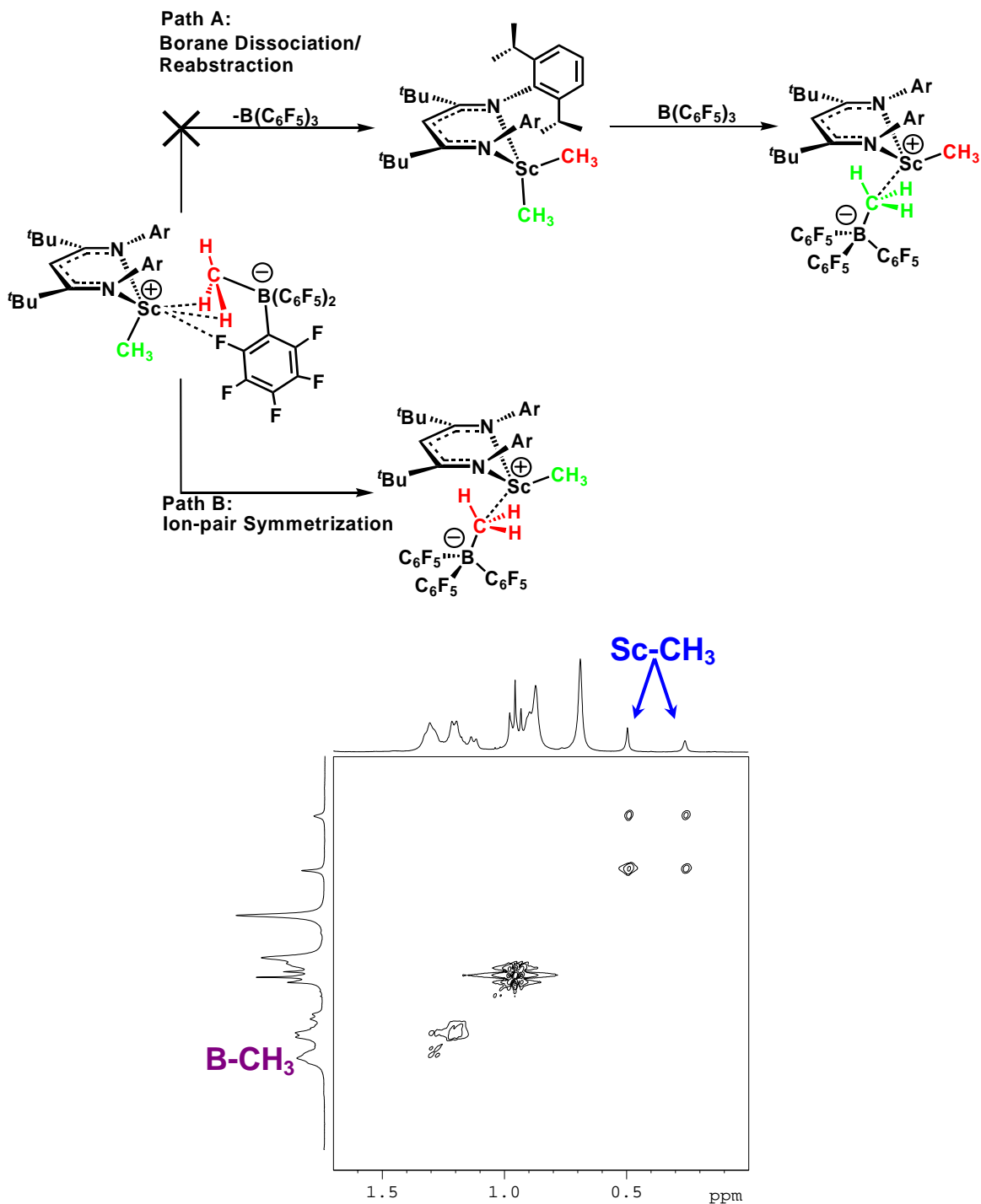
rates illustrate the dramatic effect which minute structural changes can invoke on catalyst reactivity.

3.2.6 Ion-Pair Dynamics of 10-Me

Since **10-Me** existed as two isomers in solution at low temperature it was possible to examine ion-pair dynamics for comparison with the structurally disparate zirconocene systems studied by Marks and Brintzinger. If ion-pair symmetrization was the only operative exchange process there would be exchange between the two Sc-Me and two B-Me resonances, but not between Sc-Me and B-Me peaks. If borane dissociation/reabstraction was competitive with ion-pair symmetrization, exchange between all four methyl resonances would be observed.

A low temperature ^1H - ^1H 2D EXSY experiment exhibited exchange only between

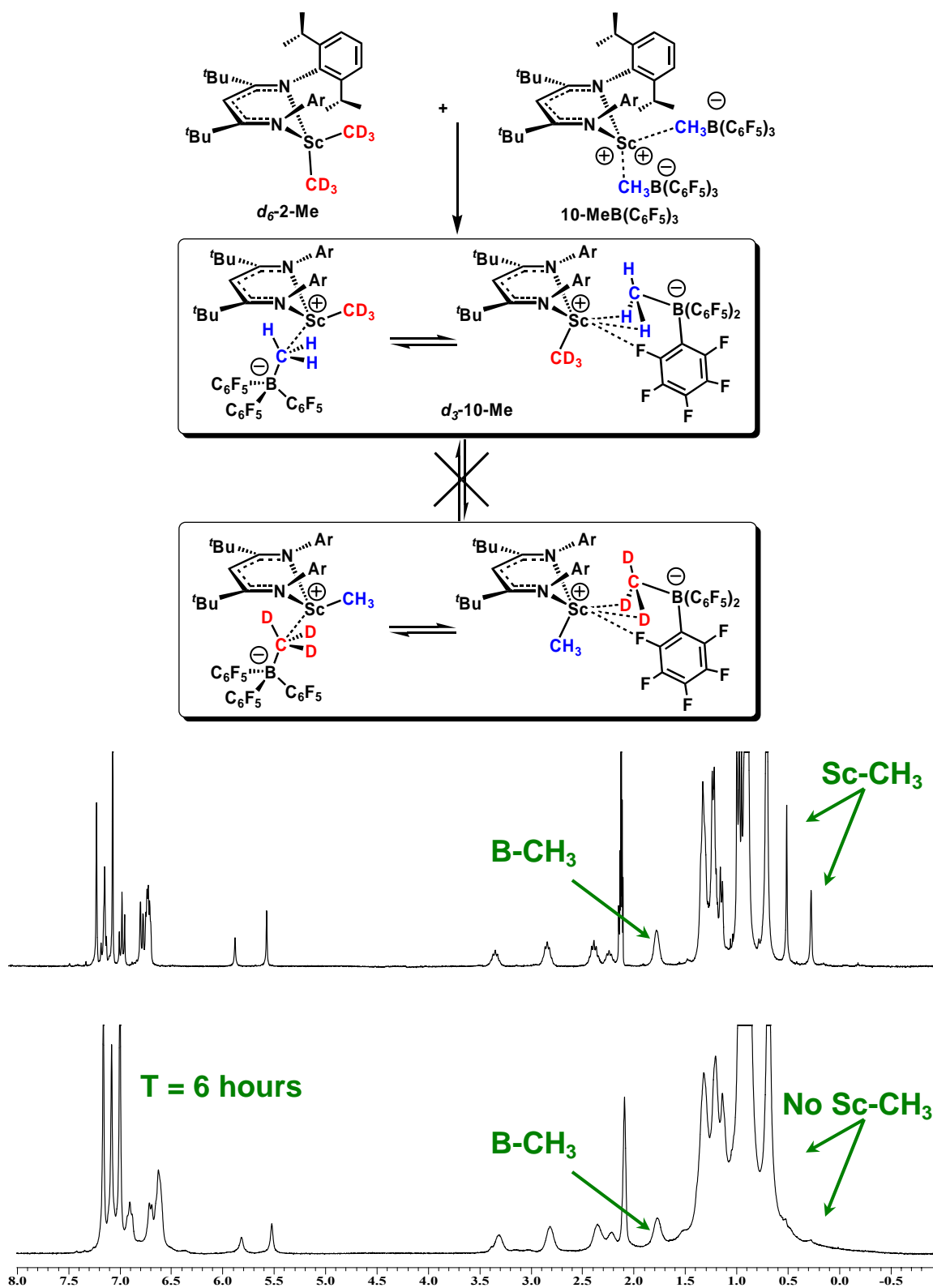
the two Sc-Me signals, suggesting that borane dissociation/reabstraction is not occurring on the NMR timescale at low temperature (Scheme 3.19). The lack of crosspeaks between the $[\text{MeB}(\text{C}_6\text{F}_5)_3]^-$ groups of the two isomers is presumably due to quadrupolar



Scheme 3.19 ^1H - ^1H 2D EXSY NMR of **10-Me**

broadening from the adjacent boron atoms (^{11}B , 80%, $I = 3/2$; ^{10}B , 20%, $I = 3$). In order to unambiguously ascertain if this mechanism was taking place on the chemical timescale, a deuterium labelling experiment was devised whereby **10-MeB(C₆F₅)₃** was reacted at low temperature with one equivalent of $\text{L}^{\text{tBu}}\text{Sc}(\text{CD}_3)_2$, ***d*₆-2-Me**, to form $[\text{L}^{\text{tBu}}\text{ScCD}_3][\text{H}_3\text{CB}(\text{C}_6\text{F}_5)_3]$, ***d*₃-10-Me**, as the exclusive product (Scheme 3.20). If a borane dissociation/reabstraction process was functioning, the deuterium label would wash from the Sc-Me into the B-Me producing an approximately statistical mixture of 1:1 (barring a significant thermodynamic equilibrium isotope effect). The ^1H NMR spectrum acquired in *d*₈-toluene definitively showed complete loss of the Sc-Me resonances with no diminution in the B-Me signals. The reaction was monitored for an additional 6 hours with periodic warming to room temperature; no evidence of deuterium label incorporation into the B-Me, nor growth of Sc-Me signals in the ^1H NMR spectrum was observed (Scheme 3.20). Thus, it can be concluded that borane exchange, if operative, occurs at a rate sufficiently slowly so as not to interfere with quantitative ion-pair symmetrization measurements.

Although the previous experiments determined it should be possible to study ion-pair symmetrization, the system was complicated because it was not possible to determine whether the observed exchange peaks were due to ion-pair symmetrization or ligand flipping. In order to unambiguously study ion-pair dissociation, it was decided that an intermolecular anion exchange would be more appropriate because anion exchange between Sc-nacnac fragments would eliminate complications from a competing ligand flip process, while still providing insight into the mechanism of anion displacement from the metal centre.



Scheme 3.20 Top: Synthesis of [L^{tBu}ScCD₃][H₃CB(C₆F₅)₃], d_3 -10-Me; Bottom: Comparison of ¹H NMR Spectra of with 10 -Me and d_3 -10-Me

Since the backbone signals for all four isomers of **10-Me** and **11-Me** were baseline resolved they could be used to examine anion exchange processes between metal centres. Although it was not experimentally determined, it was assumed that **11-Me** would be similar to **10-Me**, in that borole dissociation would be minimal and non-competitive with intermolecular anion exchange. A ^1H - ^1H 2D EXSY NMR experiment at 213 K clearly exhibited crosspeaks between all four isomers confirming intermolecular anion exchange (Figure 3.12). A comprehensive quantitative study was performed in order to obtain rate data for the various exchange processes (Table 3.6). Repeating the experiments at a variety of temperatures permitted the construction of excellent fit Eyring plots from which extraction of the activation parameters for the exchange processes shown in Figure 3.12 was possible (Table 3.7). A representative Eyring plot of the exchange between, *endo*_{Me}-**10-Me** and *endo*_{Me}-**11-Me** is shown in Figure 3.13.

The ΔS^\ddagger for the intermolecular anion exchange process is negative in all cases, however, the magnitude varies from -7(1) e.u. for exchange between *exo*_{Me}-**11-Me** and *endo*_{Me}-**10-Me** to -12(1) e.u. for exchange between *exo*_{Me}-**10-Me** and *exo*_{Me}-**11-Me** at 0.0197 M. While these values appear to correlate better with Brintzinger's findings than those of Marks' it should be realized that the ion-pair framework is completely different from either of their systems. The negative entropies of activation suggest that the exchange process involves a moderately ordered transition state relative to the ground state, which could be interpreted as associative displacement of the anion by an incoming solvent molecule to form a transient SSIP as suggested by Marks. Alternatively, the data could represent production of an ordered ion-pair quadruple, as postulated by Brintzinger. Interestingly the measured ΔS^\ddagger for exchange between isomers with the same anion

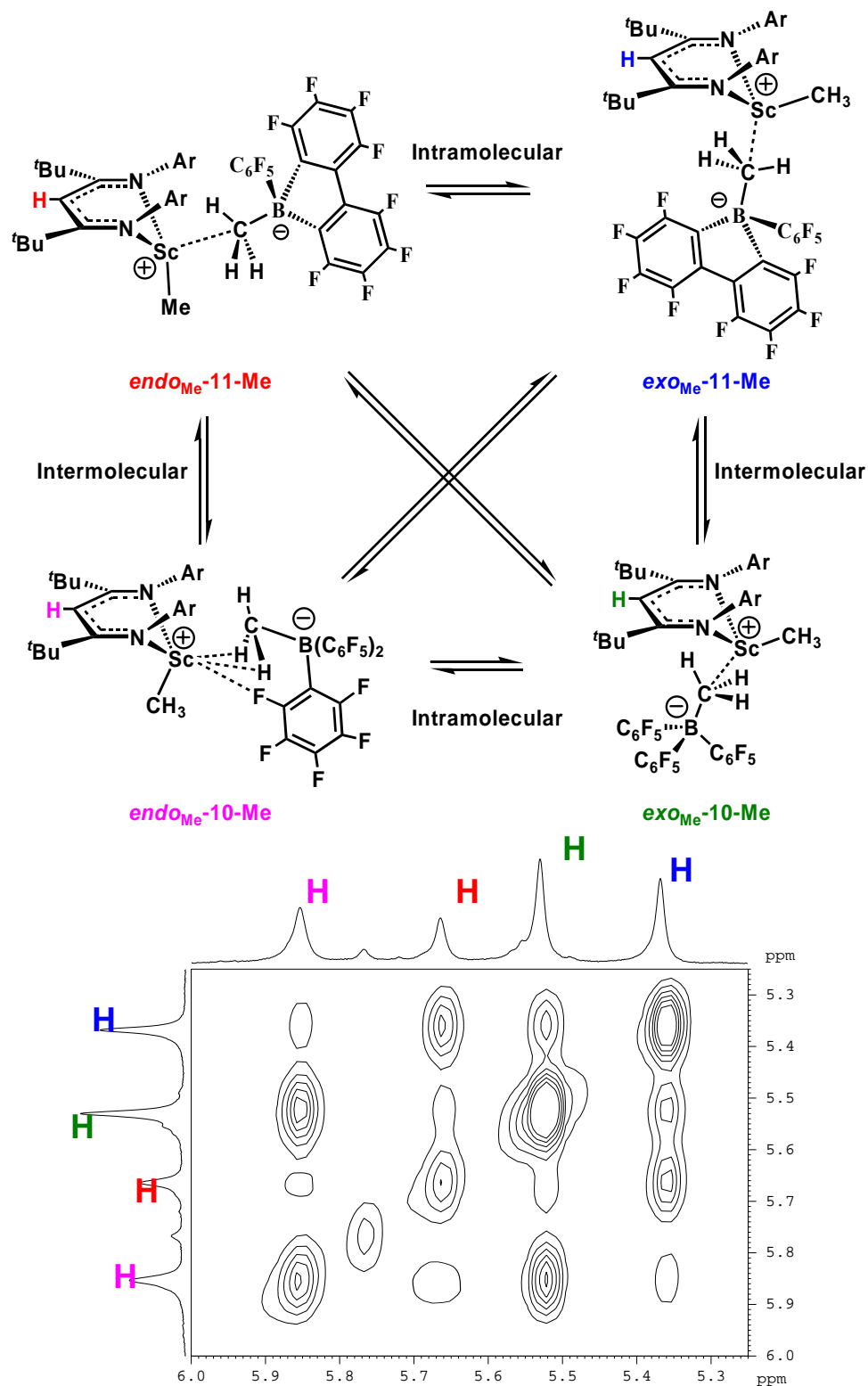


Figure 3.12 Top: Exchange Processes Between 10-Me and 11-Me; Bottom: ¹H-¹H 2D EXSY of 10-Me and 11-Me.

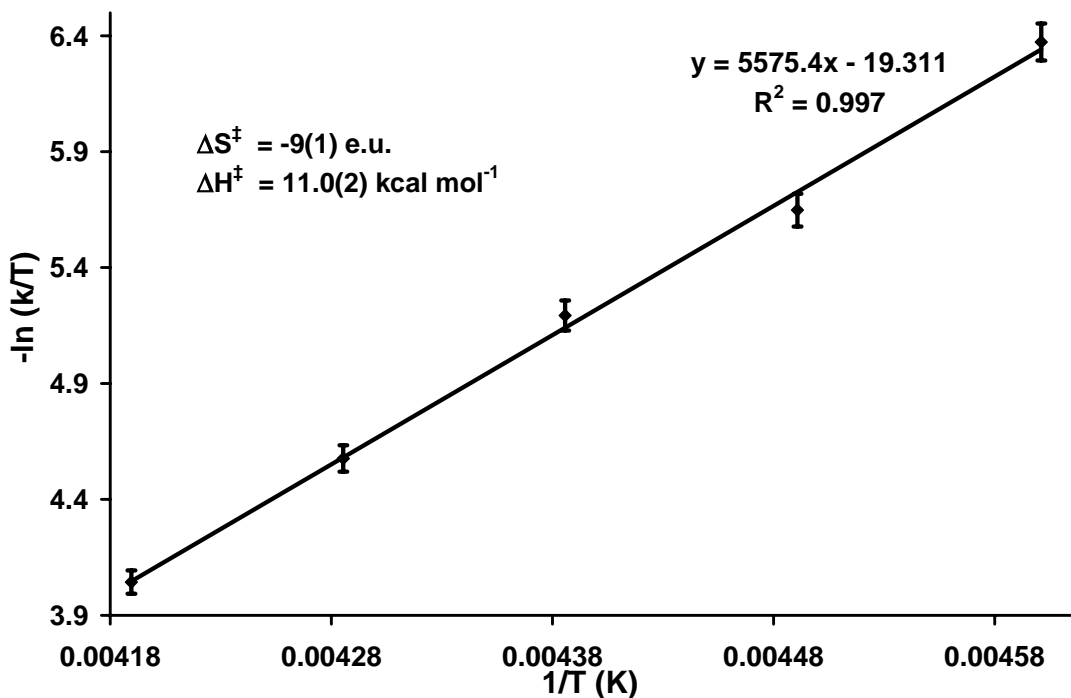


Figure 3.13 Eyring Plot of Intermolecular Anion Exchange Between *endo*_{Me}-**10-Me** and *endo*_{Me}-**11-Me**

(*exo*_{Me}-**10-Me** and *endo*_{Me}-**10-Me** or *exo*_{Me}-**11-Me** and *endo*_{Me}-**11-Me**), are almost entropically neutral with values similar to that observed for the ligand flip process of **2-CH₂SiMe₃**, ($\Delta S^\ddagger = -1.6(5)$ e.u., $\Delta H^\ddagger = 12.9(2)$ kcal mol⁻¹). This fact, combined with four-fold rate enhancements, led to the conclusion that ligand flip is the dominating exchange mechanism in these situations. The ΔH^\ddagger are similar for all of the exchange pathways with low values ranging from 10.5 – 11.8 kcal mol⁻¹.

These small, but measurable differences in the activation entropies for the different isomers suggest that anion exchange may also involve ligand flip, especially if an ion-pair quadruple mechanism is operative. For example, if *exo*_{Me}-**10-Me** and *endo*_{Me}-**11-Me** exchange, ligand flip is presumed to be involved causing an overall

Table 3.6 Rate Data for Exchange Reactions Between **10-Me** and **11-Me**

Compound A	Compound B	k_{exp} (s^{-1})	T(K)	
<i>exo</i> _{Me} -10-Me	<i>exo</i> _{Me} -11-Me	0.52(1)	222.7	} Inter
<i>exo</i> _{Me} -10-Me	<i>exo</i> _{Me} -11-Me	0.73(2)	228.0	
<i>exo</i> _{Me} -10-Me	<i>exo</i> _{Me} -11-Me	1.68(2)	233.4	
<i>exo</i> _{Me} -10-Me	<i>exo</i> _{Me} -11-Me	2.50(2)	238.7	
<i>exo</i> _{Me} -10-Me	<i>endo</i> _{Me} -11-Me	0.51(1)	222.7	
<i>exo</i> _{Me} -10-Me	<i>endo</i> _{Me} -11-Me	0.80(1)	228.0	
<i>exo</i> _{Me} -10-Me	<i>endo</i> _{Me} -11-Me	1.67(1)	233.4	
<i>exo</i> _{Me} -10-Me	<i>endo</i> _{Me} -11-Me	3.04(3)	238.7	
<i>endo</i> _{Me} -10-Me	<i>exo</i> _{Me} -11-Me	0.23(1)	217.3	
<i>endo</i> _{Me} -10-Me	<i>exo</i> _{Me} -11-Me	0.50(1)	222.7	
<i>endo</i> _{Me} -10-Me	<i>exo</i> _{Me} -11-Me	0.73(1)	228.0	
<i>endo</i> _{Me} -10-Me	<i>exo</i> _{Me} -11-Me	1.59(3)	233.4	
<i>endo</i> _{Me} -10-Me	<i>exo</i> _{Me} -11-Me	3.00(3)	238.7	
<i>endo</i> _{Me} -10-Me	<i>endo</i> _{Me} -11-Me	0.37(1)	217.3	
<i>endo</i> _{Me} -10-Me	<i>endo</i> _{Me} -11-Me	0.78(2)	222.7	
<i>endo</i> _{Me} -10-Me	<i>endo</i> _{Me} -11-Me	1.27(1)	228.0	
<i>endo</i> _{Me} -10-Me	<i>endo</i> _{Me} -11-Me	2.40(3)	233.4	
<i>endo</i> _{Me} -10-Me	<i>endo</i> _{Me} -11-Me	4.19(4)	238.7	
<i>endo</i> _{Me} -10-Me	<i>exo</i> _{Me} -10-Me	0.68(2)	217.3	} Intra
<i>endo</i> _{Me} -10-Me	<i>exo</i> _{Me} -10-Me	2.30(3)	222.7	
<i>endo</i> _{Me} -10-Me	<i>exo</i> _{Me} -10-Me	4.03(4)	228.0	
<i>endo</i> _{Me} -10-Me	<i>exo</i> _{Me} -10-Me	7.12(6)	233.4	
<i>endo</i> _{Me} -10-Me	<i>exo</i> _{Me} -10-Me	12.60(9)	238.7	
<i>endo</i> _{Me} -10-Me	<i>exo</i> _{Me} -10-Me	26.9(2)	244.0	
<i>exo</i> _{Me} -11-Me	<i>endo</i> _{Me} -11-Me	0.63(1)	217.3	
<i>exo</i> _{Me} -11-Me	<i>endo</i> _{Me} -11-Me	2.02(2)	222.7	
<i>exo</i> _{Me} -11-Me	<i>endo</i> _{Me} -11-Me	3.18(3)	228.0	
<i>exo</i> _{Me} -11-Me	<i>endo</i> _{Me} -11-Me	5.82(6)	233.4	
<i>exo</i> _{Me} -11-Me	<i>endo</i> _{Me} -11-Me	9.95(9)	238.7	
<i>exo</i> _{Me} -11-Me	<i>endo</i> _{Me} -11-Me	26.7(2)	244.0	

Table 3.7 Activation Parameters for Exchange Reactions Between **10-Me** and **11-Me**

Compound #1	Compound #2	k_{exp} at 223K (s ⁻¹)	ΔG^\ddagger (kcal mol ⁻¹)	ΔH^\ddagger (kcal mol ⁻¹)	ΔS^\ddagger (e.u.)
<i>exo</i> _{Me} -10-Me	<i>exo</i> _{Me} -11-Me	0.52(1)	13.2(3)	10.5(3)	-12(1)
<i>endo</i> _{Me} -10-Me	<i>endo</i> _{Me} -11-Me	0.78(2)	13.0(3)	11.0(2)	-9(1)
<i>endo</i> _{Me} -10-Me	<i>exo</i> _{Me} -11-Me	0.49(1)	13.3(3)	11.8(2)	-7(1)
<i>exo</i> _{Me} -10-Me	<i>endo</i> _{Me} -11-Me	0.51(1)	13.3(3)	11.6(3)	-7(1)
<i>exo</i> _{Me} -10-Me	<i>endo</i> _{Me} -10-Me	2.30(2)	12.7(2)	13.2(2)	2(1)
<i>exo</i> _{Me} -11-Me	<i>endo</i> _{Me} -11-Me	2.02(2)	12.7(2)	13.2(3)	2(1)

decrease in the entropy of activation, in comparison to cognate isomers such as *endo*_{Me}-10-Me and *endo*_{Me}-11-Me, which can presumably exchange without the added complexity of ligand flip. Since it is not possible to delineate these processes, the values obtained cannot be considered good representations of intermolecular anion exchange. Thus the study is merely considered to be qualitative evidence that intermolecular anion exchange can indeed occur within these systems. It is important to note that the actual rates are further complicated by the fact that the isomers are not present in equal concentrations which may be partially responsible for the observed variations.

Although a variety of studies were undertaken to determine the order of the reaction, it was not possible to obtain a sufficiently broad range of concentrations to unambiguously establish the dependence on metal complex concentration. These attempts were hampered by the relatively low solubility of the ion-pairs in cold hydrocarbon solvents; if the concentration exceeded $\sim 3 \times 10^{-2}$ M the compounds would begin to crystallize during the course of the time required to accurately obtain meaningful kinetic data (2 or more hours). Conversely, if the concentration was below $\sim 1.5 \times 10^{-2}$ M

it was not possible to obtain quantitative data in a realistic timeframe. For example, at these concentrations even 24 hour long EXSY experiments did not provide reliable rates. Unfortunately, 1D line broadening techniques were not possible due to the lack of sufficient separation of the backbone resonances. All other resonances were not suitable as the reaction mixture contained four different isomers, resulting in overlap of the remaining signals.

3.2.7 Ion-pair Dynamics of $10\text{-CH}_2\text{SiMe}_2\text{CH}_2\text{SiMe}_3$

In order to ascertain the feasibility of obtaining quantitative exchange measurements for the significantly more simple $10\text{-CH}_2\text{SiMe}_2\text{CH}_2\text{SiMe}_3/$

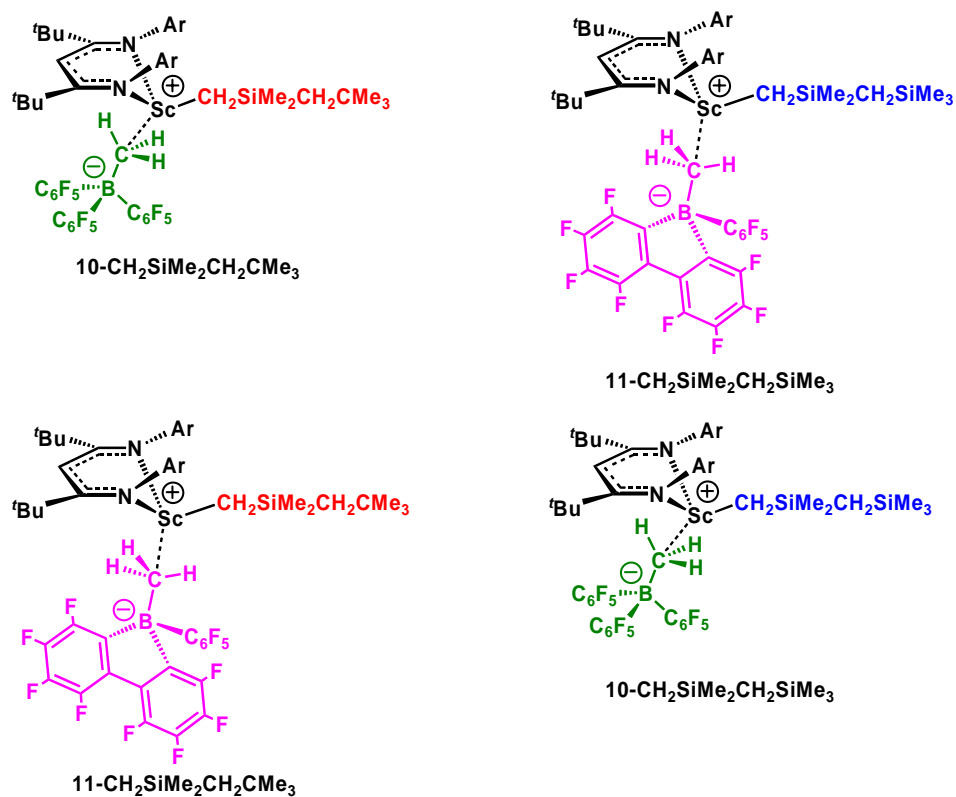


Figure 3.14 Crossover Products from Reaction of $10\text{-CH}_2\text{SiMe}_2\text{CH}_2\text{CMe}_3$ and $11\text{-CH}_2\text{SiMe}_2\text{CH}_2\text{SiMe}_3$

11-CH₂SiMe₂CH₂SiMe₃ system, a classical crossover experiment was designed to see if there was any exchange on a chemical timescale. Since a crossover experiment necessarily has two different variables it was necessary to differentiate at the metal, as well as at the borate anion. This was accomplished by using the previously synthesized

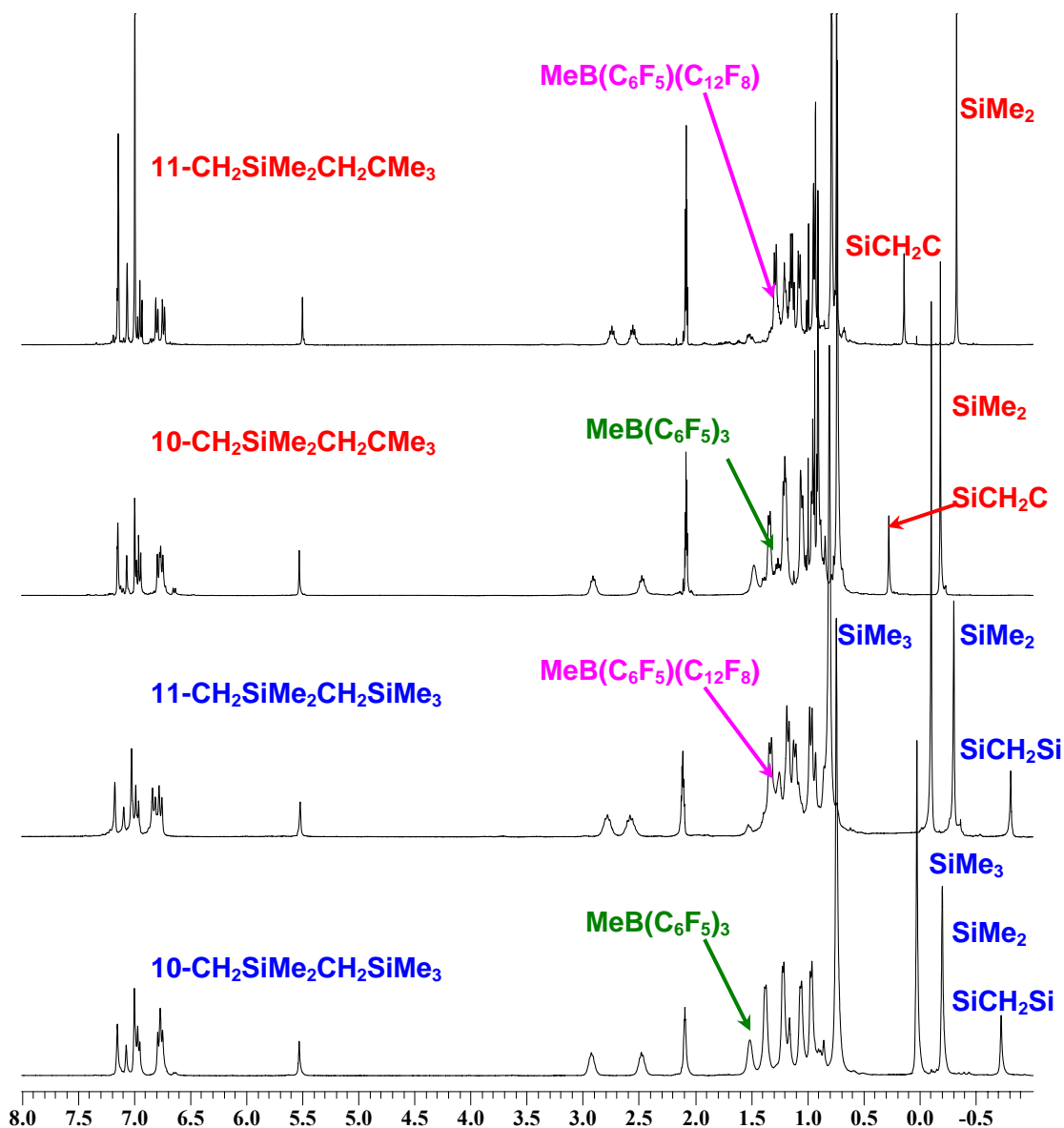


Figure 3.15 ¹H NMR Spectra of the Independently Synthesized Products from the Crossover Experiment Between **10-CH₂SiMe₂CH₂CMe₃** and **11-CH₂SiMe₂CH₂SiMe₃**

10-CH₂SiMe₂CH₂CMe₃ which differs at the metal alkyl; a carbon is in the δ position as opposed to a silicon atom in **11-CH₂SiMe₂CH₂SiMe₃**. The crossover experiment, which involved stoichiometric reaction of **10-CH₂SiMe₂CH₂CMe₃** and **11-CH₂SiMe₂CH₂SiMe₃**, was conducted; all four of the possible crossover products resulting from intermolecular anion exchange are outlined in Figure 3.14.

While the ¹H NMR spectrum of the crossover experiment appeared to indicate the presence of four species in a 1:1:1:1 statistical mixture the complexity of the spectrum

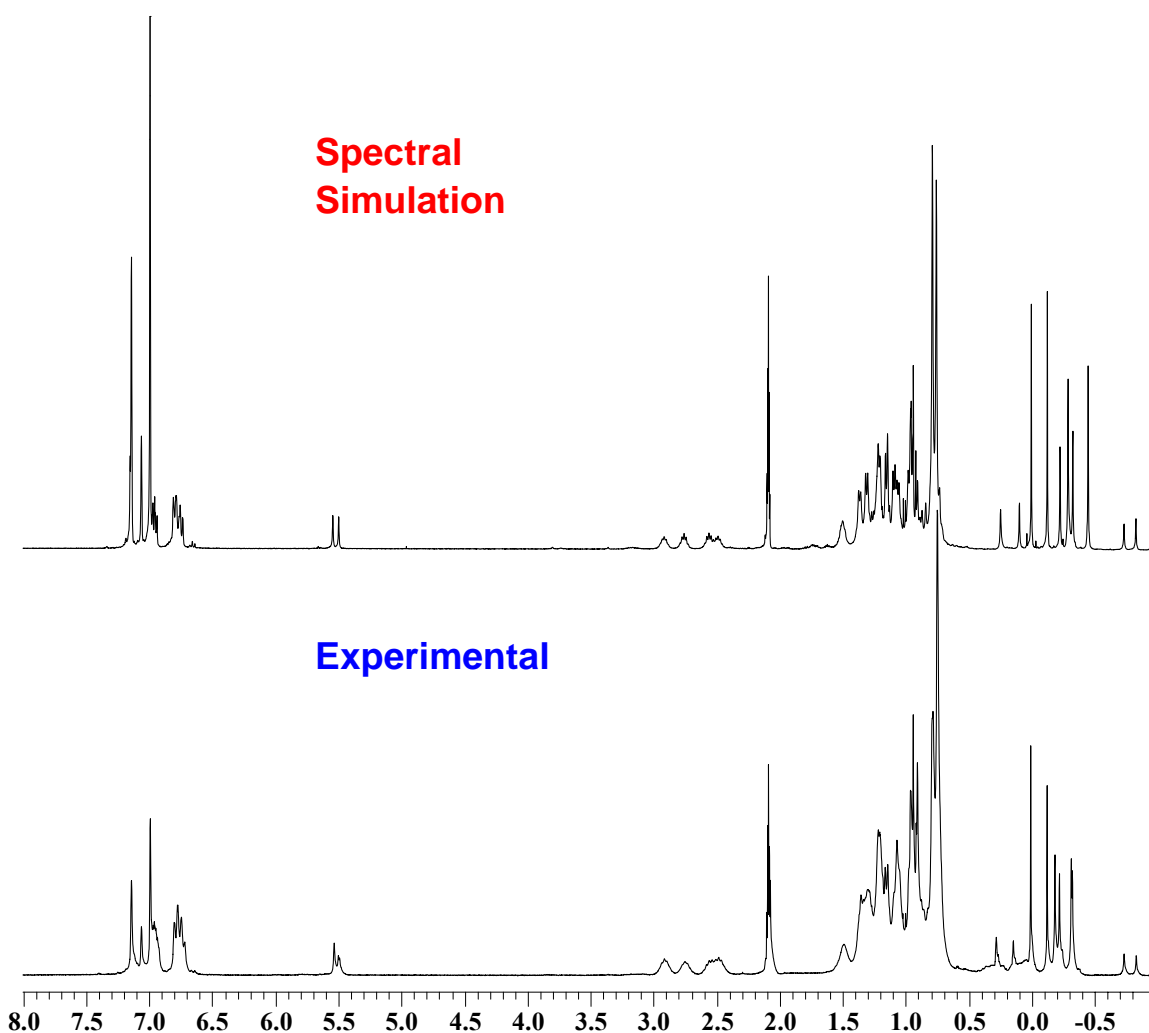


Figure 3.16 Top: Manually Summed ¹H NMR Spectra of Independently Synthesized Crossover Products. Bottom: Actual ¹H NMR Spectrum of Crossover Experiment

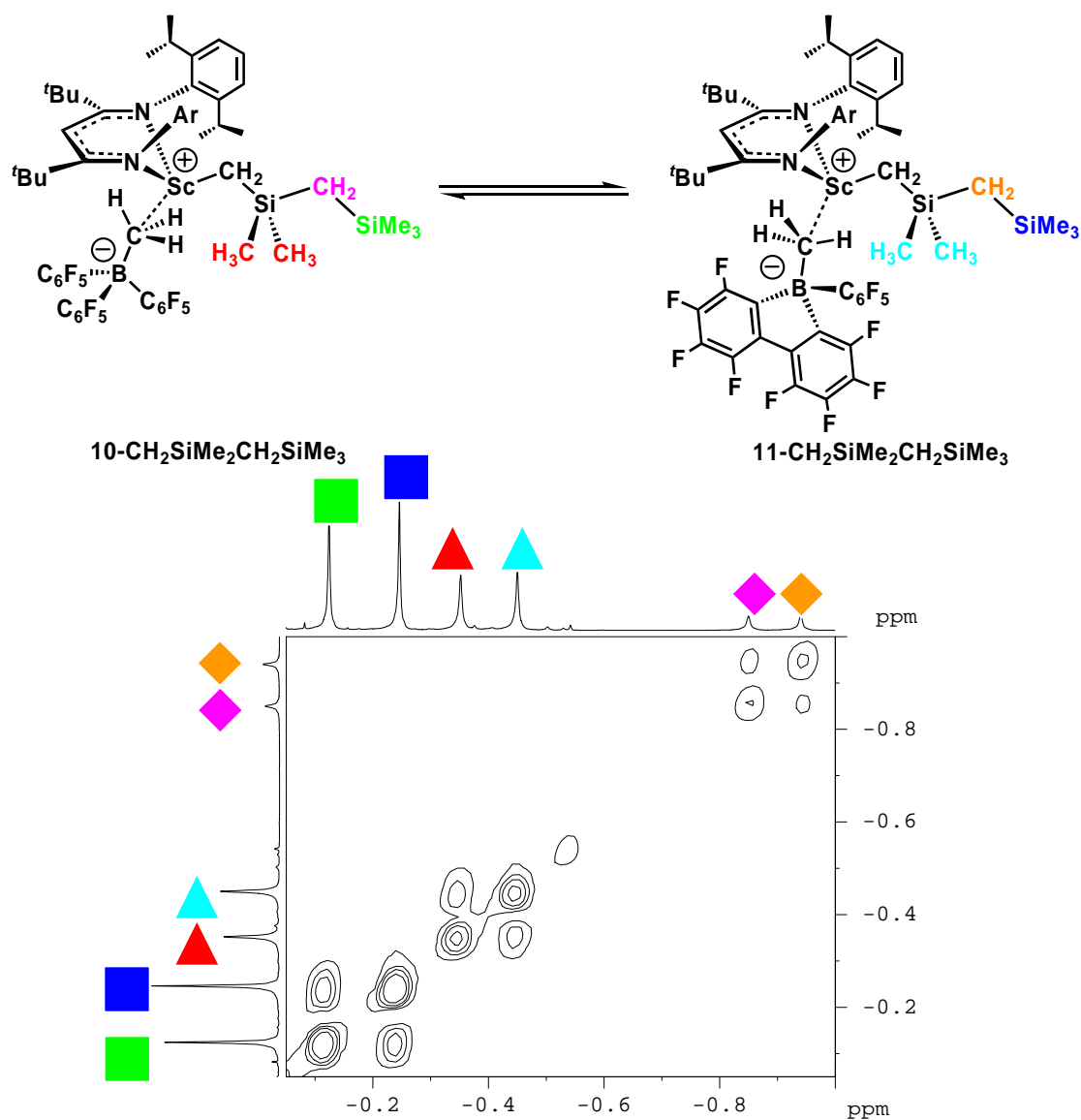


Figure 3.17 ^1H - ^1H 2D EXSY NMR Spectrum of **10-CH₂SiMe₂CH₂SiMe₃** and **11-CH₂SiMe₂CH₂SiMe₃**

made it difficult to conclude with certainty that the observed species were in fact the expected compounds. To eliminate any ambiguity all four of the species were independently synthesized, the ^1H NMR of each is shown in Figure 3.15. These spectra were then computationally summed in a 1:1:1:1 ratio for comparison with experimental results. The agreement between the simulated and experimental spectra was excellent with the most diagnostic region being upfield of 0.5 ppm where 10 resonances for the

alkyl chains were present in a 2:2:9:9:6:6:6:6:2:2 ratio. The crossover experiment unambiguously established intermolecular anion exchange between all four isomers (Figure 3.16).

Table 3.8 Rate Data for Intermolecular Anion Exchange Between **10-CH₂SiMe₂CH₂SiMe₃** and **11-CH₂SiMe₂CH₂SiMe₃**

Compound A	Compound B	k_{exp} (s ⁻¹)	T(K)
10-CH₂SiMe₂CH₂SiMe₃	11-CH₂SiMe₂CH₂SiMe₃	9.56(8)	250.4
10-CH₂SiMe₂CH₂SiMe₃	11-CH₂SiMe₂CH₂SiMe₃	5.20(4)	244.0
10-CH₂SiMe₂CH₂SiMe₃	11-CH₂SiMe₂CH₂SiMe₃	5.17(4)	244.0
10-CH₂SiMe₂CH₂SiMe₃	11-CH₂SiMe₂CH₂SiMe₃	5.12(4)	244.0
10-CH₂SiMe₂CH₂SiMe₃	11-CH₂SiMe₂CH₂SiMe₃	5.24(4)	244.0
10-CH₂SiMe₂CH₂SiMe₃	11-CH₂SiMe₂CH₂SiMe₃	2.57(3)	237
10-CH₂SiMe₂CH₂SiMe₃	11-CH₂SiMe₂CH₂SiMe₃	1.36(1)	226.4
10-CH₂SiMe₂CH₂SiMe₃	11-CH₂SiMe₂CH₂SiMe₃	0.85(1)	221.3
10-CH₂SiMe₂CH₂SiMe₃	11-CH₂SiMe₂CH₂SiMe₃	0.50(1)	217.1

Since the results of the crossover experiment proved intermolecular anion exchange indeed takes place for the bulky ion-pairs on the chemical timescale, a quantitative study of anion exchange between **10-CH₂SiMe₂CH₂SiMe₃** and **11-CH₂SiMe₂CH₂SiMe₃** (Table 3.8) was performed using ¹H-¹H 2D EXSY NMR techniques; a typical spectrum is depicted in Figure 3.17. Unlike the Sc-methyl compounds, the resonances for the CH backbone of the two compounds were not baseline resolved using a 400 MHz spectrometer, necessitating the utilization of other signals in the spectrum. Fortunately, the Sc-alkyl resonances, located upfield of 0 ppm, were well separated, providing three separate sets of peaks, integrating as 9H, 6H and 2H for the SiMe₃, SiMe₂ and SiCH₂Si groups respectively, which could be used for quantitative analysis. The presence of these peaks were beneficial for two reasons: first, the large

number of protons giving rise to each signal allowed for shorter experiment times, and second, the three sets of peaks provided a facile method to verify the precision of the data.

The 2D EXSY spectra exhibited the expected crosspeaks and thus were acquired at a variety of temperatures which provided the opportunity to construct an Eyring plot and extract the associated activation parameters for the intermolecular anion exchange process (Figure 3.18). The activation parameters ($\Delta S^\ddagger = -20(2)$ e.u., $\Delta H^\ddagger = 8.7(3)$ kcal mol⁻¹) differ substantially from those obtained for the exchange processes studied within **10-Me** and **11-Me**. The entropy of activation is significantly more negative (cf. $-7(1) - -12(1)$ e.u.) supporting the notion that the competing ligand flip process was interfering and decreasing this value in the Sc-Me compounds. Likewise, the enthalpy of activation is reflective of a lower energy process. Since the values obtained for the long chain alkyl

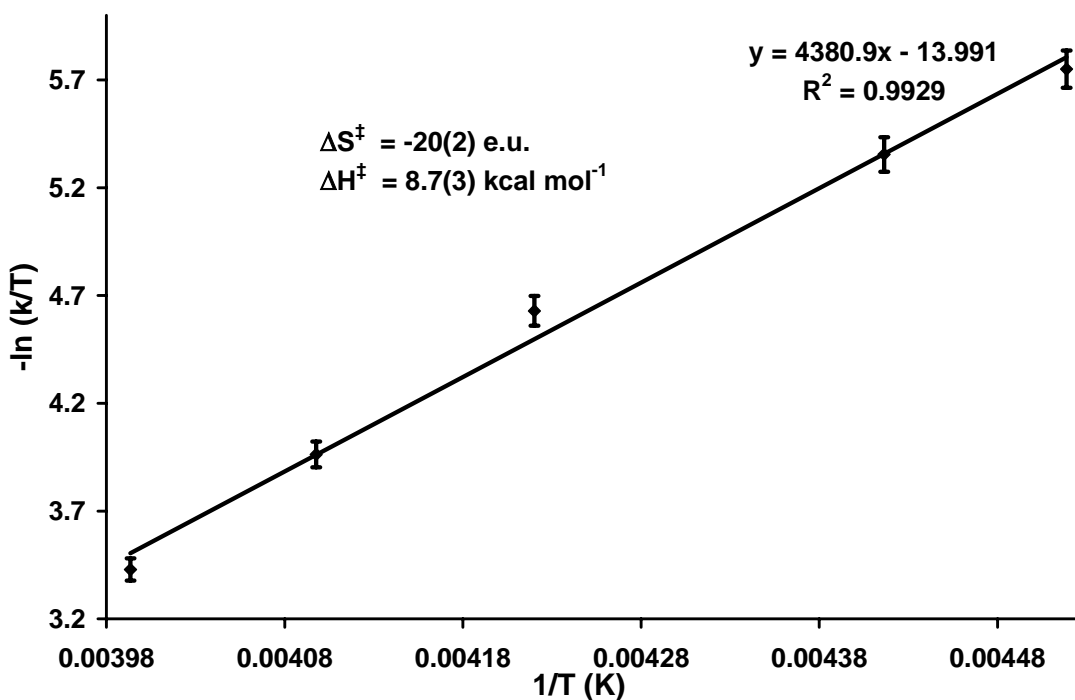


Figure 3.18 Eyring Plot of Intermolecular Anion Exchange Between **10-CH₂SiMe₂CH₂SiMe₃** and **11-CH₂SiMe₂CH₂SiMe₃**

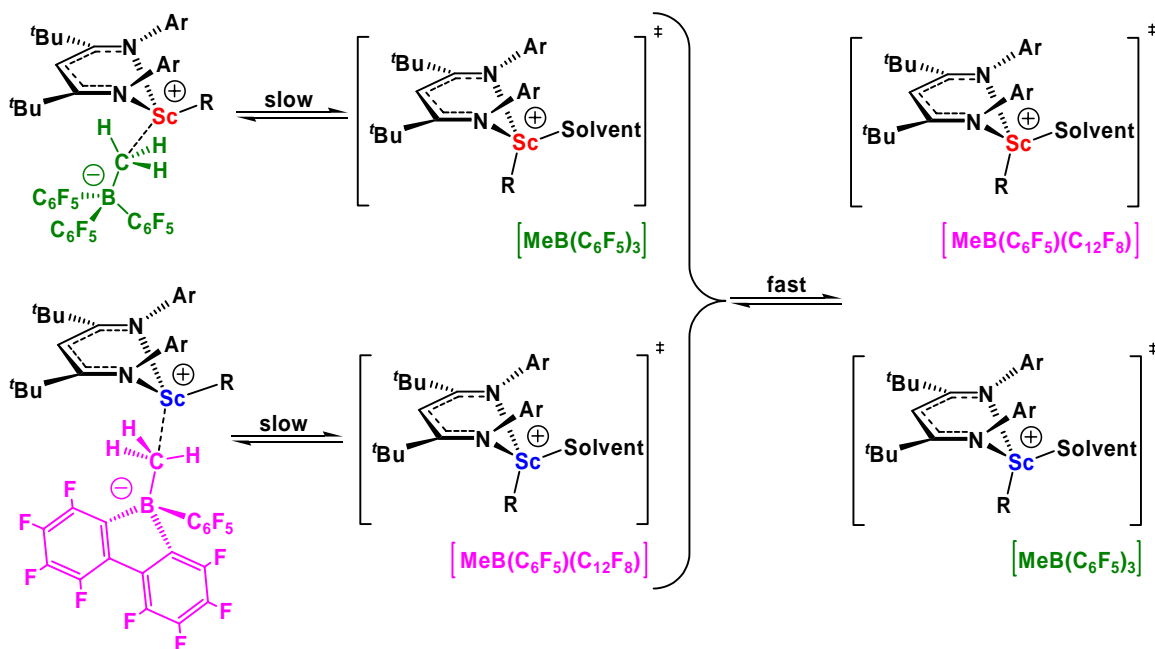
system are a better reflection of the intended intermolecular anion exchange process whereby cation – anion separation is rate limiting, it is now possible to be confident in the results and to make meaningful conclusions as to the nature of the mechanistic pathway. Unlike Marks' and Ziegler's findings with the zirconocene systems, large negative ΔS^\ddagger values are observed suggesting an associative exchange process. It is plausible that the anion displacement occurs *via* a similar pathway to the solvent assisted process (Scheme 3.2), with the major difference being that the large negative entropy value clearly suggests an associative mechanism (Scheme 3.21). The rate determining step would presumably involve an incoming solvent molecule associatively displacing the $[\text{MeB}(\text{C}_6\text{F}_5)_3]^-$ anion to form an intermediate SSIP with the solvent molecule sandwiched between the cation and anion. From this point, the anion would be free to undergo rapid productive exchange with another solvent sandwiched ion-pair. Since **11-CH₂SiMe₂CH₂SiMe₃** has a larger $\Delta\delta_{\text{m,p}}$ it is probable that the ion-pair is more tightly bound, and thus anion displacement is slower than that in **10-CH₂SiMe₂CH₂SiMe₃**.

The shift from a dissociative to an associative mechanism may be the result of significantly more cation – anion separation in the ground state, as evidenced by NMR spectroscopy and X-ray crystallography. As such, it is easier for an incoming arene to associatively displace the outgoing anion. The dramatically lower enthalpic barrier observed for this system is to be expected for the same rationale.

Once again, solubility limits precluded rigorous determination of the order in the concentration of ion-pair, however, the limited data does suggest a first order dependence in **11-CH₂SiMe₂CH₂SiMe₃**. Although the observed activation data, especially the negative ΔS^\ddagger , could be interpreted as an ion-pair quadruple transition state, the

substantially lower ΔH^\ddagger value, the greater steric bulk of the ion-pair, and the inability of Marks, Ziegler and Landis to provide evidence for ion-pair quadruples, tend to discredit this pathway in support of a solvent assisted transition state.

If scandium alkyl ion-pairs, indeed undergo a low energy associative displacement by an incoming arene molecule as the first step in olefin polymerization, the ability to experimentally study subsequent steps in the process, namely solvent displacement by incoming monomer, is paramount. This will shed light onto how the entire polymerization pathway occurs in these systems, and allow comparisons of the energetics required for each step of the process. This information is invaluable from a synthetic chemist's perspective as it will provide insight into which aspects of the catalyst system should be fine tuned, and exactly how they should be adjusted to produce a more active polymerization catalyst. The low barrier for anion dissociation would tend to



Scheme 3.21 Proposed Mechanism for Intermolecular Anion Exchange

suggest that ion-pair separation is not turnover limiting in scandium nacnac catalyzed alkene polymerization, however, further studies are required to confirm this speculation. Thus, in order to obtain information on the latter steps of the polymerization process, it was necessary to synthesize a stable aromatic solvent separated ion-pair, which could serve as a decent model for the aforementioned solvent sandwich transition state, to be used for probing arene displacement and olefin insertion. This was achieved with the successful synthesis of $[L^{\text{Me}}\text{Sc}(\text{arene})][\text{B}(\text{C}_6\text{F}_5)_4]$; complete experimental and mechanistic details are discussed at length in Chapter 4.

3.2.8 Conclusions

In conclusion, a family of highly reactive organoscandium alkyl cations has been prepared and their ion-pair dynamics quantitatively examined. While the L^{Me} ancillary lacked sufficient steric bulk to prevent deleterious deactivation pathways, most notably C_6F_5 transfer to the metal centre, the L^{tBu} derivatives were quite robust in solution. Although these species were subject to thermal decomposition *via* metallation of an *isopropyl* group and loss of RH, the process was not sufficiently rapid to hinder the development of their rich organometallic chemistry. The solution and solid state structures were studied in detail, revealing the presence of both *exo* and *endo*- $\text{MeB}(\text{C}_6\text{F}_5)_3$ isomers if the metal alkyl was small. Deuterium labeling and 2D NMR techniques established that intermolecular anion exchange processes could be probed without the interference of competitive borane dissociation/reabstraction processes. While the quantitative analysis for the energetics associated with cation – anion

dissociation were complicated with ligand flip processes, increasing the steric bulk of the metal alkyl eliminated this complexity as only the *endo*-MeB(C₆F₅)₃ isomer was observed. As such, it was established that intermolecular anion exchange occurs by way of a highly ordered transition state, most likely a low energy associative anion displacement by an incoming arene solvent molecule. In order to delve further into the deconvolution of mechanistic pathways and garner a deeper understanding of the various processes involved in nacnac supported organoscandium catalyzed olefin polymerization, a family of aromatic solvent separated ion-pairs was synthesized, the chemistry of which will be outlined in detail in the following chapter.

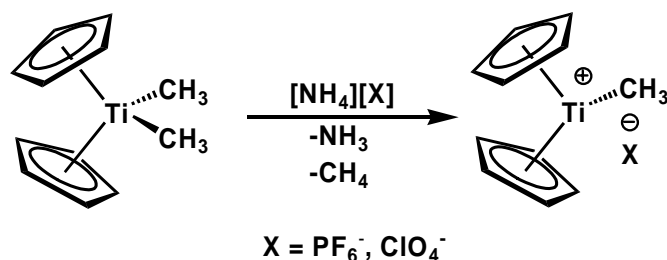
Chapter 4:

Activation of Neutral Organoscandium Complexes with Non-Borane-Based Activators

4.1 Introduction

4.1.1 Activation of Metallocenes with Protic Activators – $[\text{HNMe}_2\text{Ph}][\text{B}(\text{C}_6\text{F}_5)_4]$

Alkyl group abstraction from dialkyl metallocenes with $\text{B}(\text{C}_6\text{F}_5)_3$ to afford active olefin polymerization catalysts was preceded several years by a protonolysis approach. This strategy was first reported by Bochmann and co-workers in 1986 when Cp_2TiMe_2 was reacted with $[\text{NH}_4][\text{PF}_6]$ and $[\text{NH}_4][\text{ClO}_4]$ (Scheme 4.1).^{152,153} In this situation the



Scheme 4.1 Protic Activation of Cp_2TiMe_2 with $[\text{NH}_4][\text{X}]$; $\text{X} = \text{PF}_6^-, \text{ClO}_4^-$

activator irreversibly removes a metal alkyl fragment while instituting a loosely associated anion. Although this example proved the validity of the activation method, a less reactive anion was desired. Soon after, Marks *et al.* reported the use of trialkyl ammonium borate reagents for the transformation of Cp^*ThMe_2 to $[\text{Cp}^*\text{ThMe}][\text{BPh}_4]$.¹⁵⁴ With these activators the metal alkyl is protonated to liberate RH as in Bochmann's system, however, the more weakly coordinating and less reactive

$[\text{BPh}_4]^-$ anion is incorporated into the resultant ion-pair. Likewise, the additional steric bulk, and low basicity, of the relinquished amine (typically NMe_2Ph) was speculated to render it less likely to coordinate to the newly formed metal cation. Although these species generally react cleanly and quickly in weakly coordinating solvents, the desired cationic metal alkyls are often plagued by decomposition *via* C-H activation of the aryl groups of $[\text{BPh}_4]^-$.¹⁵⁵

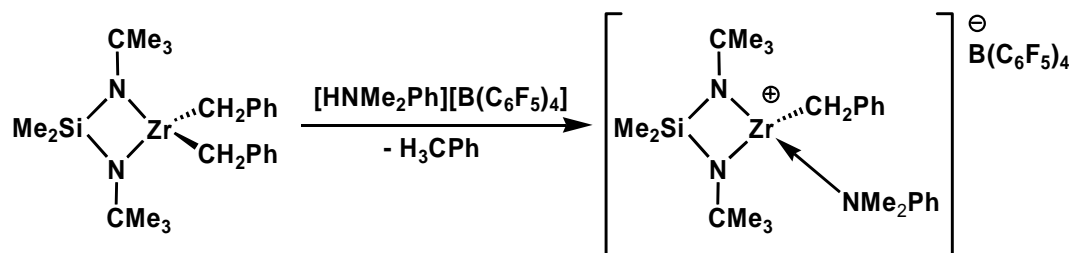
In conjunction with reports stemming from $\text{B}(\text{C}_6\text{F}_5)_3$ activated systems, the chemical community was rapidly becoming aware that the electronic and physical properties of both the cation and anion play an integral role in polymerization activity. Thus, in order to both circumvent the problematic C-H activation and produce a more weakly coordinating anion, several research groups focussed their attention on fine tuning the steric and electronic properties of Marks' ammonium borate compounds. Although a variety of similar species have since shown utility in olefin polymerization processes the most commonly employed ammonium activator from an industrial standpoint has been $[\text{HNMe}_2\text{Ph}][\text{B}(\text{C}_6\text{F}_5)_4]$.¹⁵⁶⁻¹⁵⁸ Upon activation of a dialkyl metal complex, $[\text{HNMe}_2\text{Ph}][\text{B}(\text{C}_6\text{F}_5)_4]$ installs the $[\text{B}(\text{C}_6\text{F}_5)_4]^-$ anion and liberates NMe_2Ph .

Several advantages of $[\text{HNMe}_2\text{Ph}][\text{B}(\text{C}_6\text{F}_5)_4]$ were demonstrated by Marks and colleagues when reaction with $\text{Cp}^*_2\text{ThMe}_2$ generated the desired ion-pair $[\text{Cp}^*_2\text{ThMe}][\text{B}(\text{C}_6\text{F}_5)_4]$.¹⁵⁶ As in the $[\text{BPh}_4]^-$ system, the perfluoroaryl borate appeared to impart crystallinity; the solid state structure unambiguously established weak Th-F interactions of 2.757(4) and 2.675(5) Å. The $[\text{B}(\text{C}_6\text{F}_5)_4]^-$ compounds are also advantageous in that they possess the additional NMR active nucleus, ^{19}F . The ^{11}B NMR is not particularly informative for these systems as the chemical shift is not overtly

sensitive to structural changes in the cation. The anion in these complexes is presumably quite mobile; complete dissociation is believed to occur *via* transient stabilization of the metal centre from aromatic solvent molecules, however, it is exceedingly difficult to observe such species, much less isolate them.

The inability of the $[\text{B}(\text{C}_6\text{F}_5)_4]^-$ anion to coordinate as tightly as $[\text{BPh}_4]^-$ to metal centres was apparent upon comparison of the solid state structures of $[\text{Cp}^*_2\text{ThMe}][\text{B}(\text{C}_6\text{F}_5)_4]$ and $[\text{Cp}^*_2\text{ThMe}][\text{BPh}_4]$. Significant contraction of the Th-Cp* distances, as would be expected for a more electron deficient metal centre, are observed. As anticipated, the enhanced electron deficiency and thermal stability is beneficial from a polymerization perspective; $[\text{Cp}^*_2\text{ThMe}][\text{B}(\text{C}_6\text{F}_5)_4]$ is 3300 times more active for ethylene polymerization and 4100 times more active for 1-hexene hydrogenation than its $[\text{BPh}_4]^-$ counterpart.¹⁵⁶

While a significant degree of success has been realized with $[\text{HNMe}_2\text{Ph}][\text{B}(\text{C}_6\text{F}_5)_4]$ as a co-catalyst for olefin polymerization, several problems have also surfaced, the most prevalent of which is coordination of liberated NMe_2Ph to the cationic metal centre (Scheme 4.2).^{159,160} Intuitively, one would expect the strength of amine coordination to correlate with electron deficiency and steric openness at the metal centre. This has been corroborated through variation of ligand substituents – the most

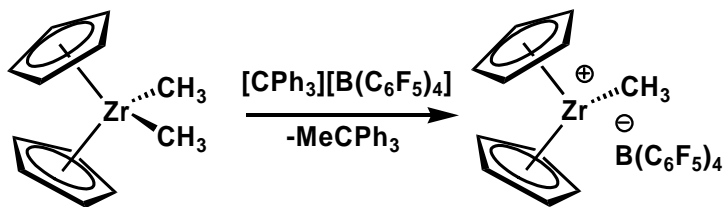


Scheme 4.2 NMe_2Ph Coordination upon Activation of $\text{Me}_2\text{Si}(\text{NCMe}_3)_2\text{Zr}(\text{CH}_2\text{Ph})_2$ with $[\text{HNMe}_2\text{Ph}][\text{B}(\text{C}_6\text{F}_5)_4]$

electron deficient and sterically accessible metal centre indeed binds the amine more tightly.¹⁶¹ While there is debate over the topic,^{162,163} the polymerization activity of certain catalyst systems appears to be hampered if the amine is capable of coordinating to the metal centre.⁷⁵ This is not surprising since a coordinating amine would serve to saturate the reactive metal centre from both steric and electronic perspectives. An additional problem with $[\text{HNMe}_2\text{Ph}][\text{B}(\text{C}_6\text{F}_5)_4]$ is that the ensuing ion-pairs are often insoluble in simple hydrocarbons necessitating the use of more expensive polar solvents (e.g. $\text{C}_6\text{H}_5\text{Br}$).⁷⁵ Likewise, the oily nature of such species frequently renders it impossible to isolate crystalline solids.¹¹⁵

4.1.2 Activation of Metallocenes with $[\text{CPh}_3][\text{B}(\text{C}_6\text{F}_5)_4]$

An alternative activation method to protonolysis involves the use of $[\text{CPh}_3][\text{B}(\text{C}_6\text{F}_5)_4]$.¹⁶⁴ As with $\text{B}(\text{C}_6\text{F}_5)_3$ the Lewis acidic trityl group $[\text{CPh}_3]^+$ abstracts a metal alkyl, however, unlike activation with boranes the abstraction is irreversible as the neutral triphenyl alkane RCPH_3 is lost and a $[\text{B}(\text{C}_6\text{F}_5)_4]^-$ counterion is added (Scheme 4.3). Although the ion-pairs are not always isolable, these activators are largely advantageous over their ammonium analogues in that now a chemically innocent alkane, MeCPH_3 , as opposed to a potentially coordinating amine, is produced. Although



Scheme 4.3 Activation of Cp_2ZrMe_2 with $[\text{CPh}_3][\text{B}(\text{C}_6\text{F}_5)_4]$

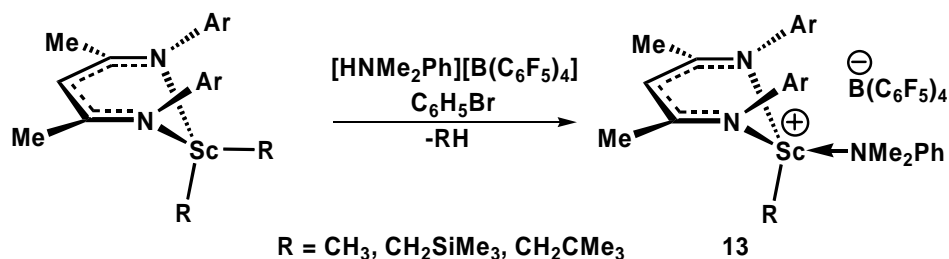
triphenylmethane has been reported to weakly coordinate to cationic metal centres through arene interactions,¹⁶⁵ this has since been disproved by Bochmann *et al.*¹⁶⁶

4.2 Results

4.2.1 Reactivity of $L^{\text{Me}}\text{ScR}_2$ with $[\text{HNMe}_2\text{Ph}][\text{B}(\text{C}_6\text{F}_5)_4]$

Since the sterically encumbered $[\text{L}^{\text{tBu}}\text{ScR}][\text{MeB}(\text{C}_6\text{F}_5)_3]$ species provided the opportunity to examine solution dynamics for a series of contact ion-pairs, it was desirable to develop a synthetic protocol for comparable SSIPs. It was hoped that such a family of compounds would allow further study of ion-pair dynamics, and perhaps provide suitable models for the proposed SSIPs thought to be involved in intermolecular anion exchange (see Chapter 3). As such, reactivity of dialkyl scandium complexes with the protic activator $[\text{HNMe}_2\text{Ph}][\text{B}(\text{C}_6\text{F}_5)_4]$ was pursued. Due to the slow decomposition of $[\text{L}^{\text{tBu}}\text{ScR}][\text{MeB}(\text{C}_6\text{F}_5)_3]$ through metallation of an aryl *isopropyl* group, it was decided that it would be prudent to first examine activation of the more thermally stable $L^{\text{Me}}\text{ScR}_2$ compounds.

Reaction of one equivalent of $L^{\text{Me}}\text{ScMe}_2$, **1-Me**, with $[\text{HNMe}_2\text{Ph}][\text{B}(\text{C}_6\text{F}_5)_4]$ in toluene resulted in the separation of an oily intractable mixture. However, upon moving



Scheme 4.4 Synthesis of $[\text{L}^{\text{Me}}\text{ScR}(\text{NMe}_2\text{Ph})][\text{B}(\text{C}_6\text{F}_5)_4]$

to bromobenzene as the reaction solvent it was possible to observe the rapid formation of a well defined ion-pair, **13-Me** (Scheme 4.4). The ^1H NMR spectrum exhibited typical nacnac ligand resonances and a diagnostic signal at -0.31 ppm assigned to the remaining Sc-Me group. A sharp singlet at 2.45 ppm integrating as 6H, along with resonances between 5.99 and 6.27 ppm were assigned to the NMe_2Ph group. These signals were shifted significantly in comparison to the free amine, indicating coordination of NMe_2Ph to the electrophilic metal centre (Figure 4.1).

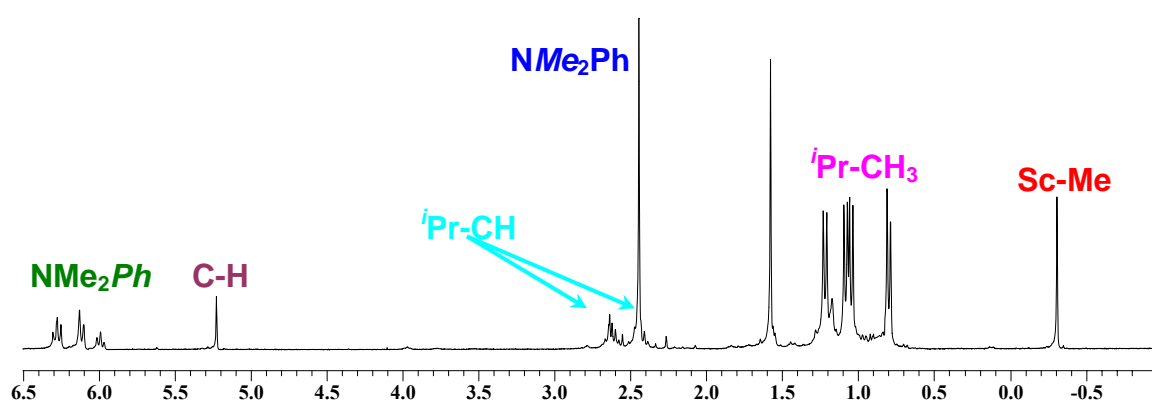


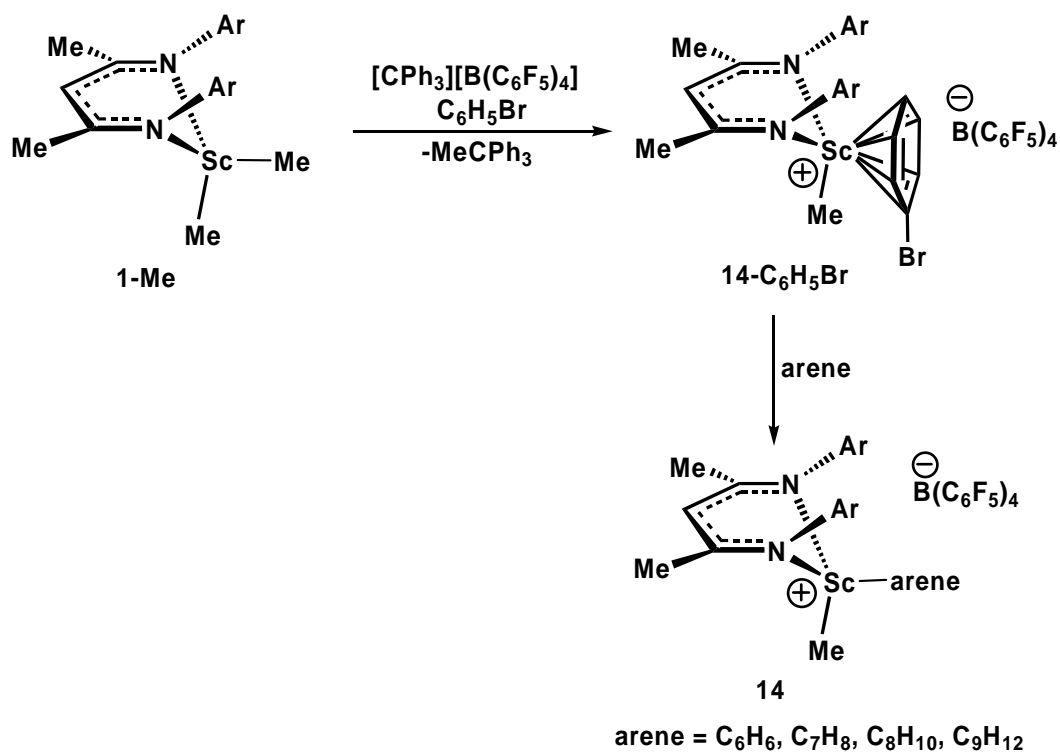
Figure 4.1 ^1H NMR Spectrum of **13-Me**

In an attempt to remove the free amine, the sample was placed under dynamic vacuum for 24 hours. Despite the prolonged exposure to reduced pressure it was not possible to remove the coordinated amine. As evidenced in group 4 metallocene chemistry, this is likely due to heightened electron deficiency at the scandium centre. Although a plethora of solvent mixtures, temperatures and crystallization techniques were explored, it was not possible to attain **13-Me** as a well defined solid. This fact, combined with amine retention, rendered **13-Me** a poor candidate for mechanistic studies. Despite these negative characteristics, however, it is interesting to note that **13-Me** was extremely thermally stable with no signs of decomposition observed after 12 hours in solution at room temperature.

In order to discourage amine coordination, and hopefully enhance the crystallinity of the ion-pair, it was decided to increase the steric bulk at the metal centre by choosing a more bulky dialkyl starting material. As such, both $L^{\text{Me}}\text{Sc}(\text{CH}_2\text{SiMe}_3)_2$, **1-CH₂SiMe₃**, and $L^{\text{Me}}\text{Sc}(\text{CH}_2\text{CMe}_3)_2$, **1-CH₂CMe₃**, were reacted with $[\text{HNMe}_2\text{Ph}][\text{B}(\text{C}_6\text{F}_5)_4]$. As with **1-Me**, the reactions progressed cleanly to afford the anticipated ion-pairs **13-CH₂SiMe₃** and **13-CH₂CMe₃**. Despite attempting Lewis base removal tactics it was still not possible to eliminate the coordinated NMe_2Ph ; the ^1H and ^{19}F NMR spectra were nearly identical to those observed for **13-Me**.

4.2.2 Reactivity of $L^{\text{Me}}\text{ScR}_2$ with $[\text{CPh}_3][\text{B}(\text{C}_6\text{F}_5)_4]$

In order to prepare a SSIP while alleviating amine retention issues, the trityl salt $[\text{CPh}_3][\text{B}(\text{C}_6\text{F}_5)_4]$, was reacted on an NMR scale with one equivalent of **1-Me** in $\text{C}_6\text{D}_5\text{Br}$ (Scheme 4.5). Characterization by multinuclear NMR spectroscopy revealed rapid reaction to afford the ion-pair $[\text{L}^{\text{Me}}\text{ScMe}(\text{C}_6\text{D}_5\text{Br})][\text{B}(\text{C}_6\text{F}_5)_4]$, **14-C₆D₅Br**, as evidenced by a characteristic peak at 2.00 ppm in the ^1H NMR spectrum attributed to triphenylethane. No indication of tight $[\text{B}(\text{C}_6\text{F}_5)_4]^-$ or solvent coordination was exhibited; retention of both top – bottom and right – left symmetry was indicated in the ^1H NMR spectrum (Figure 4.2). This species was remarkably stable with no signs of C_6F_5 transfer or metallation even at elevated temperatures for extended periods of time. It was possible to isolate **14-C₆H₅Br** by leaving a concentrated bromobenzene solution



Scheme 4.5 Synthesis of $[\text{L}^{\text{Me}}\text{ScMe(arene)}][\text{B(C}_6\text{F}_5\text{)}_4]$

layered with hexanes for approximately 24 hours at $-35\text{ }^\circ\text{C}$ whereupon the desired product quantitatively precipitated as a pale yellow microcrystalline solid. Single crystals suitable for X-ray diffraction were readily grown by a similar solvent mixture over the course of several days. The ability to isolate **14-C₆H₅Br** as a well behaved solid was a

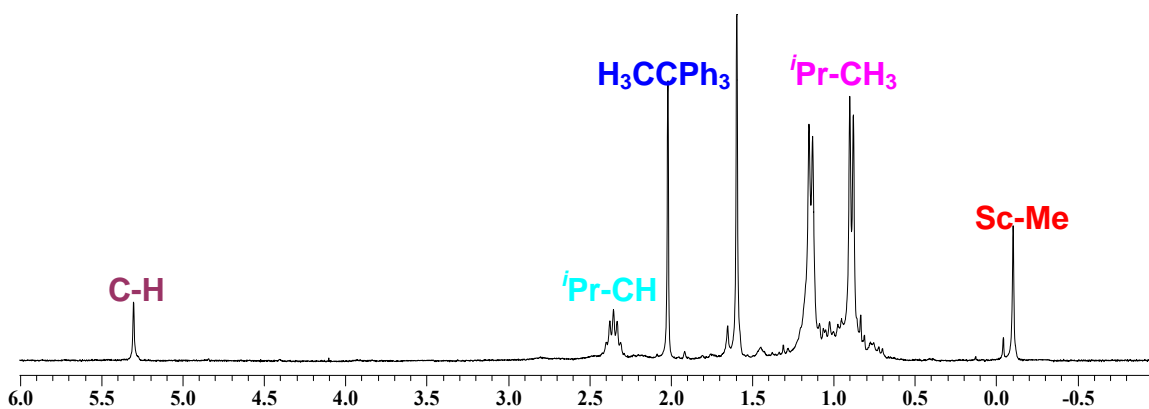


Figure 4.2 ^1H NMR Spectrum of **14-C₆D₅Br** Generated *In Situ*

key development towards studying the organometallic chemistry of scandium SSIPs.

The molecular structure of **14-C₆D₅Br** deviates from the observed ¹H NMR spectrum in that it exists as the bromobenzene adduct. The arene solvent molecule occupies the *exo* site and is bonded to the scandium centre in an unusual η^6 fashion (Figure 4.3). It is much more common for haloarenes to coordinate in an η^1 bonding mode *via* the halogen to d⁰ metals.¹⁶⁷ The preference for η^6 hapticity demonstrates the high electrophilicity and steric openness of the cation. Although the arene is best

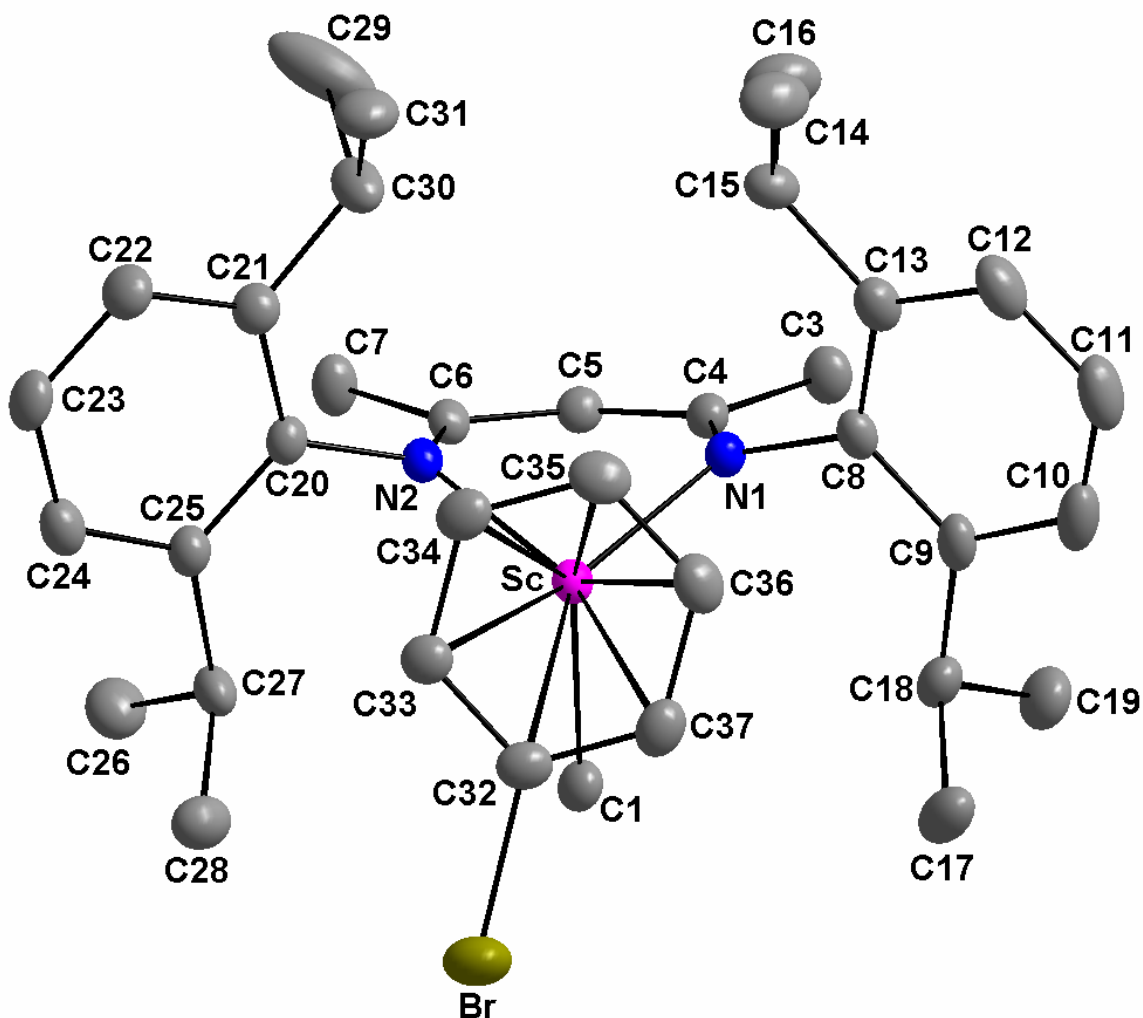


Figure 4.3 X-ray Structure of **14-C₆D₅Br**. Thermal Ellipsoids are drawn at the 30% probability level. Hydrogen atoms and [B(C₆F₅)₄]⁻ are removed for clarity.

considered η^6 bound, the bonding is not symmetrical; steric interactions cause significant tilting of the ring with Sc-C_{arene} bond distances ranging from 2.680(4) – 2.842(4) Å (Table 4.1). These distances agree well with those observed for other arene bound scandium species.⁵⁶ No close contacts (< 4.9 Å) between the borate anion and the metal centre were observed. The tipping of the 2,6-diisopropylphenyl groups towards each other above the nacnac plane (Figure 4.3) favours the observed conformation of the bromobenzene molecule where the bromine atom is nearly eclipsing the Sc-Me (C(1)-Sc-C(32)-Br = -14.4(3) °). Since there is no evidence for η^6 Sc-arene bonding in solution (even at -35 °C) it can be assumed that there is likely rapid exchange between free and bound bromobenzene on the NMR timescale with the barrier for bromobenzene dissociation being quite low.

In an attempt to examine arene binding strength **14-C₆H₅Br** was reacted with a variety of arenes (benzene, toluene, xylene, and mesitylene). The loosely coordinated bromobenzene was easily displaced by the more electron rich arenes to give the corresponding family of SSIPs (**14-C₆H₆**, **14-C₇H₈**, **14-C₈H₁₀** and **14-C₉H₁₂**). X-ray crystallography was successful in determining the solid state structures of **14-C₇H₈** and **14-C₉H₁₂** (Figure 4.4). **14-C₇H₈** is essentially isostructural with **14-C₆H₅Br**; the aromatic ring is oriented in a similar fashion with a C(1)-Sc-C(32)-C(38) torsion angle of -14.3(3) °. Although the Sc-arene still possesses significant asymmetry (Sc-arene = 2.643(4) – 2.796(4) Å) the smaller methyl group, in comparison to the bromine atom, does not necessitate the same magnitude of tilting to alleviate steric strain. The more basic toluene sits slightly closer to the cationic scandium centre (Sc-C_{arene} ave. = 2.715 cf.

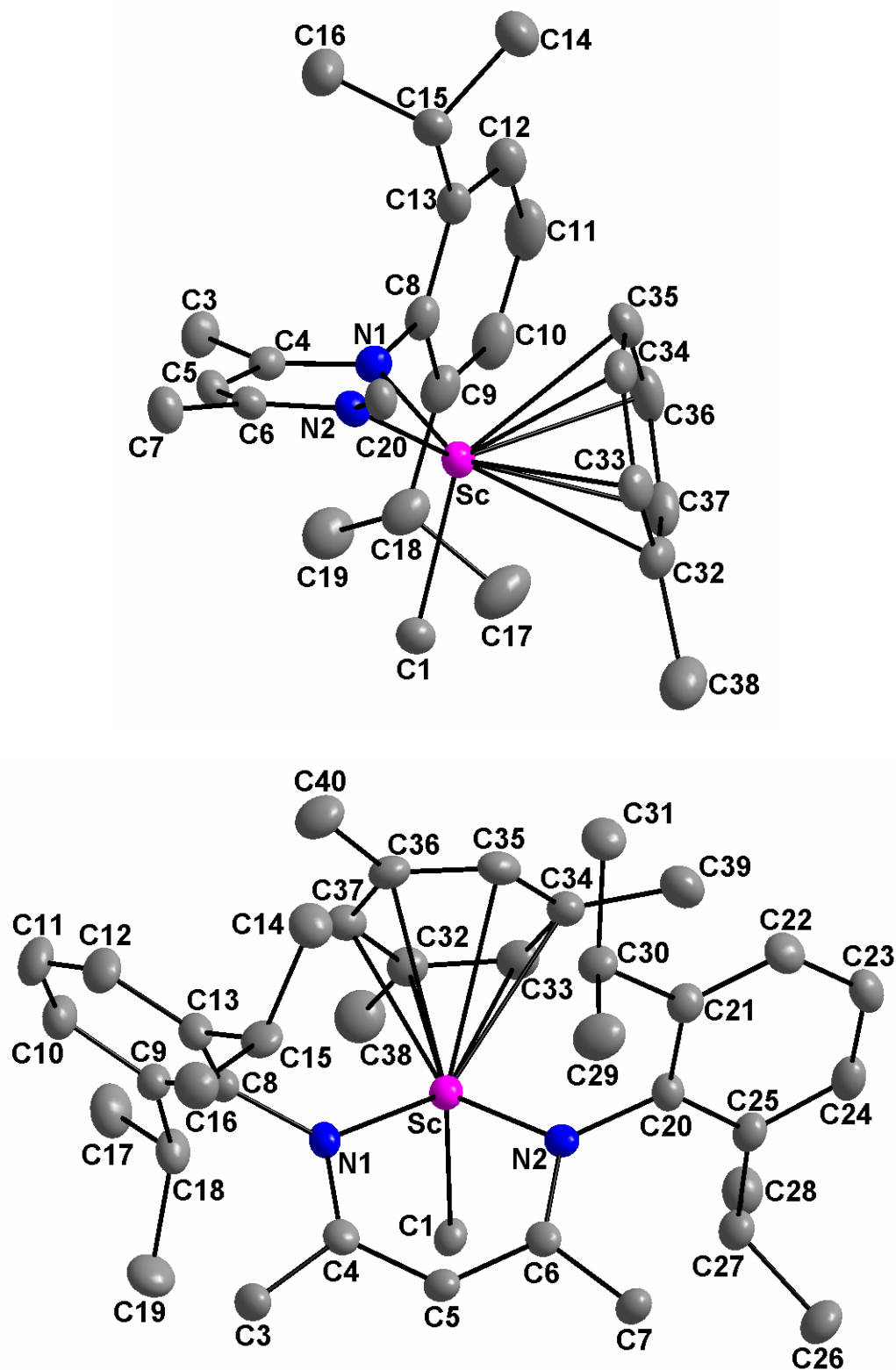


Figure 4.4 Top: X-ray structure of **14-C₇H₈**. Front aryl group, hydrogen atoms and [B(C₆F₅)₄] removed for clarity. Bottom: X-ray structure of **14-C₉H₁₂**. Hydrogen atoms and [B(C₆F₅)₄] removed for clarity. Thermal ellipsoids are at the 30% probability level.

Table 4.1 Selected Metrical Data for **14-C₆H₅Br**, **14-C₇H₈** and **14-C₉H₁₂**

Parameter ^a	14-C ₆ H ₅ Br	14-C ₇ H ₈	14-C ₉ H ₁₂
Bond Distances (Å)			
Sc-N(1)	2.100(4)	2.098(3)	2.120(4)
Sc-N(2)	2.105(4)	2.109(3)	2.097(4)
Sc-C(1)	2.162(5)	2.186(4)	2.212(4)
Sc-C _{arene}	2.640(4)	2.643(4)	2.694(5)
	2.682(4)	2.655(4)	2.701(5)
	2.715(4)	2.704(4)	2.736(5)
	2.767(4)	2.722(4)	2.773(5)
	2.802(5)	2.769(4)	2.795(5)
	2.842(4)	2.796(4)	2.843(5)
Sc-C _{arene} (ave.)	2.741(6)	2.715(6)	2.757(6)
Sc-C(4)	2.959(9)	2.973(4)	2.956(5)
Sc-C(5)	3.196(5)	3.212(4)	3.162(4)
Sc-C(6)	2.957(8)	2.970(4)	2.934(5)
Sc-N ₂ C ₃ plane	0.890(5)	0.887(4)	0.979(5)
Bond Angles (°)			
N(1)-Sc-N(2)	90.79(14)	90.48(110)	90.53(14)
N(1)-Sc-C(1)	105.22(16)	105.03(13)	102.66(16)
N(2)-Sc-C(1)	105.23(16)	104.54(13)	101.19(16)
C _{centroid} -C(32)-E	177.23(33)	174.55(44)	177.26(51)
C _{centroid} -C(34)-C(39)			172.76(45)
C _{centroid} -C(36)-C(40)			175.70(39)
N(1)-C(4)-C(5)	123.2(4)	123.1(3)	123.3(4)
C(4)-C(5)-C(6)	131.4(4)	131.1(3)	130.9(4)
C(5)-C(6)-N(2)	123.7(4)	123.6(2)	123.5(4)
Torsion Angles (°)			
C(1)-Sc-C(32)-E	-14.4(3)	-14.3(3)	23.9(4)
C(6)-N(2)-C(20)-C(25)	90.2(5)	91.4(4)	81.6(6)
C(6)-N(2)-C(20)-C(21)	-91.2(5)	-91.2(4)	-100.7(5)
C(4)-N(1)-C(8)-C(9)	93.8(5)	93.8(4)	71.5(6)
C(4)-N(1)-C(8)-C(13)	-87.9(5)	-88.7(4)	-111.1(5)

^aE = Br for **14-C₆H₅Br** and C(38) for **14-C₇H₈** and **14-C₉H₁₂**

2.741 Å for **14-C₆H₅Br**) resulting in perturbation from linearity in the C_{centroid}-C(32)-C(38) bond angle (174.55(44) °).

While the X-ray crystal structure of **14-C₉H₁₂** was similar to both **14-C₆H₅Br** and **14-C₇H₈**, several minor structural differences result from the enhanced steric bulk of this more basic arene. For example, the 1,3,5 ring substitution pattern renders it impossible to orient the molecule such that all 3 methyl groups avoid close contact with the upper *isopropyl* groups. As a consequence, there is less eclipsing of the Sc-Me group (C(1)-Sc-C(32)-C(38) = 23.9(4) °) and less tilting of the mesitylene ring (Sc-C_{arene} = 2.694(5) – 2.843(5) Å). Likewise, the N-aryl groups are forced far from orthogonal with torsion angles as low as 71.5(6) °. This deviation, which is greater than that observed for other LScR species, reflects the degree to which the coordination sphere of the metal centre is blocked. As such, at 0.979(5) Å, the scandium centre resides further from the N₂C₃ nacnac plane than in all previously characterized L^{Me}Sc compounds.

Although the additional methyl groups on the aromatic ring provide significant inductive donation, thus enhancing the Lewis basicity of the arene,^{168,169} the electronic stabilization appears to be overridden by the overwhelming steric constraints (*vide infra*). Although the difference is not statistically relevant to $\pm 3\sigma$, the longer Sc-C_{arene} ave. bond distance of 2.757(6) Å seems to support this fact.

The solution ¹H NMR spectra of **14-C₇H₈** and **14-C₉H₁₂**, in C₆D₅Br indicated C_s molecular symmetry due to loss of top – bottom equivalence on the NMR timescale, thus confirming that toluene and mesitylene bind stronger than bromobenzene to the scandium centre. The ¹H resonances for the coordinated toluene within **14-C₇H₈** were observed

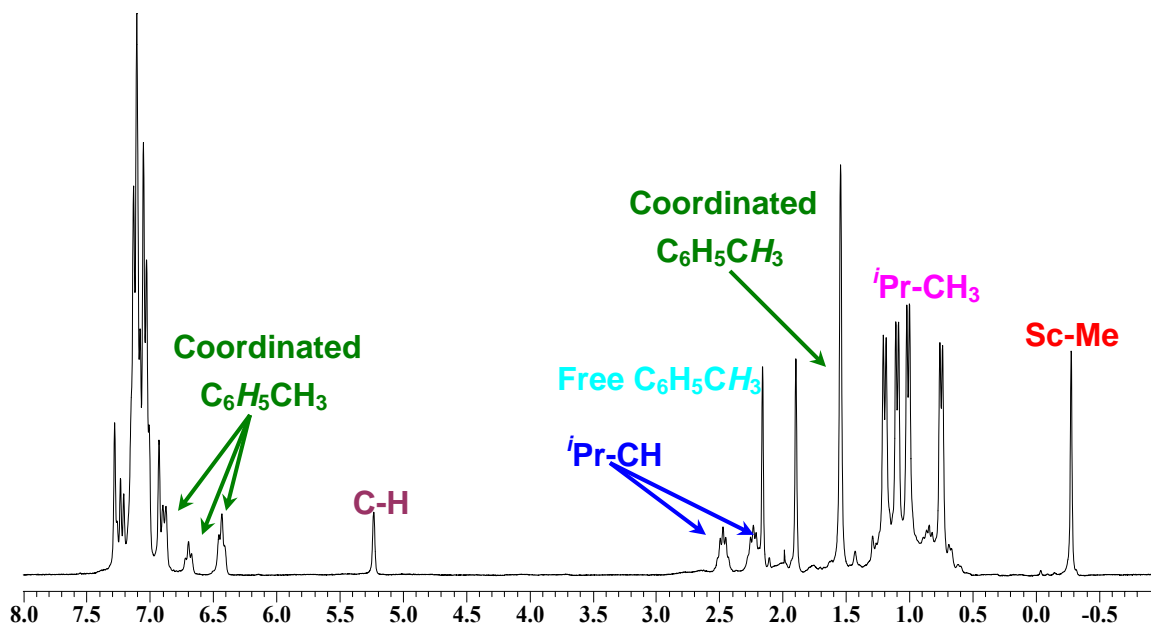


Figure 4.5 ^1H NMR Spectrum of **14-C₇H₈** in $\text{C}_6\text{D}_5\text{Br}$ at Room Temperature

upfield of free toluene at 6.81, 6.66, 6.39 and 1.85 ppm (Figure 4.5). Addition of excess d_8 -toluene at room temperature resulted in the gradual disappearance of these signals over the course of five minutes indicating exchange with free toluene.

4.2.3 Arene Exchange Between **14-C₉H₁₂** and **14-C₇H₈**

Since SSIPs are often speculated to be intimately involved in olefin polymerization processes, the ability to isolate this family of well defined SSIPs is important. Specifically, if SSIPs persist as intermediates whereby the solvent molecule has displaced the coordinating anion, the mechanism by which the arene is displaced by an incoming olefin is of keen interest. The observation of exchange between coordinated arene and free solvent brought to light that it might be possible to quantitatively study arene exchange within these systems. While studies focussing on arene exchange within

d^n metal systems are plentiful,¹⁷⁰⁻¹⁸⁶ examples of cationic d^0 complexes with relevance to olefin polymerization are exceedingly rare and in these cases the arene is bound sufficiently tight so as to stunt all organometallic reactivity.¹⁸⁷⁻¹⁸⁹ As the only previously reported scandium example, $[L^{Me}ScCH_2Ph][PhCH_2B(C_6F_5)_3]$ is totally unreactive towards H_2 and ethylene, even at elevated temperatures.⁵⁶

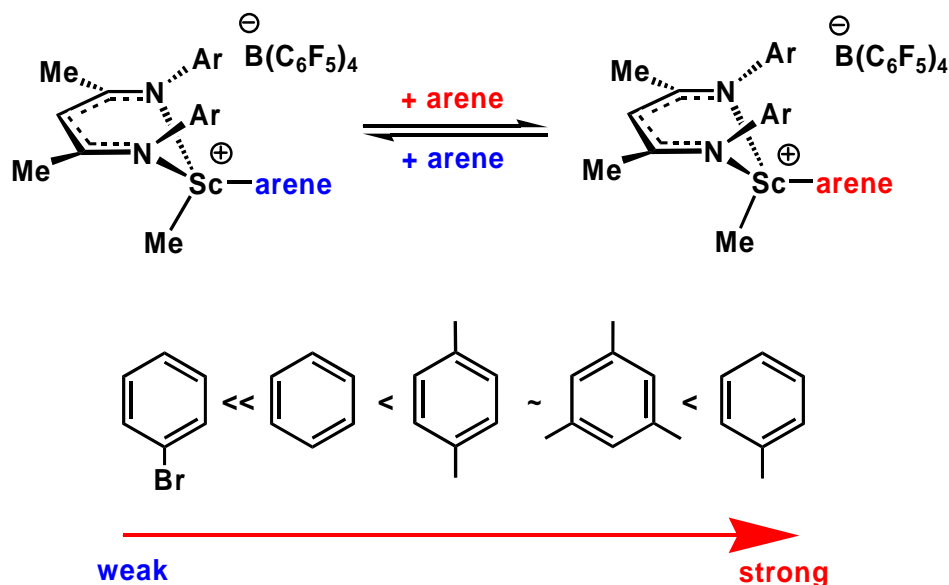


Figure 4.6 Relative Arene Binding to $[L^{Me}ScMe][B(C_6F_5)_4]$

A series of competition experiments were performed revealing the order of arene coordination to be $C_6H_5Br \ll C_6H_6 < C_8H_{10} \sim C_9H_{12} < C_7H_8$ confirming that steric factors indeed come into play on incorporation of more than one methyl group in the arene (Figure 4.6). In order to obtain the desired thermodynamic parameters for arene exchange several criteria were required. First, a system with a labile arene was necessary, second, experimental conditions which permitted exchange at a temperature and rate which could be monitored on a realistic timeframe using a compatible solvent,

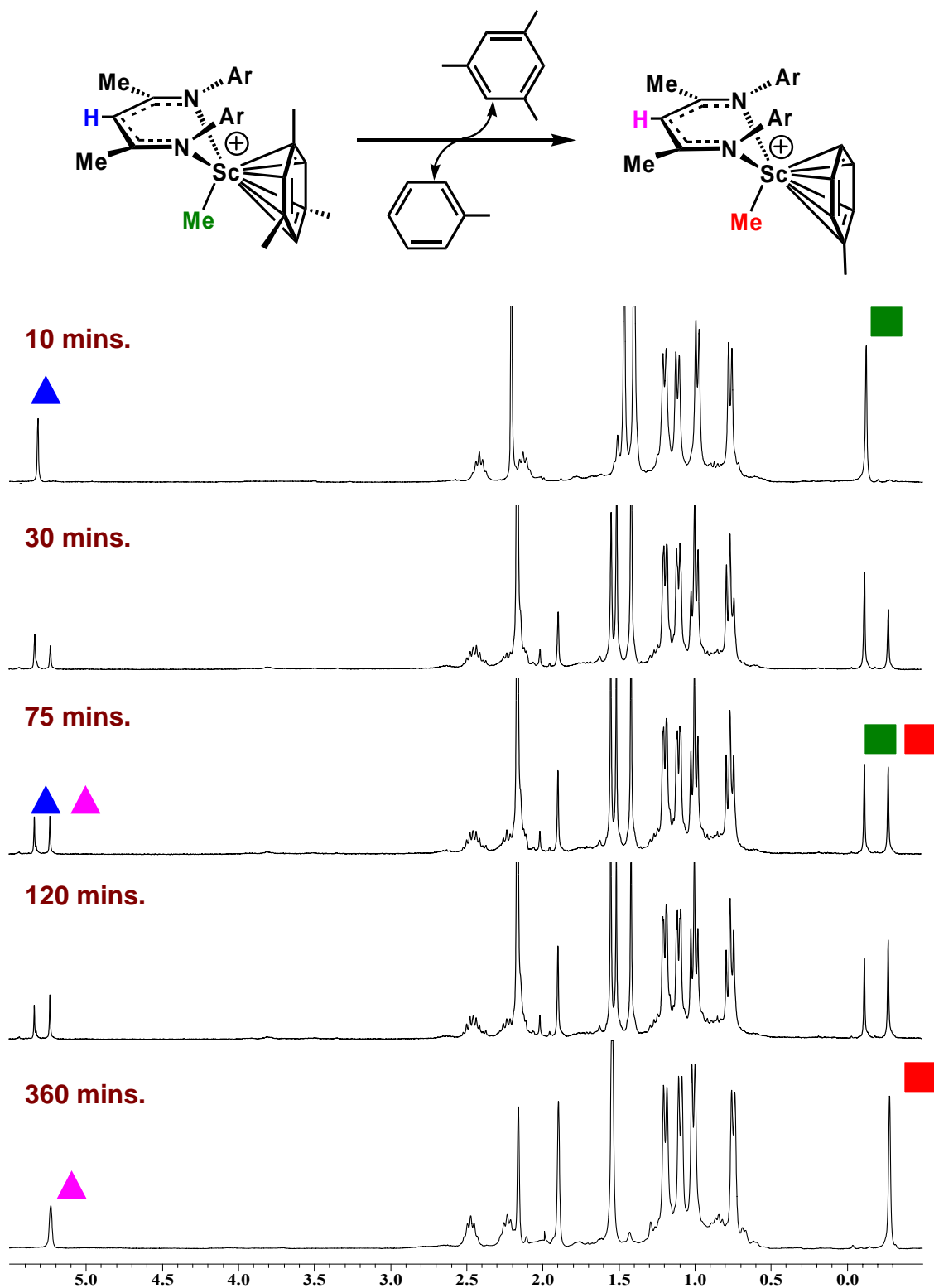


Figure 4.7 Series of ¹H NMR Spectra Exhibiting Arene Exchange from **14-C₉H₁₂** to **14-C₇H₈** at 266.0 K

and finally, it had to be possible to distinguish between the starting material and product so that the progress of reaction could be followed. In this situation, it was desired to monitor exchange utilizing ^1H NMR spectroscopy and although addition of excess toluene to **14-C₈H₁₀** proceeded at a reasonable rate in $\text{C}_6\text{D}_5\text{Br}$, overlap of signals rendered this system unamenable. Fortunately, however, displacement of mesitylene from **14-C₉H₁₂** by toluene proceeded at a comparable rate and both the backbone and Sc-Me resonances were baseline resolved.

At low temperature, the substitution of mesitylene from **14-C₉H₁₂** with toluene to afford **14-C₇H₈** was quantitatively monitored under pseudo-first-order conditions (Table 4.2) using ^1H NMR spectroscopy (Figure 4.7). Repeating the experiment at several temperatures permitted the construction of an Eyring plot (Figure 4.8) from which the activation parameters were extracted ($\Delta\text{H}^\ddagger = 21.4(2) \text{ kcal mol}^{-1}$, $\Delta\text{S}^\ddagger = 6.0(8) \text{ e.u.}$). These values are quite close to those reported for ion-pair reorganization processes within metallocenium and constrained geometry cations partnered with the $[\text{B}(\text{C}_6\text{F}_5)_4]^-$ anion¹¹⁵ suggesting that arene exchange may in fact be a good model for anion displacement by monomer. The positive entropy of activation, although relatively low in magnitude, suggests arene exchange proceeds *via* a dissociative mechanism. Since a dissociative pathway should be independent of [toluene] a concentration dependence study was completed (still under pseudo-first-order conditions) at 261 K. The findings indeed supported a dissociative type process; virtually no rate enhancement was observed upon moving from 8 to 24 equivalents of toluene (Table 4.2). In fact, a slight depression in rate was realized upon moving to higher concentrations of toluene (Figure 4.9). This diminution in rate at high concentrations is presumably a consequence of significant

changes to the dielectric constant of the medium under these reaction conditions. The experiment which had the highest concentration of toluene (203 equivalents) consisted of a solvent mixture approaching 1 : 1 bromobenzene : toluene.

The positive ΔS^\ddagger , in combination with the lack of [toluene] dependence supports a dissociative mechanism, however, the low ΔS^\ddagger is not large enough to support a fully dissociative pathway. As such, it is unlikely for a purely dissociative process involving a “naked” scandium cation to prevail. Thus, a partially dissociative pathway, which involves a rate determining ring slipping to lower hapticity, such as η^2 or η^4 , is proposed. This ring slipping produces a vacant coordination site which allows the incoming toluene molecule to coordinate, after which, complete dissociation of the mesitylene can readily occur (Scheme 4.6). The proposed transition state is consistent with expectations since the metal centre is likely too sterically encumbered to support a fully associative process

Table 4.2 Reaction Rates and Half-Lives for the Arene Exchange of **14-C₉H₁₂** to **14-C₇H₈**

Equivalents of Toluene	[Toluene] M	T(K)	k_{exp} (s ⁻¹)
8.1	0.17	261.0	4.47(4) × 10 ⁻⁴
10.0	0.21	245.6	7.58(8) × 10 ⁻⁶
10.0	0.21	252.9	2.77(3) × 10 ⁻⁵
10.0	0.21	259.7	1.00(2) × 10 ⁻⁴
10.0	0.21	266.0	2.37(4) × 10 ⁻⁴
10.0	0.21	266.0	2.46(4) × 10 ⁻⁴
10.0	0.21	266.0	2.43(4) × 10 ⁻⁴
10.0	0.21	266.0	2.42(4) × 10 ⁻⁴
16.2	0.34	261.0	4.52(4) × 10 ⁻⁴
24.3	0.51	261.0	4.49(4) × 10 ⁻⁴
32.4	0.68	261.0	3.81(3) × 10 ⁻⁴
81	1.71	261.0	3.48(4) × 10 ⁻⁴
202.5	4.27	261.0	2.19(2) × 10 ⁻⁴

while too electrophilic to favour a fully dissociative pathway.

These findings are of interest from an olefin polymerization perspective because they provide a concrete explanation as to why toluene has previously been observed to

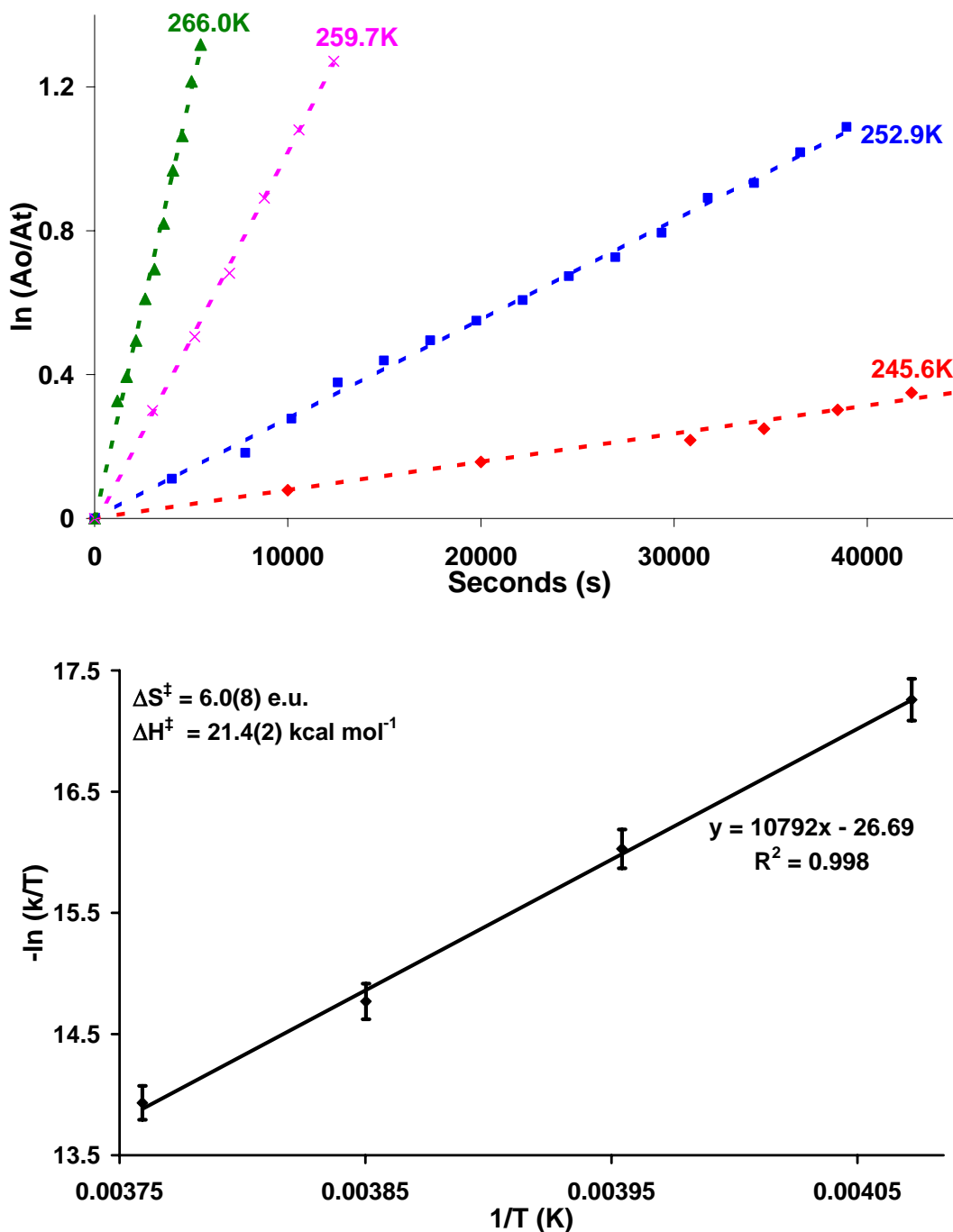


Figure 4.8 Top: Arene Exchange from $14\text{-C}_9\text{H}_{12}$ to $14\text{-C}_7\text{H}_8$, Monitored Quantitatively at Various Temperatures; Bottom: Eyring Plot of Arene Exchange from $14\text{-C}_9\text{H}_{12}$ to $14\text{-C}_7\text{H}_8$

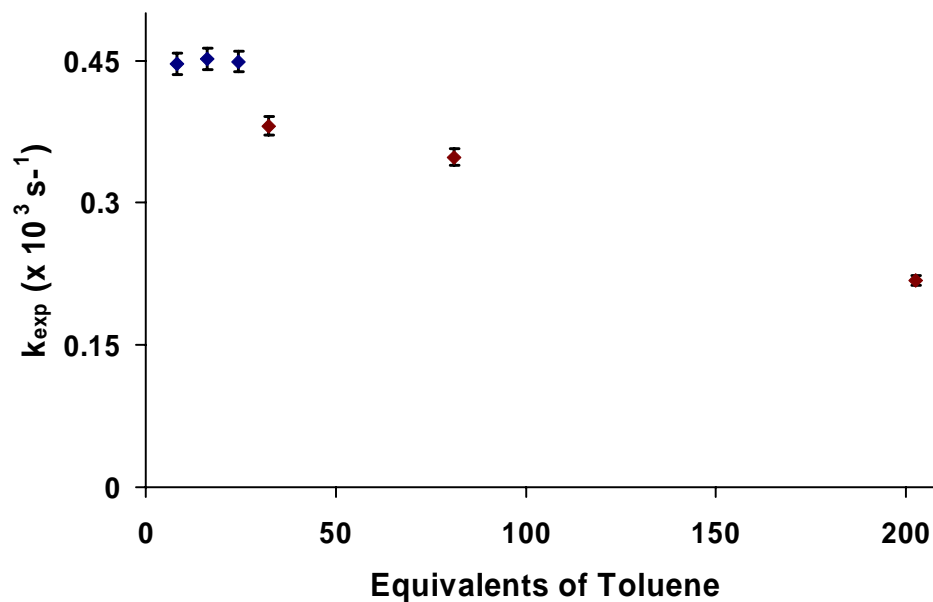
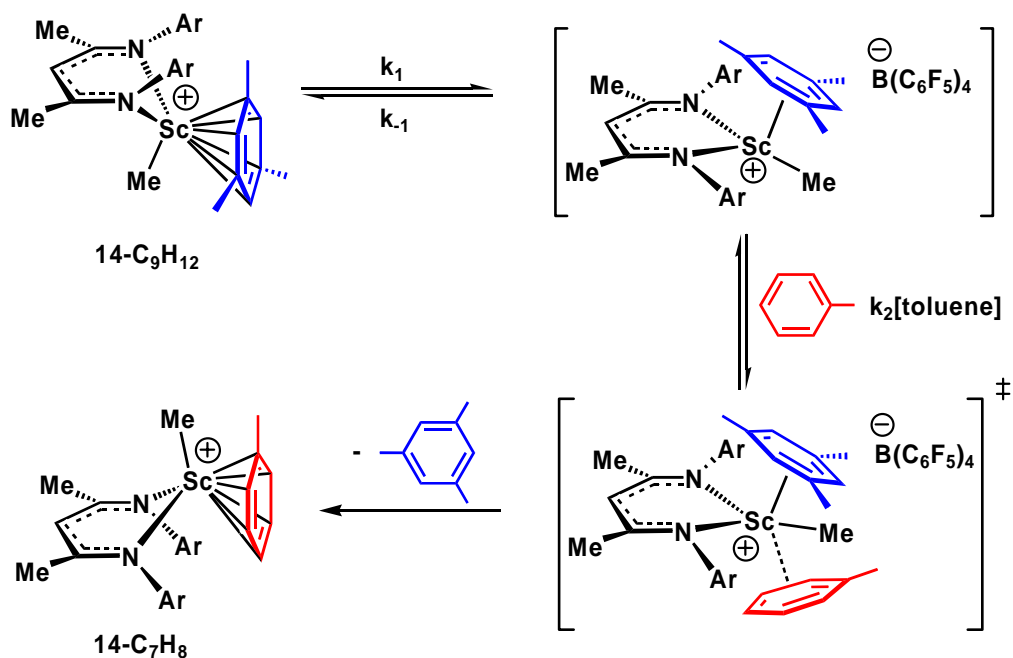


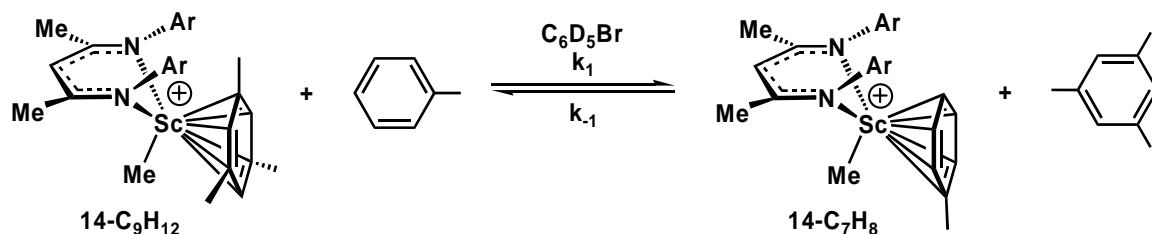
Figure 4.9 [Toluene] vs. Rate of Arene Exchange from $14\text{-C}_9\text{H}_{12}$ to $14\text{-C}_7\text{H}_8$

have a dampening effect on polymerization activity for lower coordinate sterically open catalysts.¹⁹⁰ Indeed, the competition of toluene for the cationic metal centre appears to have a dramatic effect; $14\text{-C}_9\text{H}_{12}$ exhibited significant ethylene polymerization activity



Scheme 4.6 Proposed Mechanism for Arene Exchange

when the reaction was conducted in bromobenzene, whereas activity was negligible if carried out in toluene. Evidently, ethylene is capable of displacing mesitylene, (which has a similar barrier to the $[\text{MeB}(\text{C}_6\text{F}_5)_3]^-$ anion; $\Delta H^\ddagger = 24(1) \text{ kcal mol}^{-1}$, $\Delta G^\ddagger = 18.9 \text{ kcal mol}^{-1}$)¹⁰⁰ however, it is not competitive with toluene for the active site, and activity is



Scheme 4.7 Equilibrium Upon Addition of 1 Equivalent of Toluene to **14-C₉H₁₂**

nullified. Clearly, the nature of the resting state of the active catalyst and solvent used both play significant roles in the polymerization process and must be thoroughly studied in the quest for industrially applicable catalysts.

In an effort to examine the ground state energetics of arene exchange and complete an energy profile for arene exchange, the effects of temperature upon the above equilibrium were quantitatively studied (Scheme 4.7). Addition of one equivalent of toluene to **14-C₉H₁₂** at room temperature resulted in a K_{eq} of 20.1(9) which significantly favoured product formation. As the temperature was lowered to 264 K, this value

Table 4.3 Temperature Dependence of K_{eq} for the Addition of 1 Equivalent of Toluene to **14-C₆H₅Br**

T(K)	K_{eq}
263.8	12.3(7)
288.5	15.7(8)
304.5	20.1(9)
324.4	23.5(9)

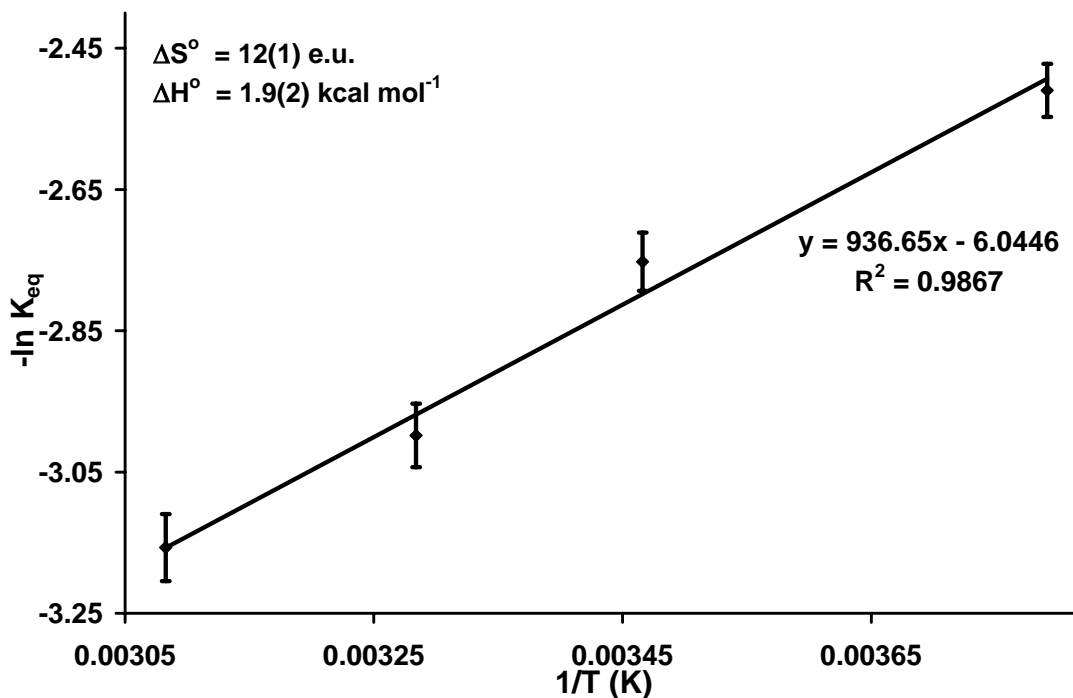
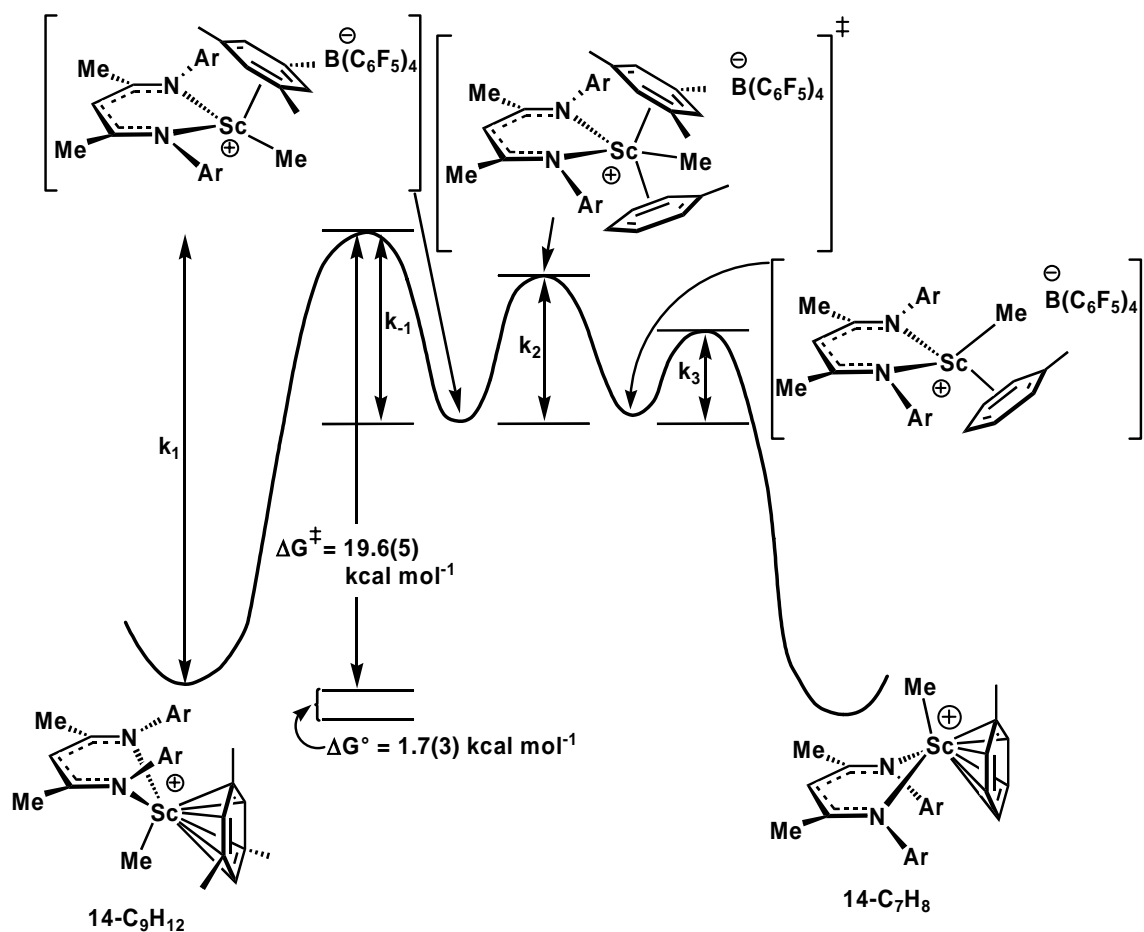


Figure 4.10 Van't Hoff Plot for the Addition of 1 Equivalent of Toluene to **14-C₆H₅Br**

decreased to 12.3(7) (Table 4.3). A Van't Hoff plot showed reasonable fit and provided the ground state parameters of $\Delta H^\circ = 1.9(2) \text{ kcal mol}^{-1}$ and $\Delta S^\circ = 12(1) \text{ e.u.}$ (Figure 4.10). Interestingly, the reaction appears to be entropically driven, despite the fact that both sides of the reaction possess the same quantity of similar molecules. Perhaps the enhanced conformational freedom enjoyed by the η^6 bound toluene molecule, in comparison to the more rigid constraints imposed on both the arene and ancillary framework in the mesitylene bound species, is sufficient to drive the reaction forward. Also, at 65.38(1) e.u.,¹⁹¹ free mesitylene has a larger molar entropy than toluene (52.4(3) e.u.).¹⁹²

The energy profile for toluene/mesitylene exchange is depicted in Scheme 4.8. The reaction is thought to proceed *via* the previously discussed pathway, with the rate

determining barrier for ring slipping measured to be $\Delta G^\ddagger = 19.6(5)$ kcal mol⁻¹. Mesitylene displacement by toluene has been established to be an entropically driven reaction spontaneously favoured at room temperature with a $\Delta G^\circ = -1.7(3)$ kcal mol⁻¹. Since very little is known about the nature of the second and third transition states and the second and third intermediates it is not possible to accurately comment on their energy levels with respect to each other. For this reason the energy levels are depicted to be similar.

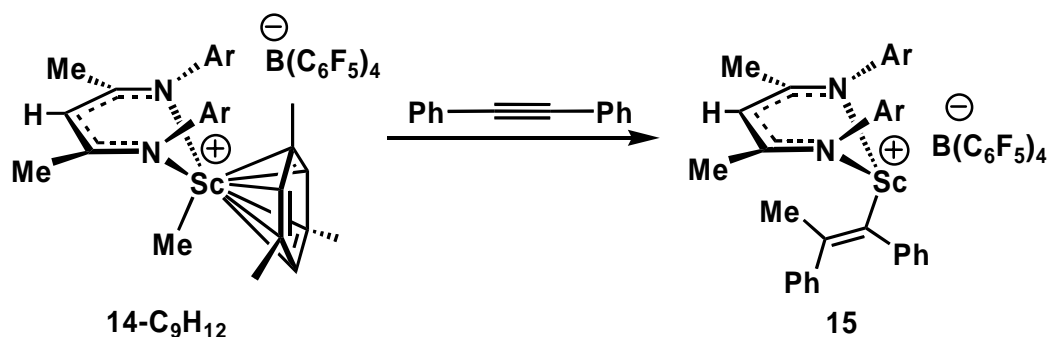


Scheme 4.8 Proposed Reaction Profile for Arene Exchange from **14-C₉H₁₂** to **14-C₇H₈** at 298 K

4.2.4 Insertion of Diphenylacetylene into 14-C₉H₁₂

Upon completing the study of arene exchange, it was decided to further probe the mechanism of arene displacement in a scenario which more closely resembled olefin polymerization. Following this rationale, it was of interest to examine the insertion of an unsaturated molecule into the Sc-Me bond. While preliminary investigations focussed upon reaction of 14-C₉H₁₂ with isocyanides, numerous reactions yielded only intractable mixtures. Subsequent experiments were conducted using diphenylacetylene for three reasons: firstly, it is a reasonable model for various olefins, secondly, it was anticipated that the steric bulk of the phenyl substituents would sufficiently retard the rate of reaction to ensure the feasibility of monitoring the progress using ¹H NMR spectroscopy, and finally, from a logistical standpoint, diphenyl acetylene, as a solid with no resonances in the aliphatic region of the ¹H NMR spectrum, was an excellent candidate as it simplified several aspects of performing the reactions.

Addition of one equivalent of diphenylacetylene to a cold (-30 °C) bromobenzene solution of 14-C₉H₁₂, cleanly produced [L^{Me}Sc(PhC=CMePh)][B(C₆F₅)₄], **15**, by insertion of the alkyne into the Sc-Me bond (Scheme 4.9). The progress of the reaction



Scheme 4.9 Reaction of 14-C₉H₁₂ with PhC≡CPh

was conveniently followed by ^1H NMR spectroscopy as the Sc-Me resonance at -0.14 ppm was gradually replaced by a new signal at 1.40 ppm. Likewise, the ligand backbone CH resonances are baseline resolved with distinct peaks at 5.25 and 5.11 ppm for the **14-C₉H₁₂** starting material and **15**, respectively. Several upfield resonances (6.73, 6.38 and 6.22 ppm) are observed for one of the phenyl rings originating from diphenylacetylene (Scheme 4.9). The chemical shift of these signals agrees well with other aromatic fragments bound to cationic β -diketiminato organoscandium species,^{56,193} such as **14-C₇H₈** (6.81, 6.66 and 6.39 ppm), and would thus seem to suggest arene interaction with the metal centre.

It was possible to scale up the above reaction in bromobenzene, and upon removal of solvent and sonication in hexanes, **15** was isolated as a deep yellow solid in 61% yield. Despite repeated attempts, the oily nature of **15** did not allow the growth of single crystals suitable for an X-ray diffraction study. Nonetheless, the identity of **15** was unambiguously confirmed through elemental analysis and ^1H , ^{11}B , ^{13}C , ^{19}F and 2D NMR experiments. The diagnostic resonances for the vinyl fragment are observed at 160.6 and 159.6 ppm in the $^{13}\text{C}\{^1\text{H}\}$ NMR spectrum and agree better with vinylic fragments which donate to the metal centre¹⁹⁴ than those that do not.¹⁹⁵

At temperatures ranging from 276 – 310 K it was possible to quantitatively monitor the reaction of diphenylacetylene with **14-C₉H₁₂** in $\text{C}_6\text{D}_5\text{Br}$ under pseudo-first-order conditions using ^1H NMR spectroscopy (Figure 4.11). It was not possible to acquire data at temperatures below 276 K as the rate of reaction became prohibitively slow, while if the temperature was raised above 310 K the reaction was completed too fast to obtain meaningful kinetic data.

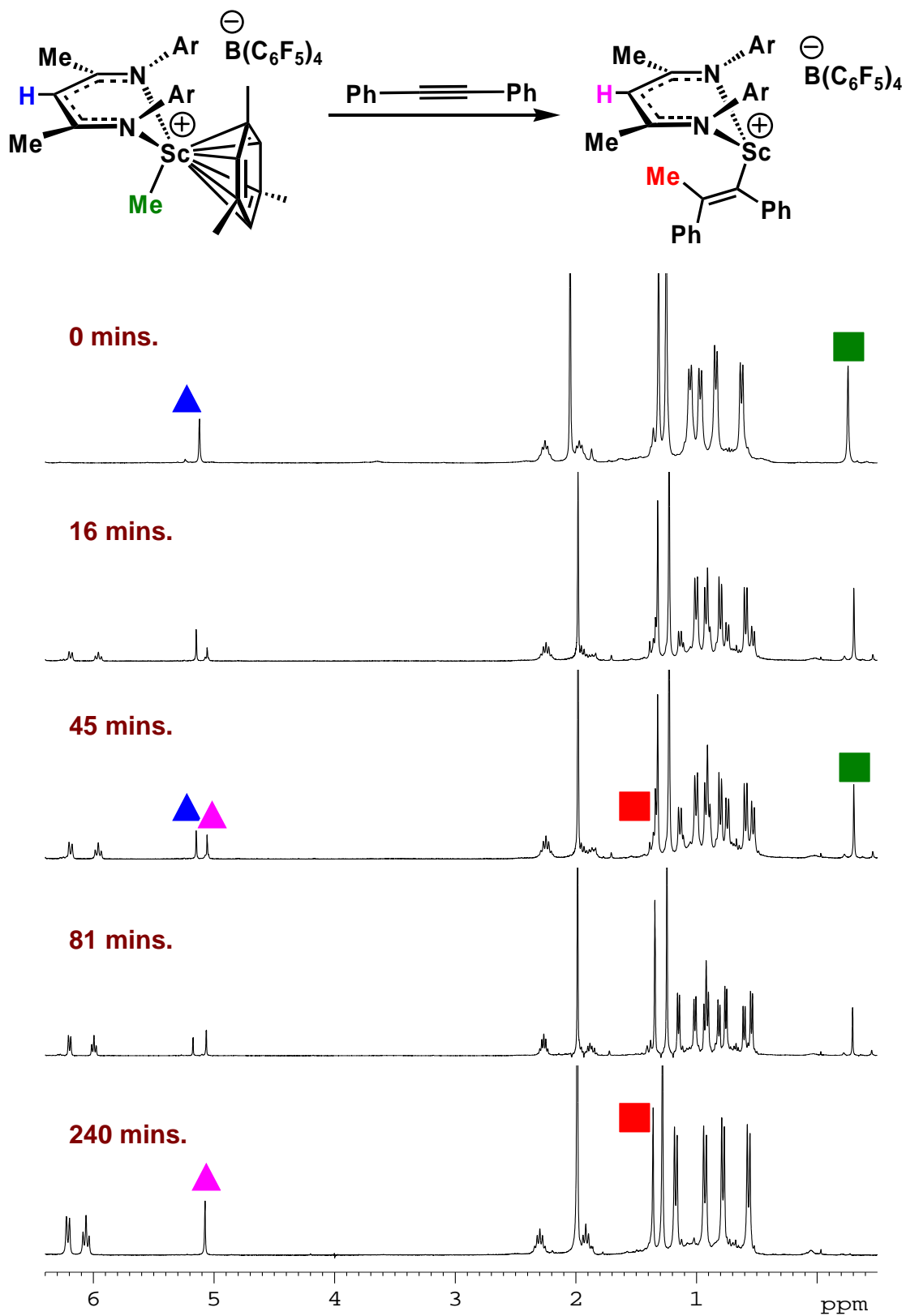


Figure 4.11 Series of ^1H NMR Spectra for Reaction of $\text{PhC}\equiv\text{CPh}$ with $14\text{-C}_9\text{H}_{12}$ at 306 K

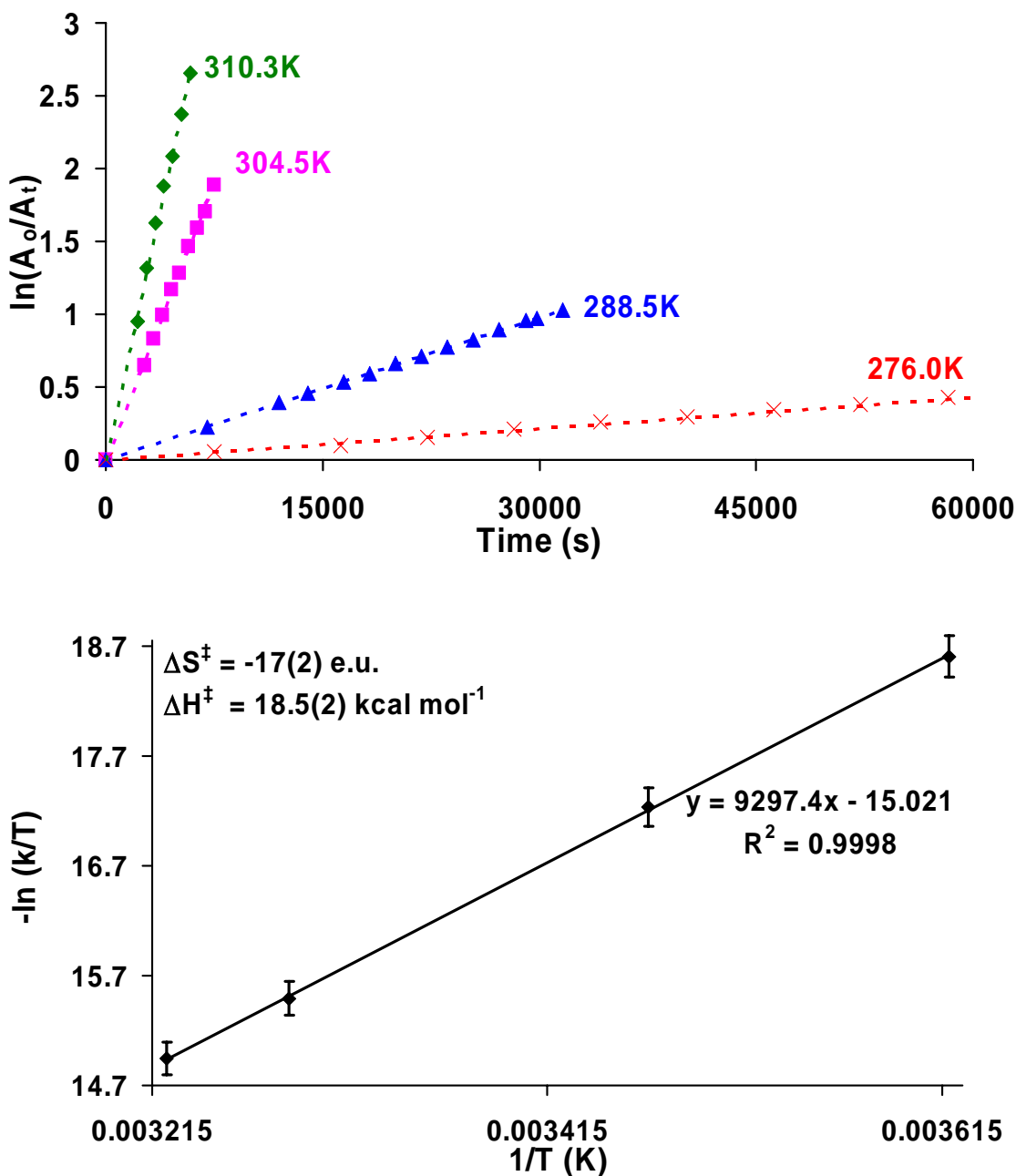


Figure 4.12 Top: Reaction of PhC≡CPh and **14-C₉H₁₂**, Monitored Quantitatively at Various Temperatures; Bottom: Eyring Plot of Reaction of PhC≡CPh and **14-C₉H₁₂**

Integration of the CH backbone resonances provided the necessary concentration data to determine reliable reaction rates for all temperatures (Table 4.4). The linear nature of the first order plots indicated that the insertion was first order in [**14-C₉H₁₂**].

For the higher temperatures, the first order rates remained linear for greater than 3 half-lives while the data for lower temperatures remained linear throughout the duration of the experiment. Construction of an Eyring plot enabled the calculation of the activation parameters ($\Delta H^\ddagger = 18.5(2)$ kcal mol⁻¹, $\Delta S^\ddagger -17(2) =$ e.u.) (Figure 4.12). The entropy of activation for alkyne insertion lies in stark contrast with that observed for arene exchange; an opposing sign for this value suggests that the rate determining transition state is not dissociative ring slipping, but rather, a process which is more associative in

Table 4.4 Reaction Rates and Half-Lives for the Reaction of PhC≡CPh with **14-C₉H₁₂**

[PhC≡CPh] (M)	T(K)	t _{1/2} (h)	k _{exp} (s ⁻¹)
0.215	276.4	26.7	7.20(7) × 10 ⁻⁶
0.215	288.5	5.9	3.26(4) × 10 ⁻⁵
0.215	304.5	0.8	2.51(2) × 10 ⁻⁴
0.215	310.3	0.4	4.55(5) × 10 ⁻⁴
0.215	310.3	0.4	4.61(5) × 10 ⁻⁴
0.215	310.3	0.4	4.47(4) × 10 ⁻⁴
0.215	310.3	0.4	4.51(4) × 10 ⁻⁴

nature. Once again, the magnitude of the activation entropy is not exceedingly large, thus, in order to further corroborate an associative mechanism, an assessment of the rates using varying quantities of diphenylacetylene at 305.5 K was conducted (Table 4.5). The expected rate acceleration was observed with a linear relationship exhibited between [diphenylacetylene] and k_{exp} over the concentrations examined (10 – 40 equivalents of diphenylacetylene) (Figure 4.13). As expected, these rate constants normalize to the same value when the differing diphenylacetylene concentrations are taken into account.

$$\text{rate} = k_{\text{exp}}[\mathbf{14-C}_9\mathbf{H}_{12}], \text{ where } k_{\text{exp}} = k_1[\text{diphenylacetylene}] \quad (4.1)$$

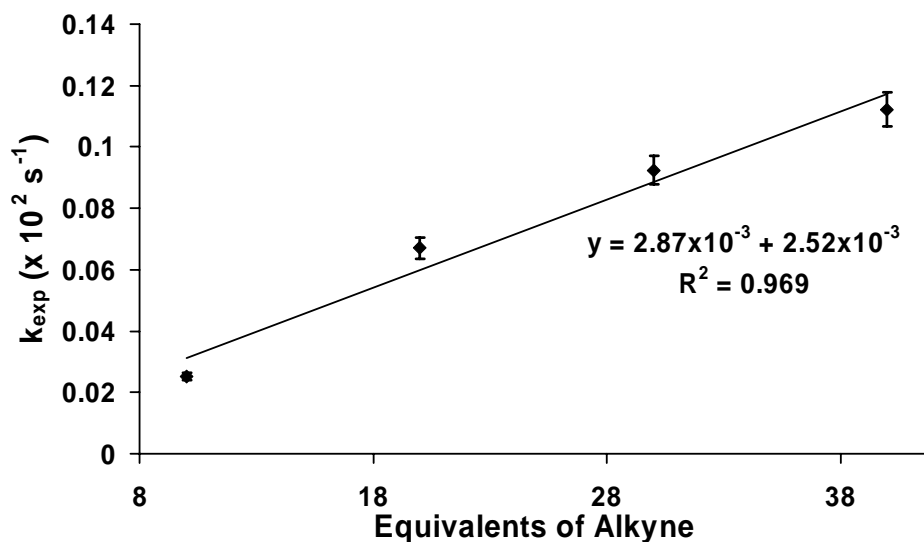


Figure 4.13 [Diphenylacetylene] vs. k_{exp} for Reaction of [Diphenylacetylene with **14-C₉H₁₂**

The rate law in equation 4.1 explains both the first order concentration dependence upon [14-C₉H₁₂] as well as the first order dependence on [diphenylacetylene]. The enthalpy of activation is similar to arene exchange while at 23.7(4) kcal mol⁻¹ the Gibb's free energy barrier is approximately 4 kcal mol⁻¹ higher than that measured for ring slipping.

The pre-equilibrium in Scheme 4.10 was supported experimentally by conducting reactions of 14-C₆H₅Br, 14-C₆H₆, and 14-C₇H₈ with diphenylacetylene. Since the ring slipping equilibrium constant (K_{slip}) contributes to k_{exp} , there should be an observable

Table 4.5 [Diphenylacetylene] vs. k_{exp} of Reaction with **14-C₉H₁₂**

Equivalents of Diphenylacetylene	[Diphenylacetylene] (M)	T(K)	$k_{\text{exp}} \text{ (s}^{-1}\text{)}$
10	0.215	305.5	$2.51(3) \times 10^{-4}$
20	0.430	305.5	$6.70(6) \times 10^{-4}$
30	0.645	305.5	$9.25(8) \times 10^{-4}$
40	0.860	305.5	$1.12(1) \times 10^{-3}$

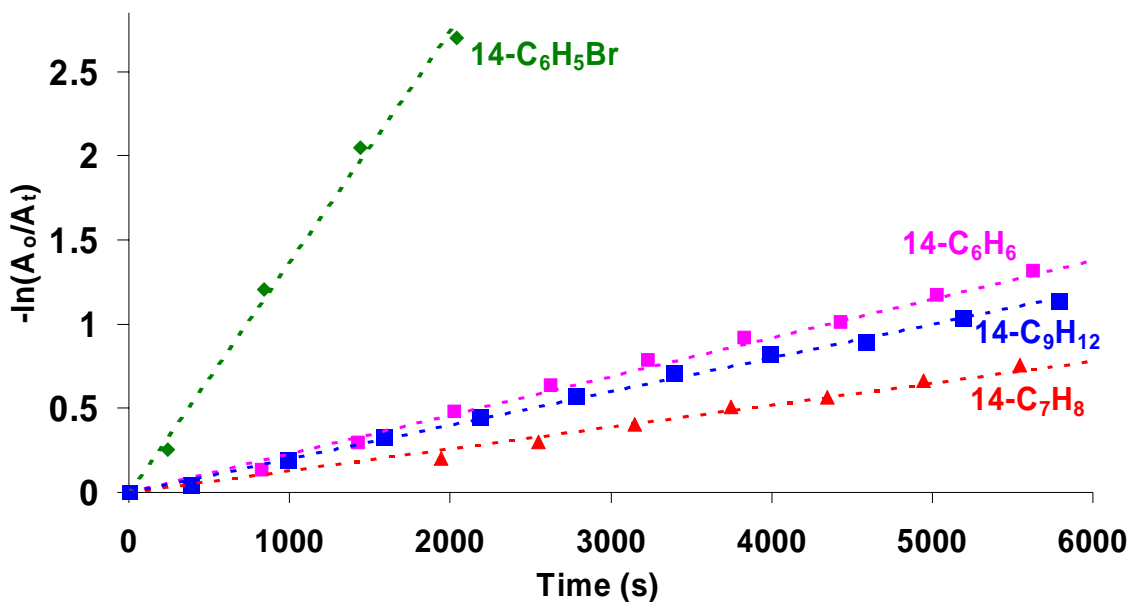


Figure 4.14 Effect of Bound Arene on k_{exp} for Alkyne Insertion

difference in the rate of reaction for the various arene bound starting materials. Indeed, k_{exp} was found to be dependent upon the scandium starting material with **14-C₆H₅Br** giving rise to the largest k_{exp} and **14-C₇H₈** the smallest (Table 4.6, Figure 4.14). These results agree with the strength of arene coordination previously determined for arene exchange (Figure 4.6).

In light of these results the proposed rate law must be modified to include a pre-equilibrium involving arene ring slipping prior to rate determining alkyne binding

Table 4.6 Reaction Rates and Half-Lives for the Reaction of PhC≡CPh with **14-arene**

Compound	[Diphenylacetylene] (M)	k_{exp} (s ⁻¹)	T(K)
14-C₆H₅Br	0.215	$1.36(5) \times 10^{-3}$	300
14-C₆H₆	0.215	$2.00(6) \times 10^{-4}$	300
14-C₉H₁₂	0.215	$2.30(8) \times 10^{-4}$	300
14-C₇H₈	0.215	$1.30(3) \times 10^{-4}$	300

(Scheme 4.10). Upon invoking a steady state approximation for the η^2 bound intermediate, the rate law simplifies to that shown in equation 4.4.^{196,197}

$$rate = k_2[\eta^2 - Sc][diphenylacetylene] \quad (4.2)$$

Steady State Approximation:

$$0 = k_1[\eta^6 - Sc] - k_{-1}[\eta^2 - Sc] - k_2[\eta^2 - Sc][diphenylacetylene]$$

$$0 = k_1[\eta^6 - Sc] - [\eta^2 - Sc](k_{-1} + k_2[diphenylacetylene])$$

$$[\eta^2 - Sc] = \frac{k_1[\eta^6 - Sc]}{k_{-1} + k_2[diphenylacetylene]}$$

Inserting into 4.2:

$$rate = \frac{k_1 k_2 [\eta^6 - Sc][diphenylacetylene]}{k_{-1} + k_2[diphenylacetylene]} \quad (4.3)$$

Under pseudo-first order conditions 4.3 simplifies to:

$$rate = k_{\text{exp}}[\eta^6 - Sc]; \text{ where } k_{\text{exp}} = \frac{k_1 k_2 [diphenylacetylene]}{k_{-1} + k_2 [diphenylacetylene]} \quad (4.4)$$

The above equation is further simplified if $k_{-1} \gg k_2[diphenylacetylene]$, and although it is not possible to delineate these two values explicitly, a double reciprocal plot of $\frac{1}{k_{\text{exp}}}$ vs.

$\frac{1}{[diphenylacetylene]}$ gives a slope = $\frac{k_{-1}}{k_1 k_2}$ and a y-intercept of $\frac{1}{k_1}$ (Figure 4.15). Since

the value of k_1 was previously determined this provides a method for comparing

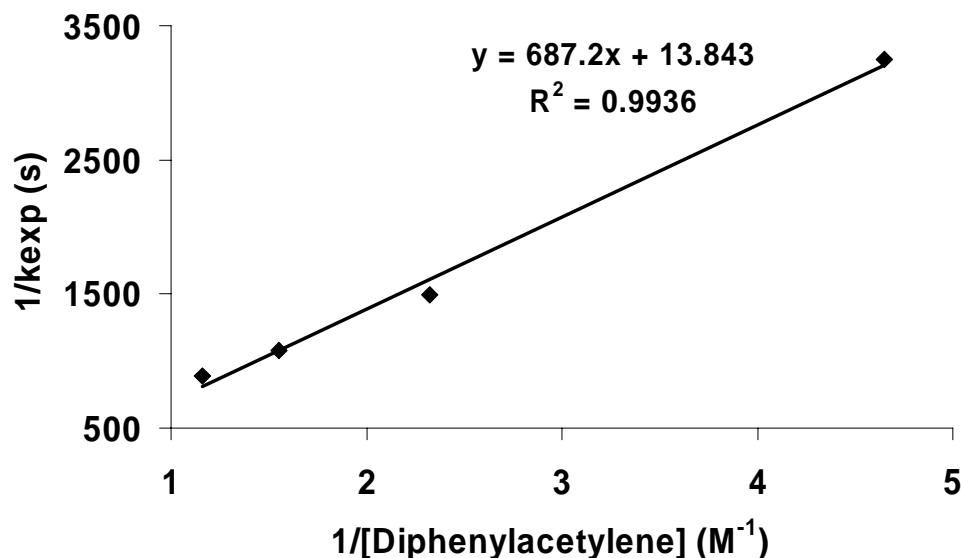
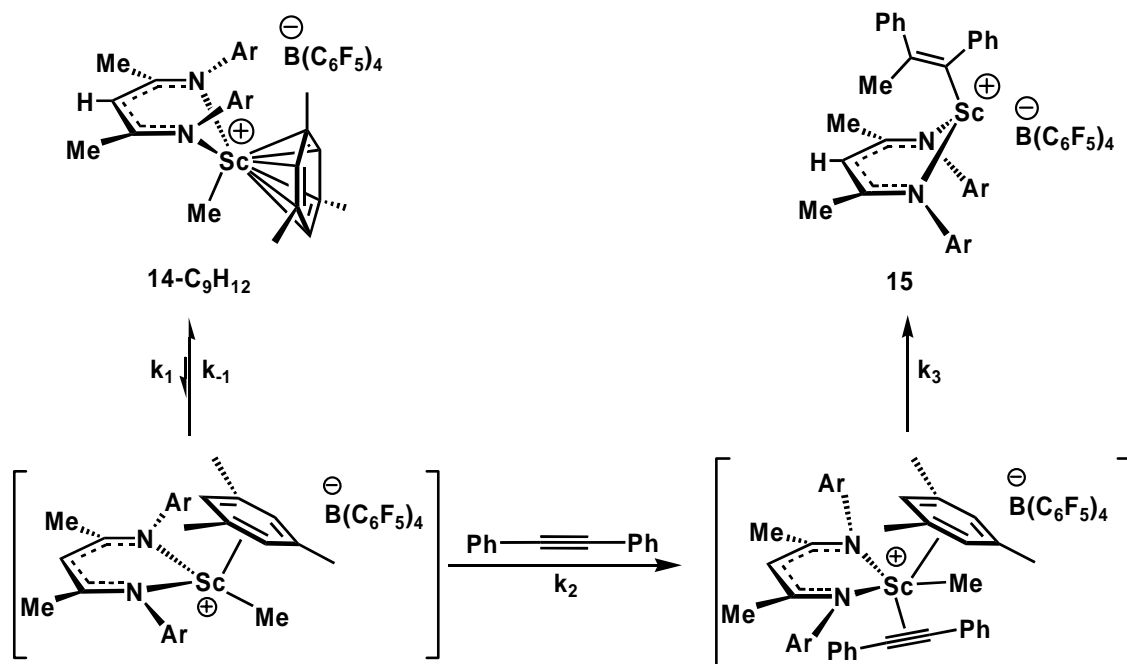


Figure 4.15 Double Reciprocal Plot ($1/k_{\text{exp}}$ vs. $1/[\text{Diphenylacetylene}]$) for Reaction of Diphenylacetylene with **14-C₉H₁₂**

this value as well as calculating the ratio of $k_2 : k_{-1}$. The observation of a rate limiting associative transition state dependent upon $[\text{diphenylacetylene}]$ necessitates that $k_2 < k_{-1}$. Indeed, upon completing the calculations, it was determined that $k_{-1} = 43.4 k_2$, thus $k_2[\text{diphenylacetylene}]$ is insignificant in comparison to k_{-1} and can be ignored.¹ The calculated value for k_1 (0.072 s^{-1}) matched quite closely with that previously measured (0.054 s^{-1}).

Since alkyne insertion into the Sc-Me bond of **14-C₉H₁₂** can be envisioned to occur in three steps (arene ring slipping, alkyne coordination and finally alkyne insertion) and the activation parameters are reflective of only the rate determining step, it is important to ensure the values are attributed to the correct process. Although one can

¹ A slight curvature of the line in Figures 4.13 and 4.15 suggest saturation behaviour, thus at very high $[\text{diphenylacetylene}]$, $k_2[\text{diphenylacetylene}]$ should be considered significant.

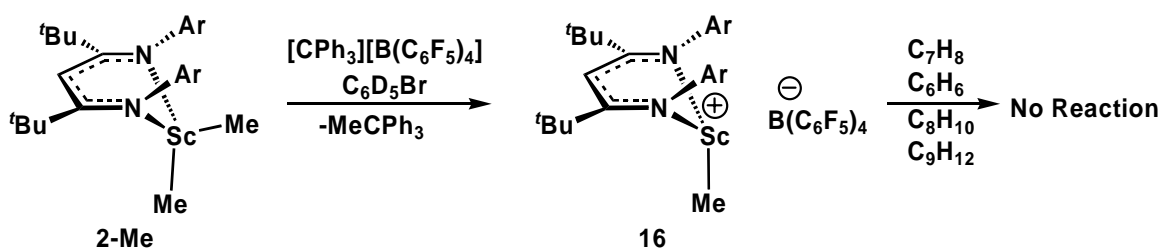


Scheme 4.10 Proposed Mechanism for Reaction of Diphenylacetylene with $14\text{-C}_9\text{H}_{12}$

envison a mechanism which involves initial coordination of diphenylacetylene through the aromatic groups prior to insertion into the Sc-Me bond, no evidence of such coordination was observed, even upon addition of reagents and subsequent monitoring at $-35\text{ }^\circ\text{C}$.

The independent measurement of arene ring slipping, established for arene exchange, confirmed the calculated values are not associated with this step. In order to lend support to the idea that alkyne coordination, and not alkyne insertion, was the rate limiting step, a study was conducted to determine how increasing the steric bulk near the metal centre would effect reaction rates. In order to achieve this, one equivalent of $\text{L}^{\text{tBu}}\text{ScMe}_2$, **2-Me**, was reacted with one equivalent of $[\text{CPh}_3][\text{B}(\text{C}_6\text{F}_5)_4]$ *in situ* at $-30\text{ }^\circ\text{C}$ in $\text{C}_6\text{D}_5\text{Br}$. Rapid loss of MeCPh_3 was observed in the ^1H NMR spectrum along with concomitant production of $[\text{L}^{\text{tBu}}\text{ScMe}][\text{B}(\text{C}_6\text{F}_5)_4]$, **16**. The spectrum exhibited 1

isopropyl methine resonance and 2 *isopropyl* methyl resonances indicative of a C_{2v} symmetric structure with no evidence of C_6D_5Br coordination. A series of experiments involving addition of C_6H_6 , C_7H_8 , C_8H_{10} and C_9H_{12} to **16** showed no evidence for arene coordination in solution (Scheme 4.11). This would seem to suggest either that the more sterically encompassing L^{tBu} ancillary crowds the scandium centre to the point whereby no close metal – arene contacts occur, or perhaps, as suggested by Ziegler,¹⁰⁹ η^2 or η^4 stabilizing interactions are present and rapidly fluxional on the NMR timescale. Nonetheless, it can be assumed that if the mechanism for either arene

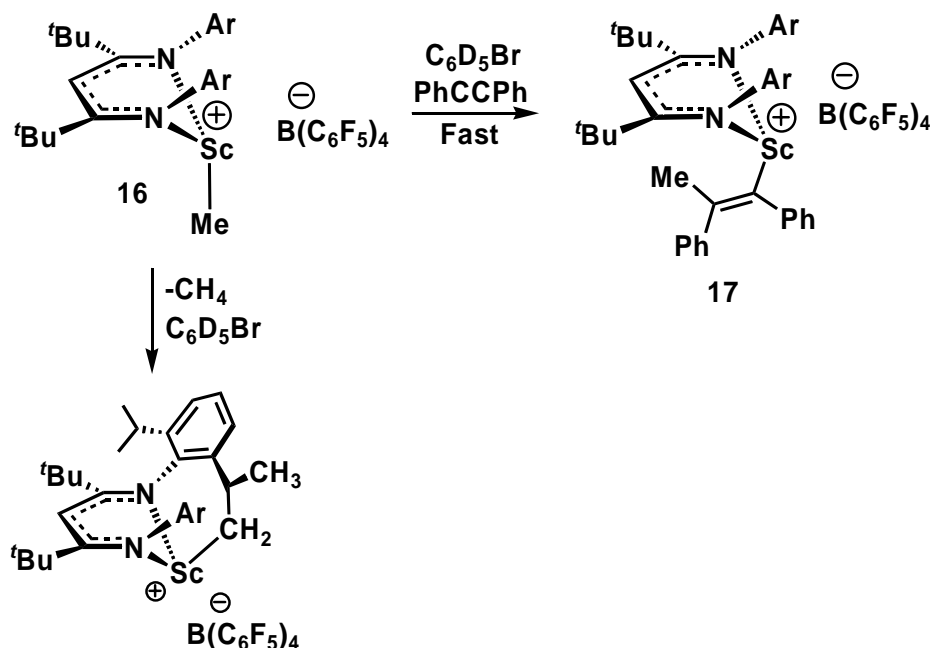


Scheme 4.11 Preparation of **16**

exchange or alkyne insertion involved complete dissociation, **16** could be viewed as a good model for the transition state whereby complete dissociation has occurred, but no coordination or insertion has yet taken place. Thus, monitoring of alkyne insertion into **16** should be representative of the barrier pertinent only to coordination and insertion.

Reaction of **16** with diphenylacetylene to afford **17** was qualitatively monitored and found to be exceedingly rapid, even at $-20\text{ }^\circ\text{C}$ (Scheme 4.12). Since the reaction rate of diphenylacetylene with the more bulky **16** is substantially greater (at least several orders of magnitude) than with **14-C₉H₁₂**, and that upon complete dissociation of the arene from **14-C₉H₁₂**, the reaction coordinate (alkyne insertion) should be similar for both compounds, it is not likely that the barriers extracted from the kinetic data (*vide*

supra) are reflective of alkyne insertion. It is therefore reasonable to assume that the rate determining step for reaction of diphenylacetylene with **14-C₉H₁₂** is association of the alkyne to a ring slipped **14-C₉H₁₂** intermediate.¹⁹⁸

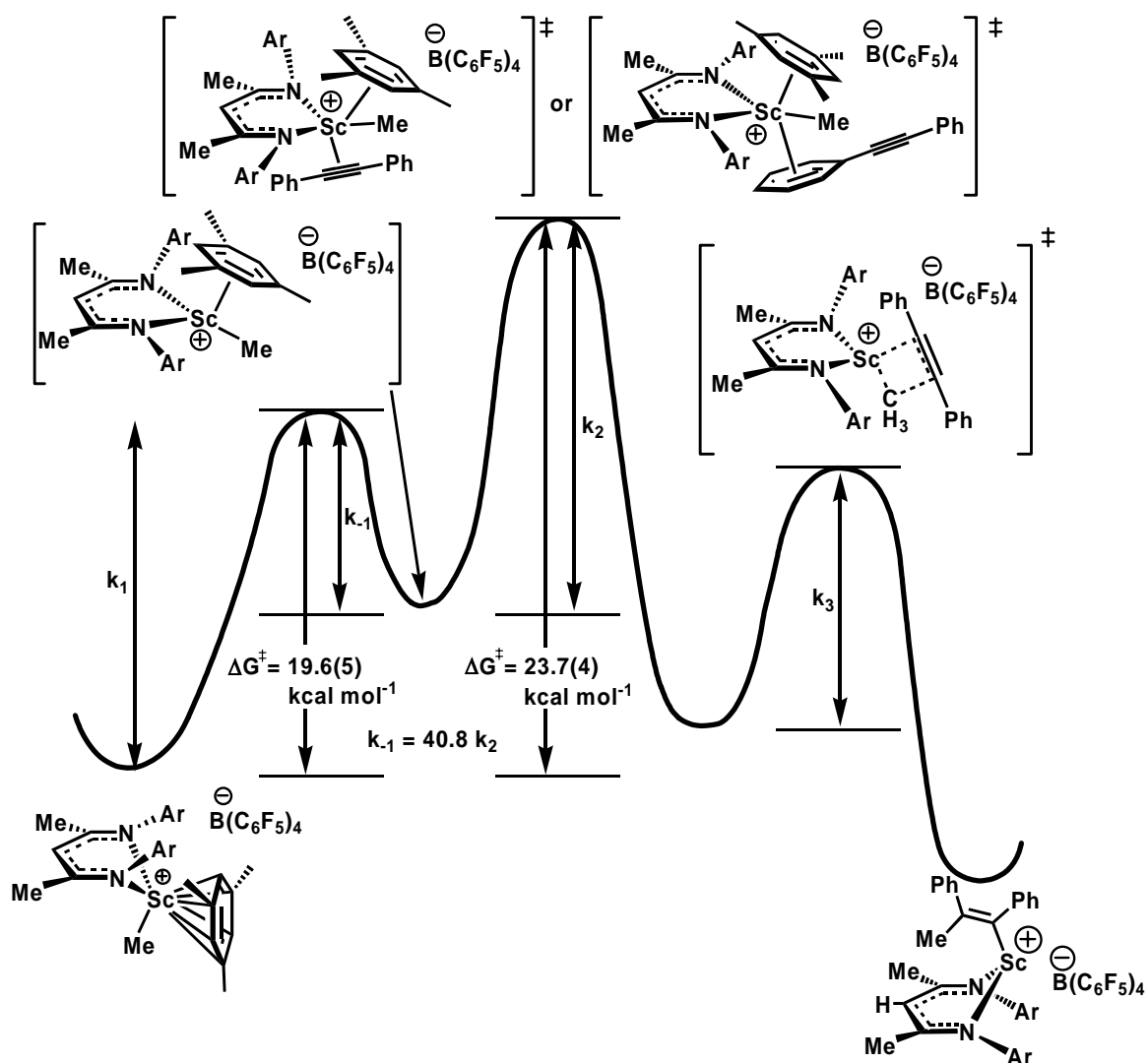


Scheme 4.12 Competing Pathways Upon Addition of $\text{PhC}\equiv\text{CPh}$ to **16**

Unfortunately, quantitative assessment of the barriers for the reaction of diphenylacetylene with **16** was not possible due to competitive decomposition *via* metallation of an aryl *isopropyl* group at temperatures above $-20\text{ }^\circ\text{C}$ (Scheme 4.12). Evidently any coordination of the solvent is very weak, and not sufficient to stabilize the molecule against typical deactivation routes. The inability of arenes to stabilize **16** through coordination appears to hold for **17**. The ^1H NMR spectrum does not exhibit any upfield resonances characteristic of phenyl interactions with the metal centre, as seen with the more sterically open **15**.

These findings are in good agreement with a kinetic study on the insertion of 2-butyne into Cp^*_2ScMe reported by Bercaw *et al.* where coordination of 2-butyne was

postulated to be the rate determining step ($\Delta G^\ddagger = 12.3(3)$ kcal mol⁻¹).^{9,198} The much larger enthalpic barrier ($\Delta H^\ddagger = 18.5(2)$ kcal mol⁻¹) observed for reaction of diphenylacetylene with **14-C₉H₁₂**, in comparison to reaction of 2-butyne with Cp*₂ScMe, ($\Delta H^\ddagger = 9.7(3)$ kcal mol⁻¹) is likely due to the increased steric bulk associated with both the alkyne and metal centre. The more negative entropy of activation ($\Delta S^\ddagger = -36(2)$ e.u.) observed by Bercaw and co-workers is indicative of a purely associative



Scheme 4.13 Proposed Reaction Profile for Reaction of PhC≡CPh with **14-C₉H₁₂**

transition state. Unlike this system, no ambiguity existed about a dissociative rate determining step because there were no dissociating molecules.

An energy profile for alkyne insertion is proposed in Scheme 4.13. This pathway involves arene ring slipping to a lower hapticity, followed by rate determining coordination of the alkyne to the metal centre. While it is certainly plausible that this coordination could be *via* an η^6 interaction with one of the aromatic groups, it seems unlikely that the barrier for this would be substantially greater than association of toluene. With the given data, however, it is impossible to disprove this scenario.

Although ring slipping is important for simple arene exchange, these findings suggest that the rate determining step for alkyne insertion, and possibly olefin polymerization, is alkyne coordination. As such, it is possible that for other β -diketiminato supported organoscandium olefin polymerization catalysts this mechanism is operative even when the SSIP is not observed.

4.2.5 Conclusions

In summary, a unique family of isolable solvent separated organoscandium methyl cations have been synthesized. These complexes are supported by a sterically bulky nacnac ligand and have been found to be resistant to both C_6F_5 transfer and metallation decomposition pathways which hamper similar ion-pairs possessing the $[MeB(C_6F_5)_3]^-$ anion. Their solution and solid state structures have been explored using multinuclear NMR and X-ray crystallography. While the molecular structures show stabilization of the alkyl cations through η^6 arene binding to the metal centre, the 1H

NMR spectrum for **14-C₆D₅Br** is indicative of a more symmetric species, indicating rapid arene exchange on the NMR timescale. In the presence of more basic arenes, however, the ¹H NMR spectra, which reveal top – bottom asymmetry, more closely resemble the C_s symmetric solid state structures.

Unlike the limited number of previously reported arene bound d⁰ complexes, the aromatic solvent molecules are bound sufficiently loose to permit the study of their chemistry. Quantitative kinetic experiments for arene exchange imply a partially dissociative mechanism whereby the rate limiting step involves dissociation to lower hapticity. The mechanism for arene displacement was further investigated upon exploring the reactivity of these SSIPs with diphenylacetylene. This process was also monitored by using NMR spectroscopy and it was determined that rate limiting coordination of the alkyne to the metal centre had a slightly higher barrier than arene ring slipping.

Chapter 5:

Future Work: Synthesis of Cationic Organoyttrium Compounds and Ethylene Polymerization Data

5.1 Introduction

5.1.1 Cationic Organoyttrium Compounds

While significant advances have recently been made in the development of organoscandium chemistry, the same is not necessarily true for the larger group 3 member yttrium. As with scandium, yttrium usually adopts a +3 oxidation state and its electrophilicity often results in complex oligomerization, and ligation of Lewis bases.⁵ Since yttrium is significantly larger than scandium (ionic radii: $Y^{3+} = 1.04 \text{ \AA}$, $Sc^{3+} = 0.89 \text{ \AA}$) these synthetic challenges are often more pronounced, resulting in a limited number of organoyttrium complexes of form LYR_2 . The larger size also results in more facile “ate” complex formation; it is frequently difficult to remove the salt by-products which form during preparations *via* salt metathesis.^{5,199}

Most progress towards the synthesis of monomeric LYR_2 species has been pioneered by a handful of scientists using salicylaldiminato,⁶⁷ anilido-imine,²⁰⁰ PNP,^{196,201} aza-18-crown-6,¹⁴⁶ *tris*(pyrazolyl)borate^{16,202} and modified amidinates ligands.^{199,203,204} The majority of these examples have required the use of rather bulky alkyl groups, thus limiting their ensuing organometallic reactivity.

While the number of dialkyl yttrium compounds is small, the number of well defined organoyttrium cations is even more limited with only several structurally characterized complexes reported.^{136,146,147,200,205} Most of these examples require at least one equivalent of a Lewis base, frequently THF, if they are to realize thermal stability for prolonged periods.^{147,200,205}

The utility of the β -diketiminato ligand in stabilizing both dialkyl (see Chapter 2) and cationic scandium species (see Chapter 3 & 4) suggested that this ancillary might be suitable for the development of well behaved dialkyl yttrium compounds. The larger size of yttrium was not anticipated to be problematic as the nacnac framework has been successfully attached to much larger metals.^{30,36,206-208} The following section describes preliminary results and future directions for the development of organoyttrium cations supported by a β -diketiminato ancillary.

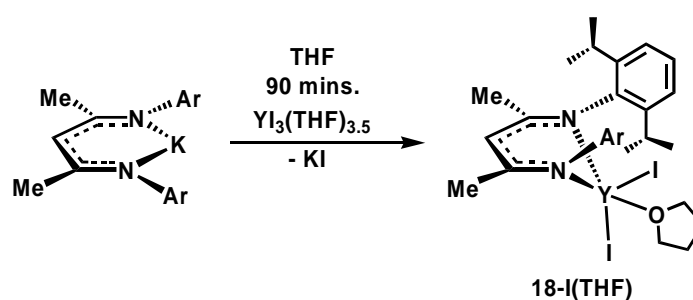
5.2 Preliminary Results

5.2.1 Synthesis and Reactivity of $L^{\text{Me}}\text{YR}_2(\text{THF})$

Initial attempts to produce L^{Me} supported yttrium compounds, including amine and alkane elimination routes, as well as salt metathesis from YCl_3 , were all unsuccessful. An yttrium species of form LYX_2 ($\text{X} = \text{halide}$) was most desirable because it would allow the greatest versatility when installing organic groups. The subsequent efforts focused upon enhancing the solubility of the yttrium starting material; YI_3 was chosen as the yttrium source. Although YI_3 is significantly more costly than YCl_3 , its greater solubility renders it more reactive. In addition, a recent report by Izod *et al.*

describes the preparation of $YI_3(THF)_{3.5}$ in 79% yield starting from the elements.²⁰⁹ Due to the reasonably high solubility of LiI in common hydrocarbon solvents, it is often difficult to separate from the desired product. Since KI is much less soluble, KL^{Me} , which is readily prepared from excess KH and HL^{Me} , was selected as a suitable nacnac starting material.

Reaction of $YI_3(THF)_{3.5}$ with KL^{Me} in THF for 90 minutes afforded $L^{Me}YI_2(THF)$, **18-I(THF)**, as a yellow crystalline solid in 44% yield (Scheme 5.1). The 1H NMR



Scheme 5.1 Synthesis of **18-I(THF)**

spectrum exhibited the anticipated nacnac resonances, as well as signals at 3.41 and 1.17 ppm attributed to one equivalent of coordinated THF (Figure 5.1). All efforts to remove

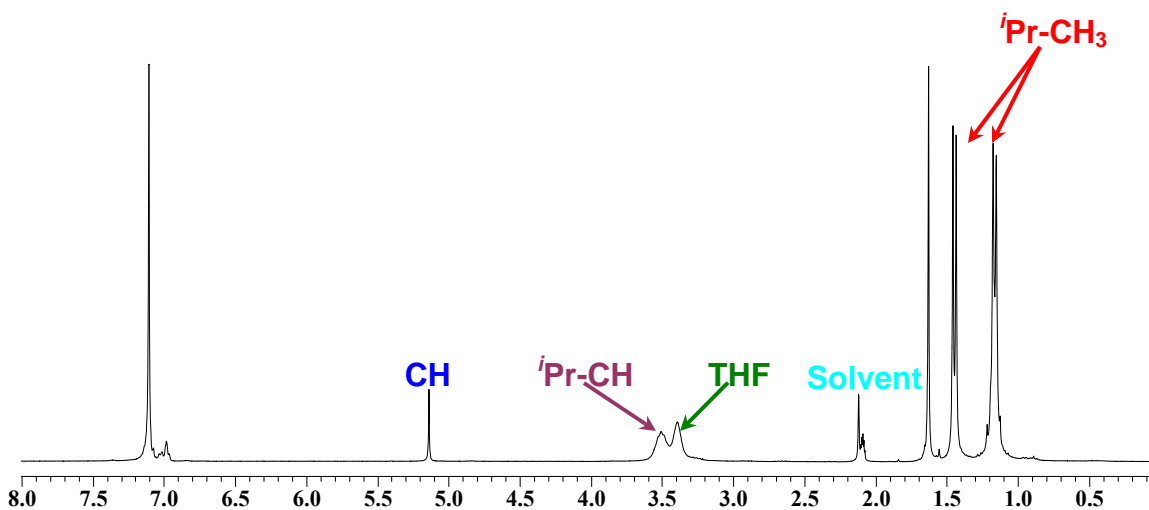


Figure 5.1 1H NMR Spectrum of **18-I(THF)**

the ligated THF, including exposure to dynamic vacuum for 3 days, were unsuccessful. The partial solubility of **18-I(THF)** in hexanes made it possible to grow single crystals suitable for an X-ray diffraction study. The molecular structure confirmed the identity of **18-I(THF)** as a monomer isostructural with **1-CI(THF)**. The yttrium centre adopts a distorted trigonal bipyramidal geometry with N(2) and O(1) comprising the axial sites and N(1), I(1) and I(2) the equatorial positions (Figure 5.2). As with the scandium

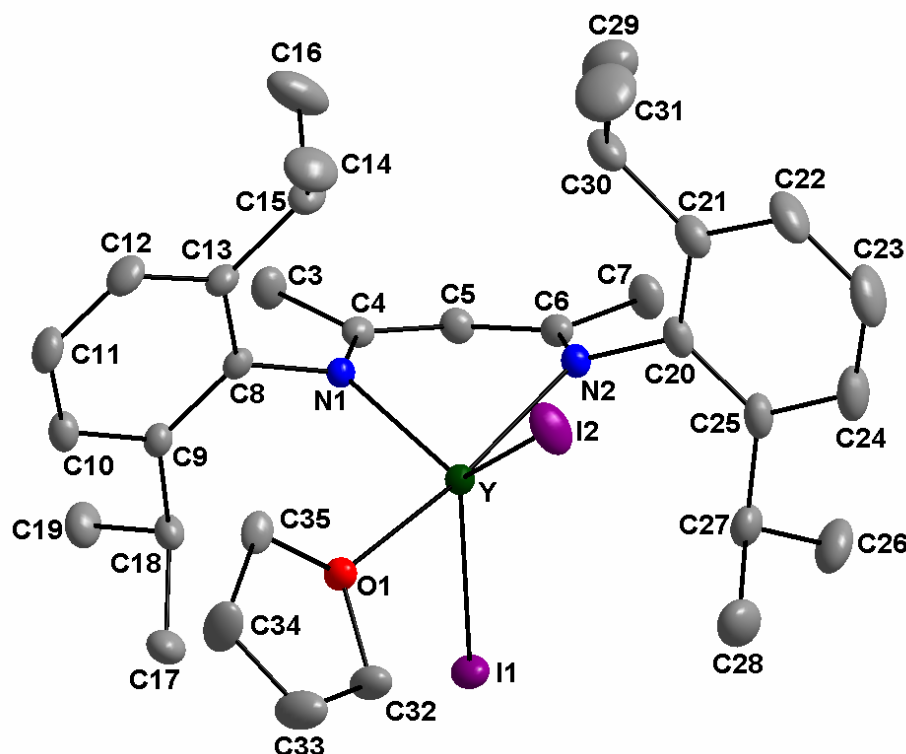


Figure 5.2 X-ray Molecular Structure of **18-I(THF)**. Thermal ellipsoids are drawn at the 30% probability level. Hydrogen atoms are removed for clarity.

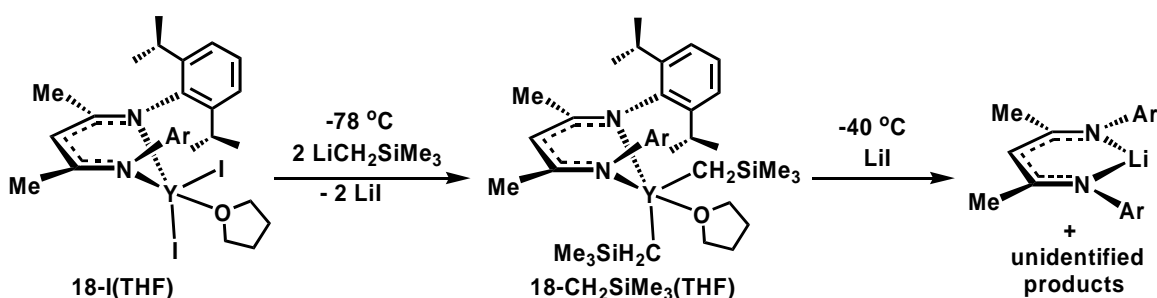
analogue, the metal centre is significantly displaced from the plane made by the nacnac backbone. This distance, at 1.017(3) Å, is longer than L^{Me} scandium species and is due to the larger metal centre and longer bond distances. The ligand is essentially symmetrically bound to yttrium with typical Y-N distances of 2.255(2) and 2.300(2) Å (Table 5.1). All other aspects of the solid state structure are unremarkable.

An NMR scale reaction of **18-I(THF)** with 2 equivalents of $\text{LiCH}_2\text{SiMe}_3$ in toluene resulted in immediate precipitation of LiI and concomitant growth of resonances attributable to **18-CH₂SiMe₃(THF)** in the ^1H NMR spectrum. Unfortunately it was not possible to isolate pure **18-CH₂SiMe₃(THF)** due to rapid production of LiL^{Me} upon

Table 5.1 Selected Metrical Data for **18-I(THF)**

Atoms	Bond Lengths (Å)	Atoms	Bond Angles (°)
Y-N(1)	2.255(2)	N(1)-Y-N(2)	82.99(8)
Y-N(2)	2.300(2)	N(1)-Y-O(1)	96.45(7)
Y-I(1)	2.9322(4)	N(2)-Y-O(1)	168.26(7)
Y-I(2)	2.9252(5)	N(1)-Y-I(1)	101.12(5)
Y-O(1)	2.3685(17)	N(1)-Y-I(2)	124.57(10)
Y-C(4)	3.167(3)	N(2)-Y-I(1)	100.72(5)
Y-C(5)	3.408(4)	N(2)-Y-I(2)	90.78(11)
Y-C(6)	3.160(3)	Y-N(1)-C(4)	121.49(17)
Y-N ₂ C ₃ Plane	1.017(3)	C(3)-C(4)-N(1)	120.6(2)
Atoms	Torsion Angles (°)	N(1)-C(4)-C(5)	123.6(2)
C(6)-N(2)-C(20)-C(25)	92.21(31)	C(4)-C(5)-C(6)	130.7(2)
C(6)-N(2)-C(20)-C(21)	-91.00(31)	C(5)-C(6)-N(2)	124.4(2)
C(4)-N(1)-C(8)-C(9)	82.13(31)	C(7)-C(6)-N(2)	119.9(2)
C(4)-N(1)-C(8)-C(13)	-102.77(28)	C(6)-N(2)-Y	118.15(17)

gradual warming of the sample above $-40\text{ }^\circ\text{C}$. Evidently the partial solubility of LiI was detrimental as it appears to have reacted with the newly formed **18-CH₂SiMe₃(THF)** to afford LiL^{Me} and unidentified yttrium species (Scheme 5.2).

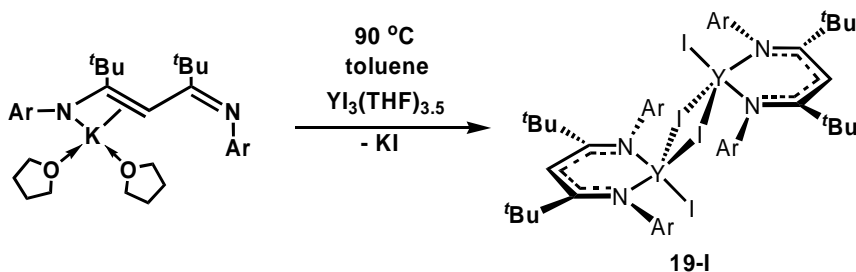


Scheme 5.2 Synthesis and Reactivity of **18-CH₂SiMe₃(THF)**

While it was not possible to overcome the production of LiL^{Me} , the use of alkyl potassium or Grignard reagents would produce KI and MgXI ($\text{X} = \text{halide}$) respectively, which may not present undesirable reactivities with the dialkyl yttrium compound. Likewise, performing the reaction in hexane, or using $\text{YBr}_3(\text{THF})_{3.5}$ as the yttrium starting material are straightforward alternatives which may alleviate the decomposition pathway through decreasing the solubility of the liberated salt.

5.2.2 Synthesis and Reactivity of $[\text{L}^{\text{tBu}}\text{YR}_2]_2$

In hopes of generating a monomeric base free dialkyl yttrium species, the more sterically demanding L^{tBu} was reacted, as its potassium salt, with one equivalent of $\text{YI}_3(\text{THF})_{3.5}$. Although no reaction occurred in THF, heating for 1 hour at $90\text{ }^\circ\text{C}$ in toluene afforded $\text{L}^{\text{tBu}}\text{YI}_2$, **19-I**, which could be isolated as a bright yellow microcrystalline solid in 55% yield (Scheme 5.3). The ^1H NMR spectrum closely mimicked that of **2-Cl**, in fact, the two are almost indistinguishable (Figure 5.3). The spectrum was quite broad at room temperature, however, at 370 K all signals were well resolved. The thermal stability of **19-I** was indicated by no evidence of decomposition over the duration required (12 hours) to obtain a variety of NMR spectra at 370K.



Scheme 5.3 Synthesis of **19-I**

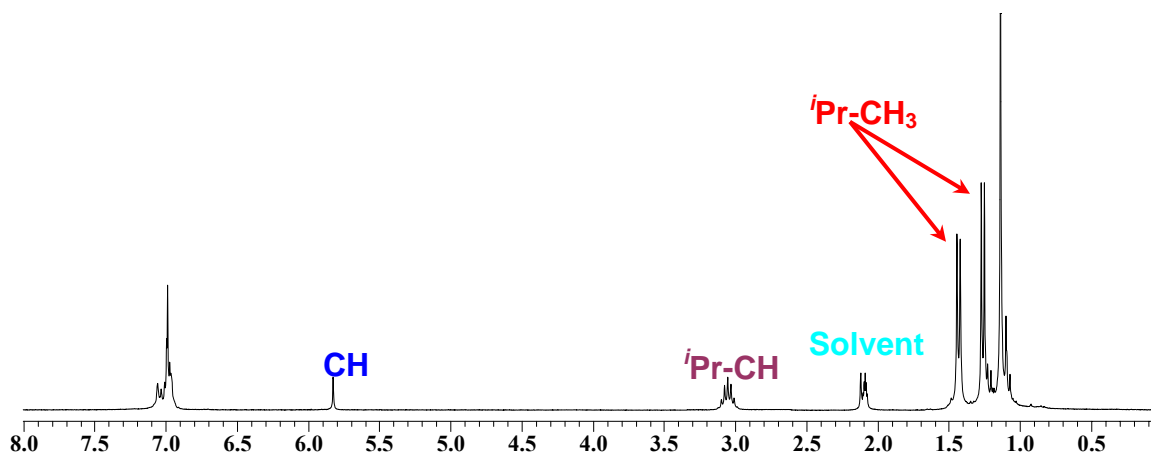


Figure 5.3 ^1H NMR Spectrum of **19-I** at 370K

Cryoscopic molecular weight measurements were not conducted, however, the inherent insolubility of **19-I** at low temperatures suggests that it may exist as a dimer in solution.

The solid state structure of **19-I** was indeed established as a dimer *via* X-ray crystallography (Figure 5.4). The yttrium centre is approximately trigonal bipyramidal,

Table 5.2 Selected Metrical Data for **19-I**

Atoms	Bond Lengths (Å)	Atoms	Bond Angles (°)
Y-N(1)	2.356(3)	N(1)-Y-N(2)	81.67(11)
Y-N(2)	2.256(3)	N(1)-Y-I(1)	93.27(8)
Y-I(1)	2.9119(7)	N(1)-Y-I(2)	90.42(8)
Y-I(2)	3.0915(7)	N(1)-Y-I(2')	169.21(8)
Y-I(2')	3.1363(7)	N(2)-Y-I(1)	122.62(8)
Y-C(4)	2.909(4)	N(2)-Y-I(2)	130.51(8)
Y-C(5)	2.673(4)	N(2)-Y-I(2')	105.43(8)
Y-C(6)	2.645(4)	Y-N(1)-C(4)	101.2(8)
Y-N ₂ C ₃ Plane	1.750(3)	C(3)-C(4)-N(1)	128.8(4)
Atoms	Torsion Angles (°)	N(1)-C(4)-C(5)	117.5(4)
C(6)-N(2)-C(20)-C(25)	146.67(43)	C(4)-C(5)-C(6)	128.7(4)
C(6)-N(2)-C(20)-C(21)	-41.67(64)	C(5)-C(6)-N(2)	119.4(4)
C(4)-N(1)-C(8)-C(9)	95.34(55)	C(7)-C(6)-N(2)	123.4(4)
C(4)-N(1)-C(8)-C(13)	-90.78(56)	C(6)-N(2)-Y	90.2(2)

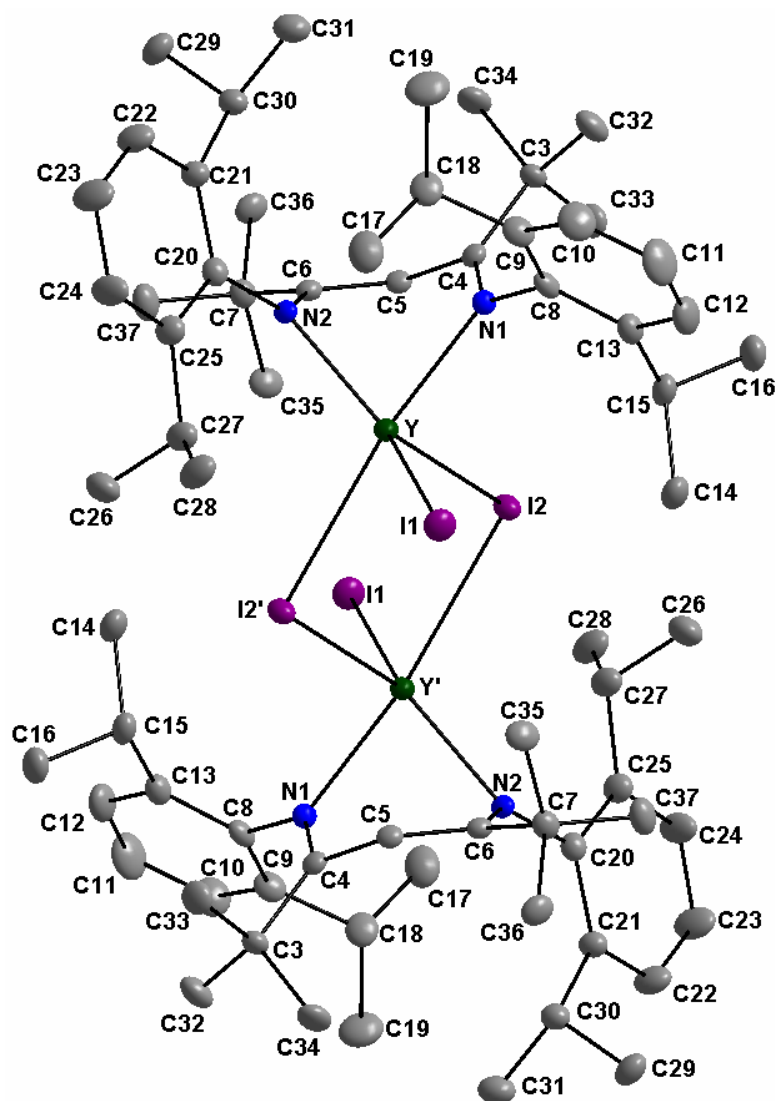
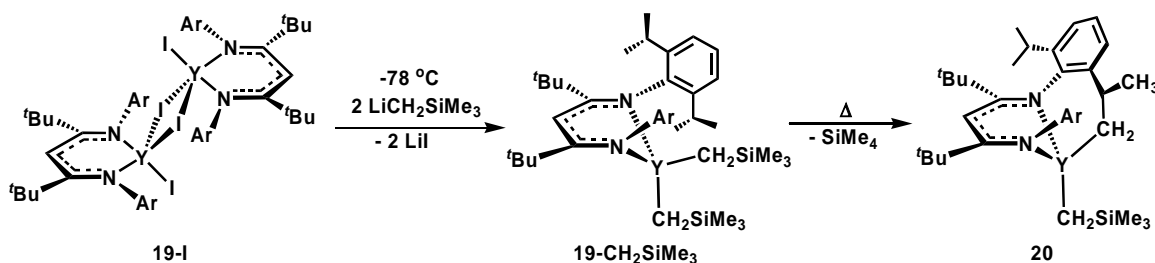


Figure 5.4 X-ray Molecular Structure of **19-I**. Thermal ellipsoids are drawn at the 30% probability level. Hydrogen atoms are removed for clarity.

however, significant steric interactions cause large distortions from the optimal geometry. Likewise, the ligand framework is substantially strained as evidenced by the severe distortion from planarity in the backbone. This flexion relieves steric strain by placing one ^tBu and one N-aryl group above the ligand framework and one beneath it. In addition, the N-aryl groups are forced far from orthogonality with torsion angles ranging from $-41.67 - 146.67^\circ$ (Table 5.2). The metal centre resides almost directly beneath the

nitrogen atoms at a distance of 1.750(3) Å from the plane made by the ancillary core. This fact is illustrated by the small Y-N(2)-C(6) angle of 90.2(2)°.

Distinct differences between the terminal (2.9119(7) Å) and bridging (3.0915(7) and 3.1363(7) Å) Y-I bond distances are observed with the terminal halides occupying the *exo* sites. The dimeric *endo-endo* structure removes the bulk of the two nacnac ligands further from each other than if they were in an *exo-exo* or *endo-exo/exo-endo* conformation. Unlike $L^{tBu}Sc(TeCH_2SiMe_3)-\mu-Te-ScL^{tBu}(TeCH_2SiMe_3)^{59}$ it is not possible to freeze out mixed *endo-exo/exo-endo* structures by NMR spectroscopy, even at very low temperatures (-90 °C). It appears that as the bridging metal-substituent lengths increase from 2.303(5)/2.364(10) Å in **1-Me** to 2.8326(4) Å in $L^{tBu}Sc(TeCH_2SiMe_3)-\mu-Te-ScL^{tBu}(TeCH_2SiMe_3)$ to 3.0915(7)/3.1363(7) Å in **19-I** the preference gradually changes from an *exo-exo* to *endo-endo* conformation.



Scheme 5.4 Synthesis and Metallation of **19-CH₂SiMe₃**

The addition of 2 equivalents of LiCH₂SiMe₃ to **19-I** led to the immediate formation of the desired dialkyl complex $L^{tBu}Y(CH_2SiMe_3)_2$, **19-CH₂SiMe₃** as indicated by ¹H NMR spectroscopy (Scheme 5.4). The ¹H NMR spectrum exhibited a diagnostic doublet (²J_{H-Y} = 2.8 Hz; ⁸⁹Y = 100%, I = ½) at -0.52 ppm assigned to the Y-CH₂ group (Figure 5.5).⁵ Although there were no complications arising from reaction of **19-CH₂SiMe₃** with LiI, gradual warming of the sample to room temperature exhibited

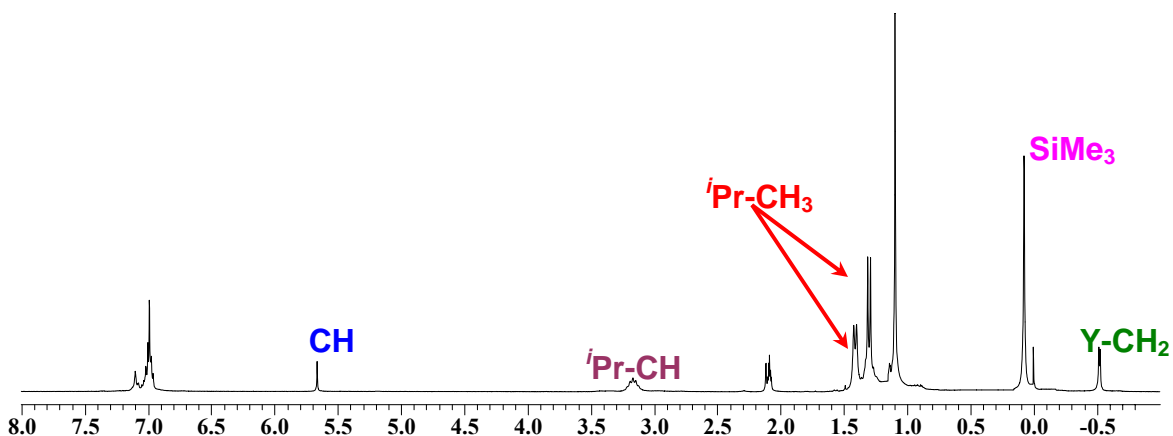


Figure 5.5 ^1H NMR Spectrum of **19-CH₂SiMe₃**

loss of SiMe_4 , along with other resonances attributed to metallation of an aryl *isopropyl* moiety and formation of $\kappa^3\text{-[ArNC}(\text{tBu})\text{CHC}(\text{tBu})\text{N-}i\text{Pr-C}_6\text{H}_3\text{]YCH}_2\text{SiMe}_3$, **20**. Kinetic experiments to quantitatively determine the rate of metallation were not conducted, however, qualitative inspection revealed that decomposition was not exceedingly rapid with an approximate half-life of 1 hour at 300 K. Cryoscopic measurements could not be performed due to the instability of **19-CH₂SiMe₃**, however, the significant enhancement in solubility suggests that **19-CH₂SiMe₃** may exist as the desired base free monomer in solution.

The ^1H NMR spectrum of **20** was quite complex as it consisted of an approximate 3 : 1 ratio of isomers. Although no attempts to assign the isomers were taken, it is likely that the major isomer is *exo*-**CH₂SiMe₃-20**, as observed for **3-CH₂SiMe₃**. Overlapping multiplets upfield of -1.5 ppm are attributed to the magnetically inequivalent Y-CH₂ of the remaining Y-CH₂SiMe₃ moiety. Although the signals seem quite complex, they nicely match the expected appearance for 4 sets of doublets of doublets of different intensities, 2 of which are overlapping (Figure 5.6). All 4 doublets of doublets have the same coupling constants ($^2J_{\text{H-H}} = 14.1$ Hz, $^2J_{\text{H-Y}} = 2.7$ Hz).

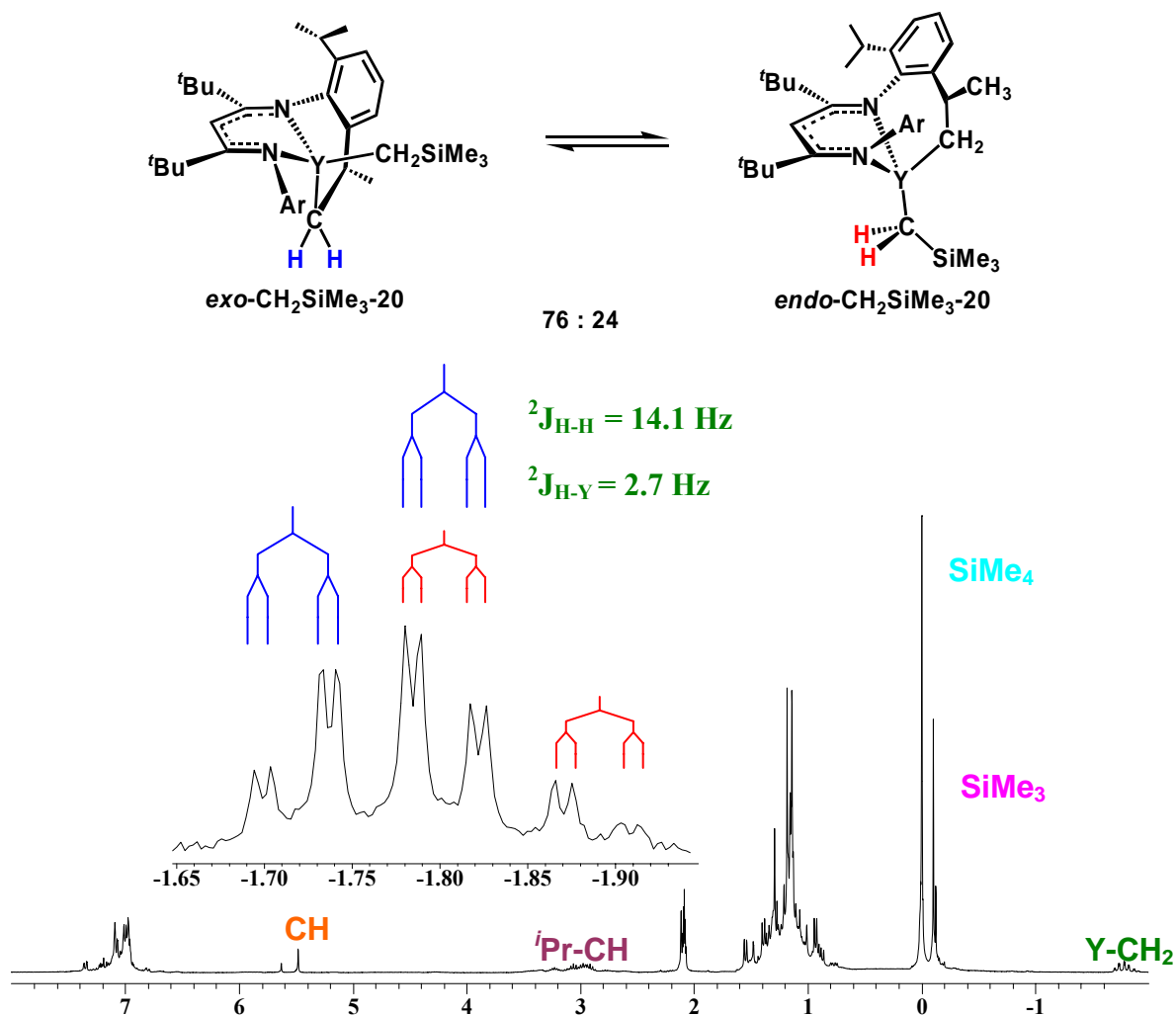


Figure 5.6 ¹H NMR Spectrum of 20

It may be possible to circumvent metallation by modification of the Y alkyl substituents, for example, benzyl groups were found to be substantially more metallation resistant in the scandium analogues. Isolation of **19-CH₂SiMe₃** should also be possible if the reaction is carefully carried out at low temperature.

5.3 Conclusions

In conclusion, the β -diketiminato ligand has proven to be potentially useful in the preparation of organoyttrium cations. Preliminary studies demonstrated facile ligand attachment protocols for both L^{Me} and the more sterically demanding L^{tBu} . Although reaction of **18-I(THF)** with alkyl lithium reagents was complicated by competing reactivity with LiI, these problems may potentially be avoided merely by fine tuning the reaction temperatures, solvents or by judicious choice of alkylating reagent. Facile alkylation of **19-I** afforded **19-CH₂SiMe₃** which showed no sign of side reactions with LiI, however, metallation of an aryl *isopropyl* group occurred at elevated temperatures. Nonetheless, this metallation process was found to proceed at a rate slow enough so that it is unlikely to significantly interfere with the synthesis of cationic derivatives. It may also be possible to circumvent metallation altogether by replacing the CH₂SiMe₃ moiety with aryl containing groups, such as CH₂Ph or CH₂SiMe₂Ph.

Chapter 6: Experimental Methods

6.1 General

6.1.1 Laboratory Equipment and Apparatus

An argon filled Innovative Technology System One glove box was employed for manipulation and storage of all oxygen and moisture sensitive compounds. All thermally unstable compounds were stored in a -35 °C freezer within the glove box. All reactions were performed on a double manifold high vacuum line using standard techniques.²¹⁰ Residual oxygen and moisture were removed from the argon stream by passage through an OxisorBW scrubber from Matheson Gas Products. Commonly utilized specialty glassware includes the swivel frit assembly, needle valves, and thick walled (5 mm) glass bombs equipped with Kontes Teflon stopcocks. All glassware was stored in a 110 °C oven for a minimum of 12 hours before immediate transfer to the glove box antechamber or assembled on the vacuum line and evacuated while hot.

6.1.2 Solvents

Toluene, hexanes, and tetrahydrofuran (THF) solvents were dried and purified using the Grubbs/Dow purification system²¹¹ and stored in evacuated 500 mL bombs over titanocene²¹² (toluene and hexanes) or sodium/benzophenone ketal (THF). Benzene, *d*₆-benzene, *d*₈-toluene, *d*₈-THF and hexamethyldisiloxane were dried and stored over sodium/benzophenone ketal in glass bombs under vacuum. Bromobenzene, *d*₅-bromobenzene, and *d*₂-methylene chloride were predried over 4Å molecular sieves, stored over calcium hydride and distilled prior to use. Diethyl ether was pre-dried over lithium aluminum hydride and stored over sodium/benzophenone ketyl in a glass bomb

under vacuum. Unless otherwise noted, solvents were introduced via vacuum transfer with condensation at $-78\text{ }^{\circ}\text{C}$.

Liquid nitrogen ($-196\text{ }^{\circ}\text{C}$), liquid nitrogen/pentane ($-130\text{ }^{\circ}\text{C}$), dry ice/acetone ($-78\text{ }^{\circ}\text{C}$) dry ice/acetonitrile ($-45\text{ }^{\circ}\text{C}$) and water/ice ($0\text{ }^{\circ}\text{C}$) baths were used for cooling receiving flasks and to maintain low temperature conditions.

6.1.3 Instrumentation and details for NMR experiments

Nuclear magnetic resonance spectroscopy (^1H , ^2H , ^{11}B , $^{13}\text{C}\{^1\text{H}\}$, ^{19}F , DEPT-135, DEPT-90, HMQC, EXSY,⁶⁵ ROESY and COSY experiments) was performed on Bruker AC-200 (^1H 200.134 MHz, $^{13}\text{C}\{^1\text{H}\}$ 50.323 MHz), Bruker AMX-300 (^1H 300.138 MHz, ^2H 46.073 MHz, $^{11}\text{B}\{^1\text{H}\}$ and ^{11}B 96.293 MHz, $^{13}\text{C}\{^1\text{H}\}$ 75.478 MHz, ^{19}F 282.371 MHz) or Bruker DRX-400 (^1H 400.134 MHz, $^{13}\text{C}\{^1\text{H}\}$ 100.614 MHz, ^{11}B 128.375 MHz) spectrometers. All 2D NMR experiments were performed using Bruker AMX-300 or Bruker-DRX 400 spectrometers. All ^1H NMR spectra were referenced to SiMe_4 through the residual ^1H resonance(s) of the employed solvent; C_6D_6 (7.16 ppm), d_8 -toluene (2.09, 6.98, 7.02 and 7.09 ppm), d_8 -THF (1.73 and 3.58 ppm), $\text{C}_6\text{D}_5\text{Br}$ (6.94, 7.02 and 7.30 ppm), or CD_2Cl_2 (5.32 ppm). ^2H NMR spectra were referenced relative to an external standard of $\text{Si}(\text{CD}_3)_4$ (0.0 ppm) in C_6D_6 prior to spectrum acquisition. ^{11}B NMR spectra were referenced to an external standard of boron trifluoride diethyl etherate (δ 0.0 ppm) in C_6D_6 prior to acquisition of the first spectrum. ^{13}C NMR spectra were referenced relative to SiMe_4 through the resonance(s) of the employed solvent; C_6D_6 (128.0 ppm), d_8 -toluene (20.4, 125.2, 128.0, 128.9, 137.5 ppm), d_8 -THF (25.4, 67.6 ppm), $\text{C}_6\text{D}_5\text{Br}$ (122.3, 126.1, 129.3, 130.9 ppm), or CD_2Cl_2 (54.0 ppm). ^{19}F NMR spectra are referenced

to CFCl_3 using an external standard of hexafluorobenzene (δ -163.0 ppm)²¹³ in C_6D_6 prior to acquisition of the first spectrum. Temperature calibration for NMR experiments was achieved by monitoring the ^1H NMR spectrum of pure methanol (below room temperature) and pure ethylene glycol (above room temperature).²¹⁴

All NMR samples were prepared in the glove box and tubes capped with rubber septa. ^1H NMR spectra are presented with the following format: chemical shift (ppm), multiplicity, J = coupling constant (Hz), number of protons, assignment. ^2H NMR spectra are listed with the following format: chemical shift (ppm), multiplicity, J = coupling constant (Hz), number of deuteriums, assignment. ^{11}B NMR spectra are listed with the following format: chemical shift (ppm), multiplicity, J = coupling constant (Hz). $^{13}\text{C}\{^1\text{H}\}$ NMR spectra are listed with the following format: chemical shift (ppm), J = coupling constant (Hz), assignment. Some ^{13}C NMR resonances (Sc-C and B-C) were assigned using the HMQC pulse sequence.²¹⁵ ^{13}C NMR resonances are not reported for carbons directly bonded to a fluorine atom. ^{19}F NMR spectra are listed with the following format: chemical shift (ppm), number of fluorines, assignment.

6.1.4 Other Instrumentation and Analysis

Elemental analyses were performed on a Control Equipment Corporation 440 Elemental Analyzer by Mrs. Dorothy Fox and Mrs. Roxanna Smith of this department. IR spectra were obtained using a NEXUS 470 FT-IR ESP spectrometer. Solid samples were pressed into KBr pellets and handled exclusively under argon. UV-Vis spectra were collected between 190 and 900 nm using a Varian Cary-1E UV-VIS spectrometer. All samples were prepared in the glove box (in hexane between 1×10^{-4} and 1×10^{-5} M) and

spectra obtained using Teflon capped quartz 10 mm cells. Thermogravimetric analysis (TGA) was performed on a Netzsch STA 449C Simultaneous Thermal Analyzer with an aluminum sample pan and an empty aluminum pan, as reference, employed. The dynamic heating programs were conducted with a constant flow of dried (CaCl_2) dinitrogen being maintained, heating from 25 to 600 °C at a rate of 10 °C/minute. The solid samples were sealed in aluminum pans in the glovebox and pierced with a small bore needle under a flow of N_2 immediately prior to insertion into the instrument. X-ray crystallographic analyses were performed on suitable crystals coated in Paratone 8277 oil (Exxon) and mounted on a glass fibre. Measurements were collected on a Rigaku AFC6S or Nonius KappaCCD diffractometer by Dr. Masood Parvez of this department or a Bruker P4/RA/SMART 1000 CCD diffractometer by Dr. Robert McDonald (University of Alberta); full details can be found in the individual tables for each crystal structure (see Appendix 1). A Fischer Scientific Ultrasonic FS-14 bath was used to sonicate reaction mixtures where indicated.

6.1.5 NMR tube Reactions

Unless otherwise noted NMR tube reactions were carried out by charging an NMR tube with the initial reagents and solvents in the glove box. Subsequent reagents were introduced by syringe to the septa sealed NMR tubes submerged in the appropriate cold bath. The tube was shaken once to ensure proper mixing prior to insertion into the NMR probe. This mixing was performed very quickly (~ 2 seconds) to avoid warming and premature reaction.

In situations where gases or low boiling liquids were to be introduced a flame-

sealable NMR tube and vacuum line adaptor were used. Once attached to the vacuum line the NMR tube was evacuated and solution degassed using a freeze-pump-thaw routine. The solution was carefully frozen with the appropriate cooling bath for the solvent in use followed by evacuation for several minutes. The frozen solution was thawed whereby dissolved gases were released into the headspace. The solution was frozen again and the vessel evacuated for several minutes. This process was repeated thrice more to ensure full degassing. Once all reagents were added the tube was flame sealed using an oxygen/natural gas torch.

NMR tube reactions which require high pressures of H₂ gas were conducted in a similar manner with the exception that after the solution was degassed approximately two thirds of the tube was cooled with a liquid nitrogen bath. One atmosphere of H₂ was introduced and then the system closed at the line adaptor using the Kontes valve. The liquid nitrogen bath was raised higher to cool approximately three quarters of the tube, thus creating a slight vacuum within. The NMR tube was then flame sealed above this point using an oxygen/natural gas torch.

6.1.6 Starting Materials

Tris(pentafluorophenyl)borane (B(C₆F₅)₃) was purchased from Boulder Scientific Co. and dried by stirring over Me₂SiHCl under an argon atmosphere for 20 minutes; the volatiles were removed *in vacuo*. The dried B(C₆F₅)₃ was then sublimed at 70 °C under a dynamic vacuum.²¹⁶ HL (L = ArNC(R)CHC(R)NAr where Ar = 2,6-*i*Pr-C₆H₃ and R = Me and *t*Bu), KL (L = ArNC(R)CHC(R)NAr where Ar = 2,6-*i*Pr-C₆H₃ and R = Me) and EtLi were prepared by literature procedures.²¹⁷⁻²¹⁹ [CPh₃][B(C₆F₅)₄] and

[HNMe₂Ph][B(C₆F₅)₄] were received as gifts from NOVA Chemicals LTD. Scandium oxide (Sc₂O₃) was purchased from Boulder Scientific Co. and used as received. All deuterated solvents for NMR experiments were purchased from Cambridge Isotopes. All other reagents were purchased from Aldrich Chemicals and used as received.

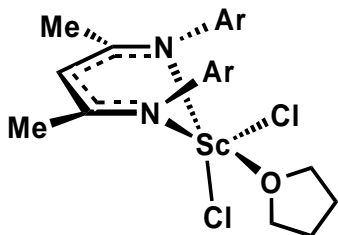
6.2 Experimental Procedures Pertaining to Chapter 2

6.2.1 Synthetic Procedures

Synthesis of ScCl₃(THF)₃:

ScCl₃(THF)₃ was made by a modified literature procedure.²²⁰ A 1 L RB flask equipped with a condenser was charged with Sc₂O₃ (20.3 g, 0.146 mol) and 6M HCl (300 mL). The reaction mixture was heated to reflux for 3 hours during which the mixture had changed from a cloudy white suspension to a clear yellow solution. The solvent was removed by rotational evaporation to give ScCl₃(H₂O)₆ as a thick yellow oil. A solution of SOCl₂ (350 mL) and THF (250 mL) was added dropwise to the oil over 2 hours (caution: extremely exothermic), during which time a large quantity of gas (SO₂) evolved with concomitant precipitation of a white solid, followed by a gradual change to a clear yellow solution. The reaction mixture was then heated at 86 °C for 18 hours and solvent removed by rotational evaporation to afford an oily yellow solid. The moisture sensitive mixture was quickly attached to a swivel frit apparatus and evacuated. Et₂O (200 mL) was added to the residue, stirred for 20 minutes and then filtered. The fine white powder was washed with Et₂O (4 x 50 mL) and solvent removed *in vacuo*. Yield: 100.8 g, 0.274 mol, 94%. The IR matched that of the published procedure.

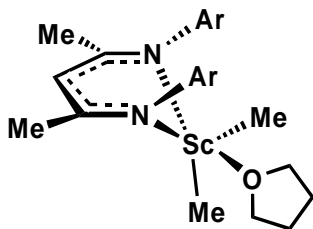
Synthesis of [ArNC(Me)CHC(Me)NAr]ScCl₂•THF (1-Cl(THF)):



Toluene (40 mL) was condensed into an evacuated flask containing LiL (2.00 g, 4.72 mmol) and ScCl₃(THF)₃ (2.00 g, 4.72 mmol) at -78 °C. The mixture was heated with stirring at 110 °C for 16 hours. The reaction mixture was

hot filtered to remove LiCl, and the toluene removed *in vacuo*. Trituration of the residue with hexanes (30 mL) followed by back filtration lead to isolation of pure **1-Cl(THF)** as a pale yellow solid (2.70 g, 4.46 mmol, 95%). ¹H NMR (C₆D₆): δ 7.21 (m, 6H; C₆H₃), 5.32 (s, 1H; CH); 3.56 (sp, 4H; CHMe₂, J_{H-H} = 6.8 Hz), 3.48 (OCH₂CH₂), 1.65 (s, 6H; NCMe), 1.48 (OCH₂CH₂) (1.39 (d, 12H; CHMe₂, J_{H-H} = 6.8 Hz), 1.17 (d, 12H; CHMe₂, J_{H-H} = 6.8 Hz). ¹³C{¹H} NMR (C₆D₆): δ 162.3 (NCMe), 143.3 (C_{ipso}), 143.3, 126.6, 124.2 (C₆H₃), 99.8 (CH), 28.6 (CHMe₂), 25.0, 24.7 (CHMe₂) 24.4 (Me). Anal. Calcd. for C₃₃H₄₉N₂Cl₂O₂Sc : C, 65.44; H, 8.15; N, 4.63. Found : C, 65.35; H, 8.61; N, 4.61.

Synthesis of [ArNC(Me)CHC(Me)NAr]ScMe₂•THF (1-Me(THF)):

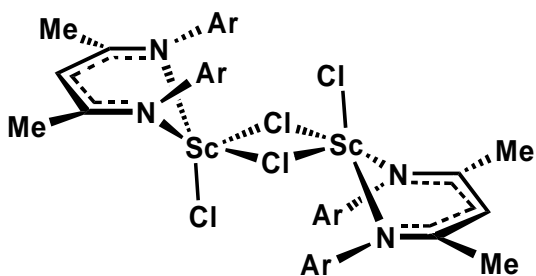


Toluene (20 mL) was condensed into an evacuated flask containing **1-Cl(THF)** (0.390 g, 0.640 mmol) and solid methyl lithium (0.028 g, 1.28 mmol) at -78 °C. The yellow mixture was gradually warmed to room temperature and

stirred for 3 hours. The solvent was removed and hexanes (10 mL) were added. The reaction mixture was cooled to -78 °C for 1 hour and resultant precipitate filtered and dried under vacuum. Yield: 0.120 g, 0.198 mmol, 31%. ¹H NMR (C₆D₆): δ 7.16 (m, 6H; C₆H₃), 5.06 (s, 1H; CH); 3.45 (sp, 4H; CHMe₂, J_{H-H} = 6.8 Hz), 3.40 (OCH₂CH₂), 1.67 (s,

6H; NCMe), 1.40 (d, 12H; CHMe₂, $J_{\text{H-H}} = 6.8$ Hz), 1.23 (OCH₂CH₂), 1.20 (d, 12H; CHMe₂, $J_{\text{H-H}} = 6.8$ Hz), -0.15 (s, 3H; ScMe). ¹³C{¹H} NMR (C₆D₆): δ 167.8 (NCMe), 143.0 (C_{ipso}), 142.7, 126.9, 124.4 (C₆H₃), 96.1 (CH), 28.6 (CHMe₂), 25.4, 25.2 (CHMe₂), 24.8 (ScMe), 24.1 (Me). Anal. Calcd. for C₃₅H₅₅N₂O₂Sc : C, 74.43; H, 9.82; N, 4.96. Found : C, 72.92; H, 9.70; N, 4.91.

Synthesis of [ArNC(Me)CHC(Me)NAr]ScCl₂ (**1-Cl**):

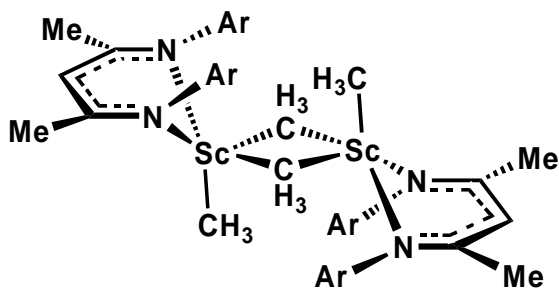


A 50 mL RB flask containing **1-Cl**(THF) (1.50 g, 2.48 mmol) was heated at 130 °C under full dynamic vacuum for 18 hours. The resultant yellow powder was washed with toluene (2 x 15 mL) and evacuated to

dryness. Yield: 1.29 g, 2.43 mmol, 98%. ¹H NMR (CD₂Cl₂): δ 7.11 (s, 6H; C₆H₃), 4.90 (s, 1H; CH), 3.11 (sp, 4H; CHMe₂, $J_{\text{H-H}} = 6.9$ Hz), 1.69 (s, 6H; NCMe), 1.21 (d, 12H; CHMe₂, $J_{\text{H-H}} = 6.6$ Hz), 1.11 (d, 12H; CHMe₂, $J_{\text{H-H}} = 6.6$ Hz). ¹³C{¹H} NMR (CD₂Cl₂): δ 161.8 (NCMe), 143.2 (C_{ipso}), 141.5, 125.7, 123.5 (C₆H₃), 94.0 (CH), 28.8 (CHMe₂), 24.6 (NCMe), 23.5, 21.1 (CHMe₂). Anal. Calcd. for C₂₉H₄₁N₂Cl₂Sc : C, 65.29; H, 7.75; N, 5.25. Found: C, 64.13; H, 6.84; N, 5.03.

Synthesis of [ArNC(Me)CHC(Me)NAr]ScMe₂ (**1-Me**):

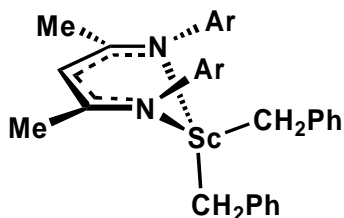
1-Cl (0.600 g, 1.13 mmol) and 2.1 equivalents of MeLi (0.0520 g, 2.37 mmol) were added to a 50 mL RB flask attached to a swivel frit apparatus. Toluene (30 mL) was



vacuum transferred onto the mixture and the resultant solution stirred for 4.5 hours. The reaction mixture was filtered and solvent removed *in vacuo* to afford 0.502 g (1.02 mmol, 91%) of **1-Me** as a yellow

crystalline solid. $^1\text{H NMR}$ (C_7D_8): δ 7.11 (s, 6H; C_6H_3), 4.91 (s, 1H; CH), 3.32 (sp, 4H; CHMe_2 , $J_{\text{H-H}} = 6.9$ Hz), 1.57 (s, 6H; NCMe), 1.35 (d, 12H; CHMe_2 , $J_{\text{H-H}} = 6.6$ Hz), 1.14 (d, 12H; CHMe_2 , $J_{\text{H-H}} = 6.6$ Hz), -0.06 (s, 6H; ScMe). $^{13}\text{C}\{^1\text{H}\}$ NMR (C_6D_6): δ 167.9 (NCMe), 143.0 (C_{ipso}), 141.4, 127.0, 124.5 (C_6H_3), 96.0 (CH), 28.8 (CHMe_2), 28.6 (ScMe), 25.6, 24.3 (CHMe_2), 23.9 (NCMe). Anal. Calcd. For $\text{C}_{31}\text{H}_{47}\text{N}_2\text{Sc}$: C, 75.57; H, 9.62; N, 5.69. Found: C, 75.00; H, 9.20; N, 5.66.

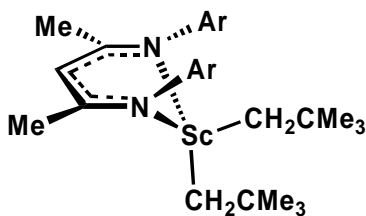
Synthesis of $[\text{ArNC}(\text{Me})\text{CHC}(\text{Me})\text{NAr}]\text{Sc}(\text{CH}_2\text{Ph})_2$ (**1-CH₂Ph**):



A two-necked flask was charged with **1-Cl**(THF) (0.400 g, 0.660 mmol) and attached to a swivel frit apparatus. A solid addition tube was loaded with benzyl potassium (0.172 g, 1.32 mmol) and attached to the second neck of the flask. The entire assemblage was evacuated, and benzene (50 mL) was vacuum distilled into the flask. After warming to room temperature, the benzyl potassium was gradually added to the solution over 30 minutes. Stirring was continued for another 4 hours. The reaction was filtered and the benzene removed under vacuum to give crude **1-CH₂Ph**. Recrystallization from hexanes afforded pure **1-CH₂Ph** (0.230 g, 0.389 mmol, 59%). $^1\text{H NMR}$ (C_6D_6): δ 7.16-6.70 (m, 16H; ScCH_2Ph , C_6H_3), 5.01 (s, 1H; CH); 3.08

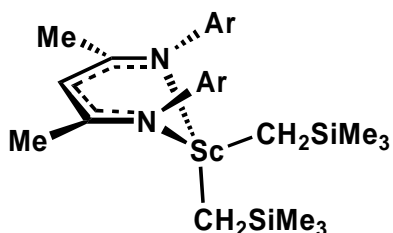
(sp, 4H; $CHMe_2$, $J_{H-H} = 6.8$ Hz), 2.10 (s, 4H; $ScCH_2Ph$), 1.58 (s, 6H; $NCMe$), 1.22 (d, 12H; $CHMe_2$, $J_{H-H} = 6.8$ Hz), 1.06 (d, 12H; $CHMe_2$, $J_{H-H} = 6.8$ Hz). $^{13}C\{^1H\}$ NMR (C_6D_6): δ 167.9 ($NCMe$), 149.3 ($ScCH_2Ph$), 143.2 (C_{ipso}), 142.2 (C_6H_3), 129.6 ($ScCH_2Ph$), 126.9 (C_6H_3), 124.9 ($ScCH_2Ph$), 124.7 (C_6H_3), 120.3 ($ScCH_2Ph$), 95.7 (CH), 61.6 ($ScCH_2Ph$), 28.8 ($CHMe_2$), 24.9, 24.8 ($CHMe_2$), 24.2 (Me). Anal. Calcd. for $C_{49}H_{67}N_2Sc$: C, 80.09; H, 8.60; N, 4.34. Found: C, 80.46; H, 8.04; N, 4.46.

Synthesis of $[ArNC(Me)CHC(Me)NAr]Sc(CH_2CMe_3)_2$ (**1-CH₂CMe₃**):



Toluene (20 mL) was condensed into an evacuated flask containing $LiCH_2CMe_3$ (0.139 g, 1.78 mmol) and **1-Cl(THF)** (0.474 g, 0.890 mmol) at -78 °C. The reaction vessel was slowly warmed to room temperature, after which stirring was continued for another 90 minutes. The solvent was removed under reduced pressure and hexanes (20 mL) was vacuum distilled into the flask. The mixture was filtered to remove $LiCl$. The solution was concentrated to 5 mL, cooled to -78 °C for 1 hour and back filtered to afford **1-CH₂CMe₃** as a white solid (0.340 g, 0.562 mmol, 64%). 1H NMR (C_6D_6): δ 7.16 (m, 6H; C_6H_3), 5.00 (s, 1H; CH), 3.47 (sp, 4H; $CHMe_2$, $J_{H-H} = 6.8$ Hz), 1.63 (s, 6H; $NCMe$), 1.47 (d, 12H; $CHMe_2$, $J_{H-H} = 6.8$ Hz), 1.17 (d, 12H; $CHMe_2$, $J_{H-H} = 6.8$ Hz), 1.03 (s, 18H; $ScCH_2CMe_3$), 0.87 (s, 4H; $ScCH_2CMe_3$). $^{13}C\{^1H\}$ NMR (C_6D_6): δ 167.1 ($NCMe$), 143.0 (C_{ipso}), 142.3, 126.8, 124.6 (C_6H_3), 94.3 (CH), 72.3 ($ScCH_2CMe_3$), 35.4 ($ScCH_2CMe_3$), 34.9 ($ScCH_2CMe_3$), 28.8 ($CHMe_2$), 25.3, 25.0 ($CHMe_2$), 24.6 (Me). Anal. Calcd. for $C_{39}H_{63}N_2Sc$: C, 77.44; H, 10.50; N, 4.63. Found: C, 77.56; H, 9.80; N, 4.73.

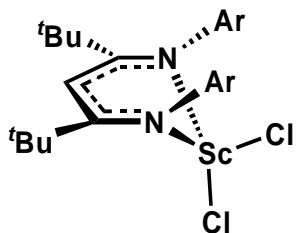
Synthesis of [ArNC(Me)CHC(Me)NAr]Sc(CH₂SiMe₃)₂ (1-CH₂SiMe₃**):**



A 100 mL flask was charged with LiCH₂SiMe₃ (0.310 g, 3.30 mmol) and **1-Cl(THF)** (1.00 g, 1.65 mmol) and evacuated. Toluene (50 mL) was condensed into the vessel at -78 °C. The solution was gradually warmed

to room temperature whereupon it was allowed to stir for 2 hours. The mixture was hot filtered to remove LiCl. The solvent was removed *in vacuo* and hexanes (5 mL) added. The mixture was cooled to -78 °C for 30 minutes and back filtered. The solvent was removed under reduced pressure to give 802 mg (1.26 mmol, 76%) of **1-CH₂SiMe₃** as a white powder. ¹H NMR (C₆D₆): δ 7.16 (m, 6H; C₆H₃), 5.00 (s, 1H; CH); 3.31 (sp, 4H; CHMe₂, J_{H-H} = 6.8 Hz), 1.59 (s, 6H; NCMe), 1.44 (d, 12H; CHMe₂, J_{H-H} = 6.8 Hz), 1.16 (d, 12H; CHMe₂, J_{H-H} = 6.8 Hz), 0.18 (s, 18H; ScCH₂SiMe₃), 0.08 (s, 4H; ScCH₂SiMe₃). ¹³C{¹H} NMR (C₆D₆): δ 167.9 (NCMe), 141.8 (C_{ipso}), 142.6, 127.1, 124.7 (C₆H₃), 95.7 (CH), 44.9 (ScCH₂SiMe₃), 28.6 (CHMe₂), 25.7, 24.9 (CHMe₂), 24.4 (Me) 3.4 (ScCH₂SiMe₃). Anal. Calcd. for C₃₇H₆₃N₂Si₂Sc : C, 69.76; H, 9.97; N, 4.40. Found : C, 69.41; H, 9.64; N, 4.55.

Synthesis of [ArNC(^tBu)CHC(^tBu)NAr]ScCl₂ (2-Cl**):**



Preparation 1: A thick-walled reactor bomb equipped with a Kontes valve was charged with LiL (11.1 g, 21.9 mmol) and ScCl₃(THF)₃ (9.38 g, 25.7 mmol) and evacuated. Toluene (400 mL) was condensed into the vessel, which was then

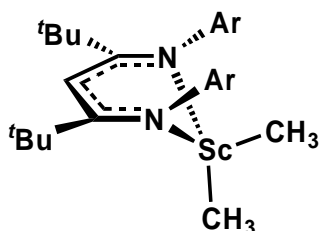
sealed and heated at 110 °C for 3 days. The mixture was cannula transferred to a swivel

frit apparatus. A hot filtration to remove the salts was performed followed by removal of toluene and trituration with hexanes to give **2-Cl** in 88% yield as a pale yellow solid (11.7 g, 18.9 mmol).

Preparation 2: The above method was used with the exception that the reaction mixture was heated at 180 °C for approximately 15 minutes and **2-Cl** was obtained in 68% yield.

^1H NMR (C_6D_6): δ 7.05 (m, 6H; C_6H_3), 6.01 (s, 1H; CH); 3.10 (sp, 4H; CHMe_2 , $J_{\text{H-H}} = 6.8$ Hz), 1.43 (d, 12H; CHMe_2 , $J_{\text{H-H}} = 6.8$ Hz), 1.26 (d, 12H; CHMe_2 , $J_{\text{H-H}} = 6.8$ Hz), 1.17 (s, 18H; NCMe_3). $^{13}\text{C}\{^1\text{H}\}$ NMR (C_6D_6): δ 174.3 (NCMe_3), 142.8 (C_{ipso}), 141.1, 127.0, 124.3 (C_6H_3), 90.8 (CH), 44.7 (CMe_3), 32.3 (CMe_3), 29.9 (CHMe_2), 26.9, 24.4 (CHMe_2).
Anal. Calcd. for $\text{C}_{35}\text{H}_{53}\text{N}_2\text{Cl}_2\text{Sc}$: C, 68.06; H, 8.65; N, 4.54. Found : C, 68.54; H, 7.98; N, 4.92.

Synthesis of $[\text{ArNC}(\text{tBu})\text{CHC}(\text{tBu})\text{NAr}]\text{ScMe}_2$ (**2-Me**):

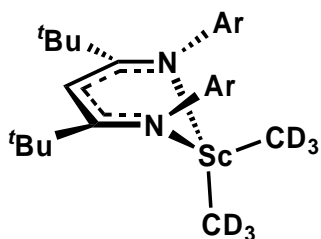


Toluene (75 mL) was condensed into an evacuated flask containing **2-Cl** (1.50 g, 2.43 mmol) and solid methyl lithium (0.200 g, 9.09 mmol) at -78 °C. The resultant mixture was allowed to warm slowly to room temperature and stirred for

three hours. The toluene was removed under vacuum to give an orange solid. Hexanes (85 mL) were added and the reaction mixture was filtered and concentrated to 10 mL. The solution was cooled to -78 °C for 2 hours and back filtered to afford 0.900 g of fine yellow powder (1.56 mmol, 64%). ^1H NMR (C_6D_6): δ 7.25 (m, 6H; C_6H_3), 5.77 (s, 1H; CH); 3.52 (sp, 4H; CHMe_2 , $J_{\text{H-H}} = 6.8$ Hz), 1.47 (d, 12H; CHMe_2 , $J_{\text{H-H}} = 6.8$ Hz), 1.41 (d, 12H; CHMe_2 , $J_{\text{H-H}} = 6.8$ Hz), 1.21 (s, 18H; NCMe_3), 0.00 (s, 3H; ScMe). $^{13}\text{C}\{^1\text{H}\}$ NMR

(C₆D₆): δ 174.1 (NCMe), 143.4 (C_{ipso}), 141.1, 126.1, 124.2 (C₆H₃), 92.7 (CH), 44.6 (CMe₃), 32.6 (CMe₃), 29.7 (CHMe₂), 27.6 (ScMe), 26.9, 24.5 (CHMe₂). Anal. Calcd. for C₃₇H₅₉N₂Sc : C, 77.04; H, 10.31; N, 4.86. Found : C, 76.55; H, 9.53; N, 4.98. TGA: 154 – 277 °C -2.1 % obs. -2.8 % calcd. for loss of 1 methane.

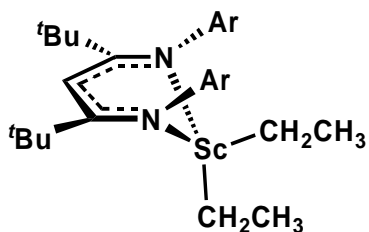
Synthesis of [ArNC(^tBu)CHC(^tBu)NAr]Sc(CD₃)₂ (*d*₆-2-Me):



This compound was prepared in an identical manner to that previously described for **2-Me**, with the exception that LiCD₃•LiI was used. The ¹H NMR spectrum matched **2-Me** except no resonances were observed for the methyl groups.

²H NMR (C₇H₈) : δ (s, 0.00).

Synthesis of [ArNC(^tBu)CHC(^tBu)NAr]Sc(CH₂CH₃)₂ (2-Et):



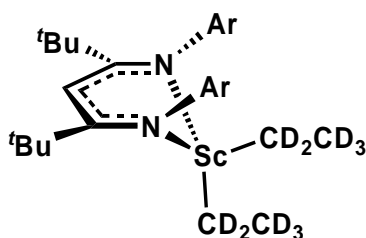
Toluene (25 mL) was condensed into an evacuated flask charged with LiCH₂CH₃ (0.058 mg, 1.62 mmol) and **2-Cl** (0.500 g, 0.809 mmol) at -78 °C. The reaction mixture was allowed to stir for 30 minutes after the vessel was

slowly warmed to room temperature. Hot filtration followed by removal of the solvent *in vacuo* and trituration with hexanes afforded an orange solid (168 mg, 0.283 mmol, 35%).

¹H NMR (C₆D₆): δ 7.26 (m, 6H; C₆H₃), 5.70 (s, 1H; CH); 3.58 (sp, 4H; CHMe₂, *J*_{H-H} = 6.8 Hz), 1.50 (d, 12H; CHMe₂, *J*_{H-H} = 6.8 Hz), 1.43 (d, 12H; CHMe₂, *J*_{H-H} = 6.8 Hz), 1.25 (t, 6H; ScCH₂CH₃, *J*_{H-H} = 8.2 Hz), 1.13 (s, 18H; NCMe₃), 0.11 (q, 4H; ScCH₂CH₃, *J*_{H-H} =

8.2 Hz). $^{13}\text{C}\{^1\text{H}\}$ NMR (C_6D_6): δ 174.2 (NCMe), 143.8 (C_{ipso}), 141.5, 126.0, 124.2 (C_6H_3), 92.5 (CH), 44.7 (CMe_3), 40.8 (ScCH_2CH_3), 32.4 (CMe_3), 29.2 (CHMe_2), 26.7, 26.6 (CHMe_2), 13.2 (ScCH_2CH_3). Anal. Calcd. for $\text{C}_{35}\text{H}_{53}\text{N}_2\text{Cl}_2\text{Sc}$: C, 77.44; H, 10.50; N, 4.63. Found: C, 77.28; H, 10.63; N, 4.74. TGA: 96 – 142 °C -5.2 % obs. -5.0 % calcd. for loss 1 ethane; 145 – 228 °C -4.5% obs. -5.0 % calcd. for loss of 1 ethane.

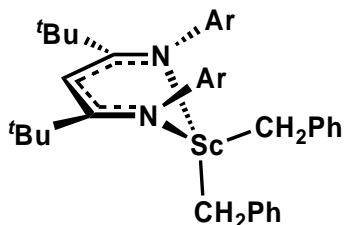
Synthesis of $[\text{ArNC}(\text{tBu})\text{CHC}(\text{tBu})\text{NAr}]\text{Sc}(\text{CD}_2\text{CD}_3)_2$ (***d*₁₀-2-Et**):



This compound was prepared in an identical manner to that previously described for **2-Et** with the exception that LiCD_2CD_3 was used. The ^1H NMR spectrum matched **2-Et** except no resonances were observed for the ethyl

groups. ^2H NMR (C_7H_8): δ 1.16 (6D; ScCD_2CD_3), 0.24 (4D; ScCD_2CD_3).

Synthesis of $[\text{ArNC}(\text{tBu})\text{CHC}(\text{tBu})\text{NAr}]\text{Sc}(\text{CH}_2\text{Ph})_2$ (**2-CH₂Ph**):

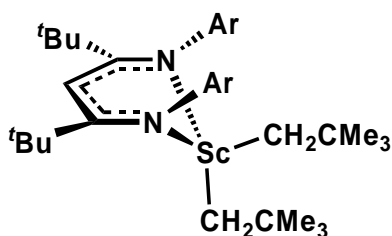


A 100 mL flask was charged with **2-Cl** (0.750 g, 1.21 mmol) and solid BnMgCl (0.366 g, 2.43 mmol). Toluene (65 mL) was condensed into the evacuated flask at -78 °C.

The mixture was slowly allowed to warm to room temperature whereby stirring was continued for another 17 hours. The toluene was removed *in vacuo* to afford an orange solid. Benzene (55 mL) was condensed into the flask and the assemblage was sonicated for 10 minutes. The reaction mixture was filtered and benzene removed under vacuum to afford **2-CH₂Ph** as an orange solid (0.605 g, 0.829 mmol, 69%). ^1H NMR (C_6D_6): δ 7.20-6.70 (m, 16H; ScCH_2Ph , C_6H_3), 5.62 (s, 1H;

CH); 3.65-2.50 (br, 4H; $CHMe_2$), 2.12 (s, 4H; $ScCH_2Ph$), 1.23-1.18 (br ov m 24H; $CHMe_2$), 1.04 (s, 18H; $NCMe_3$). $^{13}C\{^1H\}$ NMR (C_7D_8 , 265K): δ 174.8 ($NCMe$), 151.6, 149.0 ($ScCH_2Ph$), 143.2 (C_{ipso}), 142.3, 141.9 (C_6H_3), 128.7, 128.5 ($ScCH_2Ph$), 126.7 (C_6H_3), 126.0, 125.2 ($ScCH_2Ph$), 125.1, 124.7 (C_6H_3), 119.8, 119.7 ($ScCH_2Ph$), 91.3 (CH), 64.3, 57.5 ($ScCH_2Ph$), 45.0 (CMe_3), 32.3 (CMe_3), 29.8, 28.9 ($CHMe_2$), 27.0, 26.2, 25.3, 24.6 ($CHMe_2$). Anal. Calcd. for $C_{49}H_{67}N_2Sc$: C, 80.73; H, 9.26; N, 3.84. Found : C, 79.57; H, 8.91; N, 3.89.

Synthesis of $[ArNC(tBu)CHC(tBu)NAr]Sc(CH_2CMe_3)_2$ (**2-CH₂CMe₃**):

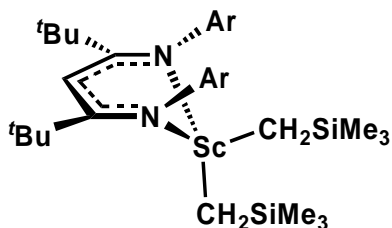


Toluene (20 mL) was condensed into an evacuated flask containing $LiCH_2CMe_3$ (0.088 g, 1.13 mmol) and **2-Cl** (0.350 g, 0.566 mmol) at -78 °C. The yellow mixture was warmed to room temperature and allowed

to stir for 1 hour. The mixture was filtered and solvent removed under vacuum. The residue was sonicated in hexanes (10 mL), cooled to -78 °C for 2 hours and back filtered to afford pure **2-CH₂CMe₃** in 42% yield (0.165 g, 0.239 mmol). 1H NMR (C_7D_8 , 242K): δ 7.20-7.00 (m, 6H; C_6H_3), 5.58 (s, 1H; CH); 4.12 (sp, 2H; $CHMe_2$, $J_{H-H} = 6.8$ Hz), 2.86 (sp, 2H; $CHMe_2$, $J_{H-H} = 6.8$ Hz), 1.74 (d, 6H; $CHMe_2$, $J_{H-H} = 6.8$ Hz), 1.46 (d, 6H; $CHMe_2$, $J_{H-H} = 6.8$ Hz), 1.23 (ov d, 12H; $CHMe_2$, $J_{H-H} = 6.8$ Hz), 1.35 (s, 18H; $ScCH_2CMe_3$), 1.11 (s, 18H; $NCMe_3$), 0.78 (s, 2H; $ScCH_2CMe_3$), 0.75 (ov s, 2H; $ScCH_2CMe_3$). $^{13}C\{^1H\}$ NMR (242K, C_7D_8): δ 174.9 ($NCMe$), 144.2 (C_{ipso}), 142.3, 141.9, 126.7, 125.1, 124.7 (C_6H_3), 93.0 (CH), 75.5 ($ScCH_2CMe_3$), 45.3 (CMe_3), 35.6 ($ScCH_2CMe_3$), 35.3 ($ScCH_2CMe_3$), 33.0 (CMe_3), 29.9, 28.8 ($CHMe_2$), 27.5, 26.7, 25.6,

25.1 (CHMe_2). Anal. Calcd. for $\text{C}_{45}\text{H}_{75}\text{N}_2\text{Sc}$: C, 78.43; H, 10.97; N, 4.07.
 Found : C, 77.50; H, 10.59; N, 4.80.

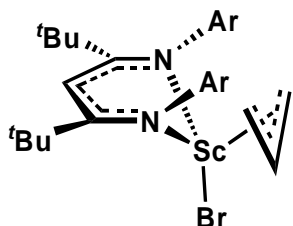
Synthesis of $[\text{ArNC}(\text{tBu})\text{CHC}(\text{tBu})\text{NAr}]\text{Sc}(\text{CH}_2\text{SiMe}_3)_2$ (2-CH₂SiMe₃**):**



To an evacuated flask at $-78\text{ }^\circ\text{C}$ containing $\text{LiCH}_2\text{SiMe}_3$ (0.480 g, 5.11 mmol) and **2-Cl** (1.50 g, 2.48 mmol) toluene (75 mL) was condensed. The reaction mixture was warmed to room temperature and

then allowed to stir for 90 minutes. The solvent was removed *in vacuo* to afford a yellow residue which was triturated with hexanes (70 mL) and filtered. The reaction mixture was concentrated to 10 mL, cooled to $-78\text{ }^\circ\text{C}$ for two hours and filtered to give **2-CH₂SiMe₃** as a yellow crystalline solid (0.901 g, 1.25 mmol, 50%). ^1H NMR (C_6D_6): δ 7.07 (m, 6H; C_6H_3), 5.68 (s, 1H; CH); 3.95-2.70 (br sp, 4H; CHMe_2), 1.75-1.20 (br ov m, 24H; CHMe_2), 1.10 (s, 18H; NCMe_3), 0.13 (s, 18H; $\text{ScCH}_2\text{SiMe}_3$), 0.00 (s, 4H; $\text{ScCH}_2\text{SiMe}_3$). $^{13}\text{C}\{^1\text{H}\}$ NMR (C_7D_8 , 233K): δ 175.6 (NCMe), 143.2 (C_{ipso}), 142.4, 142.0, 127.0, 125.1, 124.7 (C_6H_3), 93.6 (CH), 48.7 ($\text{ScCH}_2\text{SiMe}_3$), 44.8 (CMe_3), 41.8 ($\text{ScCH}_2\text{SiMe}_3$), 32.7 (CMe_3), 29.4, 28.8 (CHMe_2), 28.4, 26.5, 25.4, 24.7 (CHMe_2), 4.7 ($\text{ScCH}_2\text{SiMe}_3$), 3.4 ($\text{ScCH}_2\text{SiMe}_3$). Anal. Calcd. for $\text{C}_{43}\text{H}_{75}\text{N}_2\text{Si}_2\text{Sc}$: C, 71.61; H, 10.48; N, 3.88. Found : C, 70.76; H, 10.41; N, 4.00. TGA: 129 – 182 $^\circ\text{C}$ -22.1 % obs. -24.2 % calcd. for loss of 2 SiMe_4 .

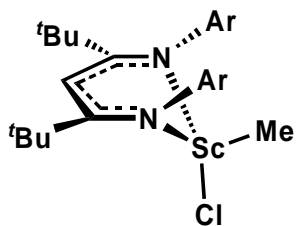
Synthesis of [ArNC(^tBu)CHC(^tBu)NAr]Sc(Br)(C₃H₅) (2-Br(C₃H₅)**):**



A 1.0 M solution of allyl magnesium bromide (1.20 mL, 1.22 mmol) in Et₂O was added to a 100 mL RB flask attached to a swivel frit apparatus. The Et₂O was removed under vacuum and **2-Cl** (0.750 g, 1.22 mmol) was added. The entire frit assemblage was evacuated and toluene (50 mL) condensed in at -78 °C. The reaction mixture was slowly warmed to room temperature, sonicated for 10 minutes, and allowed to stir for 14 hours. The yellow solution was filtered and solvent removed *in vacuo* to give a yellow-brown solid. The residue was washed with hexanes (3 x 15 mL) and dried under vacuum to afford 0.565 g (0.852 mmol, 71%) of **2-Br(C₃H₅)** as a fine yellow solid.

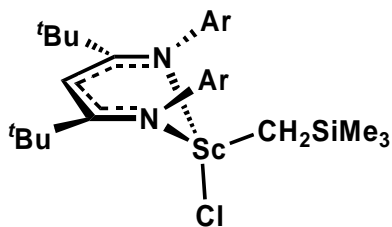
¹H NMR (C₆D₆): δ 7.06-6.94 (ov m, 6H; C₆H₃), 6.12 (quint, 1H; H₂CCHCH₂, *J*_{H-H} = 12.9 Hz), 6.10 (s, 1H; CH), 3.64 (sp, 2H; CHMe₂, *J*_{H-H} = 7.0 Hz), 3.20 (d, 4H; H₂CCHCH₂, *J*_{H-H} = 12.9 Hz), 2.89 (sp, 2H; CHMe₂, *J*_{H-H} = 7.0 Hz), 1.39 (d, 6H; CHMe₂, *J*_{H-H} = 7.0 Hz), 1.38 (d, 6H; CHMe₂, *J*_{H-H} = 7.0 Hz), 1.21 (s, 18H; NCMe₃), 1.18 (d, 6H; CHMe₂, *J*_{H-H} = 7.0 Hz), 1.12 (d, 6H; CHMe₂, *J*_{H-H} = 7.0 Hz). ¹³C{¹H} NMR (C₆D₆): δ 175.8 (NCMe), 146.2 (H₂CCHCH₂), 144.7 (C_{ipso}), 142.6, 141.0, 126.4, 124.7, 124.1 (C₆H₃), 95.0 (CH), 83.1 (H₂CCHCH₂), 45.2 (CMe₃), 32.6 (CMe₃), 29.3, 28.1 (CHMe₂), 26.6, 25.5, 25.1, 24.3 (CHMe₂). Anal. Calcd. for C₃₈H₅₈N₂BrSc: C, 68.35; H, 8.75; N, 4.20. Found : C, 68.58; H, 8.86; N, 4.05.

Synthesis of [ArNC(^tBu)CHC(^tBu)NAr]Sc(Me)Cl (2-Me(Cl)**):**



A 50 mL flask was charged with **2-Cl** (0.085g, 0.144mmol) and **2-Me** (0.089g, 0.144mmol) and 30 mL of toluene was condensed into it at $-78\text{ }^{\circ}\text{C}$. The reaction mixture was gradually warmed to room temperature and solvent removed under vacuum to afford a light yellow powder. Hexanes (25 mL) were added and the mixture was filtered to give a clear yellow solution. Removal of solvent *in vacuo* gave crude **2-Me(Cl)** as a pale yellow powder which was recrystallized from hexanes at $-35\text{ }^{\circ}\text{C}$ (0.150 g, 0.255 mmol, 89%). $^1\text{H NMR}$ (C_6D_6): δ 7.07-6.99 (m, 6H; C_6H_3), 5.87 (s, 1H; CH); 3.43 (sp, 2H; CHMe_2 , $J_{\text{H-H}} = 6.8$ Hz), 3.15 (sp, 2H; CHMe_2 , $J_{\text{H-H}} = 6.8$ Hz), 1.46 (d, 6H; CHMe_2 , $J_{\text{H-H}} = 6.8$ Hz), 1.37 (ov d, 12H; CHMe_2 , $J_{\text{H-H}} = 6.8$ Hz), 1.27 (d, 6H; CHMe_2 , $J_{\text{H-H}} = 6.8$ Hz), 1.10 (s, 18H; NCMe_3), 0.16 (s, 3H; ScMe). $^{13}\text{C}\{^1\text{H}\}$ NMR (C_6D_6): δ 174.2 (NCMe), 143.0 (C_{ipso}), 141.4, 141.1, 126.6, 124.3, 124.1 (C_6H_3), 92.1 (CH), 44.6 (CMe_3), 32.2 (CMe_3), 29.7, 29.1 (CHMe_2), 26.6, 26.3 (CHMe_2), 25.8 (ScMe), 24.1, 24.0 (CHMe_2). Anal. Calcd. for $\text{C}_{38}\text{H}_{56}\text{N}_2\text{ClSc}$: C, 72.40; H, 9.45; N, 4.61. Found: C, 72.21; H, 9.32; N, 4.61. (Note: Sample contained 5% of each **2-Cl** and **2-Me**.)

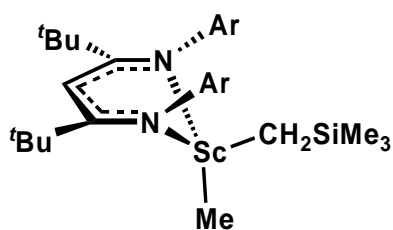
Synthesis of [ArNC(^tBu)CHC(^tBu)NAr]Sc(Cl)(CH₂SiMe₃) (2-Cl(CH₂SiMe₃)**):**



To an evacuated 100 mL RB flask at $-78\text{ }^{\circ}\text{C}$ containing **2-Cl** (0.700 g, 1.14 mmol) toluene (65 mL) was condensed. While maintaining rapid stirring a 20 mL toluene solution of $\text{LiCH}_2\text{SiMe}_3$ (0.107 g, 1.14 mmol)

was added at a rate of 0.1 mL/min using a syringe pump. Upon completion of the addition the reaction mixture was gradually warmed to room temperature for 12 hours. The solvent was removed *in vacuo*, sonicated in hexanes (25 mL) and filtered. The solvent was removed to give a sticky yellow solid, which was then sonicated in hexamethyldisiloxane (10 mL) and filtered. Removal of the solvent afforded **2-Cl(CH₂SiMe₃)** as a yellow crystalline solid (0.570 g, 0.085 mmol, 79%). ¹H NMR (C₇D₈): δ 7.09-6.97 (m, 6H; C₆H₃), 5.84 (s, 1H; CH), 3.60 (br m, 2H; CHMe₂), 3.04 (sp, 2H; CHMe₂, *J*_{H-H} = 6.7 Hz), 1.54 (d, 6H; CHMe₂, *J*_{H-H} = 6.7 Hz), 1.32 (d, 6H; CHMe₂, *J*_{H-H} = 6.7 Hz), 1.29 (d, 6H; CHMe₂, *J*_{H-H} = 6.7 Hz), 1.22 (d, 6H; CHMe₂, *J*_{H-H} = 6.7 Hz), 1.10 (s, 18H; NCM₃), 0.23 (s, 2H; ScCH₂SiMe₃), -0.04 (s, 9H; ScCH₂SiMe₃). ¹³C{¹H} NMR (C₇D₈): δ 174.8 (NCMe), 143.0 (C_{ipso}), 142.0, 141.2, 126.8, 124.6, 124.4 (C₆H₃), 93.1 (CH), 47.8 (ScCH₂SiMe₃), 44.6 (CMe₃), 32.1 (CMe₃), 31.8, 28.9 (br) (CHMe₂), 26.0 (br), 24.3, 24.2, 24.0 (br) (CHMe₂), 3.3 (ScCH₂SiMe₃). Anal. Calcd. for C₃₉H₆₄N₂ClSiSc: C, 69.97; H, 9.64; N, 4.19. Found: C, 68.29; H, 9.40; N, 4.03.

Synthesis of [ArNC(^tBu)CHC(^tBu)NAr]Sc(Me)(CH₂SiMe₃) (**2-Me(CH₂SiMe₃)**):



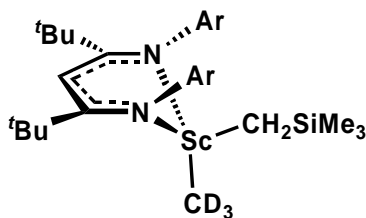
Preparation 1: A 100 mL flask was charged with **2-Me(Cl)** (0.300 g, 0.511 mmol) and LiCH₂SiMe₃ (0.053 g, 0.563 mmol) and attached to a swivel frit apparatus. The entire assemblage was evacuated, and

toluene (50 mL) was vacuum distilled into the flask. After warming to room temperature, the reaction mixture was stirred for another 45 minutes whereby the solvent was removed under vacuum to afford a thick yellow oil. Hexanes (40 mL) were added and the reaction

mixture was filtered. The volume was reduced to 25 mL and cooled to $-78\text{ }^{\circ}\text{C}$ for 30 minutes, during this time a small quantity of fine yellow powder precipitated. The mixture was back filtered and solvent removed *in vacuo* to afford **2-Me(CH₂SiMe₃)** as a light yellow powder. (0.125g, 0.193mmol, 38%).

Preparation 2: A 50 mL flask was charged with **2-Cl(CH₂SiMe₃)** (0.200 g, 0.299 mmol) and MeLi (0.013 g, 0.600 mmol) and attached to a swivel frit apparatus. The entire assemblage was evacuated, and toluene (20 mL) was vacuum distilled into the flask. After warming to room temperature, the reaction mixture was stirred for another 10 hours, filtered and solvent removed under vacuum to afford a thick yellow oil. Hexanes (10 mL) were added and the reaction mixture was sonicated. The volume was reduced to 5 mL and cooled to $-78\text{ }^{\circ}\text{C}$ for 30 minutes, during this time a small quantity of fine yellow powder precipitated. The solvent was removed *in vacuo* to afford **2-Me(CH₂SiMe₃)** as a light yellow powder. (0.080 g, 0.123 mmol, 41%). ¹H NMR (C₆D₆): δ 7.10-6.97 (m, 6H; C₆H₃), 5.73 (s, 1H; CH); 3.55 (sp, 2H; CHMe₂), $J_{\text{H-H}} = 6.8$ Hz), 3.12 (sp, 2H; CHMe₂, $J_{\text{H-H}} = 6.8$ Hz), 1.48 (d, 6H; CHMe₂, $J_{\text{H-H}} = 6.8$ Hz), 1.32 (d, 6H; CHMe₂, $J_{\text{H-H}} = 6.8$ Hz), 1.30 (d, 6H; CHMe₂, $J_{\text{H-H}} = 6.8$ Hz), 1.27 (d, 6H; CHMe₂, $J_{\text{H-H}} = 6.8$ Hz), 1.09 (s, 18H; NCM₃), 0.00 (s, 9H; ScCH₂SiMe₃), -0.08 (s, 2H; ScCH₂SiMe₃), -0.09 (s, 3H; ScMe). ¹³C{¹H} NMR (C₆D₆): δ 174.5 (NCMe), 143.2 (C_{ipso}), 141.8, 141.2, 127.0, 124.6, 124.5 (C₆H₃), 93.2 (CH), 45.5 (ScCH₂SiMe₃), 44.7 (CMe₃), 32.3 (CMe₃), 29.6, 27.0 (CHMe₂), 27.3 (ScMe), 26.6, 25.1, 24.6, 24.4 (CHMe₂), 3.9 (ScCH₂SiMe₃). Anal. Calcd. for C₄₀H₆₇N₂SiSc: C, 74.03; H, 10.41; N, 4.32. Found: C, 73.63; H, 10.29; N, 4.31.

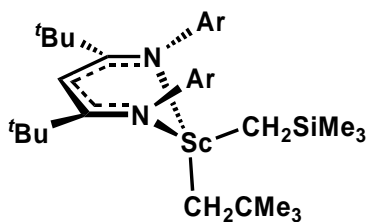
Synthesis of $\{[\text{ArNC}(\text{tBu})\text{CHC}(\text{tBu})\text{NAr}]\text{Sc}(\text{CD}_3)(\text{CH}_2\text{SiMe}_3) (d_3\text{-2-Me}(\text{CH}_2\text{SiMe}_3))\}$:



A 50 mL RB flask was charged with **2-Cl(CH₂SiMe₃)** (0.300 g, 0.448 mmol), LiCD₃(LiI) (0.142 g, 0.894 mmol) and toluene (30 mL). The reaction mixture was allowed to stir at room temperature for 20 hours whereby the solvent was removed under vacuum. Pentane (25 mL) was added, the mixture sonicated for 10 minutes and filtered. The yellow solution was then condensed to 5 mL and cooled to $-78\text{ }^\circ\text{C}$ for 16 hours. The supernatant was decanted and the fine yellow solid dried *in vacuo*. Yield: (0.049 g, 0.075 mmol, 17%). The ¹H NMR spectrum matched **2-Me(CH₂SiMe₃)** with the exception that no resonances were observed for the methyl groups. ²H NMR (C₇H₈) : δ (s, -0.09).

Synthesis of $[\text{ArNC}(\text{tBu})\text{CHC}(\text{tBu})\text{NAr}]\text{Sc}(\text{CH}_2\text{CMe}_3)(\text{CH}_2\text{SiMe}_3)$

(2-CH₂SiMe₃(CH₂CMe₃)):

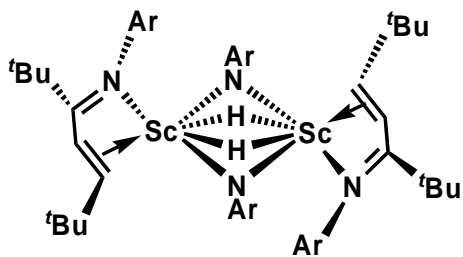


To an evacuated 100 mL RB flask at $-78\text{ }^\circ\text{C}$ containing **2-Cl** (1.21 g, 1.96 mmol) toluene (70 mL) was condensed. While maintaining rapid stirring a 25 mL toluene solution of LiCH₂SiMe₃ (0.107 g, 1.14 mmol) was added at a rate of 0.11 mL/min. Upon completion of the addition the reaction mixture was gradually warmed to room temperature and allowed to stir for another 12 hours. The reaction mixture was cooled to $-78\text{ }^\circ\text{C}$ and a 10 mL toluene solution of LiCH₂CMe₃ (0.153g, 1.96 mmol) was added dropwise. The reaction mixture was gradually warmed to room temperature, stirred for 2 hours and toluene removed under

vacuum. Hexanes (20 mL) was added and the reaction mixture filtered. Removal of the solvent gave an oily yellow solid which was triturated with hexamethyldisiloxane (10 mL) and back filtered. The solvent was removed *in vacuo* to afford **2-CH₂SiMe₃(CH₂CMe₃)** as a yellow crystalline solid (0.750 g, 1.18 mmol, 60%). ¹H NMR for Isomer A (34%) (C₇D₈, 218K): δ 7.15-6.96 (m, 6H; C₆H₃), 5.60 (s, 1H; CH), 4.05 (sp, 2H; CHMe₂, J_{H-H} = 6.4 Hz), 2.80 (sp, 2H; CHMe₂, J_{H-H} = 6.4 Hz), 1.75 (d, 6H; CHMe₂, J_{H-H} = 6.4 Hz), 1.47 (d, 6H; CHMe₂, J_{H-H} = 6.4 Hz), 1.31 (s, 9H; ScCH₂CMe₃), 1.21 (ov d, 6H; CHMe₂, J_{H-H} = 6.4 Hz), 1.20 (ov d, 6H; CHMe₂, J_{H-H} = 6.4 Hz), 1.08 (ov s, 18H; NCCMe₃), 0.79 (s, 2H; ScCH₂CMe₃), 0.29 (ov s, 2H; ScCH₂SiMe₃), -0.14 (s, 9H; ScCH₂SiMe₃). ¹H NMR for Isomer B (66%) (C₇D₈, 213K): δ 7.15-6.96 (m, 6H; C₆H₃), 5.56 (s, 1H; CH), 3.90 (sp, 2H; CHMe₂, J_{H-H} = 6.4 Hz), 2.94 (sp, 2H; CHMe₂, J_{H-H} = 6.4 Hz), 1.78 (d, 6H; CHMe₂, J_{H-H} = 6.4 Hz), 1.49 (d, 6H; CHMe₂, J_{H-H} = 6.4 Hz), 1.29 (d, 6H; CHMe₂, J_{H-H} = 6.4 Hz), 1.20 (ov d, 6H; CHMe₂, J_{H-H} = 6.4 Hz), 1.08 (ov s, 18H; NCCMe₃), 0.85 (s, 9H; ScCH₂CMe₃), 0.59 (s, 2H; ScCH₂CMe₃), 0.39 (s, 9H; ScCH₂SiMe₃) 0.29 (ov s, 2H; ScCH₂SiMe₃). Complete assignment of the ¹³C{¹H} NMR spectrum was not possible and such data is reported by carbon type: δ 143.3, 142.7 (C_{ipso}), 142.0, 141.6, 141.3, 141.1, 126.4, 126.2, 125.3, 124.5, 124.3, 124.2 (C₆H₃). All other carbon resonances were attributable to a specific isomer. ¹³C{¹H} NMR for Isomer A (34%) (C₇D₈ 218K): δ 174.0 (NCCMe₃), 92.1 (CH), 69.5 (ScCH₂CMe₃), 44.6 (CMe₃), 40.8 (ScCH₂SiMe₃), 35.9 (ScCH₂CMe₃), 35.2 (ScCH₂CMe₃), 32.2 (CMe₃), 29.4, 28.1 (CHMe₂), 27.2, 26.3, 25.0, 24.1 (CHMe₂), 2.9 (ScCH₂SiMe₃). ¹³C{¹H} NMR for Isomer B (66%) (C₇D₈, 218K): δ 175.1 (NCCMe₃), 93.5 (CH), 75.5 (ScCH₂CMe₃), 47.3 (ScCH₂SiMe₃), 44.3 (CMe₃), 35.2 (ScCH₂CMe₃), 34.7 (ScCH₂CMe₃), 32.3 (CMe₃), 28.6,

28.3 (CHMe_2), 27.6, 26.0, 25.1, 24.2 (CHMe_2), 4.2 ($\text{ScCH}_2\text{SiMe}_3$). Anal. Calcd. for $\text{C}_{44}\text{H}_{75}\text{N}_2\text{SiSc}$: C, 74.95; H, 10.72; N, 3.97. Found: C, 73.10; H, 10.69; N, 3.92.

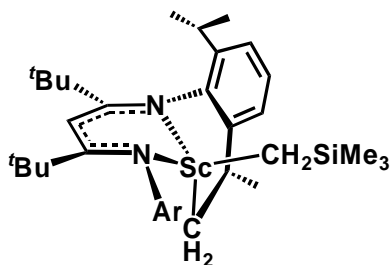
Synthesis of $[\text{ArNCH}(\text{tBu})\text{CHC}(\text{tBu})\text{NAr}]\text{ScH}$ (2-H):



To an evacuated bomb at $-196\text{ }^\circ\text{C}$ containing $2\text{-CH}_2\text{SiMe}_3$ (0.150 g, 0.208 mmol) and toluene (10 mL) H_2 was emitted. The bomb was closed and gradually warmed to room temperature

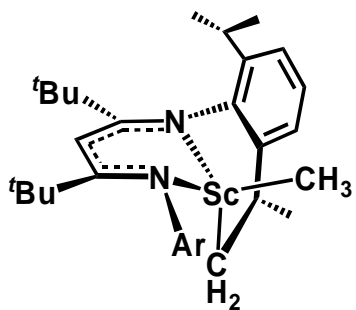
whereupon it was allowed to stir for 3 days. The solution was transferred via cannula into a 100 mL RB flask attached to a swivel frit apparatus and evacuated to dryness. Hexamethyldisiloxane (5 mL) was added and the reaction mixture sonicated (5 minutes), cooled to $-40\text{ }^\circ\text{C}$ (30 minutes) and filtered. Removal of the solvent under reduced pressure afforded 0.095 mg (0.17 mmol, 83%) of orange powder. ^1H NMR (C_7D_8) : δ 7.10-6.98 (m, 6H; C_6H_3), 5.78 (d, 1H; CH; $J_{\text{H-H}} = 16.7$ Hz), 5.68 (d, 1H; CH; $J_{\text{H-H}} = 16.7$ Hz), 2.92 (sp, 4H; CHMe_2 , $J_{\text{H-H}} = 6.9$ Hz), 1.34 (s, 9H; NCCMe_3), 1.20 (d, 24H; CHMe_2 , $J_{\text{H-H}} = 6.9$ Hz), 0.72 (s, 9H; NCCMe_3). ^2H NMR (C_7H_8) : δ 5.72, 3.04, 2.91, 1.38, 1.15. $^{13}\text{C}\{^1\text{H}\}$ NMR: δ 172.3 (NCCMe_3), 150.5 (C_{ipso}), 147.7, 134.8, 122.9, 122.8, 117.4 (C_6H_3), 44.7, 40.4 (CMe_3), 35.0 (CMe_3), 28.8, 28.5 (CHMe_2), 25.6, 23.4, 22.3(2) (CHMe_2). Anal. Calcd.: $\text{C}_{35}\text{H}_{55}\text{N}_2\text{Sc}$: C, 76.60; H, 10.10; N, 5.11. Found: C, 75.94; H, 9.99; N, 4.91.

Synthesis of κ^3 -[ArNC(*t*Bu)CHC(*t*Bu)N-*i*Pr-C₆H₃]ScCH₂SiMe₃ (3-CH₂SiMe₃**):**

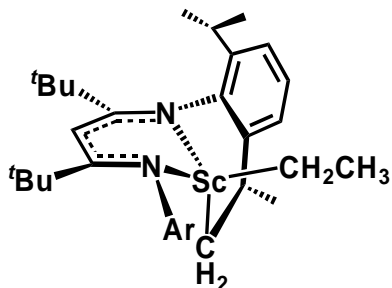


To an evacuated flask at $-78\text{ }^{\circ}\text{C}$ containing **2-CH₂SiMe₃** (0.500 g, 0.693 mmol) hexanes (25 mL) was condensed. The solution was heated at $85\text{ }^{\circ}\text{C}$ for 90 minutes and solvent removed under vacuum

yielding a red oil. Hexamethyldisiloxane (30 mL) was added, the mixture sonicated (10 minutes) and cooled to $-30\text{ }^{\circ}\text{C}$ for 1 hour. The mixture was filtered and solvent removed to afford small yellow crystals of **3-CH₂SiMe₃** (0.251 g, 0.394 mmol, 57%). ¹H NMR: δ 7.20-6.94 (m, 6H; C₆H₃), 5.57 (s, 1H; CH), 3.43 (sp, 1H; CHMe₂, $J_{\text{H-H}} = 6.8\text{ Hz}$), 3.10 (ov m, 2H; CHMe₂, CH₂CHMe), 2.84 (sp, 1H; CHMe₂, $J_{\text{H-H}} = 6.8\text{ Hz}$), 1.48 (d, 3H; CHMe₂, $J_{\text{H-H}} = 6.8\text{ Hz}$), 1.39 (d, 3H; CHMe₂, $J_{\text{H-H}} = 6.8\text{ Hz}$), 1.31 (d, 3H; CHMe₂, $J_{\text{H-H}} = 6.8\text{ Hz}$), 1.26 (d, 3H; CHMe₂, $J_{\text{H-H}} = 6.8\text{ Hz}$), 1.21 (d, 3H; CHMe₂, $J_{\text{H-H}} = 6.8\text{ Hz}$), 1.18 (d, 3H; CHMe₂, $J_{\text{H-H}} = 6.8\text{ Hz}$), 1.18 (s, 18H; NCCMe₃), 1.02 (d, 3H; CHMe₂, $J_{\text{H-H}} = 6.8\text{ Hz}$), 0.94 (dd, 1H; CH₂CHMe, $J_{\text{H-H}} = 12.3, 5.6\text{ Hz}$), 0.08 (dd, 1H; CH₂CHMe, $J_{\text{H-H}} = 12.3, 11.8\text{ Hz}$), 0.00 (s, 2H; CH₂SiMe₃), -0.25 (s, 9H; CH₂SiMe₃), -1.08 (d, 1H; CH₂CHMe, $J_{\text{H-H}} = 11.2\text{ Hz}$), -1.16 (d, 1H; CH₂CHMe, $J_{\text{H-H}} = 11.2\text{ Hz}$). ¹³C{¹H} NMR: δ 174.2, 173.9 (NCCMe₃), 147.6 (C_{ipso}), 144.9, 144.7, 142.2, 138.2, 127.7, 125.7, 125.6, 124.9, 123.9, 121.5 (C₆H₃, one peak not observed), 99.0 (CH), 45.0 (CH₂SiMe₃), 43.4, 43.2 (CMe₃), 39.7 (CH₂CHMe), 32.9, 32.2 (CMe₃), 28.9, 28.7, 28.4 (CHMe₂, one peak not observed), 26.8, 26.0, 25.7, 25.0, 24.5, 23.1 (CHMe₂, one peak not observed), 4.1 (CH₂SiMe₃). Anal. Calcd. for C₃₈H₅₆N₂ClSc : C, 74.00; H, 10.03; N, 4.43. Found: C, 74.42; H, 10.05; N, 4.47.

κ^3 -[ArNC(^tBu)CHC(^tBu)N-*i*Pr-C₆H₃]ScMe (**3-Me**):


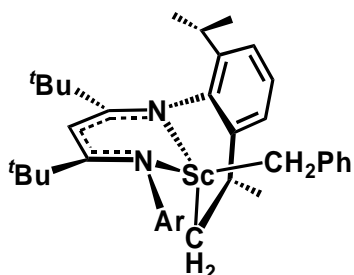
An NMR tube containing **2-Me** (0.017 g, 0.022 mmol, generated *in situ*) in 0.6 mL *d*₈-toluene was heated in the NMR probe at 335K for 3 hours. General experimental procedure 1 was followed. ¹H NMR: δ 7.27-6.98 (m, 6H; C₆H₃), 5.58 (s, 1H; CH), 3.48 (sp, 1H; CHMe₂, *J*_{H-H} = 6.8 Hz), 3.12 (ov m 2H; CHMe₂, CH₂CHMe), 2.89 (sp, 1H; CHMe₂, *J*_{H-H} = 6.8 Hz), 1.43 (d, 3H; CHMe₂, *J*_{H-H} = 6.8 Hz), 1.33 (d, 3H; CHMe₂, *J*_{H-H} = 6.8 Hz), 1.32 (d, 3H; CHMe₂, *J*_{H-H} = 6.8 Hz), 1.31 (d, 3H; CHMe₂, *J*_{H-H} = 6.8 Hz), 1.27 (d, 3H; CHMe₂, *J*_{H-H} = 6.8 Hz), 1.20 (d, 3H; CHMe₂, *J*_{H-H} = 6.8 Hz), 1.19 (s, 18H; NCCMe₃), 1.00 (d, 3H; CHMe₂, *J*_{H-H} = 6.8 Hz), 0.80 (dd, 1H; CH₂CHMe, *J*_{H-H} = 12.0, 5.6 Hz), -0.04 (dd, 1H; CH₂CHMe, *J*_{H-H} = 12.0, 11.8 Hz), -1.10 (s, 3H; ScMe). ¹³C{¹H} NMR: δ 174.2, 173.9 (NCCMe₃), 147.7, 145.2 (C_{ipso}), 144.9, 141.8, 141.4, 138.1, 127.5, 126.5, 125.9, 124.6, 124.5, 123.3 (C₆H₃), 98.8 (CH), 43.4, 43.2 (CMe₃), 39.7 (CH₂CHMe), 32.9, 32.2 (CMe₃), 29.6, 29.1, 28.9, 28.5 (CHMe₂), 26.8 (Me), 26.3, 26.1, 26.0, 25.9, 25.2, 24.4, 22.7 (CHMe₂).

 κ^3 -[ArNC(^tBu)CHC(^tBu)N-*i*Pr-C₆H₃]ScCH₂CH₃ (**3-Et**):


A similar procedure to that used for **3-Me** was followed. ¹H NMR: δ 7.35-6.86 (m, 6H; C₆H₃), 5.55 (s, 1H; CH), 3.45 (sp, 1H; CHMe₂, *J*_{H-H} = 6.8 Hz), 3.14 (ov m, 2H; CHMe₂, CH₂CHMe), 2.91 (sp, 1H; CHMe₂, *J*_{H-H} = 6.8 Hz), 1.46 (d, 3H; CHMe₂, *J*_{H-H} = 6.8 Hz), 1.45 (d, 3H; CHMe₂, *J*_{H-H} = 6.8 Hz), 1.32 (d, 3H; CHMe₂, *J*_{H-H} = 6.8 Hz), 1.31 (d, 3H;

CHMe₂, $J_{\text{H-H}} = 6.8$ Hz), 1.26 (d, 3H; CHMe₂, $J_{\text{H-H}} = 6.8$ Hz), 1.19 (d, 3H; CHMe₂, $J_{\text{H-H}} = 6.8$ Hz), 1.18 (s, 18H; NCCMe₃), 1.03 (d, 3H; CHMe₂, $J_{\text{H-H}} = 6.8$ Hz), 0.88 (dd, 1H; CH₂CHMe, $J_{\text{H-H}} = 12.0, 5.6$ Hz), 0.63 (t, 3H; CH₂CH₃, $J_{\text{H-H}} = 8.2$ Hz), 0.21 (dd, 1H; CH₂CHMe, $J_{\text{H-H}} = 12.0, 11.8$ Hz), -0.64 (d, 1H; CH₂CH₃, $J_{\text{H-H}} = 8.2$ Hz), -0.62 (d, 1H; CH₂CH₃, $J_{\text{H-H}} = 8.2$ Hz). ¹³C{¹H} NMR: δ 174.1, 173.8 (NCCMe₃), 147.8, 145.2 (C_{ipso}), 144.7, 142.2, 141.7, 139.7, 127.5, 126.8, 125.6, 125.3, 124.7, 123.3 (C₆H₃), 98.7 (CH), 43.4, 43.2 (CMe₃), 40.0 (CH₂CH₃), 39.7 (CH₂CHMe), 32.9, 32.3 (CMe₃), 29.0, 28.9, 28.6, 28.5, 26.3, 26.2, 26.0, 25.9, 25.2, 24.4, 22.8 (CHMe₂), 12.2 (CH₂CH₃).

κ^3 -[ArNC(^tBu)CHC(^tBu)N-*i*Pr-C₆H₃]ScCH₂Ph (**3-CH₂Ph**):

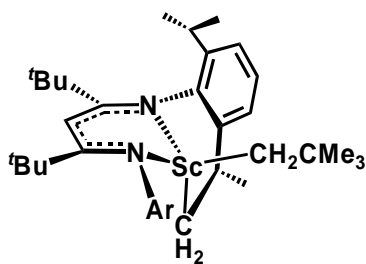


A similar procedure to that used for **3-Me** was followed.

¹H NMR: δ 7.27-6.84 (m, 11H; C₆H₃, Ph), 5.58 (s, 1H; CH), 3.13 (sp, 1H; CHMe₂, $J_{\text{H-H}} = 6.8$ Hz), 3.11 (ov m, 2H; CHMe₂, CH₂CHMe), 2.92 (sp, 1H; CHMe₂, $J_{\text{H-H}} = 6.8$ Hz), 2.12 (s, 2H; CH₂Ph) 1.39 (d, 3H; CHMe₂, $J_{\text{H-H}} = 6.8$ Hz), 1.37 (d, 3H; CHMe₂, $J_{\text{H-H}} = 6.8$ Hz), 1.31 (d, 3H; CHMe₂, $J_{\text{H-H}} = 6.8$ Hz), 1.25 (d, 3H; CHMe₂, $J_{\text{H-H}} = 6.8$ Hz), 1.24 (d, 3H; CHMe₂, $J_{\text{H-H}} = 6.8$ Hz), 1.22 (d, 3H; CHMe₂, $J_{\text{H-H}} = 6.8$ Hz), 1.21 (d, 3H; CHMe₂, $J_{\text{H-H}} = 6.8$ Hz), 1.07 (s, 18H; NCCMe₃), 0.89 (dd, 1H; CH₂CHMe, $J_{\text{H-H}} = 12.1, 5.6$ Hz), 0.07 (dd, 1H; CH₂CHMe, $J_{\text{H-H}} = 12.2, 11.8$ Hz). ¹³C{¹H} NMR: δ 175.4, 173.8 (NCCMe₃), 149.1, 146.6, 145.4 (C_{ipso}), 143.7, 142.2, 141.7, 140.8, 129.7, 129.1, 128.9, 128.7, 127.0, 126.2, 125.6, 125.0, 123.7, 120.0, 119.5 (C₆H₃, CH₂Ph), 99.4 (CH), 43.4, 43.2 (CMe₃), 39.7 (CH₂CHMe), 32.9, 32.3 (CMe₃),

29.0, 28.9, 28.7, 28.6, 26.8, 26.2, 26.0, 25.7, 25.2, 24.5, 23.6 (CHMe₂), (ScCH₂Ph not observed).

κ^3 -[ArNC(^tBu)CHC(^tBu)N-*i*Pr-C₆H₃]ScCH₂CMe₃ (3-CH₂CMe₃):



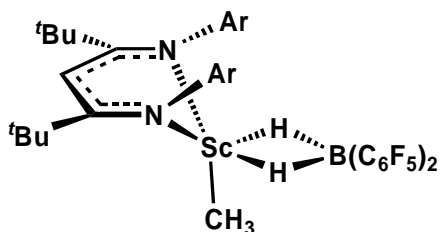
A similar procedure to that used for **3-Me** was followed. ¹H NMR: δ 7.34-6.96 (m, 6H; C₆H₃), 5.56 (s, 1H; CH), 3.50 (sp, 1H; CHMe₂, J_{H-H} = 6.8 Hz), 3.20 (ov m, 2H; CHMe₂, CH₂CHMe), 2.89 (sp, 1H; CHMe₂,

J_{H-H} = 6.8 Hz), 1.56 (d, 3H; CHMe₂, J_{H-H} = 6.8 Hz), 1.48 (d, 3H; CHMe₂, J_{H-H} = 6.8 Hz), 1.34 (d, 3H; CHMe₂, J_{H-H} = 6.8 Hz), 1.33 (d, 3H; CHMe₂, J_{H-H} = 6.8 Hz), 1.27 (d, 3H; CHMe₂, J_{H-H} = 6.8 Hz), 1.18 (d, 3H; CHMe₂, J_{H-H} = 6.8 Hz), 1.17 (s, 18H; NCCMe₃), 1.11 (d, 3H; CHMe₂, J_{H-H} = 6.8 Hz), 0.77 (s, 9H; CH₂CMe₃), 0.19 (dd, 1H; CH₂CHMe, J_{H-H} = 11.8 Hz, 1 CH₂CHMe not observed), -0.43 (d, 1H; CH₂CMe₃, J_{H-H} = 12.6 Hz), -0.55 (d, 1H; CH₂CMe₃, J_{H-H} = 12.6 Hz). ¹³C{¹H} NMR: δ 174.0, 173.8 (NCCMe₃), 147.7, 144.8 (C_{ipso}), 144.7, 142.3, 141.3, 138.7, 127.6, 126.7, 125.6, 125.0, 123.8, 123.7 (C₆H₃), 98.8 (CH), 70.8 (CH₂CMe₃) 43.4, 43.2 (CMe₃), 39.8 (CH₂CHMe), 35.7 (CH₂CMe₃), 34.6 (CH₂CMe₃), 33.1, 32.6 (CMe₃), 28.9, 28.8, 28.5, 26.5, 26.1, 26.0, 25.8, 25.7, 25.2, 24.6, 21.9 (CHMe₂).

6.3 Experimental Procedures Pertaining to Chapter 3

6.3.1 Synthetic Procedures

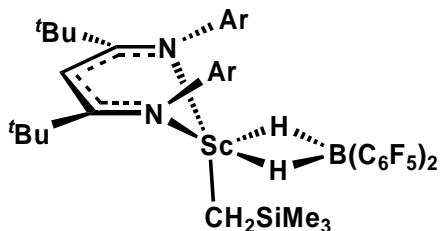
Synthesis of $[\text{ArNC}(\text{tBu})\text{CHC}(\text{tBu})\text{NAr}]\text{ScMe}(\mu\text{-H})_2\text{B}(\text{C}_6\text{F}_5)_2$ (**4-Me**):



2-Me (0.135 g, 0.233 mmol) and $\text{HB}(\text{C}_6\text{F}_5)_2$ (0.160 g, 0.466 mmol) were dissolved in THF (15 mL) and stirred for 15 minutes whereupon solvent was removed under vacuum to give an oily yellow solid.

Hexanes (20 mL) were added and the reaction mixture filtered. The solvent was removed *in vacuo* to give **4-Me** as a yellow solid which was recrystallized from hexanes. (0.112 g, 0.123 mmol, 53%). ^1H NMR (C_7D_8 , 285K): δ 7.14-6.81 (ov m, 6H; C_6H_3), 5.49 (s, 1H; CH), 3.46 (sp, 2H; CHMe_2 , $J_{\text{H-H}} = 6.4$ Hz), 2.77 (q, 2H; $\text{Sc}(\mu\text{-H})_2\text{B}(\text{C}_6\text{F}_5)_2$, $^1J_{\text{H-B}} = 69$ Hz), 2.61 (sp, 2H; CHMe_2 , $J_{\text{H-H}} = 6.4$ Hz), 1.46 (d, 6H; CHMe_2 , $J_{\text{H-H}} = 6.4$ Hz), 1.38 (d, 6H; CHMe_2 , $J_{\text{H-H}} = 6.4$ Hz), 1.10 (d, 6H; CHMe_2 , $J_{\text{H-H}} = 6.4$ Hz), 0.98 (d, 6H; CHMe_2 , $J_{\text{H-H}} = 6.4$ Hz), 0.87 (s, 18H; NCCMe_3), 0.18 (ScMe). $^{13}\text{C}\{^1\text{H}\}$ NMR (C_7D_8 , 285K, C_6F_5 resonances not reported): δ 173.9 (NCCMe_3), 142.4 (C_{ipso}), 140.1, 139.4, 126.3, 124.2, 123.6, (C_6H_3), 87.8 (CH), 43.9 (CMe_3), 32.3 (CHMe_2), 31.0 (CMe_3), 28.1 (CHMe_2), 26.1, 25.9, 24.2, 23.7 (CHMe_2), (ScMe not observed). ^{19}F NMR (C_7D_8): δ -131.2 (*o-F*), -157.5 (*p-F*), -163.7 (*m-F*). ^{11}B NMR (d^8 -THF): δ -10.9 (t, 1B; $^1J_{\text{B-H}} = 69$ Hz). Anal. Calcd. for $\text{C}_{48}\text{H}_{58}\text{N}_2\text{BF}_{10}\text{Sc}$: C, 63.45; H, 6.43; N, 3.08. Found: C, 63.15; H, 6.29; N, 2.96.

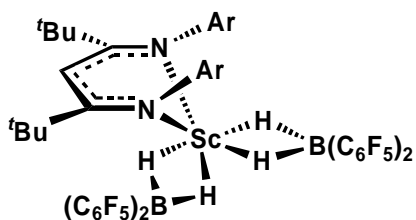
Synthesis of [ArNC(^tBu)CHC(^tBu)NAr]ScCH₂SiMe₃(μ-H)₂B(C₆F₅)₂ (4-CH₂SiMe₃):



An NMR tube was charged with **2-CH₂SiMe₃** (0.021 g, 0.029 mmol) and HB(C₆F₅)₂ (0.20 g, 0.058 mmol) in 0.5 mL *d*₈-toluene. The tube was shaken and the allowed to sit for 15 minutes. ¹H

NMR (C₆D₆): δ 7.12-6.89 (ov m, 6H; C₆H₃), 5.50 (s, 1H; CH), 3.46 (sp, 2H; CHMe₂, *J*_{H-H} = 6.4 Hz), 2.85 (q, 2H; Sc(μ-H)₂B(C₆F₅)₂, ¹*J*_{H-B} = 69 Hz), 2.68 (sp, 2H; CHMe₂, *J*_{H-H} = 6.4 Hz), 1.50 (d, 6H; CHMe₂, *J*_{H-H} = 6.4 Hz), 1.37 (d, 6H; CHMe₂, *J*_{H-H} = 6.4 Hz), 1.17 (d, 6H; CHMe₂, *J*_{H-H} = 6.4 Hz), 1.14 (d, 6H; CHMe₂, *J*_{H-H} = 6.4 Hz), 0.87 (s, 18H; NCCMe₃), -0.07 (s, 2H; ScCH₂SiMe₃), -0.38 (s, 9H; ScCH₂SiMe₃). ¹³C{¹H} NMR (C₆D₆, C₆F₅ resonances not reported): δ 175.0 (NCCMe₃), 143.3 (C_{ipso}), 141.7, 140.9, 127.2, 124.9, 124.6, (C₆H₃), 87.8 (CH), 44.6 (CMe₃), 31.6 (CMe₃), 31.1 (CHMe₂), 28.5 (CHMe₂), 26.9, 26.5, 24.4, 24.3 (CHMe₂), 2.2 (ScCH₂SiMe₃), (ScCH₂SiMe₃ not observed). ¹⁹F NMR (C₇D₈): δ -131.2 (*o*-F), -157.5 (*p*-F), -163.7 (*m*-F). ¹⁹F NMR (C₆D₆): δ -130.1 (*o*-F), -157.8 (*p*-F), -163.7 (*m*-F). ¹¹B{¹H} NMR (C₆D₆): δ -19.4 (t, 1B; ¹*J*_{B-H} = 69 Hz).

Synthesis of [ArNC(^tBu)CHC(^tBu)NAr]Sc((μ-H)₂B(C₆F₅)₂)₂ (4-H₂B(C₆F₅)₂):

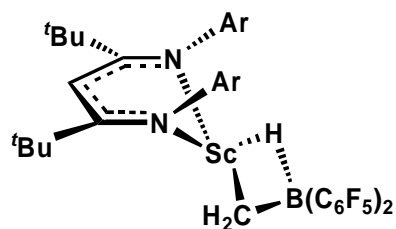


A 50 mL flask equipped with **2-Me** (0.058 g, 0.10 mmol) and HB(C₆F₅)₂ (0.140 g, 0.40 mmol) was attached to a swivel frit apparatus. The entire assemblage was evacuated, and toluene (30 mL) was

vacuum distilled into the flask. After warming to room temperature, the reaction mixture was stirred for another 30 minutes, filtered and solvent removed under vacuum to afford

a yellow powder. Hexanes (15 mL) were added and the reaction mixture was sonicated. The volume was reduced to 5 mL, cooled to $-78\text{ }^{\circ}\text{C}$ for 30 minutes, and back filtered. The solvent was removed *in vacuo* to afford **4-H₂B(C₆F₅)₂** as a light yellow powder. (0.089 g, 0.072 mmol, 72%). ¹H NMR (C₆D₆): δ 6.99 (t, 2H; C₆H₃, $J_{\text{H-H}} = 7.7$ Hz), 6.87-6.83 (ov m, 4H; C₆H₃), 5.55 (s, 1H; CH), 3.08 (sp, 2H; CHMe₂, $J_{\text{H-H}} = 6.4$ Hz), 2.52 (sp, 2H; CHMe₂, $J_{\text{H-H}} = 6.4$ Hz), 2.48 (q, 4H; Sc((μ -H)₂B(C₆F₅)₂)₂, $^1J_{\text{H-B}} = 67$ Hz), 1.34 (d, 6H; CHMe₂, $J_{\text{H-H}} = 6.4$ Hz), 1.13 (d, 6H; CHMe₂, $J_{\text{H-H}} = 6.4$ Hz), 1.04 (d, 6H; CHMe₂, $J_{\text{H-H}} = 6.4$ Hz), 1.00 (d, 6H; CHMe₂, $J_{\text{H-H}} = 6.4$ Hz), 0.82 (s, 18H; NCCMe₃). ¹³C{¹H} NMR (C₇D₈, C₆F₅ resonances not reported): δ 177.0 (NCCMe₃), 142.4 (C_{ipso}), 141.0, 140.6, 128.3, 125.3, 124.7 (C₆H₃), 82.2 (CH), 45.0 (CMe₃), 31.6 (CHMe₂), 30.7 (CMe₃), 28.7 (CHMe₂), 25.8, 25.4, 25.1, 24.6 (CHMe₂). ¹⁹F NMR (C₇D₈): δ -127.5, -130.3 (*o*-F), -156.6, -156.8 (*p*-F), -162.3, -163.4 (*m*-F). ¹¹B NMR (C₇D₈): δ -13.6 (t, 1B; $^1J_{\text{BH}} = 67$ Hz), -15.5 (t, 1B; $^1J_{\text{B-H}} = 67$ Hz). Anal. Calcd. for C₅₉H₅₇N₂B₂F₂₀Sc: C, 57.12; H, 4.63; N, 2.26. Found: C, 56.81; H, 4.55; N, 2.07.

Synthesis of [ArNC(^tBu)CHC(^tBu)NAr]Sc(μ -H)(μ -CH₂)B(C₆F₅)₂ (5):

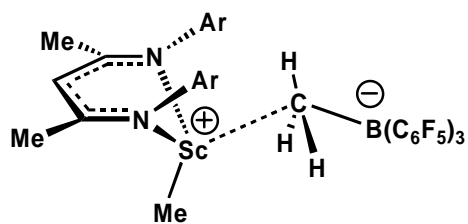


2-Me (0.350 g, 0.608 mmol) and HB(C₆F₅)₂ (0.210 g, 0.608 mmol) were dissolved in cold ($-78\text{ }^{\circ}\text{C}$) toluene (30 mL) and gradually warmed to room temperature. Upon stirring for another 80 minutes, the solvent was

removed to give a reddish foam. Hexamethyldisiloxane (15 mL) was added, the reaction mixture sonicated (15 minutes), cooled to $-35\text{ }^{\circ}\text{C}$ (30 minutes) and filtered. The solvent was removed to give a yellow powder which was recrystallized from hexanes. (0.250 g,

0.0276 mmol, 45%). ^1H NMR (C_6D_6): δ 7.11-6.64 (ov m, 6H; C_6H_3), 5.75 (s, 1H; CH), 3.19 (sp, 1H; CHMe_2 , $J_{\text{H-H}} = 6.5$ Hz), 3.07 (sp, 1H; CHMe_2 , $J_{\text{H-H}} = 6.5$ Hz), 2.95 (q, 4H; $\text{Sc}((\mu\text{-H})_2\text{B}(\text{C}_6\text{F}_5)_2)_2$, $^1J_{\text{H-B}} = 64$ Hz), 2.82 (sp, 1H; CHMe_2 , $J_{\text{H-H}} = 6.5$ Hz), 2.55 (sp, 1H; CHMe_2 , $J_{\text{H-H}} = 6.5$ Hz), 1.45 (d, 3H; CHMe_2 , $J_{\text{H-H}} = 6.5$ Hz), 1.33 (d, 3H; CHMe_2 , $J_{\text{H-H}} = 6.5$ Hz), 1.13 (d, 3H; CHMe_2 , $J_{\text{H-H}} = 6.5$ Hz), 1.01-0.97 (ov m, 30H; CHMe_2 , NCCMe_3), 0.82 (d, 3H; CHMe_2 , $J_{\text{H-H}} = 6.5$ Hz), -0.13 (br s, 2H; $\text{ScCH}_2\text{B}(\text{C}_6\text{F}_5)_2$). $^{13}\text{C}\{^1\text{H}\}$ NMR (C_7D_8 , C_6F_5 resonances not reported, ScCH_2 not observed): δ 174.8, 174.5 (NCCMe_3), 145.5, 143.9 (C_{ipso}), 143.4, 137.6, 136.9, 135.3, 129.3, 128.5, 126.0, 125.7, 124.0, 122.5 (C_6H_3), 101.3 (CH), 42.9, 39.3 (CMe_3), 32.1, 31.5 (CMe_3), 31.2, 29.2, 28.4, 27.8 (CHMe_2), 25.1, 25.0, 24.8, 24.4 (2), 24.2, 23.4 (2) (CHMe_2). ^{19}F NMR (C_7D_8 , 230K): δ -131.0 (*o-F*), -158.3 (*p-F*), -162.6 (*m-F*). ^{11}B NMR (C_7D_8): δ -21.0 (d, 1B; $^1J_{\text{B-H}} = 64$ Hz). Anal. Calcd. for $\text{C}_{48}\text{H}_{56}\text{N}_2\text{BF}_{10}\text{Sc}$: C, 63.59; H, 6.23; N, 3.09. Found: C, 63.97; H, 6.19; N, 2.94.

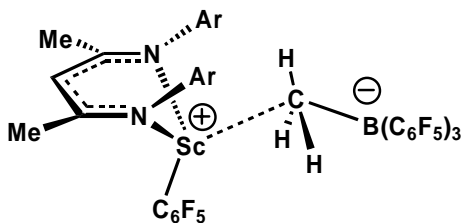
Synthesis of $\{[\text{ArNC}(\text{Me})\text{CHC}(\text{Me})\text{NAr}]\text{ScMe}\}^+[\text{MeB}(\text{C}_6\text{F}_5)_3]^-$ (7-Me) and $\{[\text{ArNC}(\text{Me})\text{CHC}(\text{Me})\text{NAr}]\text{ScC}_6\text{F}_5\}^+[\text{MeB}(\text{C}_6\text{F}_5)_3]^-$ (7-C₆F₅):



An NMR tube was charged with **1-Me** (0.010 g, 0.020 mmol) and $\text{B}(\text{C}_6\text{F}_5)_3$ (0.023 g, 0.020 mmol) to which cold (-35 °C) $\text{C}_6\text{D}_5\text{Br}$ (0.5 mL) was added. Upon mixing, the tube was inserted in the

NMR probe at -35 °C and slowly warmed to -23 °C. ^1H NMR ($\text{C}_6\text{D}_5\text{Br}$, 250K): δ 7.20-6.79 (ov m, 6H; C_6H_3), 5.19 (s, 1H; CH), 3.36 (br m, 2H; CHMe_2), 2.14 (br, 2H m; CHMe_2), 1.69 (br s, 3H; BMe), 1.56 (s, 6H; NCMe), 1.16-0.74 (ov m, 24H; CHMe_2),

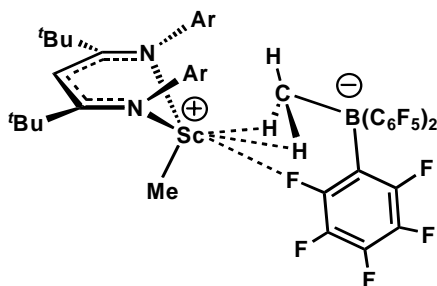
0.52 (s, 3H; ScMe). ^{19}F NMR ($\text{C}_6\text{D}_5\text{Br}$, 250K): δ -134.3 (*o-F*), -159.4 (*p-F*), -163.6 (*m-F*). $^{11}\text{B}\{^1\text{H}\}$ NMR ($\text{C}_6\text{D}_5\text{Br}$, 250K): δ -16.8 (br s).



The NMR tube was gradually warmed to RT generating **7-C₆F₅** from rapid C₆F₅ transfer and loss of free MeB(C₆F₅)₂. ^1H NMR ($\text{C}_6\text{D}_5\text{Br}$): δ 7.16-7.05 (ov m, 6H; C₆H₃), 5.69 (s, 1H; CH),

2.53 (br m, 4H; CHMe₂), 1.75 (s, 6H; NCMe), 1.27 (br s, 3H; BMe), 1.03-0.85 (ov m, 24H; CHMe₂). ^{19}F NMR ($\text{C}_6\text{D}_5\text{Br}$, 250K): δ Isomer 1 (70%): -117.1, -123.0 (2F; ScC₆F₅, *o-F*), -133.2 (6F; Me-B(C₆F₅)₃, *o-F*), -150.2 (1F; ScC₆F₅, *p-F*), -159.3 (3F; Me-B(C₆F₅)₃, *p-F*), -163.8 (6F; Me-B(C₆F₅)₃, *m-F*), -167.1 (2F; ScC₆F₅, *m-F*). Isomer 2 (30%): -125.1 (2F; ScC₆F₅, *o-F*), -134.5 (6F; Me-B(C₆F₅)₃, *o-F*), -150.9 (1F; ScC₆F₅, *p-F*), -159.6 (3F; Me-B(C₆F₅)₃, *p-F*), -164.7 (6F; Me-B(C₆F₅)₃, *m-F*), -167.1 (2F; ScC₆F₅, *m-F*). $^{11}\text{B}\{^1\text{H}\}$ NMR ($\text{C}_6\text{D}_5\text{Br}$): δ -15.2 (br s). The instability of these compounds made it impossible to acquire ^{13}C NMR spectra as further decomposition occurs over the timeframe required to collect the necessary data. Upon cooling the tube to -35 °C and layering with 1 mL of hexanes, yellow crystals suitable for X-ray diffraction were obtained after 2 weeks.

Synthesis of $\{[\text{ArNC}(\text{tBu})\text{CHC}(\text{tBu})\text{NAr}]\text{ScMe}\}^+[\text{MeB}(\text{C}_6\text{F}_5)_3]^-$ (**10-Me**):

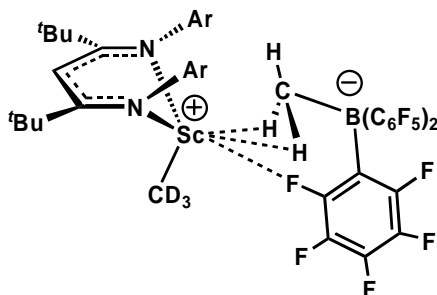


A 25 mL vial was charged with **2-Me** (0.160 g, 0.277 mmol) and hexane (9 mL). In a separate vial B(C₆F₅)₃ (0.142 g, 0.277 mmol) was dissolved in hexane (13 mL). The B(C₆F₅)₃ solution was added dropwise to the clear yellow **2-Me** solution causing

immediate formation of a pale yellow precipitate. The solution was cooled to $-35\text{ }^{\circ}\text{C}$ for 24 hours, upon which the supernatant was removed and the pale yellow crystalline solid was dried *in vacuo* to afford pure **10-Me** (0.286 g, 0.263 mmol, 95%). ^1H NMR for Isomer A (213K): δ 7.11-6.69 (m, 6H; C_6H_3), 5.85 (s, 1H; CH), 3.31 (sp, 2H; CHMe_2 , $J_{\text{H-H}} = 6.6$ Hz), 2.21 (sp, 2H; CHMe_2 , $J_{\text{H-H}} = 6.6$ Hz), 1.28 (d, 6H; CHMe_2 , $J_{\text{H-H}} = 6.6$ Hz), 1.20 (d, 6H; CHMe_2 , $J_{\text{H-H}} = 6.6$ Hz), 1.10 (br s, 3H; BMe), 1.02 (d, 6H; CHMe_2 , $J_{\text{H-H}} = 6.6$ Hz), 0.98 (s, 18H; NCCMe_3) 0.97 (d, 6H; CHMe_2 , $J_{\text{H-H}} = 6.6$ Hz), 0.24 (s, 3H; ScMe). ^1H NMR for Isomer B (213K): δ 7.11-6.69 (m, 6H; C_6H_3), 5.53 (s, 1H; CH), 2.81 (sp, 2H; CHMe_2 , $J_{\text{H-H}} = 6.6$ Hz), 2.38 (sp, 2H; CHMe_2 , $J_{\text{H-H}} = 6.6$ Hz), 1.73 (br s, 3H, BMe), 1.28 (d, 6H; CHMe_2 , $J_{\text{H-H}} = 6.6$ Hz), 1.25 (d, 6H; CHMe_2 , $J_{\text{H-H}} = 6.6$ Hz), 1.02 (d, 6H; CHMe_2 , $J_{\text{H-H}} = 6.6$ Hz), 0.97 (d, 6H; CHMe_2 , $J_{\text{H-H}} = 6.6$ Hz), 0.72 (s, 18H; NCCMe_3), 0.47 (s, 3H; ScMe). Complete assignment of the $^{13}\text{C}\{^1\text{H}\}$ NMR spectrum was not possible and such data is reported by carbon type: δ 141.7, 140.6 (C_{ipso}), 140.0, 139.8, 139.5, 139.4, 125.6, 124.7, 124.6, 124.2, 125.5 (C_6H_3 , one peak not observed). All other carbon resonances were attributable to a specific isomer. $^{13}\text{C}\{^1\text{H}\}$ NMR for Isomer A (213K; C_6F_5 resonances not reported): δ 173.9 (NCCMe_3), 90.1 (CH), 45.0 (CMe_3), 34.0 (ScMe) 31.3 (CMe_3), 29.9, 28.4 (CHMe_2), 25.7, 23.9, 23.7 (CHMe_2 , one peak not observed), (BMe not observed). $^{13}\text{C}\{^1\text{H}\}$ NMR for Isomer B (213K; C_6F_5 resonances not reported): δ 174.5 (NCCMe_3), 88.0 (CH), 45.8 (ScMe), 43.8 (CMe_3), 32.0 (CHMe_2), 30.5 (CMe_3), 28.2 (CHMe_2), 27.9 (BMe), 25.6, 23.9, 23.7 (CHMe_2 , one peak not observed). ^{19}F NMR for Isomer A (213K): δ -132.6 (*o-F*), -159.0 (*p-F*), -162.8 (*m-F*). ^{19}F NMR for Isomer B (213K): δ -133.1 (*o-F*), -158.5 (*p-F*), -163.4 (*m-F*). $^{11}\text{B}\{^1\text{H}\}$ NMR for Isomers

A & B: δ -16.6 (br s). Anal. Calcd. for $C_{55}H_{59}N_2BF_{15}Sc$: C, 60.67; H, 5.46; N, 2.57.
 Found : C, 60.80; H, 5.71; N, 2.47.

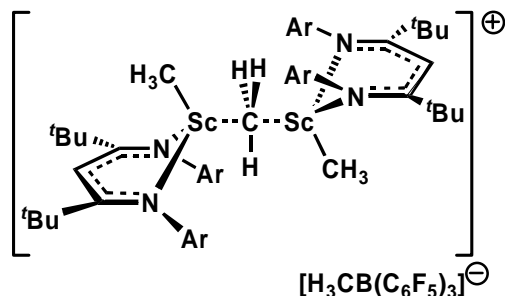
Synthesis of $\{[ArNC(tBu)CHC(tBu)NAr]ScCD_3\}^+[H_3CB(C_6F_5)_3]^-$ (*d*₃-10-Me**):**



*d*₆-**2-Me** (0.0070 g, 0.012 mmol) and **10** (0.019 g, 0.012 mmol) were dissolved in 0.5 mL cold (-78 °C) *d*₈-toluene. The ¹H NMR spectrum matched **10-Me** exception no resonances were observed for the ScMe groups (even after several hours at room

temperature). ²H NMR (C_7H_8 , 215K) Isomer A : δ 0.26. Isomer B : 0.50.

Synthesis of $\{[ArNC(tBu)CHC(tBu)NAr]ScMe_2(\mu-Me)\}^+[MeB(C_6F_5)_3]^-$ (9**):**



Preparation 1: **10-Me** (0.011 g, 0.010 mmol) and **2-Me** (0.0060 g, 0.010 mmol) were placed in an NMR tube. The tube was cooled to -30 °C, 0.5 mL of cold C_6D_5Br (-30 °C) was added and the sample was slowly allowed

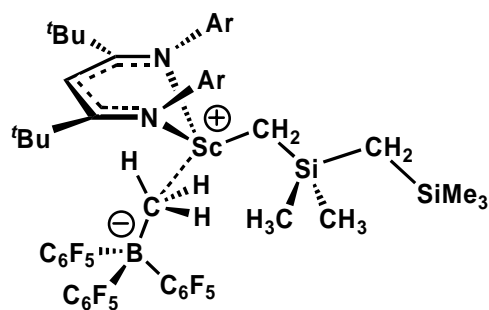
to warm to 285K.

Preparation 2: **2-Me** (0.012 g, 0.020 mmol) and $B(C_6F_5)_3$ (0.0050 g, 0.010 mmol) were placed in an NMR tube. The tube was cooled to -30 °C, 0.5 mL of cold C_6D_5Br (-30 °C) was added and the sample was slowly allowed to warm to 285K. ¹H NMR (285K, C_6D_5Br): δ 7.12-6.91 (m, 12H; C_6H_3), 5.82 (s, 2H; CH), 2.87 (br m, 4H; $CHMe_2$), 2.43 (br m, 4H; $CHMe_2$), 1.27 (br m, 12H; $CHMe_2$), 1.20 (br m, 12H; $CHMe_2$), 1.08 (br m,

24H; CHMe_2), 0.98 (s, 36H; NCCMe_3) 0.10 (s, 3H; ScMeSc), -0.29 (s, 6H; ScMe). $^{13}\text{C}\{^1\text{H}\}$ NMR ($\text{C}_6\text{D}_5\text{Br}$, 250K, C_6F_5 resonances not reported): δ 173.4 (NCCMe_3), 142.7 (C_{ipso}), 140.7, 124.7, 123.7 (C_6H_3), 91.9 (CH), 44.2 (CMe_3), 35.6 (ScMeSc $^1J_{\text{C-H}} = 132.1$ Hz), 29.4 (CHMe_2), 27.7 (ScMe , $^1J_{\text{C-H}} = 100.6$ Hz), 27.1 (CHMe_2), 24.2, 24.1, 24.0, 23.5 (CHMe_2). ^{19}F NMR ($\text{C}_6\text{D}_5\text{Br}$): δ -133.3 (*o-F*), -165.1 (*p-F*), -167.5 (*m-F*). $^{11}\text{B}\{^1\text{H}\}$ NMR ($\text{C}_6\text{D}_5\text{Br}$): δ -15.0.

Synthesis of $\{[\text{ArNC}(\text{tBu})\text{CHC}(\text{tBu})\text{NAr}]\text{ScCH}_2\text{SiMe}_2\text{CH}_2\text{SiMe}_3\}^+[\text{MeB}(\text{C}_6\text{F}_5)_3]^-$

($10\text{-CH}_2\text{SiMe}_2\text{CH}_2\text{SiMe}_3$):



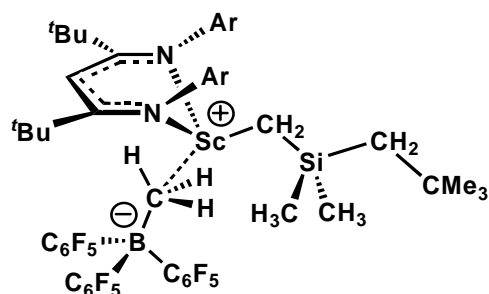
$2\text{-CH}_2\text{SiMe}_3$ (0.050 g, 0.069 mmol) was dissolved in 5 mL of hexane. In a separate vial $\text{B}(\text{C}_6\text{F}_5)_3$ (0.036 g, 0.069 mmol) was dissolved in hexane (7 mL). The $\text{B}(\text{C}_6\text{F}_5)_3$ solution was added dropwise to the clear yellow

$2\text{-CH}_2\text{SiMe}_3$ solution causing immediate formation of a pale yellow precipitate. The solution was cooled to $-35\text{ }^\circ\text{C}$ for 24 hours, upon which the supernatant was removed and the remaining residue dried *in vacuo* to afford pure $10\text{-CH}_2\text{SiMe}_2\text{CH}_2\text{SiMe}_3$ as a pale yellow solid. (0.058 g, 0.047 mmol, 68%). ^1H NMR (215K): δ 6.96-6.74 (m, 6H; C_6H_3), 5.52 (s, 1H; CH), 2.92 (sp, 2H; CHMe_2 , $J_{\text{H-H}} = 6.3$ Hz), 2.47 (sp, 2H; CHMe_2 , $J_{\text{H-H}} = 6.3$ Hz), 1.51 (br s, 3H, BMe), 1.37 (d, 6H; CHMe_2 , $J_{\text{H-H}} = 6.3$ Hz), 1.21 (d, 6H; CHMe_2 , $J_{\text{H-H}} = 6.3$ Hz), 1.16 (s, 2H; $\text{CH}_2\text{SiMe}_2\text{CH}_2\text{SiMe}_3$), 1.05 (d, 6H; CHMe_2 , $J_{\text{H-H}} = 6.3$ Hz), 0.96 (d, 6H; CHMe_2 , $J_{\text{H-H}} = 6.3$ Hz), 0.74 (s, 18H; NCCMe_3), 0.02 (s, 9H; $\text{CH}_2\text{SiMe}_2\text{CH}_2\text{SiMe}_3$), -0.20 (s, 6H; $\text{CH}_2\text{SiMe}_2\text{CH}_2\text{SiMe}_3$) -0.73 (s, 2H;

CH₂SiMe₂CH₂SiMe₃). ¹³C{¹H} NMR (215K; C₆F₅ resonances not reported): δ 175.4 (NCCMe₃), 142.0 (C_{ipso}), 139.9, 127.4, 124.6 (C₆H₃), 88.0 (CH), 73.2 (ScCH₂), 44.3 (CMe₃), 31.0 (CHMe₂), 30.9 (CMe₃), 28.5 (CHMe₂), 26.6, 25.6, 24.3, 23.9 (CHMe₂), 5.9 (CH₂SiMe₂CH₂SiMe₃), 3.0 (CH₂SiMe₂CH₂SiMe₃), 1.5 (CH₂SiMe₂CH₂SiMe₃). ¹⁹F NMR: δ -133.4 (*o*-F), -160.4 (*p*-F), -165.0 (*m*-F). ¹¹B{¹H} NMR: δ -15.2 (br s). Anal. Calcd. for C₄₃H₇₅N₂Si₂BF₁₅Sc : C, 59.41; H, 6.13; N, 2.27. Found : C, 59.78; H, 6.11; N, 2.37.

Synthesis of {[ArNC(^tBu)CHC(^tBu)NAr]ScCH₂SiMe₂CH₂CMe₃}{MeB(C₆F₅)₃}

(10-CH₂SiMe₂CH₂CMe₃):

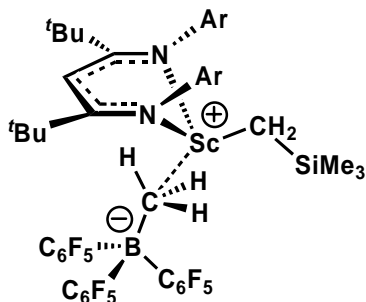


A 25 mL vial was charged with **2-CH₂SiMe₃(CH₂CMe₃)** (0.050 g, 0.071 mmol) and hexanes (8 mL). In a separate vial B(C₆F₅)₃ (0.036 g, 0.071 mmol) was dissolved in hexanes (4 mL). The scandium solution was added dropwise to the colourless B(C₆F₅)₃ solution. The solution was cooled to -35 °C for 18 hours, upon which the supernatant was decanted and the yellow crystalline solid was dried *in vacuo* to afford pure **10-CH₂SiMe₂CH₂CMe₃** (0.047 g, 0.039 mmol, 55%). ¹H NMR (C₇D₈; 233K): δ 6.95 (t, 2H; C₆H₃, J_{H-H} = 7.8 Hz), 6.79 (d, 2H; C₆H₃, J_{H-H} = 7.8 Hz), 6.75 (d, 2H; C₆H₃, J_{H-H} = 7.8 Hz), 5.54 (s, 1H; CH), 2.91 (sp, 2H; CHMe₂, J_{H-H} = 6.6 Hz), 2.41 (sp, 2H; CHMe₂, J_{H-H} = 6.6 Hz), 1.48 (br s, 3H, BMe), 1.35-1.03 (br ov m, 24H; CHMe₂), 1.03 (br s, 2H; ScCH₂SiMe₂CH₂CMe₃), 0.90 (s, 9H; ScCH₂SiMe₂CH₂CMe₃), 0.75 (s, 18H; NCCMe₃), 0.28 (s, 2H; ScCH₂SiMe₂CH₂CMe₃),

-0.19 (s, 6H; ScCH₂SiMe₂CH₂CMe₃). ¹³C{¹H} NMR (C₇D₈, 233K; CF resonances not reported): δ 175.4 (NCCMe₃), 142.2 (C_{ipso}), 140.0, 139.9, 129.1, 124.9, 124.5 (C₆H₃), 88.0 (CH), 72.1 (br s, ScCH₂SiMe₂CH₂CMe₃) 44.2 (CMe₃), 35.3 (ScCH₂SiMe₂CH₂CMe₃), 34.8 (ScCH₂SiMe₂CH₂CMe₃), 33.3 (ScCH₂SiMe₂CH₂CMe₃), 32.2 (CMe₃), 31.2, 28.4 (CHMe₂), 26.7, 25.4, 24.3, 23.8 (CH(Me)₂), 2.6 (ScCH₂SiMe₂CH₂CMe₃), (BMe not found). ¹⁹F NMR (C₇D₈, 203K) : δ -132.4 (6F; *o*-F), -158.3 (3F; *p*-F), -163.3 (6F; *m*-F). ¹¹B{¹H} NMR (C₇D₈, 240K) : δ -15.2(br s). Anal. Calcd. for C₆₂H₇₅N₂SiBF₁₅Sc : C, 61.18; H, 6.21; N, 2.30. Found : C, 59.79; H, 6.38; N, 2.32.

Synthesis of {[ArNC(^tBu)CHC(^tBu)NAr]ScCH₂SiMe₃}{H₃CB(C₆F₅)₃}

(10-CH₂SiMe₃):

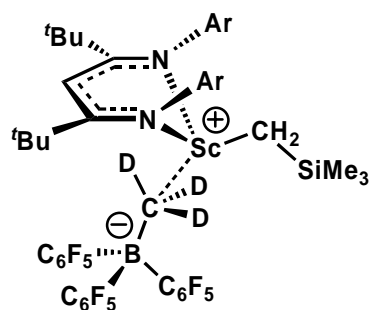


A 1 dram vial was charged with **2-Me(CH₂SiMe₃)** (0.035 g, 0.054 mmol) and hexane (1.5 mL). In a separate vial B(C₆F₅)₃ (0.028 g, 0.054 mmol) was dissolved in hexane (3.5 mL). The scandium solution was added dropwise to the B(C₆F₅)₃ solution causing immediate precipitation of a fine yellow powder. The solution was cooled to -35 °C for 24 hours, upon which the supernatant was removed and the yellow powder dried *in vacuo* to afford pure **10-CH₂SiMe₃** (0.021 g, 0.018 mmol, 33%). ¹H NMR (C₇D₈; 210K): δ 6.95 (t, 2H; C₆H₃, *J*_{H-H} = 7.5 Hz), 6.73 (d, 2H; C₆H₃, *J*_{H-H} = 7.5 Hz), 6.68 (d, 2H; C₆H₃, *J*_{H-H} = 7.5 Hz), 5.49 (s, 1H; CH), 2.96 (sp, 2H; CHMe₂, *J*_{H-H} = 6.6 Hz), 2.41 (sp, 2H; CHMe₂, *J*_{H-H} = 6.6 Hz), 1.56 (br s, 3H, BMe), 1.34 (d, 6H; CHMe₂, *J*_{H-H} = 6.6 Hz), 1.24 (d, 6H; CHMe₂, *J*_{H-H} = 6.6

Hz), 1.14 (br s, 2H; ScCH₂SiMe₃), 1.01 (d, 6H; CHMe₂, J_{H-H} = 6.6 Hz), 0.95 (d, 6H; CHMe₂, J_{H-H} = 6.6 Hz), 0.69 (s, 18H; NCCMe₃), -0.18 (s, 6H; ScCH₂SiMe₃). ¹³C{¹H} NMR (C₇D₈, 210K; C₆F₅ resonances not reported): δ 175.1 (NCCMe₃), 142.0 (C_{ipso}), 139.7, 139.6, 129.5, 128.8, 128.2 (C₆H₃), 88.6 (CH), 44.0 (CMe₃), 31.0 (CMe₃), 30.7, 30.6 (CHMe₂), 25.4, 24.3, 23.8, 23.4 (CHMe₂), 2.0 (ScCH₂SiMe₃), (ScCH₂SiMe₃, BMe not found). ¹⁹F NMR (C₇D₈) : δ -132.2 (6F; *o*-F), -159.5 (3F; *p*-F), -163.9 (6F; *m*-F). ¹¹B{¹H} NMR (C₇D₈, 210K) : δ -15.3 (br s).

Synthesis of {[ArNC(^tBu)CHC(^tBu)NAr]ScCH₂SiMe₃}{D₃CB(C₆F₅)₃}

(*d*₃-10-CH₂SiMe₃):

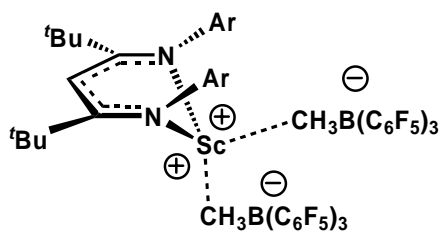


An NMR tube was charged with B(C₆F₅)₃ (0.012 g, 0.023 mmol) and 0.3 mL C₇D₈. The tube was cooled to -78 °C and *d*₃-2-Me(CH₂SiMe₃) (0.015 g, 0.023 mmol) in 0.3 mL C₇D₈ was added dropwise. The tube was slowly warmed to room temperature then placed in the

NMR probe at 210K. The ¹H NMR spectrum matched **10-Me(CH₂SiMe₃)** with the exception that no resonances were observed for the MeB(C₆F₅)₃. ²H NMR (C₇H₈, 210K) : δ (s, 1.56).

Synthesis of {[ArNC(^tBu)CHC(^tBu)NAr]Sc}⁺[MeB(C₆F₅)₃]₂⁻ (**10-MeB(C₆F₅)₃**):

Preparation 1: Toluene (30 mL) was condensed into an evacuated flask containing **2-Me** (0.150 g, 0.260 mmol) and B(C₆F₅)₃ (0.270 g, 0.520 mmol) at -78 °C. The yellow



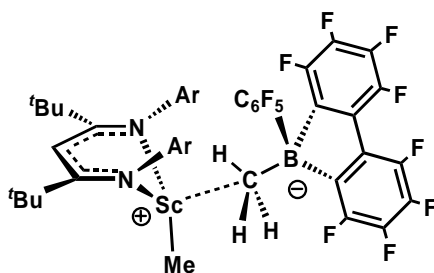
solution was warmed gradually to room temperature and then solvent removed to afford **10-MeB(C₆F₅)₃** as a fine yellow powder which was recrystallized from toluene (0.270 g, 0.170 mmol,

65%).

Preparation 2: 10-Me (0.013 g, 0.011 mmol) and B(C₆F₅)₃ (0.0060 g, 0.011 mmol) were dissolved in *d*₈-toluene (0.4 mL) in an NMR tube at -78 °C. The tube was gradually warmed to -30 °C upon which analysis by ¹H NMR spectroscopy showed only the presence of **10-MeB(C₆F₅)₃**. ¹H NMR (225K) : δ 7.02 (m, 2H; C₆H₃), 6.59 (d, 2H; C₆H₃, *J*_{H-H} = 6.9 Hz), 6.46 (d, 2H; C₆H₃, *J*_{H-H} = 6.9 Hz), 5.85 (s, 1H; CH), 2.01 (sp, 4H; CHMe₂, *J*_{H-H} = 6.9 Hz), 1.92 (br s, 3H; BMe), 1.55 (br s, 3H; BMe) 1.13 (d, 6H; CHMe₂, *J*_{H-H} = 6.9 Hz), 0.92 (d, 6H; CHMe₂, *J*_{H-H} = 6.9 Hz), 0.87 (d, 6H; CHMe₂, *J*_{H-H} = 6.9 Hz), 0.78 (d, 6H; CHMe₂, *J*_{H-H} = 6.9 Hz), 0.64 (s, 18H; NCCMe₃). ¹³C{¹H} NMR (C₆F₅ resonances not reported): δ 175.1 (NCCMe₃), 140.7 (C_{ipso}), 138.7, 137.7, 129.1, 124.9, 124.6 (C₆H₃), 84.2 (CH), 44.8 (CMe₃), 37.7 (BMe), 30.1 (CMe₃), 32.9, 28.9 (CHMe₂), 30.6 (CHMe₂), 26.2, (BMe), 25.3, 24.4, 24.0 (CHMe₂). ¹⁹F NMR: δ -132.1, -132.4 (*o*-F), -157.3, -157.6 (*p*-F), -161.6, -163.1 (*m*-F). ¹¹B{¹H} NMR: δ -14.5, -15.9. Anal. Calcd. for C₇₃H₅₉N₂B₂F₃₀Sc : C, 54.77; H, 3.71; N, 1.75. Found : C, 54.99; H, 3.66; N, 1.94.

Synthesis of {[ArNC(^tBu)CHC(^tBu)NAr]ScMe}{MeB(C₆F₅)(C₁₂F₈)} (**11-Me**):

A 25 mL vial was charged with **2-Me** (0.050 g, 0.087 mmol) and hexanes (3 mL). In a separate vial (C₆F₅)B(C₁₂F₈) (0.041g, 0.087mmol) was dissolved in hexanes (1 mL). The

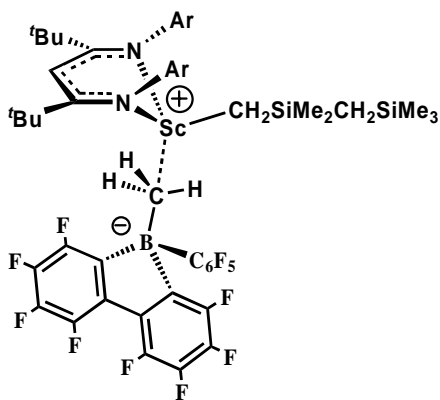


scandium solution was added dropwise to the clear yellow $(C_6F_5)B(C_{12}F_8)$ solution causing immediate formation of a pale yellow precipitate. The solution was cooled to $-35\text{ }^\circ\text{C}$ for 24 hours, upon which the

supernatant was removed and the pale yellow crystalline solid dried *in vacuo* to afford pure **11-Me** (0.082 g, 0.078 mmol, 90%). ^1H NMR for Isomer A (39%) (C_7D_8 , 215K): δ 7.15-6.61 (m, 6H; C_6H_3), 5.64 (s, 1H; CH), 3.20 (sp, 2H; $CHMe_2$, $J_{H-H} = 6.4$ Hz), 1.85 (sp, 2H; $CHMe_2$, $J_{H-H} = 6.4$ Hz), 1.21 (d, 6H; $CHMe_2$, $J_{H-H} = 6.4$ Hz), 0.95 (d, 6H; $CHMe_2$, $J_{H-H} = 6.4$ Hz), 0.81 (s, 18H; $NCCMe_3$), 0.78 (d, 6H; $CHMe_2$, $J_{H-H} = 6.4$ Hz), 0.52 (d, 6H; $CHMe_2$, $J_{H-H} = 6.4$ Hz), 0.24 (s, 3H; ScMe), (BMe not observed). ^1H NMR for Isomer B (61%) (C_7D_8 , 215K): δ 7.15-6.61 (m, 6H; C_6H_3), 5.35 (s, 1H; CH), 2.83 (sp, 2H; $CHMe_2$, $J_{H-H} = 6.4$ Hz), 2.39 (sp, 2H; $CHMe_2$, $J_{H-H} = 6.4$ Hz), 1.52 (d, 6H; $CHMe_2$, $J_{H-H} = 6.4$ Hz), 1.43 (br s, 3H, BMe), 1.34 (d, 6H; $CHMe_2$, $J_{H-H} = 6.4$ Hz), 1.21 (d, 6H; $CHMe_2$, $J_{H-H} = 6.4$ Hz), 0.89 (d, 6H; $CHMe_2$, $J_{H-H} = 6.4$ Hz), 0.67 (s, 18H; $NCCMe_3$), 0.36 (s, 3H; ScMe). Complete assignment of the $^{13}\text{C}\{^1\text{H}\}$ NMR spectrum was not possible and such data is reported by carbon type: δ 141.2, 140.4 (C_{ipso}), 139.6, 139.3, 138.9, 138.7, 129.2, 128.3, 127.3, 125.5, 124.4, 124.3 (C_6H_3). All other carbon resonances were attributable to a specific isomer. $^{13}\text{C}\{^1\text{H}\}$ NMR for Isomer A (39%) (C_7D_8 , 215K; fluorene resonances not reported): δ 173.5 ($NCCMe_3$), 87.1 (CH), 44.8 (CMe_3), 34.1 (ScMe), 31.9 ($CHMe_2$), 30.8 (CMe_3), 30.6, 27.2 ($CHMe_2$), 24.1, 23.2, 22.9 ($CHMe_2$), (BMe not observed). $^{13}\text{C}\{^1\text{H}\}$ NMR for Isomer B (61%) (C_7D_8 , 215K; CF resonances not reported): δ 174.2 ($NCCMe_3$), 87.0 (CH), 45.2 (ScMe), 44.0 (CMe_3), 32.2 ($CHMe_2$), 30.7 ($CHMe_2$), 30.5 (CMe_3), 28.6 ($CHMe_2$), 28.2 ($CHMe_2$), 26.0 (BMe), 25.4,

23.3 (CHMe₂). ¹⁹F NMR for Isomer A (39%) (C₇D₈, 245K): δ -133.4 (2F; *o*-F), -134.8, -136.6, 156.7, -158.2 (8F; C₁₂F₈), -158.8 (1F; *p*-F), -163.6 (2F; *m*-F). ¹⁹F NMR for Isomer B (61%) (C₇D₈, 245K): δ -132.0 (2F; *o*-F), -133.4, -137.7, -157.2 (2 overlapping signals) (8F; C₁₂F₈), -158.8 (1F; *p*-F), -163.3 (2F; *m*-F). ¹¹B{¹H} NMR for Isomers A & B: δ -14.9. Anal. Calcd. for C₅₅H₅₉N₂BF₁₃Sc: C, 62.86; H, 5.66; N, 2.66. Found: C, 63.31; H, 6.16; N, 2.45.

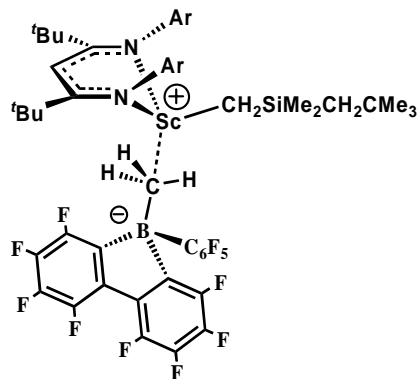
Synthesis of {[ArNC(^tBu)CHC(^tBu)NAr]ScCH₂SiMe₂CH₂SiMe₃}{MeB(C₆F₅)(C₁₂F₈)} (11-CH₂SiMe₂CH₂SiMe₃):



A 25 mL vial was charged with **2-CH₂SiMe₃** (0.050 g, 0.069 mmol) and hexanes (1 mL). In a separate vial (C₆F₅)B(C₁₂F₈) (0.033 g, 0.069 mmol) was dissolved in hexanes (1 mL). The scandium solution was added dropwise to the clear yellow (C₆F₅)B(C₁₂F₈) solution. The solution was cooled to -35 °C for 72 hours, upon which the supernatant was removed and the yellow crystalline solid was dried *in vacuo* to afford pure **11-CH₂SiMe₂CH₂SiMe₃** (0.075 g, 0.063 mmol, 91%). ¹H NMR (C₇D₈; 240K): δ 7.16-6.75 (m, 6H; C₆H₃), 5.51 (s, 1H; CH), 2.76 (sp, 2H; CHMe₂, J_{H-H} = 6.5 Hz), 2.55 (sp, 2H; CHMe₂, J_{H-H} = 6.5 Hz), 1.31 (d, 6H; CHMe₂, J_{H-H} = 6.5 Hz), 1.24 (br s, 3H, BMe), 1.15 (d, 6H; CHMe₂, J_{H-H} = 6.5 Hz), 1.10 (d, 6H; CHMe₂, J_{H-H} = 6.5 Hz), 0.96 (s, 2H; ScCH₂SiMe₂CH₂SiMe₃), 0.95 (d, 6H; CHMe₂, J_{H-H} = 6.5 Hz), 0.79 (s, 18H; NCCMe₃), -0.12 (s, 9H; ScCH₂SiMe₂CH₂SiMe₃), -0.33 (s, 6H; CH₂SiMe₂CH₂SiMe₃), -0.82 (s, 2H; ScCH₂SiMe₂CH₂SiMe₃). ¹³C{¹H}

NMR (C_7D_8 , 240K; CF resonances not reported): δ 175.4 (NCCMe₃), 141.8 (C_{ipso}), 140.1, 139.8, 129.1, 124.8, 124.5 (C₆H₃), 87.4 (CH), 72.4 (ScCH₂SiMe₂CH₂SiMe₃), 44.5 (CMe₃), 32.2 (CHMe₂), 30.9 (CMe₃), 30.2 (CHMe₂), 28.1, 26.8, 25.2, 23.9 (CHMe₂), 5.7 (ScCH₂SiMe₂CH₂SiMe₃), 3.0 (ScCH₂SiMe₂CH₂SiMe₃), 1.3 (ScCH₂SiMe₂CH₂SiMe₃). (BMe not found). ¹⁹F NMR (C_7D_8 , 230K) : δ -131.6 (2F; *o*-F), -133.2, -136.1, -156.8, -157.1 (8F; C₁₂F₈) -158.1 (1F; *p*-F), -163.2 (2F; *m*-F). ¹¹B{¹H} NMR (C_7D_8 , 240K) : δ -12.1 (br s). Anal. Calcd. for C₆₁H₇₅N₂Si₂BF₁₃Sc : C, 61.30; H, 6.32; N, 2.34. Found : C, 61.49; H, 6.75; N, 2.31.

**Synthesis of {[ArNC(^tBu)CHC(^tBu)NAr]ScCH₂SiMe₂CH₂CMe₃}[MeB(C₆F₅)(C₁₂F₈)]
(**11-CH₂SiMe₂CH₂CMe₃**):**



A 25 mL vial was charged with **2-CH₂SiMe₃(CH₂CMe₃)** (0.038 g, 0.054 mmol) and hexanes (1.5 mL). In a separate vial (C₆F₅)B(C₁₂F₈) (0.026 g, 0.054 mmol) was dissolved in hexanes (1 mL). The scandium solution was added dropwise to the clear yellow (C₆F₅)B(C₁₂F₈) solution. The

solution was cooled to -35 °C for 96 hours, upon which the supernatant was removed and the yellow crystalline solid was dried *in vacuo* to afford pure **11-CH₂SiMe₂CH₂CMe₃** (0.049 g, 0.042 mmol, 78%). ¹H NMR (C_7D_8 ; 240K): δ 6.95 (t, 2H; C₆H₃, J_{H-H} = 8.2 Hz), 6.80 (d, 2H; C₆H₃, J_{H-H} = 8.2 Hz), 6.74 (d, 2H; C₆H₃, J_{H-H} = 8.2 Hz), 5.50 (s, 1H; CH), 2.75 (sp, 2H; CHMe₂, J_{H-H} = 6.4 Hz), 2.56 (sp, 2H; CHMe₂, J_{H-H} = 6.4 Hz), 1.30 (d, 6H; CHMe₂, J_{H-H} = 6.4 Hz), 1.22 (br s, 3H, BMe), 1.15 (d, 6H; CHMe₂, J_{H-H} = 6.4 Hz), 1.08

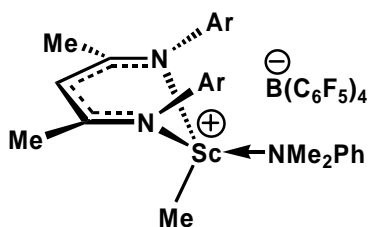
assayed by ^1H and ^{19}F NMR spectroscopy. During this time the solution gradually changed from bright yellow to dark orange and methane was produced. Two different isomers were observed and the data is reported by H type. ^1H NMR (C_6D_6): δ 7.30-6.79 (m; C_6H_3), 5.94 (s; CH), 5.67 (s; CH), 3.13 (sp; CHMe_2 , $J_{\text{H-H}} = 6.9$ Hz), 2.97 (m; CHMe_2), 2.82 (m; CHMe_2), 2.72 (m; CHMe_2), 2.58-2.52 (ov m; CHMe_2), 2.32 (sp; CHMe_2 , $J_{\text{H-H}} = 6.9$ Hz), 1.38 (br s; BMe), 1.28-1.19 (ov m; CHMe_2), 1.17 (s; NCCMe_3), 1.00 (s; NCCMe_3), 0.98-0.89 (ov m; CHMe_2), 0.69 (d; ScCH_2), 0.48 (d; ScCH_2). Complete assignment of the $^{13}\text{C}\{^1\text{H}\}$ NMR spectrum was not possible and such data is reported by carbon type: δ 174.4, 171.9 (NCCMe_3), 145.4, 145.1 (C_{ipso}), 144.5, 143.9, 132.1, 130.1, 129.4, 126.0, 125.6, 124.2 (C_6H_3), 101.5, 101.3 (CH), 42.1, 41.8 (CMe_3), 31.7, 31.2, 30.8, 30.4 (CMe_3), 28.3, 28.1, 28.0, 27.5, 27.2 (CHMe_2), 25.6, 24.7 (ScCH_2), 24.3, 24.3 (CHMe_2), 23.9 (BMe), 23.7, 23.3, 22.5, 22.4 (CHMe_2), 21.9 (BMe), 21.0 (CHMe_2). ^{19}F NMR: δ -131.4, -131.9 (*o-F*), -160.9 (*p-F*), -165.1 (*m-F*). $^{11}\text{B}\{^1\text{H}\}$ NMR: δ -16.0. Anal. Calcd. for $\text{C}_{54}\text{H}_{55}\text{N}_2\text{BF}_{15}\text{Sc}$: C, 60.46; H, 5.17; N, 2.61. Found : C, 59.74; H, 5.55; N, 2.52.

6.4 Experimental Procedures Pertaining to Chapter 4

6.4.1 Synthetic Procedures

Synthesis of $\{[\text{ArNC}(\text{Me})\text{CHC}(\text{Me})\text{NAr}]\text{Sc}(\text{Me})(\text{NMe}_2\text{Ph})\}^+[\text{B}(\text{C}_6\text{F}_5)_4]^-$ (**13-Me**):

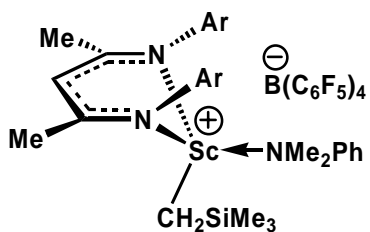
An NMR tube was charged with **1-Me** (0.010 g, 0.020 mmol), $[\text{HNMe}_2\text{Ph}][\text{B}(\text{C}_6\text{F}_5)_4]$ (0.016 g, 0.020 mmol) and 0.5 mL $\text{C}_6\text{D}_5\text{Br}$. Upon mixing the reaction mixture



immediately turned deep yellow in colour. ^1H NMR ($\text{C}_6\text{D}_5\text{Br}$): δ 7.24-7.08 (ov m, 6H; C_6H_3), 6.27 (t, 2H; *m*- NMe_2Ph , $J_{\text{H-H}} = 7.5$ Hz), 6.11 (d, 2H; *p*- NMe_2Ph , $J_{\text{H-H}} = 8.4$ Hz), 5.99 (t, 1H; *o*- NMe_2Ph , $J_{\text{H-H}} = 7.5$ Hz), 5.22 (s, 1H; CH), 2.64 (sp, 2H; CHMe_2 , $J_{\text{H-H}} = 6.5$ Hz), 2.45 (s, 6H; NMe_2Ph), 2.41 (sp, 2H; CHMe_2 , $J_{\text{H-H}} = 6.5$ Hz), 1.58 (s, 6H; NCMe), 1.21 (d, 6H; CHMe_2 , $J_{\text{H-H}} = 6.5$ Hz), 1.15 (d, 6H; CHMe_2 , $J_{\text{H-H}} = 6.5$ Hz), 1.07 (d, 6H; CHMe_2 , $J_{\text{H-H}} = 6.5$ Hz), 0.86 (d, 6H; CHMe_2 , $J_{\text{H-H}} = 6.5$ Hz), -0.31 (s, 3H; ScMe). $^{13}\text{C}\{^1\text{H}\}$ NMR ($\text{C}_6\text{D}_5\text{Br}$, 250K, C_6F_5 resonances not reported): δ 169.6 (NCMe), 151.9 (NMe_2Ph , C_{ipso}), 142.5 (C_6H_3 , C_{ipso}), 140.7, 140.2 (C_6H_3), 132.5 (NMe_2Ph), 127.9, 125.0, 124.0 (C_6H_3), 112.0, 111.8 (NMe_2Ph), 97.8 (CH), 38.8 (NMe_2Ph), 38.3 (ScMe), 28.8, 27.4 (CHMe_2), 25.2 (CHMe_2), 24.1 (NCMe), 24.0, 23.9, 22.5 (CHMe_2). ^{19}F NMR ($\text{C}_6\text{D}_5\text{Br}$): δ -132.9 (*o*-F), -163.1 (*p*-F), -166.9 (*m*-F). $^{11}\text{B}\{^1\text{H}\}$ NMR ($\text{C}_6\text{D}_5\text{Br}$): δ -17.0.

Synthesis of $\{[\text{ArNC}(\text{Me})\text{CHC}(\text{Me})\text{NAr}]\text{Sc}(\text{CH}_2\text{SiMe}_3)(\text{NMe}_2\text{Ph})\}^+[\text{B}(\text{C}_6\text{F}_5)_4]^-$

(13- CH_2SiMe_3):

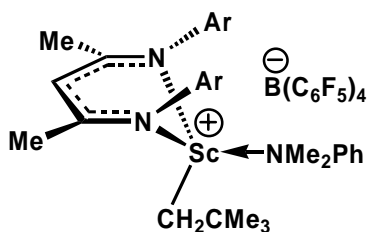


An NMR tube was charged with **1- CH_2SiMe_3** (0.012 g, 0.019 mmol), $[\text{HNMe}_2\text{Ph}][\text{B}(\text{C}_6\text{F}_5)_4]$ (0.015 g, 0.019 mmol) and 0.5 mL $\text{C}_6\text{D}_5\text{Br}$. ^1H NMR ($\text{C}_6\text{D}_5\text{Br}$): δ 7.26-7.09 (ov m, 6H; C_6H_3), 6.31 (t, 2H; *m*- NMe_2Ph , $J_{\text{H-H}} = 7.4$ Hz), 6.17 (d, 2H; *p*- NMe_2Ph , $J_{\text{H-H}} = 8.4$ Hz), 6.07 (t, 1H; *o*- NMe_2Ph , $J_{\text{H-H}} = 7.4$ Hz), 5.33 (s, 1H; CH), 2.79 (sp, 2H; CHMe_2 , $J_{\text{H-H}} = 6.6$ Hz), 2.43 (s, 6H; NMe_2Ph), 2.35 (sp, 2H; CHMe_2 , $J_{\text{H-H}} = 6.6$ Hz), 1.67 (s, 6H; NCMe), 1.20 (d, 6H; CHMe_2 , $J_{\text{H-H}} = 6.6$ Hz),

1.13 (d, 6H; CHMe_2 , $J_{\text{H-H}} = 6.6$ Hz), 1.08 (d, 6H; CHMe_2 , $J_{\text{H-H}} = 6.6$ Hz), 0.77 (d, 6H; CHMe_2 , $J_{\text{H-H}} = 6.5$ Hz), -0.06 (s, 9H; $\text{ScCH}_2\text{SiMe}_3$), -0.53 (s, 2H; $\text{ScCH}_2\text{SiMe}_3$). $^{13}\text{C}\{^1\text{H}\}$ NMR ($\text{C}_6\text{D}_5\text{Br}$, C_6F_5 resonances not reported): δ 169.6 (NCMe), 151.3 (NMe_2Ph , C_{ipso}), 142.3 (C_6H_3 , C_{ipso}), 141.7, 140.4 (C_6H_3), 132.9 (NMe_2Ph), 128.2, 125.3, 124.6 (C_6H_3), 113.8, 113.3 (NMe_2Ph), 97.0 (CH), 39.4 (NMe_2Ph), 28.6, 27.1 (CHMe_2), 25.1 (CHMe_2), 25.0 (NCMe), 24.9, 24.4, 23.1 (CHMe_2), 2.8 ($\text{ScCH}_2\text{SiMe}_3$); $\text{ScCH}_2\text{SiMe}_3$ not observed. ^{19}F NMR ($\text{C}_6\text{D}_5\text{Br}$): δ -132.9 (*o*-F), -163.1 (*p*-F), -166.9 (*m*-F). $^{11}\text{B}\{^1\text{H}\}$ NMR ($\text{C}_6\text{D}_5\text{Br}$): δ -17.0.

Synthesis of $\{[\text{ArNC}(\text{Me})\text{CHC}(\text{Me})\text{NAr}]\text{Sc}(\text{CH}_2\text{CMe}_3)(\text{NMe}_2\text{Ph})\}^+[\text{B}(\text{C}_6\text{F}_5)_4]^-$

(13- CH_2CMe_3):

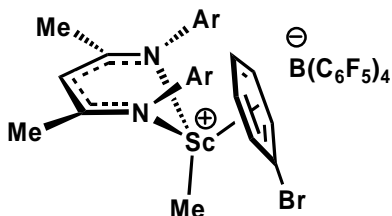


An NMR tube was charged with **1- CH_2CMe_3** (0.012 g, 0.017 mmol), $[\text{HNMe}_2\text{Ph}][\text{B}(\text{C}_6\text{F}_5)_4]$ (0.014 g, 0.017 mmol) and 0.5 mL $\text{C}_6\text{D}_5\text{Br}$. Upon mixing the reaction mixture immediately changed turned deep yellow. ^1H

NMR ($\text{C}_6\text{D}_5\text{Br}$): δ 7.25-7.08 (ov m, 6H; C_6H_3), 6.35 (t, 2H; *m*- NMe_2Ph , $J_{\text{H-H}} = 7.2$ Hz), 6.27 (d, 2H; *p*- NMe_2Ph , $J_{\text{H-H}} = 8.1$ Hz), 6.11 (t, 1H; *o*- NMe_2Ph , $J_{\text{H-H}} = 7.2$ Hz), 5.34 (s, 1H; CH), 2.91 (sp, 2H; CHMe_2 , $J_{\text{H-H}} = 6.5$ Hz), 2.48 (s, 6H; NMe_2Ph), 2.27 (sp, 2H; CHMe_2 , $J_{\text{H-H}} = 6.5$ Hz), 1.65 (s, 6H; NCMe), 1.16 (d, 12H; CHMe_2 , $J_{\text{H-H}} = 6.5$ Hz), 1.04 (d, 6H; CHMe_2 , $J_{\text{H-H}} = 6.5$ Hz), 0.82 (d, 6H; CHMe_2 , $J_{\text{H-H}} = 6.5$ Hz), 0.80 (s, 9H; $\text{ScCH}_2\text{CMe}_3$), 0.02 (s, 2H; $\text{ScCH}_2\text{CMe}_3$). $^{13}\text{C}\{^1\text{H}\}$ NMR ($\text{C}_6\text{D}_5\text{Br}$, C_6F_5 resonances not reported): δ 169.4 (NCMe), 151.0 (NMe_2Ph , C_{ipso}), 142.6 (C_6H_3 , C_{ipso}), 141.8, 140.5 (C_6H_3), 132.8 (NMe_2Ph), 128.1, 125.1, 124.6 (C_6H_3), 113.7, 112.8 (NMe_2Ph), 95.4 (CH),

39.5 (NMe_2Ph), 36.3 ($\text{ScCH}_2\text{CMe}_3$), 34.0 ($\text{ScCH}_2\text{CMe}_3$), 28.3, 27.5 (CHMe_2), 27.4 (CHMe_2), 25.3 (NCMe), 24.8, 24.3, 23.4 (CHMe_2); $\text{ScCH}_2\text{CMe}_3$ not observed. ^{19}F NMR ($\text{C}_6\text{D}_5\text{Br}$): δ -132.9 (*o*-F), -163.2 (*p*-F), -167.0 (*m*-F). $^{11}\text{B}\{^1\text{H}\}$ NMR ($\text{C}_6\text{D}_5\text{Br}$): δ -16.9.

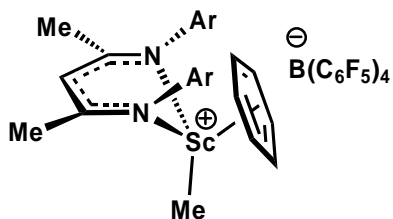
Synthesis of $\{[\text{ArNC}(\text{Me})\text{CHC}(\text{Me})\text{NAr}]\text{ScMe}\}^+[\text{B}(\text{C}_6\text{F}_5)_4]^-$ (14-C₆H₅Br**):**



A 25mL RB flask was charged with **1-Me** (0.035 g, 0.072 mmol) and $[\text{CPh}_3][\text{B}(\text{C}_6\text{F}_5)_4]$ (0.066 g, 0.072 mmol) to which bromobenzene (3 mL) was added. The solution was stirred for 5 minutes and then layered with hexanes (5 mL). The reaction mixture was cooled to -35 °C for 24 hours and solvent decanted. The yellow crystals washed with toluene (2 x 2 mL) and dried under vacuum to yield 0.067 g (0.052 mmol, 72%) of **14-C₆H₅Br** as a fine yellow powder. ^1H NMR ($\text{C}_6\text{D}_5\text{Br}$): δ 7.24-7.02 (ov m, 6H; C_6H_3), 5.30 (s, 1H; CH), 2.35 (sp, 4H; CHMe_2 , $J_{\text{H-H}} = 6.6$ Hz), 1.59 (s, 6H; NCMe), 1.14 (d, 12H; CHMe_2 , $J_{\text{H-H}} = 6.6$ Hz), 0.88 (d, 12H; CHMe_2 , $J_{\text{H-H}} = 6.6$ Hz), -0.10 (s, 3H; ScMe). $^{13}\text{C}\{^1\text{H}\}$ NMR ($\text{C}_6\text{D}_5\text{Br}$, 270K, C_6F_5 resonances not reported): δ 170.3 (NCMe), 141.1 (C_{ipso}), 139.8, 128.5, 127.7 (C_6H_3), 97.6 (CH), 45.3 (ScMe), 28.4 (CHMe_2), 24.0 (NCMe), 24.0, 23.7 (CHMe_2). ^{19}F NMR ($\text{C}_6\text{D}_5\text{Br}$): δ -132.9 (*o*-F), -163.0 (*p*-F), -166.9 (*m*-F). $^{11}\text{B}\{^1\text{H}\}$ NMR ($\text{C}_6\text{D}_5\text{Br}$): δ -17.0. Anal. Calcd. for $\text{C}_{60}\text{H}_{49}\text{N}_2\text{BF}_{20}\text{BrSc}$: C, 54.86; H, 3.76; N, 2.13. Found: C, 54.24; H, 3.80; N, 1.98.

Synthesis of $\{[\text{ArNC}(\text{Me})\text{CHC}(\text{Me})\text{NAr}]\text{Sc}(\text{Me})(\text{C}_6\text{H}_6)\}^+[\text{B}(\text{C}_6\text{F}_5)_4]^-$ (14-C₆H₆**):**

A 25mL RB flask was charged with **1-Me** (0.035 g, 0.072 mmol) and $[\text{CPh}_3][\text{B}(\text{C}_6\text{F}_5)_4]$

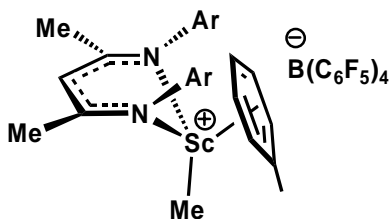


(0.066 g, 0.072 mmol) to which bromobenzene (3 mL) was added. The solution was stirred for 5 minutes during which period benzene (2 mL) was added dropwise. The reaction mixture was layered with

hexanes (5 mL), cooled to $-35\text{ }^{\circ}\text{C}$ for 24 hours and solvent decanted. The yellow crystals were washed with toluene (2 x 2 mL) and dried under vacuum to give 0.054 g (0.044 mmol, 62%) of **14-C₆H₆** as a fine yellow powder. ^1H NMR ($\text{C}_6\text{D}_5\text{Br}$, 270K): δ 7.22-7.10 (ov m, 6H; C_6H_3), 6.85 (s, 6H; C_6H_6), 5.21 (s, 1H; CH), 2.46 (sp, 2H; CHMe_2 , $J_{\text{H-H}} = 6.8$ Hz), 2.18 (sp, 2H; CHMe_2 , $J_{\text{H-H}} = 6.8$ Hz), 1.55 (s, 6H; NCMe), 1.19 (d, 6H; CHMe_2 , $J_{\text{H-H}} = 6.8$ Hz), 1.11 (d, 6H; CHMe_2 , $J_{\text{H-H}} = 6.8$ Hz), 1.01 (d, 6H; CHMe_2 , $J_{\text{H-H}} = 6.8$ Hz), 0.73 (d, 6H; CHMe_2 , $J_{\text{H-H}} = 6.8$ Hz), -0.28 (s, 3H; ScMe). $^{13}\text{C}\{^1\text{H}\}$ NMR ($\text{C}_6\text{D}_5\text{Br}$, 270K, C_6F_5 resonances not reported): δ 169.7 (NCMe), 142.4 (C_{ipso}), 140.7, 139.8 (C_6H_3), 132.2 (C_6H_6), 129.9, 127.9, 124.7 (C_6H_3), 96.9 (CH), 41.5 (ScMe) 28.4, 27.5 (CHMe_2), 24.3, 23.9 (CHMe_2), 23.8 (NCMe), 23.7, 22.4 (CHMe_2). ^{19}F NMR ($\text{C}_6\text{D}_5\text{Br}$, 250K): δ -131.1 (*o-F*), -161.0 (*p-F*), -164.9 (*m-F*). $^{11}\text{B}\{^1\text{H}\}$ NMR ($\text{C}_6\text{D}_5\text{Br}$, 250K): δ -17.0. Anal. Calcd. for $\text{C}_{60}\text{H}_{50}\text{N}_2\text{BF}_{20}\text{Sc}\cdot\text{C}_6\text{H}_5\text{Br}$: C, 56.96; H, 3.98; N, 2.01. Found: C, 54.26; H, 3.71; N, 1.86.

Synthesis of $\{[\text{ArNC}(\text{Me})\text{CHC}(\text{Me})\text{NAr}]\text{Sc}(\text{Me})(\text{C}_7\text{H}_8)\}^+[\text{B}(\text{C}_6\text{F}_5)_4]^-$ (**14-C₇H₈**):

A 25mL RB flask was charged with **1-Me** (0.035 g, 0.072 mmol) and $[\text{CPh}_3][\text{B}(\text{C}_6\text{F}_5)_4]$ (0.066 g, 0.072 mmol) to which bromobenzene (3 mL) was added. The solution was

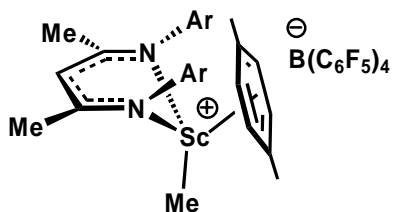


stirred for 5 minutes, toluene (2 mL) was added followed by an additional 5 minutes of stirring. The reaction mixture was layered with hexanes (5 mL), cooled to $-35\text{ }^{\circ}\text{C}$ for 24 hours and solvent decanted.

The yellow solid was washed with toluene (2 x 2 mL) and dried under vacuum to give 0.087 g (0.071 mmol, 98%) of **14-C₇H₈** as a bright yellow powder. ^1H NMR ($\text{C}_6\text{D}_5\text{Br}$, 260K): δ 7.22-7.10 (ov m, 6H; C_6H_3), 6.81 (d, 2H; *o*- C_7H_8 , $J_{\text{H-H}} = 7.5$ Hz), 6.66 (t, 1H; *p*- C_7H_8 , $J_{\text{H-H}} = 7.5$ Hz), 6.39 (t, 2H; *m*- C_7H_8 , $J_{\text{H-H}} = 7.5$ Hz), 5.18 (s, 1H; CH), 2.44 (sp, 2H; CHMe_2 , $J_{\text{H-H}} = 6.7$ Hz), 2.19 (sp, 2H; CHMe_2 , $J_{\text{H-H}} = 6.7$ Hz), 1.86 (s, 3H; *MePh*), 1.50 (s, 6H; NCMe), 1.16 (d, 6H; CHMe_2 , $J_{\text{H-H}} = 6.7$ Hz), 1.06 (d, 6H; CHMe_2 , $J_{\text{H-H}} = 6.7$ Hz), 1.01 (d, 6H; CHMe_2 , $J_{\text{H-H}} = 6.7$ Hz), 0.72 (d, 6H; CHMe_2 , $J_{\text{H-H}} = 6.7$ Hz), -0.29 (s, 3H; ScMe). $^{13}\text{C}\{^1\text{H}\}$ NMR ($\text{C}_6\text{D}_5\text{Br}$, 270K, C_6F_5 resonances not reported): δ 169.8 (NCMe), 142.3 (C_{ipso} of C_6H_3), 140.7, 139.9 (C_6H_3), 137.3 (C_{ipso} of *MePh*), 133.2, 132.7 (*MePh*), 128.3, 127.7 (C_6H_3), 126.0 (*MePh*), 125.5 (C_6H_3), 97.6 (CH), 42.7 (ScMe), 28.8, 27.8 (CHMe_2), 24.7 (CHMe_2), 24.1 (NCMe), 24.1, 24.0, 22.6 (CHMe_2), 21.3 (*PhMe*). ^{19}F NMR ($\text{C}_6\text{D}_5\text{Br}$, 250K) : δ -131.2 (*o-F*), -161.0 (*p-F*), -164.9 (*m-F*). ^{11}B NMR ($\text{C}_6\text{D}_5\text{Br}$, 250K) : δ -17.0. Anal. Calcd. for $\text{C}_{61}\text{H}_{52}\text{N}_2\text{BF}_{20}\text{Sc}\cdot\text{C}_6\text{H}_5\text{Br}$: C, 57.24; H, 4.09; N, 1.99. Found: C, 56.94; H, 3.87; N, 2.39.

Synthesis of $\{[\text{ArNC}(\text{Me})\text{CHC}(\text{Me})\text{NAr}]\text{Sc}(\text{Me})(\text{C}_8\text{H}_{10})\}^+[\text{B}(\text{C}_6\text{F}_5)_4]^-$ (**14-C₈H₁₀**):

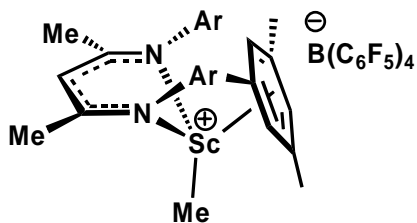
A 25mL RB flask was charged with **1-Me** (0.023 g, 0.047 mmol) and $[\text{CPh}_3][\text{B}(\text{C}_6\text{F}_5)_4]$ (0.043 g, 0.047 mmol) to which bromobenzene (3 mL) was added. The solution was



stirred for 5 minutes, *p*-xylene (2 mL) was added followed by an additional 5 minutes of stirring. The reaction mixture was layered with hexanes (5 mL), cooled to $-35\text{ }^{\circ}\text{C}$ for 36 hours and solvent decanted.

The oily yellow solid was washed with toluene (2 x 2 mL) and dried under vacuum to give 0.030 g (51%) of **14-C₈H₁₀** as a yellow powder. ^1H NMR ($\text{C}_6\text{D}_5\text{Br}$, 250K): δ 7.22-6.97 (ov m, 6H; C_6H_3), 6.65 (s, 4H; 1,4-Me- C_6H_4), 5.24 (s, 1H; CH), 2.35 (sp, 2H; CHMe_2 , $J_{\text{H-H}} = 6.6$ Hz), 2.12 (sp, 2H; CHMe_2 , $J_{\text{H-H}} = 6.6$ Hz), 1.58 (s, 6H; 1,4-Me- C_6H_4), 1.48 (s, 6H; NCMe), 1.14 (ov d, 12H; CHMe_2 , $J_{\text{H-H}} = 6.6$ Hz), 0.97 (d, 6H; CHMe_2 , $J_{\text{H-H}} = 6.6$ Hz), 0.70 (d, 6H; CHMe_2 , $J_{\text{H-H}} = 6.6$ Hz), -0.30 (s, 3H; ScMe). $^{13}\text{C}\{^1\text{H}\}$ NMR ($\text{C}_6\text{D}_5\text{Br}$, 250K, C_6F_5 resonances not reported): δ 169.7 (NCMe), 143.4 (C_{ipso} of C_6H_3), 141.6, 140.1 (C_6H_3), 132.9 (C_{ipso} of 1,4-Me- C_6H_3), 129.0 (1,4-Me- C_6H_3), 128.7, 127.9, 127.8 (C_6H_3), 97.6 (CH), 42.3 (ScMe), 30.4, 28.7 (CHMe_2), 24.6 (NCMe), 24.3, 24.2, 24.1, 22.8 (CHMe_2), 20.4 (1,4-Me- C_6H_3). ^{19}F NMR ($\text{C}_6\text{D}_5\text{Br}$, 250K) : δ -131.2 (*o*-F), -161.0 (*p*-F), -164.9 (*m*-F). ^{11}B NMR ($\text{C}_6\text{D}_5\text{Br}$, 250K) : δ -16.7. Anal. Calcd. for $\text{C}_6\text{H}_5\text{N}_2\text{BF}_2\text{Sc}\cdot\text{C}_6\text{H}_5\text{Br}$: C, 57.52; H, 4.19; N, 1.97. Found: C, 54.70; 3.81; N, 1.58.

Synthesis of $\{[\text{ArNC}(\text{Me})\text{CHC}(\text{Me})\text{NAr}]\text{Sc}(\text{Me})(\text{C}_9\text{H}_{12})\}^+[\text{B}(\text{C}_6\text{F}_5)_4]^-$ (**14-C₉H₁₂**):

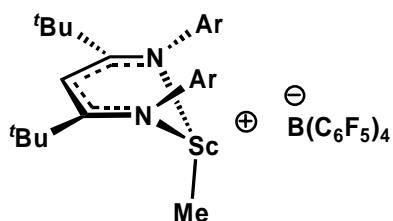


A 25mL RB flask was charged with **1-Me** (0.045 g, 0.091 mmol) and $[\text{CPh}_3][\text{B}(\text{C}_6\text{F}_5)_4]$ (0.084 g, 0.091 mmol) to which bromobenzene (5 mL) was added.

The solution was stirred for 5 minutes, mesitylene (1 mL) was added followed by an additional 5 minutes of stirring. The reaction mixture was

layered with hexanes (5 mL), cooled to $-35\text{ }^{\circ}\text{C}$ for 18 hours and solvent decanted. The large yellow crystals were washed with toluene (3 x 2 mL) and dried under vacuum to give 0.110 g (0.088 mmol) **14-C₉H₁₂** as a yellow powder in 97% yield. ^1H NMR ($\text{C}_6\text{D}_5\text{Br}$, 250K): δ 7.26-6.88 (ov m, 6H; C_6H_3), 6.59 (s, 3H; 1,3,5-Me- C_6H_3), 5.25 (s, 1H; CH), 2.37 (sp, 2H; CHMe_2 , $J_{\text{H-H}} = 6.6$ Hz), 2.09 (sp, 2H; CHMe_2 , $J_{\text{H-H}} = 6.6$ Hz), 1.43 (s, 6H; NCMe), 1.36 (s, 9H; 1,3,5-Me- C_6H_3), 1.17 (d, 6H; CHMe_2 , $J_{\text{H-H}} = 6.6$ Hz), 1.08 (d, 6H; CHMe_2 , $J_{\text{H-H}} = 6.6$ Hz), 0.95 (d, 6H; CHMe_2 , $J_{\text{H-H}} = 6.6$ Hz), 0.74 (d, 6H; CHMe_2 , $J_{\text{H-H}} = 6.6$ Hz), -0.14 (s, 3H; ScMe). $^{13}\text{C}\{^1\text{H}\}$ NMR ($\text{C}_6\text{D}_5\text{Br}$, 250K, C_6F_5 resonances not reported): δ 170.4 (NCMe), 141.7 (C_{ipso} of C_6H_3), 141.2, 140.8 (C_6H_3), 137.2 (C_{ipso} of 1,3,5-Me- C_6H_3), 130.0 (1,3,5-Me- C_6H_3), 127.0, 126.8, 124.9 (C_6H_3), 98.8 (CH), 43.5 (ScMe), 29.1, 28.3 (CHMe_2), 24.8 (NCMe), 24.6, 24.1, 23.5, 23.1 (CHMe_2), 21.4 (1,3,5-Me- C_6H_3). ^{19}F NMR ($\text{C}_6\text{D}_5\text{Br}$, 250K) : δ -131.2 (*o-F*), -161.1 (*p-F*), -165.0. ^{11}B NMR ($\text{C}_6\text{D}_5\text{Br}$, 250K) : δ -16.6. Anal. Calcd. for $\text{C}_{63}\text{H}_{56}\text{N}_2\text{BF}_{20}\text{Sc}$: C, 59.26; H, 4.42; N, 2.19. Found: C, 58.75; H, 4.34; N, 2.21.

Synthesis of $\{[\text{ArNC}(\text{tBu})\text{CHC}(\text{tBu})\text{NAr}]\text{ScMe}\}^+[\text{B}(\text{C}_6\text{F}_5)_4]^-$ (**15**):

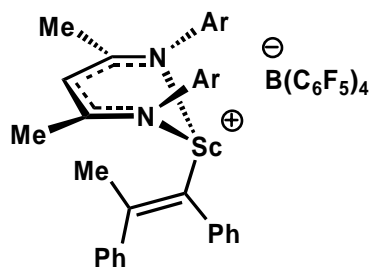


An NMR tube was charged with **1-Me** (0.010 g, 0.017 mmol) and $[\text{Ph}_3\text{C}]^+[\text{B}(\text{C}_6\text{F}_5)_4]^-$ (0.016 g, 0.017 mmol). The tube was cooled to $-30\text{ }^{\circ}\text{C}$, 0.5 mL of cold $\text{C}_6\text{D}_5\text{Br}$ ($-30\text{ }^{\circ}\text{C}$) was added and the sample was slowly allowed

to warm to 285K. ^1H NMR (285K, $\text{C}_6\text{D}_5\text{Br}$): δ 7.11-6.97 (m, 6H; C_6H_3), 5.95 (s, 1H; CH), 2.46 (sp, 4H; CHMe_2 , $J_{\text{H-H}} = 6.8$ Hz), 1.12 (d, 12H; CHMe_2 , $J_{\text{H-H}} = 6.8$ Hz), 1.02 (s, 18H; NCCMe_3), 0.82 (d, 12H; CHMe_2 , $J_{\text{H-H}} = 6.8$ Hz), -0.12 (s, 3H; ScMe). $^{13}\text{C}\{^1\text{H}\}$

NMR (C_6D_5Br , C_6F_5 resonances not reported): δ 174.5 (NCCMe₃), 140.0 (C_{ipso}), 138.8, 128.3, 124.8 (C₆H₃), 91.8 (CH), 44.5 (CMe₃), 41.1 (ScMe) 30.9 (CMe₃), 29.7 (CHMe₂), 25.7, 22.9 (CHMe₂). ¹⁹F NMR (C_6D_5Br): δ -133.2 (*o*-F), -162.4 (*p*-F), -166.3 (*m*-F). ¹¹B{¹H} NMR (C_6D_5Br): δ -17.0.

Synthesis of [{ArNC(Me)CHC(Me)NAr}Sc(PhC=CMePh)][B(C₆F₅)₄] (16**):**

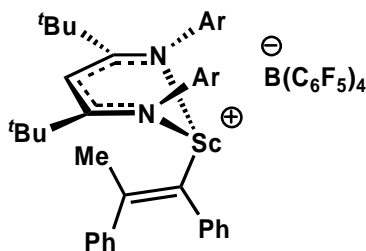


Bromobenzene (3 mL) was condensed into an evacuated flask containing **14-C₉H₁₂** (0.118 g, 0.0900 mmol) and diphenylacetylene (0.0160 g, 0.0900 mmol) at -35 °C. The yellow solution was gradually warmed to room

temperature and allowed to stir for 2 days. Removal of solvent under vacuum gave a yellow/orange oil. Hexanes (5 mL) was added and the reaction mixture sonicated (5 minutes), filtered, and solvent removed to afford 0.081 g (0.055 mmol, 61%) of **16** as a fine yellow solid. ¹H NMR (C_6D_5Br): δ 7.56 (d, 2H; Ph, $J_{H-H} = 7.4$ Hz), 7.49-6.96 (ov m, 8H; Ph), 6.80 (t, 1H; Ph, $J_{H-H} = 7.4$ Hz), 6.73 (t, 1H; Ph, $J_{H-H} = 7.7$ Hz), 6.38 (d, 2H; Ph, $J_{H-H} = 7.7$ Hz), 6.22 (t, 2H; Ph, $J_{H-H} = 7.7$ Hz), 5.25 (s, 1H; CH), 2.46 (sp, 2H; CHMe₂, $J_{H-H} = 6.7$ Hz), 2.08 (sp, 2H; CHMe₂, $J_{H-H} = 6.7$ Hz), 1.52 (s, 3H; ScC=CMe), 1.45 (s, 6H; NCMe), 1.33 (d, 6H; CHMe₂, $J_{H-H} = 6.7$ Hz), 1.09 (d, 6H; CHMe₂, $J_{H-H} = 6.7$ Hz), 0.94 (d, 6H; CHMe₂, $J_{H-H} = 6.7$ Hz), 0.73 (d, 6H; CHMe₂, $J_{H-H} = 6.7$ Hz). ¹³C{¹H} NMR (C_6D_5Br): δ 169.4 (NCMe), 160.6 (ScC=C), 159.6 (ScC=C), 143.5, 142.8, 142.3, 141.5, 139.9, 136.9, 133.2, 131.3, 129.8, 126.9, 126.6, 125.0, 124.8, 123.3 (C₆H₃, Ph), 96.8 (CH), 28.6, 28.4 (CHMe₂), 25.3 (CHMe₂), 25.1 (NCMe), 24.3, 24.2, 23.4 (CHMe₂), 23.0 (ScC=CMe). ¹⁹F NMR (C_6D_5Br): δ -132.9 (*o*-F), -163.1 (*p*-F), -167.0 (*m*-F). ¹¹B{¹H}

NMR (C_6D_5Br): δ -16.9. Anal. Calcd. for $ScN_2BF_{20}C_{68}H_{54}$: C, 61.18; H, 4.08; N, 2.10. Found : C, 60.82; H, 4.58; N, 1.85.

Synthesis of $[\{ArNC(tBu)CHC(tBu)NAr\}Sc(PhC=CMePh)][B(C_6F_5)_4]$ (17):



Cold ($-35\text{ }^\circ\text{C}$) C_6D_5Br (0.4 mL) was added to an NMR tube charged with **2-Me** (0.015 g, 0.026 mmol) and $[CPh_3][B(C_6F_5)_4]$ (0.024 g, 0.026 mmol). Upon mixing of reagents a cold ($-35\text{ }^\circ\text{C}$) C_6D_5Br (0.3 mL) solution of diphenylacetylene (0.005 g, 0.028 mmol) was added dropwise. The tube was shaken and inserted into the NMR probe at $-35\text{ }^\circ\text{C}$. 1H NMR (C_6D_5Br , 280K): δ 7.12-6.83 (ov m, 16H; Ph, C_6H_3), 5.69 (s, 1H; CH), 2.31 (br, 4H; $CHMe_2$), 1.71 (s, 3H; $ScC=CMe$), 1.08-0.95 (ov m, 24H; $CHMe_2$), 0.89 (s, 18H; $NCCMe_3$). ^{19}F NMR (C_6D_5Br): δ -132.8 (*o*-F), -163.2 (*p*-F), -167.0 (*m*-F). $^{11}B\{^1H\}$ NMR (C_6D_5Br): δ -16.8. The instability of the compound made it impossible to acquire ^{13}C NMR spectra as further decomposition occurs over the timeframe required to collect the necessary data.

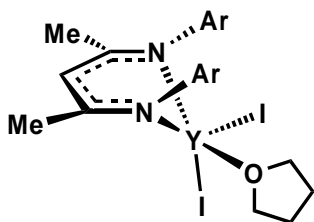
6.5 Experimental Procedures Pertaining to Chapter 5

6.5.1 Synthetic Procedures

Synthesis of $YI_3(THF)_{3.5}$:

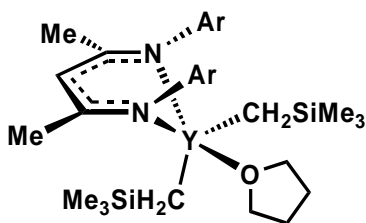
YI_3 (0.750 g, 1.60 mmol) and THF (15 mL) were added to a 50 mL RB flask and heated to $65\text{ }^\circ\text{C}$ for 8 hours. The solvent was removed under reduced pressure to give 1.14 g (1.58 mmol, 99%) of $YI_3(THF)_{3.5}$ as a fine white powder.

Synthesis of [ArNC(Me)CHC(Me)NAr]YI₂(THF) (18-I**(THF)):**



A 25 mL RB flask was charged with KL^{Me} (0.350 g, 0.771 mmol) and YI₃(THF)_{3.5} (0.550 g, 0.771 mmol) to which THF (20 mL) was added. The resultant yellow solution was stirred for 1.5 hours at which point the THF was removed *in vacuo*. The resultant yellow powder was slurried in toluene (20 mL), filtered and solvent removed. The residue was washed with hexanes (15 mL) and evacuated to dryness to give 0.285 g (0.342 mmol, 44%) of **18-I**(THF) as a white solid. ¹H NMR (C₇D₈): δ 7.13-6.96 (s, 6H; C₆H₃), 5.14 (s, 1H; CH), 3.51 (sp, 4H; CHMe₂, J_{H-H} = 6.9 Hz), 3.41 (br, 4H; OCH₂CH₂), 1.63 (s, 6H; NCMe), 1.45 (d, 12H; CHMe₂, J_{H-H} = 6.9 Hz), 1.17 (ov m, 16H; CHMe₂, OCH₂CH₂). ¹³C{¹H} NMR (CD₂Cl₂): δ 168.1 (NCMe), 143.6 (C_{ipso}), 143.5, 127.1, 124.7 (C₆H₃), 99.2 (d, ⁴J_{H-Y} = 10.0 Hz; CH), 71.8 (OCH₂CH₂), 29.1 (CHMe₂), 25.0 (NCMe), 24.9(2) (CHMe₂), 24.8 (OCH₂CH₂). Anal. Calcd. for C₃₃H₄₉N₂I₂OY : C, 47.54; H, 5.92; N, 3.36. Found: C, 46.44; H, 6.27; N, 2.99.

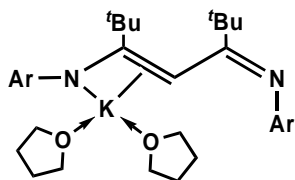
Synthesis of [ArNC(Me)CHC(Me)NAr]Y(CH₂SiMe₃)₂(THF) (18-CH₂SiMe₃**(THF)):**



An NMR tube was charged with **18-I**(THF) (0.018 g, 0.022 mmol) and *d*₈-toluene (0.3 mL). The NMR tube was cooled to -78 °C and a *d*₈-toluene (0.3 mL) solution of LiCH₂SiMe₃ (0.0040 g, 0.044 mmol) was added dropwise. Immediately upon mixing a large quantity of white precipitate formed. The tube was placed in the NMR probe at -78 °C and slowly warmed to room temperature. ¹H NMR (C₇D₈): δ 7.12-6.98 (s, 6H; C₆H₃), 5.01 (s, 1H; CH), 3.48 (br s, 4H; OCH₂CH₂),

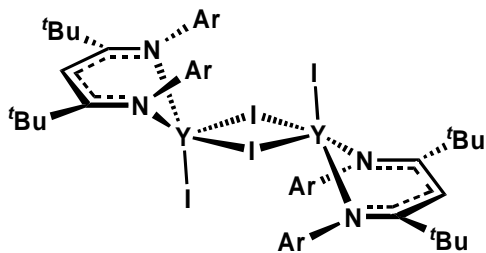
3.17 (sp, 4H; $CHMe_2$, $J_{H-H} = 6.9$ Hz), 1.64 (s, 6H; $NCMe$), 1.39 (d, 12H; $CHMe_2$, $J_{H-H} = 6.8$ Hz), 1.17 (br m, 12H; $CHMe_2$), 1.16 (br s, 4H; OCH_2CH_2), 0.02 (s, 18H; YCH_2SiMe_3), -0.44 (d, 4H; YCH_2SiMe_3 , $^2J_{H-Y} = 2.8$ Hz).

Synthesis of $K[ArNC(tBu)CHC(tBu)NAr]$, (KL^{tBu}):



This compound was made via a modified procedure.¹⁰ HL ($HArNC(tBu)CHC(tBu)NAr$) (1.03 g, 2.05 mmol) and KH (0.146 g, 3.64 mmol) were placed in a 50 mL RB flask attached to a swivel frit apparatus to which 30 mL of THF was added. The solution changed from pale to bright yellow after 30 minutes of stirring. The reaction mixture was allowed to stir for another 18 hours at which point the solvent was removed *in vacuo* to afford a bright yellow solid. Toluene (50 mL) was added and the solution filtered. Removal of solvent gave the desired product in 45% yield (0.499 g, 0.923 mmol). The 1H NMR matched that reported by the previous method: 1H NMR (C_6D_6) δ : 7.06-6.78 (m, 6H; C_6H_3), 4.94 (s, 1H; CH), 3.30 (4H; $CHMe_2$, $J_{H-H} = 6.9$ Hz), 1.38 (s, 18H; CMe_3), 1.34 (d, 12H; $CHMe_2$, $J_{H-H} = 6.9$ Hz), 0.94 (d, 12H; $CHMe_2$, $J_{H-H} = 6.9$ Hz).

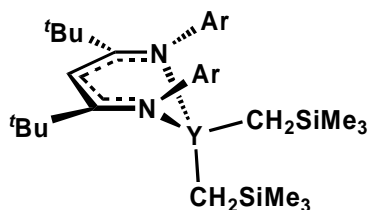
Synthesis of $[ArNC(tBu)CHC(tBu)NAr]YI_2$ (**19-I**):



A 100 mL RB flask was charged with KL^{tBu} (0.200 g, 0.370 mmol) and $YI_3(THF)_{3.5}$ (0.267 g, 0.370 mmol) to which toluene (25 mL) was added. The reaction mixture was warmed to 90 °C and stirred for 1 hour at which point the solvent was removed *in vacuo* to afford a

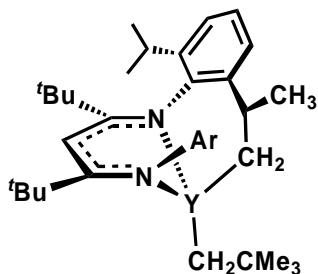
sticky yellow solid. Hexanes (20 mL) was added and the reaction mixture sonicated for 5 minutes, filtered and washed (2 x 5 mL). Removal of solvent under reduced pressure gave **19-I** as a bright yellow solid in 55% yield (0.170 g, 0.202 mmol). ^1H NMR (C_7D_8 , 343K): δ 6.99-6.96 (m, 6H; C_6H_3), 5.82 (s, 1H; CH), 3.05 (sp, 4H; CHMe_2 , $J_{\text{H-H}} = 6.7$ Hz), 1.44 (d, 12H; CHMe_2 , $J_{\text{H-H}} = 6.7$ Hz), 1.26 (d, 12H; CHMe_2 , $J_{\text{H-H}} = 6.7$ Hz), 1.13 (s, 18H; NCCMe_3). $^{13}\text{C}\{^1\text{H}\}$ NMR (C_7D_8 , 343K): δ 173.2 (NCCMe_3), 143.1 (C_{ipso}), 140.6, 126.9, 124.4 (C_6H_3), 88.0 (CH), 45.1 (NCCMe_3), 32.2 (NCCMe_3), 30.3 (CHMe_2), 27.0, 24.0 (CHMe_2). Anal. Calcd. for $\text{C}_{35}\text{H}_{53}\text{N}_2\text{I}_2\text{Y}$: C, 49.71; H, 6.32; N, 3.31. Found: C, 49.17; H, 6.44; N, 3.07.

Synthesis of $[\text{ArNC}(\text{tBu})\text{CHC}(\text{tBu})\text{NAr}]\text{Y}(\text{CH}_2\text{SiMe}_3)_2$ (19-CH₂SiMe₃**):**



19-I (0.018 g, 0.022 mmol) was dissolved in d_8 -toluene (0.3 mL) and cooled to -78 °C. A d_8 -toluene (0.3 mL) solution of $\text{LiCH}_2\text{SiMe}_3$ (0.0040 g, 0.044 mmol) was added dropwise to the yttrium solution. Immediately upon mixing a large quantity of white precipitate formed. The tube was placed in the NMR probe at -78 °C and slowly warmed to room temperature. ^1H NMR (C_7D_8 , 290K): δ 7.11-6.96 (m, 6H; C_6H_3), 5.67 (s, 1H; CH), 3.17 (sp, 4H; CHMe_2 , $J_{\text{H-H}} = 6.7$ Hz), 1.41 (d, 12H; CHMe_2 , $J_{\text{H-H}} = 6.7$ Hz), 1.30 (d, 12H; CHMe_2 , $J_{\text{H-H}} = 6.7$ Hz), 1.10 (s, 18H; NCCMe_3), 0.08 (s, 18H; $\text{Y-CH}_2\text{SiMe}_3$), -0.52 (d, 4H; $\text{YCH}_2\text{SiMe}_3$, $^2J_{\text{H-Y}} = 2.8$ Hz).

Synthesis of κ^3 -[ArNC(^tBu)CHC(^tBu)N-*i*Pr-C₆H₃]YCH₂SiMe₃ (20):



An NMR tube containing **19-CH₂SiMe₃** (0.017 g, 0.022 mmol, generated *in situ*) in 0.6 mL *d*₈-toluene was heated in the NMR probe at 320K for 3 hours. Two isomers exist in a 24 : 76 ratio which cause a very complex ¹H NMR spectrum.

As a result, the following data does not distinguish which signals result from which isomer, the peaks are only assigned to the type of H. ¹H NMR: δ 7.37-6.29 (m, 6H; C₆H₃), 5.63, 5.49 (s, 1H; CH), 3.41-2.92 (ov m, 4H; CHMe₂), 1.55 (d, 3H; CHMe₂, J_{H-H} = 6.6 Hz), 1.40 (d, 3H; CHMe₂, J_{H-H} = 6.6 Hz), 1.37-1.02 (ov m, 16H; CHMe₂, CH₂CHMe), 1.19, 1.14 (s, 18H; NCCMe₃), 0.94 (d, 3H; CHMe₂, J_{H-H} = 6.6 Hz), 0.77 (ddd, 1H; CH₂CHMe, J_{H-H} = 12.2, 5.4, 1.4 Hz), -0.10, -0.12 (s, 9H; CH₂SiMe₃), -1.75, (ddd, 1H; CH₂CHMe, J_{H-H} = 14.1, 11.4, 2.5 Hz), -1.84 (ddd, 1H; CH₂CHMe, J_{H-H} = 14.1, 10.8, 2.8 Hz).

6.6 Kinetic Experiments

Error Analysis:

For all kinetic experiments estimated error values are depicted in brackets after the rate. These values were established upon judicious choice of potential sources of experimental error including temperature accuracy, integration accuracy, mass and concentration accuracy, NMR sensitivity, and sample purity. Each of these parameters was manually calculated for maximum error and the resultant affect that had on the measurement and any subsequent calculations. The summation of all such errors generated the total estimated error in brackets. This method is beneficial over routine standard deviation

calculations in that it allows the calculation of potential systematic sources of error, such as temperature calibration of the NMR probe. In such circumstances it is possible to have high precision with low accuracy, and thus have a deceptively low standard deviation.

Before starting a kinetic experiment the T_1 of all relevant atoms was determined. A delay of at least 5 times the longest T_1 value was used in each kinetic experiment.

Ligand Flip within Neutral Dialkyl Scandium Compounds:

Method 1:

In a typical experiment, the compound of interest (0.0138 mmol) was dissolved in 0.7 mL d_8 -toluene (1.97×10^{-3} M) (0.0208 mmol) and kept at -78 °C until inserted into the NMR probe, at which time the sample was given 10 minutes to equilibrate at each temperature. Upon approaching the coalescence temperature, a spectrum was acquired at every 5 °C until an approximate coalescence temperature was determined. At this point a spectrum was acquired every 1 °C from both directions of the coalescence temperature.

Method 2:

In a typical experiment, **2-CH₂SiMe₃** (0.010g, 0.0138 mmol) was dissolved in 0.7 mL d_8 -toluene (1.97×10^{-3} M) and kept at -78 °C until inserted into the NMR probe, at which time it was given 30 minutes to equilibrate to the specified temperature. The rate was determined using 2D EXSY NMR with a delay time of 6s.

Metallation of Neutral Dialkyl Scandium Compounds:

In a typical experiment, the compound of interest (0.0208 mmol) was dissolved in 0.5 mL *d*₈-toluene (4.15 x10⁻³ M) and kept at -78 °C until inserted into the NMR probe, at which time it was given 10 minutes to equilibrate to the specified temperature. The progress of reaction was monitored by integration of the backbone peak in the ¹H spectrum. The reaction was followed until 95% completion. Although these compounds were produced via the kinetic experiments, they were not isolated and as a result only the ¹H and ¹³C NMR spectra are reported. Decomposition of the metallation products of **1-CH₂Ph**, **1-CH₂CMe₃** and **1-CH₂SiMe₃** occurred before completion of the kinetic experiments, making it impossible to obtain clean spectra. The kinetic data obtained for these species was limited to the first 65% of the metallation process and is therefore considered only semiquantitative.

Metallation of Cationic Scandium Compounds:

In a typical experiment, the compound of interest (0.0208 mmol) was dissolved in 0.5 mL *d*₈-toluene (4.15 x10⁻³ M) and kept at -78 °C until inserted into the NMR probe, at which time it was given 10 minutes to equilibrate to the specified temperature. The progress of reaction was monitored by integration of the backbone peak in the ¹H NMR spectrum. The reaction was followed until 95% completion.

Intermolecular Anion Exchange:

In a typical experiment, the compounds of interest (0.0138 mmol) were dissolved in 0.7 mL *d*₈-toluene (1.97 x10⁻³ M) and kept at -78 °C until inserted into the NMR probe, at

which time it was given 10 minutes to equilibrate to the specified temperature. The rate was determined using 2D EXSY NMR with a delay time of 6s.

[10-CH₂SiMe₂CH₂SiMe₃] Dependence Study for Intermolecular Anion Exchange :

In a typical experiment, [11-CH₂SiMe₂CH₂SiMe₃] (0.015 g, 0.013 mmol) and the desired quantity of [10-CH₂SiMe₂CH₂SiMe₃] were dissolved in 0.6 mL cold (-78 °C) *d*₈-toluene. The NMR tube was kept at -78 °C until inserted into the NMR probe, at which time it was given 10 minutes to equilibrate to the specified temperature. The rate was determined using 2D EXSY NMR with a delay time of 6s.

Exchange of 14-C₉H₁₂ with C₇H₈:

In a typical experiment, the compound of interest (0.015g, 0.0118 mmol, 2.14 x10⁻² M) was dissolved in 0.5 mL C₆D₅Br, cooled to -35 °C and cold toluene (0.05 mL, 0.471 mmol) added). The NMR tube was kept at -35 °C until inserted into the NMR probe, at which time it was given 10 minutes to equilibrate to the specified temperature. The progress of reaction was monitored by integration of the backbone peak in the ¹H NMR spectrum. The reaction was followed until 95% completion.

[C₇H₈] Dependence Study for Exchange of 14-C₉H₁₂ with C₇H₈:

In a typical experiment, the compound of interest (0.015g, 0.0118 mmol, 2.14 x10⁻² M) was dissolved in 0.5 mL C₆D₅Br, cooled to -35 °C and the desired quantity of cold toluene. The NMR tube was kept at -35 °C until inserted into the NMR probe, at which time it was given 10 minutes to equilibrate to the specified temperature. The progress of

reaction was monitored by integration of the backbone peak in the ^1H NMR spectrum. The reaction was followed until 95% completion.

Equilibrium Between 14-C₉H₁₂ and 14-C₇H₈:

In a typical experiment, **14-C₉H₁₂** (0.015g, 0.012 mmol, 2.14×10^{-2} M) was dissolved in 0.5 mL C₆D₅Br, cooled to -35 °C and 1 equivalent of cold toluene (1.2 μL , 0.012 mmol) was added. The NMR tube was kept at -35 °C until inserted into the NMR probe, at which time it was given 120 minutes to equilibrate to each temperature. K_{eq} was calculated from concentrations determined by integration of the backbone peak in the ^1H NMR spectrum. In order to ensure equilibrium had been achieved at a given temperature, a series of ^1H NMR spectra were recorded until identical results were obtained in three consecutive experiments.

Insertion of PhCCPh into 14-C₉H₁₂:

In a typical experiment, the compound of interest (0.015 g, 0.0118 mmol) was dissolved in 0.3 mL C₆D₅Br, cooled to -35 °C and a C₆D₅Br solution (0.3 mL) of diphenylacetylene (0.022 g, 0.118 mol) added. The NMR tube was kept at -35 °C until inserted into the NMR probe, at which time it was given 10 minutes to equilibrate to the specified temperature. The progress of reaction was monitored by integration of the backbone peak in the ^1H NMR spectrum. The reaction was followed until 95% completion.

[PhCCPh] Dependence Study for Insertion of PhCCPh into 14-C₉H₁₂:

In a typical experiment, the compound of interest (0.015 g, 0.0118 mmol) was dissolved in 0.3 mL C₆D₅Br, cooled to -35 °C and a C₆D₅Br solution (0.3 mL) of the desired quantity of diphenylacetylene added. The NMR tube was kept at -35 °C until inserted into the NMR probe, at which time it was given 10 minutes to equilibrate to the specified temperature. The progress of reaction was monitored by integration of the backbone peak in the ¹H NMR spectrum. The reaction was followed until 95% completion.

1. Birmingham, J. M.; Wilkinson, G. *J. Am. Chem. Soc.* **1956**, *78*, 42.
2. Piers, W. E.; Shapiro, P. J.; Bunel, E. E.; Bercaw, J. E. *Synlett.* **1990**, 74.
3. Thompson, M. E.; Bercaw, J. E. *Pure and Applied Chemistry* **1984**, *56*, 1.
4. Thompson, M. E.; Baxter, S. M.; Bulls, A. R.; Burger, B.; Nolam, M. C.; Santarsiero, B. D.; Schaefer, W. P.; Bercaw, J. E. *J. Am. Chem. Soc.* **1987**, *109*, 203.
5. Piers, W. E.; Emslie, D. J. H. *Coord. Chem. Rev.* **2002**, *233-234*, 131.
6. Mountford, P.; Ward, B. D. *Chem. Commun.* **2003**, 1797.
7. Cotton, S. A. *Polyhedron* **1999**, *18*, 1691.
8. Meehan, P. R.; Aris, D. R.; Willey, G. R. *Coord. Chem. Rev.* **1999**, *181*, 121.
9. Burger, B. J.; Thompson, M. E.; Cotter, W. D.; Bercaw, J. E. *J. Am. Chem. Soc.* **1990**, *112*, 1566.
10. Piers, W. E.; Bercaw, J. E. *J. Am. Chem. Soc.* **1990**, *112*, 9406.
11. Fryzuk, M. D.; Giesbrecht, G.; Rettig, S. J. *Organometallics* **1996**, *15*, 3329.
12. Fryzuk, M. D.; Giesbrecht, G. R.; Rettig, S. J. *Can. J. Chem.* **2000**, *78*, 1003.
13. Putzer, M. A.; Rogers, J. S.; Bazan, G. C. *J. Am. Chem. Soc.* **1999**, *121*, 8112.
14. Blackwell, J.; Lehr, C.; Sun, Y.; Piers, W. E.; Pearce-Batchilder, S. D.; Zaworotko, M. J.; Young, V. J., Jr. *Can. J. Chem.* **1997**, *75*, 702.
15. Apostolidis, C.; Rebizant, J.; Kanellakopulos, B.; von Ammon, R.; Dornberger, E.; Muller, J.; Powietzka, B.; Nuber, B. *Polyhedron* **1997**, *16*, 1057.
16. Long, D. P.; Chandrasekaran, A.; Day, R. O.; Bionconi, P. A.; Rheingold, A. L. *Inorg. Chem.* **2000**, *39*, 4476.
17. Long, D. P.; Bionconi, P. A. *J. Am. Chem. Soc.* **1996**, *118*, 12453.
18. Hajela, S.; Schaefer, W. P.; Bercaw, J. E. *J. Organomet. Chem.* **1997**, *532*, 45.
19. Lawrence, S. C.; Ward, B. D.; Dubberley, S. R.; Kozak, C. M.; Mountford, P. *Chem. Commun.* **2003**, 2880.

20. Neculai, A. M.; Neculai, D.; Roesky, H. W.; Magull, J. *Organometallics* **2002**, *21*, 2590.
21. Arnold, P. L.; Cloke, F. G. N.; Hitchcock, P. B.; Nixon, J. F. *J. Am. Chem. Soc.* **1996**, *118*, 7630.
22. Cloke, F. G. N.; Hitchcock, P. B.; Wilson, D. J. *Organometallics* **2000**, *19*, 219.
23. Cloke, F. G. N.; Kahn, K.; Perutz, R. N. *J. Chem. Soc., Chem. Commun.* **1991**, 1372.
24. Cloke, F. G. N. *Chem. Soc. Rev.* **1993**, *22*, 17.
25. Clentsmith, G. K. B.; Cloke, F. G. N.; Green, J. C.; Hanks, J.; Hitchcock, P. B.; Nixon, J. F. *Angew. Chem. Int. Ed.* **2003**, *42*, 1038.
26. Beetstra, D. J.; Meetsma, A.; Hessen, B.; Teuben, J. H. *Organometallics* **2003**, *22*, 4372.
27. Arnold, P. L.; Cloke, F. G. N.; Nixon, J. F. *Chem. Commun.* **1998**, 797.
28. McGeachin, S. G. *Can. J. Chem.* **1968**, *46*, 1903.
29. Kim, W.-K.; Fevola, M. J.; Liable-Sands, L. M.; Rheingold, A. L.; Theopold, K. H. *Organometallics* **1998**, *17*, 4541.
30. Bourget-Merle, L.; Lappert, M. F.; Severn, J. R. *Chem. Rev.* **2002**, *102*, 3031.
31. Allen, S. D.; Moore, D. R.; Lobkovsky, E. B.; Coates, G. W. *J. Am. Chem. Soc.* **2002**, *124*, 14284.
32. Moore, D. R.; Cheng, M.; Lobkovsky, E. B.; Coates, G. W. *J. Am. Chem. Soc.* **2003**, *125*, 11911.
33. Moore, D. R.; Cheng, M.; Lobkovsky, E. B.; Coates, G. W. *Angew. Chem. Int. Ed.* **2002**, *41*, 2599.
34. Budzelaar, P. H. M.; van Oort, A. B.; Orpen, A. G. *Eur. J. Inorg. Chem.* **1998**, 1485.
35. Bercaw, J. E.; Davies, D. L.; Wolczanski, P. T. *Organometallics* **1986**, *5*, 443.
36. Hitchcock, P. B.; Lappert, M. F.; Tian, S. *J. Organomet. Chem.* **1997**, *549*, 1.
37. Cui, C.; Roesky, H. W.; Schmidt, H.-G.; Noltemeyer, M.; Hao, H.; Cimpoesu, F. *Angew. Chem. Int. Ed.* **2000**, *39*, 4274.

38. Hardman, N. J.; Eichler, B. E.; Power, P. P. *Chem. Commun.* **2000**, 1991.
39. Bailey, P. J.; Coxall, R. A.; Dick, C. M.; Fabre, S.; Parsons, S. *Organometallics* **2001**, *20*, 798.
40. Gibson, V. C.; Segal, J. A.; White, A. J. P.; Williams, D. J. *J. Am. Chem. Soc.* **2000**, *122*, 7120.
41. Bailey, P. J.; Dick, C. M. E.; Fabre, S.; Parsons, S. *J. Chem. Soc., Dalton Trans.* **2000**, 1655.
42. Radzewich, C. E.; Guzei, I. A.; Jordan, R. F. *J. Am. Chem. Soc.* **1999**, *121*, 8673.
43. Radzewich, C. E.; Coles, M. P.; Jordan, R. F. *J. Am. Chem. Soc.* **1998**, *120*, 9384.
44. Qian, B.; Baek, S. W.; Smith, M. R., III *Polyhedron* **1999**, *18*, 2405.
45. Avent, A. G.; Khovostov, A. V.; Hitchcock, P. B.; Lappert, M. F. *Chem. Commun.* **2002**, 1410.
46. Prust, J.; Hohmesiter, H.; Stasch, A.; Roesky, H. W.; Magull, J.; Alexopolous, E.; Usón, I.; Schmidt, H.-G.; Noltemeyer, M. *Eur. J. Inorg. Chem.* **2002**, 2156.
47. Qian, B.; Ward, D. L.; Smith, M. R., III *Organometallics* **1998**, *17*, 3070.
48. Hitchcock, P. B.; Lappert, M. F.; Tian, S. *J. Chem. Soc., Dalton Trans.* **1997**, 1945.
49. Vollmerhaus, R.; Rahim, M.; Tomaszewski, R.; Xin, S.; Taylor, N. J.; Collins, S. *Organometallics* **2000**, *19*, 2161.
50. Rahim, M.; Taylor, N. J.; Xin, S.; Collins, S. *Organometallics* **1998**, *17*, 1315.
51. Clegg, W.; Coles, S. J.; Cope, E. K.; Mair, F. S. *Angew. Chem. Int. Ed.* **1998**, *37*, 796.
52. Qian, B.; Scanlon, W. J., IV; Smith, M. R., III *Organometallics* **1999**, *18*, 1693.
53. Deelman, B.-J.; Hitchcock, P. B.; Lappert, M. F.; Leung, W.-P.; Lee, H.-K.; Mak, T. C. W. *Organometallics* **1999**, *18*, 1444.
54. Randall, D. W.; George, S. D.; Holland, P. L.; Hedman, B.; Hodgson, K. O.; Tolman, W. B.; Solomon, E. I. *J. Am. Chem. Soc.* **2000**, *122*, 11632.
55. MacAdams, L. A.; Kim, W.-K.; Liable-Sands, L. M.; Guzei, I. A.; Rheingold, A. L.; Theopold, K. H. *Organometallics* **2002**, *21*, 952.

56. Lee, L. W. M.; Piers, W. E.; Elsegood, M. R. J.; Clegg, W.; Parvez, M. *Organometallics* **1999**, *18*, 2947.
57. Hayes, P. G.; Piers, W. E.; Lee, L. W. M.; Knight, L. K.; Parvez, M.; Elsegood, M. R. J.; Clegg, W. *Organometallics* **2001**, *20*, 2533.
58. Schlosser, M.; Hartmann, J. *Angew. Chem. Int. Ed.* **1973**, *12*, 508.
59. Knight, L. K.; Piers, W. E.; McDonald, R. *Chem. Eur. J.* **2000**, *6*, 4322.
60. Dagorne, S.; Jordan, R. F. *Organometallics* **1999**, *18*, 4619.
61. Knight, L. K.; Piers, W. E.; Fleurat-Lessard, P.; Parvez, M.; McDonald, R. *Organometallics* **2004**, *23*, 2087.
62. Knight, L. K. *Ph.D. Thesis* **2004**, University of Calgary.
63. Sandstrøm, J. *Dynamic NMR Spectroscopy*; Academic Press: New York, 1982.
64. Abrams, M. B.; Yoder, J. C.; Loeber, C.; Day, M. W.; Bercaw, J. E. *Organometallics* **1999**, *18*, 1389.
65. Perrin, C. L.; Dwyer, T. J. *Chem. Rev.* **1990**, *90*, 935.
66. Hoskin, A. J.; Stephan, D. W. *Coord. Chem. Rev.* **2002**, *233-234*, 107.
67. Emslie, D. J. H.; Piers, W. E.; Parvez, M.; McDonald, R. *Organometallics* **2002**, *21*, 4226.
68. Fekl, U.; Goldberg, K. I. *J. Am. Chem. Soc.* **2002**, *124*, 6804.
69. Fekl, U.; Kaminsky, W.; Goldberg, K. I. *J. Am. Chem. Soc.* **2003**, *125*, 15286.
70. Hart, D. W.; Schwartz, J. *J. Am. Chem. Soc.* **1974**, *96*, 8115.
71. Basuli, F.; Bailey, B. C.; Tomaszewski, J.; Huffman, J. C.; Mindiola, D. J. *J. Am. Chem. Soc.* **2003**, *125*, 6052.
72. Ibers, J. A.; DiCosimo, R.; Whitesides, G. M. *Organometallics* **1982**, *1*, 13.
73. Constable, E. C. *Polyhedron* **1984**, *3*, 1037.
74. Gagneur, S.; Montchamp, J.-L.; Negishi, E.-I. *Organometallics* **2000**, *19*, 2417.
75. Chen, E. Y. X.; Marks, T. J. *Chem. Rev.* **2000**, *100*, 1391.

76. McKnight, A. L.; Waymouth, R. M. *Chem. Rev.* **1998**, *98*, 2587.
77. Britovsek, G. J. P.; Gibson, V. C.; Wass, D. F. *Angew. Chem. Int. Ed.* **1999**, *38*, 428.
78. Hou, Z.; Wakatsuki, Y. *Coord. Chem. Rev.* **2002**, *231*, 1.
79. Sinn, H.; Kaminsky, W.; Vollmer, H. J.; Woldt, R. *Angew. Chem.* **1980**, *92*, 396.
80. Babushkin, D. E.; Semikoleova, N. V.; Zakharov, V. A.; Talsi, E. P. *Macromol. Chem. Phys.* **2000**, *201*, 558.
81. Harlan, C. J.; Bott, S. G.; Barron, A. R. *J. Am. Chem. Soc.* **1995**, *117*, 6465.
82. Sinn, H. *Macromol. Symp.* **1995**, *97*, 27.
83. Ystenes, M.; Eilertsen, J. L.; Liu, J.; Ott, M.; Rytter, E.; Stovngeng, J. A. *J. Polym. Sci.* **2000**, *38*, 3106.
84. Eilertsen, J. L.; Rytter, E.; Ystenes, M. M. *Vib. Spectrosc.* **2000**, *24*, 257.
85. Imhoff, D. W.; Simeral, L. S.; Sangokoya, S. A.; Peel, J. H. *Organometallics* **1998**, *17*, 1941.
86. Bryliakov, K. P.; Semikolenova, N. V.; Yudaev, D. V.; Zakharov, V. A.; Brintzinger, H.-H.; Ystenes, M.; Rytter, E.; Talsi, E. P. *J. Organomet. Chem.* **2003**, *683*, 92.
87. Zurek, E.; Ziegler, T. *Organometallics* **2002**, *21*, 83.
88. Zurek, E.; Ziegler, T. *Inorg. Chem.* **2001**, *40*, 3279.
89. Zurek, E.; Woo, T. K.; Firman, T. K.; Ziegler, T. *Inorg. Chem.* **2001**, *40*, 361.
90. Yang, X. M.; Stern, C. L.; Marks, T. J. *J. Am. Chem. Soc.* **1991**, *113*, 3623.
91. Ewen, J. A.; Elder, M. J. *CA-A* **1991**, *2*, 27.
92. Hlatky, G. G.; Turner, H. W. In *PCT Int. Appl. W/O 91/14713*; Exxon Chemical Co., 1991.
93. Massey, A. G.; Park, A. J.; Stone, F. G. A. *Proc. Chem. Soc.* **1963**, 212.
94. Massey, A. G.; Park, A. J. *J. Organomet. Chem.* **1964**, *2*, 245.
95. Piers, W. E. *Adv. Organomet. Chem.* **2004**, In Press.

96. Piers, W. E.; Chivers, T. *Chem. Soc. Rev.* **1997**, 26, 345.
97. Cossee, P. *J. Catal.* **1964**, 3, 80.
98. Yang, X. M.; Stern, C. L.; Marks, T. J. *J. Am. Chem. Soc.* **1994**, 116, 10015.
99. Horton, A. D. *Organometallics* **1996**, 15, 2675.
100. Deck, P. A.; Marks, T. J. *J. Am. Chem. Soc.* **1995**, 117, 6128.
101. Deck, P. A.; Beswick, C. L.; Marks, T. J. *J. Am. Chem. Soc.* **1998**, 120, 1772.
102. Beswick, C. L.; Marks, T. J. *Organometallics* **1999**, 18, 2410.
103. Beswick, C. L.; Marks, T. J. *J. Am. Chem. Soc.* **2000**, 122, 10358.
104. Beck, S.; Geyer, A.; Brintzinger, H.-H. *Chem. Commun.* **1999**, 2477.
105. Beck, S.; Lieber, S.; Schaper, F.; Geyer, A.; Brintzinger, H.-H. *J. Am. Chem. Soc.* **2001**, 123, 1483.
106. Stahl, N. G.; Zuccaccia, C.; Jensen, T. R.; Marks, T. J. *J. Am. Chem. Soc.* **2003**, 125, 5256.
107. Zuccaccia, C.; Stahl, N. G.; Macchiono, A.; Chen, M.-C.; Roberts, J. A.; Marks, T. J. *J. Am. Chem. Soc.* **2004**, 126, 1448.
108. Landis, C. R., Personal Communication, **2003**.
109. Vanka, K.; Chan, M. S. W.; Pye, C. C.; Ziegler, T. *Organometallics* **2000**, 19, 1841.
110. Chan, M. S. W.; Vanka, K.; Pye, C. C.; Ziegler, T. *Organometallics* **1999**, 18, 4624.
111. Scollard, J. D.; McConville, D. H.; Rettig, S. J. *Organometallics* **1997**, 16, 1810.
112. Thorn, M. G.; Etheridge, Z. C.; Fanwick, P. E.; Rothwell, I. P. *J. Organomet. Chem.* **1999**, 591, 148.
113. Woodman, T. J.; Thornton-Pett, M.; Bochmann, M. *Chem. Commun.* **2001**, 329.
114. Li, L.; Marks, T. J. *Organometallics* **1998**, 17, 3996.
115. Jia, L.; Yang, X. M.; Stern, C. L.; Marks, T. J. *Organometallics* **1997**, 16, 842.

116. Chen, E. Y. X.; Metz, M. V.; Li, L.; Stern, C. L.; Marks, T. J. *J. Am. Chem. Soc.* **1998**, *120*, 6287.
117. Metz, M. V.; Sun, Y.; Stern, C. L.; Marks, T. J. *Organometallics* **2002**, *21*, 3691.
118. Metz, M. V.; Schwartz, D. J.; Stern, C. L.; Nickias, P. N.; Marks, T. J. *Angew. Chem. Int. Ed.* **2000**, *39*, 1312.
119. Li, L.; Metz, M. V.; Chen, M.-C.; Marks, T. J.; Liable-Sands, L.; Rheingold, A. L. *J. Am. Chem. Soc.* **2002**, *124*, 12725.
120. Abramo, G. P.; Li, L.; Marks, T. J. *J. Am. Chem. Soc.* **2002**, *124*, 13966.
121. Chen, M.-C.; Marks, T. J. *J. Am. Chem. Soc.* **2001**, *123*, 11803.
122. Parks, D. J.; Spence, R. E. v. H.; Piers, W. E. *Angew. Chem. Int. Ed.* **1995**, *34*, 809.
123. Spence, R. E. v. H.; Piers, W. E. *Organometallics* **1995**, *14*, 4617.
124. Parks, D. J.; Piers, W. E.; Yap, G. P. A. *Organometallics* **1998**, *17*, 5492.
125. Parks, D. J.; Piers, W. E. *Tetrahedron* **1998**, *54*, 15469.
126. Spence, R. E. v. H.; Parks, D. J.; Piers, W. E.; MacDonald, M. A.; Zawortoko, M. J.; Rettig, S. J. *Angew. Chem. Int. Ed.* **1995**, *34*, 1230.
127. Spence, R. E. v. H.; Piers, W. E.; Sun, Y.; Parvez, M.; MacGillivray, L. R.; Zawortoko, M. J. *Organometallics* **1998**, *17*, 2459.
128. Chase, P. A.; Piers, W. E.; Parvez, M. *Organometallics* **2000**, *19*, 2040.
129. Douthwaite, R. E. *Polyhedron* **2000**, *19*, 1579.
130. Schrock, R. R.; Sharp, P. R. *J. Am. Chem. Soc.* **1978**, *100*, 2389.
131. Cook, K. S.; Piers, W. E.; Woo, T. K.; McDonald, R. *Organometallics* **2001**, *20*, 3927.
132. Cook, K. S.; Piers, W. E.; McDonald, R. *J. Am. Chem. Soc.* **2002**, *124*, 5411.
133. Cook, K. S.; Piers, W. E.; Hayes, P. G.; Parvez, M. *Organometallics* **2002**, *21*, 2422.
134. van der Eide, E. F.; Piers, W. E.; Romero, P. E.; Parvez, M.; McDonald, R. *Organometallics* **2004**, *23*, 314.

135. Romero, P. E.; Piers, W. E. *Unpublished results* **2004**.
136. Song, X. J.; Thornton-Pett, M.; Bochmann, M. *Organometallics* **1998**, *17*, 1004.
137. Tebbe, F. N.; Parshall, G. W.; Reddy, G. S. *J. Am. Chem. Soc.* **1978**, *100*, 3611.
138. Guérin, F.; Stephan, D. W. *Angew. Chem. Int. Ed.* **2000**, *39*, 1298.
139. Zhang, S.; Piers, W. E. *Organometallics* **2001**, *20*, 2088.
140. Bottomley, F.; Paez, D. E.; White, P. S. *J. Organomet. Chem.* **1985**, *291*, 35.
141. Hayes, P. G.; Piers, W. E.; McDonald, R. *J. Am. Chem. Soc.* **2002**, *124*, 2132.
142. Ozawa, F.; Park, J. W.; MacKenzie, P. B.; Schaefer, W. P.; Henling, L. M.; Grubbs, R. H. *J. Am. Chem. Soc.* **1989**, *111*, 1319.
143. Lide, D. R., Ed. *CRC Handbook of Chemistry and Physics*; 84 ed.; CRC Press LLC: New York, 2003-2004.
144. Bochmann, M.; Cuenca, T.; Hardy, D. T. *J. Organomet. Chem.* **1994**, *484*, C10.
145. Chase, P. A.; Piers, W. E.; Patrick, B. O. *J. Am. Chem. Soc.* **2000**, *122*, 12911.
146. Lee, L.; Berg, D. J.; Einstein, F. W.; Batchelor, R. J. *Organometallics* **1997**, *16*, 1819.
147. Arndt, S.; Spaniol, T. P.; Okuda, J. *Chem. Commun.* **2002**, 896.
148. Ankianiec, B. C.; Christou, V.; Hardy, D. T.; Thomson, S. K.; Young, G. B. *J. Am. Chem. Soc.* **1994**, *117*, 9963.
149. Gielens, E.; Tiesnitsch, J. Y.; Hessen, B.; Teuben, J. H. *Organometallics* **1998**, *17*, 1652.
150. Cameron, T. M.; Gordon, J. C.; Michalcyzk, R.; Scott, B. L. *Chem. Commun.* **2003**, 2282.
151. Huheey, J. E.; Keiter, E. A.; Keiter, R. L. *Inorganic Chemistry Principles of Structures and Reactivity*; 4th ed.; Harper Collins College Publishers, 1993.
152. Bochmann, M.; Wilson, L. M. *J. Chem Soc., Chem. Commun.* **1986**, 1610.
153. Bochmann, M.; Wilson, L. M.; Hursthouse, M. B.; Short, R. L. *Organometallics* **1987**, *6*, 2556.

154. Lin, Z.; Le Marechal, J.-F.; Sabat, M.; Marks, T. J. *J. Am. Chem. Soc.* **1987**, *109*, 4127.
155. Hlatky, G. G.; Turner, H. W.; Eckman, R. R. *J. Am. Chem. Soc.* **1989**, *111*, 2728.
156. Yang, X.; Stern, C. L.; Marks, T. J. *Organometallics* **1991**, *10*, 840.
157. Hlatky, G. G.; Upton, D. J.; Turner, H. W. In *PCT Int. Appl. W/O 91/09882*; Exxon Chemical Co., 1991.
158. Turner, H. W. In *Eur. Pat. Appl. EP 0 277 004 A1*; Exxon Chemical Co., 1988.
159. Horton, D. A.; de With, J.; van der Linden, A. J.; van de Weg, H. *Organometallics* **1996**, *15*, 2672.
160. Horton, D. A.; de With, J. *Organometallics* **1997**, *16*, 5424.
161. Bei, X.; Swenson, D. C.; Jordan, R. F. *Organometallics* **1997**, *16*, 3282.
162. Bochmann, M.; Lancaster, S. J. *J. Organomet. Chem.* **1992**, *434*, C1.
163. Ewan, J. A.; Elder, M. J. *Makromol. Chem. Macromol. Symp.* **1993**, *66*, 179.
164. Chien, J. C. W.; Tsai, W.-M.; Rausch, M. D. *J. Am. Chem. Soc.* **1991**, *113*, 8570.
165. Casey, C. P.; Carpenetti, D. W., II *J. Organomet. Chem.* **2002**, *642*, 120.
166. Lancaster, S. J.; Bochmann, M. *J. Organomet. Chem.* **2002**, *654*, 221.
167. Bouwkamp, M. W.; de Wolf, J.; del Hierro Morales, I.; Gercama, J.; Meetsma, A.; Troyanov, S. I.; Hessen, B.; Teuben, J. H. *J. Am. Chem. Soc.* **2002**, *124*, 12956.
168. Reed, C. A.; Kim, K.-C.; Stoyanov, E. S.; Stasko, D.; Tham, F. S.; Mueller, L. J.; Boyd, P. D. W. *J. Am. Chem. Soc.* **2003**, *125*, 1796.
169. Reed, C. A.; Fackler, N. L. P.; Kim, K.-C.; Stasko, D.; Evans, D. R. *J. Am. Chem. Soc.* **1999**, *121*, 6314.
170. Klabunde, K. J.; Anderson, B. B.; Bader, M.; Radonovich, L. J. *J. Am. Chem. Soc.* **1978**, *100*, 1313.
171. Traylor, T. G.; Goldberg, M. J. *Organometallics* **1987**, *6*, 2531.
172. Takahashi, T.; Hashiguchi, S.; Kasuga, K.; Tsuji, J. *J. Am. Chem. Soc.* **1978**, *100*, 7425.

173. Gastinger, R. G.; Anderson, B. B.; Klabunde, K. J. *J. Am. Chem. Soc.* **1980**, *102*, 4959.
174. Sievert, A. C.; Muetterties, E. L. *Inorg. Chem.* **1981**, *20*, 489.
175. Brezinski, M. M.; Klabunde, K. J. *Organometallics* **1983**, *2*, 1116.
176. Harrison, J. J. *J. Am. Chem. Soc.* **1984**, *106*, 1487.
177. Traylor, T. G.; Stewart, K. J.; Goldberg, M. J. *J. Am. Chem. Soc.* **1984**, *106*, 4445.
178. Traylor, T. G.; Stewart, K. *Organometallics* **1984**, *3*, 325.
179. Traylor, T. G.; Stewart, K. J.; Goldberg, M. J. *Organometallics* **1986**, *5*, 2062.
180. Traylor, T. G.; Stewart, K. J. *J. Am. Chem. Soc.* **1986**, *108*, 6977.
181. Bush, B. F.; Lynch, V. M.; Lagowski, J. J. *Organometallics* **1987**, *6*, 1267.
182. Kündig, E. P.; Desobry, V.; Grivet, C.; Rudolph, B.; Spichiger, S. *Organometallics* **1987**, *6*, 1173.
183. Sassano, C. A.; Mirkin, C. A. *J. Am. Chem. Soc.* **1995**, *117*, 11379.
184. Singewald, E. T.; Shi, X.; Mirkin, C. A.; Schofer, S. J.; Stern, C. L. *Organometallics* **1996**, *15*, 3062.
185. Semmelhack, M. F.; Chlenov, A.; Wu, L.; Ho, D. *J. Am. Chem. Soc.* **2001**, *123*, 8438.
186. Branch, C. S.; Barron, A. R. *J. Am. Chem. Soc.* **2002**, *124*, 14156.
187. Gillis, D. J.; Quyoum, R.; Tudoret, M.-J.; Wang, Q. Y.; Jeremic, D.; Roszak, A. W.; Baird, M. C. *Organometallics* **1996**, *15*, 3600.
188. Gillis, D. J.; Tudoret, M.-J.; Baird, M. C. *J. Am. Chem. Soc.* **1993**, *115*, 2543.
189. Lancaster, S. J.; Robinson, O. B.; Bochmann, M.; Coles, S. J.; Hursthouse, M. B. *Organometallics* **1995**, *14*, 2456.
190. Scollard, J. D.; McConville, D. H. *J. Am. Chem. Soc.* **1996**, *118*, 10008.
191. Taylor, R. D.; Kilpatrick, J. E. *J. Chem. Phys.* **1955**, *23*, 1232.
192. Kelley, K. K. *J. Am. Chem. Soc.* **1929**, *51*, 2738.

193. Hayes, P. G.; Piers, W. E.; Parvez, M. *J. Am. Chem. Soc.* **2003**, *125*, 5622.
194. Guram, A. S.; Jordan, R. F. *Organometallics* **1991**, *10*, 3470.
195. Doxsee, K. M.; Juliette, J. J. J.; Mouser, J. K. M.; Zientara, K. *Organometallics* **1993**, *12*, 4682.
196. Fryzuk, M. D.; Haddad, T. S.; Rettig, S. J. *Organometallics* **1991**, *10*, 2026.
197. Cook, K.; Piers, W. E.; Rettig, S. J.; McDonald, R. *Organometallics* **2000**, *19*, 2243.
198. Cotter, W. D.; Bercaw, J. E. *J. Organomet. Chem.* **1991**, *417*, C1.
199. Bambirra, S.; Brandsma, M. J. R.; Brussee, E. A. C.; Meetsma, A.; Hessen, B.; Teuben, J. H. *Organometallics* **2000**, *19*, 3197.
200. Hayes, P. G.; Welch, G. C.; Emslie, D. J. H.; Noack, C. L.; Piers, W. E.; Parvez, M. *Organometallics* **2003**, *22*, 1577.
201. Fryzuk, M. D.; Haddad, T. S.; Rettig, S. J. *Organometallics* **1992**, *11*, 2967.
202. Long, D. P.; Bionconi, P. A. *J. Am. Chem. Soc.* **1996**, *118*, 12453.
203. Duchateau, R.; van Wee, C. T.; Teuben, J. H. *Organometallics* **1996**, *15*, 2291.
204. Bambirra, S.; van Leusen, D.; Meetsma, A.; Hessen, B.; Teuben, J. H. *Chem. Commun.* **2001**, 637.
205. Arndt, S.; Spaniol, T. P.; Okuda, J. *Angew. Chem. Int. Ed.* **2003**, *42*, 5075.
206. Lappert, M. F.; Liu, D.-S. *J. Organomet. Chem.* **1995**, *500*, 203.
207. Drees, D.; Magull, J. *Z. anorg. allg. Chem.* **1994**, *620*, 814.
208. Hitchcock, P. B.; Hu, J.; Lappert, M. F.; Tian, S. *J. Organomet. Chem.* **1997**, *536*, 473.
209. Izod, K.; Liddle, S. T.; Clegg, W. *Inorg. Chem.* **2004**, *43*, 214.
210. Burger, B. J.; Bercaw, J. E. *Experimental Organometallic Chemistry*; American Chemical Society: Washington, D.C., 1987.
211. Pangborn, A. B.; Giardello, M. A.; Grubbs, R. H.; Rosen, R. K.; Timmers, F. J. *Organometallics* **1996**, *15*, 1518.

212. Marvich, R. H.; Brintzinger, H. H. *J. Am. Chem. Soc.* **1971**, *93*, 2046.
213. Harris, R. K.; Mann, B. E., Eds. *NMR and the Periodic Table*; Academic Press: New York, 1978.
214. Ammann, C.; Meier, P.; Merbach, A. E. *J. Magn. Reson.* **1982**, *46*.
215. Bax, A.; Subramanian, S. *J. Magn. Reson.* **1986**, *67*, 565.
216. Blackwell, J. M.; Foster, K. L.; Beck, V. H.; Piers, W. E. *J. Org. Chem.* **1999**, *64*, 4887.
217. Budzelaar, P. H. M.; van Oort, A. B.; Orpen, A. G. *Eur. J. Inorg. Chem.* **1998**, 1485.
218. Piers, W. E.; Cipot, J. H. *Unpublished results* **2002**.
219. Brookhart, M.; Green, M. L. H. *J. Organomet. Chem.* **1983**, *250*, 395.
220. Manzer, L. E. *Inorg. Synth* **1982**, *21*, 135.

**Appendix 1: Crystallographic Data Tables, Atomic Coordinates, Anisotropic
Displacement Parameters and Metrical Data**

Table A.1: Crystal Data and Structure Refinement for [1-Me]₂

A. Crystal Data

Crystallographer	Masood Parvez	University of Calgary
Empirical Formula	C ₃₁ H ₄₇ N ₂ Sc · 0.5 C ₆ H ₁₄	
Formula Weight	535.75	
Crystal Size	0.20 x 0.17 x 0.16 mm ³	
Crystal System	monoclinic	
Space Group	P2 ₁ /c	
Lattice Parameters	a = 13.7854(2) Å b = 13.6742(3) Å β = 103.6522(11)° c = 17.7349(3) Å	
Volume	3248.65(10) Å ³	
Z	4	
Density (calculated)	1.095 Mg/m ³	

B. Data Collection and Refinement Conditions

Diffractionmeter	Nonius Kappa CCD
Radiation (λ[Å])	Graphite-monochromated MoKα (0.71073)
Temperature	170(2) K
Reflections Collected	14041
Independent Reflections	7342 [R(int) = 0.018]
Structure Solution	Direct Methods
Refinement Method	Full-matrix least-squares on F ²
Data / Restraints / Parameters	7342 / 0 / 354
Goodness-of-Fit	1.03
Final R Indices [I>2σ(I)]	R1 = 0.054, wR2 = 0.147
R Indices (all data)	R1 = 0.068, wR2 = 0.158
Largest Difference Peak & Hole	0.53 and -0.46 e.Å ⁻³

Table A.2: Atomic Coordinates and Equivalent Isotropic Displacement Parameters for [1-Me]₂

	x	y	z	U(eq)		x	y	z	U(eq)
Sc(1)	4890(1)	4080(1)	618(1)	26(1)	C(17)	3179(2)	2746(2)	-1947(2)	58(1)
N(1)	5846(1)	2761(1)	916(1)	26(1)	C(18)	3230(2)	2460(2)	-1108(1)	52(1)
N(2)	3614(1)	3052(1)	498(1)	27(1)	C(19)	3187(4)	1370(3)	-1047(2)	102(2)
C(1)	4975(2)	4686(2)	1786(1)	49(1)	C(20)	6841(1)	2706(1)	781(1)	29(1)
C(2)	6191(4)	4913(9)	301(10)	82(4)	C(21)	7678(2)	3068(2)	1323(1)	35(1)
C(2')	6095(9)	4641(8)	-34(5)	14(3)	C(22)	8593(2)	3083(2)	1124(1)	47(1)

C(3)	6320(2)	1267(2)	1703(1)	42(1)	C(23)	8702(2)	2737(2)	419(2)	53(1)
C(4)	5563(1)	2023(1)	1314(1)	28(1)	C(24)	7889(2)	2351(2)	-97(1)	51(1)
C(5)	4587(1)	1866(1)	1382(1)	29(1)	C(25)	6945(2)	2328(2)	64(1)	38(1)
C(6)	3686(1)	2258(1)	950(1)	28(1)	C(26)	8393(2)	2904(3)	2764(2)	61(1)
C(7)	2759(2)	1684(2)	998(1)	36(1)	C(27)	7639(2)	3447(2)	2123(1)	42(1)
C(8)	2631(1)	3253(1)	11(1)	30(1)	C(28)	7848(2)	4540(2)	2206(2)	67(1)
C(9)	1908(1)	3752(2)	303(1)	34(1)	C(29)	5973(3)	2323(3)	-1336(2)	83(1)
C(10)	981(2)	3927(2)	-200(1)	43(1)	C(30)	6072(2)	1895(2)	-524(1)	48(1)
C(11)	765(2)	3618(2)	-963(1)	51(1)	C(31)	6176(4)	790(3)	-559(3)	129(2)
C(12)	1485(2)	3141(2)	-1243(1)	51(1)	C(32)	555(4)	5408(5)	3373(3)	119(2)
C(13)	2431(2)	2960(2)	-774(1)	40(1)	C(33)	-124(4)	5486(5)	3959(4)	94(2)
C(14)	2115(2)	5224(2)	1187(2)	55(1)	C(33')	776(9)	4913(10)	4188(8)	87(4)
C(15)	2081(2)	4114(2)	1137(1)	38(1)	C(34)	199(4)	5034(4)	4671(3)	111(2)
C(16)	1260(2)	3757(2)	1526(2)	52(1)					

Table A.3: Anisotropic Displacement Parameters for [1-Me]₂

Atom	U11	U22	U33	U23	U13	U12
Sc(1)	30(1)	22(1)	27(1)	0(1)	8(1)	1(1)
N(1)	27(1)	25(1)	26(1)	2(1)	10(1)	0(1)
N(2)	27(1)	28(1)	27(1)	1(1)	8(1)	1(1)
C(1)	68(2)	43(1)	37(1)	-8(1)	13(1)	4(1)
C(2)	33(2)	76(5)	131(10)	71(6)	6(3)	-2(2)
C(2')	17(4)	21(4)	6(5)	5(3)	6(3)	6(3)
C(3)	39(1)	33(1)	55(1)	17(1)	14(1)	7(1)
C(4)	32(1)	26(1)	26(1)	2(1)	9(1)	2(1)
C(5)	34(1)	27(1)	28(1)	5(1)	11(1)	-1(1)
C(6)	31(1)	26(1)	28(1)	-2(1)	11(1)	-2(1)
C(7)	34(1)	35(1)	41(1)	3(1)	12(1)	-7(1)
C(8)	28(1)	31(1)	31(1)	1(1)	5(1)	0(1)
C(9)	29(1)	37(1)	35(1)	0(1)	8(1)	0(1)
C(10)	30(1)	53(1)	43(1)	2(1)	6(1)	8(1)
C(11)	37(1)	69(2)	42(1)	1(1)	-2(1)	7(1)
C(12)	50(1)	64(2)	32(1)	-5(1)	-3(1)	7(1)
C(13)	43(1)	42(1)	32(1)	-2(1)	5(1)	6(1)
C(14)	47(1)	54(2)	67(2)	-20(1)	19(1)	-2(1)
C(15)	26(1)	51(1)	37(1)	-6(1)	10(1)	5(1)
C(16)	40(1)	76(2)	45(1)	2(1)	18(1)	4(1)
C(17)	65(2)	67(2)	45(1)	-5(1)	19(1)	8(1)
C(18)	59(2)	61(2)	33(1)	-8(1)	6(1)	19(1)
C(19)	183(4)	58(2)	87(2)	16(2)	79(3)	46(2)
C(20)	30(1)	29(1)	32(1)	5(1)	13(1)	3(1)
C(21)	31(1)	41(1)	35(1)	7(1)	12(1)	2(1)
C(22)	30(1)	68(2)	43(1)	12(1)	12(1)	-1(1)
C(23)	35(1)	83(2)	49(1)	12(1)	22(1)	5(1)
C(24)	47(1)	71(2)	41(1)	3(1)	24(1)	9(1)
C(25)	41(1)	41(1)	36(1)	1(1)	17(1)	3(1)
C(26)	47(1)	98(2)	37(1)	15(1)	7(1)	2(1)
C(27)	32(1)	58(1)	34(1)	-1(1)	6(1)	-1(1)
C(28)	63(2)	65(2)	65(2)	-18(1)	-1(1)	-2(1)
C(29)	70(2)	130(3)	45(2)	6(2)	4(1)	-24(2)

C(30)	53(1)	53(1)	41(1)	-14(1)	19(1)	-4(1)
C(31)	154(5)	58(2)	142(4)	-32(2)	-33(4)	-3(2)
C(32)	113(4)	153(5)	92(3)	-19(3)	27(3)	-32(3)
C(33)	68(3)	112(5)	89(4)	-14(4)	-5(3)	-18(3)
C(33')	74(8)	92(9)	99(10)	-19(7)	32(7)	0(6)
C(34)	127(4)	109(3)	98(3)	-33(3)	26(3)	-51(3)

Table A.4: Bond Lengths [Å] for [1-Me]₂

Sc(1)-C(1)	2.208(2)	C(6)-C(7)	1.520(3)	C(21)-C(22)	1.389(3)
Sc(1)-N(1)	2.2230(15)	C(8)-C(9)	1.404(3)	C(21)-C(27)	1.522(3)
Sc(1)-N(2)	2.2230(16)	C(8)-C(13)	1.411(3)	C(22)-C(23)	1.377(4)
Sc(1)-C(2)	2.303(5)	C(9)-C(10)	1.395(3)	C(23)-C(24)	1.374(4)
Sc(1)-C(2')#1	2.305(10)	C(9)-C(15)	1.525(3)	C(24)-C(25)	1.397(3)
Sc(1)-C(2')	2.364(10)	C(10)-C(11)	1.382(3)	C(25)-C(30)	1.515(3)
Sc(1)-C(2)#1	2.372(6)	C(11)-C(12)	1.375(4)	C(26)-C(27)	1.538(3)
Sc(1)-Sc(1)#1	3.3973(7)	C(12)-C(13)	1.394(3)	C(27)-C(28)	1.523(4)
N(1)-C(4)	1.340(2)	C(13)-C(18)	1.530(3)	C(29)-C(30)	1.530(4)
N(1)-C(20)	1.449(2)	C(14)-C(15)	1.520(3)	C(30)-C(31)	1.521(5)
N(2)-C(6)	1.339(2)	C(15)-C(16)	1.538(3)	C(32)-C(33)	1.559(8)
N(2)-C(8)	1.451(2)	C(17)-C(18)	1.524(4)	C(32)-C(33')	1.560(14)
C(3)-C(4)	1.515(3)	C(18)-C(19)	1.496(4)	C(33)-C(34)	1.382(8)
C(4)-C(5)	1.395(3)	C(20)-C(21)	1.405(3)	C(33')-C(34)	1.309(12)
C(5)-C(6)	1.403(3)	C(20)-C(25)	1.411(3)	C(34)-C(34)#2	1.407(9)

Table A.5: Bond Angles [°] for [1-Me]₂

C(1)-Sc(1)-N(1)	100.63(8)	C(4)-N(1)-C(20)	116.92(15)	C(19)-C(18)-C(17)	109.4(2)
C(1)-Sc(1)-N(2)	101.10(8)	C(4)-N(1)-Sc(1)	120.40(12)	C(19)-C(18)-C(13)	111.9(3)
N(1)-Sc(1)-N(2)	85.46(6)	C(20)-N(1)-Sc(1)	122.23(11)	C(17)-C(18)-C(13)	113.1(2)
C(1)-Sc(1)-C(2)	99.9(5)	C(6)-N(2)-C(8)	115.97(15)	C(21)-C(20)-C(25)	120.25(18)
N(1)-Sc(1)-C(2)	90.4(2)	C(6)-N(2)-Sc(1)	120.67(12)	C(21)-C(20)-N(1)	121.66(17)
N(2)-Sc(1)-C(2)	159.0(5)	C(8)-N(2)-Sc(1)	122.90(12)	C(25)-C(20)-N(1)	117.98(17)
C(1)-Sc(1)-C(2')#1	91.8(2)	N(1)-C(4)-C(5)	124.57(17)	C(22)-C(21)-C(20)	118.7(2)
N(1)-Sc(1)-C(2')#1	167.4(2)	N(1)-C(4)-C(3)	119.90(17)	C(22)-C(21)-C(27)	117.8(2)
N(2)-Sc(1)-C(2')#1	93.9(3)	C(5)-C(4)-C(3)	115.50(17)	C(20)-C(21)-C(27)	123.57(18)
C(2)-Sc(1)-C(2')#1	85.7(3)	C(4)-C(5)-C(6)	129.96(17)	C(23)-C(22)-C(21)	121.7(2)
C(1)-Sc(1)-C(2')	116.7(3)	N(2)-C(6)-C(5)	124.57(17)	C(24)-C(23)-C(22)	119.3(2)
N(1)-Sc(1)-C(2')	86.3(2)	N(2)-C(6)-C(7)	120.51(17)	C(23)-C(24)-C(25)	121.7(2)
N(2)-Sc(1)-C(2')	142.2(3)	C(5)-C(6)-C(7)	114.87(17)	C(24)-C(25)-C(20)	118.3(2)
C(2)-Sc(1)-C(2')	16.8(4)	C(9)-C(8)-C(13)	120.78(18)	C(24)-C(25)-C(30)	119.7(2)
C(2')#1-Sc(1)-C(2')	86.6(4)	C(9)-C(8)-N(2)	121.08(17)	C(20)-C(25)-C(30)	122.06(19)
C(1)-Sc(1)-C(2)#1	108.2(5)	C(13)-C(8)-N(2)	118.11(17)	C(28)-C(27)-C(21)	112.1(2)
N(1)-Sc(1)-C(2)#1	151.1(5)	C(10)-C(9)-C(8)	118.04(19)	C(28)-C(27)-C(26)	108.8(2)
N(2)-Sc(1)-C(2)#1	86.95(19)	C(10)-C(9)-C(15)	118.28(18)	C(21)-C(27)-C(26)	111.0(2)
C(2)-Sc(1)-C(2)#1	86.79(18)	C(8)-C(9)-C(15)	123.68(18)	C(25)-C(30)-C(31)	110.4(3)
C(2')#1-Sc(1)-C(2)#1	16.8(4)	C(11)-C(10)-C(9)	121.8(2)	C(25)-C(30)-C(29)	112.2(2)
C(2')-Sc(1)-C(2)#1	82.8(3)	C(12)-C(11)-C(10)	119.5(2)	C(31)-C(30)-C(29)	109.3(3)
C(1)-Sc(1)-Sc(1)#1	109.51(7)	C(11)-C(12)-C(13)	121.4(2)	C(33)-C(32)-C(33')	55.1(5)
N(1)-Sc(1)-Sc(1)#1	128.07(4)	C(12)-C(13)-C(8)	118.5(2)	C(34)-C(33)-C(32)	117.6(5)
N(2)-Sc(1)-Sc(1)#1	126.57(4)	C(12)-C(13)-C(18)	120.3(2)	C(34)-C(33')-C(32)	122.4(10)

C(2)-Sc(1)-Sc(1)#1	44.20(15)	C(8)-C(13)-C(18)	121.22(19)	C(33')-C(34)-C(33)	64.8(7)
C(2')#1-Sc(1)-Sc(1)#1	44.0(2)	C(14)-C(15)-C(9)	112.1(2)	C(33')-C(34)-C(34)2	162.0(10)
C(2'')-Sc(1)-Sc(1)#1	42.6(2)	C(14)-C(15)-C(16)	107.9(2)	C(33)-C(34)-C(34)2	133.1(8)
C(2)#1-Sc(1)-Sc(1)#1	42.60(11)	C(9)-C(15)-C(16)	111.68(18)		

Table A.6: Crystal Data and Structure Refinement for **2-Et****A. Crystal Data**

Crystallographer	Masood Parvez	University of Calgary
Empirical Formula	C ₃₉ H ₆₃ N ₂ Sc	
Formula Weight	604.9	
Crystal Dimensions (mm)	0.43 × 0.40 × 0.38	
Crystal System	monoclinic	
Space Group	<i>P</i> 2 ₁ / <i>n</i> (#14)	
Lattice Parameters		
	<i>a</i> (Å)	18.759(5)
	<i>b</i> (Å)	10.427(6)
	<i>c</i> (Å)	19.608(5)
	<i>β</i> (deg)	107.32(2)
	<i>V</i> (Å ³)	3661.4(28)
	<i>Z</i>	4
<i>D</i> _{calc}	1.097g/cm ³	
<i>μ</i> (MoK α)	2.25cm ⁻¹	

B. Data Collection and Refinement Conditions

Diffractionmeter	Rigaku AFC6S
Radiation (λ [Å])	Graphite-monochromated Mo K α (0.71069)
Temperature (°C)	-103 °C
Total Reflections	7115
Unique Reflections	6893 (<i>R</i> _{int} = 0.097)
Corrections	Lorentz-polarization Absorption (trans Factors: 0.9243 – 1.000) Decay (1.02%)
Structure Solution	Direct Methods
Refinement	Full-Matrix-Least-Squares
No. Observations	2654
No. Variables	379
Reflection/Parameter Ratio	7
Residuals: <i>R</i> ; <i>R</i> _w	0.052; 0.054
Goodness of Fit Indicator	1.89

Largest Difference Peak & Hole 0.29 and $-0.36 \text{ e } \text{\AA}^{-3}$

Table A.7: Atomic Coordinates and Equivalent Isotropic Displacement Parameters for **2-Et**

1-Me	<i>x</i>	<i>y</i>	<i>z</i>	<i>U</i> _{eq} , \AA^2
Sc(1)	0.50790(6)	-0.00902(11)	0.24371(6)	0.0267(3)
N(1)	0.4303(2)	0.1298(5)	0.1861(2)	0.0246(15)
N(2)	0.5674(2)	0.1236(5)	0.3219(2)	0.0238(14)
C(1)	0.5763(3)	-0.0892(7)	0.1774(3)	0.044(2)
C(2)	0.4497(4)	-0.1464(6)	0.2940(3)	0.042(2)
C(3)	0.4488(3)	0.3116(6)	0.1041(3)	0.0334(19)
C(4)	0.4713(3)	0.2210(6)	0.1702(3)	0.0245(17)
C(5)	0.5461(3)	0.2427(6)	0.2130(3)	0.0269(17)
C(6)	0.5895(3)	0.2140(6)	0.2842(3)	0.0254(17)
C(7)	0.6656(3)	0.2883(6)	0.3083(3)	0.0341(19)
C(8)	0.3502(3)	0.1158(6)	0.1553(3)	0.0253(17)
C(9)	0.3218(3)	0.0204(6)	0.1032(3)	0.0304(18)
C(10)	0.2444(3)	0.0106(7)	0.0743(3)	0.0380(19)
C(11)	0.1969(3)	0.0892(6)	0.0961(3)	0.036(2)
C(12)	0.2249(3)	0.1765(6)	0.1502(3)	0.0340(19)
C(13)	0.3018(3)	0.1896(6)	0.1813(3)	0.0279(18)
C(14)	0.3050(4)	0.2349(8)	0.3071(3)	0.061(3)
C(15)	0.3304(3)	0.2834(7)	0.2439(3)	0.037(2)
C(16)	0.3024(4)	0.4202(7)	0.2257(4)	0.060(3)
C(17)	0.3562(4)	-0.2080(7)	0.0921(4)	0.066(3)
C(18)	0.3702(4)	-0.0705(7)	0.0760(4)	0.047(2)
C(19)	0.3586(4)	-0.0550(8)	-0.0046(4)	0.072(3)
C(20)	0.5960(3)	0.1002(6)	0.3984(3)	0.0249(17)
C(21)	0.6518(3)	0.0068(6)	0.4235(3)	0.0314(17)
C(22)	0.6773(3)	-0.0176(7)	0.4979(3)	0.042(2)
C(23)	0.6482(4)	0.0481(7)	0.5434(3)	0.045(2)
C(24)	0.5913(4)	0.1352(6)	0.5174(3)	0.040(2)
C(25)	0.5638(3)	0.1637(6)	0.4447(3)	0.0305(19)
C(26)	0.4542(4)	0.2728(8)	0.4727(4)	0.060(3)
C(27)	0.4979(3)	0.2545(6)	0.4188(3)	0.038(2)
C(28)	0.5193(4)	0.3852(7)	0.3967(4)	0.061(3)
C(29)	0.7722(4)	-0.0679(7)	0.3995(4)	0.059(3)
C(30)	0.6863(4)	-0.0716(6)	0.3760(3)	0.041(2)
C(31)	0.6594(4)	-0.2104(7)	0.3717(4)	0.061(3)
C(32)	0.7065(3)	0.2904(7)	0.3895(3)	0.050(2)
C(33)	0.6559(4)	0.4307(7)	0.2856(4)	0.056(2)
C(34)	0.7163(3)	0.2223(7)	0.2707(4)	0.052(2)
C(35)	0.4965(4)	0.2742(8)	0.0553(3)	0.065(3)
C(36)	0.4651(4)	0.4518(7)	0.1262(4)	0.068(3)
C(37)	0.3680(4)	0.3071(7)	0.0573(3)	0.050(2)
C(38)	0.5709(4)	-0.2292(8)	0.1592(4)	0.072(3)
C(39)	0.4528(4)	-0.2926(7)	0.2945(4)	0.056(3)

Table A.8: Anisotropic Displacement Parameters for **2-Et**

Atom	<i>U</i> 11	<i>U</i> 22	<i>U</i> 33	<i>U</i> 23	<i>U</i> 13	<i>U</i> 12
Sc(1)	0.0258(6)	0.0264(7)	0.0251(6)	0.0018(7)	0.0032(4)	-0.0006(7)
N(1)	0.024(3)	0.025(3)	0.024(3)	-0.001(3)	0.006(2)	-0.002(2)
N(2)	0.026(3)	0.028(3)	0.015(3)	0.003(3)	0.002(2)	-0.001(2)
C(1)	0.029(4)	0.052(5)	0.041(4)	0.013(4)	-0.005(3)	-0.011(4)
C(2)	0.042(4)	0.039(5)	0.041(4)	0.001(4)	0.005(3)	0.004(4)
C(3)	0.027(4)	0.039(4)	0.033(4)	0.002(3)	0.006(3)	0.012(3)
C(4)	0.028(3)	0.026(4)	0.022(3)	0.003(3)	0.012(3)	0.003(3)
C(5)	0.028(3)	0.029(4)	0.022(3)	-0.004(3)	0.006(3)	0.008(3)
C(6)	0.023(3)	0.024(4)	0.029(3)	0.003(3)	0.006(3)	0.001(3)
C(7)	0.024(4)	0.038(4)	0.037(4)	-0.009(3)	0.004(3)	0.006(3)
C(8)	0.021(3)	0.025(4)	0.028(3)	-0.002(3)	0.004(3)	0.002(3)
C(9)	0.030(3)	0.029(4)	0.030(3)	0.002(3)	0.005(3)	0.000(3)
C(10)	0.026(3)	0.044(4)	0.036(4)	-0.003(4)	-0.002(3)	-0.005(4)
C(11)	0.023(4)	0.041(5)	0.040(4)	0.002(3)	0.004(3)	0.000(4)
C(12)	0.028(4)	0.036(4)	0.036(4)	0.002(3)	0.006(3)	-0.002(3)
C(13)	0.027(4)	0.034(4)	0.023(3)	0.001(3)	0.008(3)	0.002(3)
C(14)	0.063(5)	0.087(6)	0.034(4)	-0.009(5)	0.016(4)	-0.017(4)
C(15)	0.029(4)	0.047(5)	0.037(4)	0.005(3)	0.009(3)	-0.010(4)
C(16)	0.065(5)	0.045(5)	0.066(6)	0.004(4)	0.011(4)	-0.021(4)
C(17)	0.067(5)	0.045(5)	0.073(6)	0.022(4)	-0.001(4)	-0.013(5)
C(18)	0.038(4)	0.046(5)	0.048(5)	0.003(4)	-0.003(4)	-0.019(4)
C(19)	0.069(6)	0.088(7)	0.067(6)	0.018(5)	0.031(5)	-0.010(5)
C(20)	0.026(3)	0.030(4)	0.016(3)	-0.006(3)	0.003(3)	-0.001(3)
C(21)	0.033(3)	0.031(4)	0.026(3)	0.001(4)	0.002(3)	-0.009(4)
C(22)	0.047(4)	0.038(5)	0.031(4)	0.008(4)	-0.003(3)	0.003(4)
C(23)	0.058(5)	0.044(5)	0.023(4)	0.000(4)	-0.002(3)	0.004(3)
C(24)	0.053(5)	0.042(5)	0.025(4)	-0.003(4)	0.013(3)	-0.005(4)
C(25)	0.035(4)	0.032(4)	0.024(4)	-0.005(3)	0.008(3)	0.000(3)
C(26)	0.048(5)	0.084(6)	0.051(5)	0.011(5)	0.021(4)	-0.014(5)
C(27)	0.038(4)	0.043(5)	0.028(4)	0.007(4)	0.003(3)	-0.012(3)
C(28)	0.088(6)	0.048(5)	0.051(5)	0.027(5)	0.024(5)	0.007(4)
C(29)	0.041(4)	0.073(6)	0.055(5)	0.013(4)	0.004(4)	-0.006(4)
C(30)	0.042(4)	0.038(5)	0.035(4)	0.009(4)	-0.001(3)	-0.003(3)
C(31)	0.050(5)	0.063(6)	0.064(5)	0.006(4)	0.005(4)	-0.027(5)
C(32)	0.040(4)	0.059(5)	0.040(4)	-0.022(4)	-0.006(3)	0.006(4)
C(33)	0.047(5)	0.052(5)	0.060(5)	-0.023(4)	0.001(4)	0.003(4)
C(34)	0.028(4)	0.068(6)	0.056(5)	-0.010(4)	0.006(4)	0.011(4)
C(35)	0.054(5)	0.114(7)	0.031(4)	0.016(5)	0.017(4)	0.028(5)
C(36)	0.071(6)	0.041(5)	0.075(6)	-0.001(4)	-0.003(5)	0.021(4)
C(37)	0.042(4)	0.067(6)	0.034(4)	0.007(4)	0.000(3)	0.021(4)
C(38)	0.043(5)	0.084(7)	0.081(6)	-0.003(5)	0.009(4)	-0.028(5)
C(39)	0.046(5)	0.047(5)	0.076(6)	-0.001(4)	0.019(4)	0.010(4)

Table A.9: Bond Lengths (Å) for **2-Et**

Sc(1)	N(2)	2.118(5)	C(5)	C(6)	1.422(7)	C(17)	C(18)	1.508(10)
Sc(1)	N(1)	2.124(5)	C(6)	C(7)	1.568(7)	C(18)	C(19)	1.538(9)
Sc(1)	C(2)	2.204(7)	C(7)	C(32)	1.548(8)	C(20)	C(21)	1.408(7)

Sc(1)	C(1)	2.243(6)	C(7)	C(33)	1.544(9)	C(20)	C(25)	1.397(7)
N(1)	C(4)	1.317(6)	C(7)	C(34)	1.530(8)	C(21)	C(22)	1.416(7)
N(1)	C(8)	1.451(6)	C(8)	C(9)	1.411(7)	C(21)	C(30)	1.521(8)
N(2)	C(20)	1.456(6)	C(8)	C(13)	1.396(7)	C(22)	C(23)	1.360(8)
N(2)	C(6)	1.338(7)	C(9)	C(10)	1.395(7)	C(23)	C(24)	1.378(8)
C(1)	C(38)	1.499(10)	C(9)	C(18)	1.516(8)	C(24)	C(25)	1.395(7)
C(2)	C(39)	1.526(9)	C(10)	C(11)	1.370(8)	C(25)	C(27)	1.520(8)
C(3)	C(4)	1.558(7)	C(11)	C(12)	1.378(8)	C(26)	C(27)	1.530(8)
C(3)	C(35)	1.542(8)	C(12)	C(13)	1.396(7)	C(27)	C(28)	1.520(9)
C(3)	C(36)	1.530(9)	C(13)	C(15)	1.536(8)	C(29)	C(30)	1.539(8)
C(3)	C(37)	1.520(8)	C(14)	C(15)	1.539(8)	C(30)	C(31)	1.528(9)
C(4)	C(5)	1.421(7)	C(15)	C(16)	1.526(9)			

Table A.10: Bond Angles (°) for 2-Et

N(1)	Sc(1)	N(2)	94.00(16)	C(9)	C(10)	C(11)	121.6(6)
N(1)	Sc(1)	C(1)	111.4(2)	C(9)	C(18)	C(17)	111.1(6)
N(1)	Sc(1)	C(2)	109.2(2)	C(9)	C(18)	C(19)	112.3(6)
N(1)	C(4)	C(3)	126.9(5)	C(10)	C(9)	C(18)	118.1(6)
N(1)	C(4)	C(5)	121.2(5)	C(10)	C(11)	C(12)	120.1(5)
N(1)	C(8)	C(9)	119.5(5)	C(11)	C(12)	C(13)	120.5(6)
N(1)	C(8)	C(13)	119.9(5)	C(12)	C(13)	C(15)	118.7(5)
N(2)	C(6)	C(5)	120.5(5)	C(13)	C(8)	C(9)	120.4(5)
N(2)	C(6)	C(7)	125.9(5)	C(13)	C(15)	C(14)	108.5(5)
N(2)	Sc(1)	C(1)	113.2(2)	C(13)	C(15)	C(16)	113.2(5)
N(2)	Sc(1)	C(2)	108.9(2)	C(14)	C(15)	C(15)	109.2(6)
N(2)	C(20)	C(21)	118.9(5)	C(17)	C(18)	C(19)	109.6(6)
N(2)	C(20)	C(25)	119.5(5)	C(20)	C(25)	C(24)	117.6(6)
Sc(1)	N(1)	C(4)	105.2(3)	C(20)	C(25)	C(27)	122.9(5)
Sc(1)	N(1)	C(8)	127.8(4)	C(20)	C(21)	C(22)	118.2(5)
Sc(1)	C(2)	C(39)	129.0(5)	C(20)	C(21)	C(27)	124.4(5)
Sc(1)	C(1)	C(38)	119.4(5)	C(21)	C(22)	C(23)	120.4(6)
Sc(1)	N(2)	C(20)	126.1(4)	C(21)	C(30)	C(29)	113.6(5)
Sc(1)	N(2)	C(6)	104.1(3)	C(21)	C(30)	C(31)	110.4(6)
C(2)	Sc(1)	C(1)	117.5(3)	C(22)	C(23)	C(24)	120.4(6)
C(3)	C(4)	C(5)	111.8(5)	C(22)	C(21)	C(27)	117.4(6)
C(4)	C(5)	C(6)	136.3(5)	C(23)	C(24)	C(25)	121.9(6)
C(4)	C(3)	C(35)	107.4(5)	C(24)	C(25)	C(27)	119.4(6)
C(4)	C(3)	C(36)	111.2(5)	C(25)	C(27)	C(28)	113.3(5)
C(4)	C(3)	C(37)	117.3(5)	C(25)	C(27)	C(26)	113.4(5)
C(4)	N(1)	C(8)	125.5(5)	C(25)	C(20)	C(21)	121.4(5)
C(5)	C(6)	C(7)	113.3(5)	C(26)	C(27)	C(28)	109.0(6)
C(6)	C(7)	C(32)	116.4(5)	C(29)	C(30)	C(31)	109.8(6)
C(6)	C(7)	C(33)	111.7(5)	C(33)	C(7)	C(32)	105.2(5)
C(6)	C(7)	C(34)	105.8(5)	C(33)	C(7)	C(34)	109.3(6)
C(6)	N(2)	C(20)	127.4(5)	C(34)	C(7)	C(32)	108.2(5)
C(8)	C(9)	C(10)	117.9(6)	C(35)	C(3)	C(37)	106.1(5)
C(8)	C(9)	C(18)	124.0(5)	C(36)	C(3)	C(37)	106.3(6)
C(8)	C(13)	C(12)	119.1(5)	C(36)	C(3)	C(35)	108.2(6)
C(8)	C(13)	C(15)	122.2(5)				

Table A.11: Crystal Data and Structure Refinement for **2-CH₂Ph**

A. Crystal Data		
Crystallographer	Masood Parvez	University of Calgary
Empirical Formula	C ₄₉ H ₆₇ N ₂ Sc	
Formula Weight	729.01	
Crystal Dimensions (mm)	0.38 × 0.30 × 0.24	
Crystal System	monoclinic	
Space group	<i>P</i> 2 ₁ / <i>c</i> (#14)	
Lattice Parameters		
	<i>a</i> (Å)	12.653(4)
	<i>b</i> (Å)	12.096(3)
	<i>c</i> (Å)	28.069(4)
	β (deg)	90.77(2)
	<i>V</i> (Å ³)	4295.5(17)
	<i>Z</i>	4
<i>D</i> _{calc}	1.127g/cm ³	
μ (MoK α)	0.205mm ⁻¹	
B. Data Collection and Refinement Conditions		
Diffractometer	Rigaku AFC6S	
Radiation (λ [Å])	Graphite-monochromated Mo K α (0.71069)	
Temperature (°C)	-103 °C	
Total Reflections	7907	
Unique Reflections	7607 (<i>R</i> _{int} = 0.0848)	
Structure Solution	Direct Methods	
Refinement	Full-Matrix-Least-Squares	
No. Observations	2654	
No. Variables	379	
Reflection/Parameter Ratio	7	
Residuals: <i>R</i> ; <i>R</i> _w	0.0629; 0.01358	
Goodness of Fit Indicator	1.02	
Largest Difference Peak & Hole	0.252 and -0.306 e Å ⁻³	

Table A.12: Atomic Coordinates and Equivalent Isotropic Displacement Parameters for **2-CH₂Ph**

Atom	<i>x</i>	<i>y</i>	<i>z</i>	<i>U</i> _{eq} , Å ²
Sc1	0.15346(10)	0.22554(11)	0.10583(5)	0.0425(4)
N1	0.3026(4)	0.2779(5)	0.13261(18)	0.0389(14)
N2	0.0671(4)	0.3381(4)	0.14634(17)	0.0337(14)
C1	0.1254(6)	0.0625(6)	0.1383(3)	0.059(2)
C2	0.1033(5)	0.2381(6)	0.0283(2)	0.0408(18)
C3	0.4068(5)	0.4609(6)	0.1247(3)	0.048(2)

C4	0.3063(5)	0.3863(6)	0.1262(2)	0.0414(18)
C5	0.2108(5)	0.4471(6)	0.1178(2)	0.0420(19)
C6	0.1050(5)	0.4368(6)	0.1308(2)	0.0367(18)
C7	0.0366(5)	0.5420(6)	0.1207(2)	0.046(2)
C8	0.3905(5)	0.2036(6)	0.1425(3)	0.0412(19)
C9	0.4431(5)	0.1574(6)	0.1034(3)	0.045(2)
C10	0.5247(5)	0.0823(6)	0.1130(3)	0.054(2)
C11	0.5518(6)	0.0541(7)	0.1589(3)	0.064(2)
C12	0.4965(6)	0.0969(7)	0.1964(3)	0.061(2)
C13	0.4128(5)	0.1705(6)	0.1899(3)	0.047(2)
C14	0.4175(7)	0.2904(7)	0.2627(3)	0.094(3)
C15	0.3525(6)	0.2120(7)	0.2320(3)	0.059(2)
C16	0.3129(6)	0.1158(7)	0.2621(3)	0.077(3)
C17	0.3717(5)	0.0791(6)	0.0271(2)	0.062(2)
C18	0.4170(5)	0.1819(6)	0.0516(2)	0.047(2)
C19	0.5119(5)	0.2244(7)	0.0233(2)	0.067(2)
C20	-0.0250(5)	0.3257(5)	0.1753(2)	0.0393(18)
C21	-0.1181(5)	0.2777(6)	0.1569(2)	0.0488(19)
C22	-0.2053(5)	0.2696(6)	0.1864(3)	0.052(2)
C23	-0.2010(6)	0.3033(6)	0.2330(3)	0.058(2)
C24	-0.1077(6)	0.3454(6)	0.2512(3)	0.057(2)
C25	-0.0178(5)	0.3543(6)	0.2238(2)	0.0434(19)
C26	0.1135(7)	0.3278(8)	0.2906(3)	0.101(3)
C27	0.0850(6)	0.3940(7)	0.2465(3)	0.056(2)
C28	0.0835(7)	0.5150(7)	0.2604(3)	0.097(3)
C29	-0.1645(6)	0.1191(7)	0.1018(3)	0.072(3)
C30	-0.1305(5)	0.2407(6)	0.1053(3)	0.055(2)
C31	-0.2088(7)	0.3117(7)	0.0774(3)	0.092(3)
C32	0.0236(6)	0.5484(7)	0.0662(2)	0.079(3)
C33	-0.0739(5)	0.5477(6)	0.1434(2)	0.053(2)
C34	0.0947(6)	0.6476(6)	0.1378(3)	0.075(3)
C35	0.3915(6)	0.5564(6)	0.1602(3)	0.073(3)
C36	0.5121(5)	0.4047(6)	0.1382(3)	0.061(2)
C37	0.4175(5)	0.5072(6)	0.0739(3)	0.064(2)
C38	0.1739(7)	-0.0297(7)	0.1143(3)	0.058(2)
C39	0.1231(6)	-0.0752(7)	0.0737(3)	0.069(3)
C40	0.1687(9)	-0.1566(8)	0.0466(3)	0.086(3)
C41	0.2661(9)	-0.1996(8)	0.0590(4)	0.089(3)
C42	0.3197(7)	-0.1585(8)	0.0992(4)	0.082(3)
C43	0.2718(7)	-0.0753(7)	0.1267(3)	0.066(2)
C44	0.1713(6)	0.2589(7)	-0.0124(3)	0.054(2)
C45	0.1845(6)	0.1811(7)	-0.0490(3)	0.067(2)
C46	0.2532(8)	0.1987(9)	-0.0863(3)	0.086(3)
C47	0.3098(7)	0.2956(11)	-0.0898(4)	0.097(4)
C48	0.2963(7)	0.3731(9)	-0.0547(3)	0.085(3)
C49	0.2302(6)	0.3565(7)	-0.0171(3)	0.061(2)

Table A.13: Anisotropic Displacement Parameters for 2-CH₂Ph

Atom	<i>U</i> 11	<i>U</i> 22	<i>U</i> 33	<i>U</i> 23	<i>U</i> 13	<i>U</i> 12
Sc1	0.0364(8)	0.0462(8)	0.0447(9)	-0.0056(8)	0.0003(6)	0.0002(8)
N1	0.037(3)	0.037(4)	0.043(4)	0.000(3)	0.003(3)	0.005(3)
N2	0.028(3)	0.040(4)	0.033(3)	0.002(3)	0.006(3)	-0.002(3)
C1	0.043(5)	0.049(5)	0.085(7)	0.000(5)	0.002(4)	-0.002(4)
C2	0.038(4)	0.049(5)	0.035(4)	-0.002(4)	0.006(3)	0.002(4)
C3	0.041(5)	0.053(5)	0.050(5)	0.005(4)	-0.003(4)	-0.009(4)
C4	0.044(5)	0.045(5)	0.035(4)	-0.001(4)	-0.002(4)	-0.001(4)
C5	0.046(5)	0.037(5)	0.043(5)	0.005(4)	-0.001(4)	-0.003(4)
C6	0.044(5)	0.043(5)	0.023(4)	0.000(4)	0.001(3)	-0.001(4)
C7	0.055(5)	0.038(5)	0.046(5)	0.000(4)	0.010(4)	0.011(4)
C8	0.030(4)	0.038(5)	0.055(5)	0.010(4)	-0.003(4)	-0.007(4)
C9	0.030(4)	0.057(5)	0.047(5)	0.010(4)	-0.003(4)	-0.001(4)
C10	0.041(5)	0.059(6)	0.062(6)	0.003(5)	0.006(4)	0.009(4)
C11	0.045(5)	0.070(6)	0.078(7)	0.018(6)	-0.001(5)	0.014(5)
C12	0.056(5)	0.071(6)	0.056(6)	0.016(5)	-0.014(4)	0.008(5)
C13	0.038(5)	0.053(5)	0.049(5)	0.008(4)	-0.013(4)	-0.001(4)
C14	0.139(9)	0.073(7)	0.072(6)	-0.007(6)	0.005(6)	-0.023(7)
C15	0.065(5)	0.063(6)	0.049(5)	0.003(5)	0.000(4)	0.005(5)
C16	0.080(6)	0.088(7)	0.065(6)	0.011(6)	0.009(5)	-0.002(6)
C17	0.059(5)	0.078(6)	0.050(5)	0.000(5)	0.004(4)	0.001(5)
C18	0.038(4)	0.052(5)	0.051(5)	0.003(4)	0.003(4)	0.010(4)
C19	0.053(5)	0.082(6)	0.067(6)	0.020(5)	0.017(4)	0.004(5)
C20	0.035(4)	0.038(4)	0.045(5)	-0.003(4)	0.010(4)	0.003(3)
C21	0.043(5)	0.050(5)	0.054(5)	-0.003(5)	0.006(4)	0.009(4)
C22	0.035(4)	0.051(5)	0.070(6)	-0.008(5)	0.010(4)	0.001(4)
C23	0.050(5)	0.068(6)	0.056(6)	0.004(5)	0.028(4)	0.003(5)
C24	0.064(6)	0.057(6)	0.051(5)	-0.007(4)	0.020(5)	0.002(5)
C25	0.052(5)	0.041(5)	0.038(5)	0.005(4)	0.019(4)	0.002(4)
C26	0.098(8)	0.104(8)	0.100(8)	0.028(7)	-0.033(6)	-0.006(6)
C27	0.057(5)	0.073(6)	0.038(5)	-0.015(5)	0.013(4)	-0.013(5)
C28	0.118(8)	0.083(8)	0.091(8)	0.000(6)	-0.010(6)	-0.039(6)
C29	0.060(5)	0.086(7)	0.069(6)	-0.020(5)	0.004(5)	-0.003(5)
C30	0.041(4)	0.061(6)	0.062(5)	-0.016(5)	-0.006(4)	-0.003(4)
C31	0.094(7)	0.096(8)	0.085(7)	-0.013(6)	-0.041(6)	0.004(6)
C32	0.091(7)	0.099(7)	0.048(6)	0.016(5)	0.000(5)	0.048(6)
C33	0.042(5)	0.049(5)	0.069(6)	-0.001(4)	0.011(4)	0.011(4)
C34	0.078(6)	0.047(6)	0.100(7)	0.004(5)	0.041(5)	0.016(5)
C35	0.067(6)	0.066(6)	0.087(7)	-0.009(5)	-0.019(5)	-0.014(5)
C36	0.036(5)	0.063(6)	0.083(6)	0.003(5)	-0.007(4)	-0.014(4)
C37	0.048(5)	0.067(6)	0.078(6)	0.018(5)	0.008(4)	-0.012(4)
C38	0.073(7)	0.048(6)	0.053(6)	0.010(5)	0.001(5)	-0.025(5)
C39	0.057(6)	0.062(6)	0.090(7)	-0.004(6)	0.012(5)	0.000(5)
C40	0.099(8)	0.078(8)	0.082(8)	0.002(6)	0.018(6)	-0.014(6)
C41	0.103(9)	0.067(8)	0.099(9)	0.009(7)	0.030(7)	0.000(7)
C42	0.071(7)	0.062(7)	0.114(9)	0.022(6)	0.019(7)	0.001(6)
C43	0.065(6)	0.060(6)	0.071(6)	0.015(6)	0.000(5)	-0.007(5)
C44	0.050(5)	0.068(7)	0.042(5)	0.006(5)	-0.011(4)	0.007(5)
C45	0.069(6)	0.081(7)	0.051(6)	-0.012(5)	-0.005(5)	0.008(5)

C46	0.087(8)	0.125(10)	0.046(6)	-0.018(6)	-0.004(5)	0.036(7)
C47	0.068(7)	0.159(13)	0.063(7)	0.026(8)	0.020(5)	0.017(8)
C48	0.061(6)	0.129(10)	0.065(7)	0.019(7)	0.006(5)	-0.005(6)
C49	0.054(5)	0.070(7)	0.058(6)	0.006(5)	-0.007(4)	0.001(5)

Table A.14: Bond Lengths (Å) for 2-CH₂Ph

Sc1	N2	2.091(5)	C7	C32	1.539(9)	C23	C24	1.378(9)
Sc1	N1	2.118(5)	C7	C33	1.545(8)	C24	C25	1.388(9)
Sc1	C1	2.203(7)	C7	C34	1.548(9)	C25	C27	1.518(9)
Sc1	C2	2.265(6)	C8	C9	1.406(9)	C26	C27	1.515(10)
Sc1	C6	2.722(7)	C8	C13	1.413(9)	C27	C28	1.514(10)
Sc1	C5	2.796(7)	C9	C10	1.398(9)	C29	C30	1.535(9)
Sc1	C4	2.796(7)	C9	C18	1.517(9)	C30	C31	1.519(9)
N1	C4	1.325(8)	C10	C11	1.374(9)	C38	C43	1.395(10)
N1	C8	1.454(8)	C11	C12	1.372(9)	C38	C39	1.412(10)
N2	C6	1.361(8)	C12	C13	1.393(9)	C39	C40	1.375(11)
N2	C20	1.438(7)	C13	C15	1.502(9)	C40	C41	1.379(11)
C1	C38	1.443(10)	C14	C15	1.516(9)	C41	C42	1.398(12)
C2	C44	1.460(8)	C15	C16	1.527(9)	C42	C43	1.410(11)
C3	C36	1.539(9)	C17	C18	1.530(9)	C44	C45	1.405(9)
C3	C37	1.540(9)	C18	C19	1.536(8)	C44	C49	1.403(10)
C3	C35	1.540(9)	C20	C25	1.406(8)	C45	C46	1.386(11)
C3	C4	1.560(9)	C20	C21	1.406(9)	C46	C47	1.378(12)
C4	C5	1.431(9)	C21	C22	1.391(8)	C47	C48	1.373(12)
C5	C6	1.399(8)	C21	C30	1.523(9)	C48	C49	1.370(10)
C6	C7	1.562(9)	C22	C23	1.370(9)			

Table A.15: Bond Angles (°) for 2-CH₂Ph

N2	Sc1	N1	94.7(2)	C33	C7	C6	117.6(6)
N2	Sc1	C1	105.7(3)	C34	C7	C6	110.9(6)
N1	Sc1	C1	105.6(3)	C9	C8	C13	122.0(7)
N2	Sc1	C2	109.7(2)	C9	C8	N1	117.7(6)
N1	Sc1	C2	123.9(2)	C13	C8	N1	119.8(6)
C1	Sc1	C2	114.4(3)	C10	C9	C8	117.7(7)
N2	Sc1	C6	29.26(18)	C10	C9	C18	117.4(7)
N1	Sc1	C6	80.3(2)	C8	C9	C18	124.9(7)
C1	Sc1	C6	134.1(2)	C11	C10	C9	121.0(7)
C2	Sc1	C6	97.1(2)	C12	C11	C10	120.2(8)
N2	Sc1	C5	56.5(2)	C11	C12	C13	122.3(7)
N1	Sc1	C5	56.1(2)	C12	C13	C8	116.5(7)
C1	Sc1	C5	148.4(3)	C12	C13	C15	120.2(7)
C2	Sc1	C5	96.9(2)	C8	C13	C15	123.2(7)
C6	Sc1	C5	29.33(18)	C13	C15	C14	112.2(6)
N2	Sc1	C4	78.5(2)	C13	C15	C16	110.8(7)
N1	Sc1	C4	27.05(19)	C14	C15	C16	110.0(6)
C1	Sc1	C4	130.8(3)	C9	C18	C17	110.4(6)
C2	Sc1	C4	109.5(2)	C9	C18	C19	113.6(6)

C6	Sc1	C4	56.8(2)	C17	C18	C19	109.3(6)
C5	Sc1	C4	29.66(18)	C25	C20	C21	120.0(6)
C4	N1	C8	127.5(5)	C25	C20	N2	118.6(6)
C4	N1	Sc1	106.3(4)	C21	C20	N2	121.1(6)
C8	N1	Sc1	123.9(4)	C22	C21	C20	118.5(7)
C6	N2	C20	124.4(6)	C22	C21	C30	118.3(7)
C6	N2	Sc1	102.0(4)	C20	C21	C30	123.1(6)
C20	N2	Sc1	132.3(4)	C23	C22	C21	121.7(7)
C38	C1	Sc1	115.3(5)	C22	C23	C24	119.1(7)
C44	C2	Sc1	127.0(4)	C23	C24	C25	121.8(7)
C36	C3	C37	107.6(6)	C24	C25	C20	118.4(7)
C36	C3	C35	106.7(6)	C24	C25	C27	119.7(7)
C37	C3	C35	109.8(6)	C20	C25	C27	121.9(6)
C36	C3	C4	116.2(6)	C26	C27	C28	107.7(7)
C37	C3	C4	108.5(6)	C26	C27	C25	111.7(6)
C35	C3	C4	107.9(6)	C28	C27	C25	113.6(7)
N1	C4	C5	120.0(6)	C21	C30	C31	112.5(6)
N1	C4	C3	127.4(6)	C21	C30	C29	111.6(7)
C5	C4	C3	112.6(6)	C31	C30	C29	109.2(6)
N1	C4	Sc1	46.6(3)	C43	C38	C39	116.0(8)
C5	C4	Sc1	75.2(4)	C43	C38	C1	124.8(8)
C3	C4	Sc1	163.4(5)	C39	C38	C1	119.0(8)
C6	C5	C4	136.1(7)	C40	C39	C38	122.4(9)
C6	C5	Sc1	72.4(4)	C39	C40	C41	120.7(10)
C4	C5	Sc1	75.2(4)	C40	C41	C42	119.5(10)
N2	C6	C5	120.3(6)	C41	C42	C43	119.1(9)
N2	C6	C7	125.2(6)	C38	C43	C42	122.2(9)
C5	C6	C7	114.2(6)	C45	C44	C49	115.1(7)
N2	C6	Sc1	48.7(3)	C45	C44	C2	122.2(8)
C5	C6	Sc1	78.3(4)	C49	C44	C2	122.6(7)
C7	C6	Sc1	147.5(5)	C46	C45	C44	122.1(9)
C32	C7	C33	108.8(6)	C45	C46	C47	121.2(10)
C32	C7	C34	108.1(6)	C48	C47	C46	117.4(9)
C33	C7	C34	105.3(6)	C49	C48	C47	122.3(10)
C32	C7	C6	105.9(6)	C48	C49	C44	121.9(9)

Table A.16: Crystal Data and Structure Refinement for **2-Cl(CH₂SiMe₃)**

A. Crystal Data

Crystallographer	Masood Parvez	University of Calgary
Empirical Formula	C ₃₉ H ₆₄ ClN ₂ ScSi	
Formula Weight	669.42	
Crystal Size	0.28 x 0.22 x 0.20 mm ³	
Crystal System	triclinic	
Space Group	P -1	
Lattice Parameters	a = 9.63070(10) Å	α = 83.3540(10)°.

	B = 10.85800(10) Å	$\beta = 77.4090(10)^\circ$.
	C = 20.3445(2) Å	$\gamma = 78.3060(10)^\circ$.
Volume	2027.46(3) Å ³	
Z	2	
Density (calculated)	1.097 Mg/m ³	

B. Data Collection and Refinement Conditions

Diffractometer	Nonius Kappa CCD
Radiation (λ [Å])	Graphite-monochromated MoK α (0.71073)
Temperature	173(2) K
Reflections Collected	21471
Independent Reflections	11757 [R(int) = 0.023]
Structure Solution	Direct Methods
Refinement Method	Full-matrix least-squares on F ²
Data / Restraints / Parameters	11757 / 12 / 413
Goodness-of-Fit	1.07
Final R Indices [$I > 2\sigma(I)$]	R1 = 0.046, wR2 = 0.135
R Indices (all data)	R1 = 0.062, wR2 = 0.155
Largest Difference Peak & Hole	0.60 and -0.69 e.Å ⁻³

Table A.17: Atomic coordinates and equivalent isotropic displacement parameters for **2-Cl(CH₂SiMe₃)**

	x	y	z	U(eq)		x	y	z	U(eq)
Sc(1)	2148(1)	1487(1)	7630(1)	23(1)	C(21)	1267(2)	2035(1)	9513(1)	26(1)
Cl(1)	884(1)	-162(1)	8066(1)	41(1)	C(22)	510(2)	1602(2)	10135(1)	32(1)
Si(1)	5639(1)	-654(1)	7363(1)	46(1)	C(23)	-984(2)	1725(2)	10267(1)	35(1)
N(1)	1434(1)	2654(1)	6842(1)	23(1)	C(24)	-1744(2)	2286(2)	9774(1)	34(1)
N(2)	1245(1)	2895(1)	8338(1)	22(1)	C(25)	-1041(2)	2718(2)	9138(1)	28(1)
C(1)	4502(2)	890(2)	7577(1)	33(1)	C(26)	-2685(2)	2289(2)	8424(1)	51(1)
C(3)	3247(2)	3984(2)	6119(1)	33(1)	C(27)	-1952(2)	3291(2)	8616(1)	34(1)
C(4)	2282(2)	3546(1)	6796(1)	24(1)	C(28)	-3086(2)	4430(2)	8872(1)	49(1)
C(5)	2492(2)	3980(1)	7376(1)	25(1)	C(29)	3373(2)	2495(2)	9944(1)	45(1)
C(6)	1716(2)	3930(1)	8078(1)	23(1)	C(30)	2905(2)	1867(2)	9410(1)	30(1)
C(7)	1586(2)	5144(2)	8431(1)	31(1)	C(31)	3598(2)	464(2)	9418(1)	42(1)
C(8)	555(2)	2586(1)	6370(1)	25(1)	C(32)	3120(2)	5288(2)	8489(1)	48(1)
C(9)	737(2)	1472(2)	6042(1)	33(1)	C(33)	651(2)	5178(2)	9142(1)	40(1)
C(10)	-149(2)	1446(2)	5585(1)	48(1)	C(34)	924(3)	6266(2)	7997(1)	54(1)
C(11)	-1191(2)	2456(2)	5455(1)	51(1)	C(35)	4755(2)	3165(3)	6086(1)	62(1)
C(12)	-1400(2)	3519(2)	5795(1)	40(1)	C(36)	2745(2)	3813(2)	5475(1)	41(1)
C(13)	-564(2)	3610(2)	6262(1)	30(1)	C(37)	3380(3)	5373(2)	6103(1)	65(1)
C(14)	-2507(2)	4983(2)	7025(1)	55(1)	C(38)	7083(3)	-1203(4)	7842(2)	86(2)
C(15)	-940(2)	4788(2)	6646(1)	41(1)	C(39)	4599(4)	-1926(3)	7441(3)	138(3)
C(16)	-710(3)	5977(2)	6189(2)	79(1)	C(40)	6541(4)	-497(4)	6461(1)	96(2)
C(17)	1190(3)	-869(2)	6372(1)	56(1)	C(38')	7596(3)	-774(8)	7308(4)	86(2)
C(18)	1874(2)	301(2)	6137(1)	42(1)	C(39')	5045(9)	-1788(7)	8070(3)	138(3)
C(19)	3023(3)	63(2)	5492(1)	61(1)	C(40')	5439(9)	-1284(9)	6592(3)	96(2)

C(20) 469(2) 2597(1) 9015(1) 23(1) |

Table A.18: Anisotropic Displacement Parameters for 2-Cl(CH₂SiMe₃)

Atom	U11	U22	U33	U23	U13	U12
Sc(1)	28(1)	20(1)	22(1)	-1(1)	-6(1)	-2(1)
Cl(1)	56(1)	31(1)	37(1)	4(1)	-7(1)	-18(1)
Si(1)	35(1)	36(1)	65(1)	-13(1)	-15(1)	8(1)
N(1)	24(1)	23(1)	20(1)	0(1)	-5(1)	-5(1)
N(2)	22(1)	22(1)	21(1)	-1(1)	-5(1)	-5(1)
C(1)	30(1)	31(1)	36(1)	-1(1)	-7(1)	2(1)
C(3)	32(1)	43(1)	24(1)	8(1)	-2(1)	-14(1)
C(4)	23(1)	24(1)	24(1)	3(1)	-4(1)	-4(1)
C(5)	24(1)	25(1)	26(1)	2(1)	-4(1)	-9(1)
C(6)	22(1)	22(1)	25(1)	-1(1)	-6(1)	-5(1)
C(7)	38(1)	24(1)	32(1)	-6(1)	-4(1)	-11(1)
C(8)	25(1)	30(1)	21(1)	-1(1)	-4(1)	-6(1)
C(9)	37(1)	36(1)	28(1)	-7(1)	-8(1)	-5(1)
C(10)	57(1)	51(1)	44(1)	-19(1)	-23(1)	-6(1)
C(11)	53(1)	66(1)	44(1)	-12(1)	-28(1)	-8(1)
C(12)	35(1)	50(1)	36(1)	0(1)	-14(1)	-3(1)
C(13)	28(1)	34(1)	27(1)	-1(1)	-7(1)	-4(1)
C(14)	51(1)	57(1)	45(1)	-8(1)	-3(1)	13(1)
C(15)	36(1)	37(1)	51(1)	-11(1)	-18(1)	8(1)
C(16)	71(2)	38(1)	116(3)	-11(1)	11(2)	-8(1)
C(17)	84(2)	36(1)	53(1)	-11(1)	-21(1)	-8(1)
C(18)	51(1)	34(1)	41(1)	-15(1)	-15(1)	1(1)
C(19)	59(1)	58(1)	60(1)	-24(1)	-3(1)	7(1)
C(20)	27(1)	22(1)	21(1)	-2(1)	-4(1)	-8(1)
C(21)	31(1)	26(1)	23(1)	-2(1)	-6(1)	-8(1)
C(22)	41(1)	31(1)	24(1)	1(1)	-7(1)	-11(1)
C(23)	43(1)	37(1)	25(1)	0(1)	2(1)	-16(1)
C(24)	30(1)	37(1)	33(1)	-2(1)	2(1)	-13(1)
C(25)	27(1)	29(1)	27(1)	-3(1)	-3(1)	-9(1)
C(26)	48(1)	59(1)	57(1)	-8(1)	-24(1)	-16(1)
C(27)	25(1)	41(1)	35(1)	0(1)	-7(1)	-8(1)
C(28)	36(1)	50(1)	58(1)	-4(1)	-12(1)	1(1)
C(29)	43(1)	60(1)	39(1)	-5(1)	-17(1)	-19(1)
C(30)	31(1)	34(1)	27(1)	1(1)	-11(1)	-8(1)
C(31)	37(1)	41(1)	47(1)	6(1)	-14(1)	-2(1)
C(32)	51(1)	56(1)	48(1)	-16(1)	-5(1)	-31(1)
C(33)	50(1)	31(1)	40(1)	-15(1)	3(1)	-13(1)
C(34)	82(2)	23(1)	54(1)	-1(1)	-15(1)	-1(1)
C(35)	30(1)	104(2)	37(1)	17(1)	5(1)	-5(1)
C(36)	41(1)	55(1)	23(1)	6(1)	-1(1)	-15(1)
C(37)	104(2)	62(2)	37(1)	16(1)	-7(1)	-54(2)
C(38)	80(3)	77(3)	96(3)	-23(2)	-51(3)	39(2)
C(39)	57(2)	35(2)	322(10)	-44(3)	-36(4)	5(2)
C(40)	92(3)	98(4)	75(3)	-31(2)	-9(2)	39(2)
C(38')	80(3)	77(3)	96(3)	-23(2)	-51(3)	39(2)
C(39')	57(2)	35(2)	322(10)	-44(3)	-36(4)	5(2)

C(40')	92(3)	98(4)	75(3)	-31(2)	-9(2)	39(2)
--------	-------	-------	-------	--------	-------	-------

Table A.19: Bond Lengths [Å] for **2-Cl(CH₂SiMe₃)**

Sc(1)-N(1)	2.0747(12)	C(3)-C(36)	1.534(2)	C(13)-C(15)	1.516(2)
Sc(1)-N(2)	2.1435(12)	C(3)-C(35)	1.534(3)	C(14)-C(15)	1.523(3)
Sc(1)-C(1)	2.2098(16)	C(3)-C(37)	1.535(3)	C(15)-C(16)	1.526(3)
Sc(1)-Cl(1)	2.3493(5)	C(3)-C(4)	1.568(2)	C(17)-C(18)	1.529(3)
Sc(1)-C(4)	2.6528(14)	C(4)-C(5)	1.388(2)	C(18)-C(19)	1.529(3)
Sc(1)-C(5)	2.7695(15)	C(5)-C(6)	1.460(2)	C(20)-C(25)	1.403(2)
Sc(1)-C(6)	2.8262(14)	C(6)-C(7)	1.543(2)	C(20)-C(21)	1.412(2)
Si(1)-C(38)	1.8334(16)	C(7)-C(33)	1.530(2)	C(21)-C(22)	1.397(2)
Si(1)-C(39)	1.8379(17)	C(7)-C(34)	1.533(3)	C(21)-C(30)	1.521(2)
Si(1)-C(40')	1.8429(19)	C(7)-C(32)	1.547(3)	C(22)-C(23)	1.387(2)
Si(1)-C(38')	1.8429(19)	C(8)-C(9)	1.409(2)	C(23)-C(24)	1.381(3)
Si(1)-C(1)	1.8480(17)	C(8)-C(13)	1.416(2)	C(24)-C(25)	1.400(2)
Si(1)-C(39')	1.852(2)	C(9)-C(10)	1.399(2)	C(25)-C(27)	1.522(2)
Si(1)-C(40)	1.8551(17)	C(9)-C(18)	1.525(2)	C(26)-C(27)	1.538(3)
N(1)-C(4)	1.3708(19)	C(10)-C(11)	1.372(3)	C(27)-C(28)	1.532(3)
N(1)-C(8)	1.4300(18)	C(11)-C(12)	1.372(3)	C(29)-C(30)	1.535(2)
N(2)-C(6)	1.3093(18)	C(12)-C(13)	1.395(2)	C(30)-C(31)	1.535(2)
N(2)-C(20)	1.4508(18)				

Table A.20: Bond Angles [°] for **2-Cl(CH₂SiMe₃)**

N(1)-Sc(1)-N(2)	92.49(5)	C(40')-Si(1)-C(40)	46.4(3)	C(6)-C(7)-C(32)	108.45(14)
N(1)-Sc(1)-C(1)	118.75(6)	C(38')-Si(1)-C(40)	71.0(3)	C(9)-C(8)-C(13)	119.76(14)
N(2)-Sc(1)-C(1)	111.00(6)	C(1)-Si(1)-C(40)	107.57(14)	C(9)-C(8)-N(1)	120.17(14)
N(1)-Sc(1)-Cl(1)	116.32(4)	C(39')-Si(1)-C(40)	144.3(3)	C(13)-C(8)-N(1)	119.96(13)
N(2)-Sc(1)-Cl(1)	103.22(4)	C(4)-N(1)-C(8)	124.53(12)	C(10)-C(9)-C(8)	118.26(16)
C(1)-Sc(1)-Cl(1)	111.90(5)	C(4)-N(1)-Sc(1)	98.63(9)	C(10)-C(9)-C(18)	117.48(16)
N(1)-Sc(1)-C(4)	30.72(5)	C(8)-N(1)-Sc(1)	136.06(10)	C(8)-C(9)-C(18)	124.23(14)
N(2)-Sc(1)-C(4)	80.46(5)	C(6)-N(2)-C(20)	129.60(12)	C(11)-C(10)-C(9)	122.22(18)
C(1)-Sc(1)-C(4)	96.91(6)	C(6)-N(2)-Sc(1)	107.40(9)	C(12)-C(11)-C(10)	119.17(17)
Cl(1)-Sc(1)-C(4)	146.65(4)	C(20)-N(2)-Sc(1)	122.23(9)	C(11)-C(12)-C(13)	121.78(17)
N(1)-Sc(1)-C(5)	57.08(5)	Si(1)-C(1)-Sc(1)	127.99(9)	C(12)-C(13)-C(8)	118.67(16)
N(2)-Sc(1)-C(5)	56.30(4)	C(36)-C(3)-C(35)	107.05(17)	C(12)-C(13)-C(15)	117.90(15)
C(1)-Sc(1)-C(5)	90.06(6)	C(36)-C(3)-C(37)	107.66(15)	C(8)-C(13)-C(15)	123.39(14)
Cl(1)-Sc(1)-C(5)	155.25(4)	C(35)-C(3)-C(37)	108.61(19)	C(13)-C(15)-C(14)	111.08(17)
C(4)-Sc(1)-C(5)	29.57(4)	C(36)-C(3)-C(4)	115.20(13)	C(13)-C(15)-C(16)	112.85(19)
N(1)-Sc(1)-C(6)	76.56(4)	C(35)-C(3)-C(4)	106.36(13)	C(14)-C(15)-C(16)	108.23(17)
N(2)-Sc(1)-C(6)	26.24(4)	C(37)-C(3)-C(4)	111.69(15)	C(9)-C(18)-C(17)	111.70(18)
C(1)-Sc(1)-C(6)	100.43(5)	N(1)-C(4)-C(5)	120.35(12)	C(9)-C(18)-C(19)	111.78(17)
Cl(1)-Sc(1)-C(6)	128.96(3)	N(1)-C(4)-C(3)	123.50(13)	C(17)-C(18)-C(19)	109.97(17)
C(4)-Sc(1)-C(6)	56.77(4)	C(5)-C(4)-C(3)	115.52(13)	C(25)-C(20)-C(21)	121.19(13)
C(5)-Sc(1)-C(6)	30.23(4)	N(1)-C(4)-Sc(1)	50.64(7)	C(25)-C(20)-N(2)	119.38(13)
C(38)-Si(1)-C(39)	107.52(12)	C(5)-C(4)-Sc(1)	79.88(8)	C(21)-C(20)-N(2)	118.90(13)
C(38)-Si(1)-C(40')	127.2(3)	C(3)-C(4)-Sc(1)	138.67(10)	C(22)-C(21)-C(20)	118.16(14)
C(39)-Si(1)-C(40')	60.7(3)	C(4)-C(5)-C(6)	132.71(13)	C(22)-C(21)-C(30)	118.08(14)
C(38)-Si(1)-C(38')	37.3(3)	C(4)-C(5)-Sc(1)	70.55(8)	C(20)-C(21)-C(30)	123.76(13)
C(39)-Si(1)-C(38')	128.8(3)	C(6)-C(5)-Sc(1)	77.03(8)	C(23)-C(22)-C(21)	121.41(15)

C(40')-Si(1)-C(38')	106.45(15)	N(2)-C(6)-C(5)	118.60(13)	C(24)-C(23)-C(22)	119.46(15)
C(38)-Si(1)-C(1)	115.05(13)	N(2)-C(6)-C(7)	127.69(13)	C(23)-C(24)-C(25)	121.66(15)
C(39)-Si(1)-C(1)	113.52(14)	C(5)-C(6)-C(7)	113.70(12)	C(24)-C(25)-C(20)	118.11(14)
C(40')-Si(1)-C(1)	116.4(3)	N(2)-C(6)-Sc(1)	46.36(7)	C(24)-C(25)-C(27)	118.47(14)
C(38')-Si(1)-C(1)	115.8(3)	C(5)-C(6)-Sc(1)	72.74(8)	C(20)-C(25)-C(27)	123.42(14)
C(38)-Si(1)-C(39')	70.4(3)	C(7)-C(6)-Sc(1)	169.89(10)	C(25)-C(27)-C(28)	111.51(15)
C(39)-Si(1)-C(39')	46.9(3)	C(33)-C(7)-C(34)	107.67(16)	C(25)-C(27)-C(26)	110.08(15)
C(40')-Si(1)-C(39')	105.83(15)	C(33)-C(7)-C(6)	115.12(13)	C(28)-C(27)-C(26)	110.46(16)
C(38')-Si(1)-C(39')	105.89(14)	C(34)-C(7)-C(6)	108.28(14)	C(21)-C(30)-C(31)	110.72(14)
C(1)-Si(1)-C(39')	105.5(3)	C(33)-C(7)-C(32)	107.24(15)	C(21)-C(30)-C(29)	111.96(14)
C(38)-Si(1)-C(40)	106.45(11)	C(34)-C(7)-C(32)	110.03(17)	C(31)-C(30)-C(29)	109.77(15)
C(39)-Si(1)-C(40)	106.15(12)				

Table A.21: Crystal Data and Structure Refinement for **2-CH₂SiMe₃(CH₂CMe₃)**

A. Crystal Data

Crystallographer	Masood Parvez	University of Calgary
Empirical Formula	C ₄₄ H ₇₅ N ₂ ScSi	
Formula Weight	705.11	
Crystal size	0.28 x 0.25 x 0.20 mm ³	
Crystal System	orthorhombic	
Space Group	P2 ₁ 2 ₁ 2 ₁	
Lattice Parameters	a = 18.3993(2) Å b = 19.1857(2) Å c = 25.5578(4) Å	
Volume	9022.0(2) Å ³	
Z	8	
Density (calculated)	1.038 Mg/m ³	

B. Data Collection and Refinement Conditions

Diffractometer	Nonius Kappa CCD
Radiation (λ[Å])	Graphite-monochromated MoKα (0.71073)
Temperature	173(2) K
Reflections Collected	24452
Independent Reflections	24452 [R(int) = 0.00]
Structure Solution	Direct Methods
Refinement Method	Full-matrix least-squares on F ²
Data / Restraints / Parameters	24452 / 14 / 912
Goodness-of-Fit	1.01
Final R Indices [I>2σ(I)]	R1 = 0.078, wR2 = 0.1961
R Indices (all data)	R1 = 0.112, wR2 = 0.223
Largest Difference Peak & Hole	1.65 and -1.16 e.Å ⁻³

Table A.22: Atomic Coordinates and Equivalent Isotropic Displacement Parameters for 2-CH₂SiMe₃(CH₂CMe₃)

	x	y	z	U(eq)		x	y	z	U(eq)
Sc(1)	4871(1)	2708(1)	3485(1)	27(1)	Sc(1A)	129(2)	2713(2)	1381(1)	24(1)
Si(1)	6684(1)	3383(1)	3886(1)	47(1)	Si(1')	1552(1)	3598(1)	1271(1)	49(1)
N(1)	4113(1)	3428(1)	3822(1)	25(1)	C(1')	-474(3)	1940(3)	2287(1)	57(1)
N(2)	4611(1)	1906(1)	4027(1)	25(1)	C(2')	920(3)	3133(3)	1711(2)	60(1)
C(1)	4423(2)	2312(2)	2727(1)	37(1)	N(1')	-36(1)	1720(1)	1011(1)	26(1)
C(2)	6012(2)	3098(2)	3419(2)	42(1)	N(2')	-967(1)	3038(1)	1205(1)	28(1)
C(3)	3801(2)	3997(2)	4716(1)	36(1)	C(3')	270(2)	1628(2)	28(1)	41(1)
C(4)	4109(2)	3419(2)	4343(1)	26(1)	C(4')	-89(2)	1966(2)	520(1)	27(1)
C(5)	4431(2)	2858(2)	4624(1)	28(1)	C(5')	-441(2)	2596(2)	409(1)	28(1)
C(6)	4583(2)	2150(2)	4520(1)	25(1)	C(6')	-940(2)	3039(2)	687(1)	29(1)
C(7)	4763(2)	1721(2)	5022(1)	34(1)	C(7')	-1406(2)	3496(2)	304(2)	41(1)
C(8)	3745(2)	3927(2)	3486(1)	28(1)	C(8')	61(2)	996(2)	1154(1)	30(1)
C(9)	4118(2)	4529(2)	3311(1)	33(1)	C(9')	709(2)	776(2)	1392(1)	36(1)
C(10)	3739(2)	4991(2)	2983(2)	40(1)	C(10')	763(2)	77(2)	1550(2)	46(1)
C(11)	3048(2)	4869(2)	2826(2)	43(1)	C(11')	193(3)	-383(2)	1486(2)	52(1)
C(12)	2706(2)	4255(2)	2975(2)	39(1)	C(12')	-434(3)	-156(2)	1260(2)	48(1)
C(13)	3045(2)	3768(2)	3295(1)	30(1)	C(13')	-528(2)	537(2)	1092(2)	37(1)
C(14)	2275(3)	2795(3)	2938(2)	56(1)	C(14')	-1864(3)	609(3)	1257(2)	63(1)
C(15)	2651(2)	3096(2)	3423(2)	35(1)	C(15')	-1255(2)	749(2)	867(2)	48(1)
C(16)	2098(4)	3175(3)	3863(3)	80(2)	C(16')	-1438(3)	365(3)	345(2)	70(2)
C(17)	5365(2)	4785(2)	2969(2)	53(1)	C(17')	1573(3)	1295(3)	2052(2)	54(1)
C(18)	4887(2)	4718(2)	3458(2)	42(1)	C(18')	1366(2)	1236(2)	1472(2)	39(1)
C(19)	4942(3)	5399(2)	3773(2)	62(1)	C(19')	2034(3)	990(3)	1162(2)	65(1)
C(20)	4576(2)	1187(2)	3872(1)	30(1)	C(20')	-1471(2)	3426(2)	1526(1)	33(1)
C(21)	5201(2)	837(2)	3701(1)	36(1)	C(21')	-1287(2)	4108(2)	1697(2)	37(1)
C(22)	5133(3)	151(2)	3527(2)	48(1)	C(22')	-1788(3)	4469(2)	1995(2)	49(1)
C(23)	4475(3)	-187(2)	3519(2)	50(1)	C(23')	-2455(3)	4177(3)	2139(2)	58(1)
C(24)	3860(3)	157(2)	3684(2)	48(1)	C(24')	-2610(2)	3509(3)	1993(2)	52(1)
C(25)	3891(2)	852(2)	3850(2)	38(1)	C(25')	-2121(2)	3103(2)	1694(2)	38(1)
C(26)	2812(3)	912(4)	4476(3)	91(2)	C(26')	-2889(3)	2319(3)	1135(2)	68(1)
C(27)	3183(2)	1223(2)	3992(2)	53(1)	C(27')	-2320(2)	2359(2)	1569(2)	42(1)
C(28)	2651(3)	1203(3)	3539(3)	71(2)	C(28')	-2602(2)	1979(2)	2056(2)	49(1)
C(29)	6492(3)	759(3)	4045(2)	62(1)	C(29')	-671(3)	5136(3)	1252(2)	67(1)
C(30)	5953(2)	1160(2)	3705(2)	41(1)	C(30')	-571(2)	4461(2)	1576(2)	45(1)
C(31)	6259(3)	1228(3)	3146(2)	57(1)	C(31')	-172(3)	4649(2)	2081(2)	58(1)
C(32)	5505(3)	1966(3)	5221(2)	60(1)	C(32')	-877(3)	4005(3)	29(2)	61(1)
C(33)	4809(3)	928(2)	4959(2)	48(1)	C(33')	-2014(2)	3939(2)	549(2)	50(1)
C(34)	4189(3)	1846(2)	5449(2)	58(1)	C(34')	-1763(3)	3016(3)	-105(2)	65(1)
C(35)	4453(3)	4347(2)	4992(2)	56(1)	C(35')	958(4)	2058(3)	-89(3)	91(2)
C(36)	3344(2)	4577(2)	4457(2)	40(1)	C(36')	527(3)	873(2)	86(2)	47(1)
C(37)	3303(3)	3664(3)	5136(2)	62(1)	C(37')	-237(4)	1638(3)	-450(2)	82(2)
C(38)	4456(1)	2543(1)	2138(1)	49(1)	C(38')	-447(2)	2208(1)	2844(1)	117(2)
C(39)	4197(2)	3303(1)	2085(2)	58(1)	C(39')	273(2)	2354(4)	3129(3)	132(4)
C(40)	5260(1)	2487(3)	1961(2)	70(2)	C(40')	-958(2)	2857(2)	2919(2)	58(1)
C(41)	3985(2)	2065(2)	1789(2)	58(1)	C(41')	-838(4)	1605(2)	3162(3)	117(3)
C(42)	6280(3)	3869(4)	4406(3)	86(2)	C(42')	2265(3)	3016(4)	1124(4)	114(3)
C(43)	7394(3)	3934(3)	3589(3)	77(2)	C(43')	1956(6)	4338(5)	1584(4)	127(3)

C(44)	7135(3)	2641(3)	4188(3)	86(2)	C(44')	1075(4)	3911(4)	683(3)	88(2)
Sc(1')	-81(1)	2497(1)	1594(1)	24(1)					

Table A.23: Anisotropic Displacement Parameters for **2-CH₂SiMe₃(CH₂CMe₃)**

Atom	U11	U22	U33	U23	U13	U12
Sc(1)	25(1)	28(1)	29(1)	2(1)	3(1)	1(1)
Si(1)	33(1)	54(1)	54(1)	6(1)	-6(1)	-4(1)
N(1)	27(1)	23(1)	25(1)	0(1)	1(1)	0(1)
N(2)	31(1)	20(1)	25(1)	-1(1)	-1(1)	1(1)
C(1)	30(2)	42(2)	39(2)	1(2)	3(1)	-1(1)
C(2)	33(2)	45(2)	49(2)	5(2)	3(2)	-3(1)
C(3)	48(2)	30(2)	31(2)	-4(1)	3(2)	10(2)
C(4)	30(1)	24(1)	23(1)	-1(1)	1(1)	-1(1)
C(5)	37(2)	26(2)	20(1)	-3(1)	-4(1)	1(1)
C(6)	28(1)	22(1)	25(1)	1(1)	-3(1)	2(1)
C(7)	51(2)	29(2)	23(2)	5(1)	0(1)	10(1)
C(8)	32(2)	26(1)	25(1)	-1(1)	1(1)	2(1)
C(9)	45(2)	26(2)	27(2)	2(1)	-7(1)	-3(1)
C(10)	54(2)	31(2)	36(2)	7(2)	-3(2)	1(2)
C(11)	50(2)	38(2)	41(2)	9(2)	-6(2)	12(2)
C(12)	33(2)	43(2)	42(2)	2(2)	-6(2)	8(1)
C(13)	30(2)	31(2)	29(2)	-1(1)	0(1)	4(1)
C(14)	56(3)	59(3)	54(3)	1(2)	-17(2)	-20(2)
C(15)	27(2)	33(2)	43(2)	0(2)	-1(1)	0(1)
C(16)	97(4)	58(3)	86(4)	-15(3)	53(4)	-23(3)
C(17)	50(2)	56(3)	54(3)	15(2)	-10(2)	-15(2)
C(18)	52(2)	37(2)	38(2)	10(2)	-13(2)	-13(2)
C(19)	85(3)	45(2)	57(3)	4(2)	-14(3)	-28(2)
C(20)	42(2)	22(1)	25(1)	1(1)	-2(1)	3(1)
C(21)	54(2)	29(2)	26(2)	-1(1)	-4(2)	11(2)
C(22)	69(3)	34(2)	40(2)	-6(2)	-6(2)	19(2)
C(23)	82(3)	23(2)	44(2)	-6(2)	-7(2)	2(2)
C(24)	71(3)	26(2)	47(2)	1(2)	-11(2)	-8(2)
C(25)	52(2)	25(2)	36(2)	-1(1)	2(2)	-6(1)
C(26)	64(3)	134(6)	76(4)	-4(4)	18(3)	-20(4)
C(27)	43(2)	37(2)	80(3)	-6(2)	8(2)	-14(2)
C(28)	55(3)	58(3)	99(5)	-2(3)	-13(3)	1(2)
C(29)	50(2)	74(3)	60(3)	-2(3)	-12(2)	23(2)
C(30)	43(2)	43(2)	37(2)	-5(2)	1(2)	12(2)
C(31)	57(3)	76(3)	38(2)	-11(2)	7(2)	11(2)
C(32)	71(3)	51(2)	57(3)	16(2)	-28(2)	-1(2)
C(33)	79(3)	30(2)	33(2)	10(2)	0(2)	14(2)
C(34)	98(4)	44(2)	31(2)	14(2)	22(2)	19(2)
C(35)	78(3)	40(2)	49(2)	-19(2)	-21(2)	11(2)
C(36)	54(2)	31(2)	35(2)	-5(2)	3(2)	15(2)
C(37)	78(3)	57(3)	50(3)	9(2)	29(2)	27(2)
C(38)	43(1)	62(2)	42(1)	-4(1)	2(1)	1(1)
C(39)	67(3)	66(3)	42(2)	1(2)	1(2)	-14(2)
C(40)	53(3)	110(4)	47(2)	7(3)	-3(2)	4(3)
C(41)	58(3)	63(3)	52(3)	-1(2)	-3(2)	12(2)

C(42)	58(3)	123(5)	77(4)	-11(4)	-23(3)	2(3)
C(43)	55(3)	95(4)	80(4)	11(3)	-5(3)	-12(3)
C(44)	72(3)	68(3)	118(6)	22(4)	-32(4)	-18(3)
Sc(1')	27(1)	24(1)	22(1)	-2(1)	-1(1)	2(1)
Sc(1A)	24(1)	23(1)	24(2)	1(1)	-2(1)	-2(1)
Si(1')	49(1)	44(1)	55(1)	0(1)	-7(1)	-7(1)
C(1')	53(3)	66(3)	52(3)	-1(2)	3(2)	2(2)
C(2')	65(3)	51(3)	63(3)	-3(2)	-9(2)	-2(2)
N(1')	30(1)	21(1)	28(1)	1(1)	4(1)	-1(1)
N(2')	30(1)	29(1)	25(1)	0(1)	0(1)	4(1)
C(3')	65(2)	31(2)	28(2)	-3(1)	16(2)	3(2)
C(4')	29(1)	27(1)	24(1)	-3(1)	5(1)	-4(1)
C(5')	33(2)	29(2)	24(1)	1(1)	3(1)	-3(1)
C(6')	30(2)	29(2)	27(2)	5(1)	0(1)	0(1)
C(7')	43(2)	51(2)	30(2)	10(2)	-3(1)	14(2)
C(8')	45(2)	22(1)	23(1)	0(1)	8(1)	2(1)
C(9')	53(2)	28(2)	27(2)	4(1)	7(1)	9(1)
C(10')	72(3)	30(2)	35(2)	2(2)	7(2)	14(2)
C(11')	95(3)	23(2)	38(2)	6(2)	10(2)	4(2)
C(12')	76(3)	27(2)	41(2)	-5(2)	15(2)	-14(2)
C(13')	48(2)	28(2)	34(2)	-2(1)	9(2)	-6(1)
C(14')	58(3)	58(3)	72(3)	-16(3)	21(2)	-25(2)
C(15')	45(2)	42(2)	56(3)	-1(2)	7(2)	-14(2)
C(16')	57(3)	93(4)	61(3)	-9(3)	-1(2)	-17(3)
C(17')	49(2)	63(3)	50(2)	2(2)	-9(2)	0(2)
C(18')	40(2)	37(2)	39(2)	6(2)	3(2)	10(1)
C(19')	49(3)	80(3)	66(3)	-1(3)	18(2)	9(2)
C(20')	34(2)	35(2)	28(2)	5(1)	3(1)	10(1)
C(21')	46(2)	31(2)	34(2)	5(1)	8(2)	9(1)
C(22')	66(3)	37(2)	43(2)	-2(2)	10(2)	17(2)
C(23')	58(3)	61(3)	54(3)	9(2)	20(2)	29(2)
C(24')	43(2)	62(3)	52(2)	12(2)	15(2)	20(2)
C(25')	32(2)	47(2)	36(2)	8(2)	4(1)	13(2)
C(26')	68(3)	76(3)	59(3)	10(3)	-18(2)	-9(3)
C(27')	31(2)	51(2)	43(2)	7(2)	3(1)	1(2)
C(28')	38(2)	57(3)	51(2)	11(2)	8(2)	-1(2)
C(29')	91(4)	48(3)	63(3)	13(2)	12(3)	-4(2)
C(30')	58(2)	32(2)	45(2)	-8(2)	10(2)	2(2)
C(31')	74(3)	38(2)	62(3)	-8(2)	-1(2)	0(2)
C(32')	73(3)	57(3)	55(3)	29(2)	15(2)	22(2)
C(33')	48(2)	60(3)	44(2)	16(2)	-2(2)	24(2)
C(34')	53(3)	100(4)	40(2)	-6(2)	-18(2)	21(3)
C(35')	104(4)	48(3)	121(5)	-3(3)	90(4)	-8(3)
C(36')	69(3)	35(2)	36(2)	-7(2)	20(2)	6(2)
C(37')	144(6)	71(3)	31(2)	-15(2)	-12(3)	42(4)
C(38')	175(4)	58(2)	118(3)	-19(2)	-105(3)	26(2)
C(39')	56(3)	237(11)	101(6)	-89(7)	-6(3)	7(5)
C(40')	85(3)	51(3)	37(2)	-7(2)	-8(2)	4(2)
C(41')	177(9)	100(6)	76(5)	22(4)	-19(5)	-1(6)
C(42')	53(3)	83(4)	205(10)	34(5)	-20(4)	2(3)

C(43')	178(9)	112(6)	91(6)	-12(5)	19(6)	-31(6)
C(44')	97(5)	86(4)	81(4)	26(4)	7(4)	3(4)

Table A.24: Bond Lengths [Å] for **2-(CH₂SiMe₃)(CH₂CMe₃)**

Sc(1)-N(2)	2.126(3)	C(20)-C(25)	1.415(5)	C(3')-C(37')	1.537(7)
Sc(1)-N(1)	2.144(3)	C(21)-C(22)	1.395(5)	C(3')-C(35')	1.540(7)
Sc(1)-C(2)	2.234(4)	C(21)-C(30)	1.516(6)	C(3')-C(4')	1.560(4)
Sc(1)-C(1)	2.239(3)	C(22)-C(23)	1.373(7)	C(4')-C(5')	1.400(4)
Si(1)-C(42)	1.785(7)	C(23)-C(24)	1.376(7)	C(5')-C(6')	1.440(5)
Si(1)-C(2)	1.803(4)	C(24)-C(25)	1.400(5)	C(6')-C(7')	1.571(5)
Si(1)-C(44)	1.818(6)	C(25)-C(27)	1.529(6)	C(7')-C(34')	1.539(7)
Si(1)-C(43)	1.844(6)	C(26)-C(27)	1.532(8)	C(7')-C(33')	1.537(6)
N(1)-C(4)	1.332(4)	C(27)-C(28)	1.517(8)	C(7')-C(32')	1.547(6)
N(1)-C(8)	1.454(4)	C(29)-C(30)	1.527(6)	C(8')-C(9')	1.404(5)
N(2)-C(6)	1.345(4)	C(30)-C(31)	1.542(6)	C(8')-C(13')	1.405(5)
N(2)-C(20)	1.438(4)	C(38)-C(39)	1.539(2)	C(9')-C(10')	1.403(5)
C(1)-C(38)	1.571(3)	C(38)-C(41)	1.546(2)	C(9')-C(18')	1.511(6)
C(3)-C(35)	1.545(6)	C(38)-C(40)	1.550(2)	C(10')-C(11')	1.381(6)
C(3)-C(36)	1.543(5)	Sc(1')-N(1')	2.110(3)	C(11')-C(12')	1.361(7)
C(3)-C(37)	1.551(6)	Sc(1')-N(2')	2.173(3)	C(12')-C(13')	1.409(5)
C(3)-C(4)	1.568(5)	Sc(1')-C(1')	2.192(5)	C(13')-C(15')	1.512(6)
C(4)-C(5)	1.422(4)	Sc(1')-C(2')	2.227(5)	C(14')-C(15')	1.524(6)
C(5)-C(6)	1.413(4)	Sc(1')-C(38')	3.314(4)	C(15')-C(16')	1.562(7)
C(6)-C(7)	1.560(4)	Sc(1A)-C(2')	1.864(5)	C(17')-C(18')	1.535(6)
C(7)-C(32)	1.530(6)	Sc(1A)-N(1')	2.148(3)	C(18')-C(19')	1.537(6)
C(7)-C(33)	1.532(5)	Sc(1A)-N(2')	2.158(3)	C(20')-C(25')	1.413(5)
C(7)-C(34)	1.539(5)	Sc(1A)-C(4')	2.657(4)	C(20')-C(21')	1.420(5)
C(8)-C(13)	1.411(5)	Sc(1A)-C(5')	2.705(4)	C(21')-C(22')	1.382(5)
C(8)-C(9)	1.416(5)	Sc(1A)-C(6')	2.721(4)	C(21')-C(30')	1.514(6)
C(9)-C(10)	1.406(5)	Sc(1A)-Si(1')	3.133(4)	C(22')-C(23')	1.398(7)
C(9)-C(18)	1.508(5)	Si(1')-C(42')	1.763(7)	C(23')-C(24')	1.365(7)
C(10)-C(11)	1.355(6)	Si(1')-C(43')	1.791(9)	C(24')-C(25')	1.415(5)
C(11)-C(12)	1.389(6)	Si(1')-C(2')	1.848(6)	C(25')-C(27')	1.510(6)
C(12)-C(13)	1.390(5)	Si(1')-C(44')	1.840(7)	C(26')-C(27')	1.528(6)
C(13)-C(15)	1.515(5)	C(1')-C(38')	1.516(3)	C(27')-C(28')	1.532(6)
C(14)-C(15)	1.531(6)	N(1')-C(4')	1.346(4)	C(29')-C(30')	1.548(6)
C(15)-C(16)	1.524(6)	N(1')-C(8')	1.447(4)	C(30')-C(31')	1.528(7)
C(17)-C(18)	1.534(6)	N(2')-C(6')	1.323(4)	C(38')-C(39')	1.537(3)
C(18)-C(19)	1.538(6)	N(2')-C(20')	1.446(4)	C(38')-C(40')	1.573(3)
C(20)-C(21)	1.401(5)	C(3')-C(36')	1.531(5)	C(38')-C(41')	1.587(3)

Table A.25: Bond Angles [°] for **2-(CH₂SiMe₃)(CH₂CMe₃)**

N(2)-Sc(1)-N(1)	93.32(10)	C(25)-C(27)-C(26)	112.9(5)	C(36')-C(3')-C(4')	116.5(3)
N(2)-Sc(1)-C(2)	120.17(13)	C(29)-C(30)-C(21)	113.0(4)	C(37')-C(3')-C(4')	112.3(4)
N(1)-Sc(1)-C(2)	115.18(13)	C(29)-C(30)-C(31)	109.4(4)	C(35')-C(3')-C(4')	106.4(3)
N(2)-Sc(1)-C(1)	103.58(11)	C(21)-C(30)-C(31)	111.3(3)	N(1')-C(4')-C(5')	121.7(3)
N(1)-Sc(1)-C(1)	109.11(12)	C(39)-C(38)-C(41)	109.7(2)	N(1')-C(4')-C(3')	125.1(3)
C(2)-Sc(1)-C(1)	113.28(14)	C(39)-C(38)-C(40)	109.7(2)	C(5')-C(4')-C(3')	113.1(3)
C(42)-Si(1)-C(2)	111.4(2)	C(41)-C(38)-C(40)	109.0(2)	N(1')-C(4')-Sc(1A)	53.49(17)

C(42)-Si(1)-C(44)	106.4(4)	C(39)-C(38)-C(1)	109.8(3)	C(5')-C(4')-Sc(1A)	76.76(19)
C(2)-Si(1)-C(44)	110.9(2)	C(41)-C(38)-C(1)	111.3(3)	C(3')-C(4')-Sc(1A)	145.8(3)
C(42)-Si(1)-C(43)	107.5(3)	C(40)-C(38)-C(1)	107.3(3)	C(4')-C(5')-C(6')	134.8(3)
C(2)-Si(1)-C(43)	112.7(2)	N(1')-Sc(1')-N(2')	92.52(10)	C(4')-C(5')-Sc(1A)	72.97(18)
C(44)-Si(1)-C(43)	107.5(3)	N(1')-Sc(1')-C(1')	103.79(14)	C(6')-C(5')-Sc(1A)	75.24(18)
C(4)-N(1)-C(8)	126.7(3)	N(2')-Sc(1')-C(1')	110.78(16)	N(2')-C(6')-C(5')	121.0(3)
C(4)-N(1)-Sc(1)	113.4(2)	N(1')-Sc(1')-C(2')	116.71(17)	N(2')-C(6')-C(7')	127.3(3)
C(8)-N(1)-Sc(1)	119.3(2)	N(2')-Sc(1')-C(2')	114.85(17)	C(5')-C(6')-C(7')	111.7(3)
C(6)-N(2)-C(20)	126.2(3)	C(1')-Sc(1')-C(2')	115.54(19)	N(2')-C(6')-Sc(1A)	51.33(18)
C(6)-N(2)-Sc(1)	111.56(19)	N(1')-Sc(1')-C(38')	124.77(10)	C(5')-C(6')-Sc(1A)	73.98(19)
C(20)-N(2)-Sc(1)	121.7(2)	N(2')-Sc(1')-C(38')	111.64(10)	C(7')-C(6')-Sc(1A)	158.4(3)
C(38)-C(1)-Sc(1)	135.9(2)	C(1')-Sc(1')-C(38')	21.81(11)	C(34')-C(7')-C(33')	107.3(3)
Si(1)-C(2)-Sc(1)	134.1(2)	C(2')-Sc(1')-C(38')	97.48(15)	C(34')-C(7')-C(32')	109.8(4)
C(35)-C(3)-C(36)	107.8(3)	C(2')-Sc(1A)-N(1')	133.8(2)	C(33')-C(7')-C(32')	107.2(4)
C(35)-C(3)-C(37)	108.8(4)	C(2')-Sc(1A)-N(2')	134.3(2)	C(34')-C(7')-C(6')	108.7(3)
C(36)-C(3)-C(37)	105.8(3)	N(1')-Sc(1A)-N(2')	91.87(13)	C(33')-C(7')-C(6')	116.8(3)
C(35)-C(3)-C(4)	107.7(3)	C(2')-Sc(1A)-C(4')	136.5(3)	C(32')-C(7')-C(6')	107.0(3)
C(36)-C(3)-C(4)	116.5(3)	N(1')-Sc(1A)-C(4')	30.23(10)	C(9')-C(8')-C(13')	121.1(3)
C(37)-C(3)-C(4)	110.0(3)	N(2')-Sc(1A)-C(4')	80.92(12)	C(9')-C(8')-N(1')	120.2(3)
N(1)-C(4)-C(5)	120.8(3)	C(2')-Sc(1A)-C(5')	138.9(3)	C(13')-C(8')-N(1')	118.5(3)
N(1)-C(4)-C(3)	126.8(3)	N(1')-Sc(1A)-C(5')	57.88(11)	C(10')-C(9')-C(8')	118.1(4)
C(5)-C(4)-C(3)	112.3(3)	N(2')-Sc(1A)-C(5')	58.03(11)	C(10')-C(9')-C(18')	117.6(4)
C(6)-C(5)-C(4)	135.7(3)	C(4')-Sc(1A)-C(5')	30.27(10)	C(8')-C(9')-C(18')	124.2(3)
N(2)-C(6)-C(5)	121.2(3)	C(2')-Sc(1A)-C(6')	139.4(2)	C(11')-C(10')-C(9')	121.6(4)
N(2)-C(6)-C(7)	125.4(3)	N(1')-Sc(1A)-C(6')	79.38(12)	C(12')-C(11')-C(10')	119.3(3)
C(5)-C(6)-C(7)	113.2(3)	N(2')-Sc(1A)-C(6')	28.61(10)	C(11')-C(12')-C(13')	122.3(4)
C(32)-C(7)-C(33)	106.9(3)	C(4')-Sc(1A)-C(6')	58.36(11)	C(12')-C(13')-C(8')	117.6(4)
C(32)-C(7)-C(34)	109.1(4)	C(5')-Sc(1A)-C(6')	30.78(10)	C(12')-C(13')-C(15')	118.6(4)
C(33)-C(7)-C(34)	105.4(3)	C(2')-Sc(1A)-Si(1')	32.29(19)	C(8')-C(13')-C(15')	123.8(3)
C(32)-C(7)-C(6)	107.6(3)	N(1')-Sc(1A)-Si(1')	124.03(15)	C(13')-C(15')-C(14')	110.7(4)
C(33)-C(7)-C(6)	116.7(3)	N(2')-Sc(1A)-Si(1')	127.24(16)	C(13')-C(15')-C(16')	113.0(4)
C(34)-C(7)-C(6)	110.9(3)	C(4')-Sc(1A)-Si(1')	110.14(15)	C(14')-C(15')-C(16')	108.4(4)
C(13)-C(8)-C(9)	120.7(3)	C(5')-Sc(1A)-Si(1')	106.63(16)	C(9')-C(18')-C(17')	111.9(3)
C(13)-C(8)-N(1)	119.2(3)	C(6')-Sc(1A)-Si(1')	114.89(16)	C(9')-C(18')-C(19')	112.9(4)
C(9)-C(8)-N(1)	119.8(3)	C(42')-Si(1')-C(43')	106.7(5)	C(17')-C(18')-C(19')	108.8(4)
C(10)-C(9)-C(8)	117.5(3)	C(42')-Si(1')-C(2')	107.0(3)	C(25')-C(20')-C(21')	120.8(3)
C(10)-C(9)-C(18)	117.6(3)	C(43')-Si(1')-C(2')	111.8(4)	C(25')-C(20')-N(2')	119.3(3)
C(8)-C(9)-C(18)	125.0(3)	C(42')-Si(1')-C(44')	112.9(4)	C(21')-C(20')-N(2')	119.7(3)
C(11)-C(10)-C(9)	122.4(4)	C(43')-Si(1')-C(44')	107.7(4)	C(22')-C(21')-C(20')	118.2(4)
C(10)-C(11)-C(12)	119.3(3)	C(2')-Si(1')-C(44')	110.8(3)	C(22')-C(21')-C(30')	117.9(4)
C(11)-C(12)-C(13)	122.0(3)	C(42')-Si(1')-Sc(1A)	107.3(2)	C(20')-C(21')-C(30')	123.9(3)
C(12)-C(13)-C(8)	117.9(3)	C(43')-Si(1')-Sc(1A)	137.4(3)	C(21')-C(22')-C(23')	122.0(4)
C(12)-C(13)-C(15)	119.0(3)	C(2')-Si(1')-Sc(1A)	32.61(17)	C(24')-C(23')-C(22')	119.2(4)
C(8)-C(13)-C(15)	123.2(3)	C(44')-Si(1')-Sc(1A)	81.5(2)	C(23')-C(24')-C(25')	122.1(4)
C(13)-C(15)-C(16)	113.1(3)	C(38')-C(1')-Sc(1')	125.7(3)	C(20')-C(25')-C(24')	117.5(4)
C(13)-C(15)-C(14)	111.3(3)	Si(1')-C(2')-Sc(1A)	115.1(3)	C(20')-C(25')-C(27')	123.8(3)
C(16)-C(15)-C(14)	109.5(4)	Si(1')-C(2')-Sc(1')	134.6(3)	C(24')-C(25')-C(27')	118.7(4)
C(9)-C(18)-C(17)	110.8(3)	Sc(1A)-C(2')-Sc(1')	19.67(12)	C(25')-C(27')-C(28')	111.1(4)
C(9)-C(18)-C(19)	113.4(4)	C(4')-N(1')-C(8')	125.6(3)	C(25')-C(27')-C(26')	111.5(4)
C(17)-C(18)-C(19)	108.5(3)	C(4')-N(1')-Sc(1')	114.1(2)	C(28')-C(27')-C(26')	109.6(4)

C(21)-C(20)-C(25)	120.1(3)	C(8')-N(1')-Sc(1')	120.3(2)	C(21')-C(30')-C(31')	110.6(4)
C(21)-C(20)-N(2)	120.5(3)	C(4')-N(1')-Sc(1A)	96.3(2)	C(21')-C(30')-C(29')	112.4(4)
C(25)-C(20)-N(2)	119.2(3)	C(8')-N(1')-Sc(1A)	136.3(2)	C(31')-C(30')-C(29')	108.2(4)
C(22)-C(21)-C(20)	118.5(4)	Sc(1')-N(1')-Sc(1A)	21.23(9)	C(1')-C(38')-C(39')	122.3(4)
C(22)-C(21)-C(30)	118.0(3)	C(6')-N(2')-C(20')	126.1(3)	C(1')-C(38')-C(40')	111.2(3)
C(20)-C(21)-C(30)	123.5(3)	C(6')-N(2')-Sc(1A)	100.1(2)	C(39')-C(38')-C(40')	108.3(2)
C(23)-C(22)-C(21)	122.0(4)	C(20')-N(2')-Sc(1A)	129.1(2)	C(1')-C(38')-C(41')	102.7(4)
C(22)-C(23)-C(24)	119.6(3)	C(6')-N(2')-Sc(1')	115.5(2)	C(39')-C(38')-C(41')	106.4(2)
C(23)-C(24)-C(25)	121.1(4)	C(20')-N(2')-Sc(1')	117.9(2)	C(40')-C(38')-C(41')	104.2(2)
C(24)-C(25)-C(20)	118.7(4)	Sc(1A)-N(2')-Sc(1')	20.89(9)	C(1')-C(38')-Sc(1')	32.5(2)
C(24)-C(25)-C(27)	118.7(4)	C(36')-C(3')-C(37')	106.0(3)	C(39')-C(38')-Sc(1')	104.5(3)
C(20)-C(25)-C(27)	122.6(3)	C(36')-C(3')-C(35')	105.7(4)	C(40')-C(38')-Sc(1')	96.0(2)
C(28)-C(27)-C(25)	110.9(4)	C(37')-C(3')-C(35')	109.7(5)	C(41')-C(38')-Sc(1')	135.1(3)
C(28)-C(27)-C(26)	108.7(4)				

Table A.26: Crystal Data and Structure Refinement for **2-Br(C₃H₅)****A. Crystal Data**

Crystallographer	Robert McDonald	University of Alberta
Empirical Formula	C ₃₇ H ₅₈ BrN ₂ Sc	
Formula Weight	667.73	
Crystal Dimensions (mm)	0.54 × 0.50 × 0.13	
Crystal System	monoclinic	
Space Group	<i>P</i> 2 ₁ / <i>n</i> (a nonstandard setting of <i>P</i> 2 ₁ / <i>c</i> [No. 14])	
Lattice Parameters		
	<i>a</i> (Å)	12.0594 (7)
	<i>b</i> (Å)	16.2933 (10)
	<i>c</i> (Å)	19.2164 (11)
	<i>β</i> (deg)	101.1698 (12)
	<i>V</i> (Å ³)	3704.3 (4)
	<i>Z</i>	4
ρ_{calcd} (g cm ⁻³)	1.197	
μ (mm ⁻¹)	1.304	

B. Data Collection and Refinement Conditions

Diffractometer	Bruker P4/RA/SMART 1000 CCD
Radiation (λ [Å])	Graphite-monochromated Mo K α (0.71073)
Temperature (°C)	-80 °C
Total Data Collected	19795 (-15 ≤ <i>h</i> ≤ 14, -20 ≤ <i>k</i> ≤ 20, -21 ≤ <i>l</i> ≤ 24)
Independent Reflections	7573
Number of Observations (<i>NO</i>)	4916 [<i>F</i> _{o2} ≥ 2 σ (<i>F</i> _{o2})]
Structure Solution	Direct methods/fragment search (<i>DIRDIF-96c</i>)
Refinement	Full-matrix least-squares on <i>F</i> ² (<i>SHELXL-93d</i>)
Absorption Correction Method	<i>SADABS</i>
Data/Restraints/Parameters	7573 [<i>F</i> _{o2} ≥ -3 σ (<i>F</i> _{o2})] / 0 / 379

Goodness-of-Fit	0.940 [$F_{o2} \geq -3\sigma(F_{o2})$]	
Final <i>R</i> indices	<i>R</i> 1 [$F_{o2} \geq 2\sigma(F_{o2})$]	0.714
	<i>wR</i> 2 [$F_{o2} \geq -3\sigma(F_{o2})$]	0.2559
Largest Difference Peak & Hole	0.449 and $-0.820 e \text{ \AA}^{-3}$	0.0408

Table A.27: Atomic Coordinates and Equivalent Isotropic Displacement Parameters for 2-Br(C₃H₅)

Atom	<i>x</i>	<i>y</i>	<i>z</i>	<i>U</i> _{eq} , Å ²
Br	0.19181(3)	0.12485(2)	0.304698(17)	0.06675(13)*
Sc	0.00528(3)	0.13542(3)	0.21589(2)	0.02836(12)*
N1	0.03592(14)	0.22030(11)	0.13982(10)	0.0292(4)*
N2	-0.10333(14)	0.21283(11)	0.25974(9)	0.0246(4)*
C1A	-0.1366(2)	0.07120(17)	0.12463(17)	0.0513(8)*
C1B	-0.0161(3)	-0.00985(17)	0.21394(17)	0.0584(8)*
C1C	-0.1182(3)	0.01962(17)	0.18177(17)	0.0544(8)*
C3	0.1698(3)	0.34648(19)	0.16209(17)	0.0586(9)*
C4	0.07486(18)	0.28791(15)	0.17790(13)	0.0336(6)*
C5	0.03848(18)	0.30800(14)	0.24070(13)	0.0308(5)*
C6	-0.05256(17)	0.28533(14)	0.27424(12)	0.0268(5)*
C7	-0.07578(19)	0.35051(15)	0.32938(13)	0.0331(6)*
C8	0.03903(19)	0.20851(15)	0.06615(13)	0.0337(6)*
C9	-0.0314(2)	0.25641(17)	0.01423(14)	0.0417(6)*
C10	-0.0270(3)	0.24371(19)	-0.05683(15)	0.0543(8)*
C11	0.0424(3)	0.1854(2)	-0.07673(16)	0.0593(9)*
C12	0.1061(2)	0.13585(18)	-0.02662(16)	0.0497(8)*
C13	0.10509(19)	0.14500(16)	0.04551(14)	0.0379(6)*
C14	0.1631(2)	-0.00272(18)	0.07565(16)	0.0542(8)*
C15	0.1770(2)	0.08725(17)	0.09784(15)	0.0449(7)*
C16	0.3026(2)	0.1101(2)	0.1118(2)	0.0867(13)*
C17	-0.2353(3)	0.2870(2)	0.00512(19)	0.0776(11)*
C18	-0.1160(3)	0.31804(19)	0.03239(16)	0.0556(8)*
C19	-0.1034(4)	0.4042(2)	0.0015(2)	0.0877(12)*
C20	-0.20265(18)	0.18266(14)	0.28467(12)	0.0284(5)*
C21	-0.30845(18)	0.19112(15)	0.24082(13)	0.0322(6)*
C22	-0.4018(2)	0.15896(18)	0.26485(15)	0.0485(7)*
C23	-0.3906(3)	0.11823(19)	0.32807(17)	0.0590(9)*
C24	-0.2848(3)	0.10744(17)	0.36906(16)	0.0504(7)*
C25	-0.1886(2)	0.13824(15)	0.34902(13)	0.0384(6)*
C26	-0.0425(3)	0.0341(2)	0.40023(16)	0.0743(10)*
C27	-0.0748(2)	0.12411(17)	0.39761(14)	0.0463(7)*
C28	-0.0738(3)	0.1534(2)	0.47401(15)	0.0587(8)*
C29	-0.4128(2)	0.1887(2)	0.11358(15)	0.0580(8)*
C30	-0.32548(19)	0.23323(15)	0.16916(13)	0.0362(6)*
C31	-0.3598(3)	0.3227(2)	0.17366(18)	0.0735(10)*
C32	-0.0840(2)	0.43654(16)	0.29559(16)	0.0487(7)*
C33	0.0252(2)	0.34864(18)	0.39250(14)	0.0501(7)*
C34	-0.1845(2)	0.33838(16)	0.35911(14)	0.0408(6)*

C35	0.2742(3)	0.3295(3)	0.2199(2)	0.0974(15)*
C36	0.1321(4)	0.4362(2)	0.1662(2)	0.0947(15)*
C37	0.2067(3)	0.3356(2)	0.09053(18)	0.0739(11)*

Table A.28: Anisotropic Displacement Parameters for **2-Br(C₃H₅)**

	<i>U</i> 11	<i>U</i> 22	<i>U</i> 33	<i>U</i> 23	<i>U</i> 13	<i>U</i> 12
Br	0.0605(2)	0.0767(3)	0.0526(2)	-0.01046(17)	-0.01482(15)	0.03080(17)
Sc	0.0328(2)	0.0276(3)	0.0250(2)	-0.00118(19)	0.00632(18)	0.00370(19)
N1	0.0276(9)	0.0313(11)	0.0303(11)	-0.0058(9)	0.0098(8)	-0.0062(8)
N2	0.0277(9)	0.0259(10)	0.0205(10)	0.0020(8)	0.0056(8)	0.0007(8)
C1A	0.0526(16)	0.0428(17)	0.056(2)	-0.0261(15)	0.0042(14)	-0.0085(14)
C1B	0.093(2)	0.0352(17)	0.054(2)	-0.0025(14)	0.0309(18)	0.0049(16)
C1C	0.069(2)	0.0349(17)	0.068(2)	-0.0232(16)	0.0355(17)	-0.0208(15)
C3	0.0618(19)	0.060(2)	0.063(2)	-0.0276(16)	0.0362(16)	-0.0387(16)
C4	0.0301(12)	0.0336(14)	0.0396(15)	-0.0044(11)	0.0126(11)	-0.0079(10)
C5	0.0289(12)	0.0283(13)	0.0348(14)	-0.0091(10)	0.0048(10)	-0.0064(10)
C6	0.0277(11)	0.0275(13)	0.0242(13)	-0.0003(10)	0.0028(9)	0.0028(10)
C7	0.0374(13)	0.0307(14)	0.0327(14)	-0.0059(11)	0.0103(11)	-0.0004(10)
C8	0.0330(12)	0.0388(15)	0.0337(14)	-0.0053(11)	0.0169(11)	-0.0147(11)
C9	0.0525(16)	0.0416(16)	0.0344(15)	0.0014(12)	0.0164(13)	-0.0112(13)
C10	0.076(2)	0.0544(19)	0.0357(17)	0.0033(14)	0.0194(15)	-0.0129(16)
C11	0.089(2)	0.062(2)	0.0359(17)	-0.0067(15)	0.0326(17)	-0.0222(18)
C12	0.0573(17)	0.0513(18)	0.0498(19)	-0.0155(15)	0.0336(15)	-0.0161(14)
C13	0.0328(12)	0.0425(16)	0.0423(16)	-0.0131(12)	0.0175(11)	-0.0152(11)
C14	0.0530(16)	0.0549(19)	0.0562(19)	-0.0104(15)	0.0141(14)	0.0068(14)
C15	0.0324(13)	0.0562(18)	0.0484(17)	-0.0188(14)	0.0132(12)	-0.0018(12)
C16	0.0360(16)	0.094(3)	0.125(4)	-0.028(2)	0.0035(19)	-0.0043(17)
C17	0.066(2)	0.105(3)	0.063(2)	0.028(2)	0.0165(18)	0.018(2)
C18	0.070(2)	0.059(2)	0.0393(17)	0.0125(14)	0.0140(15)	0.0145(16)
C19	0.124(3)	0.060(2)	0.081(3)	0.010(2)	0.026(3)	0.016(2)
C20	0.0364(12)	0.0244(13)	0.0277(13)	-0.0056(10)	0.0145(10)	-0.0050(10)
C21	0.0327(12)	0.0319(14)	0.0349(14)	-0.0081(11)	0.0135(11)	-0.0047(10)
C22	0.0396(14)	0.0570(19)	0.0524(19)	-0.0142(15)	0.0177(13)	-0.0142(13)
C23	0.069(2)	0.061(2)	0.060(2)	-0.0158(16)	0.0421(18)	-0.0309(16)
C24	0.074(2)	0.0470(18)	0.0370(16)	-0.0027(13)	0.0274(15)	-0.0191(15)
C25	0.0574(16)	0.0305(14)	0.0306(14)	-0.0043(11)	0.0169(12)	-0.0063(12)
C26	0.128(3)	0.057(2)	0.0402(19)	0.0125(16)	0.0206(19)	0.027(2)
C27	0.0659(18)	0.0478(17)	0.0262(14)	0.0093(12)	0.0109(13)	0.0051(14)
C28	0.084(2)	0.061(2)	0.0301(16)	0.0026(14)	0.0074(15)	-0.0004(17)
C29	0.0411(15)	0.080(2)	0.0494(19)	-0.0035(16)	0.0011(13)	-0.0162(15)
C30	0.0301(12)	0.0393(15)	0.0380(15)	-0.0022(11)	0.0038(11)	-0.0014(11)
C31	0.102(3)	0.055(2)	0.057(2)	0.0026(16)	-0.001(2)	0.0233(19)
C32	0.0564(16)	0.0306(15)	0.065(2)	-0.0034(13)	0.0259(15)	0.0018(13)
C33	0.0537(16)	0.0595(19)	0.0371(16)	-0.0182(14)	0.0089(13)	-0.0078(14)
C34	0.0498(15)	0.0361(15)	0.0406(16)	-0.0100(12)	0.0192(12)	-0.0012(12)
C35	0.0503(19)	0.152(4)	0.097(3)	-0.048(3)	0.032(2)	-0.057(2)
C36	0.150(4)	0.055(2)	0.102(3)	-0.025(2)	0.082(3)	-0.058(2)
C37	0.082(2)	0.075(2)	0.082(3)	-0.0312(19)	0.059(2)	-0.0520(19)

Table A.29: Bond Lengths (Å) for 2-Br(C₃H₅)

Br	Sc	2.5524(5)	C3	C36	1.538(5)	C14	C15	1.527(4)
Sc	N1	2.0965(19)	C3	C37	1.535(4)	C15	C16	1.533(4)
Sc	N2	2.1081(18)	C4	C5	1.400(3)	C17	C18	1.519(4)
Sc	C1A	2.437(3)	C5	C6	1.425(3)	C18	C19	1.544(4)
Sc	C1B	2.381(3)	C6	C7	1.563(3)	C20	C21	1.393(3)
Sc	C1C	2.414(3)	C7	C32	1.540(3)	C20	C25	1.414(3)
Sc	C4	2.765(2)†	C7	C33	1.544(4)	C21	C22	1.398(3)
Sc	C5	2.867(2)†	C7	C34	1.541(3)	C21	C30	1.516(3)
Sc	C6	2.831(2)†	C8	C9	1.413(4)	C22	C23	1.368(4)
N1	C4	1.355(3)	C8	C13	1.409(3)	C23	C24	1.374(4)
N1	C8	1.436(3)	C9	C10	1.392(4)	C24	C25	1.386(4)
N2	C6	1.335(3)	C9	C18	1.519(4)	C25	C27	1.520(4)
N2	C20	1.459(3)	C10	C11	1.369(4)	C26	C27	1.517(4)
C1A	C1C	1.366(4)	C11	C12	1.372(4)	C27	C28	1.541(4)
C1B	C1C	1.353(4)	C12	C13	1.396(4)	C29	C30	1.530(3)
C3	C4	1.565(3)	C13	C15	1.520(4)	C30	C31	1.522(4)
C3	C35	1.534(5)						

†Nonbonded Distance

Table A.30: Bond Angles (°) for 2-Br(C₃H₅)

Br	Sc	N1	105.02(5)	C6	C7	C34	116.2(2)
Br	Sc	N2	107.97(5)	C32	C7	C33	109.0(2)
Br	Sc	C1A	149.03(7)	C32	C7	C34	106.5(2)
Br	Sc	C1B	91.28(9)	C33	C7	C34	107.7(2)
Br	Sc	C1C	123.10(9)	N1	C8	C9	119.7(2)
N1	Sc	N2	95.23(7)	N1	C8	C13	120.0(2)
N1	Sc	C1A	88.60(9)	C9	C8	C13	120.1(2)
N1	Sc	C1B	132.70(9)	C8	C9	C10	118.6(3)
N1	Sc	C1C	120.59(10)	C8	C9	C18	122.8(2)
N2	Sc	C1A	98.07(8)	C10	C9	C18	118.6(3)
N2	Sc	C1B	121.82(9)	C9	C10	C11	121.3(3)
N2	Sc	C1C	100.26(8)	C10	C11	C12	120.1(3)
C1A	Sc	C1B	60.18(11)	C11	C12	C13	121.5(3)
C1A	Sc	C1C	32.72(10)	C8	C13	C12	118.2(3)
C1B	Sc	C1C	32.78(10)	C8	C13	C15	123.3(2)
Sc	N1	C4	104.42(15)	C12	C13	C15	118.5(2)
Sc	N1	C8	129.85(15)	C13	C15	C14	113.1(2)
C4	N1	C8	124.65(19)	C13	C15	C16	112.5(3)
Sc	N2	C6	108.51(13)	C14	C15	C16	109.4(2)
Sc	N2	C20	122.87(14)	C9	C18	C17	109.5(3)
C6	N2	C20	127.03(18)	C9	C18	C19	113.1(3)
Sc	C1A	C1C	72.74(16)	C17	C18	C19	109.1(3)
Sc	C1B	C1C	74.97(17)	N2	C20	C21	118.8(2)
Sc	C1C	C1A	74.55(16)	N2	C20	C25	119.5(2)
Sc	C1C	C1B	72.25(17)	C21	C20	C25	121.3(2)
C1A	C1C	C1B	125.3(3)	C20	C21	C22	117.7(2)
C4	C3	C35	106.1(3)	C20	C21	C30	122.77(19)
C4	C3	C36	109.6(2)	C22	C21	C30	119.6(2)
C4	C3	C37	117.0(2)	C21	C22	C23	121.9(3)

C35	C3	C36	110.1(3)	C22	C23	C24	119.5(2)
C35	C3	C37	106.7(3)	C23	C24	C25	121.9(3)
C36	C3	C37	107.2(3)	C20	C25	C24	117.6(3)
N1	C4	C3	125.5(2)	C20	C25	C27	123.7(2)
N1	C4	C5	121.5(2)	C24	C25	C27	118.6(2)
C3	C4	C5	112.8(2)	C25	C27	C26	111.3(2)
C4	C5	C6	136.6(2)	C25	C27	C28	112.2(2)
N2	C6	C5	119.8(2)	C26	C27	C28	108.3(2)
N2	C6	C7	127.42(19)	C21	C30	C29	111.9(2)
C5	C6	C7	112.66(19)	C21	C30	C31	111.8(2)
C6	C7	C32	109.7(2)	C29	C30	C31	109.6(2)
C6	C7	C33	107.55(19)				

Table A.31: Crystal Data and Structure Refinement for **3-CH₂SiMe₃**

A. Crystal Data

Crystallographer	Masood Parvez	University of Calgary
Empirical Formula	C ₃₉ H ₆₃ N ₂ ScSi	
Formula Weight	632.96	
Crystal size	0.25 x 0.20 x 0.12 mm ³	
Crystal System	monoclinic	
Space Group	P2 ₁ /n	
Lattice Parameters	a = 12.1877(4) Å	β = 94.6109(13)°.
	b = 18.0214(7) Å	
	c = 17.8569(7) Å	
Volume	3909.4(3) Å ³	
Z	4	
Density (calculated)	1.075 Mg/m ³	

B. Data Collection and Refinement Conditions

Diffractometer	Nonius Kappa CCD
Radiation (λ[Å])	Graphite-monochromated MoKα (0.71073)
Temperature	173(2) K
Reflections Collected	25154
Independent Reflections	6867 [R(int) = 0.069]
Structure Solution	Direct Methods
Refinement Method	Full-matrix least-squares on F ²
Data / Restraints / Parameters	6867 / 0 / 481
Goodness-of-Fit	1.17
Final R Indices [I>2σ(I)]	R1 = 0.077, wR2 = 0.172
R Indices (all data)	R1 = 0.120, wR2 = 0.190
Largest Difference Peak & Hole	0.27 and -0.22 e.Å ⁻³

Table A.32: Atomic Coordinates and Equivalent Isotropic Displacement for **3-CH₂SiMe₃**

	x	y	z	U(eq)		x	y	z	U(eq)
Sc(1)	6184(1)	964(1)	2005(1)	48(1)	C(8)	4596(3)	1605(2)	2787(2)	51(1)
C(2)	6084(7)	-1(5)	1192(6)	59(2)	C(9)	4125(3)	912(2)	2936(2)	60(1)
C(26)	9181(5)	2533(3)	2400(3)	59(2)	C(10)	4033(4)	712(3)	3681(3)	79(2)
C(28)	9194(8)	3071(7)	1114(5)	67(2)	C(11)	4401(5)	1177(3)	4262(3)	88(2)
C(29)	6825(9)	-467(6)	-12(5)	66(2)	C(12)	4840(4)	1856(3)	4102(3)	76(1)
Sc(1')	6677(3)	1567(2)	2257(2)	56(1)	C(13)	4961(3)	2083(3)	3383(2)	61(1)
C(2')	6490(50)	-340(30)	1050(30)	250(40)	C(14)	4886(5)	3486(3)	3611(3)	93(2)
C(26')	8010(20)	2451(14)	2293(12)	91(7)	C(15)	5473(4)	2840(3)	3244(3)	69(1)
C(28')	9560(30)	2960(30)	1450(30)	132(19)	C(16)	6680(5)	2852(4)	3505(5)	130(3)
C(29')	6870(50)	-270(30)	-360(20)	170(30)	C(17)	4224(5)	-412(3)	2465(4)	96(2)
Si(1)	8335(7)	238(6)	3472(5)	63(2)	C(18)	3714(4)	372(3)	2323(3)	75(1)
C(1)	7463(18)	901(11)	2990(13)	72(5)	C(19)	2454(4)	290(3)	2285(4)	95(2)
C(37)	8077(13)	-764(10)	3054(7)	67(3)	C(20)	7695(3)	1335(2)	986(2)	46(1)
C(38)	8330(20)	325(14)	4496(8)	207(10)	C(21)	7748(3)	610(2)	709(2)	52(1)
C(39)	9708(8)	592(8)	3190(9)	135(6)	C(22)	8777(4)	292(3)	670(2)	62(1)
Si(1')	7985(9)	142(7)	3562(7)	59(2)	C(23)	9716(4)	655(3)	910(3)	71(1)
C(1')	7190(20)	658(16)	2922(19)	98(9)	C(24)	9663(3)	1363(3)	1203(2)	63(1)
C(37')	8480(30)	-733(16)	3350(20)	223(19)	C(25)	8658(3)	1725(2)	1255(2)	49(1)
C(38')	7081(17)	26(8)	4333(7)	115(7)	C(27)	8616(3)	2494(2)	1581(2)	57(1)
C(39')	9395(15)	313(10)	3995(12)	144(10)	C(30)	6685(3)	193(2)	473(3)	60(1)
N(1)	4890(3)	1751(2)	2041(2)	49(1)	C(31)	3520(4)	3464(2)	1455(3)	76(2)
N(2)	6635(2)	1647(2)	1101(2)	42(1)	C(32)	2572(3)	2350(3)	869(3)	79(2)
C(3)	3332(3)	2624(2)	1537(2)	56(1)	C(33)	2722(4)	2504(3)	2245(3)	69(1)
C(4)	4449(3)	2206(2)	1514(2)	45(1)	C(34)	7307(4)	2002(3)	-458(2)	60(1)
C(5)	4976(3)	2326(2)	854(2)	43(1)	C(35)	6390(4)	3173(2)	-144(3)	71(1)
C(6)	5993(3)	2062(2)	635(2)	42(1)	C(36)	5299(4)	2104(3)	-726(2)	76(1)
C(7)	6263(3)	2322(2)	-161(2)	53(1)					

Table A.33: Anisotropic Displacement Parameters for **3-CH₂SiMe₃**

Atom	U11	U22	U33	U23	U13	U12
Sc(1)	45(1)	49(1)	50(1)	5(1)	10(1)	5(1)
C(2)	41(3)	52(4)	86(5)	11(3)	13(3)	12(3)
C(26)	50(3)	80(4)	45(3)	-1(3)	0(2)	-12(3)
C(28)	55(6)	81(6)	64(5)	8(4)	7(4)	-14(5)
C(29)	64(5)	67(4)	67(7)	-13(4)	3(5)	5(4)
Sc(1')	38(2)	80(3)	50(2)	-1(2)	3(2)	3(2)
C(2')	290(80)	270(70)	160(50)	110(50)	-110(50)	-210(60)
C(26')	89(18)	120(20)	68(14)	-16(13)	-1(12)	7(15)
C(28')	70(30)	80(20)	260(70)	-30(40)	30(30)	-19(19)
C(29')	150(40)	240(60)	100(30)	-80(30)	-70(30)	90(40)
Si(1)	51(4)	80(4)	56(3)	3(2)	1(2)	10(3)
C(1)	76(14)	52(9)	82(8)	5(7)	-33(9)	-15(7)
C(37)	70(7)	68(7)	61(6)	-8(5)	4(5)	1(5)
C(38)	200(30)	330(30)	85(11)	-27(13)	-8(12)	10(20)
C(39)	54(7)	163(13)	185(15)	66(11)	-12(8)	4(7)
Si(1')	59(5)	61(3)	58(3)	7(2)	2(3)	1(4)

C(1')	55(11)	110(20)	124(19)	38(16)	-17(11)	-26(12)
C(37')	240(40)	73(15)	370(50)	10(30)	120(30)	30(20)
C(38')	193(19)	89(10)	73(9)	28(7)	64(10)	31(10)
C(39')	114(14)	133(14)	170(20)	-3(13)	-85(15)	-16(11)
N(1)	40(2)	58(2)	50(2)	-1(2)	14(2)	4(2)
N(2)	29(2)	51(2)	46(2)	-1(1)	5(1)	0(1)
C(3)	39(2)	57(3)	73(3)	-3(2)	16(2)	5(2)
C(4)	32(2)	46(2)	57(2)	-7(2)	7(2)	-2(2)
C(5)	35(2)	47(2)	48(2)	2(2)	5(2)	4(2)
C(6)	37(2)	46(2)	43(2)	-4(2)	4(2)	-2(2)
C(7)	49(2)	63(3)	47(2)	8(2)	9(2)	8(2)
C(8)	41(2)	61(3)	52(2)	2(2)	16(2)	3(2)
C(9)	50(3)	61(3)	70(3)	3(2)	21(2)	-3(2)
C(10)	81(4)	69(3)	91(4)	14(3)	39(3)	-2(3)
C(11)	103(4)	104(5)	60(3)	15(3)	34(3)	7(4)
C(12)	78(4)	95(4)	60(3)	-7(3)	25(3)	-10(3)
C(13)	52(3)	78(3)	55(3)	-6(2)	22(2)	-6(2)
C(14)	93(4)	83(4)	110(4)	-33(3)	43(3)	-20(3)
C(15)	71(3)	69(3)	71(3)	-18(2)	32(2)	-16(3)
C(16)	68(4)	107(5)	215(8)	-15(5)	17(5)	-26(4)
C(17)	95(4)	68(4)	130(5)	-2(3)	28(4)	-3(3)
C(18)	61(3)	71(3)	95(4)	-6(3)	19(3)	-18(3)
C(19)	63(3)	86(4)	135(5)	11(4)	4(3)	-19(3)
C(20)	33(2)	64(3)	43(2)	8(2)	9(2)	8(2)
C(21)	41(2)	63(3)	53(2)	-2(2)	6(2)	11(2)
C(22)	55(3)	69(3)	64(3)	-4(2)	8(2)	19(2)
C(23)	45(3)	96(4)	72(3)	0(3)	11(2)	26(3)
C(24)	34(2)	91(4)	63(3)	3(2)	6(2)	8(2)
C(25)	36(2)	64(3)	48(2)	3(2)	9(2)	3(2)
C(27)	41(2)	71(3)	61(3)	1(2)	10(2)	-7(2)
C(30)	50(3)	58(3)	70(3)	-6(2)	1(2)	5(2)
C(31)	69(3)	60(3)	103(4)	8(3)	33(3)	22(2)
C(32)	33(2)	110(4)	94(4)	-17(3)	2(2)	15(3)
C(33)	46(3)	74(3)	91(3)	3(3)	31(2)	10(2)
C(34)	62(3)	76(3)	44(2)	6(2)	17(2)	9(2)
C(35)	76(3)	66(3)	73(3)	18(2)	24(2)	5(2)
C(36)	66(3)	112(4)	47(3)	8(3)	-2(2)	1(3)

Table A.34: Bond Lengths [\AA] for **3-CH₂SiMe₃**

Sc(1)-N(1)	2.126(3)	Si(1)-C(38)	1.836(17)	C(8)-C(9)	1.409(6)
Sc(1)-N(2)	2.136(3)	Si(1)-C(39)	1.896(13)	C(8)-C(13)	1.412(6)
Sc(1)-C(1)	2.26(2)	Si(1)-C(37)	1.97(2)	C(9)-C(10)	1.391(6)
Sc(1)-C(2)	2.263(9)	Si(1')-C(1')	1.71(3)	C(9)-C(18)	1.521(6)
Sc(1)-C(8)	2.732(4)	Si(1')-(37')	1.74(3)	C(10)-C(11)	1.381(7)
Sc(1)-C(20)	2.773(4)	Si(1')-(38')	1.842(15)	C(11)-C(12)	1.375(7)
C(2)-C(30)	1.569(11)	Si(1')-(39')	1.853(17)	C(12)-C(13)	1.368(6)
C(26)-C(27)	1.566(6)	N(1)-C(4)	1.329(5)	C(13)-C(15)	1.528(6)
C(28)-C(27)	1.538(12)	N(1)-C(8)	1.430(5)	C(14)-C(15)	1.541(6)
C(29)-C(30)	1.489(11)	N(2)-C(6)	1.327(5)	C(15)-C(16)	1.507(7)

Sc(1')-N(2)	2.065(4)	N(2)-C(20)	1.439(4)	C(17)-C(18)	1.556(7)
Sc(1')-C(1')	2.09(3)	C(3)-C(32)	1.532(6)	C(18)-C(19)	1.539(7)
Sc(1')-N(1)	2.206(4)	C(3)-C(33)	1.534(6)	C(20)-C(21)	1.400(6)
Sc(1')-C(26')	2.27(2)	C(3)-C(31)	1.539(6)	C(20)-C(25)	1.418(5)
Sc(1')-C(20)	2.705(5)	C(3)-C(4)	1.559(5)	C(21)-C(22)	1.385(5)
Sc(1')-C(8)	2.778(5)	C(4)-C(5)	1.403(5)	C(21)-C(30)	1.527(6)
C(2')-C(30)	1.45(5)	C(5)-C(6)	1.411(5)	C(22)-C(23)	1.356(6)
C(26')-C(27)	1.52(2)	C(6)-C(7)	1.558(5)	C(23)-C(24)	1.384(6)
C(28')-C(27)	1.46(4)	C(7)-C(34)	1.530(5)	C(24)-C(25)	1.398(5)
C(29')-C(30)	1.73(5)	C(7)-C(36)	1.537(6)	C(25)-C(27)	1.507(6)
Si(1)-C(1)	1.77(3)	C(7)-C(35)	1.541(6)		

Table A.35: Bond Angles [$^{\circ}$] for **3-CH₂SiMe₃**

N(1)-Sc(1)-N(2)	82.84(12)	C(4)-N(1)-Sc(1)	130.5(2)	C(12)-C(13)-C(15)	119.7(4)
N(1)-Sc(1)-C(1)	118.5(6)	C(8)-N(1)-Sc(1)	98.5(2)	C(8)-C(13)-C(15)	122.0(4)
N(2)-Sc(1)-C(1)	114.5(5)	C(4)-N(1)-Sc(1')	123.6(3)	C(16)-C(15)-C(13)	111.4(5)
N(1)-Sc(1)-C(2)	122.0(2)	C(8)-N(1)-Sc(1')	97.3(2)	C(16)-C(15)-C(14)	109.4(5)
N(2)-Sc(1)-C(2)	87.8(3)	Sc(1)-N(1)-Sc(1')	34.97(11)	C(13)-C(15)-C(14)	113.3(4)
C(1)-Sc(1)-C(2)	117.4(6)	C(6)-N(2)-C(20)	128.4(3)	C(9)-C(18)-C(19)	111.2(4)
N(1)-Sc(1)-C(8)	31.20(12)	C(6)-N(2)-Sc(1')	129.2(3)	C(9)-C(18)-C(17)	111.1(4)
N(2)-Sc(1)-C(8)	112.24(12)	C(20)-N(2)-Sc(1')	99.5(2)	C(19)-C(18)-C(17)	107.7(4)
C(1)-Sc(1)-C(8)	95.5(7)	C(6)-N(2)-Sc(1)	128.6(2)	C(21)-C(20)-C(25)	121.5(3)
C(2)-Sc(1)-C(8)	130.5(2)	C(20)-N(2)-Sc(1)	99.9(2)	C(21)-C(20)-N(2)	118.8(3)
N(1)-Sc(1)-C(20)	113.12(12)	Sc(1')-N(2)-Sc(1)	36.11(12)	C(25)-C(20)-N(2)	119.1(3)
N(2)-Sc(1)-C(20)	30.74(11)	C(32)-C(3)-C(33)	107.1(4)	C(21)-C(20)-Sc(1')	118.5(3)
C(1)-Sc(1)-C(20)	94.0(6)	C(32)-C(3)-C(31)	109.2(4)	C(25)-C(20)-Sc(1')	93.6(2)
C(2)-Sc(1)-C(20)	76.6(3)	C(33)-C(3)-C(31)	107.7(4)	N(2)-C(20)-Sc(1')	48.82(17)
C(8)-Sc(1)-C(20)	140.23(13)	C(32)-C(3)-C(4)	107.3(3)	C(21)-C(20)-Sc(1)	93.4(2)
C(30)-C(2)-Sc(1)	110.4(5)	C(33)-C(3)-C(4)	115.8(4)	C(25)-C(20)-Sc(1)	118.2(3)
N(2)-Sc(1')-C(1')	127.1(10)	C(31)-C(3)-C(4)	109.6(3)	N(2)-C(20)-Sc(1)	49.36(16)
N(2)-Sc(1')-N(1)	82.57(16)	N(1)-C(4)-C(5)	120.2(3)	Sc(1')-C(20)-Sc(1)	27.50(9)
C(1')-Sc(1')-N(1)	117.7(8)	N(1)-C(4)-C(3)	125.7(3)	C(22)-C(21)-C(20)	118.1(4)
N(2)-Sc(1')-C(26')	86.6(6)	C(5)-C(4)-C(3)	114.1(3)	C(22)-C(21)-C(30)	122.3(4)
C(1')-Sc(1')-(26')	110.5(9)	C(4)-C(5)-C(6)	130.8(4)	C(20)-C(21)-C(30)	119.6(3)
N(1)-Sc(1')-C(26')	126.4(7)	N(2)-C(6)-C(5)	120.1(3)	C(23)-C(22)-C(21)	122.0(4)
N(2)-Sc(1')-C(20)	31.64(12)	N(2)-C(6)-C(7)	125.8(3)	C(22)-C(23)-C(24)	120.0(4)
C(1')-Sc(1')-C(20)	102.5(10)	C(5)-C(6)-C(7)	114.0(3)	C(23)-C(24)-C(25)	121.5(4)
N(1)-Sc(1')-C(20)	112.96(17)	C(34)-C(7)-C(36)	106.8(4)	C(24)-C(25)-C(20)	116.9(4)
C(26')-Sc(1')-C(20)	75.9(6)	C(34)-C(7)-C(35)	107.3(4)	C(24)-C(25)-C(27)	120.8(4)
N(2)-Sc(1')-C(8)	112.89(17)	C(36)-C(7)-C(35)	109.8(4)	C(20)-C(25)-C(27)	122.3(3)
C(1')-Sc(1')-C(8)	93.9(9)	C(34)-C(7)-C(6)	116.4(3)	C(28')-C(27)-C(25)	114.8(19)
N(1)-Sc(1')-C(8)	30.71(12)	C(36)-C(7)-C(6)	108.4(3)	C(28')-C(27)-C(26')	127(2)
C(26')-Sc(1')-C(8)	130.1(6)	C(35)-C(7)-C(6)	108.0(3)	C(25)-C(27)-C(26')	108.0(10)
C(20)-Sc(1')-C(8)	141.50(18)	C(9)-C(8)-C(13)	120.4(4)	C(28')-C(27)-C(28)	28.4(17)
C(27)-C(26')-Sc(1')	114.0(12)	C(9)-C(8)-N(1)	118.4(4)	C(25)-C(27)-C(28)	112.4(6)
C(1)-Si(1)-C(38)	112.1(12)	C(13)-C(8)-N(1)	120.1(4)	C(26')-C(27)-C(28)	139.6(11)
C(1)-Si(1)-C(39)	98.7(8)	C(9)-C(8)-Sc(1)	92.2(3)	C(28')-C(27)-C(26)	80.4(19)
C(38)-Si(1)-C(39)	107.9(10)	C(13)-C(8)-Sc(1)	116.7(3)	C(25)-C(27)-C(26)	112.1(4)
C(1)-Si(1)-C(37)	111.3(8)	N(1)-C(8)-Sc(1)	50.34(17)	C(26')-C(27)-C(26)	55.2(9)

C(38)-Si(1)-C(37)	116.3(10)	C(9)-C(8)-Sc(1')	116.1(3)	C(28)-C(27)-C(26)	106.9(5)
C(39)-Si(1)-C(37)	109.0(8)	C(13)-C(8)-Sc(1')	91.8(3)	C(2')-C(30)-C(29)	85(3)
Si(1)-C(1)-Sc(1)	139.5(10)	N(1)-C(8)-Sc(1')	51.97(18)	C(2')-C(30)-C(21)	108.4(19)
C(1')-Si(1')-C(37')	122.2(18)	Sc(1)-C(8)-Sc(1')	27.36(9)	C(29)-C(30)-C(21)	114.8(5)
C(1')-Si(1')-C(38')	102.9(13)	C(10)-C(9)-C(8)	118.4(4)	C(2')-C(30)-C(2)	32(3)
C(37')-Si(1')-C(38')	107.4(13)	C(10)-C(9)-C(18)	118.4(4)	C(29)-C(30)-C(2)	112.3(6)
C(1')-Si(1')-C(39')	130.0(11)	C(8)-C(9)-C(18)	123.1(4)	C(21)-C(30)-C(2)	109.0(5)
C(37')-Si(1')-C(39')	85.1(17)	C(11)-C(10)-C(9)	121.0(5)	C(2')-C(30)-C(29')	109(3)
C(38')-Si(1')-C(39')	107.3(12)	C(12)-C(11)-C(10)	119.5(5)	C(29)-C(30)-C(29')	24.6(19)
Si(1')-C(1')-Sc(1')	159.1(13)	C(13)-C(12)-C(11)	122.3(5)	C(21)-C(30)-C(29')	108(2)
C(4)-N(1)-C(8)	131.0(3)	C(12)-C(13)-C(8)	118.3(4)	C(2)-C(30)-C(29')	134(2)

Table A.36: Crystal Data and Structure Refinement for **4-H₂B(C₆F₅)₂**

A. Crystal Data

Crystallographer	Masood Parvez	University of Calgary
Empirical Formula	C ₅₉ H ₅₇ B ₂ F ₂₀ N ₂ Sc•C ₆ H ₁₄	
Formula Weight	1326.82	
Crystal Size	0.27 x 0.22 x 0.20 mm ³	
Crystal System	monoclinic	
Space Group	P21/n	
Lattice Parameters	a = 13.47120(10) Å	α = 90°.
	b = 18.5810(2) Å	β = 90.8990(10)°.
	c = 26.1801(2) Å	γ = 90°.
Volume	6552.29(10) Å ³	
Z	4	
Density (calculated)	1.345 Mg/m ³	

B. Data Collection and Refinement Conditions

Diffractometer	Nonius Kappa CCD
Radiation (λ[Å])	Graphite-monochromated MoKα (0.71073)
Temperature	173(2) K
Reflections Collected	35187
Independent Reflections	18604 [R(int) = 0.037]
Structure Solution	Direct Methods
Refinement Method	Full-matrix least-squares on F ²
Data / Restraints / Parameters	18604 / 0 / 822
Goodness-of-Fit	1.02
Final R Indices [I>2σ(I)]	R1 = 0.057, wR2 = 0.144
R Indices (all data)	R1 = 0.097, wR2 = 0.165
Largest Difference Peak & Hole	0.40 and -0.42 e.Å ⁻³

Table A.37: Atomic Coordinates and Equivalent Isotropic Displacement for **4-H₂B(C₆F₅)₂**

	x	y	z	U(eq)		x	y	z	U(eq)
Sc(1)	-1902(1)	2169(1)	742(1)	24(1)	C(26)	-1961(2)	2627(2)	2799(1)	61(1)
F(1)	2162(1)	1513(1)	941(1)	59(1)	C(27)	-1382(2)	2455(1)	2315(1)	44(1)
F(2)	2576(1)	415(1)	1560(1)	70(1)	C(28)	-519(2)	1945(1)	2451(1)	50(1)
F(3)	1108(1)	-280(1)	2059(1)	69(1)	C(29)	-1724(3)	5119(2)	888(1)	83(1)
F(4)	-822(1)	147(1)	1919(1)	58(1)	C(30)	-1394(2)	4326(1)	858(1)	51(1)
F(5)	-1240(1)	1271(1)	1293(1)	38(1)	C(31)	-590(2)	4255(2)	457(1)	62(1)
F(6)	899(1)	1660(1)	-270(1)	60(1)	C(32)	-3138(2)	4155(2)	1950(1)	61(1)
F(7)	2331(2)	2367(1)	-762(1)	91(1)	C(33)	-4212(2)	4215(2)	1167(1)	65(1)
F(8)	3185(1)	3548(1)	-331(1)	106(1)	C(34)	-4506(2)	3272(2)	1838(1)	66(1)
F(9)	2569(2)	4022(1)	585(1)	123(1)	C(35)	-4560(2)	1181(1)	102(1)	48(1)
F(10)	1131(1)	3320(1)	1080(1)	83(1)	C(36)	-5459(2)	1366(2)	916(1)	54(1)
F(11)	-3030(1)	4081(1)	-25(1)	61(1)	C(37)	-5347(2)	2349(2)	288(1)	51(1)
F(12)	-4659(2)	4561(1)	-511(1)	94(1)	C(38)	431(1)	1422(1)	1080(1)	34(1)
F(13)	-5631(1)	3720(1)	-1207(1)	101(1)	C(39)	1396(2)	1182(1)	1170(1)	42(1)
F(14)	-4965(1)	2353(1)	-1387(1)	86(1)	C(40)	1628(2)	621(2)	1490(1)	49(1)
F(15)	-3308(1)	1881(1)	-924(1)	57(1)	C(41)	886(2)	260(1)	1743(1)	48(1)
F(16)	-1165(1)	3834(1)	-713(1)	58(1)	C(42)	-86(2)	475(1)	1672(1)	41(1)
F(17)	108(1)	3750(1)	-1489(1)	72(1)	C(43)	-265(1)	1046(1)	1349(1)	35(1)
F(18)	714(1)	2454(1)	-1837(1)	76(1)	C(44)	907(2)	2487(1)	410(1)	40(1)
F(19)	33(2)	1230(1)	-1393(1)	79(1)	C(45)	1262(2)	2268(1)	-55(1)	45(1)
F(20)	-1253(1)	1298(1)	-633(1)	59(1)	C(46)	2015(2)	2619(2)	-310(1)	61(1)
N(1)	-3049(1)	1511(1)	950(1)	27(1)	C(47)	2443(2)	3209(2)	-93(1)	71(1)
N(2)	-2140(1)	2974(1)	1316(1)	30(1)	C(48)	2138(2)	3449(2)	371(1)	72(1)
C(3)	-4773(1)	1722(1)	533(1)	38(1)	C(49)	1383(2)	3079(2)	618(1)	57(1)
C(4)	-3799(1)	1968(1)	811(1)	29(1)	C(50)	-3104(2)	2954(1)	-447(1)	41(1)
C(5)	-3679(1)	2703(1)	900(1)	32(1)	C(51)	-3487(2)	3633(1)	-362(1)	49(1)
C(6)	-3087(1)	3123(1)	1267(1)	32(1)	C(52)	-4330(2)	3896(2)	-608(1)	64(1)
C(7)	-3703(2)	3697(1)	1552(1)	47(1)	C(53)	-4823(2)	3467(2)	-960(1)	72(1)
C(8)	-3177(1)	749(1)	1055(1)	33(1)	C(54)	-4482(2)	2787(2)	-1054(1)	62(1)
C(9)	-2830(2)	221(1)	713(1)	38(1)	C(55)	-3629(2)	2546(2)	-807(1)	48(1)
C(10)	-2977(2)	-504(1)	830(1)	55(1)	C(56)	-1252(2)	2571(1)	-627(1)	35(1)
C(11)	-3434(2)	-711(1)	1271(1)	69(1)	C(57)	-874(2)	3177(1)	-865(1)	42(1)
C(12)	-3726(2)	-193(2)	1617(1)	61(1)	C(58)	-216(2)	3146(1)	-1266(1)	50(1)
C(13)	-3591(2)	540(1)	1525(1)	42(1)	C(59)	79(2)	2492(2)	-1448(1)	51(1)
C(14)	-3066(2)	958(2)	2386(1)	65(1)	C(60)	-271(2)	1874(1)	-1228(1)	52(1)
C(15)	-3818(2)	1064(1)	1951(1)	47(1)	C(61)	-932(2)	1926(1)	-828(1)	42(1)
C(16)	-4863(2)	986(2)	2173(1)	69(1)	B(1)	49(2)	2060(1)	707(1)	33(1)
C(17)	-1193(2)	168(1)	263(1)	47(1)	B(2)	-2098(2)	2635(1)	-195(1)	32(1)
C(18)	-2286(2)	389(1)	221(1)	38(1)	C(1S)	-7837(5)	77(3)	3346(2)	146(2)
C(19)	-2740(2)	7(2)	-252(1)	56(1)	C(2S)	-7494(8)	647(6)	3105(3)	234(5)
C(20)	-1400(1)	3398(1)	1595(1)	35(1)	C(3S)	-7700(6)	1258(4)	2964(4)	179(3)
C(21)	-1033(2)	4028(1)	1372(1)	42(1)	C(4S)	-7383(4)	1885(5)	2723(2)	140(2)
C(22)	-275(2)	4396(1)	1631(1)	50(1)	C(5S)	-7649(7)	2539(8)	2812(5)	121(4)
C(23)	105(2)	4151(1)	2092(1)	54(1)	C(5S')	-7380(17)	2472(10)	2396(9)	240(11)
C(24)	-258(2)	3530(1)	2301(1)	49(1)	C(6S)	-7218(5)	3119(4)	2359(4)	206(4)
C(25)	-1011(2)	3131(1)	2059(1)	39(1)					

Table A.38: Anisotropic Displacement Parameters for **4-H₂B(C₆F₅)₂**

Atom	U11	U22	U33	U23	U13	U12
Sc(1)	22(1)	27(1)	24(1)	0(1)	1(1)	0(1)
F(1)	24(1)	80(1)	75(1)	2(1)	6(1)	4(1)
F(2)	39(1)	93(1)	76(1)	-1(1)	-13(1)	29(1)
F(3)	70(1)	68(1)	69(1)	16(1)	-16(1)	26(1)
F(4)	54(1)	56(1)	65(1)	23(1)	7(1)	5(1)
F(5)	24(1)	43(1)	46(1)	8(1)	3(1)	4(1)
F(6)	57(1)	63(1)	59(1)	-15(1)	15(1)	9(1)
F(7)	80(1)	114(2)	80(1)	24(1)	49(1)	27(1)
F(8)	57(1)	84(1)	178(2)	62(1)	54(1)	5(1)
F(9)	82(2)	80(2)	207(3)	-31(2)	30(2)	-47(1)
F(10)	65(1)	91(1)	95(1)	-46(1)	16(1)	-31(1)
F(11)	74(1)	54(1)	55(1)	-1(1)	-8(1)	23(1)
F(12)	98(1)	105(2)	78(1)	24(1)	0(1)	62(1)
F(13)	61(1)	182(2)	61(1)	43(1)	-14(1)	35(1)
F(14)	69(1)	144(2)	44(1)	10(1)	-25(1)	-22(1)
F(15)	61(1)	71(1)	39(1)	-7(1)	-5(1)	-10(1)
F(16)	90(1)	37(1)	49(1)	1(1)	15(1)	-5(1)
F(17)	97(1)	65(1)	55(1)	7(1)	24(1)	-36(1)
F(18)	72(1)	97(1)	59(1)	-8(1)	39(1)	-16(1)
F(19)	98(1)	62(1)	80(1)	-16(1)	41(1)	10(1)
F(20)	80(1)	37(1)	62(1)	0(1)	29(1)	-5(1)
N(1)	22(1)	30(1)	29(1)	2(1)	3(1)	1(1)
N(2)	30(1)	32(1)	29(1)	-4(1)	-2(1)	4(1)
C(3)	23(1)	48(1)	43(1)	0(1)	-4(1)	-1(1)
C(4)	22(1)	36(1)	27(1)	3(1)	2(1)	2(1)
C(5)	26(1)	37(1)	33(1)	2(1)	-3(1)	6(1)
C(6)	34(1)	32(1)	30(1)	-2(1)	0(1)	9(1)
C(7)	42(1)	48(1)	49(1)	-13(1)	0(1)	19(1)
C(8)	26(1)	33(1)	38(1)	5(1)	4(1)	-3(1)
C(9)	37(1)	32(1)	43(1)	2(1)	7(1)	-4(1)
C(10)	70(2)	31(1)	66(2)	2(1)	15(1)	-4(1)
C(11)	92(2)	35(1)	81(2)	13(1)	23(2)	-9(1)
C(12)	72(2)	51(2)	60(2)	17(1)	22(1)	-7(1)
C(13)	38(1)	44(1)	43(1)	10(1)	10(1)	-1(1)
C(14)	62(2)	80(2)	53(2)	2(1)	4(1)	-3(2)
C(15)	51(1)	52(1)	39(1)	11(1)	16(1)	4(1)
C(16)	56(2)	101(2)	50(1)	12(1)	23(1)	15(2)
C(17)	45(1)	36(1)	61(1)	-8(1)	11(1)	1(1)
C(18)	42(1)	31(1)	42(1)	-6(1)	10(1)	-4(1)
C(19)	57(2)	56(2)	55(1)	-15(1)	7(1)	-7(1)
C(20)	32(1)	37(1)	37(1)	-13(1)	-4(1)	5(1)
C(21)	45(1)	32(1)	48(1)	-10(1)	-6(1)	0(1)
C(22)	52(1)	37(1)	61(1)	-13(1)	-6(1)	-6(1)
C(23)	45(1)	56(2)	59(1)	-25(1)	-10(1)	-5(1)
C(24)	44(1)	62(2)	40(1)	-16(1)	-11(1)	4(1)
C(25)	36(1)	47(1)	35(1)	-11(1)	-4(1)	6(1)
C(26)	50(1)	87(2)	45(1)	0(1)	6(1)	10(1)
C(27)	46(1)	56(1)	29(1)	-3(1)	-8(1)	1(1)

C(28)	56(1)	58(2)	37(1)	-5(1)	-10(1)	6(1)
C(29)	108(3)	35(1)	104(2)	7(1)	-33(2)	3(2)
C(30)	64(2)	30(1)	58(1)	3(1)	-14(1)	-7(1)
C(31)	79(2)	55(2)	52(1)	12(1)	-10(1)	-24(1)
C(32)	64(2)	59(2)	60(2)	-28(1)	-4(1)	25(1)
C(33)	65(2)	55(2)	74(2)	-14(1)	-14(1)	36(1)
C(34)	54(2)	84(2)	62(2)	-16(1)	20(1)	16(1)
C(35)	36(1)	63(2)	45(1)	-9(1)	-6(1)	-5(1)
C(36)	29(1)	75(2)	58(1)	2(1)	3(1)	-9(1)
C(37)	33(1)	67(2)	53(1)	0(1)	-12(1)	7(1)
C(38)	25(1)	40(1)	36(1)	-8(1)	0(1)	3(1)
C(39)	26(1)	55(1)	45(1)	-8(1)	1(1)	6(1)
C(40)	32(1)	63(2)	52(1)	-9(1)	-7(1)	16(1)
C(41)	53(1)	47(1)	45(1)	1(1)	-12(1)	19(1)
C(42)	41(1)	44(1)	40(1)	3(1)	0(1)	4(1)
C(43)	25(1)	39(1)	39(1)	-2(1)	-2(1)	7(1)
C(44)	29(1)	37(1)	53(1)	1(1)	8(1)	1(1)
C(45)	35(1)	43(1)	58(1)	8(1)	11(1)	11(1)
C(46)	46(1)	67(2)	71(2)	26(1)	27(1)	21(1)
C(47)	42(1)	55(2)	116(2)	35(2)	30(2)	9(1)
C(48)	45(1)	47(2)	123(3)	0(2)	13(2)	-13(1)
C(49)	38(1)	52(2)	82(2)	-10(1)	12(1)	-10(1)
C(50)	38(1)	58(1)	26(1)	7(1)	2(1)	5(1)
C(51)	49(1)	63(2)	35(1)	9(1)	-1(1)	12(1)
C(52)	62(2)	85(2)	46(1)	21(1)	5(1)	32(2)
C(53)	48(1)	129(3)	38(1)	28(2)	-4(1)	20(2)
C(54)	48(1)	106(2)	32(1)	14(1)	-8(1)	-6(2)
C(55)	44(1)	70(2)	29(1)	7(1)	-1(1)	-1(1)
C(56)	35(1)	42(1)	29(1)	2(1)	2(1)	-3(1)
C(57)	50(1)	42(1)	35(1)	0(1)	5(1)	-7(1)
C(58)	56(1)	56(2)	38(1)	4(1)	9(1)	-19(1)
C(59)	48(1)	68(2)	38(1)	-3(1)	16(1)	-10(1)
C(60)	56(1)	50(1)	50(1)	-9(1)	15(1)	-1(1)
C(61)	46(1)	40(1)	41(1)	2(1)	11(1)	-4(1)
B(1)	26(1)	36(1)	37(1)	-5(1)	3(1)	0(1)
B(2)	33(1)	36(1)	27(1)	2(1)	1(1)	-1(1)
C(1S)	186(6)	108(4)	145(5)	-15(4)	16(4)	9(4)
C(2S)	318(14)	196(10)	185(7)	63(7)	-80(8)	-20(10)
C(3S)	155(6)	107(5)	273(10)	-30(6)	-58(6)	27(5)
C(4S)	92(4)	194(8)	136(5)	8(5)	2(3)	14(5)
C(5S)	58(5)	151(11)	154(10)	-28(8)	24(5)	-3(6)
C(5S')	280(20)	121(13)	320(30)	81(17)	100(20)	1(14)
C(6S)	106(5)	158(7)	355(12)	53(8)	7(6)	-18(5)

Table A.39: Bond Lengths [\AA] for $4\text{-H}_2\text{B}(\text{C}_6\text{F}_5)_2$

Sc(1)-N(1)	2.0517(15)	C(3)-C(4)	1.559(3)	C(38)-B(1)	1.615(3)
Sc(1)-N(2)	2.1475(15)	C(4)-C(5)	1.394(3)	C(39)-C(40)	1.372(3)
Sc(1)-F(5)	2.3704(12)	C(5)-C(6)	1.463(3)	C(40)-C(41)	1.380(4)
Sc(1)-C(4)	2.5911(17)	C(6)-C(7)	1.552(3)	C(41)-C(42)	1.378(3)

Sc(1)-C(5)	2.6302(18)	C(7)-C(32)	1.537(3)	C(42)-C(43)	1.376(3)
Sc(1)-C(6)	2.7642(18)	C(7)-C(34)	1.542(4)	C(44)-C(45)	1.377(3)
F(1)-C(39)	1.349(3)	C(7)-C(33)	1.547(3)	C(44)-C(49)	1.381(3)
F(2)-C(40)	1.341(2)	C(8)-C(9)	1.413(3)	C(44)-B(1)	1.612(3)
F(3)-C(41)	1.333(3)	C(8)-C(13)	1.414(3)	C(45)-C(46)	1.385(3)
F(4)-C(42)	1.339(3)	C(9)-C(10)	1.396(3)	C(46)-C(47)	1.358(5)
F(5)-C(43)	1.385(2)	C(9)-C(18)	1.523(3)	C(47)-C(48)	1.365(5)
F(6)-C(45)	1.351(3)	C(10)-C(11)	1.372(4)	C(48)-C(49)	1.395(4)
F(7)-C(46)	1.349(3)	C(11)-C(12)	1.382(4)	C(50)-C(51)	1.381(3)
F(8)-C(47)	1.343(3)	C(12)-C(13)	1.396(3)	C(50)-C(55)	1.395(3)
F(9)-C(48)	1.332(3)	C(13)-C(15)	1.514(3)	C(50)-B(2)	1.610(3)
F(10)-C(49)	1.338(3)	C(14)-C(15)	1.526(4)	C(51)-C(52)	1.387(3)
F(11)-C(51)	1.353(3)	C(15)-C(16)	1.539(3)	C(52)-C(53)	1.381(5)
F(12)-C(52)	1.339(3)	C(17)-C(18)	1.531(3)	C(53)-C(54)	1.367(5)
F(13)-C(53)	1.343(3)	C(18)-C(19)	1.543(3)	C(54)-C(55)	1.383(3)
F(14)-C(54)	1.350(3)	C(20)-C(21)	1.401(3)	C(56)-C(61)	1.381(3)
F(15)-C(55)	1.346(3)	C(20)-C(25)	1.408(3)	C(56)-C(57)	1.388(3)
F(16)-C(57)	1.346(3)	C(21)-C(22)	1.397(3)	C(56)-B(2)	1.622(3)
F(17)-C(58)	1.341(3)	C(21)-C(30)	1.528(3)	C(57)-C(58)	1.385(3)
F(18)-C(59)	1.343(2)	C(22)-C(23)	1.380(4)	C(58)-C(59)	1.367(4)
F(19)-C(60)	1.340(3)	C(23)-C(24)	1.370(4)	C(59)-C(60)	1.373(4)
F(20)-C(61)	1.346(2)	C(24)-C(25)	1.400(3)	C(60)-C(61)	1.387(3)
N(1)-C(4)	1.365(2)	C(25)-C(27)	1.511(3)	C(1S)-C(2S)	1.320(9)
N(1)-C(8)	1.453(2)	C(26)-C(27)	1.534(3)	C(2S)-C(3S)	1.225(9)
N(2)-C(6)	1.309(2)	C(27)-C(28)	1.537(3)	C(3S)-C(4S)	1.394(9)
N(2)-C(20)	1.457(2)	C(29)-C(30)	1.542(4)	C(4S)-C(5S)	1.289(13)
C(3)-C(36)	1.524(3)	C(30)-C(31)	1.525(4)	C(4S)-C(5S')	1.388(16)
C(3)-C(37)	1.534(3)	C(38)-C(43)	1.373(3)	C(5S)-C(6S)	1.710(16)
C(3)-C(35)	1.543(3)	C(38)-C(39)	1.391(3)	C(5S')-C(6S)	1.226(16)

Table A.40: Bond Angles [°] for **4-H₂B(C₆F₅)₂**

N(1)-Sc(1)-N(2)	96.18(6)	C(10)-C(11)-C(12)	119.4(2)	F(8)-C(47)-C(46)	120.0(3)
N(1)-Sc(1)-F(5)	72.28(5)	C(11)-C(12)-C(13)	121.9(2)	F(8)-C(47)-C(48)	119.7(3)
N(2)-Sc(1)-F(5)	97.08(5)	C(12)-C(13)-C(8)	118.1(2)	C(46)-C(47)-C(48)	120.2(2)
N(1)-Sc(1)-C(4)	31.55(6)	C(12)-C(13)-C(15)	118.27(19)	F(9)-C(48)-C(47)	120.0(3)
N(2)-Sc(1)-C(4)	83.85(6)	C(8)-C(13)-C(15)	123.5(2)	F(9)-C(48)-C(49)	121.0(3)
F(5)-Sc(1)-C(4)	102.55(5)	C(13)-C(15)-C(14)	109.1(2)	C(47)-C(48)-C(49)	118.9(3)
N(1)-Sc(1)-C(5)	59.46(6)	C(13)-C(15)-C(16)	114.4(2)	F(10)-C(49)-C(44)	120.0(2)
N(2)-Sc(1)-C(5)	58.72(6)	C(14)-C(15)-C(16)	107.86(19)	F(10)-C(49)-C(48)	116.8(2)
F(5)-Sc(1)-C(5)	120.27(5)	C(9)-C(18)-C(17)	111.04(18)	C(44)-C(49)-C(48)	123.2(3)
C(4)-Sc(1)-C(5)	30.96(6)	C(9)-C(18)-C(19)	113.23(18)	C(51)-C(50)-C(55)	114.8(2)
N(1)-Sc(1)-C(6)	78.87(6)	C(17)-C(18)-C(19)	107.62(18)	C(51)-C(50)-B(2)	125.7(2)
N(2)-Sc(1)-C(6)	27.41(6)	C(21)-C(20)-C(25)	121.62(19)	C(55)-C(50)-B(2)	119.4(2)
F(5)-Sc(1)-C(6)	111.30(5)	C(21)-C(20)-N(2)	119.12(17)	F(11)-C(51)-C(50)	120.0(2)
C(4)-Sc(1)-C(6)	58.67(6)	C(25)-C(20)-N(2)	119.03(19)	F(11)-C(51)-C(52)	116.5(2)
C(5)-Sc(1)-C(6)	31.35(6)	C(22)-C(21)-C(20)	117.9(2)	C(50)-C(51)-C(52)	123.5(3)
C(43)-F(5)-Sc(1)	128.68(11)	C(22)-C(21)-C(30)	118.0(2)	F(12)-C(52)-C(53)	120.2(3)
C(4)-N(1)-C(8)	124.59(15)	C(20)-C(21)-C(30)	124.04(19)	F(12)-C(52)-C(51)	120.6(3)
C(4)-N(1)-Sc(1)	96.58(11)	C(23)-C(22)-C(21)	121.4(2)	C(53)-C(52)-C(51)	119.2(3)

C(8)-N(1)-Sc(1)	136.35(12)	C(24)-C(23)-C(22)	119.7(2)	F(13)-C(53)-C(54)	120.6(3)
C(6)-N(2)-C(20)	126.35(16)	C(23)-C(24)-C(25)	121.8(2)	F(13)-C(53)-C(52)	119.7(3)
C(6)-N(2)-Sc(1)	103.54(12)	C(24)-C(25)-C(20)	117.5(2)	C(54)-C(53)-C(52)	119.6(2)
C(20)-N(2)-Sc(1)	128.18(12)	C(24)-C(25)-C(27)	118.92(19)	F(14)-C(54)-C(53)	120.6(3)
C(36)-C(3)-C(37)	107.28(18)	C(20)-C(25)-C(27)	123.59(18)	F(14)-C(54)-C(55)	119.7(3)
C(36)-C(3)-C(35)	108.7(2)	C(25)-C(27)-C(26)	111.6(2)	C(53)-C(54)-C(55)	119.7(3)
C(37)-C(3)-C(35)	106.72(18)	C(25)-C(27)-C(28)	111.2(2)	F(15)-C(55)-C(54)	117.4(2)
C(36)-C(3)-C(4)	109.61(16)	C(26)-C(27)-C(28)	109.22(18)	F(15)-C(55)-C(50)	119.4(2)
C(37)-C(3)-C(4)	112.81(18)	C(31)-C(30)-C(21)	110.9(2)	C(54)-C(55)-C(50)	123.2(3)
C(35)-C(3)-C(4)	111.58(16)	C(31)-C(30)-C(29)	109.0(2)	C(61)-C(56)-C(57)	114.44(18)
N(1)-C(4)-C(5)	118.86(16)	C(21)-C(30)-C(29)	112.9(2)	C(61)-C(56)-B(2)	123.81(18)
N(1)-C(4)-C(3)	123.75(17)	C(43)-C(38)-C(39)	113.26(19)	C(57)-C(56)-B(2)	121.38(19)
C(5)-C(4)-C(3)	117.32(16)	C(43)-C(38)-B(1)	118.01(16)	F(16)-C(57)-C(58)	117.0(2)
N(1)-C(4)-Sc(1)	51.87(8)	C(39)-C(38)-B(1)	128.72(18)	F(16)-C(57)-C(56)	119.51(19)
C(5)-C(4)-Sc(1)	76.07(10)	F(1)-C(39)-C(40)	116.67(19)	C(58)-C(57)-C(56)	123.5(2)
C(3)-C(4)-Sc(1)	146.41(12)	F(1)-C(39)-C(38)	119.9(2)	F(17)-C(58)-C(59)	119.5(2)
C(4)-C(5)-C(6)	133.75(17)	C(40)-C(39)-C(38)	123.4(2)	F(17)-C(58)-C(57)	120.8(2)
C(4)-C(5)-Sc(1)	72.97(10)	F(2)-C(40)-C(39)	120.4(2)	C(59)-C(58)-C(57)	119.6(2)
C(6)-C(5)-Sc(1)	79.38(10)	F(2)-C(40)-C(41)	119.4(2)	F(18)-C(59)-C(58)	120.3(2)
N(2)-C(6)-C(5)	118.20(16)	C(39)-C(40)-C(41)	120.1(2)	F(18)-C(59)-C(60)	120.2(2)
N(2)-C(6)-C(7)	128.73(18)	F(3)-C(41)-C(42)	120.2(2)	C(58)-C(59)-C(60)	119.5(2)
C(5)-C(6)-C(7)	113.07(16)	F(3)-C(41)-C(40)	120.4(2)	F(19)-C(60)-C(59)	120.2(2)
N(2)-C(6)-Sc(1)	49.05(9)	C(42)-C(41)-C(40)	119.3(2)	F(19)-C(60)-C(61)	120.6(2)
C(5)-C(6)-Sc(1)	69.26(10)	F(4)-C(42)-C(43)	121.55(19)	C(59)-C(60)-C(61)	119.2(2)
C(7)-C(6)-Sc(1)	176.29(15)	F(4)-C(42)-C(41)	120.9(2)	F(20)-C(61)-C(56)	120.23(18)
C(32)-C(7)-C(34)	107.4(2)	C(43)-C(42)-C(41)	117.5(2)	F(20)-C(61)-C(60)	116.1(2)
C(32)-C(7)-C(33)	107.9(2)	C(38)-C(43)-C(42)	126.38(18)	C(56)-C(61)-C(60)	123.7(2)
C(34)-C(7)-C(33)	109.1(2)	C(38)-C(43)-F(5)	116.51(17)	C(44)-B(1)-C(38)	115.39(16)
C(32)-C(7)-C(6)	116.37(18)	C(42)-C(43)-F(5)	117.11(17)	C(50)-B(2)-C(56)	109.77(15)
C(34)-C(7)-C(6)	105.44(19)	C(45)-C(44)-C(49)	114.7(2)	C(3S)-C(2S)-C(1S)	143.9(12)
C(33)-C(7)-C(6)	110.40(18)	C(45)-C(44)-B(1)	122.86(19)	C(2S)-C(3S)-C(4S)	147.3(10)
C(9)-C(8)-C(13)	120.12(18)	C(49)-C(44)-B(1)	122.30(19)	C(5S)-C(4S)-C(5S')	51.2(10)
C(9)-C(8)-N(1)	120.97(16)	F(6)-C(45)-C(44)	119.10(19)	C(5S)-C(4S)-C(3S)	128.2(9)
C(13)-C(8)-N(1)	118.76(17)	F(6)-C(45)-C(46)	117.2(2)	C(5S')-C(4S)-C(3S)	160.0(12)
C(10)-C(9)-C(8)	118.65(19)	C(44)-C(45)-C(46)	123.6(2)	C(4S)-C(5S)-C(6S)	111.8(8)
C(10)-C(9)-C(18)	117.06(19)	F(7)-C(46)-C(47)	120.5(2)	C(6S)-C(5S')-C(4S)	145(2)
C(8)-C(9)-C(18)	124.28(18)	F(7)-C(46)-C(45)	120.2(3)	C(5S')-C(6S)-C(5S)	42.7(12)
C(11)-C(10)-C(9)	121.6(2)	C(47)-C(46)-C(45)	119.3(3)		

Table A.41: Crystal Data and Structure Refinement for **7-C₆F₅****A. Crystal Data**

Crystallographer	Masood Parvez	University of Calgary
Empirical Formula	C ₅₄ H ₄₄ BF ₂₀ N ₂ Sc · 0.25 C ₆ H ₁₄	
Formula Weight	1178.22	
Crystal Size	0.30 x 0.25 x 0.20 mm ³	
Crystal System	triclinic	
Space Group	P -1	

Lattice Parameters	a = 12.2225(2) Å	$\alpha = 82.7740(6)^\circ$.
	b = 13.9703(2) Å	$\beta = 73.6650(6)^\circ$.
	c = 16.9809(3) Å	$\gamma = 73.6860(8)^\circ$.
Volume	2667.00(7) Å ³	
Z	2	
Density (calculated)	1.467 Mg/m ³	

B. Data Collection and Refinement Conditions

Diffractometer	Nonius Kappa CCD
Radiation (λ [Å])	Graphite-monochromated MoK α (0.71073)
Temperature	170(2) K
Reflections Collected	16150
Independent Reflections	8321 [R(int) = 0.023]
Structure Solution	Direct Methods
Refinement Method	Full-matrix least-squares on F ²
Data / Restraints / Parameters	8321 / 0 / 716
Goodness-of-Fit	1.09
Final R Indices [I>2sigma(I)]	R1 = 0.074, wR2 = 0.233
R Indices (all data)	R1 = 0.090, wR2 = 0.252
Largest Difference Peak and Hole	0.70 and -0.70 e.Å ⁻³

Table A.42: Atomic Coordinates and Equivalent Isotropic Displacement for 7-C₆F₅

	x	y	z	U(eq)		x	y	z	U(eq)
Sc(1)	8476(1)	2132(1)	2464(1)	32(1)	C(39)	6605(4)	6149(3)	2257(3)	42(1)
B(1)	8207(4)	4947(3)	2953(3)	33(1)	C(40)	5491(5)	6720(4)	2211(3)	57(1)
N(1)	7298(3)	1228(2)	2852(2)	34(1)	C(41)	4574(4)	6825(4)	2902(4)	57(1)
N(2)	8347(3)	2089(2)	1270(2)	33(1)	C(42)	4786(4)	6384(4)	3629(3)	55(1)
C(1)	8465(4)	4082(3)	2290(2)	35(1)	C(43)	5917(4)	5826(3)	3648(3)	43(1)
C(3)	6458(4)	-157(4)	2735(3)	52(1)	C(44)	9248(4)	5556(3)	2635(2)	37(1)
C(4)	7163(4)	604(3)	2372(3)	40(1)	C(45)	9092(4)	6578(4)	2506(3)	45(1)
C(5)	7642(4)	604(3)	1520(3)	39(1)	C(46)	10002(6)	7041(4)	2235(3)	58(1)
C(6)	8143(4)	1300(3)	999(3)	37(1)	C(47)	11149(5)	6478(5)	2098(3)	62(2)
C(7)	8435(5)	1177(4)	87(3)	52(1)	C(48)	11361(4)	5459(5)	2230(3)	59(1)
C(8)	8554(4)	2914(3)	674(2)	35(1)	C(49)	10424(4)	5030(4)	2494(3)	44(1)
C(9)	7575(4)	3634(3)	525(3)	41(1)	C(50)	10247(4)	1156(4)	2491(3)	48(1)
C(10)	7780(5)	4466(3)	-1(3)	50(1)	C(51)	10983(6)	1321(5)	2898(4)	72(2)
C(11)	8892(5)	4556(3)	-356(3)	51(1)	C(52)	12091(6)	772(5)	2931(4)	73(2)
C(12)	9855(5)	3819(3)	-224(3)	47(1)	C(53)	12597(6)	-105(5)	2493(5)	83(2)
C(13)	9713(4)	2985(3)	289(2)	39(1)	C(54)	11935(6)	-358(5)	2049(5)	79(2)
C(14)	5719(6)	3481(5)	230(5)	81(2)	C(55)	10803(6)	246(5)	2056(4)	71(2)
C(15)	6312(4)	3553(4)	895(3)	49(1)	F(1)	8072(2)	2823(2)	3657(1)	42(1)
C(16)	5564(4)	4444(4)	1421(3)	56(1)	F(2)	8495(3)	2036(2)	5061(2)	56(1)
C(17)	11541(5)	1746(4)	-439(3)	62(2)	F(3)	8892(3)	3126(2)	6129(2)	61(1)
C(18)	10800(4)	2187(3)	386(3)	44(1)	F(4)	8804(3)	5098(2)	5734(2)	62(1)
C(19)	11579(4)	2580(4)	777(3)	53(1)	F(5)	8392(3)	5936(2)	4317(2)	55(1)
C(20)	6688(4)	1232(3)	3723(3)	38(1)	F(6)	7464(3)	6075(2)	1543(2)	56(1)

C(21)	5681(4)	2013(3)	3993(3)	45(1)	F(7)	5311(3)	7151(3)	1482(2)	83(1)
C(22)	5118(5)	2040(4)	4823(3)	58(1)	F(8)	3482(3)	7357(3)	2879(3)	85(1)
C(23)	5552(5)	1315(4)	5378(3)	65(2)	F(9)	3905(3)	6471(3)	4318(2)	78(1)
C(24)	6522(5)	549(4)	5106(3)	58(1)	F(10)	6014(2)	5416(2)	4397(2)	58(1)
C(25)	7132(4)	482(3)	4274(3)	46(1)	F(11)	7995(3)	7210(2)	2652(2)	61(1)
C(26)	4348(8)	2474(6)	3051(7)	112(3)	F(12)	9768(4)	8043(3)	2128(2)	86(1)
C(27)	5180(4)	2808(3)	3389(3)	48(1)	F(13)	12043(3)	6911(3)	1829(2)	90(1)
C(28)	4648(7)	3832(4)	3735(4)	83(2)	F(14)	12475(3)	4888(3)	2099(2)	87(1)
C(29)	9229(5)	-281(4)	4351(4)	65(2)	F(15)	10713(2)	4023(2)	2618(2)	57(1)
C(30)	8232(4)	-365(3)	4019(3)	51(1)	F(16)	10563(4)	2170(3)	3345(3)	95(1)
C(31)	7983(6)	-1407(4)	4291(4)	68(2)	F(17)	12721(4)	1031(3)	3352(3)	99(1)
C(32)	8303(3)	4425(3)	3869(2)	34(1)	F(18)	13660(4)	-625(3)	2498(3)	112(2)
C(33)	8312(3)	3455(3)	4138(2)	33(1)	F(19)	12409(4)	-1178(3)	1606(3)	118(2)
C(34)	8514(4)	2993(3)	4866(2)	39(1)	F(20)	10209(4)	-53(3)	1612(3)	89(1)
C(35)	8707(4)	3546(4)	5404(3)	44(1)	C(56)	4800(18)	164(15)	432(11)	115(5)
C(36)	8663(4)	4530(4)	5201(3)	43(1)	C(57)	4990(20)	1022(19)	321(17)	154(8)
C(37)	8459(4)	4949(3)	4461(3)	40(1)	C(58)	4650(30)	1210(20)	1100(20)	192(12)

Table A.43: Anisotropic Displacement Parameters for 7-C₆F₅

Atom	U11	U22	U33	U23	U13	U12
Sc(1)	35(1)	34(1)	28(1)	2(1)	-10(1)	-11(1)
B(1)	35(2)	39(2)	27(2)	-2(2)	-4(2)	-15(2)
N(1)	38(2)	35(2)	31(2)	3(1)	-10(2)	-12(2)
N(2)	39(2)	29(2)	28(2)	2(1)	-9(1)	-6(1)
C(1)	40(2)	40(2)	25(2)	1(2)	-6(2)	-11(2)
C(3)	58(3)	53(3)	54(3)	1(2)	-15(2)	-29(2)
C(4)	39(2)	35(2)	45(3)	4(2)	-13(2)	-11(2)
C(5)	48(2)	30(2)	43(2)	-5(2)	-15(2)	-10(2)
C(6)	42(2)	32(2)	34(2)	-3(2)	-11(2)	-2(2)
C(7)	75(3)	46(3)	39(3)	-9(2)	-15(2)	-16(2)
C(8)	51(2)	29(2)	23(2)	-2(2)	-11(2)	-5(2)
C(9)	55(3)	38(2)	33(2)	-4(2)	-21(2)	-3(2)
C(10)	80(4)	35(2)	38(2)	1(2)	-29(3)	-5(2)
C(11)	86(4)	37(2)	28(2)	6(2)	-14(2)	-16(2)
C(12)	69(3)	35(2)	30(2)	-3(2)	-3(2)	-12(2)
C(13)	59(3)	33(2)	23(2)	-5(2)	-4(2)	-11(2)
C(14)	78(4)	83(4)	98(5)	-28(4)	-55(4)	-1(3)
C(15)	49(3)	46(3)	54(3)	0(2)	-28(2)	-4(2)
C(16)	51(3)	59(3)	56(3)	-4(2)	-22(2)	-1(2)
C(17)	67(3)	43(3)	56(3)	-13(2)	9(3)	-6(2)
C(18)	48(3)	35(2)	39(2)	-1(2)	2(2)	-8(2)
C(19)	45(3)	52(3)	55(3)	-5(2)	-6(2)	-8(2)
C(20)	43(2)	41(2)	35(2)	5(2)	-10(2)	-20(2)
C(21)	50(3)	46(3)	40(2)	0(2)	-7(2)	-20(2)
C(22)	63(3)	53(3)	49(3)	2(2)	3(2)	-22(2)
C(23)	81(4)	68(4)	41(3)	9(3)	0(3)	-32(3)
C(24)	78(4)	60(3)	41(3)	16(2)	-14(3)	-33(3)
C(25)	57(3)	46(3)	42(3)	9(2)	-17(2)	-25(2)
C(26)	112(6)	88(5)	172(9)	20(5)	-95(6)	-33(5)
C(27)	47(3)	46(3)	44(3)	1(2)	-9(2)	-6(2)

C(28)	114(5)	59(4)	62(4)	-5(3)	-21(4)	2(3)
C(29)	71(4)	58(3)	75(4)	18(3)	-42(3)	-18(3)
C(30)	61(3)	43(3)	53(3)	13(2)	-25(2)	-17(2)
C(31)	88(4)	48(3)	73(4)	15(3)	-27(3)	-25(3)
C(32)	29(2)	43(2)	28(2)	-6(2)	-1(2)	-10(2)
C(33)	31(2)	42(2)	25(2)	-6(2)	-3(2)	-8(2)
C(34)	37(2)	43(2)	29(2)	1(2)	-4(2)	-4(2)
C(35)	39(2)	66(3)	25(2)	2(2)	-11(2)	-8(2)
C(36)	39(2)	69(3)	26(2)	-11(2)	-6(2)	-19(2)
C(37)	42(2)	49(3)	30(2)	-6(2)	-3(2)	-17(2)
C(38)	37(2)	35(2)	36(2)	-2(2)	-9(2)	-12(2)
C(39)	48(3)	42(2)	37(2)	-1(2)	-12(2)	-11(2)
C(40)	68(3)	48(3)	59(3)	5(2)	-31(3)	-9(2)
C(41)	43(3)	46(3)	80(4)	-5(3)	-25(3)	0(2)
C(42)	36(2)	55(3)	67(3)	-10(3)	-4(2)	-8(2)
C(43)	39(2)	44(2)	40(2)	-4(2)	-4(2)	-9(2)
C(44)	43(2)	49(3)	23(2)	-3(2)	-6(2)	-20(2)
C(45)	54(3)	54(3)	34(2)	-2(2)	-9(2)	-24(2)
C(46)	90(4)	58(3)	43(3)	9(2)	-20(3)	-47(3)
C(47)	71(4)	102(5)	34(3)	5(3)	-11(2)	-61(4)
C(48)	41(3)	103(5)	38(3)	-5(3)	-8(2)	-31(3)
C(49)	44(3)	61(3)	31(2)	0(2)	-10(2)	-20(2)
C(50)	43(2)	60(3)	44(3)	14(2)	-18(2)	-19(2)
C(51)	81(4)	63(4)	64(4)	-3(3)	-6(3)	-18(3)
C(52)	73(4)	77(4)	84(4)	7(3)	-41(3)	-26(3)
C(53)	73(4)	66(4)	108(6)	6(4)	-37(4)	-8(3)
C(54)	91(5)	57(4)	91(5)	-8(3)	-31(4)	-11(3)
C(55)	78(4)	69(4)	78(4)	0(3)	-36(3)	-22(3)
F(1)	56(2)	45(1)	29(1)	0(1)	-10(1)	-22(1)
F(2)	77(2)	46(2)	40(2)	8(1)	-16(1)	-9(1)
F(3)	68(2)	81(2)	34(1)	5(1)	-26(1)	-12(2)
F(4)	80(2)	86(2)	34(1)	-10(1)	-18(1)	-37(2)
F(5)	86(2)	50(2)	35(1)	-7(1)	-9(1)	-29(1)
F(6)	66(2)	62(2)	34(1)	10(1)	-10(1)	-10(1)
F(7)	90(2)	80(2)	76(2)	19(2)	-48(2)	-4(2)
F(8)	53(2)	77(2)	120(3)	3(2)	-38(2)	3(2)
F(9)	40(2)	88(2)	81(2)	-4(2)	9(2)	-2(2)
F(10)	44(2)	79(2)	35(1)	0(1)	3(1)	-5(1)
F(11)	70(2)	41(2)	73(2)	-3(1)	-17(2)	-19(1)
F(12)	129(3)	77(2)	78(2)	18(2)	-34(2)	-71(2)
F(13)	91(3)	143(3)	67(2)	12(2)	-16(2)	-89(3)
F(14)	40(2)	138(3)	82(2)	-6(2)	-7(2)	-31(2)
F(15)	40(1)	64(2)	64(2)	-6(1)	-13(1)	-7(1)
F(16)	102(3)	88(3)	95(3)	-19(2)	-27(2)	-18(2)
F(17)	105(3)	105(3)	108(3)	9(2)	-52(3)	-43(2)
F(18)	91(3)	97(3)	150(4)	2(3)	-54(3)	-9(2)
F(19)	119(4)	82(3)	146(4)	-26(3)	-44(3)	4(2)
F(20)	98(3)	80(2)	97(3)	-3(2)	-44(2)	-20(2)

Table A.44: Bond Lengths [Å] for **7-C₆F₅**

Sc(1)-N(2)	2.087(3)	C(20)-C(25)	1.409(6)	C(41)-C(42)	1.367(8)
Sc(1)-N(1)	2.094(3)	C(21)-C(22)	1.383(7)	C(42)-F(9)	1.340(6)
Sc(1)-C(50)	2.220(5)	C(21)-C(27)	1.532(7)	C(42)-C(43)	1.391(7)
Sc(1)-F(1)	2.221(2)	C(22)-C(23)	1.391(8)	C(43)-F(10)	1.351(5)
B(1)-C(44)	1.655(6)	C(23)-C(24)	1.366(8)	C(44)-C(45)	1.384(6)
B(1)-C(32)	1.654(6)	C(24)-C(25)	1.402(7)	C(44)-C(49)	1.386(6)
B(1)-C(38)	1.655(6)	C(25)-C(30)	1.518(7)	C(45)-F(11)	1.358(6)
B(1)-C(1)	1.660(6)	C(26)-C(27)	1.498(9)	C(45)-C(46)	1.381(7)
N(1)-C(4)	1.337(6)	C(27)-C(28)	1.512(7)	C(46)-F(12)	1.346(6)
N(1)-C(20)	1.457(5)	C(29)-C(30)	1.517(7)	C(46)-C(47)	1.372(8)
N(2)-C(6)	1.354(5)	C(30)-C(31)	1.557(7)	C(47)-F(13)	1.338(6)
N(2)-C(8)	1.465(5)	C(32)-C(33)	1.373(6)	C(47)-C(48)	1.375(8)
C(3)-C(4)	1.518(6)	C(32)-C(37)	1.398(6)	C(48)-F(14)	1.343(6)
C(4)-C(5)	1.399(6)	C(33)-C(34)	1.374(6)	C(48)-C(49)	1.378(7)
C(5)-C(6)	1.385(6)	C(33)-F(1)	1.413(5)	C(49)-F(15)	1.355(6)
C(6)-C(7)	1.509(6)	C(34)-F(2)	1.341(5)	C(50)-C(51)	1.359(8)
C(8)-C(9)	1.391(6)	C(34)-C(35)	1.375(7)	C(50)-C(55)	1.447(8)
C(8)-C(13)	1.409(6)	C(35)-F(3)	1.346(5)	C(51)-C(52)	1.368(9)
C(9)-C(10)	1.410(6)	C(35)-C(36)	1.364(7)	C(51)-F(16)	1.382(7)
C(9)-C(15)	1.525(7)	C(36)-F(4)	1.349(5)	C(52)-F(17)	1.329(7)
C(10)-C(11)	1.358(8)	C(36)-C(37)	1.376(6)	C(52)-C(53)	1.407(10)
C(11)-C(12)	1.380(7)	C(37)-F(5)	1.352(5)	C(53)-F(18)	1.300(8)
C(12)-C(13)	1.385(6)	C(38)-C(43)	1.382(6)	C(53)-C(54)	1.386(10)
C(13)-C(18)	1.510(6)	C(38)-C(39)	1.380(6)	C(54)-F(19)	1.346(8)
C(14)-C(15)	1.529(7)	C(39)-F(6)	1.355(5)	C(54)-C(55)	1.401(9)
C(15)-C(16)	1.538(7)	C(39)-C(40)	1.389(7)	C(55)-F(20)	1.351(7)
C(17)-C(18)	1.533(6)	C(40)-F(7)	1.355(6)	C(56)-C(57)	1.26(3)
C(18)-C(19)	1.546(7)	C(40)-C(41)	1.366(8)	C(56)-C(56)#1	1.50(4)
C(20)-C(21)	1.403(6)	C(41)-F(8)	1.341(6)	C(57)-C(58)	1.31(3)

Table A.45: Bond Angles [°] for **7-C₆F₅**

N(2)-Sc(1)-N(1)	87.92(13)	C(22)-C(21)-C(20)	118.6(4)	F(9)-C(42)-C(43)	120.0(5)
N(2)-Sc(1)-C(50)	105.23(16)	C(22)-C(21)-C(27)	119.9(4)	C(41)-C(42)-C(43)	119.7(5)
N(1)-Sc(1)-C(50)	106.49(15)	C(20)-C(21)-C(27)	121.5(4)	F(10)-C(43)-C(38)	121.5(4)
N(2)-Sc(1)-F(1)	154.64(12)	C(21)-C(22)-C(23)	120.6(5)	F(10)-C(43)-C(42)	114.3(4)
N(1)-Sc(1)-F(1)	96.67(11)	C(24)-C(23)-C(22)	120.2(5)	C(38)-C(43)-C(42)	124.2(4)
C(50)-Sc(1)-F(1)	97.37(15)	C(23)-C(24)-C(25)	121.8(5)	C(45)-C(44)-C(49)	113.1(4)
C(44)-B(1)-C(32)	106.7(3)	C(24)-C(25)-C(20)	117.0(5)	C(45)-C(44)-B(1)	127.2(4)
C(44)-B(1)-C(38)	112.7(3)	C(24)-C(25)-C(30)	119.0(4)	C(49)-C(44)-B(1)	119.7(4)
C(32)-B(1)-C(38)	112.4(3)	C(20)-C(25)-C(30)	124.0(4)	F(11)-C(45)-C(46)	114.6(4)
C(44)-B(1)-C(1)	108.3(3)	C(26)-C(27)-C(28)	112.6(6)	F(11)-C(45)-C(44)	120.9(4)
C(32)-B(1)-C(1)	110.7(3)	C(26)-C(27)-C(21)	111.2(5)	C(46)-C(45)-C(44)	124.5(5)
C(38)-B(1)-C(1)	106.0(3)	C(28)-C(27)-C(21)	113.4(4)	F(12)-C(46)-C(47)	119.9(5)
C(4)-N(1)-C(20)	119.7(3)	C(29)-C(30)-C(25)	112.2(4)	F(12)-C(46)-C(45)	120.4(5)
C(4)-N(1)-Sc(1)	124.1(3)	C(29)-C(30)-C(31)	109.2(4)	C(47)-C(46)-C(45)	119.6(5)
C(20)-N(1)-Sc(1)	115.9(3)	C(25)-C(30)-C(31)	112.1(4)	F(13)-C(47)-C(46)	120.6(6)
C(6)-N(2)-C(8)	117.5(3)	C(33)-C(32)-C(37)	111.5(4)	F(13)-C(47)-C(48)	120.8(6)
C(6)-N(2)-Sc(1)	123.0(3)	C(33)-C(32)-B(1)	127.0(4)	C(46)-C(47)-C(48)	118.6(4)

C(8)-N(2)-Sc(1)	119.4(3)	C(37)-C(32)-B(1)	121.4(4)	F(14)-C(48)-C(47)	119.9(5)
N(1)-C(4)-C(5)	123.5(4)	C(32)-C(33)-C(34)	127.0(4)	F(14)-C(48)-C(49)	120.5(5)
N(1)-C(4)-C(3)	120.7(4)	C(32)-C(33)-F(1)	120.2(3)	C(47)-C(48)-C(49)	119.6(5)
C(5)-C(4)-C(3)	115.8(4)	C(34)-C(33)-F(1)	112.8(3)	F(15)-C(49)-C(48)	115.6(4)
C(6)-C(5)-C(4)	129.2(4)	F(2)-C(34)-C(35)	120.5(4)	F(15)-C(49)-C(44)	119.8(4)
N(2)-C(6)-C(5)	123.2(4)	F(2)-C(34)-C(33)	121.3(4)	C(48)-C(49)-C(44)	124.6(5)
N(2)-C(6)-C(7)	119.4(4)	C(35)-C(34)-C(33)	118.1(4)	C(51)-C(50)-C(55)	109.6(5)
C(5)-C(6)-C(7)	117.4(4)	F(3)-C(35)-C(36)	121.2(4)	C(51)-C(50)-Sc(1)	126.0(4)
C(9)-C(8)-C(13)	121.7(4)	F(3)-C(35)-C(34)	120.0(4)	C(55)-C(50)-Sc(1)	124.4(4)
C(9)-C(8)-N(2)	117.9(4)	C(36)-C(35)-C(34)	118.8(4)	C(50)-C(51)-C(52)	129.5(6)
C(13)-C(8)-N(2)	120.4(4)	F(4)-C(36)-C(35)	119.8(4)	C(50)-C(51)-F(16)	115.9(6)
C(8)-C(9)-C(10)	117.6(4)	F(4)-C(36)-C(37)	119.9(4)	C(52)-C(51)-F(16)	114.6(6)
C(8)-C(9)-C(15)	123.1(4)	C(35)-C(36)-C(37)	120.3(4)	F(17)-C(52)-C(51)	123.1(6)
C(10)-C(9)-C(15)	119.3(4)	F(5)-C(37)-C(36)	116.7(4)	F(17)-C(52)-C(53)	118.1(6)
C(11)-C(10)-C(9)	121.2(4)	F(5)-C(37)-C(32)	119.1(4)	C(51)-C(52)-C(53)	118.8(6)
C(10)-C(11)-C(12)	120.5(4)	C(36)-C(37)-C(32)	124.2(4)	F(18)-C(53)-C(54)	122.7(7)
C(11)-C(12)-C(13)	121.1(5)	C(43)-C(38)-C(39)	113.2(4)	F(18)-C(53)-C(52)	119.9(7)
C(12)-C(13)-C(8)	117.9(4)	C(43)-C(38)-B(1)	125.5(4)	C(54)-C(53)-C(52)	117.4(6)
C(12)-C(13)-C(18)	118.7(4)	C(39)-C(38)-B(1)	121.1(4)	F(19)-C(54)-C(53)	118.8(6)
C(8)-C(13)-C(18)	123.4(4)	F(6)-C(39)-C(38)	119.6(4)	F(19)-C(54)-C(55)	121.4(6)
C(14)-C(15)-C(9)	111.6(5)	F(6)-C(39)-C(40)	115.9(4)	C(53)-C(54)-C(55)	119.9(6)
C(14)-C(15)-C(16)	109.4(4)	C(38)-C(39)-C(40)	124.5(4)	F(20)-C(55)-C(54)	116.4(6)
C(9)-C(15)-C(16)	111.4(4)	F(7)-C(40)-C(41)	120.3(5)	F(20)-C(55)-C(50)	118.8(5)
C(13)-C(18)-C(17)	111.5(4)	F(7)-C(40)-C(39)	120.1(5)	C(54)-C(55)-C(50)	124.8(6)
C(13)-C(18)-C(19)	112.1(4)	C(41)-C(40)-C(39)	119.5(5)	C(33)-F(1)-Sc(1)	149.2(2)
C(17)-C(18)-C(19)	109.3(4)	F(8)-C(41)-C(42)	119.9(5)	C(57)-C(56)-C(56)#1	101(2)
C(21)-C(20)-C(25)	121.7(4)	F(8)-C(41)-C(40)	121.2(5)	C(56)#1-C(56)-C(58)	144(2)
C(21)-C(20)-N(1)	118.2(4)	C(42)-C(41)-C(40)	118.8(4)	C(56)-C(57)-C(58)	95(2)
C(25)-C(20)-N(1)	120.0(4)	F(9)-C(42)-C(41)	120.3(4)		

Table A.46: Crystal Data and Structure Refinement for **10-Me****A. Crystal Data**

Crystallographer	Robert McDonald	University of Alberta
Empirical Formula	C ₅₈ H ₆₆ BF ₁₅ N ₂ Sc	
Formula Weight	1131.9	
Crystal Dimensions (mm)	0.58 × 0.13 × 0.12	
Crystal System	monoclinic	
Space Group	<i>P</i> 2 ₁ / <i>c</i> (No. 14)	
Lattice Parameters		
	<i>a</i> (Å)	13.6896 (10)
	<i>b</i> (Å)	17.6084 (13)
	<i>c</i> (Å)	25.0796 (16)
	β (deg)	92.0504 (15)
	<i>V</i> (Å ³)	6041.6 (7)
	<i>Z</i>	4
ρ_{calcd} (g cm ⁻³)	1.244	

μ (mm ⁻¹)	0.204	
B. Data Collection and Refinement Conditions		
Diffractometer	Bruker P4/RA/SMART 1000 CCD	
Radiation (λ [Å])	Graphite-monochromated Mo K α (0.71073)	
Temperature (°C)	−80 °C	
Total Data Collected	33569 ($-16 \leq h \leq 17$, $-22 \leq k \leq 21$, $-31 \leq l \leq 21$)	
Independent Reflections	12367	
Number of Observations (<i>NO</i>)	4098 [$F_{o2} \geq 2\sigma(F_{o2})$]	
Structure Solution	Direct methods/fragment search (<i>DIRDIF-96c</i>)	
Refinement	Full-matrix least-squares on F^2 (<i>SHELXL-93d</i>)	
Absorption Correction Method	<i>SADABS</i>	
Data/Restraints/Parameters	12367 [$F_{o2} \geq -3\sigma(F_{o2})$] / 9_e / 689	
Extinction Coefficient	0.0018 (3)	
Goodness-of-Fit	0.956 [$F_{o2} \geq -3\sigma(F_{o2})$]	
Final <i>R</i> Indices	R_1 [$F_{o2} \geq 2\sigma(F_{o2})$]	0.0714
	wR_2 [$F_{o2} \geq -3\sigma(F_{o2})$]	0.2559
Largest Difference Peak & Hole	0.871 and −0.282 e Å ⁻³	

Table A.47: Atomic Coordinates and Equivalent Isotropic Displacement Parameters for **10-Me**

Atom	<i>x</i>	<i>y</i>	<i>z</i>	<i>U</i> _{eq} , Å ²
Sc	0.24182(8)	0.23203(6)	0.11735(4)	0.0403(3)*
F42	0.3711(3)	0.2061(2)	0.05840(14)	0.0649(11)*
F43	0.3911(4)	0.1422(3)	-0.03482(17)	0.0976(15)*
F44	0.5526(4)	0.1666(3)	-0.09298(16)	0.1045(17)*
F45	0.6963(3)	0.2621(2)	-0.05393(15)	0.0862(14)*
F46	0.6821(3)	0.3252(2)	0.04174(13)	0.0545(10)*
F52	0.3876(2)	0.41666(18)	0.04987(12)	0.0470(9)*
F53	0.4073(2)	0.56477(18)	0.03183(13)	0.0521(10)*
F54	0.5728(3)	0.63922(18)	0.06389(13)	0.0558(10)*
F55	0.7195(3)	0.5599(2)	0.11622(14)	0.0621(11)*
F56	0.6979(2)	0.41590(19)	0.14016(13)	0.0544(10)*
F62	0.5434(3)	0.3787(2)	0.21880(13)	0.0604(11)*
F63	0.6466(3)	0.3204(2)	0.30128(13)	0.0735(12)*
F64	0.7621(3)	0.1971(2)	0.28847(14)	0.0682(11)*
F65	0.7684(3)	0.1310(2)	0.19133(14)	0.0723(12)*
F66	0.6631(3)	0.1831(2)	0.10901(13)	0.0584(10)*
N1	0.2393(4)	0.2065(3)	0.19743(19)	0.0447(13)*
N2	0.1522(3)	0.3279(3)	0.12232(17)	0.0361(12)*
C1	0.1664(4)	0.1417(3)	0.0697(2)	0.0357(14)*
C2	0.4100(4)	0.3089(3)	0.1372(2)	0.0441(16)*
C3	0.1012(5)	0.1325(4)	0.2404(3)	0.0573(19)*
C4	0.1446(5)	0.1946(3)	0.2048(2)	0.0475(17)*
C5	0.0726(4)	0.2356(3)	0.1749(2)	0.0459(16)*

C6	0.0713(4)	0.3037(3)	0.1440(2)	0.0410(15)*
C7	-0.0342(5)	0.3365(4)	0.1362(3)	0.0523(18)*
C8	0.3215(5)	0.1856(4)	0.2330(3)	0.0501(18)*
C9	0.3839(5)	0.1260(4)	0.2191(3)	0.0543(19)*
C10	0.4625(5)	0.1101(5)	0.2538(3)	0.070(2)*
C11	0.4797(6)	0.1502(5)	0.2996(3)	0.077(3)*
C12	0.4213(5)	0.2092(5)	0.3119(3)	0.067(2)*
C13	0.3408(5)	0.2283(4)	0.2788(3)	0.0564(19)*
C14	0.2256(7)	0.2828(6)	0.3468(3)	0.117(4)*
C15	0.2807(6)	0.2978(5)	0.2939(3)	0.073(2)*
C16	0.3434(6)	0.3680(5)	0.2996(3)	0.087(3)*
C17	0.4627(6)	0.0810(4)	0.1347(3)	0.087(3)*
C18	0.3700(6)	0.0805(4)	0.1684(3)	0.072(2)*
C19	0.3409(7)	-0.0043(4)	0.1817(4)	0.118(4)*
C20	0.1644(4)	0.3987(3)	0.0944(2)	0.0390(15)*
C21	0.1462(4)	0.4002(4)	0.0380(3)	0.0500(17)*
C22	0.1594(5)	0.4707(5)	0.0124(3)	0.066(2)*
C23	0.1869(5)	0.5335(5)	0.0401(4)	0.073(2)*
C24	0.2075(5)	0.5300(4)	0.0945(3)	0.060(2)*
C25	0.1985(4)	0.4619(3)	0.1218(3)	0.0449(16)*
C26	0.2071(6)	0.2975(4)	-0.0192(3)	0.075(2)*
C27	0.1185(5)	0.3303(4)	0.0065(3)	0.0574(19)*
C28	0.0365(7)	0.3453(5)	-0.0376(3)	0.105(3)*
C29	0.1465(5)	0.4862(4)	0.2153(3)	0.080(2)*
C30	0.2287(5)	0.4580(4)	0.1803(3)	0.0490(17)*
C31	0.3221(5)	0.5030(4)	0.1932(3)	0.064(2)*
C32	0.0597(5)	0.0711(4)	0.2037(3)	0.076(2)*
C33	0.0203(5)	0.1660(4)	0.2750(3)	0.071(2)*
C34	0.1725(5)	0.0930(4)	0.2806(3)	0.083(3)*
C35	-0.0823(5)	0.3437(4)	0.1907(3)	0.067(2)*
C36	-0.0442(5)	0.4157(4)	0.1097(3)	0.065(2)*
C37	-0.0955(5)	0.2806(4)	0.1017(3)	0.068(2)*
C41	0.5259(4)	0.2722(3)	0.0550(2)	0.0363(14)*
C42	0.4568(5)	0.2243(4)	0.0324(3)	0.0509(17)*
C43	0.4635(6)	0.1886(4)	-0.0158(3)	0.064(2)*
C44	0.5429(7)	0.2000(4)	-0.0450(3)	0.066(2)*
C45	0.6164(6)	0.2490(4)	-0.0251(3)	0.061(2)*
C46	0.6057(5)	0.2817(3)	0.0239(2)	0.0427(16)*
C51	0.5393(4)	0.4084(3)	0.0998(2)	0.0335(14)*
C52	0.4700(4)	0.4509(3)	0.0709(2)	0.0365(14)*
C53	0.4789(5)	0.5277(4)	0.0597(2)	0.0397(15)*
C54	0.5625(5)	0.5651(3)	0.0750(2)	0.0423(16)*
C55	0.6343(5)	0.5254(4)	0.1022(2)	0.0433(16)*
C56	0.6214(4)	0.4495(4)	0.1138(2)	0.0418(16)*
C61	0.5941(4)	0.2831(3)	0.1588(2)	0.0348(14)*
C62	0.5964(5)	0.3150(3)	0.2099(2)	0.0429(16)*
C63	0.6503(5)	0.2882(3)	0.2531(2)	0.0475(17)*
C64	0.7068(5)	0.2262(4)	0.2472(2)	0.0464(16)*
C65	0.7109(5)	0.1923(3)	0.1984(3)	0.0468(16)*
C66	0.6548(4)	0.2211(3)	0.1553(2)	0.0398(15)*

B	0.5187(5)	0.3172(4)	0.1120(3)	0.0383(17)*
C1Sa	0.2154(12)	-0.0097(11)	-0.0752(6)	0.140(3)
C2Sa	0.2250(8)	-0.0595(11)	-0.0249(7)	0.140(3)
C3Sa	0.1243(9)	-0.0695(10)	-0.0005(5)	0.140(3)
C4Sa	0.1302(13)	-0.1292(7)	0.0442(5)	0.140(3)
C5Sa	0.0623(13)	-0.1071(10)	0.0892(5)	0.140(3)
C6Sa	0.0828(14)	-0.1578(11)	0.1383(5)	0.140(3)

Table A.48: Anisotropic Displacement Parameters for 10-Me

Atom	U11	U22	U33	U23	U13	U12
Sc	0.0362(7)	0.0368(7)	0.0475(7)	0.0064(6)	-0.0049(6)	-0.0005(6)
F42	0.059(3)	0.069(3)	0.066(2)	-0.002(2)	-0.005(2)	-0.016(2)
F43	0.115(4)	0.100(4)	0.076(3)	-0.025(3)	-0.023(3)	-0.014(3)
F44	0.149(5)	0.112(4)	0.052(3)	-0.024(3)	0.001(3)	0.023(3)
F45	0.090(3)	0.106(3)	0.065(3)	0.004(2)	0.035(3)	0.024(3)
F46	0.040(2)	0.065(2)	0.059(2)	0.0072(19)	0.0148(19)	0.005(2)
F52	0.037(2)	0.054(2)	0.049(2)	0.0160(17)	-0.0046(18)	0.0003(17)
F53	0.047(2)	0.052(2)	0.058(2)	0.0207(18)	0.0034(19)	0.0121(18)
F54	0.075(3)	0.035(2)	0.058(2)	0.0067(17)	0.005(2)	-0.0018(19)
F55	0.061(3)	0.061(2)	0.063(2)	0.0089(19)	-0.015(2)	-0.020(2)
F56	0.038(2)	0.060(2)	0.064(2)	0.0181(18)	-0.0141(19)	-0.0023(18)
F62	0.079(3)	0.056(2)	0.046(2)	-0.0008(17)	0.004(2)	0.023(2)
F63	0.114(4)	0.065(3)	0.041(2)	-0.0064(19)	-0.009(2)	0.014(2)
F64	0.076(3)	0.072(3)	0.055(2)	0.017(2)	-0.021(2)	0.005(2)
F65	0.080(3)	0.072(3)	0.064(2)	0.009(2)	-0.008(2)	0.038(2)
F66	0.070(3)	0.061(2)	0.043(2)	-0.0031(18)	-0.0037(19)	0.024(2)
N1	0.035(3)	0.046(3)	0.053(3)	0.014(2)	-0.006(3)	-0.001(3)
N2	0.027(3)	0.038(3)	0.043(3)	0.011(2)	-0.001(2)	-0.003(2)
C1	0.035(4)	0.031(3)	0.041(3)	0.003(3)	-0.004(3)	-0.005(3)
C2	0.035(4)	0.044(4)	0.053(4)	0.015(3)	0.004(3)	0.001(3)
C3	0.044(4)	0.059(5)	0.069(5)	0.027(4)	-0.006(4)	-0.011(4)
C4	0.034(4)	0.052(4)	0.057(4)	0.021(3)	-0.001(3)	-0.007(3)
C5	0.029(4)	0.052(4)	0.057(4)	0.015(3)	-0.002(3)	-0.007(3)
C6	0.030(4)	0.047(4)	0.045(4)	0.004(3)	-0.005(3)	-0.005(3)
C7	0.032(4)	0.061(5)	0.065(4)	0.017(4)	0.005(4)	0.003(3)
C8	0.032(4)	0.061(5)	0.057(4)	0.031(4)	-0.003(4)	-0.007(3)
C9	0.042(4)	0.053(4)	0.068(5)	0.025(4)	-0.006(4)	0.009(4)
C10	0.042(5)	0.078(6)	0.092(6)	0.037(5)	-0.002(5)	0.009(4)
C11	0.042(5)	0.118(8)	0.071(6)	0.045(5)	-0.010(5)	0.002(5)
C12	0.041(5)	0.111(7)	0.047(4)	0.021(4)	-0.003(4)	-0.001(5)
C13	0.042(4)	0.080(5)	0.047(4)	0.022(4)	0.001(4)	0.001(4)
C14	0.100(7)	0.161(10)	0.093(6)	-0.045(6)	0.040(6)	-0.037(7)
C15	0.057(5)	0.121(7)	0.041(4)	-0.002(4)	-0.003(4)	0.002(5)
C16	0.093(7)	0.091(6)	0.079(6)	0.012(5)	0.017(5)	0.005(6)
C17	0.087(7)	0.074(6)	0.101(6)	0.007(5)	-0.009(6)	0.016(5)
C18	0.055(5)	0.047(5)	0.112(7)	0.014(4)	-0.019(5)	0.008(4)
C19	0.099(8)	0.055(6)	0.200(11)	0.001(6)	0.012(7)	-0.010(5)
C20	0.022(3)	0.043(4)	0.053(4)	0.013(3)	0.003(3)	0.007(3)
C21	0.030(4)	0.058(5)	0.062(5)	0.014(4)	0.000(3)	0.005(3)
C22	0.037(4)	0.087(6)	0.074(5)	0.044(5)	0.002(4)	0.009(4)

C23	0.041(5)	0.056(5)	0.121(8)	0.041(5)	0.011(5)	0.005(4)
C24	0.041(4)	0.049(5)	0.092(6)	0.019(4)	0.013(4)	0.006(3)
C25	0.032(4)	0.039(4)	0.065(4)	0.006(3)	0.010(3)	0.007(3)
C26	0.078(6)	0.078(5)	0.071(5)	0.007(4)	0.014(5)	0.005(5)
C27	0.047(5)	0.076(5)	0.048(4)	0.012(4)	-0.008(4)	0.003(4)
C28	0.099(7)	0.126(8)	0.088(6)	-0.001(6)	-0.041(6)	0.012(6)
C29	0.051(5)	0.098(6)	0.094(6)	-0.023(5)	0.017(5)	0.005(5)
C30	0.040(4)	0.044(4)	0.064(4)	-0.008(3)	0.013(4)	0.001(3)
C31	0.056(5)	0.058(5)	0.080(5)	-0.005(4)	0.009(4)	-0.006(4)
C32	0.065(5)	0.066(5)	0.096(6)	0.038(5)	0.008(5)	-0.007(4)
C33	0.059(5)	0.086(6)	0.071(5)	0.024(4)	0.013(4)	-0.015(4)
C34	0.056(5)	0.092(6)	0.101(6)	0.065(5)	-0.009(5)	-0.016(4)
C35	0.050(5)	0.074(5)	0.078(5)	0.020(4)	0.007(4)	0.014(4)
C36	0.041(4)	0.071(5)	0.083(5)	0.025(4)	0.002(4)	0.015(4)
C37	0.037(4)	0.086(6)	0.081(5)	0.019(4)	-0.015(4)	-0.009(4)
C41	0.031(4)	0.040(4)	0.037(3)	0.012(3)	-0.005(3)	0.003(3)
C42	0.051(5)	0.060(4)	0.042(4)	0.008(4)	-0.005(4)	0.007(4)
C43	0.073(6)	0.060(5)	0.057(5)	-0.003(4)	-0.013(5)	-0.003(4)
C44	0.084(6)	0.077(6)	0.038(4)	-0.006(4)	0.000(5)	0.021(5)
C45	0.064(5)	0.075(6)	0.045(4)	0.011(4)	0.008(4)	0.021(4)
C46	0.053(5)	0.035(4)	0.039(4)	0.003(3)	0.000(4)	0.015(3)
C51	0.027(4)	0.043(4)	0.030(3)	0.006(3)	0.003(3)	0.005(3)
C52	0.029(4)	0.050(4)	0.031(3)	0.000(3)	0.004(3)	-0.002(3)
C53	0.036(4)	0.050(4)	0.034(3)	0.012(3)	0.011(3)	0.012(3)
C54	0.055(5)	0.035(4)	0.037(4)	0.005(3)	0.007(3)	0.002(3)
C55	0.040(4)	0.048(4)	0.041(4)	0.004(3)	-0.004(3)	-0.013(3)
C56	0.034(4)	0.053(4)	0.038(3)	0.007(3)	-0.005(3)	0.006(3)
C61	0.032(4)	0.039(4)	0.034(3)	0.003(3)	0.005(3)	0.002(3)
C62	0.046(4)	0.036(4)	0.047(4)	0.011(3)	0.004(3)	0.007(3)
C63	0.063(5)	0.038(4)	0.043(4)	0.005(3)	0.007(4)	0.005(3)
C64	0.051(4)	0.052(4)	0.036(4)	0.014(3)	-0.013(3)	-0.010(4)
C65	0.039(4)	0.040(4)	0.061(4)	0.011(3)	-0.001(4)	0.014(3)
C66	0.036(4)	0.043(4)	0.040(4)	0.005(3)	-0.001(3)	0.004(3)
B	0.030(4)	0.044(4)	0.040(4)	0.004(3)	0.000(3)	0.008(3)

Table A.49: Bond Lengths for 10-Me

Sc	F42	2.390(4)	C2	B	1.643(9)	C23	C24	1.384(10)
Sc	N1	2.060(5)	C3	C4	1.543(8)	C24	C25	1.387(8)
Sc	N2	2.093(5)	C3	C32	1.518(9)	C25	C30	1.512(8)
Sc	C1	2.221(5)	C3	C33	1.547(9)	C26	C27	1.507(9)
Sc	C2	2.703(6)†	C3	C34	1.544(9)	C27	C28	1.569(9)
Sc	C4	2.688(6)†	C4	C5	1.416(8)	C29	C30	1.535(8)
Sc	C5	2.773(6)†	C5	C6	1.427(8)	C30	C31	1.529(8)
Sc	C6	2.757(6)†	C6	C7	1.561(8)	C41	C42	1.376(8)
Sc	H2A	2.3	C7	C35	1.545(8)	C41	C46	1.376(8)
Sc	H2B	2.3	C7	C36	1.547(8)	C41	B	1.641(9)
F42	C42	1.400(7)	C7	C37	1.540(9)	C42	C43	1.367(9)
F43	C43	1.358(8)	C8	C9	1.405(9)	C43	C44	1.347(10)
F44	C44	1.350(7)	C8	C13	1.390(9)	C44	C45	1.403(10)
F45	C45	1.352(8)	C9	C10	1.387(9)	C45	C46	1.370(9)

F46	C46	1.358(7)	C9	C18	1.510(10)	C51	C52	1.391(7)
F52	C52	1.368(6)	C10	C11	1.362(10)	C51	C56	1.372(8)
F53	C53	1.352(6)	C11	C12	1.353(10)	C51	B	1.661(9)
F54	C54	1.343(6)	C12	C13	1.397(9)	C52	C53	1.388(8)
F55	C55	1.350(6)	C13	C15	1.529(10)	C53	C54	1.364(8)
F56	C56	1.353(6)	C14	C15	1.571(10)	C54	C55	1.369(8)
F62	C62	1.359(6)	C15	C16	1.509(10)	C55	C56	1.382(8)
F63	C63	1.337(7)	C17	C18	1.549(10)	C61	C62	1.398(8)
F64	C64	1.360(6)	C18	C19	1.584(10)	C61	C66	1.377(7)
F65	C65	1.351(6)	C20	C21	1.427(8)	C61	B	1.647(8)
F66	C66	1.349(6)	C20	C25	1.381(8)	C62	C63	1.374(8)
N1	C4	1.333(7)	C21	C22	1.413(9)	C63	C64	1.349(8)
N1	C8	1.457(7)	C21	C27	1.505(9)	C64	C65	1.366(8)
N2	C6	1.322(7)	C22	C23	1.352(10)	C65	C66	1.397(8)
N2	C20	1.443(7)						

†Nonbonded Distance

Table A.50: Bond Angles (°) for 10-Me

F42	Sc	N1	126.86(17)	C26	C27	C28	109.3(6)
F42	Sc	N2	129.72(16)	C25	C30	C29	111.1(6)
F42	Sc	C1	82.60(17)	C25	C30	C31	112.2(5)
N1	Sc	N2	95.06(19)	C29	C30	C31	109.6(5)
N1	Sc	C1	110.14(19)	C42	C41	C46	112.9(6)
N2	Sc	C1	110.32(19)	C42	C41	B	126.4(6)
Sc	F42	C42	153.7(4)	C46	C41	B	120.7(5)
Sc	N1	C4	102.7(4)	F42	C42	C41	121.5(6)
Sc	N1	C8	127.8(4)	F42	C42	C43	113.0(7)
C4	N1	C8	127.5(5)	C41	C42	C43	125.4(7)
Sc	N2	C6	105.4(4)	F43	C43	C42	121.0(8)
Sc	N2	C20	126.1(4)	F43	C43	C44	119.4(7)
C6	N2	C20	126.3(5)	C42	C43	C44	119.5(7)
C4	C3	C32	107.4(6)	F44	C44	C43	121.8(8)
C4	C3	C33	110.7(6)	F44	C44	C45	119.5(8)
C4	C3	C34	116.7(5)	C43	C44	C45	118.7(7)
C32	C3	C33	110.6(6)	F45	C45	C44	119.9(7)
C32	C3	C34	106.8(6)	F45	C45	C46	121.5(7)
C33	C3	C34	104.7(6)	C44	C45	C46	118.6(7)
N1	C4	C3	126.1(5)	F46	C46	C41	119.9(5)
N1	C4	C5	120.5(5)	F46	C46	C45	115.3(6)
C3	C4	C5	113.1(5)	C41	C46	C45	124.8(7)
C4	C5	C6	135.4(6)	C52	C51	C56	112.8(5)
N2	C6	C5	120.0(5)	C52	C51	B	119.9(5)
N2	C6	C7	127.8(5)	C56	C51	B	127.3(5)
C5	C6	C7	111.9(5)	F52	C52	C51	120.1(5)
C6	C7	C35	109.9(5)	F52	C52	C53	115.3(5)
C6	C7	C36	117.1(5)	C51	C52	C53	124.5(6)
C6	C7	C37	108.5(5)	F53	C53	C52	120.6(6)
C35	C7	C36	105.8(5)	F53	C53	C54	119.8(5)
C35	C7	C37	107.9(5)	C52	C53	C54	119.5(6)
C36	C7	C37	107.3(5)	F54	C54	C53	120.3(6)

N1	C8	C9	119.9(6)	F54	C54	C55	121.4(6)
N1	C8	C13	119.3(6)	C53	C54	C55	118.3(6)
C9	C8	C13	120.6(6)	F55	C55	C54	119.9(6)
C8	C9	C10	117.4(7)	F55	C55	C56	119.8(6)
C8	C9	C18	123.1(6)	C54	C55	C56	120.3(6)
C10	C9	C18	119.6(7)	F56	C56	C51	120.5(5)
C9	C10	C11	122.1(8)	F56	C56	C55	115.0(5)
C10	C11	C12	120.3(7)	C51	C56	C55	124.5(6)
C11	C12	C13	120.6(8)	C62	C61	C66	112.4(5)
C8	C13	C12	118.9(7)	C62	C61	B	120.0(5)
C8	C13	C15	123.3(6)	C66	C61	B	127.5(5)
C12	C13	C15	117.8(7)	F62	C62	C61	119.2(5)
C13	C15	C14	110.7(7)	F62	C62	C63	115.4(5)
C13	C15	C16	111.7(6)	C61	C62	C63	125.5(6)
C14	C15	C16	110.2(6)	F63	C63	C62	122.1(6)
C9	C18	C17	112.0(6)	F63	C63	C64	118.8(6)
C9	C18	C19	110.3(7)	C62	C63	C64	119.0(6)
C17	C18	C19	109.7(6)	F64	C64	C63	121.8(6)
N2	C20	C21	118.5(5)	F64	C64	C65	118.6(6)
N2	C20	C25	119.8(5)	C63	C64	C65	119.6(6)
C21	C20	C25	121.5(6)	F65	C65	C64	120.6(6)
C20	C21	C22	116.5(6)	F65	C65	C66	119.7(6)
C20	C21	C27	122.5(6)	C64	C65	C66	119.7(6)
C22	C21	C27	120.9(6)	F66	C66	C61	121.1(5)
C21	C22	C23	121.5(7)	F66	C66	C65	115.1(5)
C22	C23	C24	120.9(7)	C61	C66	C65	123.8(6)
C23	C24	C25	120.4(7)	C2	B	C41	112.0(5)
C20	C25	C24	119.0(6)	C2	B	C51	108.6(5)
C20	C25	C30	121.4(5)	C2	B	C61	104.4(4)
C24	C25	C30	119.6(6)	C41	B	C51	106.8(5)
C21	C27	C26	110.3(6)	C41	B	C61	112.9(5)
C21	C27	C28	113.1(6)	C51	B	C61	112.2(5)

Table A.51: Crystal Data and Structure Refinement for **10-CH₂SiMe₂CH₂SiMe₃****A. Crystal Data**

Crystallographer	Masood Parvez	University of Calgary
Empirical Formula	C ₆₁ H ₇₅ BF ₁₅ N ₂ ScSi ₂	
Formula Weight	1233.18	
Crystal size	0.20 x 0.18 x 0.15 mm ³	
Crystal System	triclinic	
Space Group	P-1	
Lattice Parameters	a = 12.75520(10) Å	α = 77.7032(5)°.
	b = 14.0148(2) Å	β = 76.5540(5)°.
	c = 19.7212(3) Å	γ = 68.6369(8)°.
Volume	3160.99(7) Å ³	
Z	2	

Density (calculated) 1.296 Mg/m³

B. Data Collection and Refinement Conditions

Diffractionmeter	Nonius Kappa CCD
Radiation (λ [Å])	Graphite-monochromated MoK α (0.71073)
Temperature	173(2) K
Reflections Collected	27049
Independent Reflections	14404 [R(int) = 0.026]
Structure Solution	Direct Methods
Refinement Method	Full-matrix least-squares on F ²
Data / Restraints / Parameters	14404 / 12 / 764
Goodness-of-Fit	1.01
Final R Indices [$I > 2\sigma(I)$]	R1 = 0.060, wR2 = 0.163
R Indices (all data)	R1 = 0.083, wR2 = 0.183
Largest diff. peak and hole	0.97 and -0.80 e.Å ⁻³

Table A.52: Atomic Coordinates and Equivalent Isotropic Displacement Parameters for **10-CH₂SiMe₂CH₂SiMe₃**

	x	y	z	U(eq)		x	y	z	U(eq)
Sc(1)	3206(1)	3445(1)	7564(1)	23(1)	C(15)	3808(2)	157(2)	7794(2)	44(1)
F(1)	414(1)	6224(1)	6467(1)	45(1)	C(16)	3955(4)	-661(5)	8436(2)	117(2)
F(2)	772(2)	7181(2)	5161(1)	74(1)	C(17)	29(3)	4122(2)	7205(2)	50(1)
F(3)	1944(2)	8551(2)	4855(1)	90(1)	C(18)	207(2)	3412(2)	7902(2)	36(1)
F(4)	2801(2)	8882(2)	5902(1)	86(1)	C(19)	-955(2)	3509(3)	8379(2)	54(1)
F(5)	2458(2)	7941(1)	7197(1)	51(1)	C(20)	5855(2)	2953(2)	7434(1)	27(1)
F(6)	2719(1)	5509(1)	8784(1)	49(1)	C(21)	6006(2)	3925(2)	7205(1)	31(1)
F(7)	2958(2)	6463(2)	9733(1)	64(1)	C(22)	7019(2)	3964(2)	6758(1)	37(1)
F(8)	1708(2)	8492(2)	9827(1)	57(1)	C(23)	7854(2)	3086(2)	6536(1)	40(1)
F(9)	181(2)	9536(1)	8940(1)	48(1)	C(24)	7680(2)	2137(2)	6749(1)	38(1)
F(10)	-65(1)	8596(1)	7970(1)	41(1)	C(25)	6678(2)	2048(2)	7193(1)	31(1)
F(11)	-1116(1)	7842(1)	7094(1)	46(1)	C(26)	7067(6)	344(3)	7993(3)	119(2)
F(12)	-3201(1)	7800(2)	7627(1)	63(1)	C(27)	6512(2)	999(2)	7380(2)	42(1)
F(13)	-3634(1)	6600(2)	8859(1)	61(1)	C(28)	6929(5)	410(3)	6764(2)	95(2)
F(14)	-1867(1)	5375(1)	9545(1)	48(1)	C(29)	5605(3)	5578(3)	7713(2)	58(1)
F(15)	254(1)	5343(1)	9009(1)	37(1)	C(30)	5121(2)	4936(2)	7405(1)	36(1)
N(1)	2620(2)	2264(1)	8140(1)	24(1)	C(31)	4588(3)	5577(2)	6767(2)	52(1)
N(2)	4795(2)	2888(1)	7884(1)	24(1)	C(32)	4753(2)	3804(2)	9421(2)	43(1)
C(1)	1896(2)	5252(2)	7682(1)	27(1)	C(33)	6562(2)	2759(3)	8756(1)	41(1)
C(2)	3497(3)	3052(2)	6533(1)	48(1)	C(34)	5435(3)	1865(3)	9681(2)	50(1)
Si(1)	3924(1)	3455(1)	5592(1)	35(1)	C(35)	1038(2)	2917(2)	9743(2)	43(1)
Si(2)	2642(2)	2392(2)	4860(1)	89(1)	C(36)	1269(2)	1238(2)	9385(1)	40(1)
C(40)	3993(4)	2507(3)	5035(2)	61(1)	C(37)	2637(3)	1302(3)	10064(2)	55(1)
C(41)	1600(5)	2333(5)	5657(3)	88(2)	C(38)	5396(3)	3520(3)	5437(2)	64(1)
C(42)	2095(7)	3425(6)	4141(4)	121(2)	C(39)	2869(3)	4738(3)	5327(2)	74(1)
C(43)	3021(9)	1133(7)	4523(5)	153(3)	C(44)	1338(2)	7082(2)	6918(1)	32(1)
Si(1')	3405(6)	3220(4)	5632(3)	39(2)	C(45)	983(2)	6907(2)	6357(1)	38(1)
Si(2')	2556(6)	1675(5)	5042(3)	56(2)	C(46)	1169(3)	7385(3)	5671(2)	52(1)

C(40')	2631(15)	2277(13)	5787(8)	45(4)	C(47)	1762(3)	8070(3)	5519(2)	59(1)
C(41')	1408(17)	1099(18)	5325(13)	70(6)	C(48)	2182(3)	8246(2)	6044(2)	57(1)
C(42')	2438(19)	2625(16)	4181(9)	60(5)	C(49)	1969(2)	7752(2)	6721(1)	40(1)
C(43')	3833(14)	593(13)	4760(10)	46(4)	C(50)	1314(2)	7003(2)	8319(1)	28(1)
C(3)	1923(2)	1914(2)	9484(1)	33(1)	C(51)	2061(2)	6520(2)	8790(1)	35(1)
C(4)	2704(2)	2254(2)	8811(1)	26(1)	C(52)	2208(2)	6998(2)	9291(1)	41(1)
C(5)	3500(2)	2653(2)	8953(1)	28(1)	C(53)	1581(2)	8016(2)	9343(1)	40(1)
C(6)	4564(2)	2772(2)	8587(1)	26(1)	C(54)	809(2)	8548(2)	8893(1)	35(1)
C(7)	5331(2)	2799(2)	9093(1)	33(1)	C(55)	696(2)	8032(2)	8402(1)	31(1)
C(8)	1990(2)	1756(2)	7901(1)	27(1)	C(56)	-283(2)	6537(2)	7994(1)	28(1)
C(9)	870(2)	2297(2)	7778(1)	29(1)	C(57)	-1230(2)	7171(2)	7686(1)	35(1)
C(10)	304(2)	1782(2)	7530(1)	38(1)	C(58)	-2333(2)	7183(2)	7963(2)	42(1)
C(11)	828(2)	773(2)	7404(2)	42(1)	C(59)	-2559(2)	6581(2)	8585(2)	42(1)
C(12)	1955(3)	260(2)	7501(2)	42(1)	C(60)	-1670(2)	5967(2)	8930(1)	36(1)
C(13)	2563(2)	743(2)	7736(1)	33(1)	C(61)	-570(2)	5961(2)	8627(1)	30(1)
C(14)	4444(3)	-344(4)	7147(2)	84(1)	B(1)	1071(2)	6480(2)	7722(1)	26(1)

Table A.53: Anisotropic Displacement Parameters for **10-CH₂SiMe₂CH₂SiMe₃**

Atom	U11	U22	U33	U23	U13	U12
Sc(1)	23(1)	23(1)	22(1)	-2(1)	-5(1)	-8(1)
F(1)	55(1)	51(1)	37(1)	-8(1)	-16(1)	-19(1)
F(2)	91(2)	98(2)	30(1)	-6(1)	-19(1)	-22(1)
F(3)	132(2)	83(2)	33(1)	17(1)	6(1)	-35(2)
F(4)	131(2)	71(1)	61(1)	-3(1)	24(1)	-68(2)
F(5)	70(1)	48(1)	46(1)	-14(1)	7(1)	-39(1)
F(6)	49(1)	44(1)	52(1)	-15(1)	-26(1)	3(1)
F(7)	60(1)	78(1)	64(1)	-24(1)	-37(1)	-11(1)
F(8)	71(1)	70(1)	50(1)	-27(1)	-10(1)	-37(1)
F(9)	73(1)	32(1)	40(1)	-12(1)	2(1)	-22(1)
F(10)	55(1)	26(1)	39(1)	-4(1)	-14(1)	-6(1)
F(11)	42(1)	42(1)	44(1)	6(1)	-15(1)	-2(1)
F(12)	35(1)	71(1)	72(1)	-7(1)	-21(1)	2(1)
F(13)	31(1)	88(1)	65(1)	-25(1)	3(1)	-21(1)
F(14)	51(1)	60(1)	36(1)	-7(1)	6(1)	-29(1)
F(15)	36(1)	40(1)	31(1)	2(1)	-8(1)	-11(1)
N(1)	24(1)	25(1)	26(1)	-2(1)	-6(1)	-10(1)
N(2)	24(1)	28(1)	22(1)	-2(1)	-3(1)	-11(1)
C(1)	29(1)	25(1)	28(1)	-4(1)	-6(1)	-9(1)
C(2)	55(2)	52(2)	32(1)	-10(1)	-11(1)	-7(1)
Si(1)	39(1)	44(1)	23(1)	-5(1)	-5(1)	-15(1)
Si(2)	142(1)	148(2)	29(1)	-13(1)	-1(1)	-117(1)
Si(1')	41(3)	45(3)	31(2)	-2(2)	-7(2)	-14(2)
Si(2')	87(4)	51(4)	43(3)	-13(3)	-14(3)	-32(3)
C(3)	35(1)	38(1)	27(1)	-1(1)	0(1)	-19(1)
C(4)	25(1)	25(1)	25(1)	-3(1)	-2(1)	-8(1)
C(5)	26(1)	33(1)	24(1)	-2(1)	-4(1)	-12(1)
C(6)	26(1)	28(1)	24(1)	-3(1)	-5(1)	-9(1)
C(7)	28(1)	49(2)	24(1)	-2(1)	-9(1)	-15(1)
C(8)	30(1)	27(1)	27(1)	-4(1)	-3(1)	-16(1)
C(9)	30(1)	29(1)	34(1)	-5(1)	-5(1)	-14(1)

C(10)	41(1)	39(1)	43(1)	-5(1)	-10(1)	-23(1)
C(11)	53(2)	39(2)	46(2)	-7(1)	-12(1)	-27(1)
C(12)	55(2)	34(1)	45(2)	-8(1)	-6(1)	-22(1)
C(13)	37(1)	28(1)	35(1)	-4(1)	-4(1)	-14(1)
C(14)	54(2)	100(3)	68(2)	-29(2)	-1(2)	13(2)
C(15)	38(1)	32(1)	56(2)	-10(1)	-5(1)	-6(1)
C(16)	67(3)	144(5)	60(3)	17(3)	-6(2)	36(3)
C(17)	53(2)	34(2)	71(2)	-2(1)	-30(2)	-15(1)
C(18)	27(1)	33(1)	54(2)	-11(1)	-11(1)	-12(1)
C(19)	31(1)	52(2)	85(2)	-28(2)	-3(1)	-13(1)
C(20)	23(1)	38(1)	21(1)	-2(1)	-5(1)	-13(1)
C(21)	29(1)	41(1)	24(1)	-3(1)	-5(1)	-16(1)
C(22)	35(1)	51(2)	31(1)	-2(1)	-3(1)	-25(1)
C(23)	28(1)	64(2)	31(1)	-9(1)	-2(1)	-19(1)
C(24)	28(1)	54(2)	32(1)	-7(1)	-4(1)	-13(1)
C(25)	26(1)	40(1)	25(1)	-5(1)	-6(1)	-9(1)
C(26)	232(7)	46(2)	91(3)	21(2)	-90(4)	-39(3)
C(27)	37(1)	34(1)	45(2)	-4(1)	1(1)	-7(1)
C(28)	176(5)	66(3)	59(2)	-17(2)	2(3)	-68(3)
C(29)	65(2)	52(2)	70(2)	-20(2)	2(2)	-36(2)
C(30)	36(1)	35(1)	39(1)	-5(1)	1(1)	-19(1)
C(31)	45(2)	46(2)	50(2)	7(1)	-1(1)	-10(1)
C(32)	37(1)	64(2)	38(1)	-17(1)	-11(1)	-20(1)
C(33)	28(1)	70(2)	31(1)	-7(1)	-10(1)	-18(1)
C(34)	43(2)	65(2)	37(2)	14(1)	-18(1)	-18(1)
C(35)	43(2)	53(2)	37(1)	-16(1)	12(1)	-27(1)
C(36)	48(2)	42(2)	34(1)	-5(1)	6(1)	-27(1)
C(37)	61(2)	70(2)	36(2)	20(1)	-12(1)	-36(2)
C(38)	56(2)	89(3)	50(2)	-11(2)	-3(2)	-29(2)
C(39)	73(2)	72(2)	52(2)	12(2)	-13(2)	-6(2)
C(44)	39(1)	24(1)	28(1)	-4(1)	-3(1)	-7(1)
C(45)	44(1)	35(1)	30(1)	-3(1)	-8(1)	-8(1)
C(46)	61(2)	55(2)	29(1)	-3(1)	-10(1)	-7(2)
C(47)	80(2)	50(2)	29(1)	6(1)	5(1)	-14(2)
C(48)	78(2)	42(2)	42(2)	-1(1)	13(2)	-27(2)
C(49)	53(2)	30(1)	34(1)	-8(1)	3(1)	-16(1)
C(50)	30(1)	30(1)	27(1)	-4(1)	-2(1)	-14(1)
C(51)	34(1)	35(1)	37(1)	-10(1)	-8(1)	-9(1)
C(52)	40(1)	54(2)	38(1)	-10(1)	-13(1)	-18(1)
C(53)	50(2)	52(2)	33(1)	-16(1)	0(1)	-31(1)
C(54)	45(1)	31(1)	33(1)	-10(1)	6(1)	-19(1)
C(55)	37(1)	29(1)	27(1)	-3(1)	-2(1)	-13(1)
C(56)	31(1)	24(1)	29(1)	-8(1)	-7(1)	-7(1)
C(57)	36(1)	30(1)	35(1)	-7(1)	-9(1)	-4(1)
C(58)	31(1)	44(2)	48(2)	-14(1)	-14(1)	-1(1)
C(59)	29(1)	53(2)	48(2)	-23(1)	2(1)	-13(1)
C(60)	39(1)	41(1)	31(1)	-12(1)	1(1)	-17(1)
C(61)	30(1)	29(1)	30(1)	-7(1)	-7(1)	-7(1)
B(1)	29(1)	23(1)	27(1)	-4(1)	-6(1)	-7(1)

Table A.54: Bond Lengths [\AA] for **10-CH₂SiMe₂CH₂SiMe₃**

Sc(1)-N(1)	2.0722(18)	Si(2)-C(42)	1.855(8)	C(20)-C(25)	1.411(3)
Sc(1)-N(2)	2.0858(18)	Si(2)-C(43)	1.875(9)	C(21)-C(22)	1.397(3)
Sc(1)-C(2)	2.133(3)	Si(2)-C(40)	1.902(4)	C(21)-C(30)	1.518(4)
Sc(1)-C(1)	2.499(2)	Si(1')-(40')	1.859(14)	C(22)-C(23)	1.377(4)
Sc(1)-C(4)	2.746(2)	Si(1')-C(39)	1.985(7)	C(23)-C(24)	1.388(4)
Sc(1)-C(6)	2.755(2)	Si(2')-(43')	1.844(14)	C(24)-C(25)	1.402(3)
Sc(1)-C(5)	2.785(2)	Si(2')-(41')	1.841(15)	C(25)-C(27)	1.517(4)
F(1)-C(45)	1.355(3)	Si(2')-(40')	1.880(13)	C(26)-C(27)	1.502(5)
F(2)-C(46)	1.346(4)	Si(2')-(42')	1.922(15)	C(27)-C(28)	1.499(5)
F(3)-C(47)	1.349(3)	C(3)-C(36)	1.536(3)	C(29)-C(30)	1.540(4)
F(4)-C(48)	1.341(4)	C(3)-C(37)	1.540(4)	C(30)-C(31)	1.526(4)
F(5)-C(49)	1.357(3)	C(3)-C(35)	1.546(4)	C(44)-C(45)	1.384(4)
F(6)-C(51)	1.360(3)	C(3)-C(4)	1.562(3)	C(44)-C(49)	1.390(4)
F(7)-C(52)	1.351(3)	C(4)-C(5)	1.427(3)	C(44)-B(1)	1.653(3)
F(8)-C(53)	1.344(3)	C(5)-C(6)	1.431(3)	C(45)-C(46)	1.383(4)
F(9)-C(54)	1.334(3)	C(6)-C(7)	1.565(3)	C(46)-C(47)	1.373(5)
F(10)-C(55)	1.354(3)	C(7)-C(32)	1.534(4)	C(47)-C(48)	1.373(5)
F(11)-C(57)	1.350(3)	C(7)-C(34)	1.542(4)	C(48)-C(49)	1.383(4)
F(12)-C(58)	1.347(3)	C(7)-C(33)	1.542(3)	C(50)-C(51)	1.380(3)
F(13)-C(59)	1.344(3)	C(8)-C(9)	1.403(3)	C(50)-C(55)	1.393(3)
F(14)-C(60)	1.343(3)	C(8)-C(13)	1.409(3)	C(50)-B(1)	1.649(3)
F(15)-C(61)	1.359(3)	C(9)-C(10)	1.405(3)	C(51)-C(52)	1.384(4)
N(1)-C(4)	1.349(3)	C(9)-C(18)	1.523(3)	C(52)-C(53)	1.371(4)
N(1)-C(8)	1.452(3)	C(10)-C(11)	1.376(4)	C(53)-C(54)	1.379(4)
N(2)-C(6)	1.337(3)	C(11)-C(12)	1.392(4)	C(54)-C(55)	1.386(3)
N(2)-C(20)	1.456(3)	C(12)-C(13)	1.398(4)	C(56)-C(61)	1.384(3)
C(1)-B(1)	1.667(3)	C(13)-C(15)	1.519(4)	C(56)-C(57)	1.395(3)
C(2)-Si(1')	1.768(6)	C(14)-C(15)	1.504(5)	C(56)-B(1)	1.663(3)
C(2)-Si(1)	1.834(3)	C(15)-C(16)	1.513(5)	C(57)-C(58)	1.380(4)
Si(1)-C(40)	1.864(4)	C(17)-C(18)	1.525(4)	C(58)-C(59)	1.368(4)
Si(1)-C(38)	1.864(4)	C(18)-C(19)	1.537(4)	C(59)-C(60)	1.374(4)
Si(1)-C(39)	1.866(4)	C(20)-C(21)	1.409(3)	C(60)-C(61)	1.389(3)
Si(2)-C(41)	1.815(6)				

Table A.55: Bond Angles [$^{\circ}$] for **10-CH₂SiMe₂CH₂SiMe₃**

N(1)-Sc(1)-N(2)	96.65(7)	N(1)-C(4)-C(5)	120.06(19)	C(45)-C(44)-B(1)	121.3(2)
N(1)-Sc(1)-C(2)	99.29(11)	N(1)-C(4)-C(3)	125.7(2)	C(49)-C(44)-B(1)	125.4(2)
N(2)-Sc(1)-C(2)	106.34(10)	C(5)-C(4)-C(3)	114.02(19)	F(1)-C(45)-C(46)	116.0(2)
N(1)-Sc(1)-C(1)	116.51(8)	N(1)-C(4)-Sc(1)	46.84(10)	F(1)-C(45)-C(44)	119.4(2)
N(2)-Sc(1)-C(1)	121.29(8)	C(5)-C(4)-Sc(1)	76.55(13)	C(46)-C(45)-C(44)	124.6(3)
C(2)-Sc(1)-C(1)	113.49(10)	C(3)-C(4)-Sc(1)	156.14(16)	F(2)-C(46)-C(47)	120.5(3)
N(1)-Sc(1)-C(4)	28.35(7)	C(4)-C(5)-C(6)	135.2(2)	F(2)-C(46)-C(45)	120.4(3)
N(2)-Sc(1)-C(4)	80.57(7)	C(4)-C(5)-Sc(1)	73.56(13)	C(47)-C(46)-C(45)	119.1(3)
C(2)-Sc(1)-C(4)	126.25(10)	C(6)-C(5)-Sc(1)	73.86(12)	F(3)-C(47)-C(48)	120.4(3)
C(1)-Sc(1)-C(4)	106.12(7)	N(2)-C(6)-C(5)	120.28(19)	F(3)-C(47)-C(46)	120.0(3)
N(1)-Sc(1)-C(6)	80.54(7)	N(2)-C(6)-C(7)	126.68(19)	C(48)-C(47)-C(46)	119.5(3)
N(2)-Sc(1)-C(6)	27.95(7)	C(5)-C(6)-C(7)	112.98(19)	F(4)-C(48)-C(47)	120.6(3)
C(2)-Sc(1)-C(6)	131.44(10)	N(2)-C(6)-Sc(1)	46.98(10)	F(4)-C(48)-C(49)	120.3(3)

C(1)-Sc(1)-C(6)	109.41(7)	C(5)-C(6)-Sc(1)	76.20(12)	C(47)-C(48)-C(49)	119.1(3)
C(4)-Sc(1)-C(6)	57.42(7)	C(7)-C(6)-Sc(1)	159.40(16)	F(5)-C(49)-C(48)	114.8(3)
N(1)-Sc(1)-C(5)	57.12(7)	C(32)-C(7)-C(34)	109.3(2)	F(5)-C(49)-C(44)	120.7(2)
N(2)-Sc(1)-C(5)	56.92(7)	C(32)-C(7)-C(33)	107.3(2)	C(48)-C(49)-C(44)	124.4(3)
C(2)-Sc(1)-C(5)	144.31(10)	C(34)-C(7)-C(33)	106.2(2)	C(51)-C(50)-C(55)	113.0(2)
C(1)-Sc(1)-C(5)	101.59(8)	C(32)-C(7)-C(6)	108.19(19)	C(51)-C(50)-B(1)	127.2(2)
C(4)-Sc(1)-C(5)	29.89(7)	C(34)-C(7)-C(6)	109.3(2)	C(55)-C(50)-B(1)	119.7(2)
C(6)-Sc(1)-C(5)	29.93(6)	C(33)-C(7)-C(6)	116.34(19)	F(6)-C(51)-C(50)	120.3(2)
C(4)-N(1)-C(8)	127.09(18)	C(9)-C(8)-C(13)	120.8(2)	F(6)-C(51)-C(52)	115.3(2)
C(4)-N(1)-Sc(1)	104.81(14)	C(9)-C(8)-N(1)	120.5(2)	C(50)-C(51)-C(52)	124.4(2)
C(8)-N(1)-Sc(1)	126.37(14)	C(13)-C(8)-N(1)	118.5(2)	F(7)-C(52)-C(53)	119.8(2)
C(6)-N(2)-C(20)	127.32(18)	C(8)-C(9)-C(10)	118.5(2)	F(7)-C(52)-C(51)	120.4(3)
C(6)-N(2)-Sc(1)	105.07(14)	C(8)-C(9)-C(18)	124.6(2)	C(53)-C(52)-C(51)	119.8(2)
C(20)-N(2)-Sc(1)	124.77(14)	C(10)-C(9)-C(18)	116.9(2)	F(8)-C(53)-C(52)	120.7(3)
B(1)-C(1)-Sc(1)	176.77(17)	C(11)-C(10)-C(9)	121.4(2)	F(8)-C(53)-C(54)	120.2(3)
Si(1')-C(2)-Si(1)	26.3(2)	C(10)-C(11)-C(12)	119.4(2)	C(52)-C(53)-C(54)	119.1(2)
Si(1')-C(2)-Sc(1)	158.3(3)	C(11)-C(12)-C(13)	121.4(2)	F(9)-C(54)-C(53)	120.0(2)
Si(1)-C(2)-Sc(1)	144.47(19)	C(12)-C(13)-C(8)	118.3(2)	F(9)-C(54)-C(55)	121.3(2)
C(2)-Si(1)-C(40)	112.47(18)	C(12)-C(13)-C(15)	118.6(2)	C(53)-C(54)-C(55)	118.7(2)
C(2)-Si(1)-C(38)	109.25(16)	C(8)-C(13)-C(15)	123.2(2)	F(10)-C(55)-C(54)	116.0(2)
C(40)-Si(1)-C(38)	105.77(19)	C(14)-C(15)-C(16)	109.0(3)	F(10)-C(55)-C(50)	119.0(2)
C(2)-Si(1)-C(39)	108.28(16)	C(14)-C(15)-C(13)	111.2(3)	C(54)-C(55)-C(50)	125.0(2)
C(40)-Si(1)-C(39)	109.5(2)	C(16)-C(15)-C(13)	112.7(3)	C(61)-C(56)-C(57)	113.0(2)
C(38)-Si(1)-C(39)	111.6(2)	C(17)-C(18)-C(9)	110.9(2)	C(61)-C(56)-B(1)	119.0(2)
C(41)-Si(2)-C(42)	114.7(3)	C(17)-C(18)-C(19)	109.6(2)	C(57)-C(56)-B(1)	127.8(2)
C(41)-Si(2)-C(43)	105.3(4)	C(9)-C(18)-C(19)	111.6(2)	F(11)-C(57)-C(58)	115.5(2)
C(42)-Si(2)-C(43)	106.2(4)	C(21)-C(20)-C(25)	121.1(2)	F(11)-C(57)-C(56)	120.9(2)
C(41)-Si(2)-C(40)	112.5(2)	C(21)-C(20)-N(2)	119.7(2)	C(58)-C(57)-C(56)	123.6(2)
C(42)-Si(2)-C(40)	109.2(3)	C(25)-C(20)-N(2)	119.1(2)	F(12)-C(58)-C(59)	119.3(2)
C(43)-Si(2)-C(40)	108.6(3)	C(22)-C(21)-C(20)	118.2(2)	F(12)-C(58)-C(57)	120.2(3)
Si(1)-C(40)-Si(2)	121.3(2)	C(22)-C(21)-C(30)	118.0(2)	C(59)-C(58)-C(57)	120.6(2)
C(2)-Si(1')-C(40')	92.6(5)	C(20)-C(21)-C(30)	123.7(2)	F(13)-C(59)-C(58)	120.6(3)
C(2)-Si(1')-C(39)	105.9(3)	C(23)-C(22)-C(21)	121.8(3)	F(13)-C(59)-C(60)	120.6(3)
C(40')-Si(1')-(39)	129.7(7)	C(22)-C(23)-C(24)	119.5(2)	C(58)-C(59)-C(60)	118.8(2)
C(43')-Si(2')-(41')	104.1(10)	C(23)-C(24)-C(25)	121.5(2)	F(14)-C(60)-C(59)	120.2(2)
C(43')-Si(2')-(40')	116.1(9)	C(24)-C(25)-C(20)	117.9(2)	F(14)-C(60)-C(61)	121.0(2)
C(41')-Si(2')-(40')	108.9(9)	C(24)-C(25)-C(27)	119.1(2)	C(59)-C(60)-C(61)	118.9(2)
C(43')-Si(2')-(42')	101.1(9)	C(20)-C(25)-C(27)	123.0(2)	F(15)-C(61)-C(56)	120.1(2)
C(41')-Si(2')-(42')	114.4(10)	C(28)-C(27)-C(26)	109.4(3)	F(15)-C(61)-C(60)	114.9(2)
C(40')-Si(2')-(42')	112.1(9)	C(28)-C(27)-C(25)	112.0(3)	C(56)-C(61)-C(60)	125.1(2)
Si(1')-C(40')-Si(2')	121.1(9)	C(26)-C(27)-C(25)	113.0(3)	C(50)-B(1)-C(44)	111.92(19)
C(36)-C(3)-C(37)	106.7(2)	C(21)-C(30)-C(31)	109.9(2)	C(50)-B(1)-C(56)	103.28(18)
C(36)-C(3)-C(35)	108.1(2)	C(21)-C(30)-C(29)	113.3(2)	C(44)-B(1)-C(56)	114.58(19)
C(37)-C(3)-C(35)	108.9(2)	C(31)-C(30)-C(29)	109.8(3)	C(50)-B(1)-C(1)	113.65(19)
C(36)-C(3)-C(4)	116.0(2)	Si(1)-C(39)-Si(1')	24.4(2)	C(44)-B(1)-C(1)	104.35(18)
C(37)-C(3)-C(4)	110.2(2)	C(45)-C(44)-C(49)	113.2(2)	C(56)-B(1)-C(1)	109.36(18)
C(35)-C(3)-C(4)	106.78(19)				

Table A.56: Crystal Data and Structure Refinement for **14-C₆D₅Br**

A. Crystal Data	
Crystallographer	Masood Parvez University of Calgary
Empirical Formula	C ₆₆ H ₄₄ D ₁₀ BBr ₂ F ₂₀ N ₂ Sc
Formula Weight	1480.76
Crystal Size	0.12 x 0.10 x 0.09 mm ³
Crystal System	monoclinic
Space Group	P2 ₁ /n
Lattice Parameters	a = 18.789(3) Å b = 14.249(3) Å β = 106.697(11)° c = 24.539(4) Å
Volume	6293(2) Å ³
Z	4
Density (calculated)	1.562 Mg/m ³
B. Data Collection and Refinement Conditions	
Diffractometer	Nonius Kappa CCD
Radiation (λ[Å])	Graphite-monochromated MoKα (0.71073)
Temperature	173(2) K
Reflections Collected	21312
Independent Reflections	11042 [R(int) = 0.0502]
Structure Solution	Direct Methods
Refinement method	Full-matrix least-squares on F ²
Data / Restraints / Parameters	11042 / 0 / 848
Goodness-of-Fit	1.014
Final R Indices [I>2σ(I)]	R1 = 0.0533, wR2 = 0.1289
R Indices (all data)	R1 = 0.1072, wR2 = 0.1608
Largest Difference Peak & Hole	0.443 and -0.884 e.Å ⁻³

Table A.57: Atomic Coordinates and Equivalent Isotropic Displacement Parameters for **14-C₆D₅Br**

	x	y	z	U(eq)		x	y	z	U(eq)
Sc(1)	4305(1)	6966(1)	1429(1)	30(1)	C(44)	2348(2)	3991(3)	-521(2)	35(1)
N(1)	5308(2)	6428(2)	1955(1)	32(1)	C(45)	2376(2)	4843(3)	-791(2)	37(1)
N(2)	4872(2)	8090(2)	1184(1)	31(1)	C(46)	3030(3)	5279(3)	-798(2)	41(1)
C(1)	4000(3)	6041(3)	701(2)	41(1)	C(47)	3703(2)	4888(4)	-529(2)	41(1)
C(3)	6545(3)	5815(3)	1983(2)	43(1)	C(48)	3712(2)	4052(4)	-247(2)	41(1)
C(4)	5901(2)	6472(3)	1756(2)	33(1)	C(49)	3057(2)	3629(3)	-254(2)	38(1)
C(5)	5963(2)	7116(3)	1337(2)	32(1)	C(50)	804(2)	3857(3)	-838(2)	30(1)
C(6)	5526(2)	7886(3)	1094(2)	31(1)	C(51)	652(2)	4676(3)	-586(2)	33(1)
C(7)	5835(3)	8516(3)	725(2)	42(1)	C(52)	-17(3)	5142(3)	-744(2)	37(1)
C(8)	5342(2)	5854(3)	2454(2)	35(1)	C(53)	-594(2)	4780(3)	-1171(2)	37(1)
C(9)	5151(2)	4899(3)	2395(2)	40(1)	C(54)	-485(2)	3966(3)	-1423(2)	36(1)

C(10)	5169(3)	4409(4)	2891(3)	54(1)	C(55)	198(2)	3533(3)	-1264(2)	32(1)
C(11)	5367(3)	4831(4)	3414(2)	59(2)	C(56)	1760(2)	2507(3)	-1018(2)	33(1)
C(12)	5555(3)	5773(4)	3463(2)	51(1)	C(57)	1985(2)	1583(3)	-898(2)	35(1)
C(13)	5553(2)	6310(4)	2990(2)	41(1)	C(58)	2172(2)	984(3)	-1282(2)	43(1)
C(14)	5584(3)	7822(4)	3556(2)	61(2)	C(59)	2164(3)	1313(4)	-1808(2)	46(1)
C(15)	5773(3)	7334(4)	3059(2)	44(1)	C(60)	1946(3)	2210(4)	-1956(2)	44(1)
C(16)	6597(3)	7470(5)	3125(3)	66(2)	C(61)	1750(2)	2781(3)	-1573(2)	38(1)
C(17)	4136(3)	4009(4)	1680(3)	67(2)	F(1)	2449(2)	3930(2)	643(1)	49(1)
C(18)	4934(3)	4383(3)	1829(2)	48(1)	F(2)	2240(2)	3218(2)	1579(1)	62(1)
C(19)	5463(3)	3561(4)	1814(3)	61(2)	F(3)	1187(2)	1878(2)	1528(1)	66(1)
C(20)	4540(2)	8999(3)	1013(2)	32(1)	F(4)	358(2)	1237(2)	494(1)	58(1)
C(21)	4707(3)	9737(3)	1415(2)	38(1)	F(5)	597(1)	1882(2)	-458(1)	41(1)
C(22)	4364(3)	10601(3)	1258(2)	46(1)	F(6)	1748(1)	5293(2)	-1084(1)	44(1)
C(23)	3873(3)	10744(3)	723(2)	43(1)	F(7)	3010(2)	6101(2)	-1084(1)	55(1)
C(24)	3720(3)	10022(3)	339(2)	43(1)	F(8)	4336(2)	5304(2)	-551(1)	58(1)
C(25)	4051(2)	9136(3)	465(2)	37(1)	F(9)	4366(1)	3640(2)	26(1)	53(1)
C(26)	4122(3)	8700(4)	-517(2)	59(2)	F(10)	3108(1)	2783(2)	7(1)	43(1)
C(27)	3887(3)	8382(3)	8(2)	44(1)	F(11)	1186(1)	5049(2)	-149(1)	43(1)
C(28)	3058(3)	8133(4)	-185(2)	57(1)	F(12)	-109(2)	5953(2)	-482(1)	49(1)
C(29)	6005(3)	10068(7)	2007(3)	112(3)	F(13)	-1257(2)	5228(2)	-1336(1)	56(1)
C(30)	5266(3)	9617(4)	1998(2)	52(1)	F(14)	-1055(1)	3585(2)	-1840(1)	53(1)
C(31)	5009(3)	10027(4)	2484(2)	56(1)	F(15)	242(1)	2727(2)	-1554(1)	38(1)
C(32)	2748(2)	6920(4)	1280(2)	41(1)	F(16)	2046(2)	1215(2)	-380(1)	46(1)
C(33)	2960(2)	7848(3)	1327(2)	38(1)	F(17)	2388(2)	101(2)	-1127(1)	60(1)
C(34)	3473(2)	8173(4)	1822(2)	41(1)	F(18)	2355(2)	738(2)	-2183(1)	65(1)
C(35)	3783(3)	7551(4)	2261(2)	46(1)	F(19)	1941(2)	2550(2)	-2472(1)	58(1)
C(36)	3575(3)	6617(4)	2216(2)	44(1)	F(20)	1547(2)	3661(2)	-1746(1)	43(1)
C(37)	3059(3)	6301(4)	1722(2)	45(1)	Br(2)	2790(1)	610(2)	2094(1)	89(1)
Br(1)	2027(1)	6479(1)	636(1)	62(1)	Br(2A)	2101(8)	-737(9)	2334(3)	163(7)
B(1)	1615(3)	3324(4)	-586(2)	31(1)	Br(2B)	2654(6)	38(13)	2330(5)	89(3)
C(38)	1557(2)	2914(3)	34(2)	33(1)	C(62)	2117(3)	-100(5)	1512(3)	72(2)
C(39)	1940(3)	3232(3)	572(2)	38(1)	C(63)	2094(3)	94(4)	967(4)	76(2)
C(40)	1833(3)	2883(4)	1071(2)	45(1)	C(64)	1585(4)	-411(5)	491(3)	79(2)
C(41)	1306(3)	2223(4)	1044(2)	46(1)	C(65)	1164(3)	-1043(5)	617(4)	82(2)
C(42)	889(3)	1885(3)	525(2)	42(1)	C(66)	1192(4)	-1256(5)	1186(4)	87(2)
C(43)	1026(2)	2241(3)	43(2)	35(1)	C(67)	1668(4)	-776(6)	1633(4)	88(2)

Table A.58: Anisotropic Displacement Parameters for 14-C₆D₅Br

Atom	U11	U22	U33	U23	U13	U12
Sc(1)	30(1)	31(1)	29(1)	1(1)	9(1)	1(1)
N(1)	31(2)	31(2)	32(2)	2(2)	9(2)	-1(2)
N(2)	35(2)	29(2)	27(2)	-2(2)	9(2)	2(2)
C(1)	41(3)	33(3)	47(3)	1(2)	10(2)	3(2)
C(3)	37(3)	46(3)	49(3)	5(2)	16(2)	6(2)
C(4)	34(2)	29(3)	36(2)	-1(2)	7(2)	1(2)
C(5)	34(2)	35(3)	31(2)	-4(2)	14(2)	0(2)
C(6)	36(2)	33(3)	25(2)	0(2)	9(2)	1(2)
C(7)	38(3)	46(3)	48(3)	12(2)	22(2)	6(2)
C(8)	28(2)	41(3)	34(2)	9(2)	7(2)	2(2)
C(9)	34(3)	38(3)	47(3)	14(2)	10(2)	6(2)

C(10)	43(3)	44(3)	76(4)	25(3)	20(3)	4(2)
C(11)	52(3)	71(4)	56(4)	30(3)	22(3)	13(3)
C(12)	44(3)	73(4)	38(3)	14(3)	14(2)	9(3)
C(13)	32(2)	51(3)	39(3)	8(2)	11(2)	0(2)
C(14)	63(4)	77(4)	48(3)	-15(3)	27(3)	-16(3)
C(15)	43(3)	52(3)	35(3)	-7(2)	8(2)	-8(2)
C(16)	54(3)	85(5)	67(4)	-22(3)	30(3)	-24(3)
C(17)	51(3)	40(3)	98(5)	1(3)	0(3)	-4(3)
C(18)	48(3)	32(3)	58(3)	4(2)	7(3)	-5(2)
C(19)	65(4)	40(3)	73(4)	2(3)	14(3)	7(3)
C(20)	34(2)	31(3)	34(2)	3(2)	14(2)	0(2)
C(21)	39(3)	38(3)	39(3)	-3(2)	15(2)	4(2)
C(22)	51(3)	38(3)	49(3)	-5(2)	15(3)	6(2)
C(23)	45(3)	32(3)	56(3)	6(2)	20(3)	10(2)
C(24)	40(3)	49(3)	41(3)	10(2)	12(2)	4(2)
C(25)	39(3)	34(3)	38(3)	4(2)	11(2)	2(2)
C(26)	71(4)	65(4)	45(3)	-6(3)	20(3)	-1(3)
C(27)	52(3)	38(3)	34(3)	2(2)	1(2)	7(2)
C(28)	62(4)	59(4)	49(3)	-3(3)	16(3)	-17(3)
C(29)	44(4)	236(10)	54(4)	-39(5)	9(3)	14(5)
C(30)	65(4)	46(3)	39(3)	-10(2)	6(3)	15(3)
C(31)	60(3)	61(4)	46(3)	-17(3)	16(3)	-11(3)
C(32)	34(3)	48(3)	43(3)	-10(2)	17(2)	-6(2)
C(33)	31(2)	42(3)	43(3)	-6(2)	14(2)	2(2)
C(34)	33(3)	42(3)	52(3)	-9(2)	20(2)	1(2)
C(35)	41(3)	65(4)	39(3)	-12(3)	20(2)	-2(3)
C(36)	41(3)	57(3)	38(3)	7(2)	19(2)	5(2)
C(37)	44(3)	40(3)	57(3)	3(3)	22(3)	-3(2)
Br(1)	49(1)	68(1)	65(1)	-16(1)	9(1)	-16(1)
B(1)	31(3)	32(3)	30(3)	-2(2)	8(2)	4(2)
C(38)	32(2)	32(3)	34(2)	-2(2)	8(2)	8(2)
C(39)	36(3)	40(3)	37(3)	-5(2)	7(2)	11(2)
C(40)	43(3)	60(3)	27(3)	-6(2)	4(2)	18(3)
C(41)	48(3)	57(3)	34(3)	10(2)	16(2)	19(3)
C(42)	40(3)	45(3)	43(3)	7(2)	17(2)	8(2)
C(43)	35(2)	40(3)	29(2)	2(2)	7(2)	7(2)
C(44)	32(2)	33(3)	37(2)	-6(2)	7(2)	2(2)
C(45)	33(3)	38(3)	42(3)	-7(2)	12(2)	1(2)
C(46)	43(3)	33(3)	50(3)	-3(2)	18(2)	-5(2)
C(47)	31(3)	50(3)	44(3)	-16(2)	12(2)	-12(2)
C(48)	29(3)	47(3)	43(3)	-15(2)	6(2)	1(2)
C(49)	36(3)	37(3)	41(3)	-10(2)	11(2)	-2(2)
C(50)	30(2)	31(3)	29(2)	-1(2)	6(2)	3(2)
C(51)	30(2)	36(3)	32(2)	0(2)	10(2)	-2(2)
C(52)	44(3)	29(3)	43(3)	0(2)	22(2)	8(2)
C(53)	32(2)	40(3)	42(3)	11(2)	12(2)	12(2)
C(54)	31(3)	41(3)	32(2)	7(2)	4(2)	0(2)
C(55)	39(3)	27(2)	30(2)	1(2)	11(2)	2(2)
C(56)	23(2)	37(3)	39(3)	-5(2)	9(2)	-1(2)
C(57)	28(2)	35(3)	40(3)	-5(2)	6(2)	1(2)

C(58)	29(2)	31(3)	59(3)	-13(2)	0(2)	6(2)
C(59)	29(2)	59(4)	47(3)	-25(3)	7(2)	2(2)
C(60)	34(3)	56(4)	42(3)	-12(2)	12(2)	-10(2)
C(61)	32(2)	39(3)	42(3)	-4(2)	11(2)	1(2)
F(1)	48(2)	50(2)	41(2)	-12(1)	3(1)	1(1)
F(2)	66(2)	82(2)	30(2)	-9(1)	1(1)	23(2)
F(3)	76(2)	92(2)	37(2)	20(2)	27(2)	28(2)
F(4)	53(2)	69(2)	57(2)	19(2)	26(2)	1(2)
F(5)	42(2)	43(2)	38(1)	0(1)	12(1)	-6(1)
F(6)	37(2)	37(2)	58(2)	10(1)	13(1)	5(1)
F(7)	52(2)	44(2)	74(2)	5(2)	24(2)	-8(1)
F(8)	37(2)	69(2)	71(2)	-12(2)	21(2)	-17(1)
F(9)	29(2)	63(2)	62(2)	-10(2)	4(1)	2(1)
F(10)	37(2)	36(2)	51(2)	2(1)	6(1)	8(1)
F(11)	41(2)	41(2)	44(2)	-15(1)	8(1)	0(1)
F(12)	56(2)	38(2)	56(2)	-3(1)	23(2)	14(1)
F(13)	41(2)	60(2)	62(2)	6(2)	8(1)	21(1)
F(14)	37(2)	60(2)	51(2)	-4(1)	-4(1)	0(1)
F(15)	37(1)	36(2)	38(1)	-9(1)	4(1)	1(1)
F(16)	51(2)	37(2)	48(2)	5(1)	11(1)	9(1)
F(17)	55(2)	39(2)	77(2)	-14(2)	4(2)	13(1)
F(18)	52(2)	78(2)	64(2)	-41(2)	15(2)	8(2)
F(19)	59(2)	79(2)	42(2)	-16(2)	24(2)	-14(2)
F(20)	52(2)	41(2)	38(1)	3(1)	15(1)	1(1)
Br(2)	53(1)	107(2)	97(1)	-51(1)	4(1)	20(1)
Br(2A)	230(13)	194(13)	81(5)	37(6)	73(7)	135(11)
Br(2B)	79(5)	110(7)	77(5)	-35(5)	19(4)	40(5)
C(62)	49(4)	74(5)	91(5)	-22(4)	17(4)	23(3)
C(63)	52(4)	48(4)	135(7)	-7(4)	40(4)	4(3)
C(64)	92(5)	62(5)	95(5)	23(4)	46(5)	35(4)
C(65)	40(4)	73(5)	120(7)	-26(5)	1(4)	7(3)
C(66)	50(4)	74(5)	145(8)	11(5)	42(5)	3(4)
C(67)	73(5)	98(6)	103(6)	8(5)	43(5)	30(5)

Table A.59: Bond Distances (Å) for **14-C₆D₅Br**

Sc(1)-N(1)	2.100(4)	C(24)-C(25)	1.402(6)	C(47)-C(48)	1.376(7)
Sc(1)-N(2)	2.105(4)	C(25)-C(27)	1.519(6)	C(48)-F(9)	1.352(5)
Sc(1)-C(1)	2.162(5)	C(26)-C(27)	1.544(7)	C(48)-C(49)	1.367(6)
Sc(1)-C(35)	2.640(4)	C(27)-C(28)	1.535(7)	C(49)-F(10)	1.354(5)
Sc(1)-C(34)	2.682(4)	C(29)-C(30)	1.525(9)	C(50)-C(55)	1.385(6)
Sc(1)-C(36)	2.715(4)	C(30)-C(31)	1.524(7)	C(50)-C(51)	1.389(6)
Sc(1)-C(33)	2.767(4)	C(32)-C(33)	1.376(6)	C(51)-F(11)	1.348(5)
Sc(1)-C(37)	2.802(5)	C(32)-C(37)	1.389(7)	C(51)-C(52)	1.376(6)
Sc(1)-C(32)	2.842(4)	C(32)-Br(1)	1.871(5)	C(52)-F(12)	1.358(5)
N(1)-C(4)	1.339(5)	C(33)-C(34)	1.395(6)	C(52)-C(53)	1.374(6)
N(1)-C(8)	1.459(5)	C(34)-C(35)	1.389(7)	C(53)-F(13)	1.354(5)
N(2)-C(6)	1.340(5)	C(35)-C(36)	1.382(7)	C(53)-C(54)	1.357(6)
N(2)-C(20)	1.447(5)	C(36)-C(37)	1.392(7)	C(54)-F(14)	1.362(5)
C(3)-C(4)	1.503(6)	B(1)-C(44)	1.643(7)	C(54)-C(55)	1.376(6)
C(4)-C(5)	1.409(6)	B(1)-C(56)	1.649(6)	C(55)-F(15)	1.365(5)

C(5)-C(6)	1.397(6)	B(1)-C(50)	1.654(6)	C(56)-C(57)	1.388(6)
C(6)-C(7)	1.506(6)	B(1)-C(38)	1.663(6)	C(56)-C(61)	1.411(6)
C(8)-C(9)	1.405(6)	C(38)-C(39)	1.388(6)	C(57)-F(16)	1.349(5)
C(8)-C(13)	1.417(6)	C(38)-C(43)	1.389(6)	C(57)-C(58)	1.391(6)
C(9)-C(10)	1.394(7)	C(39)-F(1)	1.356(5)	C(58)-F(17)	1.343(5)
C(9)-C(18)	1.520(7)	C(39)-C(40)	1.387(7)	C(58)-C(59)	1.368(7)
C(10)-C(11)	1.369(8)	C(40)-F(2)	1.348(5)	C(59)-F(18)	1.354(5)
C(11)-C(12)	1.384(8)	C(40)-C(41)	1.355(7)	C(59)-C(60)	1.360(7)
C(12)-C(13)	1.389(6)	C(41)-F(3)	1.361(5)	C(60)-F(19)	1.353(5)
C(13)-C(15)	1.513(7)	C(41)-C(42)	1.377(7)	C(60)-C(61)	1.369(6)
C(14)-C(15)	1.532(6)	C(42)-F(4)	1.345(6)	C(61)-F(20)	1.344(5)
C(15)-C(16)	1.522(7)	C(42)-C(43)	1.376(6)	Br(2)-C(62)	1.903(7)
C(17)-C(18)	1.533(7)	C(43)-F(5)	1.361(5)	Br(2A)-C(62)	2.221(12)
C(18)-C(19)	1.543(7)	C(44)-C(45)	1.391(6)	Br(2B)-C(62)	1.982(11)
C(20)-C(25)	1.407(6)	C(44)-C(49)	1.403(6)	C(62)-C(63)	1.354(9)
C(20)-C(21)	1.413(6)	C(45)-F(6)	1.353(5)	C(62)-C(67)	1.368(10)
C(21)-C(22)	1.392(7)	C(45)-C(46)	1.381(6)	C(63)-C(64)	1.468(10)
C(21)-C(30)	1.523(7)	C(46)-F(7)	1.360(5)	C(64)-C(65)	1.294(10)
C(22)-C(23)	1.386(7)	C(46)-C(47)	1.366(7)	C(65)-C(66)	1.416(10)
C(23)-C(24)	1.370(7)	C(47)-F(8)	1.344(5)	C(66)-C(67)	1.381(11)

Table A.60: Bond Angles (°) for 14-C₆D₅Br

N(1)-Sc(1)-N(2)	90.79(14)	C(9)-C(18)-C(19)	112.6(4)	C(45)-C(44)-C(49)	112.5(4)
N(1)-Sc(1)-C(1)	105.22(16)	C(17)-C(18)-C(19)	108.8(4)	C(45)-C(44)-B(1)	127.1(4)
N(2)-Sc(1)-C(1)	105.23(16)	C(25)-C(20)-C(21)	121.1(4)	C(49)-C(44)-B(1)	119.3(4)
N(1)-Sc(1)-C(35)	96.21(15)	C(25)-C(20)-N(2)	120.7(4)	F(6)-C(45)-C(46)	115.1(4)
N(2)-Sc(1)-C(35)	108.18(15)	C(21)-C(20)-N(2)	118.2(4)	F(6)-C(45)-C(44)	121.3(4)
C(1)-Sc(1)-C(35)	139.74(17)	C(22)-C(21)-C(20)	118.3(4)	C(46)-C(45)-C(44)	123.6(4)
N(1)-Sc(1)-C(34)	121.82(14)	C(22)-C(21)-C(30)	119.9(4)	F(7)-C(46)-C(47)	119.0(4)
N(2)-Sc(1)-C(34)	90.59(14)	C(20)-C(21)-C(30)	121.8(4)	F(7)-C(46)-C(45)	120.1(4)
C(1)-Sc(1)-C(34)	130.15(16)	C(23)-C(22)-C(21)	121.4(5)	C(47)-C(46)-C(45)	120.9(5)
C(35)-Sc(1)-C(34)	30.23(15)	C(24)-C(23)-C(22)	119.5(5)	F(8)-C(47)-C(46)	120.6(5)
N(1)-Sc(1)-C(36)	92.57(14)	C(23)-C(24)-C(25)	122.1(5)	F(8)-C(47)-C(48)	121.2(4)
N(2)-Sc(1)-C(36)	138.00(15)	C(24)-C(25)-C(20)	117.6(4)	C(46)-C(47)-C(48)	118.2(4)
C(1)-Sc(1)-C(36)	114.12(17)	C(24)-C(25)-C(27)	119.3(4)	F(9)-C(48)-C(49)	120.1(5)
C(35)-Sc(1)-C(36)	29.87(15)	C(20)-C(25)-C(27)	123.1(4)	F(9)-C(48)-C(47)	120.2(4)
C(34)-Sc(1)-C(36)	52.90(15)	C(25)-C(27)-C(28)	111.4(4)	C(49)-C(48)-C(47)	119.6(4)
N(1)-Sc(1)-C(33)	149.00(14)	C(25)-C(27)-C(26)	111.3(4)	F(10)-C(49)-C(48)	116.4(4)
N(2)-Sc(1)-C(33)	98.80(14)	C(28)-C(27)-C(26)	108.6(4)	F(10)-C(49)-C(44)	118.5(4)
C(1)-Sc(1)-C(33)	100.59(16)	C(31)-C(30)-C(29)	108.6(5)	C(48)-C(49)-C(44)	125.1(5)
C(35)-Sc(1)-C(33)	52.79(15)	C(31)-C(30)-C(21)	113.9(4)	C(55)-C(50)-C(51)	112.7(4)
C(34)-Sc(1)-C(33)	29.61(13)	C(29)-C(30)-C(21)	110.3(5)	C(55)-C(50)-B(1)	126.7(4)
C(36)-Sc(1)-C(33)	60.89(14)	C(33)-C(32)-C(37)	119.9(5)	C(51)-C(50)-B(1)	120.3(4)
N(1)-Sc(1)-C(37)	112.84(14)	C(33)-C(32)-Br(1)	121.0(4)	F(11)-C(51)-C(52)	116.4(4)
N(2)-Sc(1)-C(37)	149.23(14)	C(37)-C(32)-Br(1)	119.1(4)	F(11)-C(51)-C(50)	119.0(4)
C(1)-Sc(1)-C(37)	87.91(17)	C(33)-C(32)-Sc(1)	72.8(2)	C(52)-C(51)-C(50)	124.6(4)
C(35)-Sc(1)-C(37)	52.13(16)	C(37)-C(32)-Sc(1)	74.2(3)	F(12)-C(52)-C(53)	120.1(4)
C(34)-Sc(1)-C(37)	60.61(15)	Br(1)-C(32)-Sc(1)	125.8(2)	F(12)-C(52)-C(51)	120.5(4)
C(36)-Sc(1)-C(37)	29.17(15)	C(32)-C(33)-C(34)	120.2(5)	C(53)-C(52)-C(51)	119.4(4)
C(33)-Sc(1)-C(37)	50.89(14)	C(32)-C(33)-Sc(1)	78.8(3)	F(13)-C(53)-C(54)	120.9(4)

N(1)-Sc(1)-C(32)	141.28(14)	C(34)-C(33)-Sc(1)	71.8(2)	F(13)-C(53)-C(52)	120.5(4)
N(2)-Sc(1)-C(32)	124.61(14)	C(35)-C(34)-C(33)	119.7(5)	C(54)-C(53)-C(52)	118.6(4)
C(1)-Sc(1)-C(32)	82.02(16)	C(35)-C(34)-Sc(1)	73.2(3)	C(53)-C(54)-F(14)	119.6(4)
C(35)-Sc(1)-C(32)	60.67(14)	C(33)-C(34)-Sc(1)	78.6(3)	C(53)-C(54)-C(55)	120.3(4)
C(34)-Sc(1)-C(32)	51.45(14)	C(36)-C(35)-C(34)	120.4(5)	F(14)-C(54)-C(55)	120.1(4)
C(36)-Sc(1)-C(32)	51.40(14)	C(36)-C(35)-Sc(1)	78.1(3)	F(15)-C(55)-C(54)	114.8(4)
C(33)-Sc(1)-C(32)	28.37(13)	C(34)-C(35)-Sc(1)	76.5(3)	F(15)-C(55)-C(50)	120.9(4)
C(37)-Sc(1)-C(32)	28.48(14)	C(35)-C(36)-C(37)	119.5(5)	C(54)-C(55)-C(50)	124.3(4)
C(4)-N(1)-C(8)	119.4(4)	C(35)-C(36)-Sc(1)	72.1(3)	C(57)-C(56)-C(61)	112.7(4)
C(4)-N(1)-Sc(1)	117.0(3)	C(37)-C(36)-Sc(1)	78.9(3)	C(57)-C(56)-B(1)	129.0(4)
C(8)-N(1)-Sc(1)	122.3(3)	C(32)-C(37)-C(36)	120.4(5)	C(61)-C(56)-B(1)	117.8(4)
C(6)-N(2)-C(20)	119.0(3)	C(32)-C(37)-Sc(1)	77.4(3)	F(16)-C(57)-C(56)	120.5(4)
C(6)-N(2)-Sc(1)	116.5(3)	C(36)-C(37)-Sc(1)	72.0(3)	F(16)-C(57)-C(58)	115.5(4)
C(20)-N(2)-Sc(1)	123.6(3)	C(44)-B(1)-C(56)	100.5(3)	C(56)-C(57)-C(58)	123.9(4)
N(1)-C(4)-C(5)	123.2(4)	C(44)-B(1)-C(50)	115.3(4)	F(17)-C(58)-C(59)	120.6(4)
N(1)-C(4)-C(3)	120.1(4)	C(56)-B(1)-C(50)	112.9(4)	F(17)-C(58)-C(57)	119.8(5)
C(5)-C(4)-C(3)	116.7(4)	C(44)-B(1)-C(38)	112.8(4)	C(59)-C(58)-C(57)	119.6(5)
C(6)-C(5)-C(4)	131.4(4)	C(56)-B(1)-C(38)	114.0(4)	F(18)-C(59)-C(60)	120.4(5)
N(2)-C(6)-C(5)	123.7(4)	C(50)-B(1)-C(38)	102.0(3)	F(18)-C(59)-C(58)	120.0(5)
N(2)-C(6)-C(7)	120.0(4)	C(39)-C(38)-C(43)	112.9(4)	C(60)-C(59)-C(58)	119.6(4)
C(5)-C(6)-C(7)	116.3(4)	C(39)-C(38)-B(1)	127.1(4)	F(19)-C(60)-C(59)	120.4(4)
C(9)-C(8)-C(13)	122.3(4)	C(43)-C(38)-B(1)	119.6(4)	F(19)-C(60)-C(61)	119.9(5)
C(9)-C(8)-N(1)	120.5(4)	F(1)-C(39)-C(40)	115.2(4)	C(59)-C(60)-C(61)	119.7(5)
C(13)-C(8)-N(1)	117.1(4)	F(1)-C(39)-C(38)	121.1(4)	F(20)-C(61)-C(60)	116.5(4)
C(10)-C(9)-C(8)	117.0(5)	C(40)-C(39)-C(38)	123.7(5)	F(20)-C(61)-C(56)	119.0(4)
C(10)-C(9)-C(18)	119.2(5)	F(2)-C(40)-C(41)	120.2(5)	C(60)-C(61)-C(56)	124.5(5)
C(8)-C(9)-C(18)	123.8(4)	F(2)-C(40)-C(39)	120.1(5)	C(63)-C(62)-C(67)	120.8(7)
C(11)-C(10)-C(9)	122.0(5)	C(41)-C(40)-C(39)	119.8(4)	C(63)-C(62)-Br(2)	117.3(6)
C(10)-C(11)-C(12)	120.0(5)	C(40)-C(41)-F(3)	120.7(5)	C(67)-C(62)-Br(2)	121.9(7)
C(11)-C(12)-C(13)	121.5(5)	C(40)-C(41)-C(42)	120.0(4)	C(63)-C(62)-Br(2B)	147.5(9)
C(12)-C(13)-C(8)	117.1(5)	F(3)-C(41)-C(42)	119.3(5)	C(67)-C(62)-Br(2B)	90.9(9)
C(12)-C(13)-C(15)	120.2(5)	F(4)-C(42)-C(41)	120.4(4)	C(63)-C(62)-Br(2A)	167.4(7)
C(8)-C(13)-C(15)	122.7(4)	F(4)-C(42)-C(43)	121.6(4)	C(62)-C(63)-C(64)	121.0(6)
C(13)-C(15)-C(16)	111.8(4)	C(41)-C(42)-C(43)	118.0(5)	C(65)-C(64)-C(63)	117.0(7)
C(13)-C(15)-C(14)	114.1(4)	F(5)-C(43)-C(42)	115.4(4)	C(64)-C(65)-C(66)	122.2(7)
C(16)-C(15)-C(14)	108.6(4)	F(5)-C(43)-C(38)	119.1(4)	C(67)-C(66)-C(65)	120.6(7)
C(9)-C(18)-C(17)	112.0(5)	C(42)-C(43)-C(38)	125.5(4)	C(62)-C(67)-C(66)	118.4(7)

Table A.61: Crystal Data and Structure Refinement for **14-C₇H₈****A. Crystal Data**

Crystallographer	Masood Parvez	University of Calgary
Empirical Formula	C ₆₇ H ₅₇ BBrF ₂₀ N ₂ Sc	
Formula Weight	1405.83	
Crystal Size	0.20 x 0.20 x 0.18 mm ³	
Crystal System	monoclinic	
Space Group	P2 ₁ /n	
Lattice Parameters	a = 18.9115(4) Å	

	$b = 14.0831(3) \text{ \AA}$	$\beta = 107.0566(9)^\circ$
	$c = 24.6274(6) \text{ \AA}$	
Volume	$6270.6(2) \text{ \AA}^3$	
Z	4	
Density (calculated)	1.489 Mg/m^3	

B. Data Collection and Refinement Conditions

Diffractometer	Nonius Kappa CCD
Radiation (λ [\AA])	Graphite-monochromated MoK α (0.71073)
Temperature	173(2) K
Reflections Collected	18966
Independent Reflections	10673 [R(int) = 0.040]
Structure Solution	Direct Methods
Refinement Method	Full-matrix least-squares on F ²
Data / Restraints / Parameters	10673 / 0 / 835
Goodness-of-Fit	1.02
Final R Indices [$I > 2\sigma(I)$]	R1 = 0.056, wR2 = 0.130
R Indices (all data)	R1 = 0.104, wR2 = 0.156
Largest Difference Peak & Hole	0.53 and -0.58 e. \AA^{-3}

Table A.62: Atomic Coordinates and Equivalent Isotropic Displacement Parameters for **14-C₇H₈**

	x	y	z	U(eq)		x	y	z	U(eq)
Sc(1)	-4296(1)	-3079(1)	3570(1)	33(1)	F(8)	-2372(1)	761(2)	7173(1)	70(1)
N(1)	-5300(2)	-3613(2)	3045(1)	35(1)	F(9)	-1955(1)	2591(2)	7457(1)	60(1)
N(2)	-4858(2)	-1935(2)	3812(1)	33(1)	F(10)	-1559(1)	3711(2)	6731(1)	48(1)
C(1)	-4003(2)	-4016(3)	4310(2)	39(1)	F(11)	-3133(1)	2795(2)	4989(1)	46(1)
C(3)	-6544(2)	-4214(3)	3005(2)	44(1)	F(12)	-4386(1)	3640(2)	4992(1)	58(1)
C(4)	-5897(2)	-3560(2)	3238(2)	35(1)	F(13)	-4356(1)	5308(2)	5572(1)	64(1)
C(5)	-5954(2)	-2913(2)	3656(2)	36(1)	F(14)	-3032(1)	6131(2)	6094(1)	61(1)
C(6)	-5513(2)	-2131(2)	3898(1)	33(1)	F(15)	-1775(1)	5346(2)	6068(1)	49(1)
C(7)	-5818(2)	-1492(3)	4264(2)	45(1)	F(16)	-1240(1)	5103(2)	5120(1)	51(1)
C(8)	-5346(2)	-4190(3)	2547(2)	40(1)	F(17)	49(1)	6025(2)	5437(1)	60(1)
C(9)	-5160(2)	-5169(3)	2609(2)	45(1)	F(18)	1210(1)	5301(2)	6284(1)	70(1)
C(10)	-5176(2)	-5675(3)	2116(2)	58(1)	F(19)	1026(1)	3660(2)	6806(1)	61(1)
C(11)	-5364(3)	-5238(4)	1594(2)	64(1)	F(20)	-262(1)	2781(2)	6534(1)	45(1)
C(12)	-5548(2)	-4289(4)	1544(2)	57(1)	B(1)	-1640(2)	3354(3)	5568(2)	35(1)
C(13)	-5549(2)	-3741(3)	2013(2)	43(1)	C(39)	-1586(2)	2933(3)	4956(2)	36(1)
C(14)	-5565(3)	-2207(4)	1447(2)	67(1)	C(40)	-1056(2)	2256(3)	4950(2)	39(1)
C(15)	-5761(2)	-2703(3)	1945(2)	48(1)	C(41)	-928(2)	1901(3)	4465(2)	46(1)
C(16)	-6585(3)	-2565(4)	1877(2)	75(2)	C(42)	-1353(3)	2225(3)	3945(2)	51(1)
C(17)	-4156(3)	-6090(4)	3322(2)	76(2)	C(43)	-1879(2)	2887(3)	3921(2)	49(1)
C(18)	-4955(2)	-5691(3)	3173(2)	53(1)	C(44)	-1978(2)	3247(3)	4417(2)	43(1)
C(19)	-5487(3)	-6509(3)	3180(2)	65(1)	C(45)	-1772(2)	2536(3)	6013(2)	35(1)
C(20)	-4529(2)	-1007(3)	3986(2)	34(1)	C(46)	-1999(2)	1598(3)	5895(2)	39(1)
C(21)	-4693(2)	-268(3)	3586(2)	41(1)	C(47)	-2185(2)	1004(3)	6277(2)	44(1)

C(22)	-4360(2)	610(3)	3742(2)	49(1)	C(48)	-2176(2)	1328(3)	6799(2)	48(1)
C(23)	-3874(2)	742(3)	4275(2)	51(1)	C(49)	-1962(2)	2245(3)	6944(2)	45(1)
C(24)	-3716(2)	23(3)	4664(2)	45(1)	C(50)	-1761(2)	2814(3)	6560(2)	39(1)
C(25)	-4036(2)	-874(3)	4533(2)	39(1)	C(51)	-2381(2)	4027(3)	5515(2)	37(1)
C(26)	-4109(3)	-1321(4)	5513(2)	66(1)	C(52)	-3081(2)	3648(3)	5253(2)	39(1)
C(27)	-3868(2)	-1637(3)	4990(2)	49(1)	C(53)	-3732(2)	4062(3)	5256(2)	45(1)
C(28)	-3051(3)	-1891(3)	5183(2)	63(1)	C(54)	-3724(2)	4897(3)	5542(2)	48(1)
C(29)	-5997(3)	72(6)	2985(2)	111(3)	C(55)	-3054(2)	5310(3)	5805(2)	45(1)
C(30)	-5255(3)	-384(3)	3004(2)	58(1)	C(56)	-2407(2)	4882(3)	5783(2)	42(1)
C(31)	-5003(3)	14(4)	2516(2)	64(1)	C(57)	-838(2)	3912(2)	5820(2)	34(1)
C(32)	-2770(2)	-3167(3)	3734(2)	49(1)	C(58)	-698(2)	4732(3)	5559(2)	39(1)
C(33)	-2975(2)	-2216(3)	3674(2)	46(1)	C(59)	-29(2)	5208(3)	5706(2)	44(1)
C(34)	-3478(2)	-1885(3)	3174(2)	46(1)	C(60)	548(2)	4849(3)	6129(2)	46(1)
C(35)	-3785(2)	-2508(3)	2734(2)	53(1)	C(61)	451(2)	4029(3)	6392(2)	43(1)
C(36)	-3582(3)	-3455(4)	2790(2)	56(1)	C(62)	-227(2)	3585(3)	6238(2)	36(1)
C(37)	-3085(2)	-3783(3)	3284(2)	54(1)	Br(1)	-2216(1)	5550(1)	2103(1)	107(1)
C(38)	-2173(3)	-3529(4)	4254(2)	76(2)	Br(1A)	-3006(6)	4135(8)	2272(3)	162(4)
F(1)	-623(1)	1905(2)	5448(1)	45(1)	Br(1B)	-2399(5)	4917(6)	2319(3)	114(2)
F(2)	-399(1)	1249(2)	4497(1)	63(1)	C(63)	-2889(2)	4850(3)	1510(2)	90(2)
F(3)	-1235(2)	1882(2)	3468(1)	74(1)	C(64)	-3359(3)	4158(4)	1611(2)	97(2)
F(4)	-2291(2)	3224(2)	3413(1)	68(1)	C(65)	-3838(2)	3675(3)	1159(3)	102(2)
F(5)	-2491(1)	3951(2)	4345(1)	54(1)	C(66)	-3847(2)	3884(3)	605(2)	96(2)
F(6)	-2059(1)	1219(2)	5375(1)	50(1)	C(67)	-3377(3)	4577(3)	504(2)	102(2)
F(7)	-2400(1)	101(2)	6126(1)	63(1)	C(68)	-2898(2)	5060(2)	956(3)	86(2)

Table A.63: Anisotropic Displacement Parameters for 14-C₇H₈

Atom	U11	U22	U33	U23	U13	U12
Sc(1)	33(1)	36(1)	32(1)	-1(1)	10(1)	-1(1)
N(1)	36(2)	34(2)	33(2)	-3(1)	8(1)	1(1)
N(2)	38(2)	32(2)	29(2)	-1(1)	10(1)	-5(1)
C(1)	43(2)	40(2)	33(2)	1(2)	8(2)	0(2)
C(3)	38(2)	42(2)	52(2)	-7(2)	13(2)	-6(2)
C(4)	36(2)	33(2)	33(2)	4(2)	7(2)	1(2)
C(5)	37(2)	37(2)	35(2)	2(2)	16(2)	-2(2)
C(6)	36(2)	35(2)	29(2)	3(2)	9(2)	2(2)
C(7)	46(2)	46(2)	47(2)	-6(2)	22(2)	-4(2)
C(8)	32(2)	45(2)	43(2)	-11(2)	11(2)	-3(2)
C(9)	35(2)	42(2)	55(3)	-15(2)	8(2)	-5(2)
C(10)	50(3)	54(3)	71(3)	-23(3)	20(2)	-4(2)
C(11)	58(3)	77(4)	64(3)	-33(3)	26(3)	-9(3)
C(12)	49(3)	77(3)	44(3)	-10(2)	15(2)	-2(2)
C(13)	34(2)	59(3)	34(2)	-7(2)	10(2)	-1(2)
C(14)	69(3)	84(4)	55(3)	16(3)	27(3)	11(3)
C(15)	45(2)	64(3)	32(2)	4(2)	10(2)	7(2)
C(16)	58(3)	95(4)	76(3)	25(3)	28(3)	23(3)
C(17)	54(3)	58(3)	100(4)	-1(3)	-1(3)	4(2)
C(18)	49(3)	39(2)	65(3)	-6(2)	5(2)	3(2)
C(19)	65(3)	46(3)	78(3)	-1(2)	13(3)	-6(2)
C(20)	35(2)	35(2)	36(2)	-6(2)	15(2)	-3(2)
C(21)	45(2)	38(2)	41(2)	2(2)	14(2)	-4(2)

C(22)	58(3)	40(2)	54(3)	5(2)	22(2)	-4(2)
C(23)	56(3)	38(2)	64(3)	-11(2)	23(2)	-15(2)
C(24)	47(2)	43(2)	45(2)	-10(2)	12(2)	-7(2)
C(25)	41(2)	38(2)	41(2)	-6(2)	15(2)	-4(2)
C(26)	74(3)	80(3)	45(3)	3(2)	19(2)	-6(3)
C(27)	53(3)	46(2)	39(2)	-2(2)	1(2)	-7(2)
C(28)	69(3)	69(3)	48(3)	5(2)	13(2)	10(3)
C(29)	45(3)	218(8)	66(4)	45(4)	8(3)	-11(4)
C(30)	76(3)	45(2)	48(3)	12(2)	9(2)	-15(2)
C(31)	68(3)	77(3)	49(3)	14(2)	19(2)	12(3)
C(32)	34(2)	57(3)	54(3)	7(2)	13(2)	2(2)
C(33)	38(2)	53(3)	50(2)	-2(2)	17(2)	-10(2)
C(34)	38(2)	50(2)	56(3)	9(2)	22(2)	-1(2)
C(35)	45(3)	76(3)	43(2)	7(2)	19(2)	-7(2)
C(36)	53(3)	75(3)	50(3)	-19(2)	30(2)	-13(2)
C(37)	53(3)	47(2)	72(3)	-6(2)	36(3)	1(2)
C(38)	64(3)	70(3)	96(4)	18(3)	28(3)	12(3)
F(1)	44(1)	49(1)	40(1)	-3(1)	11(1)	5(1)
F(2)	61(2)	73(2)	62(2)	-20(1)	30(1)	-2(1)
F(3)	86(2)	101(2)	44(1)	-23(1)	34(1)	-30(2)
F(4)	73(2)	91(2)	32(1)	9(1)	3(1)	-21(2)
F(5)	53(2)	59(2)	43(1)	14(1)	4(1)	-3(1)
F(6)	52(1)	41(1)	53(1)	-5(1)	11(1)	-12(1)
F(7)	56(2)	44(1)	79(2)	16(1)	6(1)	-14(1)
F(8)	55(2)	83(2)	71(2)	44(2)	19(1)	-5(1)
F(9)	62(2)	83(2)	43(1)	14(1)	25(1)	11(1)
F(10)	58(2)	47(1)	42(1)	-4(1)	18(1)	-2(1)
F(11)	40(1)	43(1)	51(1)	-1(1)	7(1)	-9(1)
F(12)	35(1)	68(2)	65(2)	9(1)	4(1)	-3(1)
F(13)	47(2)	71(2)	74(2)	10(1)	21(1)	18(1)
F(14)	64(2)	47(1)	75(2)	-2(1)	28(1)	7(1)
F(15)	44(1)	42(1)	61(2)	-7(1)	16(1)	-6(1)
F(16)	54(2)	48(1)	50(1)	11(1)	15(1)	-7(1)
F(17)	73(2)	51(1)	63(2)	1(1)	33(1)	-22(1)
F(18)	51(2)	78(2)	77(2)	-8(2)	15(1)	-33(1)
F(19)	41(1)	72(2)	60(2)	0(1)	-2(1)	-7(1)
F(20)	41(1)	44(1)	45(1)	5(1)	7(1)	-4(1)
B(1)	35(2)	38(2)	31(2)	0(2)	8(2)	-4(2)
C(39)	37(2)	37(2)	35(2)	-2(2)	10(2)	-13(2)
C(40)	40(2)	44(2)	32(2)	0(2)	8(2)	-10(2)
C(41)	44(2)	50(2)	50(3)	-13(2)	22(2)	-9(2)
C(42)	62(3)	62(3)	36(2)	-12(2)	24(2)	-24(2)
C(43)	52(3)	63(3)	31(2)	3(2)	8(2)	-24(2)
C(44)	43(2)	43(2)	41(2)	6(2)	10(2)	-11(2)
C(45)	26(2)	39(2)	39(2)	4(2)	9(2)	-1(2)
C(46)	32(2)	42(2)	41(2)	5(2)	6(2)	-1(2)
C(47)	29(2)	37(2)	61(3)	12(2)	5(2)	-10(2)
C(48)	33(2)	60(3)	49(3)	26(2)	10(2)	1(2)
C(49)	34(2)	63(3)	38(2)	10(2)	12(2)	8(2)
C(50)	32(2)	42(2)	41(2)	5(2)	10(2)	0(2)

C(51)	37(2)	34(2)	39(2)	6(2)	12(2)	-5(2)
C(52)	42(2)	37(2)	39(2)	9(2)	12(2)	-1(2)
C(53)	36(2)	49(2)	48(2)	16(2)	8(2)	-2(2)
C(54)	37(2)	49(3)	59(3)	19(2)	17(2)	12(2)
C(55)	55(3)	33(2)	50(2)	4(2)	20(2)	6(2)
C(56)	38(2)	41(2)	46(2)	8(2)	11(2)	-2(2)
C(57)	37(2)	33(2)	34(2)	-7(2)	14(2)	-7(2)
C(58)	42(2)	40(2)	35(2)	1(2)	12(2)	0(2)
C(59)	56(3)	36(2)	47(2)	-6(2)	29(2)	-15(2)
C(60)	38(2)	53(3)	50(3)	-10(2)	16(2)	-15(2)
C(61)	38(2)	54(3)	36(2)	-6(2)	7(2)	-3(2)
C(62)	37(2)	35(2)	36(2)	-5(2)	12(2)	-5(2)
Br(1)	63(1)	124(1)	121(1)	-62(1)	9(1)	24(1)
Br(1A)	192(8)	204(9)	109(5)	30(5)	72(6)	108(8)
Br(1B)	133(6)	113(5)	112(5)	-27(4)	61(4)	36(5)
C(63)	53(4)	95(5)	122(6)	-26(4)	23(4)	28(3)
C(64)	76(4)	114(5)	114(6)	18(5)	49(4)	36(4)
C(65)	65(4)	96(5)	157(7)	2(5)	50(5)	1(4)
C(66)	34(3)	86(4)	155(7)	-40(5)	6(3)	9(3)
C(67)	132(6)	78(4)	114(5)	42(4)	66(5)	60(4)
C(68)	65(4)	63(3)	134(6)	-12(4)	35(4)	8(3)

Table A.64: Bond Lengths [\AA] for 14-C₇H₈

Sc(1)-N(1)	2.098(3)	C(25)-C(27)	1.520(5)	C(39)-C(40)	1.387(5)
Sc(1)-N(2)	2.109(3)	C(26)-C(27)	1.553(6)	C(39)-C(44)	1.388(5)
Sc(1)-C(1)	2.186(4)	C(27)-C(28)	1.519(6)	C(40)-C(41)	1.378(5)
Sc(1)-C(35)	2.643(4)	C(29)-C(30)	1.532(8)	C(41)-C(42)	1.376(6)
Sc(1)-C(34)	2.655(4)	C(30)-C(31)	1.524(6)	C(42)-C(43)	1.352(6)
Sc(1)-C(36)	2.704(4)	C(32)-C(33)	1.389(6)	C(43)-C(44)	1.386(6)
Sc(1)-C(33)	2.722(4)	C(32)-C(37)	1.395(6)	C(45)-C(46)	1.393(5)
Sc(1)-C(37)	2.769(4)	C(32)-C(38)	1.526(6)	C(45)-C(50)	1.398(5)
Sc(1)-C(32)	2.796(4)	C(33)-C(34)	1.397(6)	C(46)-C(47)	1.381(5)
N(1)-C(4)	1.349(4)	C(34)-C(35)	1.383(6)	C(47)-C(48)	1.359(6)
N(1)-C(8)	1.452(5)	C(35)-C(36)	1.384(6)	C(48)-C(49)	1.370(6)
N(2)-C(6)	1.345(4)	C(36)-C(37)	1.381(6)	C(49)-C(50)	1.374(5)
N(2)-C(20)	1.456(4)	F(1)-C(40)	1.353(4)	C(51)-C(56)	1.380(5)
C(3)-C(4)	1.504(5)	F(2)-C(41)	1.343(5)	C(51)-C(52)	1.399(5)
C(4)-C(5)	1.402(5)	F(3)-C(42)	1.347(4)	C(52)-C(53)	1.365(6)
C(5)-C(6)	1.404(5)	F(4)-C(43)	1.351(5)	C(53)-C(54)	1.368(6)
C(6)-C(7)	1.504(5)	F(5)-C(44)	1.362(5)	C(54)-C(55)	1.373(6)
C(8)-C(13)	1.407(5)	F(6)-C(46)	1.360(4)	C(55)-C(56)	1.379(6)
C(8)-C(9)	1.420(5)	F(7)-C(47)	1.353(4)	C(57)-C(62)	1.382(5)
C(9)-C(10)	1.401(6)	F(8)-C(48)	1.351(4)	C(57)-C(58)	1.385(5)
C(9)-C(18)	1.516(6)	F(9)-C(49)	1.351(4)	C(58)-C(59)	1.383(5)
C(10)-C(11)	1.373(7)	F(10)-C(50)	1.352(4)	C(59)-C(60)	1.366(6)
C(11)-C(12)	1.378(7)	F(11)-C(52)	1.355(4)	C(60)-C(61)	1.362(6)
C(12)-C(13)	1.390(6)	F(12)-C(53)	1.353(4)	C(61)-C(62)	1.376(5)
C(13)-C(15)	1.512(6)	F(13)-C(54)	1.349(4)	Br(1)-Br(1B)	1.142(9)
C(14)-C(15)	1.548(6)	F(14)-C(55)	1.353(4)	Br(1)-C(63)	1.907(4)

C(15)-C(16)	1.529(6)	F(15)-C(56)	1.363(4)	Br(1)-Br(1A)	2.598(12)
C(17)-C(18)	1.552(6)	F(16)-C(58)	1.358(4)	Br(1A)-Br(1B)	1.571(13)
C(18)-C(19)	1.534(6)	F(17)-C(59)	1.357(4)	Br(1A)-C(63)	2.198(10)
C(20)-C(21)	1.403(5)	F(18)-C(60)	1.356(4)	Br(1B)-C(63)	1.937(9)
C(20)-C(25)	1.409(5)	F(19)-C(61)	1.357(4)	C(63)-C(64)	1.39
C(21)-C(22)	1.391(5)	F(20)-C(62)	1.358(4)	C(63)-C(68)	1.39
C(21)-C(30)	1.522(6)	B(1)-C(39)	1.651(5)	C(64)-C(65)	1.39
C(22)-C(23)	1.376(6)	B(1)-C(45)	1.657(5)	C(65)-C(66)	1.39
C(23)-C(24)	1.367(6)	B(1)-C(57)	1.658(5)	C(66)-C(67)	1.39
C(24)-C(25)	1.397(5)	B(1)-C(51)	1.664(6)	C(67)-C(68)	1.39

Table A.65: Bond Angles [°] for **14-C₇H₈**

N(1)-Sc(1)-N(2)	90.48(11)	C(22)-C(21)-C(20)	118.5(4)	F(8)-C(48)-C(47)	121.1(4)
N(1)-Sc(1)-C(1)	105.03(13)	C(22)-C(21)-C(30)	119.4(4)	F(8)-C(48)-C(49)	120.0(4)
N(2)-Sc(1)-C(1)	104.54(13)	C(20)-C(21)-C(30)	122.1(3)	C(47)-C(48)-C(49)	118.9(4)
N(1)-Sc(1)-C(35)	95.79(13)	C(23)-C(22)-C(21)	120.4(4)	F(9)-C(49)-C(48)	120.3(4)
N(2)-Sc(1)-C(35)	108.51(13)	C(24)-C(23)-C(22)	121.1(4)	F(9)-C(49)-C(50)	120.4(4)
C(1)-Sc(1)-C(35)	140.51(15)	C(23)-C(24)-C(25)	121.1(4)	C(48)-C(49)-C(50)	119.4(4)
N(1)-Sc(1)-C(34)	121.37(12)	C(24)-C(25)-C(20)	117.5(4)	F(10)-C(50)-C(49)	116.1(3)
N(2)-Sc(1)-C(34)	90.93(12)	C(24)-C(25)-C(27)	119.0(3)	F(10)-C(50)-C(45)	119.0(3)
C(1)-Sc(1)-C(34)	130.94(14)	C(20)-C(25)-C(27)	123.4(3)	C(49)-C(50)-C(45)	124.9(4)
C(35)-Sc(1)-C(34)	30.27(13)	C(25)-C(27)-C(28)	111.8(4)	C(56)-C(51)-C(52)	113.1(3)
N(1)-Sc(1)-C(36)	92.43(13)	C(25)-C(27)-C(26)	111.3(4)	C(56)-C(51)-B(1)	127.4(3)
N(2)-Sc(1)-C(36)	138.42(14)	C(28)-C(27)-C(26)	109.1(3)	C(52)-C(51)-B(1)	118.7(3)
C(1)-Sc(1)-C(36)	114.60(15)	C(21)-C(30)-C(31)	114.2(4)	F(11)-C(52)-C(53)	116.3(3)
C(35)-Sc(1)-C(36)	29.96(14)	C(21)-C(30)-C(29)	111.4(4)	F(11)-C(52)-C(51)	119.1(3)
C(34)-Sc(1)-C(36)	52.95(14)	C(31)-C(30)-C(29)	108.5(4)	C(53)-C(52)-C(51)	124.6(4)
N(1)-Sc(1)-C(33)	149.09(12)	C(33)-C(32)-C(37)	118.3(4)	F(12)-C(53)-C(52)	120.5(4)
N(2)-Sc(1)-C(33)	99.05(12)	C(33)-C(32)-C(38)	121.7(4)	F(12)-C(53)-C(54)	119.7(4)
C(1)-Sc(1)-C(33)	100.91(14)	C(37)-C(32)-C(38)	119.8(4)	C(52)-C(53)-C(54)	119.8(4)
C(35)-Sc(1)-C(33)	53.30(13)	C(33)-C(32)-Sc(1)	72.5(2)	F(13)-C(54)-C(53)	121.4(4)
C(34)-Sc(1)-C(33)	30.08(12)	C(37)-C(32)-Sc(1)	74.4(2)	F(13)-C(54)-C(55)	120.1(4)
C(36)-Sc(1)-C(33)	61.21(13)	C(38)-C(32)-Sc(1)	128.0(3)	C(53)-C(54)-C(55)	118.5(4)
N(1)-Sc(1)-C(37)	112.42(13)	C(32)-C(33)-C(34)	120.8(4)	F(14)-C(55)-C(54)	119.5(4)
N(2)-Sc(1)-C(37)	150.21(12)	C(32)-C(33)-Sc(1)	78.4(2)	F(14)-C(55)-C(56)	120.3(4)
C(1)-Sc(1)-C(37)	88.22(14)	C(34)-C(33)-Sc(1)	72.3(2)	C(54)-C(55)-C(56)	120.2(4)
C(35)-Sc(1)-C(37)	52.60(14)	C(35)-C(34)-C(33)	120.0(4)	F(15)-C(56)-C(51)	121.1(3)
C(34)-Sc(1)-C(37)	61.27(13)	C(35)-C(34)-Sc(1)	74.4(2)	F(15)-C(56)-C(55)	115.0(3)
C(36)-Sc(1)-C(37)	29.20(13)	C(33)-C(34)-Sc(1)	77.6(2)	C(51)-C(56)-C(55)	123.8(4)
C(33)-Sc(1)-C(37)	51.59(13)	C(34)-C(35)-C(36)	119.5(4)	C(62)-C(57)-C(58)	113.1(3)
N(1)-Sc(1)-C(32)	141.45(12)	C(34)-C(35)-Sc(1)	75.4(2)	C(62)-C(57)-B(1)	126.4(3)
N(2)-Sc(1)-C(32)	125.23(12)	C(36)-C(35)-Sc(1)	77.5(2)	C(58)-C(57)-B(1)	120.0(3)
C(1)-Sc(1)-C(32)	81.59(14)	C(37)-C(36)-C(35)	120.5(4)	F(16)-C(58)-C(59)	116.2(3)
C(35)-Sc(1)-C(32)	61.89(13)	C(37)-C(36)-Sc(1)	78.0(2)	F(16)-C(58)-C(57)	119.2(3)
C(34)-Sc(1)-C(32)	52.68(12)	C(35)-C(36)-Sc(1)	72.6(2)	C(59)-C(58)-C(57)	124.6(4)
C(36)-Sc(1)-C(32)	52.06(13)	C(36)-C(37)-C(32)	120.9(4)	F(17)-C(59)-C(60)	120.6(4)
C(33)-Sc(1)-C(32)	29.11(12)	C(36)-C(37)-Sc(1)	72.8(2)	F(17)-C(59)-C(58)	120.3(4)
C(37)-Sc(1)-C(32)	29.03(13)	C(32)-C(37)-Sc(1)	76.6(2)	C(60)-C(59)-C(58)	119.0(4)
C(4)-N(1)-C(8)	118.6(3)	C(39)-B(1)-C(45)	114.6(3)	F(18)-C(60)-C(59)	120.4(4)

C(4)-N(1)-Sc(1)	117.6(2)	C(39)-B(1)-C(57)	102.5(3)	F(18)-C(60)-C(61)	120.4(4)
C(8)-N(1)-Sc(1)	122.7(2)	C(45)-B(1)-C(57)	112.3(3)	C(59)-C(60)-C(61)	119.2(4)
C(6)-N(2)-C(20)	118.2(3)	C(39)-B(1)-C(51)	114.2(3)	F(19)-C(61)-C(60)	119.4(4)
C(6)-N(2)-Sc(1)	116.8(2)	C(45)-B(1)-C(51)	99.3(3)	F(19)-C(61)-C(62)	120.6(4)
C(20)-N(2)-Sc(1)	124.1(2)	C(57)-B(1)-C(51)	114.5(3)	C(60)-C(61)-C(62)	120.0(4)
N(1)-C(4)-C(5)	123.1(3)	C(40)-C(39)-C(44)	113.2(3)	F(20)-C(62)-C(61)	114.8(3)
N(1)-C(4)-C(3)	120.2(3)	C(40)-C(39)-B(1)	119.7(3)	F(20)-C(62)-C(57)	121.1(3)
C(5)-C(4)-C(3)	116.7(3)	C(44)-C(39)-B(1)	126.8(3)	C(61)-C(62)-C(57)	124.1(3)
C(4)-C(5)-C(6)	131.1(3)	F(1)-C(40)-C(41)	116.1(3)	Br(1B)-Br(1)-C(63)	74.2(4)
N(2)-C(6)-C(5)	123.6(3)	F(1)-C(40)-C(39)	119.2(3)	Br(1B)-Br(1)-Br(1A)	19.8(5)
N(2)-C(6)-C(7)	120.4(3)	C(41)-C(40)-C(39)	124.7(4)	C(63)-Br(1)-Br(1A)	55.9(3)
C(5)-C(6)-C(7)	116.1(3)	F(2)-C(41)-C(42)	120.1(4)	Br(1B)-Br(1A)-C(63)	59.1(4)
C(13)-C(8)-C(9)	121.9(4)	F(2)-C(41)-C(40)	121.0(4)	Br(1B)-Br(1A)-Br(1)	14.3(3)
C(13)-C(8)-N(1)	118.1(3)	C(42)-C(41)-C(40)	118.9(4)	C(63)-Br(1A)-Br(1)	45.9(2)
C(9)-C(8)-N(1)	120.0(3)	F(3)-C(42)-C(43)	121.1(4)	Br(1)-Br(1B)-Br(1A)	145.9(7)
C(10)-C(9)-C(8)	117.3(4)	F(3)-C(42)-C(41)	119.5(4)	Br(1)-Br(1B)-C(63)	71.3(4)
C(10)-C(9)-C(18)	118.8(4)	C(43)-C(42)-C(41)	119.4(4)	Br(1A)-Br(1B)-C(63)	76.8(5)
C(8)-C(9)-C(18)	124.0(4)	C(42)-C(43)-F(4)	120.0(4)	C(64)-C(63)-C(68)	120
C(11)-C(10)-C(9)	121.2(4)	C(42)-C(43)-C(44)	120.0(4)	C(64)-C(63)-Br(1)	123.0(4)
C(10)-C(11)-C(12)	120.5(4)	F(4)-C(43)-C(44)	119.9(4)	C(68)-C(63)-Br(1)	117.0(4)
C(11)-C(12)-C(13)	121.7(4)	F(5)-C(44)-C(43)	115.2(4)	C(64)-C(63)-Br(1B)	89.3(5)
C(12)-C(13)-C(8)	117.5(4)	F(5)-C(44)-C(39)	121.2(4)	C(68)-C(63)-Br(1B)	149.6(5)
C(12)-C(13)-C(15)	120.6(4)	C(43)-C(44)-C(39)	123.7(4)	Br(1)-C(63)-Br(1B)	34.6(3)
C(8)-C(13)-C(15)	121.9(3)	C(46)-C(45)-C(50)	112.4(3)	C(64)-C(63)-Br(1A)	45.2(4)
C(13)-C(15)-C(16)	111.3(4)	C(46)-C(45)-B(1)	128.2(3)	C(68)-C(63)-Br(1A)	163.6(4)
C(13)-C(15)-C(14)	114.0(3)	C(50)-C(45)-B(1)	118.7(3)	Br(1)-C(63)-Br(1A)	78.2(4)
C(16)-C(15)-C(14)	109.2(4)	F(6)-C(46)-C(47)	115.8(3)	Br(1B)-C(63)-Br(1A)	44.1(4)
C(9)-C(18)-C(19)	112.5(4)	F(6)-C(46)-C(45)	120.2(3)	C(65)-C(64)-C(63)	120
C(9)-C(18)-C(17)	111.3(4)	C(47)-C(46)-C(45)	123.9(4)	C(64)-C(65)-C(66)	120
C(19)-C(18)-C(17)	108.7(4)	F(7)-C(47)-C(48)	119.8(4)	C(67)-C(66)-C(65)	120
C(21)-C(20)-C(25)	121.4(3)	F(7)-C(47)-C(46)	119.8(4)	C(68)-C(67)-C(66)	120
C(21)-C(20)-N(2)	118.2(3)	C(48)-C(47)-C(46)	120.4(4)	C(67)-C(68)-C(63)	120
C(25)-C(20)-N(2)	120.4(3)				

Table A.66: Crystal Data and Structure Refinement for **14-C₉H₁₂****A. Crystal Data**

Crystallographer	Masood Parvez	University of Calgary
Empirical Formula	C ₆₉ H ₆₁ BBrF ₂₀ N ₂ Sc	
Formula Weight	1433.88	
Crystal size	0.18 x 0.08 x 0.06 mm ³	
Crystal System	Triclinic	
Space Group	P - 1	
Lattice Parameters	a = 13.744(4) Å	α = 82.391(12)°.
	b = 13.999(4) Å	β = 72.792(13)°.
	c = 17.774(6) Å	γ = 78.948(14)°.
Volume	3195.6(17) Å ³	

Z	2
Density (calculated)	1.490 Mg/m ³

B. Data Collection and Refinement Conditions

Diffractometer	Nonius Kappa CCD
Radiation (λ [Å])	Graphite-monochromated MoK α (0.71073)
Temperature	173(2) K
Reflections Collected	21619
Independent Reflections	11318 [R(int) = 0.082]
Structure Solution	Direct Methods
Refinement Method	Full-matrix least-squares on F ²
Data / Restraints / Parameters	11318 / 0 / 860
Goodness-of-Fit	1.01
Final R Indices [$I > 2\sigma(I)$]	R1 = 0.063, wR2 = 0.143
R Indices (all data)	R1 = 0.149, wR2 = 0.181
Largest Difference Peak & Hole	0.71 and -0.86 e.Å ⁻³

Table A.67: Atomic Coordinates and Equivalent Isotropic Displacement Parameters for **14-C₉H₁₂**

	x	y	z	U(eq)		x	y	z	U(eq)
Br(1)	4428(1)	1850(1)	5514(1)	102(1)	C(25)	7283(4)	6247(3)	2144(3)	36(1)
Sc(1)	5643(1)	4255(1)	2124(1)	33(1)	C(26)	6942(5)	7794(3)	1287(3)	57(2)
F(1)	-1331(2)	8548(2)	2916(2)	43(1)	C(27)	6492(4)	6910(3)	1790(3)	40(1)
F(2)	-2847(2)	9814(2)	3702(2)	48(1)	C(28)	5518(4)	7281(4)	2427(3)	52(1)
F(3)	-2472(2)	11126(2)	4544(2)	57(1)	C(29)	9540(5)	3460(4)	1437(3)	62(2)
F(4)	-496(2)	11196(2)	4509(2)	62(1)	C(30)	8695(4)	3570(3)	2213(3)	41(1)
F(5)	1067(2)	10014(2)	3635(2)	58(1)	C(31)	9064(5)	2940(4)	2879(3)	53(2)
F(6)	680(2)	10698(2)	2064(2)	50(1)	C(32)	3957(4)	4239(3)	3448(3)	41(1)
F(7)	1989(2)	11524(2)	873(2)	62(1)	C(33)	4512(4)	4896(4)	3604(3)	45(1)
F(8)	3895(3)	10537(2)	198(2)	67(1)	C(34)	5499(4)	4627(3)	3690(3)	42(1)
F(9)	4436(2)	8646(2)	735(2)	57(1)	C(35)	5964(4)	3661(4)	3572(3)	42(1)
F(10)	3089(2)	7753(2)	1867(2)	45(1)	C(36)	5457(4)	2974(3)	3416(3)	40(1)
F(11)	-69(2)	9186(2)	1516(2)	43(1)	C(37)	4449(4)	3290(4)	3356(3)	41(1)
F(12)	-480(2)	8138(2)	534(2)	53(1)	C(38)	2850(5)	4566(4)	3417(4)	63(2)
F(13)	170(2)	6173(2)	563(2)	57(1)	C(39)	5993(5)	5309(4)	3983(3)	56(2)
F(14)	1257(2)	5289(2)	1595(2)	53(1)	C(40)	5935(5)	1914(4)	3375(3)	56(2)
F(15)	1661(2)	6297(2)	2573(2)	49(1)	C(41)	-33(4)	9232(3)	3199(3)	36(1)
F(16)	19(2)	7108(2)	3821(2)	50(1)	C(42)	-1053(4)	9203(3)	3282(3)	35(1)
F(17)	619(3)	6040(3)	5009(2)	80(1)	C(43)	-1873(4)	9842(3)	3709(3)	36(1)
F(18)	2441(3)	6205(3)	5259(2)	95(1)	C(44)	-1692(4)	10513(3)	4119(3)	41(1)
F(19)	3601(3)	7498(3)	4325(2)	85(1)	C(45)	-690(4)	10544(3)	4101(3)	44(1)
F(20)	2985(2)	8638(2)	3181(2)	60(1)	C(46)	95(4)	9921(4)	3652(3)	43(1)
N(1)	6079(3)	3180(2)	1299(2)	32(1)	C(47)	1826(4)	9167(3)	2047(3)	37(1)
N(2)	7053(3)	4764(2)	1622(2)	32(1)	C(48)	1604(4)	10135(4)	1760(3)	43(1)
C(1)	4587(4)	5388(3)	1629(3)	35(1)	C(49)	2281(5)	10587(4)	1142(3)	48(1)
C(3)	6617(4)	2943(3)	-141(3)	41(1)	C(50)	3234(4)	10092(4)	791(3)	50(1)
C(4)	6554(4)	3481(3)	554(3)	35(1)	C(51)	3501(4)	9142(4)	1063(3)	43(1)

C(5)	7050(4)	4305(3)	358(3)	35(1)	C(52)	2794(4)	8717(3)	1655(3)	39(1)
C(6)	7365(4)	4845(3)	828(3)	33(1)	C(53)	775(4)	7805(3)	2130(3)	33(1)
C(7)	8117(4)	5532(3)	384(3)	39(1)	C(54)	263(4)	8208(3)	1568(3)	36(1)
C(8)	5799(4)	2206(3)	1451(3)	35(1)	C(55)	55(4)	7683(4)	1049(3)	39(1)
C(9)	4755(4)	2111(3)	1667(3)	39(1)	C(56)	386(4)	6694(4)	1065(3)	42(1)
C(10)	4496(5)	1164(4)	1897(3)	51(2)	C(57)	913(4)	6258(3)	1583(3)	37(1)
C(11)	5257(5)	359(4)	1887(4)	55(2)	C(58)	1099(4)	6815(3)	2094(3)	36(1)
C(12)	6282(5)	470(3)	1633(3)	51(2)	C(59)	1485(4)	7902(3)	3417(3)	41(1)
C(13)	6587(4)	1380(3)	1408(3)	38(1)	C(60)	922(4)	7243(4)	3930(3)	44(1)
C(14)	8270(4)	1131(4)	1772(3)	52(1)	C(61)	1199(5)	6681(4)	4545(4)	56(2)
C(15)	7733(4)	1425(3)	1117(3)	43(1)	C(62)	2108(6)	6767(5)	4679(4)	66(2)
C(16)	8281(4)	777(4)	422(3)	53(1)	C(63)	2688(5)	7409(5)	4212(4)	60(2)
C(17)	2822(4)	2800(4)	2098(4)	60(2)	C(64)	2367(4)	7984(4)	3594(3)	49(1)
C(18)	3902(4)	2971(3)	1612(3)	45(1)	C(65)	3462(6)	1747(5)	4979(4)	68(2)
C(19)	3917(5)	3271(4)	757(3)	59(2)	C(66)	2608(7)	2434(6)	5054(4)	90(2)
C(20)	7575(4)	5236(3)	2043(3)	33(1)	C(67)	1880(6)	2363(7)	4649(5)	97(2)
C(21)	8336(4)	4659(3)	2364(3)	37(1)	C(68)	2049(7)	1608(7)	4217(5)	90(2)
C(22)	8799(4)	5094(4)	2794(3)	44(1)	C(69)	2892(8)	914(6)	4132(4)	89(2)
C(23)	8524(4)	6088(4)	2903(3)	43(1)	C(70)	3625(6)	974(5)	4526(4)	75(2)
C(24)	7786(4)	6646(4)	2581(3)	42(1)	B(1)	1013(5)	8525(4)	2707(4)	38(1)

Table A.68: Anisotropic Displacement Parameters for **14-C₉H₁₂**

Atom	U11	U22	U33	U23	U13	U12
Br(1)	116(1)	139(1)	71(1)	-19(1)	-21(1)	-68(1)
Sc(1)	39(1)	26(1)	35(1)	-2(1)	-14(1)	-2(1)
F(1)	42(2)	39(2)	50(2)	-12(1)	-14(1)	-7(1)
F(2)	34(2)	48(2)	58(2)	-7(1)	-10(2)	-2(1)
F(3)	47(2)	54(2)	62(2)	-25(2)	-7(2)	8(2)
F(4)	60(2)	62(2)	71(2)	-39(2)	-21(2)	1(2)
F(5)	41(2)	64(2)	77(2)	-36(2)	-22(2)	0(2)
F(6)	44(2)	35(2)	67(2)	-8(1)	-13(2)	2(1)
F(7)	66(2)	45(2)	75(2)	4(2)	-21(2)	-12(2)
F(8)	56(2)	69(2)	69(2)	2(2)	-4(2)	-23(2)
F(9)	38(2)	67(2)	64(2)	-20(2)	-4(2)	-8(2)
F(10)	38(2)	42(2)	53(2)	-16(1)	-11(1)	2(1)
F(11)	49(2)	32(2)	49(2)	-4(1)	-20(2)	2(1)
F(12)	56(2)	65(2)	46(2)	-9(2)	-28(2)	0(2)
F(13)	61(2)	62(2)	57(2)	-28(2)	-19(2)	-12(2)
F(14)	66(2)	30(2)	59(2)	-13(1)	-11(2)	-2(1)
F(15)	63(2)	39(2)	46(2)	-7(1)	-25(2)	10(1)
F(16)	55(2)	50(2)	46(2)	-1(1)	-18(2)	-7(2)
F(17)	100(3)	76(2)	51(2)	13(2)	-23(2)	8(2)
F(18)	107(3)	115(3)	58(2)	-10(2)	-50(2)	41(2)
F(19)	58(2)	128(3)	80(3)	-53(2)	-43(2)	26(2)
F(20)	42(2)	76(2)	71(2)	-34(2)	-24(2)	1(2)
N(1)	38(2)	23(2)	38(3)	-5(2)	-17(2)	0(2)
N(2)	40(2)	23(2)	32(2)	-3(2)	-14(2)	3(2)
C(1)	37(3)	26(2)	42(3)	-1(2)	-13(2)	-4(2)
C(3)	57(4)	32(3)	37(3)	-5(2)	-16(3)	-5(2)
C(4)	37(3)	31(3)	40(3)	-2(2)	-19(3)	2(2)

C(5)	47(3)	26(2)	32(3)	0(2)	-14(2)	-1(2)
C(6)	39(3)	23(2)	36(3)	-5(2)	-14(2)	5(2)
C(7)	52(3)	32(3)	33(3)	0(2)	-9(3)	-10(2)
C(8)	47(3)	29(3)	31(3)	-4(2)	-15(2)	-3(2)
C(9)	50(4)	31(3)	41(3)	0(2)	-20(3)	-8(2)
C(10)	59(4)	43(3)	62(4)	2(3)	-28(3)	-18(3)
C(11)	66(4)	31(3)	75(4)	1(3)	-27(3)	-14(3)
C(12)	65(4)	27(3)	67(4)	-3(3)	-30(3)	-1(3)
C(13)	45(3)	29(3)	43(3)	-3(2)	-21(3)	-2(2)
C(14)	53(4)	45(3)	60(4)	-5(3)	-24(3)	3(3)
C(15)	53(4)	25(3)	49(3)	1(2)	-21(3)	7(2)
C(16)	57(4)	46(3)	55(4)	-11(3)	-16(3)	2(3)
C(17)	49(4)	54(3)	82(5)	-12(3)	-28(3)	-3(3)
C(18)	43(3)	38(3)	62(4)	-5(3)	-26(3)	-6(2)
C(19)	60(4)	57(4)	65(4)	2(3)	-38(3)	3(3)
C(20)	35(3)	29(3)	36(3)	-6(2)	-10(2)	-4(2)
C(21)	35(3)	34(3)	40(3)	-4(2)	-8(2)	-3(2)
C(22)	41(3)	48(3)	47(3)	-3(3)	-19(3)	-4(3)
C(23)	44(3)	48(3)	43(3)	-9(2)	-15(3)	-12(3)
C(24)	47(3)	35(3)	42(3)	-9(2)	-4(3)	-11(3)
C(25)	40(3)	28(2)	39(3)	-4(2)	-8(2)	-5(2)
C(26)	75(4)	32(3)	63(4)	5(3)	-24(3)	-9(3)
C(27)	47(3)	29(3)	42(3)	-6(2)	-12(3)	-3(2)
C(28)	53(4)	42(3)	62(4)	-10(3)	-19(3)	-1(3)
C(29)	69(4)	47(3)	57(4)	-6(3)	-11(3)	9(3)
C(30)	50(3)	30(3)	41(3)	-3(2)	-15(3)	2(2)
C(31)	61(4)	43(3)	57(4)	-3(3)	-28(3)	3(3)
C(32)	39(3)	40(3)	38(3)	-4(2)	-7(3)	0(2)
C(33)	57(4)	36(3)	36(3)	-6(2)	-8(3)	1(3)
C(34)	55(4)	37(3)	35(3)	1(2)	-17(3)	-8(3)
C(35)	43(3)	51(3)	32(3)	4(2)	-14(3)	-5(3)
C(36)	47(3)	36(3)	33(3)	5(2)	-10(3)	-3(2)
C(37)	41(3)	43(3)	36(3)	2(2)	-13(3)	-3(2)
C(38)	53(4)	56(4)	73(4)	-9(3)	-15(3)	7(3)
C(39)	69(4)	60(4)	43(3)	-6(3)	-20(3)	-11(3)
C(40)	62(4)	39(3)	58(4)	4(3)	-13(3)	3(3)
C(41)	36(3)	35(3)	40(3)	-3(2)	-16(2)	-2(2)
C(42)	40(3)	30(3)	38(3)	-3(2)	-16(3)	-5(2)
C(43)	30(3)	37(3)	39(3)	1(2)	-8(2)	-4(2)
C(44)	41(3)	38(3)	39(3)	-9(2)	-8(3)	6(2)
C(45)	47(4)	41(3)	47(3)	-17(3)	-12(3)	-3(3)
C(46)	33(3)	49(3)	48(3)	-16(3)	-12(3)	0(3)
C(47)	36(3)	34(3)	41(3)	-11(2)	-15(3)	2(2)
C(48)	40(3)	43(3)	50(3)	-15(3)	-14(3)	-6(3)
C(49)	55(4)	36(3)	57(4)	-3(3)	-18(3)	-10(3)
C(50)	44(4)	59(4)	50(4)	-9(3)	-9(3)	-21(3)
C(51)	27(3)	50(3)	57(4)	-21(3)	-13(3)	-1(3)
C(52)	39(3)	38(3)	44(3)	-13(2)	-16(3)	-5(3)
C(53)	32(3)	32(3)	34(3)	-3(2)	-9(2)	-3(2)
C(54)	36(3)	32(3)	38(3)	-6(2)	-11(2)	1(2)

C(55)	29(3)	53(3)	33(3)	-8(2)	-10(2)	0(2)
C(56)	41(3)	47(3)	39(3)	-17(2)	-7(3)	-8(3)
C(57)	40(3)	30(3)	40(3)	-8(2)	-8(3)	0(2)
C(58)	34(3)	34(3)	38(3)	-4(2)	-11(2)	0(2)
C(59)	43(3)	42(3)	41(3)	-18(2)	-20(3)	8(2)
C(60)	48(4)	43(3)	40(3)	-12(3)	-19(3)	9(3)
C(61)	61(4)	56(4)	46(4)	-17(3)	-18(3)	12(3)
C(62)	78(5)	76(4)	40(4)	-18(3)	-31(4)	28(4)
C(63)	43(4)	88(5)	57(4)	-42(4)	-30(3)	23(3)
C(64)	43(4)	54(3)	51(4)	-25(3)	-20(3)	11(3)
C(65)	78(5)	71(4)	52(4)	-13(3)	1(4)	-33(4)
C(66)	103(7)	94(6)	57(5)	-9(4)	16(5)	-35(5)
C(67)	70(6)	109(7)	92(6)	10(5)	5(5)	-25(5)
C(68)	96(7)	102(6)	80(6)	0(5)	-12(5)	-59(6)
C(69)	136(8)	79(5)	65(5)	-6(4)	-25(5)	-56(6)
C(70)	102(6)	67(4)	61(4)	-4(3)	-14(4)	-41(4)
B(1)	36(4)	37(3)	46(4)	-11(3)	-19(3)	2(3)

Table A.69: Bond Lengths [\AA] for **14-C₉H₁₂**

Br(1)-C(65)	1.884(7)	C(4)-C(5)	1.404(6)	C(36)-C(40)	1.505(7)
Sc(1)-N(2)	2.097(4)	C(5)-C(6)	1.401(6)	C(41)-C(42)	1.373(6)
Sc(1)-N(1)	2.120(4)	C(6)-C(7)	1.520(6)	C(41)-C(46)	1.400(6)
Sc(1)-C(1)	2.212(4)	C(8)-C(9)	1.400(7)	C(41)-B(1)	1.659(7)
Sc(1)-C(37)	2.694(5)	C(8)-C(13)	1.417(6)	C(42)-C(43)	1.391(7)
Sc(1)-C(36)	2.701(5)	C(9)-C(10)	1.416(6)	C(43)-C(44)	1.361(6)
Sc(1)-C(35)	2.736(5)	C(9)-C(18)	1.526(7)	C(44)-C(45)	1.376(7)
Sc(1)-C(32)	2.773(5)	C(10)-C(11)	1.381(7)	C(45)-C(46)	1.369(7)
Sc(1)-C(33)	2.795(5)	C(11)-C(12)	1.378(8)	C(47)-C(52)	1.378(7)
Sc(1)-C(34)	2.843(5)	C(12)-C(13)	1.389(6)	C(47)-C(48)	1.393(7)
F(1)-C(42)	1.361(5)	C(13)-C(15)	1.517(7)	C(47)-B(1)	1.663(8)
F(2)-C(43)	1.350(5)	C(14)-C(15)	1.529(7)	C(48)-C(49)	1.382(7)
F(3)-C(44)	1.341(5)	C(15)-C(16)	1.549(7)	C(49)-C(50)	1.366(8)
F(4)-C(45)	1.347(5)	C(17)-C(18)	1.526(7)	C(50)-C(51)	1.373(7)
F(5)-C(46)	1.358(5)	C(18)-C(19)	1.517(7)	C(51)-C(52)	1.363(7)
F(6)-C(48)	1.360(6)	C(20)-C(21)	1.407(6)	C(53)-C(58)	1.376(6)
F(7)-C(49)	1.363(6)	C(20)-C(25)	1.415(6)	C(53)-C(54)	1.388(6)
F(8)-C(50)	1.342(6)	C(21)-C(22)	1.385(6)	C(53)-B(1)	1.666(7)
F(9)-C(51)	1.340(6)	C(21)-C(30)	1.543(6)	C(54)-C(55)	1.374(6)
F(10)-C(52)	1.369(5)	C(22)-C(23)	1.393(7)	C(55)-C(56)	1.371(7)
F(11)-C(54)	1.356(5)	C(23)-C(24)	1.375(7)	C(56)-C(57)	1.351(7)
F(12)-C(55)	1.360(5)	C(24)-C(25)	1.406(6)	C(57)-C(58)	1.379(6)
F(13)-C(56)	1.351(5)	C(25)-C(27)	1.516(7)	C(59)-C(64)	1.367(7)
F(14)-C(57)	1.349(5)	C(26)-C(27)	1.545(7)	C(59)-C(60)	1.383(7)
F(15)-C(58)	1.362(5)	C(27)-C(28)	1.528(7)	C(59)-B(1)	1.658(7)
F(16)-C(60)	1.362(6)	C(29)-C(30)	1.521(7)	C(60)-C(61)	1.364(7)
F(17)-C(61)	1.345(7)	C(30)-C(31)	1.532(7)	C(61)-C(62)	1.369(9)
F(18)-C(62)	1.348(7)	C(32)-C(37)	1.378(7)	C(62)-C(63)	1.348(9)
F(19)-C(63)	1.360(6)	C(32)-C(33)	1.401(7)	C(63)-C(64)	1.403(8)
F(20)-C(64)	1.360(6)	C(32)-C(38)	1.518(7)	C(65)-C(66)	1.353(10)

N(1)-C(4)	1.343(6)	C(33)-C(34)	1.385(7)	C(65)-C(70)	1.378(8)
N(1)-C(8)	1.456(5)	C(34)-C(35)	1.396(7)	C(66)-C(67)	1.417(11)
N(2)-C(6)	1.344(6)	C(34)-C(39)	1.495(7)	C(67)-C(68)	1.334(11)
N(2)-C(20)	1.462(5)	C(35)-C(36)	1.389(6)	C(68)-C(69)	1.347(11)
C(3)-C(4)	1.503(6)	C(36)-C(37)	1.403(7)	C(69)-C(70)	1.406(10)

Table A.70: Bond Angles [°] for 14-C₉H₁₂

N(2)-Sc(1)-N(1)	90.53(14)	C(9)-C(18)-C(17)	114.4(4)	C(48)-C(47)-B(1)	126.6(5)
N(2)-Sc(1)-C(1)	101.19(16)	C(21)-C(20)-C(25)	121.4(4)	F(6)-C(48)-C(49)	115.2(5)
N(1)-Sc(1)-C(1)	102.66(16)	C(21)-C(20)-N(2)	118.7(4)	F(6)-C(48)-C(47)	121.5(5)
N(2)-Sc(1)-C(37)	147.55(15)	C(25)-C(20)-N(2)	119.8(4)	C(49)-C(48)-C(47)	123.3(5)
N(1)-Sc(1)-C(37)	99.24(15)	C(22)-C(21)-C(20)	118.9(4)	F(7)-C(49)-C(50)	119.9(5)
C(1)-Sc(1)-C(37)	106.62(17)	C(22)-C(21)-C(30)	119.8(4)	F(7)-C(49)-C(48)	119.8(5)
N(2)-Sc(1)-C(36)	118.56(15)	C(20)-C(21)-C(30)	121.2(4)	C(50)-C(49)-C(48)	120.3(5)
N(1)-Sc(1)-C(36)	95.45(15)	C(21)-C(22)-C(23)	120.9(5)	F(8)-C(50)-C(49)	120.2(5)
C(1)-Sc(1)-C(36)	136.00(17)	C(24)-C(23)-C(22)	119.8(4)	F(8)-C(50)-C(51)	121.0(5)
C(37)-Sc(1)-C(36)	30.14(14)	C(23)-C(24)-C(25)	122.1(4)	C(49)-C(50)-C(51)	118.8(5)
N(2)-Sc(1)-C(35)	95.80(15)	C(24)-C(25)-C(20)	116.9(4)	F(9)-C(51)-C(52)	121.3(5)
N(1)-Sc(1)-C(35)	116.26(15)	C(24)-C(25)-C(27)	119.3(4)	F(9)-C(51)-C(50)	119.9(5)
C(1)-Sc(1)-C(35)	137.19(17)	C(20)-C(25)-C(27)	123.8(4)	C(52)-C(51)-C(50)	118.8(5)
C(37)-Sc(1)-C(35)	52.14(15)	C(25)-C(27)-C(28)	111.8(4)	C(51)-C(52)-F(10)	115.8(4)
C(36)-Sc(1)-C(35)	29.59(14)	C(25)-C(27)-C(26)	111.3(4)	C(51)-C(52)-C(47)	126.0(5)
N(2)-Sc(1)-C(32)	144.66(14)	C(28)-C(27)-C(26)	109.0(4)	F(10)-C(52)-C(47)	118.2(4)
N(1)-Sc(1)-C(32)	122.79(15)	C(29)-C(30)-C(31)	109.6(4)	C(58)-C(53)-C(54)	112.8(4)
C(1)-Sc(1)-C(32)	83.93(17)	C(29)-C(30)-C(21)	110.3(4)	C(58)-C(53)-B(1)	127.1(4)
C(37)-Sc(1)-C(32)	29.14(14)	C(31)-C(30)-C(21)	114.3(4)	C(54)-C(53)-B(1)	119.9(4)
C(36)-Sc(1)-C(32)	52.90(15)	C(37)-C(32)-C(33)	117.0(5)	F(11)-C(54)-C(55)	116.3(4)
C(35)-Sc(1)-C(32)	60.80(15)	C(37)-C(32)-C(38)	122.3(5)	F(11)-C(54)-C(53)	119.2(4)
N(2)-Sc(1)-C(33)	115.65(15)	C(33)-C(32)-C(38)	120.6(5)	C(55)-C(54)-C(53)	124.5(4)
N(1)-Sc(1)-C(33)	150.26(15)	C(37)-C(32)-Sc(1)	72.2(3)	F(12)-C(55)-C(56)	120.6(4)
C(1)-Sc(1)-C(33)	86.60(17)	C(33)-C(32)-Sc(1)	76.3(3)	F(12)-C(55)-C(54)	120.4(4)
C(37)-Sc(1)-C(33)	51.10(15)	C(38)-C(32)-Sc(1)	123.2(4)	C(56)-C(55)-C(54)	119.1(4)
C(36)-Sc(1)-C(33)	60.52(15)	C(34)-C(33)-C(32)	123.3(5)	C(57)-C(56)-F(13)	121.3(4)
C(35)-Sc(1)-C(33)	50.72(16)	C(34)-C(33)-Sc(1)	77.7(3)	C(57)-C(56)-C(55)	119.5(4)
C(32)-Sc(1)-C(33)	29.14(14)	C(32)-C(33)-Sc(1)	74.6(3)	F(13)-C(56)-C(55)	119.2(5)
N(2)-Sc(1)-C(34)	94.59(15)	C(33)-C(34)-C(35)	116.9(4)	F(14)-C(57)-C(56)	120.1(4)
N(1)-Sc(1)-C(34)	145.12(14)	C(33)-C(34)-C(39)	121.3(5)	F(14)-C(57)-C(58)	120.6(4)
C(1)-Sc(1)-C(34)	110.07(17)	C(35)-C(34)-C(39)	121.5(5)	C(56)-C(57)-C(58)	119.3(4)
C(37)-Sc(1)-C(34)	60.41(14)	C(33)-C(34)-Sc(1)	73.9(3)	F(15)-C(58)-C(53)	121.4(4)
C(36)-Sc(1)-C(34)	52.19(14)	C(35)-C(34)-Sc(1)	71.3(3)	F(15)-C(58)-C(57)	113.8(4)
C(35)-Sc(1)-C(34)	28.90(14)	C(39)-C(34)-Sc(1)	130.6(3)	C(53)-C(58)-C(57)	124.8(4)
C(32)-Sc(1)-C(34)	51.76(15)	C(36)-C(35)-C(34)	122.6(5)	C(64)-C(59)-C(60)	113.6(5)
C(33)-Sc(1)-C(34)	28.42(15)	C(36)-C(35)-Sc(1)	73.8(3)	C(64)-C(59)-B(1)	127.8(5)
C(4)-N(1)-C(8)	118.4(4)	C(34)-C(35)-Sc(1)	79.8(3)	C(60)-C(59)-B(1)	118.5(4)
C(4)-N(1)-Sc(1)	115.4(3)	C(35)-C(36)-C(37)	117.5(5)	F(16)-C(60)-C(61)	115.2(5)
C(8)-N(1)-Sc(1)	125.8(3)	C(35)-C(36)-C(40)	121.5(5)	F(16)-C(60)-C(59)	119.1(4)
C(6)-N(2)-C(20)	117.9(4)	C(37)-C(36)-C(40)	120.9(4)	C(61)-C(60)-C(59)	125.7(5)
C(6)-N(2)-Sc(1)	115.2(3)	C(35)-C(36)-Sc(1)	76.6(3)	F(17)-C(61)-C(60)	122.2(5)
C(20)-N(2)-Sc(1)	125.3(3)	C(37)-C(36)-Sc(1)	74.6(3)	F(17)-C(61)-C(62)	119.5(6)

N(1)-C(4)-C(5)	123.3(4)	C(40)-C(36)-Sc(1)	122.6(3)	C(60)-C(61)-C(62)	118.3(6)
N(1)-C(4)-C(3)	122.3(4)	C(32)-C(37)-C(36)	122.6(5)	C(63)-C(62)-F(18)	119.6(6)
C(5)-C(4)-C(3)	114.4(4)	C(32)-C(37)-Sc(1)	78.6(3)	C(63)-C(62)-C(61)	119.4(6)
C(6)-C(5)-C(4)	130.9(4)	C(36)-C(37)-Sc(1)	75.2(3)	F(18)-C(62)-C(61)	121.0(7)
N(2)-C(6)-C(5)	123.5(4)	C(42)-C(41)-C(46)	112.6(4)	C(62)-C(63)-F(19)	120.5(6)
N(2)-C(6)-C(7)	120.8(4)	C(42)-C(41)-B(1)	129.2(4)	C(62)-C(63)-C(64)	120.5(5)
C(5)-C(6)-C(7)	115.7(4)	C(46)-C(41)-B(1)	118.1(4)	F(19)-C(63)-C(64)	118.9(7)
C(9)-C(8)-C(13)	121.6(4)	F(1)-C(42)-C(41)	121.1(4)	F(20)-C(64)-C(59)	121.8(5)
C(9)-C(8)-N(1)	119.0(4)	F(1)-C(42)-C(43)	114.6(4)	F(20)-C(64)-C(63)	115.8(5)
C(13)-C(8)-N(1)	119.3(4)	C(41)-C(42)-C(43)	124.3(4)	C(59)-C(64)-C(63)	122.4(6)
C(8)-C(9)-C(10)	118.0(5)	F(2)-C(43)-C(44)	119.9(4)	C(66)-C(65)-C(70)	121.0(7)
C(8)-C(9)-C(18)	122.7(4)	F(2)-C(43)-C(42)	120.1(4)	C(66)-C(65)-Br(1)	119.0(6)
C(10)-C(9)-C(18)	119.2(5)	C(44)-C(43)-C(42)	119.9(4)	C(70)-C(65)-Br(1)	120.0(6)
C(11)-C(10)-C(9)	120.6(5)	F(3)-C(44)-C(43)	120.9(5)	C(65)-C(66)-C(67)	119.3(7)
C(12)-C(11)-C(10)	120.1(5)	F(3)-C(44)-C(45)	120.2(4)	C(68)-C(67)-C(66)	118.8(9)
C(11)-C(12)-C(13)	122.1(5)	C(43)-C(44)-C(45)	118.9(5)	C(67)-C(68)-C(69)	123.1(8)
C(12)-C(13)-C(8)	117.4(5)	F(4)-C(45)-C(46)	121.2(5)	C(68)-C(69)-C(70)	118.9(7)
C(12)-C(13)-C(15)	118.3(4)	F(4)-C(45)-C(44)	119.7(5)	C(65)-C(70)-C(69)	118.9(7)
C(8)-C(13)-C(15)	124.3(4)	C(46)-C(45)-C(44)	119.1(4)	C(59)-B(1)-C(41)	103.3(4)
C(13)-C(15)-C(14)	112.5(4)	F(5)-C(46)-C(45)	116.1(4)	C(59)-B(1)-C(47)	114.4(4)
C(13)-C(15)-C(16)	111.6(4)	F(5)-C(46)-C(41)	118.7(4)	C(41)-B(1)-C(47)	112.1(4)
C(14)-C(15)-C(16)	109.2(4)	C(45)-C(46)-C(41)	125.1(5)	C(59)-B(1)-C(53)	112.8(4)
C(19)-C(18)-C(9)	110.7(4)	C(52)-C(47)-C(48)	112.8(5)	C(41)-B(1)-C(53)	113.6(4)
C(19)-C(18)-C(17)	110.1(4)	C(52)-C(47)-B(1)	120.2(4)	C(47)-B(1)-C(53)	101.1(4)

Table A.71: Crystal Data and Structure Refinement for **18-I(THF)****A. Crystal Data**

Crystallographer	Masood Parvez	University of Calgary
Empirical Formula	$C_{33}H_{49}I_2N_2OY \cdot 0.5 C_7H_8$	
Formula Weight	878.52	
Crystal size	0.16 x 0.14 x 0.14 mm ³	
Crystal System	monoclinic	
Space Group	P2 ₁ /c	
Lattice Parameters	a = 14.995(2) Å b = 12.339(2) Å β = 102.309(5)° c = 21.238(2) Å	
Volume	3839.2(9) Å ³	
Z	4	
Density (calculated)	1.520 Mg/m ³	

B. Data Collection and Refinement Conditions

Diffractometer	Nonius Kappa CCD
Radiation (λ[Å])	Graphite-monochromated MoKα (0.71073)
Temperature	173(2) K
Reflections Collected	32944

Independent Reflections	8820 [R(int) = 0.042]
Structure Solution	Direct Methods
Refinement Method	Full-matrix least-squares on F ²
Data / Restraints / Parameters	8820 / 14 / 422
Goodness-of-Fit	1.03
Final R Indices [I>2σ(I)]	R1 = 0.030, wR2 = 0.064
R Indices (all data)	R1 = 0.048, wR2 = 0.070
Largest Difference Peak & Hole	0.57 and -0.68 e.Å ⁻³

Table A.72: Atomic Coordinates and Equivalent Isotropic Displacement Parameters for **18-I(THF)**

	x	y	z	U(eq)		x	y	z	U(eq)
I(1)	2676(1)	5978(1)	5160(1)	37(1)	C(23)	3367(3)	8964(3)	2346(2)	65(1)
I(2)	1110(3)	6411(4)	2628(2)	50(1)	C(24)	3386(3)	9055(3)	2992(2)	55(1)
I(2')	1074(5)	6589(13)	2720(7)	66(2)	C(25)	3485(2)	8140(2)	3390(2)	38(1)
Y(1)	2291(1)	5447(1)	3783(1)	24(1)	C(26)	4201(3)	9127(3)	4422(2)	64(1)
N(1)	3048(1)	3866(2)	3793(1)	24(1)	C(27)	3501(2)	8291(2)	4105(2)	43(1)
N(2)	3569(2)	6141(2)	3493(1)	26(1)	C(28)	2553(3)	8594(3)	4208(2)	66(1)
C(3)	4420(2)	2729(2)	4172(2)	39(1)	C(29)	4556(3)	5606(4)	2124(2)	83(1)
C(4)	3955(2)	3810(2)	3998(1)	26(1)	C(30)	3588(2)	5926(3)	2132(2)	48(1)
C(5)	4532(2)	4713(2)	4058(1)	30(1)	C(31)	3000(4)	5854(4)	1458(2)	91(2)
C(6)	4385(2)	5756(2)	3790(1)	29(1)	O(1)	867(1)	4680(2)	3852(1)	31(1)
C(7)	5229(2)	6456(3)	3846(2)	41(1)	C(32)	248(2)	5351(2)	4122(2)	47(1)
C(8)	2515(2)	2878(2)	3669(1)	25(1)	C(33)	-698(3)	4991(9)	3818(8)	55(5)
C(9)	2250(2)	2302(2)	4172(1)	27(1)	C(34)	-582(4)	3834(7)	3642(7)	54(3)
C(10)	1678(2)	1406(2)	4013(1)	34(1)	C(35)	365(4)	3805(7)	3502(6)	32(3)
C(11)	1382(2)	1083(2)	3383(2)	40(1)	C(33')	-680(4)	4845(13)	3938(9)	58(5)
C(12)	1643(2)	1648(2)	2896(1)	39(1)	C(34')	-632(3)	4261(7)	3291(4)	43(2)
C(13)	2207(2)	2556(2)	3021(1)	29(1)	C(35')	288(6)	3949(8)	3348(6)	27(3)
C(14)	1713(3)	3246(4)	1875(2)	63(1)	C(1S)	44(7)	4537(9)	444(5)	69(2)
C(15)	2480(2)	3165(3)	2469(1)	39(1)	C(2S)	488(7)	5511(10)	595(6)	75(3)
C(16)	3323(3)	2691(4)	2305(2)	79(1)	C(3S)	332(6)	5680(8)	175(5)	67(2)
C(17)	1739(2)	2972(3)	5158(2)	45(1)	C(4S)	629(13)	6436(17)	-27(10)	63(5)
C(18)	2547(2)	2603(2)	4879(1)	32(1)	C(1S')	-233(6)	3946(7)	559(4)	63(2)
C(19)	3019(2)	1644(3)	5279(2)	45(1)	C(2S')	248(6)	4963(8)	668(4)	47(2)
C(20)	3543(2)	7122(2)	3109(1)	31(1)	C(3S')	660(11)	6301(15)	247(8)	104(5)
C(21)	3529(2)	7019(3)	2447(1)	41(1)	C(4S')	803(11)	6854(15)	372(8)	56(4)
C(22)	3447(3)	7962(3)	2075(2)	56(1)					

Table A.73: Anisotropic Displacement Parameters for **18-I(THF)**

Atom	U11	U22	U33	U23	U13	U12
I(1)	39(1)	43(1)	29(1)	-8(1)	7(1)	-3(1)
I(2)	34(1)	66(1)	43(1)	24(1)	-6(1)	-1(1)
I(2')	33(1)	76(3)	78(3)	47(2)	-9(2)	-2(1)
Y(1)	22(1)	26(1)	25(1)	1(1)	4(1)	2(1)
N(1)	24(1)	24(1)	22(1)	1(1)	4(1)	2(1)
N(2)	25(1)	27(1)	27(1)	1(1)	3(1)	-1(1)

C(3)	31(2)	34(2)	49(2)	7(1)	5(1)	8(1)
C(4)	27(1)	31(1)	22(1)	4(1)	4(1)	5(1)
C(5)	23(1)	37(2)	28(1)	3(1)	1(1)	1(1)
C(6)	26(1)	33(2)	28(1)	-4(1)	6(1)	-4(1)
C(7)	27(2)	44(2)	52(2)	5(2)	5(1)	-7(1)
C(8)	26(1)	22(1)	26(1)	-2(1)	2(1)	6(1)
C(9)	29(1)	24(1)	29(1)	0(1)	4(1)	1(1)
C(10)	33(2)	29(2)	38(2)	4(1)	4(1)	-2(1)
C(11)	43(2)	28(2)	44(2)	-4(1)	-3(1)	-7(1)
C(12)	44(2)	36(2)	32(2)	-9(1)	-5(1)	3(1)
C(13)	34(2)	28(1)	24(1)	-4(1)	3(1)	6(1)
C(14)	69(3)	87(3)	32(2)	12(2)	6(2)	12(2)
C(15)	55(2)	39(2)	24(1)	-3(1)	7(1)	2(2)
C(16)	64(3)	119(4)	62(3)	31(3)	34(2)	27(3)
C(17)	55(2)	48(2)	37(2)	2(2)	21(2)	1(2)
C(18)	39(2)	30(2)	26(1)	1(1)	7(1)	-6(1)
C(19)	55(2)	41(2)	33(2)	7(1)	-1(1)	-2(2)
C(20)	23(1)	34(2)	34(2)	9(1)	1(1)	-5(1)
C(21)	38(2)	48(2)	35(2)	8(1)	4(1)	-10(1)
C(22)	64(2)	65(2)	36(2)	16(2)	2(2)	-18(2)
C(23)	72(3)	52(2)	65(3)	28(2)	-1(2)	-9(2)
C(24)	60(2)	34(2)	65(2)	12(2)	3(2)	-3(2)
C(25)	37(2)	29(2)	46(2)	9(1)	4(1)	-3(1)
C(26)	89(3)	38(2)	60(2)	-8(2)	4(2)	-8(2)
C(27)	53(2)	27(2)	51(2)	0(1)	13(2)	3(1)
C(28)	75(3)	49(2)	80(3)	6(2)	28(2)	17(2)
C(29)	73(3)	86(3)	92(4)	-23(3)	24(3)	-2(3)
C(30)	54(2)	56(2)	33(2)	2(2)	12(2)	-15(2)
C(31)	109(4)	105(4)	48(2)	-21(2)	-8(2)	-6(3)
O(1)	27(1)	33(1)	35(1)	-4(1)	9(1)	-2(1)
C(32)	39(2)	52(2)	55(2)	-14(2)	23(2)	-4(2)
C(33)	30(7)	95(11)	43(7)	-6(6)	12(4)	18(6)
C(34)	24(4)	44(5)	93(9)	-6(5)	12(4)	1(3)
C(35)	31(5)	30(5)	26(7)	5(4)	-11(3)	3(3)
C(33')	39(7)	82(8)	55(8)	-24(6)	14(4)	-10(6)
C(34')	26(3)	36(4)	60(5)	-2(3)	-5(3)	7(3)
C(35')	33(4)	27(4)	20(5)	0(4)	0(3)	2(3)

Table A.74: Bond Lengths [\AA] for **18-I(THF)**

I(1)-Y(1)	2.9322(4)	C(12)-C(13)	1.394(4)	O(1)-C(35')	1.522(8)
I(2)-Y(1)	2.952(5)	C(13)-C(15)	1.521(4)	C(32)-C(33)	1.496(5)
I(2')-Y(1)	2.943(7)	C(14)-C(15)	1.519(4)	C(32)-C(33')	1.499(7)
Y(1)-N(1)	2.255(2)	C(15)-C(16)	1.499(5)	C(33)-C(34)	1.495(5)
Y(1)-N(2)	2.300(2)	C(17)-C(18)	1.527(4)	C(34)-C(35)	1.512(4)
Y(1)-O(1)	2.3685(17)	C(18)-C(19)	1.539(4)	C(33')-C(34')	1.568(14)
N(1)-C(4)	1.339(3)	C(20)-C(25)	1.401(4)	C(34')-C(35')	1.411(9)
N(1)-C(8)	1.451(3)	C(20)-C(21)	1.407(4)	C(1S)-C(3S)#1	1.341(12)
N(2)-C(6)	1.338(3)	C(21)-C(22)	1.398(4)	C(1S)-C(2S)	1.377(15)
N(2)-C(20)	1.455(3)	C(21)-C(30)	1.517(5)	C(1S)-C(3S)	1.614(14)
C(3)-C(4)	1.514(4)	C(22)-C(23)	1.379(6)	C(1S)-C(4S)#1	1.69(2)

C(4)-C(5)	1.399(4)	C(23)-C(24)	1.371(6)	C(2S)-C(3S)	0.897(12)
C(5)-C(6)	1.405(4)	C(24)-C(25)	1.399(4)	C(2S)-C(4S)	1.79(2)
C(6)-C(7)	1.515(4)	C(25)-C(27)	1.527(4)	C(3S)-C(4S)	1.16(2)
C(8)-C(9)	1.408(4)	C(26)-C(27)	1.523(5)	C(3S)-C(1S)#1	1.341(12)
C(8)-C(13)	1.414(3)	C(27)-C(28)	1.530(5)	C(4S)-C(1S)#1	1.69(2)
C(9)-C(10)	1.396(4)	C(29)-C(30)	1.507(6)	C(1S')-C(2S')	1.442(13)
C(9)-C(18)	1.519(4)	C(30)-C(31)	1.516(5)	C(1S')-C(3S')#1	1.722(19)
C(10)-C(11)	1.376(4)	O(1)-C(35)	1.430(4)	C(2S')-C(3S')	2.035(19)
C(11)-C(12)	1.373(4)	O(1)-C(32)	1.450(3)	C(3S')-C(1S')#1	1.722(19)

Table A.75: Bond Angles [°] for **18-I(THF)**

N(1)-Y(1)-N(2)	82.99(8)	C(10)-C(9)-C(8)	118.4(2)	C(29)-C(30)-C(31)	110.0(4)
N(1)-Y(1)-O(1)	96.45(7)	C(10)-C(9)-C(18)	117.9(2)	C(29)-C(30)-C(21)	112.6(3)
N(2)-Y(1)-O(1)	168.26(7)	C(8)-C(9)-C(18)	123.8(2)	C(31)-C(30)-C(21)	113.1(3)
N(1)-Y(1)-I(1)	101.12(5)	C(11)-C(10)-C(9)	121.2(3)	C(35)-O(1)-C(32)	109.0(2)
N(2)-Y(1)-I(1)	100.72(5)	C(12)-C(11)-C(10)	120.1(3)	C(35)-O(1)-C(35')	13.9(10)
O(1)-Y(1)-I(1)	90.91(4)	C(11)-C(12)-C(13)	121.6(3)	C(32)-O(1)-C(35')	107.4(3)
N(1)-Y(1)-I(2')	130.5(4)	C(12)-C(13)-C(8)	118.1(3)	C(35)-O(1)-Y(1)	130.6(3)
N(2)-Y(1)-I(2')	91.83(17)	C(12)-C(13)-C(15)	120.2(2)	C(32)-O(1)-Y(1)	117.21(14)
O(1)-Y(1)-I(2')	79.58(16)	C(8)-C(13)-C(15)	121.8(2)	C(35')-O(1)-Y(1)	125.5(4)
I(1)-Y(1)-I(2')	128.0(4)	C(16)-C(15)-C(14)	111.1(3)	O(1)-C(32)-C(33)	106.8(3)
N(1)-Y(1)-I(2)	124.57(10)	C(16)-C(15)-C(13)	111.4(3)	O(1)-C(32)-C(33')	107.2(3)
N(2)-Y(1)-I(2)	90.78(11)	C(14)-C(15)-C(13)	113.0(3)	C(33)-C(32)-C(33')	11.9(15)
O(1)-Y(1)-I(2)	79.84(11)	C(9)-C(18)-C(17)	111.6(2)	C(34)-C(33)-C(32)	103.9(4)
I(1)-Y(1)-I(2)	133.99(9)	C(9)-C(18)-C(19)	111.2(2)	C(33)-C(34)-C(35)	103.7(4)
I(2')-Y(1)-I(2)	6.0(4)	C(17)-C(18)-C(19)	109.0(2)	O(1)-C(35)-C(34)	107.0(3)
C(4)-N(1)-C(8)	119.9(2)	C(25)-C(20)-C(21)	121.1(3)	C(32)-C(33')-C(34')	101.9(7)
C(4)-N(1)-Y(1)	121.49(17)	C(25)-C(20)-N(2)	120.3(2)	C(35')-C(34')-C(33')	106.1(6)
C(8)-N(1)-Y(1)	117.93(15)	C(21)-C(20)-N(2)	118.5(3)	C(34')-C(35')-O(1)	107.5(5)
C(6)-N(2)-C(20)	118.2(2)	C(22)-C(21)-C(20)	118.1(3)	C(3S)#1-C(1S)-C(2S)	118.9(10)
C(6)-N(2)-Y(1)	118.15(17)	C(22)-C(21)-C(30)	119.8(3)	C(3S)-C(1S)-C(4S)#1	127.5(11)
C(20)-N(2)-Y(1)	122.35(16)	C(20)-C(21)-C(30)	122.1(3)	C(1S)-C(2S)-C(4S)	120.7(11)
N(1)-C(4)-C(5)	123.6(2)	C(23)-C(22)-C(21)	121.1(3)	C(2S)-C(3S)-C(4S)	121.1(18)
N(1)-C(4)-C(3)	120.6(2)	C(24)-C(23)-C(22)	120.3(3)	C(2S)-C(3S)-C(1S)#1	153.3(15)
C(5)-C(4)-C(3)	115.8(2)	C(23)-C(24)-C(25)	121.0(3)	C(2S)-C(3S)-C(3S)#1	100.2(13)
C(4)-C(5)-C(6)	130.7(2)	C(24)-C(25)-C(20)	118.4(3)	C(4S)-C(3S)-C(3S)#1	137.5(15)
N(2)-C(6)-C(5)	124.4(2)	C(24)-C(25)-C(27)	118.7(3)	C(2S')-C(1S')-(3S')#1	112.4(9)
N(2)-C(6)-C(7)	119.9(2)	C(20)-C(25)-C(27)	122.9(3)	C(1S')-C(2S')-C(3S')	145.5(8)
C(5)-C(6)-C(7)	115.7(2)	C(26)-C(27)-C(25)	112.7(3)	C(4S')-C(3S')-(1S')#1	122(2)
C(9)-C(8)-C(13)	120.7(2)	C(26)-C(27)-C(28)	110.2(3)	C(4S')-C(3S')-C(2S')	133(3)
C(9)-C(8)-N(1)	121.4(2)	C(25)-C(27)-C(28)	110.8(3)	C(1S')#1-C(3S')C(2S')	102.1(10)
C(13)-C(8)-N(1)	117.7(2)				

Table A.76: Crystal Data and Structure Refinement for **19-I****A. Crystal Data**

Crystallographer	Masood Parvez	University of Calgary
Empirical Formula	C ₄₂ H ₆₁ I ₂ N ₂ Y	
Formula Weight	936.64	

Crystal Size	0.20 x 0.18 x 0.08 mm ³
Crystal System	Monoclinic
Space Group	P2 ₁ /n
Lattice Parameters	a = 13.131(2) Å b = 20.410(4) Å β = 112.410(8)° c = 16.979(4) Å
Volume	4206.8(14) Å ³
Z	4
Density (calculated)	1.479 Mg/m ³

B. Data Collection and Refinement Conditions

Diffractometer	Nonius Kappa CCD
Radiation (λ[Å])	Graphite-monochromated MoKα (0.71073)
Temperature	173(2) K
Reflections Collected	18313
Independent Reflections	9616 [R(int) = 0.055]
Structure Solution	Direct Methods
Refinement Method	Full-matrix least-squares on F ²
Data / Restraints / Parameters	9616 / 0 / 417
Goodness-of-Fit	0.99
Final R Indices [I>2σ(I)]	R1 = 0.042, wR2 = 0.080
R Indices (all data)	R1 = 0.089, wR2 = 0.094
Largest Difference Peak & Hole	0.94 and -0.55 e.Å ⁻³

Table A.77: Atomic Coordinates and Equivalent Isotropic Displacement Parameters for **19-I**

	x	y	z	U(eq)		x	y	z	U(eq)
I(1)	4747(1)	-1101(1)	2917(1)	36(1)	C(25)	7144(4)	750(2)	2795(3)	35(1)
I(2)	3424(1)	207(1)	4686(1)	30(1)	C(26)	8433(4)	263(3)	4171(3)	52(1)
Y(1)	4796(1)	227(1)	3557(1)	22(1)	C(27)	7390(4)	155(2)	3370(3)	39(1)
N(1)	3231(3)	553(2)	2374(2)	23(1)	C(28)	7474(4)	-476(2)	2925(4)	51(1)
N(2)	5556(3)	1073(2)	3120(2)	21(1)	C(29)	6029(4)	3002(2)	2294(3)	44(1)
C(3)	2035(3)	1586(2)	2223(3)	27(1)	C(30)	5405(4)	2344(2)	2094(3)	33(1)
C(4)	3070(3)	1145(2)	2603(3)	24(1)	C(31)	4524(4)	2385(2)	1192(3)	45(1)
C(5)	3960(3)	1438(2)	3347(2)	22(1)	C(32)	1275(4)	1403(2)	1312(3)	41(1)
C(6)	5075(3)	1507(2)	3492(2)	23(1)	C(33)	1402(4)	1534(2)	2810(3)	39(1)
C(7)	5743(3)	1993(2)	4214(3)	28(1)	C(34)	2394(4)	2301(2)	2212(3)	42(1)
C(8)	2540(3)	183(2)	1628(3)	27(1)	C(35)	5703(4)	1718(2)	5046(3)	36(1)
C(9)	2795(4)	200(2)	897(3)	33(1)	C(36)	5247(4)	2685(2)	4086(3)	34(1)
C(10)	2181(4)	-190(2)	220(3)	47(1)	C(37)	6958(3)	2040(2)	4324(3)	40(1)
C(11)	1353(4)	-589(3)	247(3)	56(2)	C(38)	5441(10)	2384(6)	9133(7)	42(3)
C(12)	1123(4)	-613(2)	971(3)	46(1)	C(39)	6550(12)	2019(6)	9357(8)	42(3)
C(13)	1713(3)	-229(2)	1681(3)	31(1)	C(40)	7639(13)	2323(8)	9918(10)	56(4)
C(14)	1695(4)	-962(2)	2874(3)	44(1)	C(41)	7505(14)	2970(8)	10216(7)	42(3)
C(15)	1415(4)	-287(2)	2464(3)	36(1)	C(42)	6463(15)	3267(6)	9972(9)	42(3)

C(16)	189(4)	-140(2)	2249(4)	46(1)	C(43)	5381(15)	3073(8)	9437(10)	71(4)
C(17)	4748(4)	179(3)	1019(3)	53(2)	C(44)	4341(10)	2197(6)	8627(8)	67(3)
C(18)	3733(4)	605(2)	842(3)	39(1)	C(38')	5653(11)	2643(8)	9355(9)	56(4)
C(19)	3427(5)	945(3)	-26(3)	58(2)	C(39')	6115(10)	2142(5)	9261(6)	25(2)
C(20)	6320(3)	1220(2)	2733(3)	28(1)	C(40')	7279(17)	2177(8)	9694(11)	71(5)
C(21)	6204(4)	1773(2)	2200(3)	31(1)	C(41')	7847(13)	2708(10)	10219(9)	67(4)
C(22)	6870(4)	1820(2)	1733(3)	47(1)	C(42')	7050(15)	3174(7)	10172(8)	46(3)
C(23)	7659(5)	1356(3)	1786(4)	53(2)	C(43')	5995(18)	3113(9)	9738(12)	68(5)
C(24)	7798(4)	836(3)	2327(3)	48(1)	C(44')	4520(20)	2741(13)	8948(16)	180(10)

Table A.78: Anisotropic Displacement Parameters for 19-I

Atom	U11	U22	U33	U23	U13	U12
I(1)	43(1)	27(1)	39(1)	-6(1)	16(1)	1(1)
I(2)	28(1)	37(1)	25(1)	7(1)	11(1)	6(1)
Y(1)	24(1)	21(1)	21(1)	2(1)	9(1)	2(1)
N(1)	24(2)	23(2)	21(2)	0(2)	8(2)	0(2)
N(2)	21(2)	23(2)	24(2)	4(2)	14(2)	4(2)
C(3)	26(2)	24(2)	29(2)	5(2)	8(2)	7(2)
C(4)	26(2)	25(2)	26(2)	5(2)	15(2)	0(2)
C(5)	28(2)	23(2)	18(2)	1(2)	12(2)	3(2)
C(6)	28(2)	21(2)	21(2)	4(2)	9(2)	2(2)
C(7)	29(2)	24(2)	29(2)	-4(2)	9(2)	1(2)
C(8)	25(2)	24(2)	24(2)	-3(2)	-1(2)	3(2)
C(9)	39(3)	36(3)	21(2)	-5(2)	9(2)	5(2)
C(10)	57(3)	56(3)	28(3)	-12(2)	16(2)	1(3)
C(11)	52(4)	62(4)	43(3)	-28(3)	6(3)	-11(3)
C(12)	36(3)	38(3)	53(3)	-9(3)	5(3)	-12(2)
C(13)	27(2)	28(2)	34(2)	-4(2)	7(2)	0(2)
C(14)	36(3)	32(3)	63(4)	7(2)	19(3)	-5(2)
C(15)	27(2)	30(2)	51(3)	2(2)	17(2)	-2(2)
C(16)	28(3)	47(3)	65(4)	6(3)	19(3)	1(2)
C(17)	51(3)	73(4)	42(3)	-5(3)	25(3)	-3(3)
C(18)	45(3)	50(3)	25(2)	-4(2)	18(2)	-1(3)
C(19)	84(4)	60(4)	35(3)	6(3)	30(3)	1(3)
C(20)	27(2)	32(2)	26(2)	-1(2)	11(2)	1(2)
C(21)	32(3)	30(2)	34(3)	7(2)	16(2)	6(2)
C(22)	55(3)	45(3)	53(3)	20(3)	37(3)	13(3)
C(23)	65(4)	56(3)	61(4)	21(3)	50(3)	19(3)
C(24)	46(3)	53(3)	61(4)	23(3)	39(3)	25(3)
C(25)	34(3)	36(3)	41(3)	6(2)	22(2)	7(2)
C(26)	39(3)	59(3)	55(3)	23(3)	15(3)	15(3)
C(27)	36(3)	39(3)	52(3)	13(2)	27(2)	11(2)
C(28)	53(3)	42(3)	77(4)	17(3)	47(3)	11(3)
C(29)	46(3)	32(3)	61(3)	9(2)	30(3)	-2(2)
C(30)	33(3)	34(3)	34(3)	9(2)	14(2)	6(2)
C(31)	52(3)	44(3)	42(3)	13(2)	20(3)	12(3)
C(32)	34(3)	40(3)	37(3)	1(2)	0(2)	11(2)
C(33)	33(3)	44(3)	49(3)	3(2)	25(2)	11(2)
C(34)	42(3)	26(2)	51(3)	9(2)	9(2)	12(2)
C(35)	47(3)	31(2)	24(2)	-6(2)	8(2)	-1(2)

C(36)	47(3)	24(2)	34(3)	-5(2)	17(2)	-5(2)
C(37)	30(3)	39(3)	47(3)	-9(2)	8(2)	-4(2)

Table A.79: Bond Lengths [Å] for 19-I

I(1)-Y(1)	2.9119(7)	C(7)-C(37)	1.537(6)	C(25)-C(27)	1.514(6)
I(2)-Y(1)	3.0915(7)	C(7)-C(35)	1.539(6)	C(26)-C(27)	1.535(7)
I(2)-Y(1)#1	3.1363(7)	C(8)-C(13)	1.403(6)	C(27)-C(28)	1.518(7)
Y(1)-N(2)	2.256(3)	C(8)-C(9)	1.403(6)	C(29)-C(30)	1.541(6)
Y(1)-N(1)	2.356(3)	C(9)-C(10)	1.379(6)	C(30)-C(31)	1.529(6)
Y(1)-C(6)	2.645(4)	C(9)-C(18)	1.515(6)	C(38)-C(44)	1.422(16)
Y(1)-C(5)	2.673(4)	C(10)-C(11)	1.373(7)	C(38)-C(43)	1.511(19)
Y(1)-C(4)	2.909(4)	C(11)-C(12)	1.374(7)	C(38)-C(39)	1.549(16)
Y(1)-I(2)#1	3.1363(7)	C(12)-C(13)	1.399(6)	C(39)-C(40)	1.517(19)
N(1)-C(4)	1.310(5)	C(13)-C(15)	1.526(6)	C(40)-C(41)	1.45(2)
N(1)-C(8)	1.458(5)	C(14)-C(15)	1.524(6)	C(41)-C(42)	1.407(18)
N(2)-C(6)	1.373(5)	C(15)-C(16)	1.540(6)	C(42)-C(43)	1.42(2)
N(2)-C(20)	1.425(5)	C(17)-C(18)	1.523(7)	C(38')-C(43')	1.15(2)
C(3)-C(33)	1.525(6)	C(18)-C(19)	1.537(6)	C(38')-C(39')	1.230(18)
C(3)-C(32)	1.534(6)	C(20)-C(21)	1.418(6)	C(38')-C(44')	1.40(3)
C(3)-C(34)	1.535(6)	C(20)-C(25)	1.420(6)	C(39')-C(40')	1.42(2)
C(3)-C(4)	1.552(5)	C(21)-C(22)	1.389(6)	C(40')-C(41')	1.42(2)
C(4)-C(5)	1.481(5)	C(21)-C(30)	1.533(6)	C(41')-C(42')	1.39(2)
C(5)-C(6)	1.395(5)	C(22)-C(23)	1.380(7)	C(42')-C(43')	1.30(2)
C(6)-C(7)	1.562(5)	C(23)-C(24)	1.371(7)	C(43')-C(44')	2.04(3)
C(7)-C(36)	1.536(6)	C(24)-C(25)	1.386(6)		

Table A.80: Bond Angles [°] for 19-I

Y(1)-I(2)-Y(1)#1	101.21(2)	C(32)-C(3)-C(4)	114.0(4)	C(9)-C(18)-C(19)	112.6(4)
N(2)-Y(1)-N(1)	81.67(11)	C(34)-C(3)-C(4)	109.4(3)	C(17)-C(18)-C(19)	109.7(4)
N(2)-Y(1)-C(6)	31.28(12)	N(1)-C(4)-C(5)	117.5(4)	C(21)-C(20)-C(25)	118.6(4)
N(1)-Y(1)-C(6)	77.02(11)	N(1)-C(4)-C(3)	128.8(4)	C(21)-C(20)-N(2)	122.6(4)
N(2)-Y(1)-C(5)	57.25(12)	C(5)-C(4)-C(3)	113.6(3)	C(25)-C(20)-N(2)	118.3(4)
N(1)-Y(1)-C(5)	56.27(11)	N(1)-C(4)-Y(1)	52.6(2)	C(22)-C(21)-C(20)	118.8(4)
C(6)-Y(1)-C(5)	30.42(12)	C(5)-C(4)-Y(1)	65.9(2)	C(22)-C(21)-C(30)	115.6(4)
N(2)-Y(1)-C(4)	70.91(11)	C(3)-C(4)-Y(1)	168.0(3)	C(20)-C(21)-C(30)	125.6(4)
N(1)-Y(1)-C(4)	26.21(11)	C(6)-C(5)-C(4)	128.7(4)	C(23)-C(22)-C(21)	122.4(5)
C(6)-Y(1)-C(4)	55.41(12)	C(6)-C(5)-Y(1)	73.7(2)	C(24)-C(23)-C(22)	118.7(5)
C(5)-Y(1)-C(4)	30.39(11)	C(4)-C(5)-Y(1)	83.7(2)	C(23)-C(24)-C(25)	121.9(4)
N(2)-Y(1)-I(1)	122.62(8)	N(2)-C(6)-C(5)	119.4(4)	C(24)-C(25)-C(20)	119.6(4)
N(1)-Y(1)-I(1)	93.27(8)	N(2)-C(6)-C(7)	123.4(4)	C(24)-C(25)-C(27)	116.3(4)
C(6)-Y(1)-I(1)	152.52(9)	C(5)-C(6)-C(7)	116.1(4)	C(20)-C(25)-C(27)	124.1(4)
C(5)-Y(1)-I(1)	149.51(8)	N(2)-C(6)-Y(1)	58.56(19)	C(25)-C(27)-C(28)	113.5(4)
C(4)-Y(1)-I(1)	119.34(8)	C(5)-C(6)-Y(1)	75.9(2)	C(25)-C(27)-C(26)	110.8(4)
N(2)-Y(1)-I(2)	130.51(8)	C(7)-C(6)-Y(1)	129.8(3)	C(28)-C(27)-C(26)	110.7(4)
N(1)-Y(1)-I(2)	90.42(8)	C(36)-C(7)-C(37)	109.0(4)	C(31)-C(30)-C(21)	112.4(4)
C(6)-Y(1)-I(2)	99.31(9)	C(36)-C(7)-C(35)	107.6(4)	C(31)-C(30)-C(29)	108.1(4)
C(5)-Y(1)-I(2)	77.80(9)	C(37)-C(7)-C(35)	107.9(4)	C(21)-C(30)-C(29)	110.8(4)

C(4)-Y(1)-I(2)	80.76(8)	C(36)-C(7)-C(6)	113.1(3)	C(44)-C(38)-C(43)	106.4(11)
I(1)-Y(1)-I(2)	106.49(2)	C(37)-C(7)-C(6)	112.5(4)	C(44)-C(38)-C(39)	131.5(12)
N(2)-Y(1)-I(2)#1	105.42(8)	C(35)-C(7)-C(6)	106.4(3)	C(43)-C(38)-C(39)	122.1(12)
N(1)-Y(1)-I(2)#1	169.21(8)	C(13)-C(8)-C(9)	121.6(4)	C(40)-C(39)-C(38)	122.0(10)
C(6)-Y(1)-I(2)#1	104.69(8)	C(13)-C(8)-N(1)	119.7(4)	C(41)-C(40)-C(39)	112.4(12)
C(5)-Y(1)-I(2)#1	120.50(8)	C(9)-C(8)-N(1)	118.4(4)	C(42)-C(41)-C(40)	121.6(12)
C(4)-Y(1)-I(2)#1	148.35(8)	C(10)-C(9)-C(8)	117.5(4)	C(41)-C(42)-C(43)	133.7(12)
I(1)-Y(1)-I(2)#1	89.67(2)	C(10)-C(9)-C(18)	119.6(4)	C(42)-C(43)-C(38)	108.0(13)
I(2)-Y(1)-I(2)#1	78.79(2)	C(8)-C(9)-C(18)	122.9(4)	C(43')-C(38')-C(39')	131.4(17)
C(4)-N(1)-C(8)	128.3(3)	C(11)-C(10)-C(9)	122.2(5)	C(43')-C(38')-C(44')	105.9(19)
C(4)-N(1)-Y(1)	101.2(2)	C(12)-C(11)-C(10)	119.9(5)	C(39')-C(38')-C(44')	122.7(19)
C(8)-N(1)-Y(1)	130.2(2)	C(11)-C(12)-C(13)	120.9(5)	C(38')-C(39')-C(40')	112.2(12)
C(6)-N(2)-C(20)	127.2(3)	C(12)-C(13)-C(8)	117.9(4)	C(41')-C(40')-C(39')	124.5(14)
C(6)-N(2)-Y(1)	90.2(2)	C(12)-C(13)-C(15)	117.8(4)	C(42')-C(41')-C(40')	106.3(12)
C(20)-N(2)-Y(1)	142.2(3)	C(8)-C(13)-C(15)	124.3(4)	C(43')-C(42')-C(41')	125.5(13)
C(33)-C(3)-C(32)	109.6(4)	C(14)-C(15)-C(13)	111.7(4)	C(38')-C(43')-C(42')	120.0(17)
C(33)-C(3)-C(34)	108.7(4)	C(14)-C(15)-C(16)	109.5(4)	C(38')-C(43')-C(44')	41.3(12)
C(32)-C(3)-C(34)	107.7(4)	C(13)-C(15)-C(16)	111.8(4)	C(42')-C(43')-C(44')	161.2(17)
C(33)-C(3)-C(4)	107.3(3)	C(9)-C(18)-C(17)	110.3(4)	C(38')-C(44')-C(43')	32.9(10)

Appendix 2: Publications Arising from Thesis

Author's Contribution to Publications Contained in Appendix 2

The author's contribution to publication #1 is the basis of the majority of this publication. Several of the compounds were not synthesized by the author. In addition, the author did not perform the X-ray crystal data collection and analysis. The author was responsible for all material, except the X-ray crystal data collection and analysis, presented in publications #2 and #3.

Publications:

1. Hayes, P. G.; Piers, W. E.; Lee, L. W. M.; Knight, L. K.; Parvez, M.; Elsegood, M. R. J.; Clegg, W. "Synthesis, Characterization and Thermal Stability of a New Family of Organoscandium Complexes" *Organometallics* **2001**, 20, 2533-2544.
2. Hayes, P. G.; Piers, W. E.; McDonald, R. "Cationic Scandium Methyl Complexes Supported by a β -Diketiminato ("Nacnac") Ligand Framework" *J. Am. Chem. Soc.* **2002**, 124, 2132-2133.
3. Hayes, P.G.; Piers, W.E.; Parvez, M. "Cationic Organoscandium β -Diketiminato Chemistry: Arene Exchange in Solvent Separated Ion Pairs" *J. Am. Chem. Soc.* **2003**, 125, 5622-5623.

Dialkylscandium Complexes Supported by β -Diketiminato Ligands: Synthesis, Characterization, and Thermal Stability of a New Family of Organoscandium Complexes

Paul G. Hayes,[†] Warren E. Piers,^{*,†,1} Lawrence W. M. Lee,[†] Lisa K. Knight,[†] Masood Parvez,[†] Mark R. J. Elsegood,^{‡,2} and William Clegg[‡]

Departments of Chemistry, University of Calgary, 2500 University Drive NW, Calgary, Alberta T2N 1N4, Canada, and University of Newcastle, Newcastle upon Tyne NE1 7RU, U.K.

Received February 9, 2001

Several diorganoscandium complexes stabilized by the β -diketiminato ligands (Ar)NC(R)-CHC(R)N(Ar) (Ar = 2,6-*i*Pr-C₆H₃; R = CH₃ (ligand **a**), R = *t*Bu (ligand **b**)) have been synthesized. Reaction of the lithium salts of the ligands with ScCl₃·3THF leads to the complexes LScCl₂(THF)_{*m*}, which may be readily alkylated to form the dialkyl derivatives. Most are isolated as base-free, four-coordinate complexes. Several have been characterized via X-ray crystallography, and a detailed discussion of their structures is presented. Steric interactions between Ar and the Sc-alkyl groups force the scandium to adopt an out-of-plane bonding mode. In solution, this is manifested via a fluxional process which equilibrates the two diastereotopic alkyl groups and ligand groups as well. The barriers to this process roughly correlate with the steric bulk of the alkyl substituents. At elevated temperatures, the dialkyl derivatives LScR₂ undergo a metalation process whereby one of the alkyl groups is eliminated as RH, and a ligand *i*Pr group is metalated in the methyl position. These reactions are first order in scandium complex, and activation parameters of $\Delta H^\ddagger = 19.7(6)$ kcal mol⁻¹ and $\Delta S^\ddagger = -17(2)$ cal mol⁻¹ K⁻¹ were measured for the loss of Me₄Si from (Ligb)-Sc(CH₂SiMe₃)₂.

Introduction

Organoscandium chemistry has to date been dominated by complexes with a dianionic complement of ancillary ligands and one hydrocarbyl ligand.^{3,4} While much elegant chemistry of fundamental importance has been uncovered, the inherent limitations of only one reactive organyl group has been a roadblock toward further development of the organometallic chemistry of scandium in comparison to the group 4 elements, where dialkyl derivatives are plentiful.

The difficulty in synthesizing well-defined compounds of general formula LScR₂, where L is a monoanionic ancillary ligand, stems from the tendency of these types of compounds to undergo redistribution reactions, to

dimerize or oligomerize, or to retain molecules of donor ligand in the metal's coordination sphere. Indeed, this is also a long standing set of problems for organoyttrium and organolanthanide chemistry.⁵ The circumvention of these problems is mainly a question of ligand choice; desirable ligands offer enough steric bulk and electron donation to prevent the aforementioned chemical problems, but not so much as to shut down organometallic reactivity. Thus, while some examples of LScR₂ complexes exist in the literature,⁶ the ligand modifications necessary to achieve these targets have also resulted in rather uninteresting compounds from an organometallic reactivity point of view.

We recently turned to the β -diketiminato ligand framework as a promising template for developing the organometallic chemistry of the ScR₂ molecular fragment.⁷ This family of ligands, imine analogues of the ubiquitous "acac" grouping of ligands, has been known for some time,⁸ but their coordination chemistry has only recently begun to be developed. When the nitrogen substituents are sterically bulky, they are particularly suited to stabilizing organometallic compounds of Lewis

* To whom correspondence should be addressed. Phone: 403-220-5746. FAX: 403-289-9488. E-mail: wpiers@ucalgary.ca.

[†] University of Calgary.

[‡] University of Newcastle.

(1) Phone: 403-220-5746. Fax: 403-289-9488. E-mail: wpiers@ucalgary.ca. S. Robert Blair Professor of Chemistry 2000–2005.

(2) Present address: University of Loughborough, Department of Chemistry, Loughborough, Leicestershire LE1 3TU, U.K.

(3) Reviews: (a) Piers, W. E.; Shapiro, P. J.; Bunel, E. E.; Bercaw, J. E. *Synlett* **1990**, 74. (b) Meehan, P. R.; Aris, D. R.; Willey, G. R. *Coord. Chem. Rev.* **1999**, 181, 121. (c) Edelmann, F. T. In *Comprehensive Organometallic Chemistry II*; Abel, E. W., Stone, F. G. A., Wilkinson, G., Lappert, M. F., Eds.; Elsevier Science: New York, 1995; Vol. 4. (d) Cotton, S. A. *Polyhedron* **1999**, 18, 1691.

(4) Recent papers: (a) Herberich, G. E.; Englert, U.; Fischer, A.; Ni, J.; Schmitz, A. *Organometallics* **1999**, 18, 5496. (b) Abrams, M. B.; Yoder, J. C.; Loeber, C.; Day, M. E.; Bercaw, J. E. *Organometallics* **1999**, 18, 1389. (c) Yoder, J. C.; Day, M. W.; Bercaw, J. E. *Organometallics* **1998**, 17, 4946. (d) Fryzuk, M. D.; Geisbrecht, G. R.; Rettig, S. J. *Can. J. Chem.* **2000**, 78, 1003.

(5) Bambirra, S.; Brandsma, M. J. R.; Brussee, E. A. C.; Meetsma, A.; Hessen, B.; Teuben, J. H. *Organometallics* **2000**, 19, 3197 and references therein.

(6) (a) Blackwell, J.; Lehr, C.; Sun, Y.; Piers, W. E.; Pearce-Batchilder, S. D.; Zaworotko, M. J.; Young, V. G., Jr. *Can. J. Chem.* **1997**, 75, 702. (b) Fryzuk, M. D.; Giesbrecht, G. R.; Rettig, S. J. *Organometallics* **1996**, 15, 3329.

(7) Lee, L. W. M.; Piers, W. E.; Elsegood, M. R. J.; Clegg, W.; Parvez, M. *Organometallics* **1999**, 18, 2947.

(8) McGeachin, S. G. *Can. J. Chem.* **1968**, 46, 1903.

acidic metals in group 2,⁹ group 4,¹⁰ and group 13.¹¹ Herein we describe the synthesis of several β -diketiminato-supported bis(hydrocarbyl)scandium derivatives, where use of 2,6-*i*-PrC₆H₃ aryl groups on nitrogen offers adequate steric protection to the metal center. While a bis-Cp* scandocene derivative containing a β -diketiminato ligand has been reported,¹² the compounds reported here are the first of scandium supported by a β -diketiminato ancillary ligand.

Results and Discussion

Synthesis and General Properties. The β -diketiminato ligands employed in this study incorporate the bulky 2,6-diisopropylphenyl group as the substituent on nitrogen and differ only in the nature of the backbone substituent R. The "a" series of compounds utilizes methyl groups in these positions, while the "b" series exploits the bulkier *tert*-butyl group, which renders the aryl groups more sterically active about the metal center by pushing them forward and holding them more upright with respect to the N–C–C–N plane of the ligand.^{10b,13} The lithium salts of these ligands^{10b} may be used in conjunction with ScCl₃·3THF to attach the β -diketiminato framework to the scandium metal (Scheme 1). For the methyl-substituted ligand, dichloride **1a** retains one THF donor, while the more sterically demanding *t*Bu-adorned ligand precludes THF ligation and the "base-free" dichloride complex **1b** is obtained. This is consistent with the greater steric demands of the **b** ligand, as are the somewhat more forcing conditions required to institute this donor into the scandium coordination sphere.

Dichlorides **1** serve as starting materials for the preparation of a variety of base-free dialkylscandium derivatives. Reactions between the dichlorides and 2 equiv of R'Li or PhCH₂MgCl occur under mild conditions (room temperature, 0.5–2 h) to give the products in moderate to good yields. Only in one reaction involving

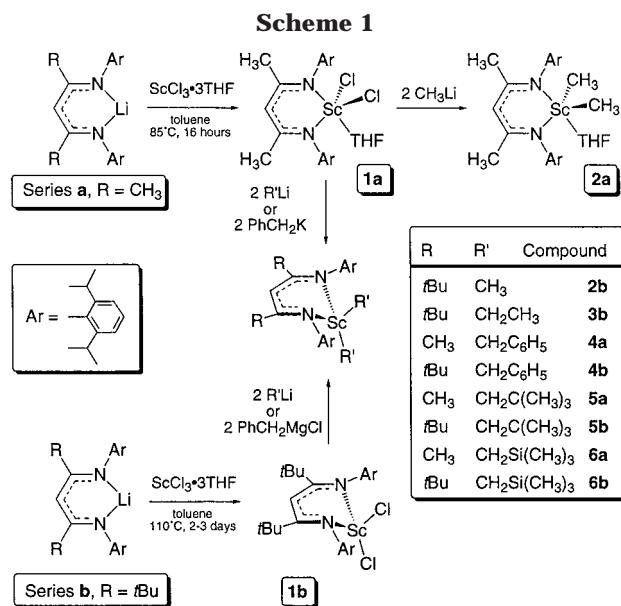


Table 1. UV–Vis Data for **1a**, **2a**, **4a**, **5a**, and **1b–6b**

compd	λ	ϵ	compd	λ	ϵ
1a	322	3800	1b	358	10 800
2a	318	20 600	2b	366	11 000
4a	348	4300	3b	366	20 800
5a	346	28 900	4b	366	11 300
6a	344	19 400	5b	367	22 100
			6b	370	22 200

the **a** series, that producing the dimethyl derivative **2a**, is the THF ligand in the starting dichloride retained. For the dibenzyl, dineopentyl, and bis((trimethylsilyl)methyl) examples, the alkyl group is large enough to preclude THF coordination; compounds **4a–6a** are isolated base-free as formally eight-electron complexes, assuming the diketiminato ligand donates four electrons to the scandium center (vide infra). In the *t*Bu-substituted **b** series, all of the dialkyl complexes remain base-free, even when exposed to THF, attesting again to the greater steric saturation about the metal center with this ligand. Notably, the diethyl derivative **3b** is also accessible and stable toward decomposition pathways involving β -elimination (vide infra).

The compounds are all white to pale yellow solids which exhibit intense LMCT absorptions in the UV–visible spectra taken in hexane (Table 1). Maximum absorptions for five-coordinate compounds **1a** and **2a** are at shorter wavelength than the four-coordinate species due to the different geometry and greater electronic saturation at the metal. λ_{\max} for the dialkyl members of the **a** series is about 10–15 nm lower (higher energy) than the values for the **b** series.

The mixed-alkyl derivative L_bSc(CH₃)CH₂SiMe₃ (**8b**) was prepared via the pathway shown in Scheme 2. A solution of **1b** and **2b** in a 1:1 ratio underwent almost complete comproportionation to give solutions which were comprised of about 85% of the mixed methyl–chloro derivative **7b** and residual starting materials. This appears to be an equilibrium ratio, as the addition of B(C₆F₅)₃ as a catalyst¹⁴ did not drive the reaction further toward the mixed species. Alkylation of the

(9) (a) Gibson, V. C.; Segal, J. A.; White, A. J. P.; Williams, D. J. *J. Am. Chem. Soc.* **2000**, *122*, 7120. (b) Bailey, P. J.; Dick, C. M. E.; Fabre, S.; Parsons, S. *J. Chem. Soc., Dalton Trans.* **2000**, 1655. (c) Caro, C. F.; Hitchcock, P. B.; Lappert, M. F. *Chem. Commun.* **1999**, 1433. (d) Chisholm, M. H.; Huffman, J. C.; Phomphrai, K. *J. Chem. Soc., Dalton Trans.* **2001**, 222.

(10) (a) Qian, B.; Scanlon, W. J.; Smith, M. R., III. *Organometallics* **1999**, *18*, 1693. (b) Budzelaar, P. H. M.; van Oort, A. B.; Orpen, A. G. *Eur. J. Inorg. Chem.* **1998**, 1485. (c) Kakaliou, L.; Scanlon, W. J.; Qian, B.; Back, S. W.; Smith, M. R., III; Motry, D. H. *Inorg. Chem.* **1999**, *38*, 5964. (d) Rahim, M.; Taylor, N. J.; Xin, S.; Collins, S. *Organometallics* **1998**, *17*, 1315. (e) Lappert, M. F.; Liu, D. S. *J. Organomet. Chem.* **1995**, *500*, 203. (f) Hitchcock, P. B.; Lappert, M. F.; Liu, D.-S. *J. Chem. Soc., Chem. Commun.* **1994**, 2637. (g) Kim, W.-K.; Fevola, M. J.; Liable-Sands, L. M.; Rheingold, A. L.; Theopold, K. H. *Organometallics* **1998**, *17*, 4541. (h) Vollmerhaus, R.; Rahim, M.; Tomaszewski, R.; Xin, S.; Taylor, N. J.; Collins, S. *Organometallics* **2000**, *19*, 2161.

(11) (a) Hardman, N. J.; Eichler, B. E.; Power, P. P. *Chem. Commun.* **2000**, 1991. (b) Cui, C.; Roesky, H. W.; Schmidt, H.-G.; Noltemeyer, M.; Hao, H.; Cimposesu, F. *Angew. Chem., Int. Ed.* **2000**, *39*, 4274. (c) Yalpani, M.; Köster, R.; Boese, R. *Chem. Ber.* **1992**, *125*, 15. (d) Radzewich, C. E.; Coles, M. P.; Jordan, R. F. *J. Am. Chem. Soc.* **1998**, *120*, 9384. (e) Cosledan, F.; Hitchcock, P. B.; Lappert, M. F. *Chem. Commun.* **1999**, 705. (f) Radzewich, C. E.; Guzei, I. A.; Jordan, R. F. *J. Am. Chem. Soc.* **2000**, *122*, 8673. (g) Qian, B.; Ward, D. L.; Smith, M. R., III. *Organometallics* **1998**, *17*, 3070. (h) Cui, C.; Roesky, H. W.; Hao, H.; Schmidt, H. G.; Noltemeyer, M. *Angew. Chem., Int. Ed.* **2000**, *39*, 1815. (i) Qian, B.; Baek, S. W.; Smith, M. R., III. *Polyhedron* **1999**, *18*, 2405.

(12) Bercaw, J. E.; Davies, D. L.; Wolczanski, P. T. *Organometallics* **1986**, *5*, 443.

(13) A similar phenomenon is observed and used in related amidinate ligands: Dagorne, S.; Guzei, I. A.; Coles, M. P.; Jordan, R. F. *J. Am. Chem. Soc.* **2000**, *122*, 274.

(14) Zhang, S.; Piers, W. E.; Gao, X.; Parvez, M. *J. Am. Chem. Soc.* **2000**, *122*, 5499.

Scheme 2

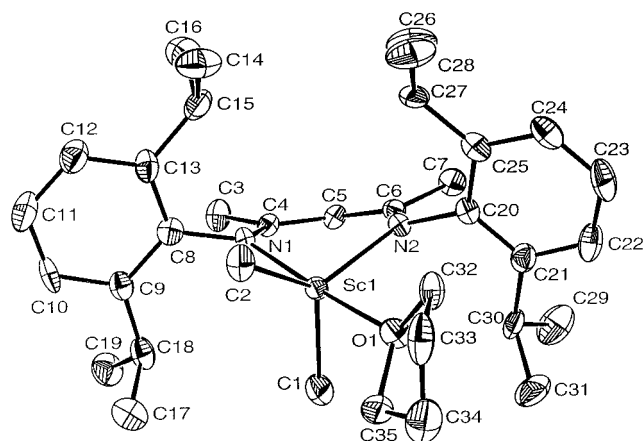
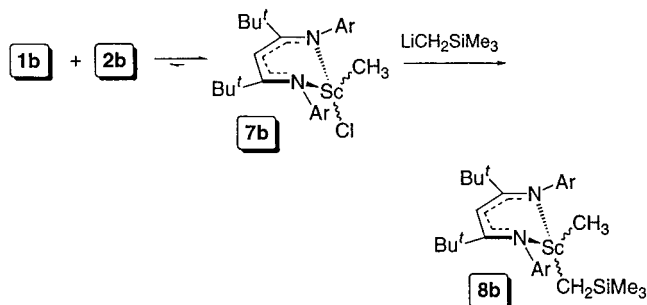


Figure 1. ORTEP diagram of the five-coordinate complex **2a** (30% ellipsoids).

mixture with $\text{LiCH}_2\text{SiMe}_3$ gave samples of **8b** contaminated with **2b** and **6b**. The mixed-alkyl species **8b** could be obtained about 95% pure via successive recrystallizations; discussion of the solution structure of this compound is presented below. Interestingly, **8b** cannot be prepared via redistribution between the two dialkyls **2b** and **6b**, even in the presence of catalytic $\text{B}(\text{C}_6\text{F}_5)_3$; evidently, a ligand capable of bridging the scandium centers is required for this process.

X-ray Crystal Structures. Several of the derivatives prepared as shown in Scheme 1 have been structurally characterized.

The structure of the five-coordinate dichloride **1a** was reported in a preliminary account;⁷ the structural features of the dimethyl congener are comparable, and an ORTEP diagram of **2a** is shown in Figure 1. Table 2 gives selected metrical data for both of these compounds for comparison; full details for **2a** and all of the other compounds reported herein can be found in the Supporting Information. The scandium center in **2a** has a distorted-trigonal-bipyramidal geometry, with N(1) and O(1) occupying the apical sites ($\text{N}(1)\text{--Sc}(1)\text{--O}(1) = 175.5(3)^\circ$). Perusal of the Sc(1) to ligand atom distances (bonding distances to N(1) and N(2) and nonbonding distances to the three carbon atoms) suggests that the ligand is essentially symmetrically bound to the scandium center; additionally, the five ligand atoms are virtually coplanar, with the highest deviation from the plane defined by these atoms being 0.064(8) Å for C(6). The scandium atom sits 0.815 Å out of this plane (cf. 0.694 Å for **1a**), somewhat less than the values for this parameter observed for the four-coordinate complexes discussed below. The torsion angles included in Table 2 are an indication as to how "upright" the aryl moieties

Table 2. Selected Metrical Parameters for Five-Coordinate Structures **1a** and **2a**

param ^a	1a	2a
Bond Distances (Å)		
Sc–N(1)	2.175(4)	2.201(6)
Sc–N(2)	2.107(4)	2.190(7)
Sc–O(1)	2.203(4)	2.228(5)
Sc–E(1)	2.3556(17)	2.210(9)
Sc–E(2)	2.3795(18)	2.245(9)
Sc–C(4)	3.066(5)	3.116(9)
Sc–C(5)	3.327(6)	3.383(9)
Sc–C(6)	3.062(6)	3.098(9)
N(1)–C(4)	1.312(7)	1.337(9)
C(4)–C(5)	1.399(8)	1.385(10)
C(5)–C(6)	1.387(7)	1.414(10)
C(6)–N(2)	1.363(6)	1.311(9)
Bond Angles (deg)		
E(1)–Sc–E(2)	131.47(8)	123.8(4)
N(1)–Sc–E(1)	94.85(13)	96.4(3)
N(1)–Sc–E(2)	92.33(12)	93.1(3)
N(2)–Sc–E(1)	104.53(13)	105.9(3)
N(2)–Sc–E(2)	123.79(13)	130.1(3)
N(1)–Sc–N(2)	86.77(17)	85.2(3)
N(1)–Sc–O(1)	175.31(16)	175.5(3)
N(2)–Sc–O(1)	95.82(16)	93.7(2)
Sc–N(1)–C(4)	121.1(4)	121.5(6)
N(1)–C(4)–C(3)	120.2(5)	119.6(8)
N(1)–C(4)–C(5)	123.5(5)	124.0(8)
C(3)–C(4)–C(5)	116.3(5)	116.4(8)
C(4)–C(5)–C(6)	130.4(5)	129.3(8)
C(5)–C(6)–C(7)	116.3(5)	113.3(8)
C(5)–C(6)–N(2)	122.9(5)	124.7(8)
C(7)–C(6)–N(2)	120.7(5)	122.0(8)
C(6)–N(2)–Sc	122.4(3)	122.6(6)
Torsion Angles (deg)		
C(6)–N(2)–C(20)–C(25)	82.2(6)	99.0(9)
C(6)–N(2)–C(20)–C(21)	–100.9(6)	–81.0(11)
C(4)–N(1)–C(8)–C(9)	90.0(6)	94.1(11)
C(4)–N(1)–C(8)–C(13)	–92.6(7)	–89.1(10)

^a E = Cl for **1a** and C for **2a**.

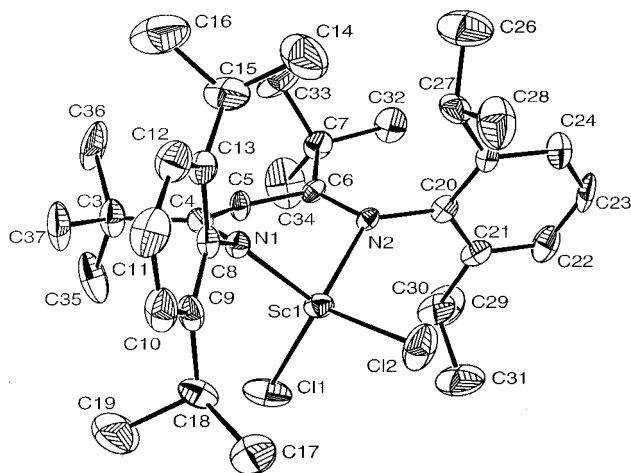


Figure 2. ORTEP diagram of the four-coordinate complex **1b** (30% ellipsoids).

are with respect to the NCCCN ligand plane. The values are close to $90(\pm 10)^\circ$, indicating that the rings are essentially perpendicular to the ligand plane.

The molecular structures of the THF-free, four-coordinate derivatives **1b–4b** and **6a,b** have also been determined; ORTEP diagrams of these compounds showing the structures from various perspectives are given in Figures 2–7, and Table 3 lists selected metrical parameters for these complexes. The scandium centers adopt distorted-tetrahedral geometries where the N–Sc–N

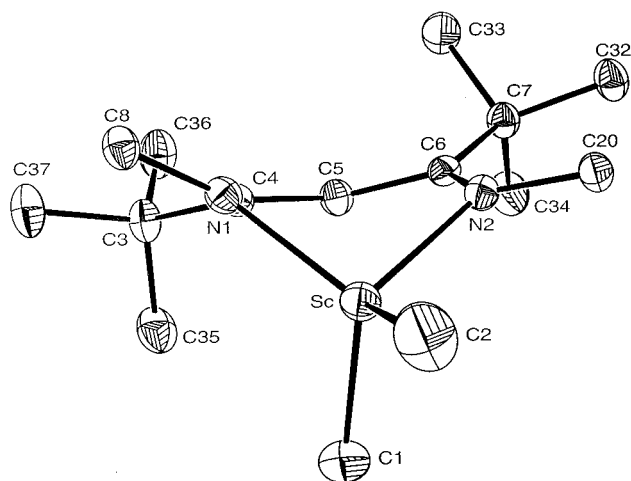


Figure 3. ORTEP diagram of the four-coordinate complex **2b** (30% ellipsoids). Only the *ipso* carbons of the N aryl groups are shown for clarity.

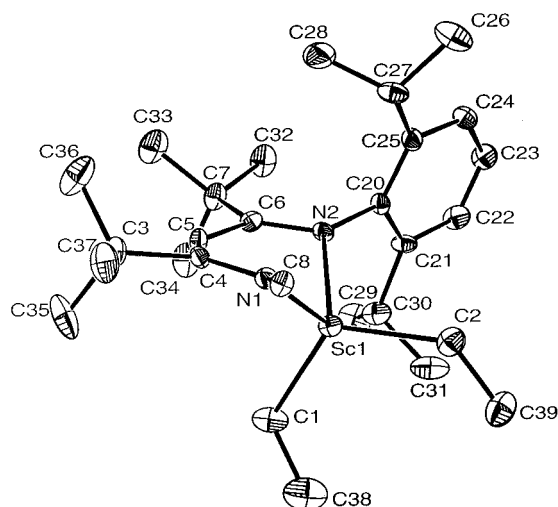


Figure 4. ORTEP diagram of the four-coordinate complex **3b** (30% ellipsoids). Only the *ipso* carbon of the forward N aryl group is shown for clarity.

angles are $\sim 92\text{--}96^\circ$ for the **b** series complexes and are about $4\text{--}5^\circ$ less at $90.71(4)^\circ$ for **6a**. The widening of the N–Sc–N angle in the *t*Bu-substituted compounds is a compensation for the increased steric interaction between the bulky aryl groups and the scandium alkyl ligands in the **b** series caused by the larger C(4)–N(1)–C(8) and C(6)–N(2)–C(20) angles (by $\sim 4\text{--}7^\circ$) compared to those in **6a**. C(1)–Sc–C(2) angles hover around the ideal tetrahedral angle of 109° , and the bond distances to scandium are typical of Sc–N, Sc–C, or Sc–Cl single bonds.^{3b} For the diethyl derivative **3b** (Figure 4) large Sc–C(1)–C(38) and Sc–C(2)–C(39) angles of $119.4(5)$ and $129.0(5)^\circ$, respectively, suggest that β -agostic interactions are absent. Similarly, normal Sc–C(1)–C(38) and Sc–C(2)–C(44) angles of $127.0(4)$ and $115.3(5)^\circ$ in the dibenzyl compound **4b** (Figure 5) argue against any η^2 bonding of these ligands to scandium.

In all of these compounds, the scandium atom is situated out of the ligand plane significantly (by $\sim 1.1\text{--}1.25$ Å; see Table 3), rendering the alkyl or chloride substituents inequivalent. In this paper and others,¹⁵

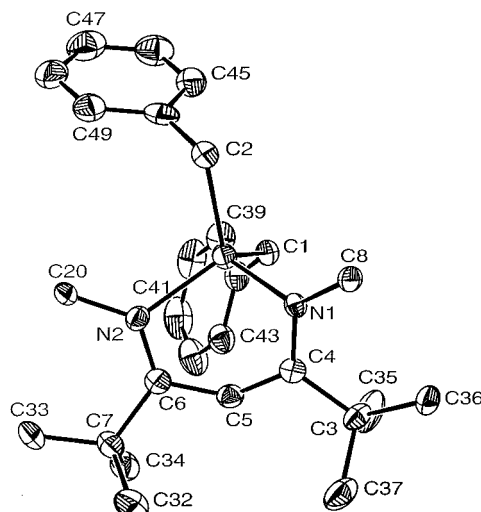


Figure 5. ORTEP diagram of the four-coordinate complex **4b** (30% ellipsoids). Only the *ipso* carbons of the N aryl groups are shown for clarity.

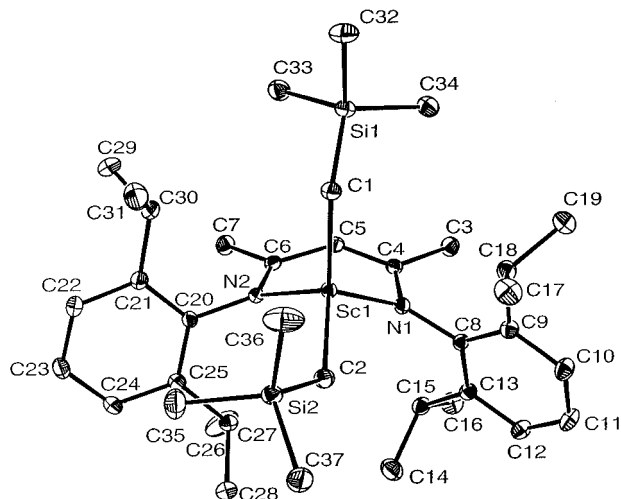


Figure 6. ORTEP diagram of the four-coordinate complex **6a** (30% ellipsoids).

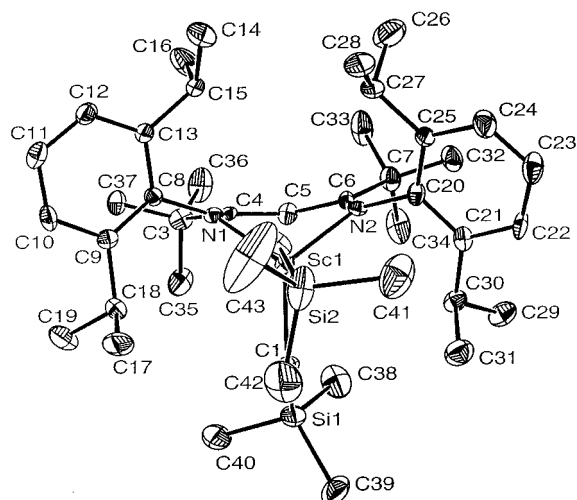


Figure 7. ORTEP diagram of the four-coordinate complex **6b** (30% ellipsoids).

we refer to the substituent which occupies the site “underneath” the β -diketiminato ligand as the *endo* group, while the other is defined as the *exo* site; the

(15) Knight, L. K.; Piers, W. E.; McDonald, R. *Chem. Eur. J.* **2000**, *6*, 4322.

Table 3. Selected Metrical Parameters for Four-Coordinate Structures 1b–4b and 6a,b

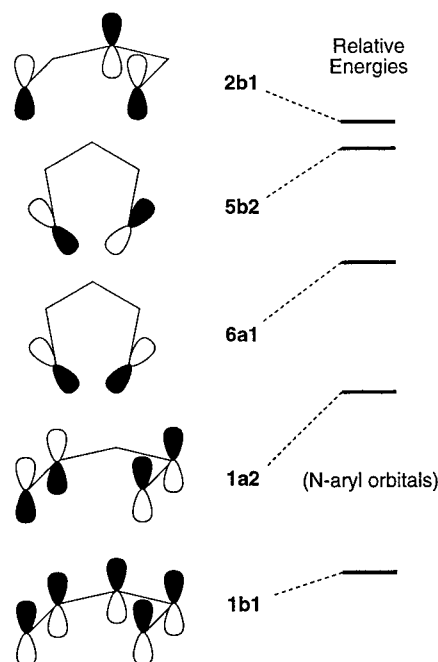
param ^a	1b	2b	3b	4b	6a	6b
Bond Distances (Å)						
Sc–N(1)	2.046(6)	2.1029(10)	2.125(5)	2.091(5)	2.1130(10)	2.091(5)
Sc–N(2)	2.099(6)	2.1451(10)	2.118(5)	2.118(5)	2.1320(10)	2.144(5)
Sc–E(1)	2.352(3)	2.2197(15)	2.244(6)	2.265(6)	2.2446(13)	2.229(7)
Sc–E(2)	2.326(3)	2.2219(16)	2.204(6)	2.203(7)	2.1954(14)	2.202(7)
Sc–C(4)	2.628(7)	2.7289(12)	2.777(7)	2.722(7)	2.8732(12)	2.808(7)
Sc–C(5)	2.700(7)	2.8775(12)	2.832(6)	2.796(7)	3.0793(13)	2.934(7)
Sc–C(6)	2.738(7)	2.8770(12)	2.767(7)	2.796(7)	2.9176(12)	2.890(7)
N(1)–C(4)	1.333(9)	1.3622(15)	1.318(6)	1.361(8)	1.3417(16)	1.349(8)
C(4)–C(5)	1.433(10)	1.3962(16)	1.418(7)	1.399(8)	1.4049(17)	1.400(9)
C(5)–C(6)	1.422(10)	1.4475(16)	1.423(7)	1.431(9)	1.4188(17)	1.447(8)
C(6)–N(2)	1.319(9)	1.3127(15)	1.338(7)	1.325(8)	1.3288(16)	1.325(7)
N ₂ C ₃ plane–Sc	1.295(6)	1.2621(12)	1.240(5)	1.244(4)	1.1152(14)	1.146(6)
Bond Angles (deg)						
E(1)–Sc–E(2)	115.00(12)	109.46(6)	117.6(3)	114.4(3)	114.84(5)	109.4(3)
N(1)–Sc–E(1)	113.5(2)	110.80(5)	111.4(2)	109.7(2)	117.18(5)	119.3(2)
N(1)–Sc–E(2)	112.2(2)	123.27(6)	109.2(2)	105.7(3)	107.58(5)	105.3(3)
N(2)–Sc–E(1)	116.0(2)	112.64(5)	113.2(2)	123.9(2)	113.12(5)	120.2(2)
N(2)–Sc–E(2)	102.2(2)	107.17(5)	108.9(2)	105.6(3)	110.91(5)	107.3(2)
N(1)–Sc–N(2)	95.9(2)	92.20(4)	94.00(16)	94.7(2)	90.71(4)	93.5(2)
Sc–N(1)–C(4)	100.0(5)	101.77(7)	105.1(3)	102.0(4)	110.55(8)	107.4(4)
C(6)–N(2)–Sc	104.2(5)	110.28(8)	104.1(3)	106.3(4)	112.86(8)	110.6(4)
N(1)–C(4)–C(3)	126.4(8)	124.60(10)	126.8(5)	125.2(6)	119.86(11)	124.6(6)
N(1)–C(4)–C(5)	120.0(8)	121.33(11)	121.2(5)	120.3(6)	123.53(11)	120.9(6)
C(3)–C(4)–C(5)	113.0(8)	113.71(10)	111.9(5)	114.2(6)	116.61(11)	114.2(6)
C(4)–C(5)–C(6)	134.8(8)	133.43(11)	136.4(5)	136.1(7)	130.74(12)	134.7(6)
C(5)–C(6)–C(7)	112.6(7)	113.28(10)	113.4(5)	112.6(6)	115.39(11)	112.0(6)
C(5)–C(6)–N(2)	119.7(8)	119.23(10)	120.5(5)	120.0(6)	123.28(11)	120.2(6)
C(7)–C(6)–N(2)	127.7(8)	127.50(10)	125.9(5)	127.4(6)	121.33(11)	127.8(6)
C(4)–N(1)–C(8)	125.3(7)	124.47(10)	125.6(5)	124.4(6)	120.06(10)	125.5(5)
C(6)–N(2)–C(20)	126.9(7)	127.52(10)	127.4(5)	127.5(5)	120.73(10)	126.3(6)
Torsion Angles (deg)						
C(6)–N(2)–C(20)–C(25)	95(1)	98.31(15)	89.3(7)	98.2(8)	99.9(1)	94.2(8)
C(6)–N(2)–C(20)–C(21)	–92.0(10)	–87.90(15)	–95.4(7)	–88.8(9)	–83.5(1)	–91.5(9)
C(4)–N(1)–C(8)–C(9)	115.1(9)	124.69(13)	104.1(7)	110.7(8)	109.5(2)	105.7(7)
C(4)–N(1)–C(8)–C(13)	–69.6(11)	–59.56(16)	–80.8(7)	–74.3(9)	–74(2)	–82.0(8)

^a E = Cl for **1b** and C for **2b–4b** and **6a,b**.

differences are best illustrated by the view of **3b** shown in Figure 4 and that of **4b** in Figure 5.

Several factors can potentially contribute to the extent to which out-of-plane bonding is present in these β -diketiminato complexes. For example, some authors have invoked a six-electron η^5 -bonding mode to account for out-of-plane bonding modes in the group 4 metal coordination chemistry of these ligands, in analogy with η^5 -pentadienyl complexes.¹⁰ However, a DFT treatment of the bonding of these ligands to Cu(I) centers recently presented by Tolman and Solomon et al.¹⁶ suggest that a description akin to that found in η^5 -pentadienyl bonding is not applicable. Tolman and Solomon show that five occupied orbitals are associated with the β -diketimide ligand (Chart 1). In this orbital set, the 2b1, 1a2, and 1b1 orbitals are out-of-plane π orbitals which could function as donors in “pentadienyl-like” bonding to a metal, while the two in-plane orbitals (5b2 and 6a1) are associated with the nitrogen lone pairs. In principle, then, the β -diketimide ligand can function as a 10-electron donor; in practice, the out-of-plane 1a2 and 1b1 orbitals are low in energy and do not figure into the ligand–metal bonding picture significantly. The majority of the bonding occurs through the in-plane orbitals 5b2 and 6a1, which form σ -bonds to the metal center; such in-plane bonding means that the ligand functions as a 4-electron donor.¹⁷ The flexibility of the

Chart 1



ligand backbone and the σ -symmetry of these orbitals allow metals to move out of the ligand plane without

(16) Randall, D. W.; DeBeer George, S.; Holland, P. L.; Hedman, B.; Hodgson, K. O.; Tolman, W. B.; Solomon, E. L. *J. Am. Chem. Soc.* **2000**, *122*, 11632.

(17) In another DFT treatment of LM–R cations (M = Ti, V, Cr), in-plane bonding was determined to be the ground-state bonding mode: Deng, L.; Schmid, R.; Ziegler, T. *Organometallics* **2000**, *19*, 3069.

significant disruption of these bonding interactions, but potentially turning on π -bonding interactions between the 2b1 ligand orbital and an orbital of appropriate symmetry on the metal. This out-of-plane 2b1 orbital is associated with the two ligand nitrogens and the central ligand backbone carbon. Indeed, those structures which have been described as η^5 structures for Ti and Zr complexes are characterized by a significant puckering of this central backbone carbon toward the metal, suggesting a 6-electron, $2\sigma-\pi$ bonding description is most appropriate. For the present scandium complexes, although they are electron-deficient, the rather long distances from the scandium center to the ligand backbone carbons C(4), C(5), and C(6) and the lack of distinct puckering of C(5) toward the Sc center (Table 3) suggest that a tendency toward a $2\sigma-\pi$ bonding mode is not the overriding cause of scandium's deviation from the ligand plane in these complexes.

Another potential contributing factor to out-of-plane bonding could be the size of the metal ion the β -diketiminato ligand is chelating. If the metal ion is too large for the ligand's maximum bite angle, it could alleviate the situation by popping up out of the ligand plane. This phenomenon accounts for out-of-plane binding of metals with an ionic radius >1.0 Å in porphyrin compounds¹⁸ or the extent to which metals deviate from the N_4 plane in related tmtaa complexes.¹⁹ While we do not observe any in-plane bonding to scandium in this series of compounds, the ionic radius of Sc^{3+} is similar to that of Zr^{4+} , for which several η^2 σ -bound β -diketiminato ligand complexes have been characterized,^{10c,d,h} suggesting that, in principle, β -diketiminato ligands can accommodate relatively large metal ions.

In light of the above discussion, it appears the most important factor dictating the adoption of an out-of-plane bonding mode is the steric interaction between the N-aryl groups and the other substituents on the metal. Several four-coordinate complexes of ligand **a** with metal ions ranging from Ti and V(III)^{10b} to Cu(II)^{16,20} and Zn(II)²¹ and into the p block with Al(III)¹¹ have been structurally characterized, and *all* assume the out-of-plane bonding mode to varying degrees. Interestingly, in lower coordinate complexes of this ligand, in-plane postures are assumed.^{9,10b,22}

To our knowledge, the complexes reported herein are the first four-coordinate compounds of the more sterically demanding ligand **b** which have been prepared and structurally characterized.²³ The successful preparation of **1b** stands in contrast to the failed attempts to attach this ligand to Ti(III) or V(III);^{10b} evidently the slightly larger effective ionic radius of Sc(III) compared to the Ti(III) and V(III) ions²⁴ is enough to allow for complexation. While the Sc(III) ion can be accommodated by this ligand, the unfavorable interactions between the aryl

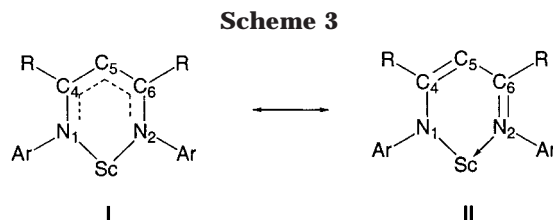


Table 4. Internal Comparison of Ligand Bond Distances (Å) for Four-Coordinate Dialkyl Complexes $LScR_2$

	2b	6b	4b	6a	3b
Sc–N(2)	2.1451(10)	2.144(5)	2.118(5)	2.1320(10)	2.118(5)
Sc–N(1)	2.1029(10)	2.091(5)	2.091(5)	2.1130(10)	2.125(5)
Δ	0.0422	0.053	0.027	0.019	–0.007
N(1)–C(4)	1.3622(15)	1.349(8)	1.361(8)	1.3417(16)	1.318(6)
N(2)–C(6)	1.3127(15)	1.325(7)	1.325(8)	1.3288(16)	1.338(7)
Δ	0.0495	0.024	0.036	0.0129	–0.02
C(5)–C(6)	1.4475(16)	1.447(8)	1.431(9)	1.4188(17)	1.423(7)
C(4)–C(5)	1.3962(16)	1.400(9)	1.399(8)	1.4049(17)	1.418(7)
Δ	0.0513	0.047	0.032	0.0139	0.005
Sc–C(6)	2.8770(12)	2.890(7)	2.796(7)	2.9176(12)	2.767(7)
Sc–C(4)	2.7289(12)	2.808(7)	2.722(7)	2.8732(12)	2.777(7)
Δ	0.1481	0.082	0.074	0.0444	–0.01

isopropyl groups and the metal substituents cause the metal to assume its position out of plane. As the metal dips below the ligand plane, the N-aryl groups tilt upward, allowing the N–Sc σ bonding interactions to be maintained. This structural perturbation alleviates steric interactions by permitting the isopropyl groups on the side of the ligand plane opposite the metal to rotate inward toward the metal, above the *exo* R group. The isopropyl groups on the same side of the metal center rotate away from the *endo* substituent. This phenomenon is best illustrated by the view of **6b** in Figure 7. When another ligand is present on scandium, as in the five-coordinate compounds **1a** and **2a**, the aryl groups cannot rotate in this fashion without encountering the fifth ligand and the deviation of scandium from the ligand plane is less (~ 0.69 Å) in these complexes.

Close inspection of the metrical parameters associated with the ligand backbone reveals that contributions to the ground-state structure from an amido–imide resonance structure (**II**; Scheme 3) in addition to the symmetric, delocalized resonance contributor **I** may be significant. Bond distances within the ligands for the dialkyl complexes suggest that bonding of the ligand to the metal is not entirely symmetrical for some of the compounds. As Table 4 shows, the phenomenon is most extreme for the dimethyl derivative **2b** and least pronounced for diethyl complex **3b**. For **2b**, the Sc–N(1) distance is slightly shorter than the Sc–N(2) distance and N(2)–C(6) and C(4)–C(5) are shorter than N(1)–C(4) and C(5)–C(6), respectively, indicating an alternating, more localized distribution of electrons in the ligand. The ligand “plane” is also somewhat disrupted; C(6) deviates significantly by 0.321 Å from the plane defined by the other four ligand atoms, which are essentially coplanar. This is seen most clearly in the view of **2b** given in Figure 3. The distortions within the ligands diminish as one progresses across Table 4; for the last entry, **3b**, the ligand is more symmetrically bound to the metal center, indicative of a delocalized electron distribution. The extent to which **II** contributes

(18) Brothers, P. J. *Adv. Organomet. Chem.* **2000**, *46*, 223.

(19) Cotton, F. A.; Czuchajowska, J. *Polyhedron* **1990**, *21*, 2553.

(20) Holland, P. L.; Tolman, W. B. *J. Am. Chem. Soc.* **2000**, *120*, 6331.

(21) (a) Cheng, M.; Lobkovsky, E. B.; Coates, G. W. *J. Am. Chem. Soc.* **1998**, *120*, 11018. (b) Cheng, M.; Attygalle, A. B.; Lobkovsky, E. B.; Coates, G. W. *J. Am. Chem. Soc.* **1999**, *121*, 11583.

(22) Holland, P. L.; Tolman, W. B. *J. Am. Chem. Soc.* **1999**, *121*, 7270.

(23) Budzelaar, who introduced ligand **b**, has reported its three-coordinate lithium salt (THF adduct), which assumes an in-plane bonding mode.

(24) Shannon, R. D. *Acta Crystallogr.* **1976**, *A32*, 751.

Table 5. ^1H NMR Data for $\text{LSc}(\text{CH}_2\text{R})_2$ Complexes^a

compd	H _L ^b	R _L ^c	Ar H	CH <i>i</i> Pr ^d	CH ₃ <i>i</i> Pr	Sc-CH ₂	R
1a ^e	5.32	1.65	7.21	3.56	1.17, 1.39		
1b	6.01	1.17	7.05	3.10	1.26, 1.43		
2a ^f	5.06	1.67	7.16	3.45	1.20, 1.40	-0.15	
2b	5.85	1.21	7.25	3.52	1.41, 1.47	0.11	
3b	5.70	1.13	7.26	3.38	1.43, 1.50	0.32 ^g	1.25
4a	5.01	1.58	7.15	3.08	1.06, 1.22	2.10	6.70-7.16
4b	5.62	1.04	7.12	2.50, 3.65	1.18, 1.23	2.12	6.70-7.20
5a	5.00	1.63	7.16	3.47	1.17, 1.47	0.87	1.03
5b ^h	5.58	1.11	7.00-7.20	2.86, 4.12	1.23, 1.23, 1.46, 1.74	0.75, 0.78	1.35
6a	5.00	1.59	7.16	3.31	1.16, 1.44	0.18	0.08
6b	5.68	1.10	7.07	2.70, 3.95	1.20, 1.75	0.00	0.13
7b	5.87	1.10	6.99-7.07	3.15, 3.43	1.27, 1.37, 1.37, 1.46	0.16	
8b	5.73	1.09	6.97-7.10	3.12, 3.55	1.27, 1.30, 1.32, 1.48	-0.08, -0.09 ⁱ	0.00
<i>exo</i> _{Me} - 8b ^j	5.69	1.05	6.85-7.09	2.87, 3.91	1.18, 1.38, 1.73, 1.74	0.12, 0.03	0.09
<i>endo</i> _{Me} - 8b ^j	5.74	1.03	6.85-7.09	2.73, 3.79	1.18, 1.34, 1.46, 1.69	0.12, 0.01	0.50

^a Spectra accumulated in C₆D₆ and at room temperature unless otherwise noted. ^b Ligand backbone proton. ^c Ligand backbone substituent: **a**, R₁ = CH₃; **b**, R₁ = ^tBu. ^d $J_{\text{H-H}} = 6.8(1)$ Hz. ^e Coordinated THF resonances at 1.49 and 3.48 ppm. ^f Coordinated THF resonances at 1.23 and 3.40 ppm. ^g $J_{\text{H-H}} = 8.20$ Hz. ^h Solvent C₇D₈, $T = 242$ K. ⁱ CH₃. ^j Solvent C₇D₈, $T = 200$ K.

Table 6. $^{13}\text{C}\{^1\text{H}\}$ NMR Data for $\text{LSc}(\text{CH}_2\text{R})_2$ Complexes^a

compd	C _{4/6}	C ₅	C _{ipso}	C _{Ar}	C _P ^d	R _L ^b	Sc-C	R
1a ^c	162.3	99.8	143.3	124.2, 126.6, 143.3	24.7, 25.0, 28.6	24.4		
1b	174.3	90.8	142.8	124.3, 127.0, 141.1	24.4, 26.9, 29.9	44.7, 32.3		
2a ^d	167.8	96.1	143.0	124.4, 126.9, 142.7	25.2, 25.4, 28.6	24.1	24.8	
2b	174.1	92.7	143.4	124.2, 126.1, 141.1	24.5, 26.9, 29.7	44.6, 32.6	27.6	
3b	174.2	92.5	143.8	124.2, 126.0, 141.5	26.6, 26.7, 29.2	44.7, 32.4	40.8	13.2
4a	167.9	95.7	143.2	124.7, 126.9, 142.2	24.8, 24.9, 28.8	24.2	61.6	149.3, 120.3, 124.9, 129.6
4b ^e	174.8	91.3	143.2	124.7, 125.1, 126.9, 141.2, 141.9	24.6, 25.3, 26.2, 27.0, 28.9, 29.8	45.0, 32.3	57.5, 64.3	151.6, 149.0, 128.5, 128.7, 126.0, 125.2, 119.8, 119.7
5a	167.1	94.3	143.0	124.6, 126.8, 142.3	25.0, 25.3, 28.8	24.6	72.3	35.4, 34.9
5b ^f	174.9	93.0	144.2	124.7, 125.1, 126.7, 141.9, 142.3	25.1, 25.6, 26.7, 27.5, 28.8, 29.9	45.3, 33.0	69.9, 75.5	35.6, 35.3, 36.6, 35.4
6a	167.9	95.7	141.8	124.7, 127.1, 142.6	24.9, 25.7, 28.6	24.4	44.9	3.4
6b ^g	175.6	93.6	143.2	124.7, 125.1, 127.0, 142.0, 142.4	24.7, 25.4, 26.5, 28.4, 28.8, 29.4	44.8, 32.7	41.8, 48.7	3.4, 4.7
7b	174.2	92.1	143.0	124.1, 124.3, 126.6, 141.1, 141.4	24.0, 24.1, 26.3, 26.6, 29.1, 29.7	44.6, 32.2	25.8	
8b	174.5	93.3	143.2	124.5, 124.6, 127.0, 141.2, 141.8	24.4, 24.6, 25.1, 26.6, 27.0, 29.6	44.7, 32.3	27.3, 45.5	3.9

^a Spectra accumulated in C₆D₆ or C₇D₈ and at room temperature, unless otherwise noted. ^b For the **b** series, the values are for the quaternary and primary ^tBu carbons, respectively. ^c Coordinated THF resonances at 67.0 and 24.8 ppm. ^d Coordinated THF resonances at 67.0 and 24.8 ppm. ^e $T = 265$ K. ^f $T = 242$ K. ^g $T = 233$ K.

to the structure thus does not appear to correlate well with the steric properties of the alkyl group and the energetic difference between **I** and **II** is likely small.

Solution Structures and Dynamic Behavior. Solution NMR spectra for the dialkyl structures discussed above should be reflective of the low symmetry inherent to the out-of-plane bonding mode observed. Because rotation of the N-aryl groups is precluded due to the steric properties of these ligands, the isopropyl methyl groups pointing inward at the metal are in different chemical environments than those directed away from the molecular core, and two signals would be expected for an in-plane solution structure. As the metal deviates from the ligand plane, "top-bottom" asymmetry is introduced and four separate doublets for the isopropyl methyl groups would be predicted. Also, distinct resonances for the two different (*endo* and *exo*) alkyl substituents would be expected for this structure.

Tables 5 and 6 give the ^1H and $^{13}\text{C}\{^1\text{H}\}$ NMR data for all of the dialkyl derivatives reported herein, as well as the two dichloride precursors. As can be seen, for most of these compounds, spectra consistent with a symmetrical, in-plane structure are observed at room temperature. For bis(trimethylsilyl)methyl complex **6b**, however, the ^1H NMR spectrum at room temperature is broad and featureless, a manifestation of dynamic behavior. Indeed, variable-temperature spectroscopy

on these complexes reveals coalescence behavior consistent with equilibration of two equivalent out-of-plane structures via a C_{2v} symmetric, in-plane transition state. Figure 8 shows an illustrative series of spectra using **3b** as an example; the proposed fluxional process is also depicted. In the fast-exchange regime, the ethyl groups are equivalent, and only one and two resonances are observed for the isopropyl methine and methyl groups, respectively. As the sample is cooled, signals for the now inequivalent ethyl groups emerge and the pattern for the ligand isopropyl moieties morphs into what would be expected for a structure akin to that found in the solid state as discussed above. The barrier for this process can be extracted from the NMR data;²⁵ a ΔG^\ddagger value of 10.6(5) kcal mol⁻¹ at the coalescence temperature of 240 K was measured for the diethyl compound **3b**.

The barriers for this process in each of the four-coordinate compounds was measured using variable-temperature ^1H NMR spectroscopy, and the results are shown in Table 7. In addition, barriers normalized to 298 K are given. Although there are some anomalies, generally the barriers track the steric bulk of R, with higher barriers observed as R gets larger. This is

(25) Sandström, J. *Dynamic NMR Spectroscopy*; Academic Press: New York, 1982.

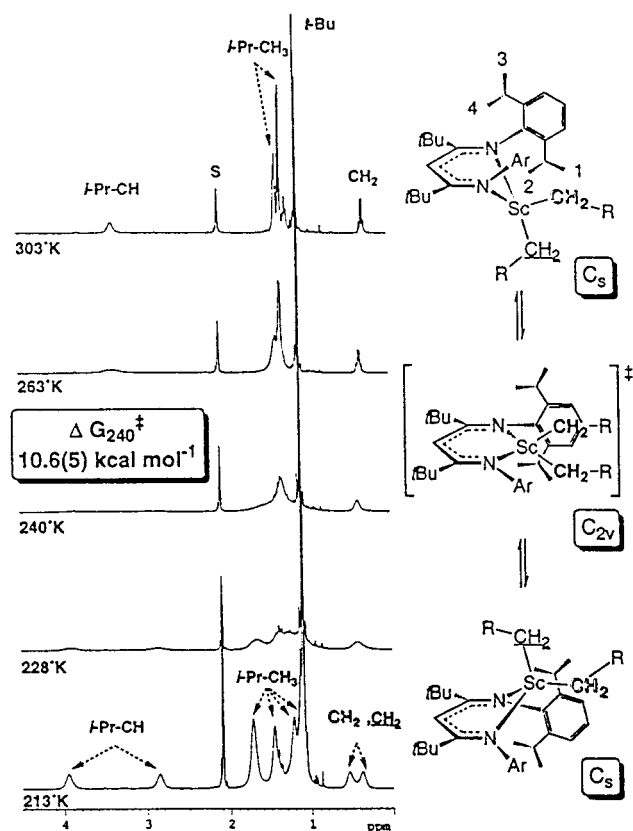


Figure 8. Representative series of ^1H NMR spectra of diethyl complex **3b** (400 MHz, C_7D_8), depicting the coalescence behavior of the spectrum and the postulated dynamic process accounting for this behavior.

Table 7. Free Energies of the Fluxional Process in LScR_2

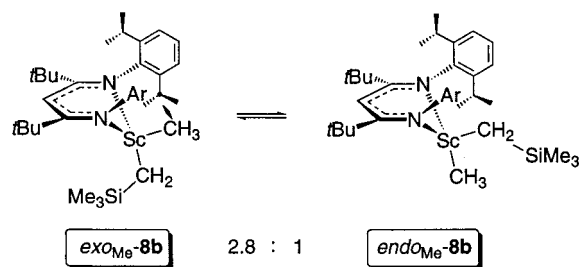
compd	R	T_c (K)	$\Delta G^\ddagger_{T_c}$ (kcal mol $^{-1}$)	$\Delta G^\ddagger_{\text{norm}}^b$
4a	CH_2Ph	187	8.2 ^c	5.2 ^c
5a	CH_2CMe_3	275	12.3	11.4
6a	CH_2SiMe_3	210	9.5	6.7
1b	Cl	263	12.3	10.8
2b	CH_3	213	9.6	6.9
3b	CH_2CH_3	240	10.6	8.6
4b	CH_2Ph	298	13.4	13.4
5b	CH_2CMe_3	242	10.7	8.7
6b	CH_2SiMe_3	303	13.7	13.9

^a In kcal mol $^{-1}$. ^b In kcal mol $^{-1}$, normalized to 298 K. ^c Upper limit due to inability to observe the low-temperature-limit spectrum of **4a**.

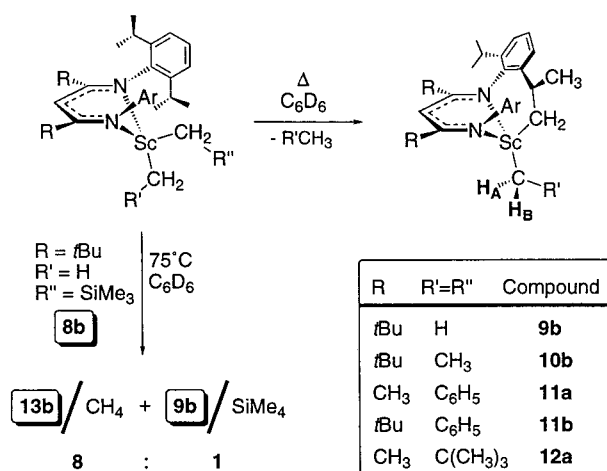
consistent with the notion that the ScR_2 fragment deviates from the NCCCN ligand plane in order to avoid steric interactions with the aryl isopropyl groups (vide supra). The anomalous values (e.g. those found for **4a** and **1b**) imply that electronic factors are also playing a role in determining the barrier to the process. Interestingly, in the related complex $\text{L}_p\text{Sc}(\text{TeCH}_2\text{SiMe}_3)_2$, where the two scandium substituents are π -donating and bulky tellurolate ligands, the barrier to their equilibration cannot be measured via this technique and a static out-of-plane structure is also observed at room temperature in solution.¹⁵

The NMR spectra for the mixed-ligand derivatives **7b** and **8b** exhibit aryl isopropyl resonance patterns expected on the basis of the now broken top-bottom symmetry, even in the averaged structure. These compounds undergo a related dynamic process which ex-

Scheme 4



Scheme 5



changes diastereomeric rather than equivalent structures (Scheme 4). As samples of **8b** are cooled, coalescence behavior is observed (255 K) and signals for the two isomers $\text{exo}_{\text{Me}}\text{-8b}$ and $\text{endo}_{\text{Me}}\text{-8b}$ emerge at 210 K; the isomers are present in a 2.8:1 ratio. The assignment of the major species as the exo_{Me} diastereomer was made on the basis of a low-temperature ROESY experiment, which clearly showed correlation between the methyl group and the lower isopropyl methine group pointing inward toward the exo position in the major isomer. Because of this relatively close contact, the exo position is the most sterically crowded, and positioning of the larger CH_2SiMe_3 group in the endo site is favored on this basis.

The four-coordinate dialkyl complexes are somewhat thermally unstable in benzene solution, initially undergoing a metalation process with one of the C-H bonds of an aryl isopropyl group and eliminating 1 equiv of R-H (Scheme 5). For dialkyls in the **a** series, further ill-defined processes compete with the metalation at later stages of the reaction, but in the **b** series, metalation to compounds **9b-13b** is relatively clean. Because of lowered symmetry, the ^1H NMR spectra for these compounds are complex, exhibiting seven doublets for the isopropyl methyl groups and four multiplets for the methines. For compounds **10b-13b**, a diagnostic AB quartet ($^2J_{\text{HH}} = 11-12$ Hz) for the diastereotopic $\text{Sc}-\text{CH}_2\text{R}$ protons of the remaining unmetalated alkyl group appears upfield of 0 ppm (this signal is at 2.12 ppm for **11b**). An X-ray structural analysis of **13b** was carried out, and while the data were not refinable to an

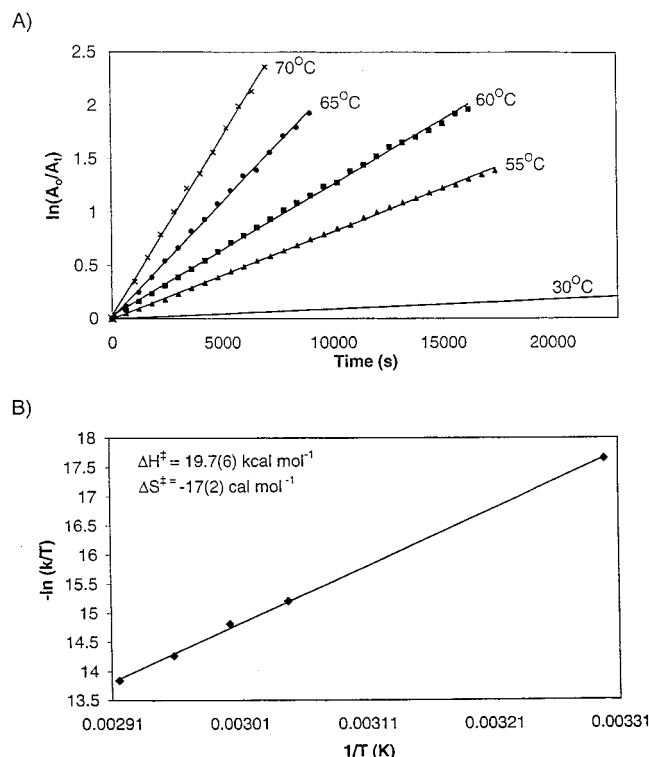


Figure 9. (A) First-order kinetic plots for the metalation of **6b** to produce **13b** and SiMe_4 at various temperatures. The complete data set for the run at 30°C is not shown in the figure; this run took over 80 000 s to go to 5 half-lives. (B) Eyring plot of the temperature dependence of the rate constants.

acceptable level, analysis did confirm the connectivity of this compound as formulated.

The metalation process for bis((trimethylsilyl)methyl) derivative **6b** was monitored quantitatively by ^1H NMR spectroscopy; these studies indicate that the process is first order in the dialkyl species, consistent with an intramolecular reaction. The reaction was followed at various temperatures (Figure 9A), and an Eyring plot (Figure 9B) allowed for extraction of the activation parameters $\Delta H^\ddagger = 19.7(6)$ kcal mol $^{-1}$ and $\Delta S^\ddagger = -17(2)$ cal mol $^{-1}$ K $^{-1}$. The ΔH^\ddagger value compares well to that found for the σ -bond metathesis reaction between $d_{30}\text{-Cp}^*\text{ScCH}_3$ and C_6H_6 ($\Delta H^\ddagger = 18.9(2)$ kcal mol $^{-1}$).²⁶ However, the ΔS^\ddagger value is more negative than one would expect for an intramolecular reaction (cf. the value of $-23(2)$ cal mol $^{-1}$ K $^{-1}$ found for ΔS^\ddagger in the intermolecular reaction). Perhaps the fluxionality of these complexes contributes to the more negative activation entropy observed.

For the ligand **a** series of compounds, the metalation process was not as clean as for the **b** series. At the higher temperatures required to induce metalation in the **a** series, other decomposition processes complicate the situation somewhat; however, semiquantitative estimates of the half-lives of these reactions are obtainable (Table 8). In general, the THF-free complexes incorporating ligand **a** are more resistant to metalation than those of the **b** series. For example, when solutions of **6a** and **6b** are heated at 360 K (concentration $4.16 \times$

Table 8. Half-Lives and k_{obsd} (Calculated) for Metalation Reactions

compd	R	T (K)	$t_{1/2}$ (h)	k_{obsd} (s $^{-1}$)
4a	CH_2Ph	360	7.2	2.68×10^{-5}
5a	CH_2CMe_3	360	0.37	5.32×10^{-4}
6a	CH_2SiMe_3	360	3.8	5.09×10^{-5}
6b	CH_2SiMe_3	360	0.13	1.47×10^{-3}
2b	CH_3	333	0.53	3.59×10^{-4}
3b	CH_2CH_3	333	0.15	1.34×10^{-3}
4b	CH_2Ph	333	11.7	1.65×10^{-5}
5b	CH_2CMe_3	333	0.33	5.86×10^{-4}
6b	CH_2SiMe_3	333	1.6	1.22×10^{-4}

10^{-3} M), the observed half-lives are ~ 3.8 h and 8 min, respectively. Much precedence exists for the notion that steric crowding about a metal center favors metalation processes,²⁷ and this observation is another manifestation of the significantly higher steric impact of the **b** ligand vs that of the **a** donor. Given the complex interplay of steric and electronic effects on the fluxionality observed for these compounds (vide supra) and likely on the energetics of the σ -bond metathesis transition state, meaningful conclusions regarding the trends observed within each series are difficult to come by. However, the almost complete lack of correlation between the observed barriers to *endo/exo* ligand exchange and the rates of metalation suggest that metalation does not occur from the in-plane C_{2v} structure. Interestingly, when the mixed-alkyl complex **8b** is induced to undergo metalation at 75°C , methane elimination to produce **13b** is preferred over loss of SiMe_4 to give **9b** by an 8:1 margin (Scheme 5). We speculate that the metalation transition state occurs from an out-of-plane structure and preferentially involves loss of the *exo* alkyl substituent. In fact, as many of the ORTEP diagrams in Figures 2–7 show, the *exo* alkyl group is closely proximal to the lower isopropyl groups, facilitating metalation from this structure.

As the only example in the series which contains β -hydrogen-containing alkyl groups, diethyl derivative **3b** deserves special comment. Although alternate mechanistic possibilities involving β -hydride elimination²⁸ or abstraction²⁹ in the metalation chemistry observed for diethyl complex **3b** are feasible, it appears that metalation via direct σ -bond metathesis is operative for this derivative as well. This is indicated by the results of the metalation of d_{10} -**3b**, specifically deuterated in the ethyl groups. When this compound was allowed to undergo metalation, only d_5 -**10b** was observed in the ^2H NMR spectrum, as indicated by two signals appearing at 0.6 and -0.6 ppm (integrating in a 3:2 ratio) in the $^2\text{H}\{^1\text{H}\}$ NMR spectrum. Also produced was $\text{CD}_3\text{-CD}_2\text{H}$ (identified in the ^1H NMR spectrum). If this reaction proceeded, for example, by initial β -elimination of CD_3CD_3 , followed by metalation of the resulting scandacyclopropane, d_4 -**10b** would have been expected. Interestingly, the only other $\text{LSc}(\text{CH}_2\text{CH}_3)_2$ reported in the literature⁶ also appeared to be immune to β -elimination pathways.

(27) (a) Constable, E. C. *Polyhedron* **1984**, *3*, 1037. (b) Ibers, J. A.; DiCosimo, R.; Whitesides, G. M. *Organometallics* **1982**, *1*, 13.

(28) Burger, B. J.; Thompson, M. E.; Cotter, W. D.; Bercaw, J. E. *J. Am. Chem. Soc.* **1990**, *112*, 1566.

(29) By analogy to the loss of butane/1-butene from $\text{Cp}_2\text{Zr}(\text{tBu})_2$: (a) Negishi, E.-I.; Takahashi, T. *Acc. Chem. Res.* **1994**, *27*, 124. (b) Dioumaev, V. K.; Harrod, J. F. *Organometallics* **1997**, *16*, 1452.

(26) Thompson, M. E.; Baxter, S. M.; Bulls, A. R.; Burger, B. J.; Nolan, M. C.; Santarsiero, B. D.; Schaefer, W. P.; Bercaw, J. E. *J. Am. Chem. Soc.* **1987**, *109*, 203.

Summary and Conclusions. Facile routes to base-free dialkyl derivatives have been developed, opening up opportunities to study the organoscandium chemistry of these species in detail. Several structural determinations have shown that the β -diketiminato ligand framework, equipped with bulky 2,6-*i*-PrC₆H₃ groups, is well-suited to the stabilization of lower-coordinate, electronically unsaturated ScR₂ fragments. These compounds exhibit complex solution behavior that can be understood in terms of a dynamic process by which out-of-plane bonding modes are equilibrated via an in-plane transition state. Although these highly electrophilic species undergo intramolecular metalation reactions, eliminating RH, in solution, these processes are slow enough on the chemical time scale that the organometallic chemistry of these compounds is rich.¹⁵ In particular, this ligand can be viewed as a monoanionic version of the successful diamido ligand set employed by McConville in living titanium olefin polymerization catalysts,³⁰ and we have shown that stable scandium alkyl cations can be generated via reaction of compounds **4a**,⁷ **2b**, and **6b** with the strong organometallic Lewis acid B(C₆F₅)₃.³¹ We are also exploring new, more metalation resistant β -diketiminato ligands.

Experimental Section

General Procedures. All operations were performed under a purified argon atmosphere using glovebox or vacuum-line techniques. Toluene, hexane, and THF solvents were dried and purified by passing through activated alumina and Q5 columns.³² NMR spectra were recorded in dry, oxygen-free C₆D₆, unless otherwise noted. ¹H, ²H, ¹³C{¹H}, HMQC, ROESY, and COSY NMR experiments were performed on Bruker AC-200, AMX-300, and WH-400 or Varian 200 MHz spectrometers. Data are given in ppm relative to solvent signals for ¹H and ¹³C spectra. UV spectra were obtained on a Hewlett-Packard Model 8452A diode array spectrophotometer interfaced to a PC computer in hexanes solutions with concentrations between 1 × 10⁻⁵ and 1 × 10⁻⁴ M. Elemental analyses were performed by Mrs. Dorothy Fox of this department. The ligands HL^{10b} (L = ArNC(R)CHC(R)NAr, where Ar = 2,6-*i*-Pr-C₆H₃ and R = CH₃, Bu⁹), and benzylpotassium³³ were prepared by literature procedures. The protio ligands were converted to their lithium salts by treatment with *n*-BuLi in hexanes. All other materials were obtained from Sigma-Aldrich and purified according to standard procedures.

Synthesis of [ArNC(CH₃)CHC(CH₃)NAr]ScCl₂·THF (1a**).** Toluene (20 mL) was condensed into an evacuated flask containing LiL (3.50 g, 8.26 mmol) and ScCl₃·3THF (3.03 g, 8.26 mmol) at -78 °C. The mixture was heated with stirring at 85 °C for 16 h. The reaction mixture was hot-filtered to remove LiCl and the toluene removed in vacuo. Trituration of the residue with hexanes followed by filtration led to isolation of pure **1a** as a pale yellow solid (3.23 g, 5.34 mmol, 65%). Anal. Calcd for C₃₃H₄₉N₂Cl₂Osc: C, 65.44; H, 8.15; N, 4.63. Found: C, 65.35; H, 8.71; N, 4.61.

Synthesis of [ArNC(Bu⁹)CHC(Bu⁹)NAr]ScCl₂ (1b**).** A thick-walled reactor bomb equipped with a Kontes valve was charged with LiL (5.70 g, 11.2 mmol) and ScCl₃·3THF (4.70 g,

12.8 mmol) and evacuated. Toluene (300 mL) was condensed into the vessel, which was then sealed and heated to 110 °C for 3 days. The mixture was then cannula-transferred to a swivel frit apparatus. A hot filtration to remove the salts was performed, followed by removal of toluene and trituration with hexanes to give **1b** in 77% yield as a pale yellow solid (5.35 g, 8.66 mmol). Anal. Calcd for C₃₅H₅₃N₂Cl₂Sc: C, 68.06; H, 8.65; N, 4.54. Found: C, 68.54; H, 7.98; N, 4.92.

Synthesis of [ArNC(CH₃)CHC(CH₃)NAr]Sc(CH₃)₂·THF (2a**).** Hexanes (10 mL) and THF (10 mL) were condensed into an evacuated flask containing **1a** (0.390 g, 0.640 mmol) and solid methyllithium (0.028 g, 1.28 mmol) at -78 °C. The yellow mixture was warmed gradually to room temperature and stirred for 1 h before removal of the solvent mixture under reduced pressure. The residue was suspended in toluene and filtered. The filtrate was concentrated, and hexanes were added to induce crystallization of the product. Cold filtration (-30 °C) gave **2a** (0.120 g, 0.198 mmol, 31%). Anal. Calcd for C₃₅H₅₅N₂Osc: C, 74.43; H, 9.82; N, 4.96. Found: C, 72.52; H, 9.70; N, 4.98. Repeated attempts consistently gave low carbon analyses for this compound.

Synthesis of [ArNC(Bu⁹)CHC(Bu⁹)NAr]Sc(CH₃)₂ (2b**).** Toluene (30 mL) was condensed into an evacuated flask containing **1b** (1.00 g, 1.62 mmol) and solid methyllithium (0.132 g, 6.00 mmol) at -78 °C. The resultant mixture was warmed slowly to room temperature and stirred for 1 h. The reaction mixture was filtered and the toluene removed in vacuo. The residue was recrystallized from hexanes, affording yellow crystals of **2b** (0.480 g, 0.832 mmol, 51%). Anal. Calcd for C₃₇H₅₉N₂Sc: C, 77.04; H, 10.31; N, 4.86. Found: C, 76.55; H, 9.53; N, 4.98.

Synthesis of [ArNC(Bu⁹)CHC(Bu⁹)NAr]Sc(CH₂CH₃)₂ (3b**).** Toluene (25 mL) was condensed into an evacuated flask charged with LiCH₂CH₃ (0.058 mg, 1.62 mmol) and **1b** (0.500 g, 0.809 mmol) at -78 °C. The reaction mixture was stirred for 30 min after the vessel was slowly warmed to room temperature. Hot filtration followed by removal of the solvent in vacuo and trituration with hexanes afforded an orange solid (168 mg, 0.283 mmol, 35%). Anal. Calcd for C₃₅H₅₃N₂Cl₂Sc: C, 77.44; H, 10.50; N, 4.63. Found: C, 77.28; H, 10.63; N, 4.74.

Synthesis of [ArNC(Bu⁹)CHC(Bu⁹)NAr]Sc(CD₂CD₃)₂ (d₁₀-3b**).** This compound was prepared in a manner identical with that previously described for **3b**, with the exception that LiCD₂-CD₃ was used. The ¹H NMR spectrum matched **3b**, with the exception that no resonances were observed for the ethyl groups.

Synthesis of [ArNC(CH₃)CHC(CH₃)NAr]Sc(CH₂C₆H₅)₂ (4a**).** A two-necked flask was charged with **1a** (0.400 g, 0.660 mmol) and attached to a swivel frit apparatus. A solid addition tube was loaded with benzylpotassium (0.172 g, 1.32 mmol) and attached to the second port on the flask. The entire assemblage was evacuated, and benzene (50 mL) was vacuum-distilled into the flask. After it was warmed to room temperature, benzylpotassium was gradually added to the solution over 30 min. Stirring was continued for another 4 h. The reaction mixture was filtered and the benzene removed under vacuum to give crude **4a**. Recrystallization from hexanes afforded pure **4a** (0.230 g, 0.389 mmol, 59%). Anal. Calcd for C₄₉H₆₇N₂Sc: C, 80.09; H, 8.60; N, 4.34. Found: C, 80.46; H, 8.04; N, 4.46.

Synthesis of [ArNC(Bu⁹)CHC(Bu⁹)NAr]Sc(CH₂C₆H₅)₂ (4b**).** A 100 mL flask was charged with **1b** (0.750 g, 1.21 mmol) and BnMgCl (0.366 g, 2.43 mmol). Toluene (65 mL) was condensed into the evacuated flask at -78 °C. The mixture was slowly warmed to room temperature, whereby stirring was continued for another 17 h. The toluene was removed in vacuo to afford an orange solid. Benzene (55 mL) was condensed into the flask, and the assemblage was sonicated for 10 min. The reaction mixture was filtered and benzene removed under vacuum to afford **4b** as an orange solid (0.605 g, 0.829 mmol,

(30) Scollard, J. D.; McConville, D. H.; Payne, N. C.; Vittal, J. J. *Macromolecules* **1996**, *29*, 5241.

(31) Piers, W. E.; Hayes, P. G.; Clegg, W. Abstracts of OCOP 2000, Organometallic Catalysts and Olefin Polymerization, June 18–22, 2000, Oslo, Norway.

(32) Pangborn, A. B.; Giardello, M. A.; Grubbs, R. H.; Rosen, R. K.; Timmers, F. J. *Organometallics* **1996**, *15*, 1518.

(33) Schlosser, M.; Hartmann, J. *Angew. Chem., Int. Ed. Engl.* **1973**, *12*, 508.

69%). Anal. Calcd for $C_{49}H_{67}N_2Sc$: C, 80.73; H, 9.26; N, 3.84. Found: C, 79.57; H, 8.91; N, 3.89.

Synthesis of $[ArNC(CH_3)CHC(CH_3)NAr]Sc(CH_2C(CH_3)_2)_2$ (5a**).** Toluene (20 mL) was condensed into an evacuated flask containing $LiCH_2C(CH_3)_3$ (0.139 g, 1.78 mmol) and **1a** (0.474 g, 0.890 mmol) at $-78^\circ C$. The reaction vessel was slowly warmed to room temperature, after which stirring was continued for another 90 min. The solvent was removed under reduced pressure, and hexanes (20 mL) was vacuum-distilled into the flask. The mixture was filtered to remove LiCl. The solvent was removed in vacuo and the residue triturated with hexanes to afford **5a** as a white crystalline solid (0.340 g, 0.562 mmol, 64%). Anal. Calcd for $C_{39}H_{63}N_2Sc$: C, 77.44; H, 10.50; N, 4.63. Found: C, 77.56; H, 9.80; N, 4.73.

Synthesis of $[ArNC(Bu^t)CHC(Bu^t)NAr]Sc(CH_2C(CH_3)_2)_2$ (5b**).** Toluene (20 mL) was condensed into an evacuated flask containing $LiCH_2C(CH_3)_3$ (0.088 g, 1.13 mmol) and **1b** (0.350 g, 0.566 mmol) at $-78^\circ C$. The yellow mixture was warmed to room temperature and stirred for 1 h. Removal of solvent followed by trituration with cold hexanes permitted isolation of crude **5b** as a pale yellow solid. Recrystallization from hexanes at $-35^\circ C$ afforded **5b** in 42% yield (0.165 g, 0.239 mmol). Anal. Calcd for $C_{45}H_{75}N_2Sc$: C, 78.43; H, 10.97; N, 4.07. Found: C, 77.50; H, 10.59; N, 4.80.

Synthesis of $[ArNC(CH_3)CHC(CH_3)NAr]Sc(CH_2SiMe_3)_2$ (6a**).** A 50 mL flask was charged with $LiCH_2Si(CH_3)_3$ (0.128 g, 1.36 mmol) and **1a** (0.410 g, 0.680 mmol) and evacuated. Toluene (25 mL) was condensed into the vessel at $-78^\circ C$. The solution was gradually warmed to room temperature, whereupon it was stirred for 2 h. The mixture was hot-filtered to remove LiCl. The solvent was removed in vacuo, and the residue was triturated with hexanes to give 250 mg (0.392 mmol, 58%) of **6a** as a white powder. Anal. Calcd for $C_{37}H_{63}N_2Si_2Sc$: C, 69.76; H, 9.97; N, 4.40. Found: C, 69.11; H, 9.34; N, 4.58.

Synthesis of $[ArNC(Bu^t)CHC(Bu^t)NAr]Sc(CH_2SiMe_3)_2$ (6b**).** In an evacuated flask at $-78^\circ C$ containing $LiCH_2Si(CH_3)_3$ (0.058 g, 0.616 mmol) and **1b** (0.190 g, 0.308 mmol) was condensed toluene (15 mL). The reaction mixture was warmed to room temperature and then stirred for 90 min. The mixture was filtered, and the solvent was removed in vacuo to afford a yellow residue which was triturated with hexanes to give **6b** as a yellow crystalline solid (0.109 g, 0.151 mmol, 49%). Anal. Calcd for $C_{43}H_{75}N_2Si_2Sc$: C, 71.61; H, 10.48; N, 3.88. Found: C, 70.76; H, 10.41; N, 4.00.

Synthesis of $[ArNC(Bu^t)CHC(Bu^t)NAr]Sc(CH_3)Cl$ (7b**).** A 50 mL flask was charged with **1b** (0.085 g, 0.144 mmol) and **2b** (0.089 g, 0.144 mmol), and 30 mL of toluene was condensed into it at $-78^\circ C$. The reaction mixture was gradually warmed to room temperature and solvent removed under vacuum to afford a light yellow powder. Hexanes (25 mL) were added, and the mixture was filtered to give a clear yellow solution. Removal of solvent in vacuo gave crude **7b** as a pale yellow powder, which was then recrystallized from hexanes at $-35^\circ C$ (0.150 g, 0.255 mmol, 89%). Anal. Calcd for $C_{38}H_{56}N_2ClSc$: C, 72.40; H, 9.45; N, 4.61. Found: C, 72.21; H, 9.32; N, 4.61. (Note: the sample contained 5% of both **1b** and **2b**.)

Synthesis of $[ArNC(Bu^t)CHC(Bu^t)NAr]Sc(CH_3)(CH_2SiMe_3)$ (8b**).** A 100 mL flask was charged with **7b** (0.300 g, 0.511 mmol) and $LiCH_2Si(CH_3)_3$ (0.053 g, 0.563 mmol) and attached to a swivel frit apparatus. The entire assemblage was evacuated, and toluene (50 mL) was vacuum-distilled into the flask. After it was warmed to room temperature, the reaction mixture was stirred for another 45 min, whereby the solvent was removed under vacuum to afford a thick yellow oil. Hexanes (40 mL) were added, and the reaction mixture was filtered. The volume was reduced to 25 mL and the mixture cooled to $-78^\circ C$ for 30 min; during this time a small quantity of fine yellow powder precipitated. The mixture was back-filtered and solvent removed in vacuo to afford **8b** as a light

yellow powder. This material was further recrystallized from hexanes (0.125 g, 0.193 mmol, 38%).

Synthesis of $[\eta^3-ArNC(Bu^t)CHC(Bu^t)NC_6H_5C_3H_6]Sc-CH_2SiMe_3$ (13b**).** In an evacuated flask at $-78^\circ C$ containing **6b** (0.150 g, 0.208 mmol) was condensed toluene (25 mL). The solution was heated to $65^\circ C$ for 3 h and solvent removed under vacuum, yielding a red oil. Recrystallization from hexanes at $-35^\circ C$ afforded small yellow crystals of **13b** (0.032 g, 0.0505 mmol, 24%). 1H NMR: δ 7.20–6.94 (m, 6H; C_6H_5), 5.57 (s, 1H; CH), 3.43 (sp, 1H; $CH(CH_3)_2$, $J_{H-H} = 6.8$ Hz), 3.10 (m, 2H; $CH(CH_3)_2$, $CH_2CH(CH_3)$, $J_{H-H} = 6.8$ Hz), 2.84 (sp, 1H; $CH(CH_3)_2$, $J_{H-H} = 6.8$ Hz), 1.48 (d, 3H; $CH(CH_3)_2$, $J_{H-H} = 6.8$ Hz), 1.39 (d, 3H; $CH(CH_3)_2$, $J_{H-H} = 6.8$ Hz), 1.31 (d, 3H; $CH(CH_3)_2$, $J_{H-H} = 6.8$ Hz), 1.26 (d, 3H; $CH(CH_3)_2$, $J_{H-H} = 6.8$ Hz), 1.21 (d, 3H; $CH(CH_3)_2$, $J_{H-H} = 6.8$ Hz), 1.18 (d, 3H; $CH(CH_3)_2$, $J_{H-H} = 6.8$ Hz), 1.18 (s, 18H; $NCC(CH_3)_3$), 1.02 (d, 3H; $CH(CH_3)_2$, $J_{H-H} = 6.8$ Hz), 0.95, 0.93 (dd, 1H; $CH_2CH(CH_3)$, $J_{H-H} = 11.8$ Hz), 0.09, 0.06 (dd, 1H; $CH_2CH(CH_3)$, $J_{H-H} = 11.8$ Hz), 0.00 (s, 2H; $CH_2Si(CH_3)_3$), -0.25 (s, 9H; $CH_2Si(CH_3)_3$), -1.08 , -1.16 (dd, 2H; $CH_2Si(CH_3)_3$, $J_{H-H} = 11.2$ Hz). $^{13}C\{^1H\}$ NMR: δ 174.2, 173.9 ($NCC(CH_3)_3$), 147.6 (C_{ipso}), 144.9, 144.7, 142.2, 138.2, 127.7, 125.7, 125.6, 124.9, 123.9, 121.5 (C_6H_5), 99.0 (CH), 45.0 ($CH_2Si(CH_3)_3$), 43.4, 43.2 ($C(CH_3)_3$), 39.7 ($CH_2CH(CH_3)$), 32.9, 32.2 ($C(CH_3)_3$), 28.9, 28.7, 28.4 ($CH(CH_3)_2$, one peak not observed), 26.8, 26.0, 25.7, 25.0, 24.5, 23.1 ($CH(CH_3)_2$, one peak not observed), 4.1 ($CH_2Si(CH_3)_3$). Anal. Calcd for $C_{38}H_{56}N_2ClSc$: C, 74.00; H, 10.03; N, 4.43. Found: C, 74.42; H, 10.05; N, 4.47.

Kinetic Experiments. In a typical experiment, the compound of interest (0.0208 mmol) was dissolved in 0.5 mL of toluene- d_8 (4.15×10^{-3} M) and kept at $-78^\circ C$ until inserted into the NMR probe, at which time it was given 10 min to equilibrate to the specified temperature. The progress of reaction was monitored by integration of the ligand backbone peak in the 1H spectrum. The reaction was followed until 95% completion. Although compounds **9b**, **10b**, **11b**, and **12b** were produced via the kinetic experiments, they were not isolated and as a result only the 1H and ^{13}C NMR spectra are reported. Unfortunately, further decomposition of **11a**, **12a**, and **13a** occurred before completion of the kinetic experiments, making it impossible to obtain clean spectra. The kinetic data obtained for these species were limited to the first 65% of the metalation process and are therefore considered only semiquantitative. In the spectroscopic data presented below, the $^3J_{H-H}$ coupling constant between methyl and methine protons in the aryl Pr^t groups was invariably 6.6–7.0 Hz.

9b: 1H NMR δ 7.27–6.98 (m, 6H; C_6H_5), 5.58 (s, 1H; CH), 3.48 (sp, 1H; $CH(CH_3)_2$), 3.12 (m, 2H; $CH(CH_3)_2$, $CH_2CH(CH_3)$), 2.89 (sp, 1H; $CH(CH_3)_2$), 1.43 (d, 3H; $CH(CH_3)_2$), 1.33 (d, 3H; $CH(CH_3)_2$), 1.32 (d, 3H; $CH(CH_3)_2$), 1.31 (d, 3H; $CH(CH_3)_2$), 1.27 (d, 3H; $CH(CH_3)_2$), 1.20 (d, 3H; $CH(CH_3)_2$), 1.19 (s, 18H; $NCC(CH_3)_3$), 1.00 (d, 3H; $CH(CH_3)_2$), 0.81, 0.80 (dd, 1H; $CH_2CH(CH_3)$, $J_{H-H} = 11.8$ Hz), -0.02 , -0.05 (dd, 1H; $CH_2CH(CH_3)$, $J_{H-H} = 11.8$ Hz), -1.10 (s, 3H; CH_3); $^{13}C\{^1H\}$ NMR δ 174.2, 173.9 ($NCC(CH_3)_3$), 147.7, 145.2 (C_{ipso}), 144.9, 141.8, 141.4, 138.1, 127.5, 126.5, 125.9, 124.6, 124.5, 123.3 (C_6H_5), 98.8 (CH), 43.4, 43.2 ($C(CH_3)_3$), 39.7 ($CH_2CH(CH_3)$), 32.9, 32.2 ($C(CH_3)_3$), 29.6, 29.1, 28.9, 28.5 ($CH(CH_3)_2$), 26.8 (CH_3), 26.3, 26.1, 26.0, 25.9, 25.2, 24.4, 22.7 ($CH(CH_3)_2$).

10b: 1H NMR δ 7.35–6.86 (m, 6H; C_6H_5), 5.55 (s, 1H; CH), 3.45 (sp, 1H; $CH(CH_3)_2$), 3.14 (m, 2H; $CH(CH_3)_2$, $CH_2CH(CH_3)$), 2.91 (sp, 1H; $CH(CH_3)_2$), 1.46 (d, 3H; $CH(CH_3)_2$), 1.45 (d, 3H; $CH(CH_3)_2$), 1.32 (d, 3H; $CH(CH_3)_2$), 1.31 (d, 3H; $CH(CH_3)_2$), 1.26 (d, 3H; $CH(CH_3)_2$), 1.19 (d, 3H; $CH(CH_3)_2$), 1.18 (s, 18H; $NCC(CH_3)_3$), 1.03 (d, 3H; $CH(CH_3)_2$), 0.88, 0.87 (dd, 1H; $CH_2CH(CH_3)$, $J_{H-H} = 11.8$ Hz), 0.63 (t, 3H; CH_2CH_3 , $J_{H-H} = 8.2$ Hz), 0.22 (dd, 1H; $CH_2CH(CH_3)$, $J_{H-H} = 11.8$ Hz), -0.63 (q, 1H; CH_2CH_3 , $J_{H-H} = 8.2$ Hz), -0.62 (q, 1H; CH_2CH_3 , $J_{H-H} = 8.2$ Hz); $^{13}C\{^1H\}$ NMR: δ 174.1, 173.8 ($NCC(CH_3)_3$), 147.8, 145.2 (C_{ipso}), 144.7, 142.2, 141.7, 139.7, 127.5, 126.3, 125.6, 124.7, 123.3, 122.1 (C_6H_5), 98.7 (CH), 43.4, 43.2 ($C(CH_3)_3$), 40.0 (CH_2CH_3), 39.7 ($CH_2CH(CH_3)$), 32.9, 32.3 ($C(CH_3)_3$), 29.0, 28.9,

Table 9. Summary of Data Collection and Structure Refinement Details for 1b, 2a, 2b–4b, and 6a,b

	1b	2a	2b	3b	4b	6a	6b
formula	C ₃₅ H ₅₃ N ₂ Cl ₂ Sc	C ₃₅ H ₅₅ N ₂ Osc	C ₃₇ H ₅₉ N ₂ Sc	C ₃₉ H ₆₃ N ₂ Sc	C ₄₉ H ₆₇ N ₂ Sc	C ₃₇ H ₆₃ N ₂ ScSi ₂	C ₄₃ H ₇₅ N ₂ ScSi ₂
fw	617.68	564.79	576.82	604.90	729.04	637.03	721.21
cryst syst	monoclinic	tetragonal	monoclinic	monoclinic	monoclinic	triclinic	monoclinic
<i>a</i> , Å	11.916(2)	27.692(3)	12.9021(10)	18.759(5)	12.653(4)	10.4634(6)	13.469(6)
<i>b</i> , Å	16.243(3)		11.0349(9)	10.427(6)	12.096(3)	11.1017(6)	17.939(6)
<i>c</i> , Å	19.108(4)	17.954(4)	25.341(2)	19.608(5)	28.069(4)	18.0333(10)	19.132(5)
α , deg						80.055(2)	
β , deg	101.353(15)		98.147(2)	107.32(2)	90.77(2)	79.994(2)	90.93(3)
γ , deg						72.406(2)	
<i>V</i> , Å ³	3626.0(11)	13768(4)	3571.5(5)	3661.4(28)	4296(2)	1950.23(19)	4622(3)
space group	<i>P</i> 2 ₁ / <i>n</i>	<i>I</i> / <i>a</i>	<i>P</i> 2 ₁ / <i>n</i>	<i>P</i> 2 ₁ / <i>n</i>	<i>P</i> 2 ₁ / <i>c</i>	<i>P</i> 1	<i>P</i> 2 ₁ / <i>c</i>
<i>Z</i>	4	16	4	4	2	2	4
<i>d</i> _{calcd} , Mg m ⁻³	1.131	1.090	1.073	1.097	1.127	1.085	1.036
μ , mm ⁻¹	0.373	0.238	0.231	0.225	0.205	0.275	0.236
<i>R</i>	0.056	0.053		0.052	0.063		0.060
<i>R</i> _w	0.054	0.048		0.054	0.136		0.059
R1			0.0364			0.0351	
wR2			0.1022			0.0915	
GOF	2.02	1.76	1.090	1.89	1.02	1.051	2.18

28.6, 28.5 (CH(CH₃)₂), 26.3, 26.2, 26.0, 25.9, 25.2, 24.4, 22.8 (CH(CH₃)₂), 12.2 (CH₂CH₃).

11b: ¹H NMR δ 7.27–6.84 (m, 11H; C₆H₃, C₆H₅), 5.58 (s, 1H; CH), 3.13 (sp, 1H; CH(CH₃)₂), 3.11 (m, 2H; CH(CH₃)₂, CH₂CH(CH₃)), 2.92 (sp, 1H; CH(CH₃)₂), 2.12 (s, 2H; CH₂C₆H₅) 1.39 (d, 3H; CH(CH₃)₂), 1.37 (d, 3H; CH(CH₃)₂), 1.31 (d, 3H; CH(CH₃)₂), 1.25 (d, 3H; CH(CH₃)₂), 1.24 (d, 3H; CH(CH₃)₂), 1.22 (d, 3H; CH(CH₃)₂), 1.21 (d, 3H; CH(CH₃)₂), 1.07 (s, 18H; NCC(CH₃)₃), 0.90, 0.89 (dd, 1H; CH₂CH(CH₃), *J*_{H–H} = 11.8 Hz), 0.09, 0.05 (dd, 1H; CH₂CH(CH₃), *J*_{H–H} = 11.8 Hz); ¹³C{¹H} NMR δ 175.4, 173.8 (NCC(CH₃)₃), 149.1, 146.6, 145.4 (C_{ipso}), 143.7, 142.2, 141.7, 140.8, 129.7, 129.1, 128.9, 128.7, 127.0, 126.2, 125.6, 125.0, 123.7, 120.0, 119.5 (C₆H₃, CH₂C₆H₅), 99.4 (CH), 43.4, 43.2 (C(CH₃)₃), 39.7 (CH₂CH(CH₃)), 32.9, 32.3 (C(CH₃)₃), 29.0, 28.9, 28.7, 28.6, (CH(CH₃)₂), 26.8, 26.2, 26.0, 25.7, 25.2, 24.5, 23.6 (CH(CH₃)₂), CH₂C₆H₅ not observed.

12b: ¹H NMR δ 7.34–6.96 (m, 6H; C₆H₃), 5.56 (s, 1H; CH), 3.50 (sp, 1H; CH(CH₃)₂), 3.20 (m, 2H; CH(CH₃)₂, CH₂CH(CH₃)), 2.89 (sp, 1H; CH(CH₃)₂), 1.56 (d, 3H; CH(CH₃)₂), 1.48 (d, 3H; CH(CH₃)₂), 1.34 (d, 3H; CH(CH₃)₂), 1.33 (d, 3H; CH(CH₃)₂), 1.27 (d, 3H; CH(CH₃)₂), 1.18 (d, 3H; CH(CH₃)₂), 1.17 (s, 18H; NCC(CH₃)₃), 1.11 (d, 3H; CH(CH₃)₂), 0.77 (s, 9H; CH₂C(CH₃)₃), 0.21, 0.17 (dd, 1H; CH₂CH(CH₃), *J*_{H–H} = 11.8 Hz), –0.43, –0.55 (dd, 2H; CH₂C(CH₃)₃, *J*_{H–H} = 12.6 Hz), 1H of CH₂CH(CH₃) not observed; ¹³C{¹H} NMR δ 174.0, 173.8 (NCC(CH₃)₃), 147.7, 144.8 (C_{ipso}), 144.7, 142.3, 141.3, 138.7, 128.2, 127.6, 125.6, 123.8, 123.7, 122.1 (C₆H₃), 98.8 (CH), 70.8 (CH₂C(CH₃)₃) 43.4, 43.2 (C(CH₃)₃), 39.8 (CH₂CH(CH₃)), 35.7 (CH₂C(CH₃)₃), 32.6 (C(CH₃)₃), 28.9, 28.8, 28.5, 26.5, (CH(CH₃)₂); 26.1, 26.0, 25.8, 25.7, 25.2, 24.6, 21.9 (CH(CH₃)₂).

X-ray Crystallography. A summary of crystal data and refinement details for all structures is given in Table 9. Suitable crystals were covered in Paratone oil, mounted on a glass fiber, and immediately placed in a cold stream on the diffractometer employed.

1b. Crystals of **1b** were grown from a hexanes solution at –35 °C. Measurements were made using a Rigaku AFC6S diffractometer with a graphite-monochromated Mo K α radiation (λ = 0.710 69 Å) source at –103 °C with the ω –2 θ scan technique to a maximum 2 θ value of 55.1°. The structure was solved by direct methods and expanded using Fourier techniques. The non-hydrogen atoms were refined anisotropically; hydrogen atoms were included at geometrically idealized positions with C–H = 0.95 Å and were not refined. All calculations were performed using the teXsan crystallographic software package of Molecular Structure Corp.

2b. Crystals of **2b** were grown from a hexanes solution at –35 °C. Measurements were made using a Bruker AXS SMART CCD area-detector diffractometer using a graphite-monochromated Mo K α radiation (λ = 0.710 73 Å) source at

–113 °C with a θ range from 1.62 to 28.42°. The structure was solved by Patterson synthesis and refined on *F*² values by full-matrix least squares for all unique data. Programs used were standard Bruker SMART (control) and SAINT (integration), SHELXTL for structure solution, refinement and molecular graphics, and local programs.

3b. Crystals of **3b** were grown from a hexanes solution at –35 °C. Measurements were made at –103 °C with the ω –2 θ scan technique to a maximum 2 θ value of 50.1°. The structure was solved by direct methods and expanded using Fourier techniques. The non-hydrogen atoms were refined anisotropically; hydrogen atoms were included at geometrically idealized positions with C–H = 0.95 Å and were not refined.

4b. Crystals of **4b** were grown from a hexanes solution at –35 °C. Measurements were made at –103 °C with the ω –2 θ scan technique to a maximum 2 θ value of 50.1°. The structure was solved by direct methods and expanded using Fourier techniques. The non-hydrogen atoms were refined anisotropically; hydrogen atoms were included at geometrically idealized positions with C–H = 0.95 Å and were not refined.

6a. Crystals of **6a** were grown from a hexanes solution at –35 °C. Measurements were made using a Bruker AXS SMART CCD area-detector diffractometer at –113 °C with a θ range from 2.42 to 28.89°. The structure was solved by direct methods and refined on *F*² values by full-matrix least squares for all unique data.

6b. Crystals of **6b** were grown from a hexanes solution at –30 °C. Measurements were made at –103 °C with the ω –2 θ scan technique to a maximum 2 θ value of 55.1°. The structure was solved by direct methods and expanded using Fourier techniques. The non-hydrogen atoms were refined anisotropically; hydrogen atoms were included at geometrically idealized positions with C–H = 0.95 Å and were not refined.

Acknowledgment. This work was generously supported by the NOVA Research & Technology Corporation of Calgary, Alberta, Canada, the NSERC of Canada's Research Partnerships office (CRD program), and the EPSRC of the U.K.

Supporting Information Available: Tables of atomic coordinates, anisotropic displacement parameters, and all bond distances and angles for **2a**, **1b–4b**, and **6a,b**. This material is available free of charge via the Internet at <http://pubs.acs.org>.

OM0101310

Cationic Scandium Methyl Complexes Supported by a β -Diketiminato (“Nacnac”) Ligand Framework

Paul G. Hayes,[†] Warren E. Piers,^{*,†} and Robert McDonald[‡]

Department of Chemistry, University of Calgary, 2500 University Drive N.W., Calgary, Alberta, Canada T2N 1N4, and X-ray Structure Laboratory, Department of Chemistry, University of Alberta, Edmonton, Alberta, Canada T6G 2G2

Received September 21, 2001

Alkyl cations of group 4 metals play a crucial role in olefin polymerization catalysis,¹ and the cationic nature of these species is critical to their productivity in this process. This is underscored by the fact that their neutral group 3 metal congeners are generally much less active catalysts.² While this has been recognized for some time, suitable ligand modifications to allow for generation of well-defined group 3 metal cations have been slow to develop. Nonetheless, there are a few recently reported systems for which cationic alkyl scandium³ or yttrium^{3c,4} complexes have been implicated spectroscopically and by higher polymerization activities.

We have recently reported a family of base-free β -diketiminato, “nacnac”, supported dialkyl scandium complexes⁵ and shown that one of the dibenzyl derivatives may be activated with $B(C_6F_5)_3$ to form an ion pair.^{2a} The X-ray structure of this material shows that the $[PhCH_2B(C_6F_5)_3]^-$ counteranion is strongly η^6 coordinated to the cationic scandium center, a feature that is manifested in this ion pair’s complete lack of reactivity toward olefins. Using a sterically more bulky nacnac donor with ^tBu groups in the ligand backbone allows for the isolation of the THF-free dimethyl compound **1**; here we discuss this material’s reactions with varying amounts of the activator $B(C_6F_5)_3$ ⁶ and report the first structural characterization of a scandium methyl cation, along with a preliminary assessment of its solution dynamic behavior. In addition, we show that **1** has ethylene polymerization activities comparable to those of metallocenes under borane activation.

Dimethyl scandium compound **1** reacts with varying equivalencies of $B(C_6F_5)_3$ to form different ion pairs as shown in Scheme 1. Upon reaction with 0.5 equiv of borane, a μ -methyl dimer (**2**) is formed,⁷ as indicated by a characteristic set of resonances for the terminal Sc-Me groups (-0.29 ppm, 6H) and the bridging Sc-Me-Sc group (0.10 ppm, $^1J_{CH} = 132(1)$ Hz, 3H). Dimer **2** could not be isolated as a well-behaved solid and slowly evolves CH_4 in bromobenzene solution,⁷ yielding an as yet uncharacterized product. When **1** is treated with a full equivalent of $B(C_6F_5)_3$, however, a monomeric ion pair $[L^tBuScCH_3]^+[H_3CB(C_6F_5)_3]^-$, **3**, is produced in excellent isolated yield when precipitated from hexane.⁸

As a yellow crystalline solid, **3** is stable for long periods of time at -30 °C. Its solid-state structure is shown in Figure 1 along with selected metrical data. The scandium atom sits 1.232 Å out of the plane defined by the C_3N_2 ligand atoms (mean deviation from plane = 0.053 Å) mainly for steric reasons and not because of any bonding interactions with the ligand backbone CH moiety ($Sc-C(5) = 2.773(6)$ Å).⁵ The $Sc-CH_3$ group occupies the *endo* coordination site (pointing in toward the ligand) while the methyl-

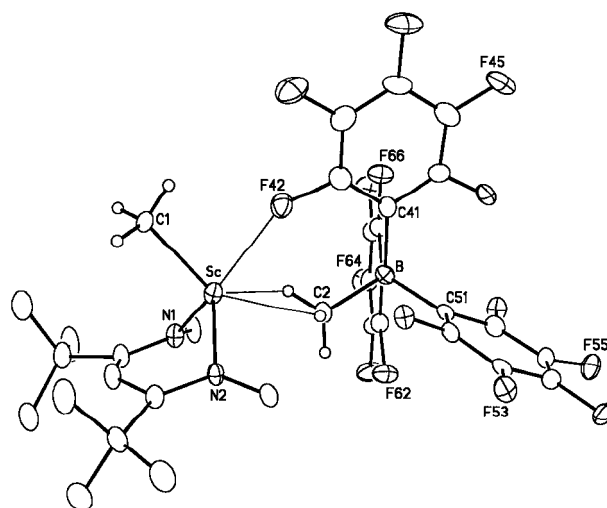
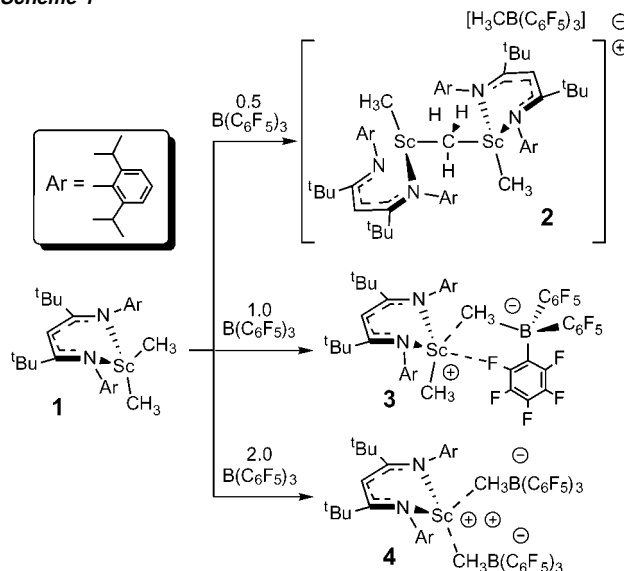


Figure 1. Molecular structure of ion pair **3**; aryl groups have been removed for clarity. Selected bond distances (Å): Sc–N(1), 2.060(5); Sc–N(2), 2.093(5); Sc–C(1), 2.221(5); Sc–C(2), 2.703(6); Sc–F(42), 2.390(4); B–C(2), 1.643(9). Selected bond angles (deg): N(1)–Sc–N(2), 95.06(19); Sc–C(2)–B, 138.72(18); Sc–F(42)–C(42), 153.7(4).

Scheme 1

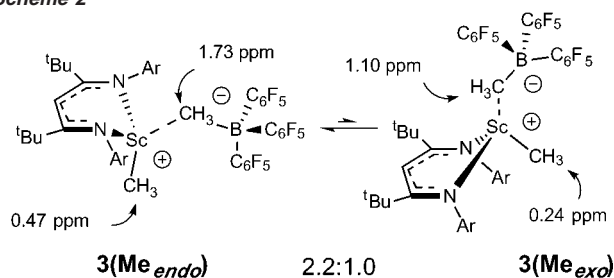


borate counteranion is situated in the sterically more open *exo* site. The methyl group is more closely associated with the boron atom ($B-C(2) = 1.643(9)$ Å) than the scandium atom ($Sc-C(2) = 2.703(6)$ Å), but is not linearly bridged between the two as is

[†] University of Calgary.

[‡] University of Alberta.

Scheme 2



commonly observed in metallocene structures⁷ ($\text{Sc}-\text{C}(2)-\text{B} = 138.72(18)^\circ$). The bending at this angle allows for a weak stabilizing interaction between an *ortho* fluorine group and the scandium center ($\text{Sc}-\text{F}(42) = 2.390(4) \text{ \AA}$); such a bonding mode for the $[\text{H}_3\text{CB}(\text{C}_6\text{F}_5)_3]^-$ anion has been observed previously in an yttrocene derivative.⁹ In **3**, we could find no evidence for such a motif in solution by ^{19}F NMR spectroscopy.

Ion pair **3** exhibits complex dynamic behavior in solution. The ^1H NMR spectrum at room temperature is broad and essentially featureless, although signals for the bridging and terminal methyl groups can be identified at 1.40 and 0.28 ppm, respectively. These signals do not coalesce under any conditions, suggesting that borane dissociation¹⁰ is a high barrier process in this system. When the sample is cooled to 213 K, the spectrum sharpens into a pattern consistent with the presence of two diastereomers (ratio 2.2:1.0) that differ in the *endo/exo* disposition of the terminal methyl group and the anion (Scheme 2). ROESY experiments show that the major diastereomer is the *endo*-Me, *exo*-anion isomer found in the solid state. Analysis of the NMR spectra at various temperatures reveals that exchange of the isomers occurs with a barrier of 12.4(5) kcal mol^{-1} at 263 K. Likely, these diastereomers interconvert via a ligand flipping mechanism similar to that proposed for the neutral dialkyl complexes,⁵ although an associative ion pair reorganization process¹¹ via ion pair quadruples¹² may also be contributing to this exchange; further experiments are underway to unravel the details of this dynamic behavior more completely. Although stable as a solid for long periods, in solution **3** undergoes methane loss via metalation with a ligand isopropyl group⁵ over the course of an hour at room temperature.

Although borane dissociation appears not to occur in these systems, we explored the possibility that excess free $\text{B}(\text{C}_6\text{F}_5)_3$ may catalyze the interconversion of the cationic diastereomers of **3**. Instead, we found that the second scandium methyl group can be abstracted to form the dicationic species **4** (Scheme 1) as an analytically pure white solid. This is indicated by the absence of an upfield $\text{Sc}-\text{CH}_3$ resonance in the ^1H NMR spectrum, and the appearance of signals for two diastereotopic $[\text{MeB}(\text{C}_6\text{F}_5)_3]^-$ anions in the ^1H , ^{11}B , and ^{19}F NMR spectra of the compound. We have observed high barriers to *endo/exo* group exchange in other sterically congested scandium nacnac compounds.¹³ This double abstraction phenomenon has precedent in a non-Cp titanium-based system,¹⁴ but unlike this system, compound **4** is moderately active for ethylene polymerization under ambient conditions (room temperature, 1 atm).

Compound **1** is an effective catalyst for ethylene polymerization under $\text{B}(\text{C}_6\text{F}_5)_3$, trityl borate, or PMAO-IP activation (Table 1) in a slurry batch reactor at 50 °C. Molecular weights are relatively high, and the polydispersities are consistent with a single site catalysis model. Activities are somewhat lower when the dichloride precursor is employed under MAO type activation, indicating that alkylation of the scandium center by organoaluminum reagents is slow. The activities in general, however, approach those observed

Table 1. Ethylene Polymerization with **1** and Various Cocatalysts

E	cat.	CoCat	act. ^a	$M_w (\times 10^{-3})$	M_w/M_n
1 ^{b,c}	LS ScCl_2	PMAO-IP	9.9×10^4	1357	2.2
2 ^{b,c}	1	PMAO-IP	1.2×10^6	1866	1.98
3 ^{b,d}	1	$\text{B}(\text{C}_6\text{F}_5)_3$	3.0×10^5	1051	1.7
4 ^{b,d}	1	TB ^e	4.8×10^5	851	2.48

^a Activity in g PE/mol Sc·h. ^b Polymerization conditions: 50 °C, 300 psi, cyclohexane/toluene, $[\text{Sc}] = 300 \mu\text{M}$, stir rate = 2000 rpm. ^c AI/M = 20. ^d $[\text{Cocatalyst}] = 315 \mu\text{M}$, $[\text{PMAO-IP}] = 1 \text{ mM}$ as scavenger. ^e $[\text{Ph}_3\text{C}][\text{B}(\text{C}_6\text{F}_5)_4]$.

for metallocene and other group 4 based catalysts, demonstrating that scandium cations can be highly effective catalysts. Notably, these activities are observed in the presence of the potentially coordinating solvent toluene,^{3a,15} which was necessary to solubilize the catalyst.

In summary, we have prepared a family of highly reactive organoscandium methyl cations supported by a bulky nacnac ligand and examined their solution and solid-state structures. These represent a new class of cationic organometallic compounds whose rich chemistry we are further exploring.

Acknowledgment. Financial support for this work was provided by Nova Chemicals Ltd. (Calgary, Alberta) and NSERC of Canada in the form of a CRD Grant. NSERC is also acknowledged for an E. W. R. Steacie Memorial Fellowship to W.E.P. (2001–2003) and a PGS A fellowship to P.G.H. Dr. Q. Wang of Nova performed the polymerization experiments.

Supporting Information Available: Experimental details, tables of crystal data, atomic coordinates, bond lengths and angles, and anisotropic displacement parameters for **3** (PDF). This material is available free of charge via the Internet at <http://pubs.acs.org>.

References

- (a) Guram, A. S.; Jordan, R. F. In *Comprehensive Organometallic Chemistry II*; Lappert, M. F., Ed.; Elsevier Scientific Ltd: Oxford, 1995; Vol. 4, p 589. (b) Resconi, L.; Cavallo, L.; Fait, A.; Piemontesi, F. *Chem. Rev.* **2000**, *100*, 1253.
- Shapiro, P. J.; Cotter, W. D.; Schaefer, W. P.; Labinger, J. A.; Bercaw, J. E. *J. Am. Chem. Soc.* **1994**, *116*, 4623.
- (a) Lee, L. W. M.; Piers, W. E.; Elsegood, M. R. J.; Clegg, W.; Parvez, M. *Organometallics* **1999**, *18*, 2947. (b) Canich, J. A. M.; Schaffer, T. D.; Christopher, J. N.; Squire, K. R. World Patent WO0018808, 2000 (Exxon). (c) Hajela, S.; Schaefer, W. P.; Bercaw, J. E. *J. Organomet. Chem.* **1997**, *532*, 45.
- (a) Bambirra, S.; van Leusen, D.; Meetsma, A.; Hessen, B.; Teuben, J. H. *Chem. Commun.* **2001**, 637. (b) Lee, L.; Berg, D. J.; Einstein, F. W.; Batchelor, R. J. *Organometallics* **1997**, *18*, 11819.
- Hayes, P. G.; Lee, L. W. M.; Knight, L. K.; Piers, W. E.; Parvez, M.; Elsegood, M. R. J.; Clegg, W.; MacDonald, R. *Organometallics* **2001**, *20*, 2533.
- Chen, E. Y.-X.; Marks, T. J. *Chem. Rev.* **2000**, *100*, 1391.
- For leading references on μ -methyl dimers in group 4 alkyl cation chemistry, see: Zhang, S.; Piers, W. E.; Parvez, M. *Organometallics* **2001**, *20*, 2088.
- For related aluminum chemistry, see: (a) Korolev, A. V.; Ihara, E.; Guzei, I. A.; Young, V. G., Jr.; Jordan, R. F. *J. Am. Chem. Soc.* **2001**, *123*, 8291. (b) Radzewich, C. E.; Guzei, I. A.; Jordan, R. F. *J. Am. Chem. Soc.* **1999**, *121*, 8673. (c) Dagorne, S.; Guzei, I. A.; Coles, M. P.; Jordan, R. F. *J. Am. Chem. Soc.* **2000**, *122*, 274.
- Song, X.; Thornton-Pett, M.; Bochmann, M. *Organometallics* **1998**, *17*, 1004.
- Deck, P. A.; Beswick, C. L.; Marks, T. J. *J. Am. Chem. Soc.* **1998**, *120*, 1772.
- (a) Beck, S.; Lieber, S.; Schaper, F.; Geyer, A.; Brintzinger, H. H. *J. Am. Chem. Soc.* **2001**, *123*, 1483. (b) Luo, L.; Marks, T. J. *Top. Catal.* **1999**, *7*, 97.
- Beck, S.; Geyer, A.; Brintzinger, H.-H. *Chem. Commun.* **1999**, 2477.
- Knight, L. K.; Piers, W. E.; MacDonald, R. *Chem. Eur. J.* **2000**, *6*, 4322.
- Guerin, F.; Stewart, J. C.; Beddie, C.; Stephan, D. W. *Organometallics* **2000**, *19*, 2994.
- Scollard, J. D.; McConville, D. H. *J. Am. Chem. Soc.* **1996**, *118*, 10008.

JA017128G

Cationic Organoscandium β -Diketiminato Chemistry: Arene Exchange Kinetics in Solvent Separated Ion Pairs

Paul G. Hayes, Warren E. Piers,* and Masood Parvez

Department of Chemistry, University of Calgary, 2500 University Drive NW, Calgary, Alberta, T2N 1N4, Canada

Received February 14, 2003; E-mail: wpiers@ucalgary.ca

It is well established that early transition metal organometallic ion pairs with weakly coordinating anions are the active species in olefin polymerization processes.¹ Increasingly, it is becoming apparent that subtle interplay between cation/anion interactions and solvent effects has a significant impact on ion pair dynamics, which in turn profoundly influence the activity and selectivity of a given catalyst system.² While these effects have been studied experimentally and computationally in some detail for metallocene³ and constrained geometry catalysts families,⁴ some controversy remains concerning the relative importance of contact ion pairs (CIP) versus solvent separated ion pairs (SSIP) in the initiation and propagation steps of a polymerization reaction.⁵ Of the two classes of ion pair, the CIPs are the more well understood from a structural and dynamic perspective. SSIPs formed in relevant nonpolar solvents are more ephemeral species, with few experimentally well-characterized examples in the literature.⁶

Recently, we reported a family of base-free dialkyl organoscandium complexes supported by bulky β -diketiminato ligands incorporating 2,6-diisopropylphenyl groups on nitrogen, and either Me (L^1) or t Bu (L^2) substituents in the 2,4 positions of the ligand backbone.⁷ Activation of the monomeric t Bu-substituted dimethyl compound L^2ScMe_2 with $B(C_6F_5)_3$ gave a well-defined CIP which was highly active for ethylene polymerization.⁸ Here we describe the activation chemistry of the less sterically encumbered scandium dimethyl derivative supported by L^1 , which gives rise to stable SSIPs in arene solvents, providing the opportunity to probe solvent exchange processes in these rare species.

Previously, the compounds L^1ScCl_2 and L^1ScMe_2 were only available as THF adducts,⁷ but we have subsequently discovered that prolonged exposure of $L^1ScCl_2 \cdot THF$ to 10^{-4} Torr at 130 °C removes the base completely. Alkylation of the resulting oligomeric $[L^1ScCl_2]_n$ with MeLi in toluene cleanly affords the base-free dimethyl derivative $[L^1ScMe_2]_2$ in 90% yield. The dimethyl compound is dimeric in the solid state, but, in solution, the terminal and bridging methyl groups are not distinguishable by NMR spectroscopy, suggesting a rapid dimer/monomer equilibrium or an intramolecular exchange process. In any event, reaction of $[L^1ScMe_2]_2$ with common activators yields products consistent with reaction through a monomeric organoscandium compound.

For example, reaction with 1 equiv of $B(C_6F_5)_3$ ⁹ at 240 K showed the formation of the expected CIP $[L^1ScMe]^+[MeB(C_6F_5)_3]^-$. Upon warming to 270 K, however, rapid C_6F_5 transfer from the borate counterion to the metal center, along with production of $MeB(C_6F_5)_2$, was observed.¹⁰ Addition of a second equivalent of borane results in abstraction of the remaining methyl group and formation of the CIP $[L^1Sc-C_6F_5][MeB(C_6F_5)_3]$. Evidently, the lower steric impact of L^1 versus L^2 reduces the barrier for C_6F_5 back-transfer because we do not observe this in the $[L^2ScMe][MeB(C_6F_5)_3]$ CIP.⁸

By contrast, activation of $[L^1ScMe_2]_2$ in d_5 -bromobenzene with 1 equiv of the trityl borate activator, $[CPh_3][B(C_6F_5)_4]$,¹¹ cleanly produces an ion pair (**1a**) which shows no evidence for C_6F_5 transfer

Scheme 1

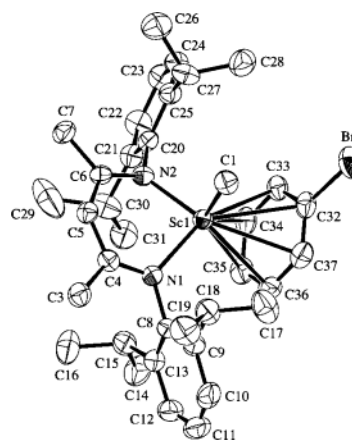
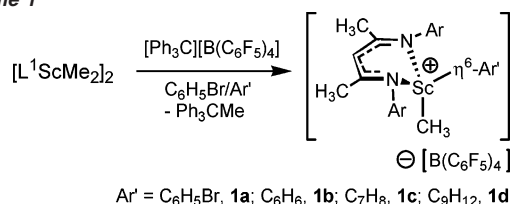


Figure 1. Molecular structure of **1a** (counterion omitted for clarity). Selected bond distances (Å) and angles (deg): Sc(1)–N(1), 2.100(4); Sc(1)–N(2), 2.105(4); Sc(1)–C(1), 2.162(5); Sc(1)–C(32), 2.842(4); Sc(1)–C(33), 2.767(4); Sc(1)–C(34), 2.682(4); Sc(1)–C(35), 2.640(4); Sc(1)–C(36), 2.715(4); Sc(1)–C(37), 2.802(5); N(1)–Sc(1)–N(2), 90.79(14); N(1)–Sc(1)–C(1), 105.22(16); N(2)–Sc(1)–C(1), 105.23(16).

even at elevated temperatures (Scheme 1). X-ray crystallography reveals that in **1a** the bromobenzene solvent, surprisingly, coordinates the cationic Sc center in an η^6 bonding mode (Figure 1). Usually, haloarenes coordinate in an η^1 fashion via the halogen to d^0 metals;¹² the preference for η^6 hapticity here demonstrates the high electrophilicity and steric openness of these cations. Although the aromatic fragment is η^6 bound, steric interactions invoke significant ring tilting ($Sc-C_{\text{arene}} = 2.640(4)–2.842(4)$ Å).¹³ There are no close contacts (≤ 4.9 Å) between the borate anion and the metal center.

The ¹H NMR spectra for SSIP **1a** at various temperatures exhibit a pattern consistent with rapid exchange between free and bound arene. Indeed, upon addition of more basic arenes to **1a**, the bromobenzene is displaced to give new SSIPs **1b–d** (Scheme 1).¹⁴ X-ray crystallography shows that the toluene adduct **1c** is essentially isostructural with **1a**,¹⁵ but the increased basicity of toluene¹⁶ leads to C_s symmetry in the ¹H NMR spectrum at ambient temperatures. Upfield shifted resonances for the η^6 toluene are observed at 6.81, 6.66, 6.39, and 1.85 ppm in C_6D_5Br . Addition of excess d_8 -toluene to this sample of **1c** results in the disappearance of the signals for coordinated toluene over the course of 5 min, indicating exchange with free toluene. Competition experiments show that the order of

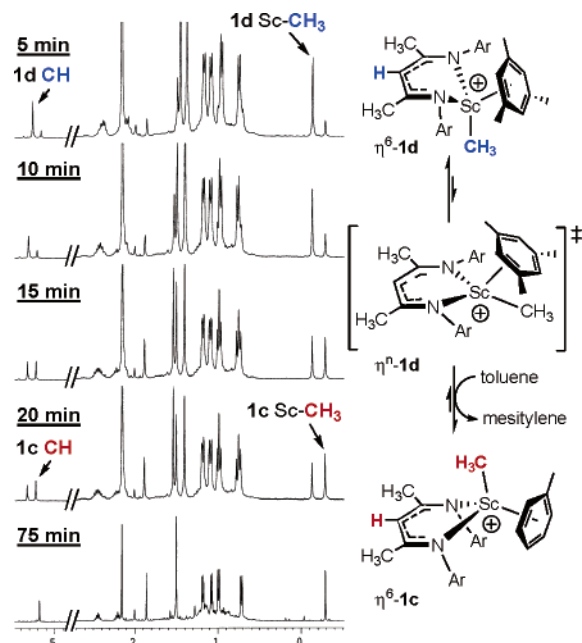


Figure 2. Representative series of ^1H NMR spectra (300 MHz, 270 K, $\text{C}_6\text{D}_5\text{Br}$) for the arene exchange of **1d** to **1c** (left). Proposed mechanism of exchange (right).

arene coordination is $\text{C}_6\text{H}_5\text{Br} \ll \text{C}_6\text{H}_6$ (**1b**) < C_9H_{12} (**1d**) < C_7H_8 , showing that steric factors come into play on incorporation of more than one methyl group in the arene.

At low temperatures, it is possible to quantitatively monitor the displacement of mesitylene from **1d** by toluene to give **1c** under pseudo-first-order conditions by ^1H NMR spectroscopy (Figure 2). The reaction was followed at various temperatures, and an Eyring plot allowed for extraction of the activation parameters ($\Delta H^\ddagger = 21.4(6) \text{ kcal mol}^{-1}$ and $\Delta S^\ddagger = 6(1) \text{ cal mol}^{-1} \text{ K}^{-1}$) which are quite close to those found for ion pair reorganization processes in metallocenium and constrained geometry cations partnered with the $[\text{B}(\text{C}_6\text{F}_5)_4]^-$ anion.¹⁷ Assessment of the rate using varying amounts of toluene (still pseudo-first-order) at the same temperature (261 K) indicates there is no dependence on [toluene]; in fact, at very high [toluene], the rate is slightly depressed, probably because the dielectric constant of the medium has changed significantly under these conditions. Although ΔS^\ddagger is not large enough to support a fully dissociative mechanism, it is slightly positive; in combination with the lack of [toluene] dependence, a mechanism involving partial slippage of the outgoing η^6 arene to a lower hapticity mode before displacement by the more basic toluene (Figure 2) is consistent with our results.

Thermodynamic parameters for arene exchange in cationic d^0 complexes of relevance to olefin polymerization have not been reported to date; indeed, previous examples do not undergo arene exchange readily.⁶ It has been previously noted that toluene has a dampening effect on olefin polymerization activity in lower coordinate, sterically open catalysts,¹⁸ and these results provide a

concrete explanation for this observation. Indeed, preliminary studies using mesitylene complex **1d** as a catalyst show that there is significant polymerization activity when the experiment is conducted in bromobenzene whereas activity is negligible when carried out in more coordinating toluene. Thus, while ethylene is able to displace mesitylene, which has a barrier similar to that of the coordinating anion $[\text{MeB}(\text{C}_6\text{F}_5)_3]^-$, it cannot compete with toluene for the active site, and activity is nullified.

Acknowledgment. This work is dedicated to Prof. Hans H. Brintzinger for his outstanding contributions to organometallic chemistry. Financial support for this work came from the NSERC of Canada in the form of a Discovery Grant and an E. W. R. Steacie Fellowship to W.E.P. (2001–2003), and scholarship support to P.G.H. (PGS-A and PGS-B). P.G.H. also thanks the Alberta Heritage Foundation for a Steinhauer Award and the Sir Izaak Walton Killam Foundation for a Fellowship.

Supporting Information Available: Experimental details, tables of crystal data, atomic coordinates, bond lengths and angles, and anisotropic parameters for **1a** and **1c** (PDF and CIF). This material is available free of charge via the Internet at <http://pubs.acs.org>.

References

- (1) (a) Guram, A. S.; Jordan, R. F. In *Comprehensive Organometallic Chemistry II*; Lappert, M. F., Ed.; Elsevier Scientific Ltd: Oxford, 1995; Vol. 4, p 589. (b) Resconi, L.; Cavallo, L.; Fait, A.; Piemontesi, F. *Chem. Rev.* **2000**, *100*, 1253.
- (2) (a) Beck, S.; Lieber, S.; Schaper, F.; Geyer, A.; Brintzinger, H.-H. *J. Am. Chem. Soc.* **2001**, *123*, 1483. (b) Schaper, F.; Geyer, A.; Brintzinger, H.-H. *Organometallics* **2002**, *21*, 473. (c) Chen, M.-C.; Marks, T. J. *J. Am. Chem. Soc.* **2001**, *123*, 11803. (d) Lanza, G.; Fragalà, I. L.; Marks, T. J. *J. Am. Chem. Soc.* **2000**, *122*, 12764. (e) Lanza, G.; Fragalà, I. L.; Marks, T. J. *J. Am. Chem. Soc.* **1998**, *120*, 8257.
- (3) Chan, M. S. W.; Vanka, K.; Pye, C. C.; Ziegler, T. *Organometallics* **1999**, *18*, 4624.
- (4) Lanza, G.; Fragalà, I. L.; Marks, T. J. *Organometallics* **2002**, *21*, 5594.
- (5) Landis, C. R.; Rossaaen, K. A.; Sillars, D. R. *J. Am. Chem. Soc.* **2003**, *125*, 1710.
- (6) (a) Lancaster, S. J.; Robinson, O. B.; Bochmann, M. *Organometallics* **1995**, *14*, 2456. (b) Gillis, D. J.; Quyoum, R.; Tudoret, M.-J.; Wang, Q.; Jeremic, D.; Roszak, A. W.; Baird, M. C. *Organometallics* **1996**, *15*, 3600.
- (7) Hayes, P. G.; Lee, L. W. M.; Knight, L. K.; Piers, W. E.; Parvez, M.; Elsegood, M. R. J.; Clegg, W.; MacDonald, R. *Organometallics* **2001**, *20*, 2533.
- (8) Hayes, P. G.; Piers, W. E.; McDonald, R. *J. Am. Chem. Soc.* **2002**, *124*, 2132.
- (9) Chen, E. Y. X.; Marks, T. J. *Chem. Rev.* **2000**, *100*, 1391.
- (10) Yang, X.; Stern, C. L.; Marks, T. J. *J. Am. Chem. Soc.* **1994**, *116*, 10015.
- (11) Chien, J. C. W.; Rausch, M. D.; Tsai, W.-M. *J. Am. Chem. Soc.* **1991**, *113*, 8570.
- (12) Bouwkamp, M. W.; de Wolf, J.; del Hierro Morales, I.; Gercama, J.; Meetsma, A.; Troyanov, S. I.; Hessen, B.; Teuben, J. H. *J. Am. Chem. Soc.* **2002**, *124*, 12956 and references therein.
- (13) Lee, L. W. M.; Piers, W. E.; Elsegood, M. R. J.; Clegg, W.; Parvez, M. *Organometallics* **1999**, *18*, 2947.
- (14) While arene exchange in d^0 metals is rare, several studies involving d^0 metals exist, see for leading references: Traylor, T. G.; Stewart, K. J. *J. Am. Chem. Soc.* **1986**, *108*, 6977.
- (15) See Supporting Information for details.
- (16) Brouwer, D. M.; Mackor, E. L.; MacLean, C. In *Carbonium Ions*; Olah, G. A.; Schleyer, P. v. R., Eds.; Wiley: New York, 1970; Vol. 2, p 837.
- (17) Jia, L.; Yang, X.; Stern, C. L.; Marks, T. J. *Organometallics* **1997**, *16*, 842.
- (18) Scollard, J. D.; McConville, D. H. *J. Am. Chem. Soc.* **1996**, *118*, 10008.

JA034680S